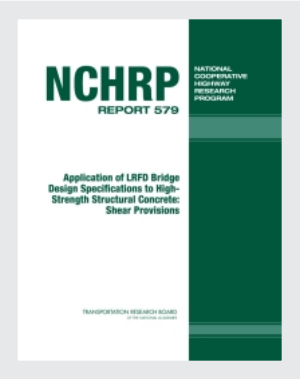

Application of LRFD Bridge Design Specifications to High-Strength Structural Concrete: Shear Provisions

DETAILS

197 pages | | PAPERBACK

ISBN 978-0-309-42282-6 | DOI 10.17226/17616

AUTHORS

Neil M Hawkins; Daniel A Kuchma; Transportation Research Board

NATIONAL COOPERATIVE HIGHWAY RESEARCH PROGRAM

NCHRP REPORT 579

Application of LRFD Bridge Design Specifications to High-Strength Structural Concrete: Shear Provisions

Neil M. Hawkins
Daniel A. Kuchma
UNIVERSITY OF ILLINOIS
Urbana, IL

Subject Areas
Bridges, Other Structures, and Hydraulics and Hydrology

Research sponsored by the American Association of State Highway and Transportation Officials
in cooperation with the Federal Highway Administration

TRANSPORTATION RESEARCH BOARD

WASHINGTON, D.C.
2007
www.TRB.org

NATIONAL COOPERATIVE HIGHWAY RESEARCH PROGRAM

Systematic, well-designed research provides the most effective approach to the solution of many problems facing highway administrators and engineers. Often, highway problems are of local interest and can best be studied by highway departments individually or in cooperation with their state universities and others. However, the accelerating growth of highway transportation develops increasingly complex problems of wide interest to highway authorities. These problems are best studied through a coordinated program of cooperative research.

In recognition of these needs, the highway administrators of the American Association of State Highway and Transportation Officials initiated in 1962 an objective national highway research program employing modern scientific techniques. This program is supported on a continuing basis by funds from participating member states of the Association and it receives the full cooperation and support of the Federal Highway Administration, United States Department of Transportation.

The Transportation Research Board of the National Academies was requested by the Association to administer the research program because of the Board's recognized objectivity and understanding of modern research practices. The Board is uniquely suited for this purpose as it maintains an extensive committee structure from which authorities on any highway transportation subject may be drawn; it possesses avenues of communications and cooperation with federal, state and local governmental agencies, universities, and industry; its relationship to the National Research Council is an insurance of objectivity; it maintains a full-time research correlation staff of specialists in highway transportation matters to bring the findings of research directly to those who are in a position to use them.

The program is developed on the basis of research needs identified by chief administrators of the highway and transportation departments and by committees of AASHTO. Each year, specific areas of research needs to be included in the program are proposed to the National Research Council and the Board by the American Association of State Highway and Transportation Officials. Research projects to fulfill these needs are defined by the Board, and qualified research agencies are selected from those that have submitted proposals. Administration and surveillance of research contracts are the responsibilities of the National Research Council and the Transportation Research Board.

The needs for highway research are many, and the National Cooperative Highway Research Program can make significant contributions to the solution of highway transportation problems of mutual concern to many responsible groups. The program, however, is intended to complement rather than to substitute for or duplicate other highway research programs.

NCHRP REPORT 579

Project 12-56
ISSN 0077-5614
ISBN 978-0-309-09886-1
Library of Congress Control Number 2007928891

COPYRIGHT PERMISSION

NOTICE

The project that is the subject of this report was a part of the National Cooperative Highway Research Program conducted by the Transportation Research Board with the approval of the Governing Board of the National Research Council. Such approval reflects the Governing Board's judgment that the program concerned is of national importance and appropriate with respect to both the purposes and resources of the National Research Council.

The members of the technical committee selected to monitor this project and to review this report were chosen for recognized scholarly competence and with due consideration for the balance of disciplines appropriate to the project. The opinions and conclusions expressed or implied are those of the research agency that performed the research, and, while they have been accepted as appropriate by the technical committee, they are not necessarily those of the Transportation Research Board, the National Research Council, the American Association of State Highway and Transportation Officials, or the Federal Highway Administration, U.S. Department of Transportation.

Each report is reviewed and accepted for publication by the technical committee according to procedures established and monitored by the Transportation Research Board Executive Committee and the Governing Board of the National Research Council.

The Transportation Research Board of the National Academies, the National Research Council, the Federal Highway Administration, the American Association of State Highway and Transportation Officials, and the individual states participating in the National Cooperative Highway Research Program do not endorse products or manufacturers. Trade or manufacturers' names appear herein solely because they are considered essential to the object of this report.

Published reports of the

NATIONAL COOPERATIVE HIGHWAY RESEARCH PROGRAM

are available from:

Transportation Research Board
Business Office
500 Fifth Street, NW
Washington, DC 20001

and can be ordered through the Internet at:

http://www.national-academies.org/trb/bookstore

Printed in the United States of America

THE NATIONAL ACADEMIES

Advisers to the Nation on Science, Engineering, and Medicine

The **National Academy of Sciences** is a private, nonprofit, self-perpetuating society of distinguished scholars engaged in scientific and engineering research, dedicated to the furtherance of science and technology and to their use for the general welfare. On the authority of the charter granted to it by the Congress in 1863, the Academy has a mandate that requires it to advise the federal government on scientific and technical matters. Dr. Ralph J. Cicerone is president of the National Academy of Sciences.

The **National Academy of Engineering** was established in 1964, under the charter of the National Academy of Sciences, as a parallel organization of outstanding engineers. It is autonomous in its administration and in the selection of its members, sharing with the National Academy of Sciences the responsibility for advising the federal government. The National Academy of Engineering also sponsors engineering programs aimed at meeting national needs, encourages education and research, and recognizes the superior achievements of engineers. Dr. William A. Wulf is president of the National Academy of Engineering.

The **Institute of Medicine** was established in 1970 by the National Academy of Sciences to secure the services of eminent members of appropriate professions in the examination of policy matters pertaining to the health of the public. The Institute acts under the responsibility given to the National Academy of Sciences by its congressional charter to be an adviser to the federal government and, on its own initiative, to identify issues of medical care, research, and education. Dr. Harvey V. Fineberg is president of the Institute of Medicine.

The **National Research Council** was organized by the National Academy of Sciences in 1916 to associate the broad community of science and technology with the Academy's purposes of furthering knowledge and advising the federal government. Functioning in accordance with general policies determined by the Academy, the Council has become the principal operating agency of both the National Academy of Sciences and the National Academy of Engineering in providing services to the government, the public, and the scientific and engineering communities. The Council is administered jointly by both the Academies and the Institute of Medicine. Dr. Ralph J. Cicerone and Dr. William A. Wulf are chair and vice chair, respectively, of the National Research Council.

The **Transportation Research Board** is a division of the National Research Council, which serves the National Academy of Sciences and the National Academy of Engineering. The Board's mission is to promote innovation and progress in transportation through research. In an objective and interdisciplinary setting, the Board facilitates the sharing of information on transportation practice and policy by researchers and practitioners; stimulates research and offers research management services that promote technical excellence; provides expert advice on transportation policy and programs; and disseminates research results broadly and encourages their implementation. The Board's varied activities annually engage more than 5,000 engineers, scientists, and other transportation researchers and practitioners from the public and private sectors and academia, all of whom contribute their expertise in the public interest. The program is supported by state transportation departments, federal agencies including the component administrations of the U.S. Department of Transportation, and other organizations and individuals interested in the development of transportation. **www.TRB.org**

www.national-academies.org

CRP STAFF FOR NCHRP REPORT 579

Christopher W. Jenks, *Director, Cooperative Research Programs*
Crawford F. Jencks, *Deputy Director, Cooperative Research Programs*
David B. Beal, *Senior Program Officer*
Eileen P. Delaney, *Director of Publications*
Beth Hatch, *Editor*

NCHRP PROJECT 12-56 PANEL
Field of Design—Area of Bridges

Julius F. J. Volgyi, Jr., *Virginia DOT* (Chair)
David Hohmann, *Texas DOT*
Ralph J. DeStefano, *Pennsylvania DOT*
Fouad H. Fouad, *University of Alabama–Birmingham*
Jen-Chi Hsieh, *Washington State DOT*
Jay Puckett, *BridgeTech, Inc., Laramie, WY*
Madhwesh Raghavendrachar, *California DOT*
Bala Sivakumar, *Lichtenstein Consulting Engineers, Inc., Paramus, NJ*
Joey Hartmann, *FHWA Liaison*
Stephen F. Maher, *TRB Liaison*

AUTHOR ACKNOWLEDGMENTS

The research reported herein was performed under NCHRP Project 12-56 by the Department of Civil and Environmental Engineering (CEE) at the University of Illinois at Urbana-Champaign (UIUC), with subcontracting and consulting services provided by Wiss, Janney, Elstner Associates and Henry Russell.

The Principal Investigators (PIs) on this project were Neil M. Hawkins (PI) and Daniel A. Kuchma (Co-PI) from the University of Illinois at Urbana-Champaign. The other Co-PIs and authors of this report are Gary Klein, Neal Anderson, and Henry Russell.

The work was done under the general supervision of Neil M. Hawkins and Daniel A. Kuchma, with the additional leadership by four PhD students, Kang Su Kim, Tom Nagle, Shaoyun Sun, and Heui Hwang Lee. Other student assistants on this project were Nathan Carroll, Joe Wilkey, Justin Barton, Monica Lim, Ayodele Ogunsola, Katrina Willenborg, Chris Wu, Charlie McLean, Sang Ho Kim, Jun Ji, Zhenhua Huang, Joe Podge, Tina Kidwell, Markus Haiden, and Ken Marley. The PIs also wish to express their sincere appreciation to Prestress Engineering Corporation for fabrication of the test girders, to the CEE machine shop for assistance in preparation of the test set-up and girder handling, to the CEE department for support of undergraduate research assistants, to the Precast/Prestressed Concrete Institute for substantial financial support, to the National Science Foundation for support on a synergistic project, and to the NCHRP project panel and manager, David Beal, for their project oversight and valuable insight and feedback.

FOREWORD

By David B. Beal
Staff Officer
Transportation Research Board

This report contains the findings of research performed to extend the applicability of shear design provisions for reinforced and prestressed concrete structures in the *AASHTO LRFD Bridge Design Specifications* to concrete compressive strengths greater than 10 ksi. The report details the research performed and includes recommended revisions to the specifications. The material in this report will be of immediate interest to bridge designers.

The *AASHTO LRFD Bridge Design Specifications* state: "Concrete strengths above 10.0 ksi shall be used only when physical tests are made to establish the relationships between the concrete strength and other properties." When the LRFD specifications were written, the data were insufficient to demonstrate that the provisions were applicable to concrete compressive strengths above 10 ksi (high-strength concrete). Nevertheless, recent research has started to address design issues with high-strength concrete, and the FHWA Showcase Projects are encouraging the use of high-strength concrete in bridge structures. There is a need to expand the LRFD specifications to allow greater use of high-strength concrete.

The objective of this research was to develop recommended revisions to the *AASHTO LRFD Bridge Design Specifications* to extend the applicability of shear design provisions for reinforced and prestressed concrete structures to concrete compressive strengths greater than 10 ksi. The research effort also included an article-by-article review of Section 5 of the specifications to identify all provisions that directly or indirectly have the potential for preventing the extension of the specifications to high-strength concrete. Companion NCHRP projects 12-60 and 12-64 address transfer and development length, and flexure and compression, respectively; these projects are scheduled for completion in 2007.

This research was performed by the University of Illinois at Urbana-Champaign. The report fully documents the research leading to the recommended specifications. The recommendations are under consideration for possible adoption by the AASHTO Highway Subcommittee on Bridges and Structures in 2007.

CONTENTS

SUMMARY

The use of high-strength concrete (HSC) offers considerable economic advantages in the design, construction, and maintenance of bridge structures. The use of HSC, rather than normal-strength concrete, enables a section of a given size to support larger loads or span longer distances. In addition, the improved durability usually associated with HSC increases the lifespan of structures and increases the ability to meet larger future loading demands.

Concretes with compressive strengths up to 24 ksi were commercially available as of 2004. However, designers and bridge owners have not taken full advantage of HSC. One reason has been a lack of experience in the use of HSC in bridge structures. This problem was addressed in a series of showcase projects that were completed throughout the United States to demonstrate the advantages and methods for the effective use of HSC. A technical barrier to the use of concrete strengths in excess of 10 ksi is the *AASHTO LRFD Bridge Design Specifications* (*1*), which generally limit the cylinder compressive strength (f'_c) that can be used in design expressions to 10 ksi. The principal reason for this limitation is that many existing provisions are based on experimental test data and very little of this data is from tests on specimens cast with HSC. To overcome this problem, the American Association of State Highway and Transportation Officials (AASHTO) sponsored a series of National Cooperative Highway Research Program (NCHRP) projects aimed at extending provisions to permit the use of concrete strengths much higher than 10 ksi. Within these projects, the experiments necessary for extension of the provisions have been conducted, and revised provisions have been developed to enable the use of HSC.

The primary goal of NCHRP Project 12-56 was the extension of the shear provisions in the *AASHTO LRFD Bridge Design Specifications* to concrete strengths greater than 10 ksi. This action principally involved the extension of the Sectional Design Model, which is the specified procedure for determining the required amounts of shear reinforcement, to higher concrete strengths. The Sectional Design Model shear procedure was introduced to the U.S. bridge community with the LRFD specifications. The model was derived from the Modified Compression Field Theory (MCFT) (*2*), which is a comprehensive behavioral model for predicting the shear response of diagonally cracked concrete. Compared with the traditional shear design model of the AASHTO *Standard Specifications for Highway Bridges* (17th Edition, 2002), the Sectional Design Model provided newer strain-based relationships for evaluating the contribution of concrete and vertical transverse reinforcement to the shear capacity, as well as newer limits for minimum shear reinforcement and maximum shear design strength.

This summary contains a brief discussion of key issues relevant to the extension of the Sectional Design Model to HSC, an overview of the research program, a summary of the results, and a summary of the proposed changes to the *AASHTO LRFD Bridge Design*

Specifications resulting from this project. Potential difficulties for the extension of the Sectional Design Model to HSC can be divided into five primary areas:

1. **Contribution of concrete (V_c).** In the LRFD Sectional Design Model, the concrete contribution to shear resistance is determined from the tensile stress that can be carried perpendicular to the field of diagonal compression. Between cracks, this tension is carried by tensile stresses in the concrete, while at crack locations the tension is assumed to be carried by a combination of local increases in reinforcement stresses and shear on the faces of the cracks. The resistance to shear slip on the crack face is evaluated in the LRFD provisions as a function of crack width, concrete compressive strength, and maximum aggregate size, where crack width is taken as the average principal tensile strain in the concrete multiplied by the crack spacing. The crack spacing is assumed to be 12 inches for members with shear reinforcement. A potential concern for the extension of this concept to HSC was that cracks in HSC were likely to be smoother and more widely spaced than in regular-strength concrete, which could lead to a decreased shear slip capacity and, thus, a smaller concrete contribution to shear resistance.
2. **Contribution of shear reinforcement (V_s).** Codes of practice throughout the world use a parallel chord truss model for evaluating the contribution of shear reinforcement to shear resistance. By this approach, the contribution of the shear reinforcement to resistance is equal to the yield capacity of an individual stirrup ($A_v f_y$) times the number of stirrups crossing the diagonal compression field ($d_v \cot\theta/s$) where d_v is the flexural lever arm or shear depth, s is the spacing of the stirrups, and θ is the angle of diagonal compression. In the LRFD Sectional Design Model, θ can be taken to be as low as 18.1 degrees, and in this case stirrups are calculated to provide approximately three times the shear strength, V_s, than they would be calculated to provide in accordance with the AASHTO *Standard Specifications for Highway Bridges* (*3*), in which θ is assumed to be 45 degrees. With the extension to HSC, the accuracy of the LRFD-based values for θ are more critical because, with the higher shear design forces permitted by the LRFD Sectional Design Model, larger contributions from the shear reinforcement are required.
3. **Minimum shear reinforcement.** The LRFD specifications increase the minimum required amount of shear reinforcement over that required by the AASHTO standard specifications. However, no evaluation has been made as to whether the same level of reinforcement is appropriate for very high-strength concretes in which the energy released at diagonal cracking is much larger and cracks are smoother and more widely spaced than in normal-strength concretes.
4. **Maximum shear strength limit.** In the AASHTO standard specifications, the maximum design shear force is controlled by a limit on the contribution of the shear reinforcement, V_s, of $8\sqrt{f'_c}\, b_v d_v$ where f'_c is in psi units. By contrast, in the LRFD specifications, the maximum shear design stress is $0.25f'_c$ plus the vertical component of the prestressing steel. The ratio of these two limits (LRFD limit to standard specification limit) increases as the concrete strength increases, from 1.42, to 2.25, to 3.18 for reinforced concrete members cast with 4, 10, and 20 ksi concrete, respectively. Thus, it was very important to investigate if the LRFD shear stress limit was appropriate for the design of HSC structures.
5. **Validity of assumptions made in derivation of LRFD model.** It can be argued that because the LRFD specifications are derived from a comprehensive behavioral model they are more likely to be applicable for structures that use new or high-strength materials. It can also be argued that because there has been considerably less field experience in the use of the LRFD specifications and because the assumptions made in the derivation of the Sectional Design Model (*4*) may not be appropriate for high-strength concrete, there is a marked need to evaluate this methodology for members cast with HSC.

In order to determine what experiments were most useful for extending the LRFD Sectional Design Model to HSC, a large experimental shear database of existing results from prior shear tests was assembled and then used to evaluate the effect of concrete strength on the safety of the existing LRFD provisions. Based on the results of this review, and from consideration of where HSC may be of greatest economic advantage, it was decided to conduct shear tests on uniformly loaded precast prestressed concrete bulb-tee girders. The largest bulb-tee girders that could be successfully tested, considering economic and testing resources, were girders 63 inches deep and 52 feet long. These girders were uniformly loaded because the resulting design shear forces at the first critical section were often in excess of 500 kips and a uniformly distributed load produces a pattern of cracking and a loading regime more representative of what is likely in field structures.

The principal variables in the testing program were the design shear stress level, the amount of shear reinforcement ($\rho_v f_y$ = 100 to 2,500 psi), the specified strength of the concrete (f'_c = 10 through 18 ksi), and the end anchorage conditions (straight and bonded strands, debonded strands, draped strands, additional bottom tension reinforcement, additional longitudinal reinforcement distributed over the depth of the girder, and anchorage enhancing steel spirals positioned within the transfer length of the strand). The girders were designed to evaluate the LRFD Sectional Design Model for the full range of possible failure modes permitted by the LRFD specifications, including yielding and rupture of shear reinforcement, crushing of a uniform diagonal compression field, local crushing above the support with and without stirrup yielding, and failure driven by slip of the prestressing strands. All members were designed to satisfy the requirements of the *AASHTO LRFD Bridge Design Specifications*, Second Edition, including the 2001 Interim Revisions (*5*).

In order to generate the data necessary for a thorough evaluation of the LRFD Sectional Design Model, significant experimental and materials testing, additional to the girder testing, were conducted and the girders were extensively instrumented. The material tests included compression tests, split cylinder tests, fracture tests, and shear friction tests. The instrumentation on each girder during its testing consisted of more than 100 strain gages on stirrups, two dozen displacement transducers, concrete surface strain gages, and the use of distributed deformation measurement systems. Further, most girders were instrumented so that the loss in prestress from release through the time of testing was known. One of the deformation measurement systems was capable of measuring the x, y, z coordinates of hundreds of points to a very high accuracy so that strain and deformation distributions over the depth of the girder, and for a significant length adjacent to the support, were measured over the duration of a test. This information proved vital to understanding the mechanisms of shear resistance; assessing the performance of end regions; evaluating angles of diagonal compression; and assessing the accuracy of the AASHTO LRFD, AASHTO standard, and other shear design specifications.

After review of the experimental test data collected from this and previous experimental research programs, the following conclusions were drawn:

- The limit in the 1996 AASHTO LRFD specifications and its interim revisions through 2006 on the compressive strength of concrete used in the Sectional Design Model can be raised to 18 ksi for normal weight concretes without a decrease in the accuracy of these provisions.
- The LRFD Sectional Design Model, with an f'_c limit of 18 ksi, is reasonably accurate and conservative except when designing for very high shear design stresses, $v_u > 0.18f'_c$, or when the staggered shear design concept is used away from end regions.
- The shear design provisions in the AASHTO standard specifications, the 2004 Canadian standards specifications (*6*), and the recommended simplified shear specifications

described in *NCHRP Report 549* (*7*) provide similarly conservative estimates of the shear capacity of the test beams subject to the same limitations as those described in the previous bulleted conclusion.
- Designing members for shear stresses in excess of $v_u = 0.15 f'_c$ can result in shear cracking and localized stirrup yielding under service load levels.
- While the LRFD specifications permit the design of end regions for shear by the Sectional Design Model, these regions are better designed by considering the flow of forces in that region, as can be done using a strut-and-tie design approach such as that provided in Article 5.6.3 of the LRFD specifications. This conclusion illustrates what was observed experimentally, which is that draping reinforcement over the height of the web and the bulb and providing additional end region longitudinal reinforcement significantly improve the behavior and strength of end regions.

Based on these conclusions, the following changes are recommended to the *AASHTO LRFD Bridge Design Specifications*:

- The limit on f'_c for the Sectional Design Model should be raised to 18 ksi for normal weight concretes.
- For members that are not cast integrally with supports, the maximum nominal shear stress resistance should be reduced to $v_u = 0.18 f'_c + v_p$ unless the end region is designed by the strut-and-tie method (S5.6.3).
- The option for the use of the staggered shear design method away from the support region should be removed.

CHAPTER 1

Introduction and Research Approach

The current limitation of 10 ksi on the compressive strength of concrete that may be used in the *AASHTO LRFD Bridge Design Specifications* (also referred to as "LRFD specifications") is a barrier to advancements in highway design and construction practice. The relaxation of this limitation would enable bridge members of a given depth to span longer distances, support heavier loads, and have longer design lives, thereby providing considerable economic benefits. This project was one of several projects sponsored through the National Cooperative Highway Research Program (NCHRP) by the Federal Highway Administration (FHWA) that were aimed at enabling the use of high-strength concrete (HSC) in the LRFD specifications.

Section 1.1 discusses those elements of the LRFD Sectional Design Model that require examination for their extension to HSC, and Section 1.2 provides a summary of project objectives and a task-by-task description of the research methodology. Chapter 2 presents the results from a review of practice, discusses areas to which the LRFD specifications can be extended with data available prior to this study, the plan of research for the project, and the results of the experimental and analytical work of the project. Chapter 3 presents proposed changes to the LRFD specifications. Chapter 4 presents overall conclusions, identifies concerns with current practice, and suggests where further research is desirable.

1.1 AASHTO LRFD Shear Design Specifications

To extend the LRFD shear provisions to HSC, it is useful to begin by examining the details of these provisions and identifying where additional study is likely to be warranted for the extension of these provisions. With the LRFD specifications, a new methodology for shear design, the Sectional Design Model, was introduced to the U.S. bridge design community. This method was derived from the Modified Compression Field Theory (MCFT) and is a significant departure from the shear design procedures in AASHTO's *Standard Specifications for Highway Bridges* (also referred to as "AASHTO Standard Specifications"). In this Sectional Design Model, the concrete contribution to shear resistance is based on the ability of cracked concrete to carry diagonal tension in the web of a member, the steel contribution to shear resistance is calculated using a variable angle truss model, a size effect is considered for members without shear reinforcement, the use of a staggered shear design approach over the entire length of a member is permitted, the minimum and maximum shear limits are substantially changed from those of the AASHTO Standard Specifications, and the longitudinal reinforcement requirements must consider the effect of all sectional force demands. Further changes in the LRFD Sectional Design Model are expected to stem from the outcome of the NCHRP 12-61 study, "Simplified Shear Design of Structural Concrete Members."

The foregoing and other aspects of the LRFD Sectional Design Model are discussed in Sections 1.1.1 through 1.1.9 of this report. Within each of these sections, potential issues for the extension of the model to HSC are identified. When relevant, differences between the LRFD specifications and AASHTO Standard Specifications are discussed. The LRFD Sectional Design Model has not been as fully field-tested as the AASHTO Standard Specifications method, and the extension of the LRFD Sectional Design Model to HSC typically enlarges the differences between the two methods. In Section 1.1.10, the impact of the outcome of the NCHRP 12-61 study is presented because the results of that study and this study are closely related.

1.1.1 Derivation of the LRFD Sectional Design Model

The LRFD Sectional Design Model was derived from the MCFT. That theory is a model for predicting the complete load-deformation response of diagonally cracked concrete.

The MCFT can be fully implemented in membrane elements that are subjected to in-plane shear and axial forces in two directions. To fully use the MCFT for predicting the behavior of a real structure requires the use of a nonlinear finite element program. Thus, when a design procedure was derived from the MCFT, it was necessary to make several simplifications and assumptions. For the extension of the LRFD Sectional Design Model to HSC, it is important to assess both (a) whether the underlying relationships in the MCFT are applicable to HSC and (b) whether the assumptions made in the derivation of the LRFD Sectional Design Model are as applicable to the design of HSC structures as they are to customary concrete strength structures. A brief summary of the MCFT and the assumptions made in the derivation of the LRFD Sectional Design Model from the MCFT is now presented.

The MCFT is an extension of the Compression Field Theory (CFT) (*8*), which provided a solution to the nearly century old problem of how to assess the angle of the diagonal compression flow (θ) in a reinforced or prestressed concrete beam. Prior to the CFT, it was not possible to evaluate θ because equilibrium provided only three equations, and for any member subjected to a known shear, there are four or five unknowns (i.e., diagonal compressive stress, angle of diagonal compression, stresses in the deformed longitudinal and shear reinforcement, and stress in the prestressing steel). The CFT introduced the use of strain compatibility relationships and material constitutive relationships that provided the additional relationships necessary to solve for θ and the other unknowns (i.e., the principal diagonal compressive stress, the inclination of the principal compressive stresses θ, the tensile force in the longitudinal reinforcement, and the stress in the stirrups). In the CFT, the entire shear resistance was calculated as being provided by the shear reinforcement. The MCFT added a concrete component to resistance by considering the diagonal tensile stress that the concrete could carry perpendicular to the direction of diagonal compression (or cracking). The MCFT assumes that the directions of principal strain and stress coincide and also considers the effects of compression softening and tension stiffening. The equilibrium, constitutive, and compatibility relations of the MCFT are presented in Figure 1. In summary, the MCFT allows the state of strain $\{\varepsilon_x, \varepsilon_y, \gamma_{xy}\}$ or $\{\varepsilon_1, \varepsilon_2, \theta\}$ to be calculated from the applied stress $\{f_x, f_y, v_{xy}\}$ or $\{f_1, f_2, v\}$, as described in Figure 1(a), or visa versa. More generally, if any combination of three values is known, then the other three can be found from the MCFT. This concept was used in the derivation of the LRFD Sectional Design Model—where, for members with shear reinforcement, v_{xy} and ε_x are evaluated by the designer and f_y is taken as zero—and then the MCFT is used to determine all other values, including the angle of diagonal compression (θ) and f_1 from which β is evaluated. A parabolic stress-strain relationship is assumed for the compressive response of concrete, and the maximum aggregate size is considered to represent the roughness of the crack in evaluating the resistance to shear slip. These issues are relevant for the extension of the MCFT to HSC because, for HSC, the stress-strain response up to peak stress is close to linear and cracks propagate through aggregates.

The development of a hand-based design procedure from the MCFT required that several assumptions be made. The primary assumptions are as follows:

- There is a linear distribution of strain over the depth of a member (plane sections remain plane).
- The flow of forces in a diagonal compression field is uniform such that the diagonal compressive stresses are equal at the top and the bottom of a web along the same diagonal flow path.
- While calculation of the distribution of shear stress over the depth of the member needs to consider the longitudinal strain at many levels, it is reasonable to characterize the state of shear at the ultimate limit state by considering the longitudinal strain at mid-depth only.
- Stirrups yield prior to diagonal crushing of the concrete and at a strain of 0.002.
- The strain at peak stress in concrete is –0.002.
- The crack spacing in members without transverse shear reinforcement is proportional to the depth of the member or the spacing between layers of longitudinal reinforcement, whichever is less; this assumption leads to a depth effect in shear for members without transverse shear reinforcement.
- The crack spacing in members containing at least the minimum required amount of shear reinforcement can be conservatively taken as 12 inches; this assumption implies that there is no depth effect in shear for members with minimum, or greater, amounts of shear reinforcement.
- A staggered shear design method may be used to evaluate shear demands in all design regions.

The separate validation of each of these assumptions for HSC (or for normal-strength concrete) for all possible design cases is not feasible or necessary. Rather, as with any other shear design methods, the most useful validation is success in providing conservative and accurate estimates of the strength of members that have been tested to failure. Nevertheless, the examination of these assumptions is useful as it helps identify areas of possible concern for extending the LRFD Sectional Design Model for the use of HSC. Areas of potential concern are further discussed in the following sections and in Chapter 2, where the findings from this research are presented.

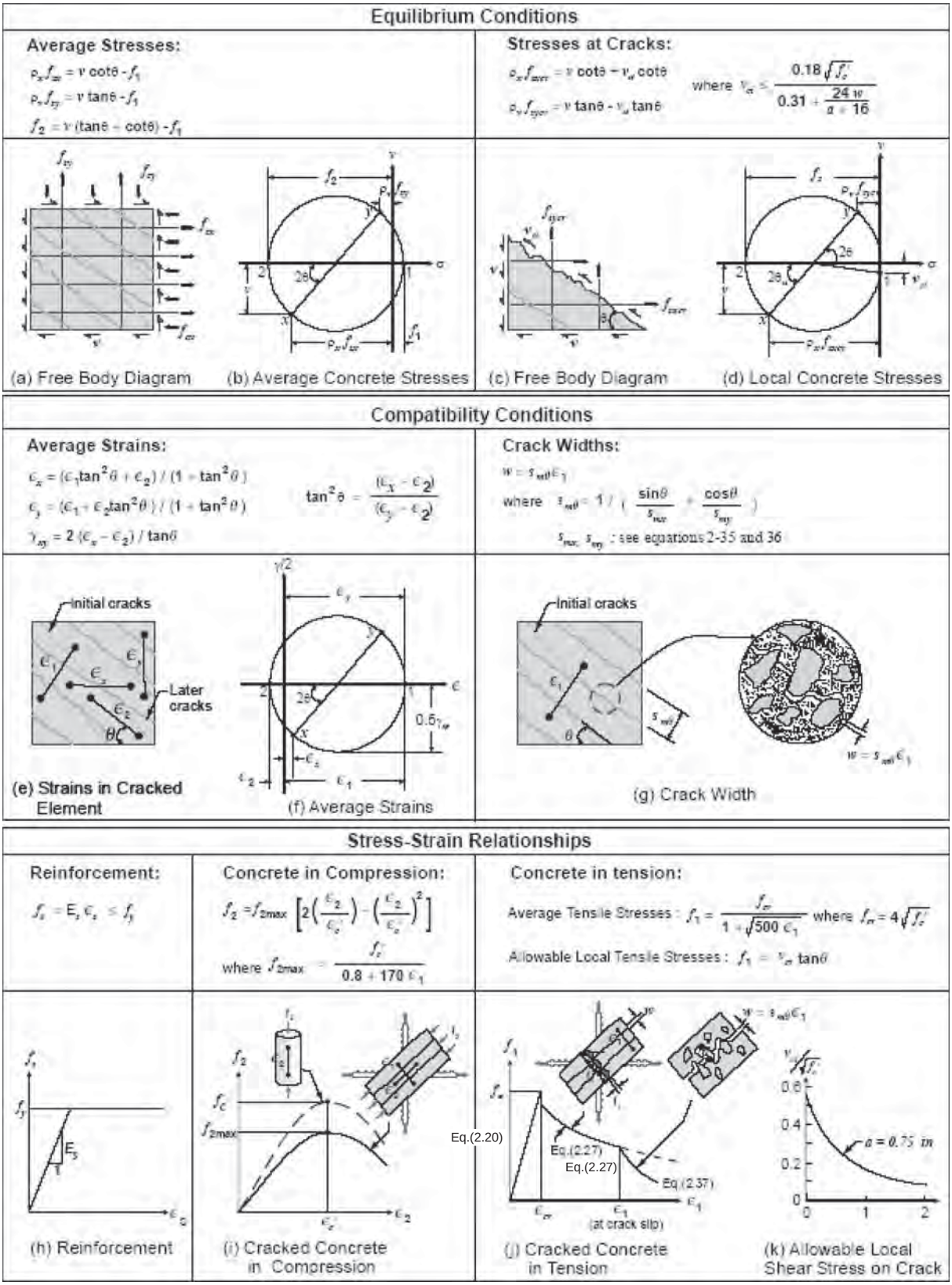

Figure 1. Description of Modified Compression Field Theory (2).

1.1.2 Concrete Contribution to Shear Resistance

In traditional U.S. design practice, the concrete contribution to shear resistance is taken as the estimated shear force at diagonal cracking. This approach is very rational for members without shear reinforcement. However, for members with shear reinforcement, there is no mechanistic reason that the diagonal cracking load should be related to the concrete contribution at the ultimate limit state, but because earlier test data (*9*) indicates that it is safe to do this, the nominal shear capacity in traditional practice has been taken as the sum of the diagonal cracking strength and the resistance provided by the transverse shear reinforcement based on a 45-degree parallel chord truss model (*10*).

In the LRFD Sectional Design Model, the concrete contribution to resistance is calculated as the capacity of the concrete to carry tension in a direction perpendicular to the direction of principal compression. This approach is analogous to the approach for considering the contribution of tensile stresses to shear in the web of a steel I-beam, except that the contribution of the tensile stresses in concrete (f_{c1}) is small relative to the magnitude of the principal diagonal compressive stresses (f_{c2}). It has been experimentally observed that the average tensile stress that can be carried in cracked concrete is a function of the cracking strength of the concrete and the principal tensile strain, as described in Equation 1.

$$f_{c1} = \frac{f_{cr}}{1+\sqrt{500\varepsilon_1}} \tag{1}$$

The assumed distribution of stress in the concrete is shown in Figure 1(j), where it is illustrated that there is a large direct tensile stress in the concrete between cracks and no direct tensile stress in the concrete at crack locations. It is possible to carry a direct tensile stress, f_{c1}, across a crack through a combination of local increases in forces in the reinforcement and in the shear on a crack face, as shown in Figure 1(c and d). In the derivation of the LRFD Sectional Design Model, it is assumed that stirrups yield and thus provide no resistance to opening of the crack. As a result, the ability to carry tension across the crack is limited either by yielding of longitudinal and transverse reinforcement or by yielding of transverse reinforcement and slip along the crack, as described in Equations 2 through 5.

$$\rho_x f_{sxcr} = v\cot\theta + v_{ci}\cot\theta \tag{2}$$

$$\rho_y f_{sycr} = v\tan\theta - v_{ci}\tan\theta \tag{3}$$

$$v_{ci} \le \frac{2.16\sqrt{f'_c}}{0.3+\frac{24w}{a+0.63}} \tag{4}$$

$$V_c = f_1 b_v d_v \cot\theta = \beta\sqrt{f'_c}\, b_v d_v \tag{5}$$

where:

f_{sxcr} = steel stress in the x-direction reinforcement at the crack location,
f_{sycr} = steel stress in the y-direction reinforcement at the crack location,
v_{ci} = interface shear stress on the crack surface,
ρ_x = steel ratio for the x-direction,
ρ_y = steel ratio for the y-direction, and
f_1 = stress in direction 1 = principal tensile stress.

The resistance to crack slip is taken as a function of the crack width *w*, the compressive strength of the concrete, and the maximum aggregate size, as given in Equation 4. The effect of this limitation on f_{c1} is illustrated in Figure 1(j). The concrete contribution can then be evaluated from equilibrium by using f_{c1} and the angle of diagonal compression θ. See Equation 5.

The LRFD Sectional Design Model provides two different tables for evaluating the contribution of the concrete, V_c, to shear resistance. For members with less than the minimum required amount of shear reinforcement, V_c is evaluated from the calculated longitudinal strain at mid-depth, ε_x, and the estimated cracking spacing, $s_{m\theta}$. The latter is proportional to the distance between layers of crack control reinforcement and is calculated using either the depth of the member or the spacing between layers of distributed horizontal reinforcement when such layers are provided. See Table 1 and Figure 2. The concrete contribution to resistance is then calculated from the slip resistance capacity given by Equation 6:

$$\beta = \frac{4\cot\theta}{1+\sqrt{500\varepsilon_1}} \le \frac{2.16}{0.3+\frac{24w}{a+0.63}} \tag{6}$$

where the crack width is taken as ε_1 times $s_{m\theta}$; where ε_1 is evaluated from Mohr's circle of strain and the MCFT using ε_x, θ, and v/f'_c; and where $s_{m\theta}$ is taken as $s_x/\sin\theta$. The significant number of steps in making these calculations, and the iterative nature of the solution method, encouraged the development of tables in an effort to simplify the design process. For members with at least minimum shear reinforcement, a similar evaluation is completed, but where the crack spacing is assumed equal to 12 inches and the level of the shear stress ratio (v/f'_c) is used in evaluating which row of tabular values should be used in selecting β and θ.

HSC issues: The concrete contribution is most often controlled by the resistance to shear slip, as is calculated using Equation 4 for v_{ci} and using the assumptions for crack spacing as described in the foregoing. With the use of HSC, cracks may be smoother than assumed in the LRFD derivation because of through aggregate cracking, and the spacing

Table 1. Values of β and θ for members with less than minimum shear reinforcement.

s_{xe}* (in)		Longitudinal Strain, $\varepsilon_x \times 1{,}000$										
		≤ -0.20	≤ -0.10	≤ -0.05	≤ 0	≤ 0.125	≤ 0.25	≤ 0.50	≤ 0.75	≤ 1.00	≤ 1.50	≤ 2.00
≤ 5	θ	25.4°	25.5°	25.9°	26.4°	27.7°	28.9°	30.9°	32.4°	33.7°	35.6°	37.2°
	β	6.36	6.06	5.56	5.15	4.41	3.90	3.26	2.86	2.58	2.21	1.96
≤ 10	θ	27.6°	27.6°	28.3°	29.3°	31.6°	33.5°	36.3°	38.4°	40.1°	42.7°	44.7°
	β	5.78	5.78	5.38	4.89	4.05	3.52	2.88	2.50	2.23	1.88	1.65
≤ 15	θ	29.5°	29.5°	29.7°	31.1°	34.1°	36.5°	39.9°	42.4°	44.4°	47.4°	49.7°
	β	5.34	5.34	5.27	4.73	3.82	3.27	2.64	2.27	2.01	1.68	1.46
≤ 20	θ	31.2°	31.2°	31.2°	32.3°	36.0°	38.8°	42.7°	45.5°	47.6°	50.9°	53.4°
	β	4.99	4.99	4.99	4.61	3.65	3.09	2.46	2.09	1.85	1.52	1.31
≤ 30	θ	34.1°	34.1°	34.1°	34.2°	38.9°	42.3°	46.9°	50.1°	52.6°	56.2°	59.0°
	β	4.46	4.46	4.46	4.43	3.39	2.82	2.19	1.84	1.61	1.30	1.10
≤ 40	θ	36.6°	36.6°	36.6°	36.6°	41.1°	45.0°	50.2°	53.7°	56.3°	60.2°	63.0°
	β	4.06	4.06	4.06	4.06	3.20	2.62	2.00	1.66	1.43	1.14	0.95
≤ 60	θ	40.8°	40.8°	40.8°	40.8°	44.5°	49.2°	55.1°	58.9°	61.8°	65.8°	68.6°
	β	3.50	3.50	3.50	3.50	2.92	2.32	1.72	1.40	1.18	0.92	0.75
≤ 80	θ	44.3°	44.3°	44.3°	44.3°	47.1°	52.3°	58.7°	62.8°	65.7°	69.7°	72.4°
	β	3.10	3.10	3.10	3.10	2.71	2.11	1.52	1.21	1.01	0.76	0.62

* $s_{xe} = \dfrac{1.38 s_x}{0.63 + a_g}$ (in inches), where

s_x = the lesser of d_v and the maximum distance between layers of crack control reinforcement (in inches) and

a_g = maximum aggregate size (in inches).

between cracks may be greater due to the larger tensile strength of the concrete. These effects could reduce shear slip resistance and needed to be investigated.

Further, although the LRFD Sectional Design Model indicates that the concrete contribution to resistance is principally through interface shear transfer, other researchers suggest that a significant portion of the load is carried by shear in the top and bottom compression zones and through dowel action (*11*). Still other researchers contend that shear is principally a fracture process that is better captured by examining the energy released with cracking than the energy required to propagate a crack (*12*). These different approaches also suggest that shear capacity may not increase in proportion to the square root of the concrete compressive strength.

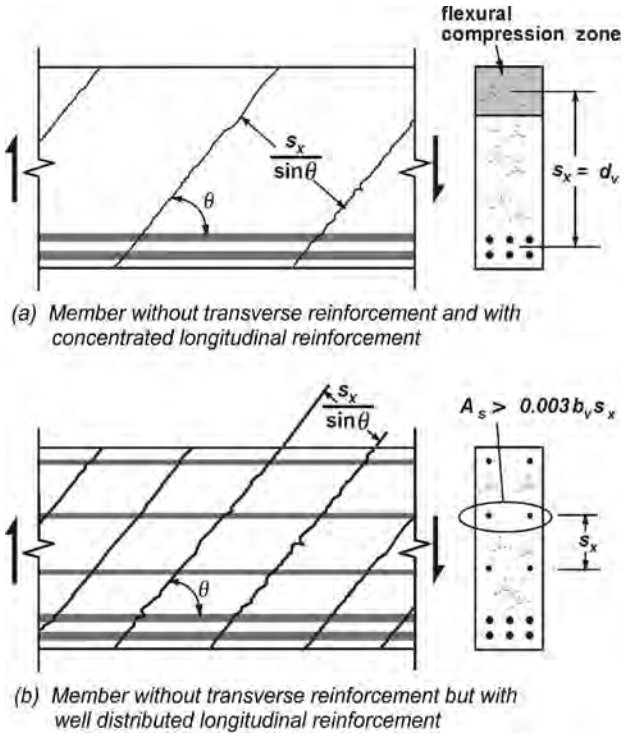

Figure 2. Crack spacing without the minimum required shear reinforcement.

1.1.3 Variable Angle Truss Model for Evaluating Contribution of Shear Reinforcement

The traditional model used throughout the world for evaluating the contribution of shear reinforcement to capacity is the parallel chord truss model that was introduced by Ritter and Mörsch (*10, 13, 14*). See Figure 3. The capacity provided by the shear reinforcement is given by Equation 7, in which both the stress in the reinforcement and the angle of diagonal compression are variables.

$$V_s = \frac{A_v f_v}{s} d_v \cot\theta \qquad (7)$$

where:

d = distance from the compression face to the centroid of tension reinforcement and

s = stirrup spacing.

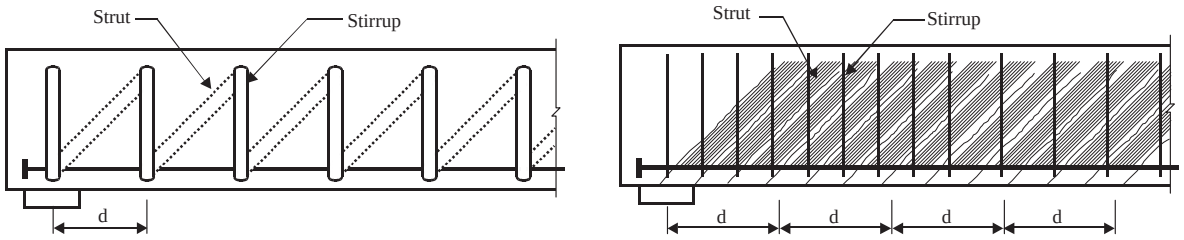

(a) Discrete Diagonal Compressive Struts **(b) Continuous Field of Diagonal Compression**

Figure 3. Parallel chord truss model.

In traditional U.S. design practice and as used in ACI 318-05 and the AASHTO Standard Specifications 17th Edition, the stirrups are taken as yielding and the angle of diagonal compression is assumed to be 45 degrees. Thus, the number of stirrups for each vertical tie is d/s and the capacity provided by shear reinforcement is evaluated using Equation 8.

$$V_s = \frac{A_v f_y}{s} d \tag{8}$$

To guard against diagonal compression failures, a limit on the nominal shear capacity is imposed in U.S. practice.

A variable truss model has been used in Eurocode 2 (*15*) and other national codes (*16*) to evaluate the contribution of shear reinforcement to shear resistance. The LRFD Sectional Design Model introduces the use of a variable angle truss model to U.S. design practice, and the impact of this change can be very significant. Because the angle of diagonal compression, θ, may be taken as low as 18.1 degrees [cot(18.1) = 3.06], a given quantity of shear reinforcement is evaluated by the LRFD Sectional Design Model as providing up to three times as much strength as that calculated using the AASHTO Standard Specifications.

HSC Issues: The use of HSC directly impacts the importance of the accuracy of the LRFD variable angle truss model for evaluating the contribution of the shear reinforcement. If the LRFD approach is somewhat unconservative (i.e., θ is too low and cotθ is too high) for normal-strength concrete, where V_c is a larger component of V_n than for HSC, then the LRFD approach will be even more unconservative for HSC, where V_s can be a larger fraction of total calculated resistance. For example, in a member cast with 20-ksi concrete that is designed up to the maximum shear design stress of $0.25f'_c$ (2.5 ksi), V_s needs to provide over 2 ksi (80 percent) of the shear capacity. Thus, it was important in this research to determine if measured angles of diagonal compression and cracking supported the shear reinforcement contributions derived from the LRFD Sectional Design Model.

1.1.4 Depth Effects

For members without shear reinforcement, traditional design practice has taken the shear stress at failure to be proportional to the square root of the cylinder compressive strength; thus, a member that is twice as deep as another is evaluated to be twice as strong. Over the last couple of decades, researchers have conducted a significant number of tests on larger members, and it has been repeatedly illustrated (*17*) that the shear stress at failure in members without shear reinforcement decreases as the size of the member increases, such as was observed in the tests by Shioya et al. (*18*). See Figure 4. Many international codes and the LRFD Sectional Design Model consider a size effect in shear for beams without shear reinforcement. This fact is illustrated in Table 1, where, because the crack spacing is proportional to s_x (the lesser of the depth of member or the spacing of the longitudinal reinforcement), as s_x increases, the value of β (the concrete contribution to shear resistance) decreases. The LRFD Sectional Design Model basis for this change is that as the distance between layers of crack control reinforcement decreases, the spacing of cracks, and thus the width of cracks, increases. According to Equation 4, as the width of a crack increases, the resistance to shear slip decreases.

For members with at least the minimum required amount of shear reinforcement, it is generally assumed in international codes, as is done in the LRFD specifications, that there is no size effect in shear.

HSC Issues: For deep members without shear reinforcement, it has also been illustrated that the traditional assumption that shear resistance is proportional to the square root of the cylinder compressive strength may not be conservative. This fact is further illustrated in Figure 5, where the results of two different test series (*19*, *20*) are shown; one series (*19*) was used as part of the justification of this traditional assumption, and the other (*20*) was on larger members cast with higher-strength concretes. The results from the second series of tests reveal that the shear strength is not always proportional to the square root of the cylinder compressive strength. The LRFD Sectional Design Model does not currently predict the pattern seen from this second series of tests, but the basis of the method would imply that for HSC, where cracks can run directly through aggregates, it is no longer reasonable to use the maximum size of the aggregate in Equation 4 for determining shear slip resistance. The shear design provisions of the 2004 Canadian Standards

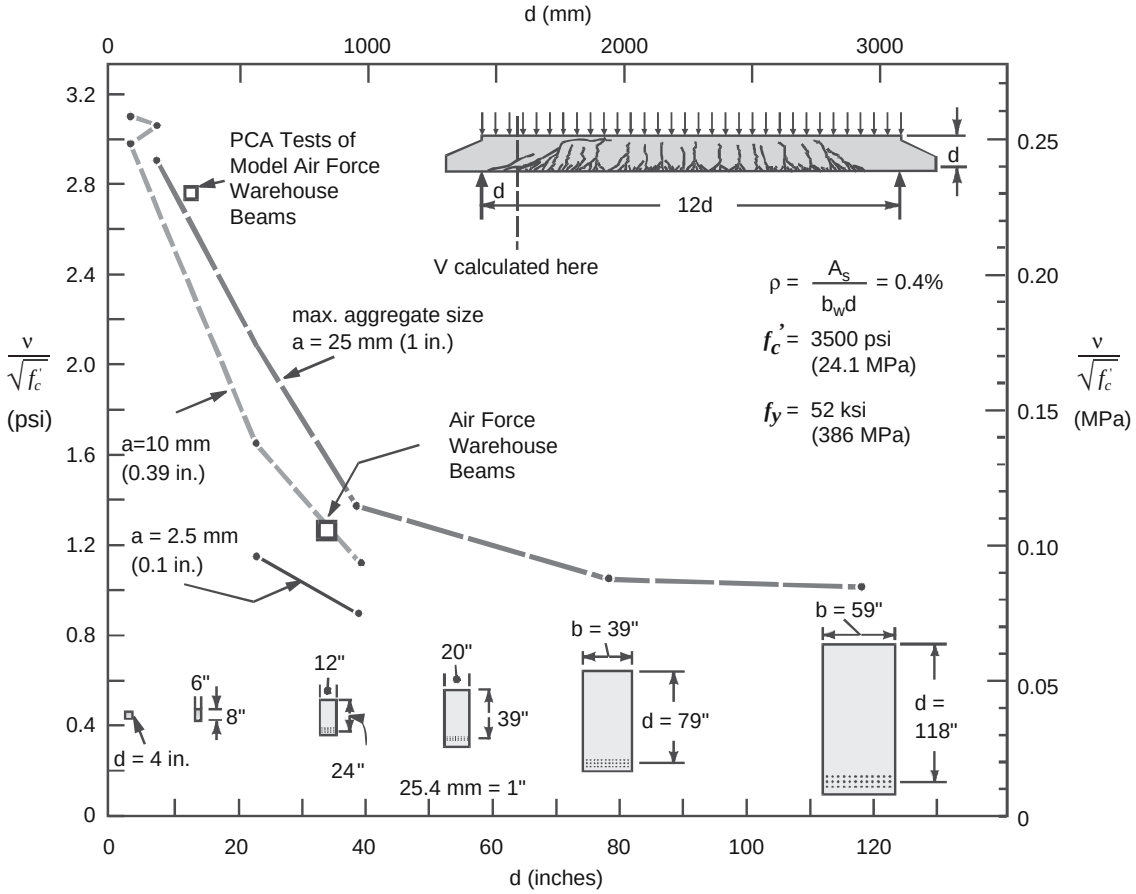

Figure 4. Influence of depth on shear capacity.

Association (*6*), which were also derived from the MCFT and are similar to the LRFD Sectional Design Model, try to account for this high-strength concrete influence by stating that the aggregate size should be taken as zero when the compressive strength is greater than 10 ksi. The appropriate approach for use in the LRFD specifications was examined in this study.

1.1.5 Minimum Shear Reinforcement Requirement

The LRFD Sectional Design Model requires a substantial increase in the minimum amount of shear reinforcement over what is required by the AASHTO Standard Specifications, as illustrated in Figure 6. This difference is opposite to what could have been expected because in the AASHTO Standard Specifications, V_c is typically higher than in the LRFD specifications, particularly for prestressed concrete members. Thus, it could have been expected that the minimum amount of shear reinforcement required to ensure that this V_c is maintained after cracking would be higher for the AASHTO Standard Specifications than for the LRFD specifications.

HSC Issues: With the use of HSC, cracks are expected to be smoother, more widely spaced, and wider than for normal-strength concretes. This suggests that minimum shear reinforcement requirements may need to be increased substantially for very high-strength concretes. This issue was investigated in this study. The minimum required amount of shear reinforcement is particularly important for prestressed concrete members for which large portions of their length may only contain the minimum requirement.

1.1.6 Maximum Shear Design Stress Limit

The LRFD Sectional Design Model permits the design of members up to a shear stress of $0.25f'_c$ plus the vertical component of the prestressing steel, as given in Equation 9.

$$V_r = V_c + V_s + V_p \le 0.25 f'_c b_v d_v + V_p \quad (9)$$

This is a substantial increase from the maximum shear stress permitted in the AASHTO Standard Specifications, in which the contribution of the shear reinforcement is limited to $8\sqrt{f'_c}\, b_w d$ (psi units). The limit in the AASHTO Standard Specifications was imposed for two reasons. First, the limit was to prevent the member from being overly reinforced in shear and failing by diagonal crushing of the concrete or another means before the full contribution of the shear

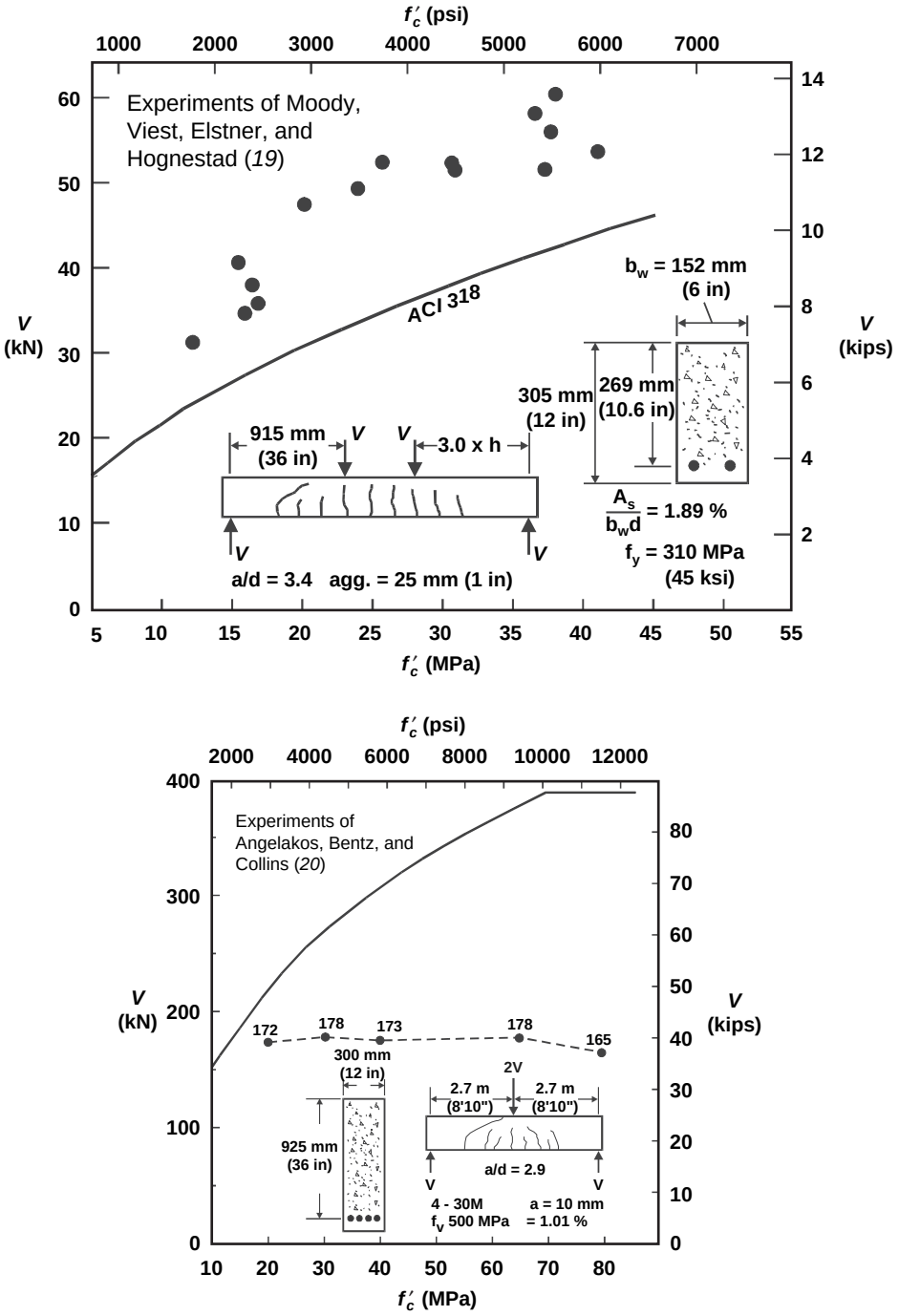

Figure 5. Influence of concrete strength on shear capacity of members without A_v.

reinforcement was realized through yielding of the stirrups. The second reason was to ensure good performance under service load levels (*21*).

HSC Issues: As the compressive strength of the concrete increases, the difference in the maximum shear design limits between the LRFD specifications and AASHTO Standard Specification limits also increases. The effect is illustrated in Figure 7, in which no limit is imposed on f'_c. The ratio of the maximum shear stresses, as permitted by the LRFD specifications and the AASHTO Standard Specifications, increases from approximately 1.5 for a 4-ksi reinforced concrete beam to 3.5 for a 20-ksi reinforced concrete beam. The wide discrepancy between these trends and the comparatively limited field experience with members designed for large stress levels by the LRFD Sectional Design Model suggested that it was important to evaluate this limit. Since the limit in the

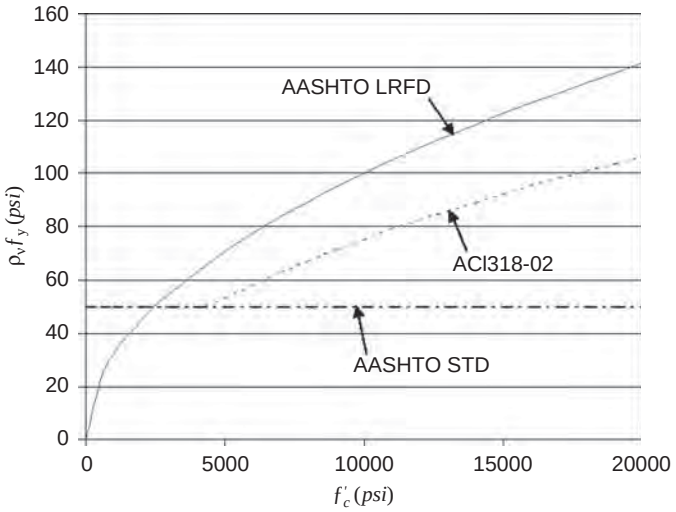

Figure 6. Minimum required amount of shear reinforcement.

AASHTO Standard Specifications was also imposed to address serviceability issues, it was also important to evaluate the condition at the service load of members designed for high shear stress levels.

1.1.7 Staggered Shear Design Concept

In traditional U.S. bridge design practice, the end region of a member is designed for the shear force that is at a longitudinal distance *d* (for reinforced concrete) or *h*/2 (for prestressed concrete) from the support. The reason for this approach is that any superimposed load that lies within this distance from the support is considered to directly flow to the support and does not need to be lifted up across a diagonal crack. In the LRFD Sectional Design Model, this concept is

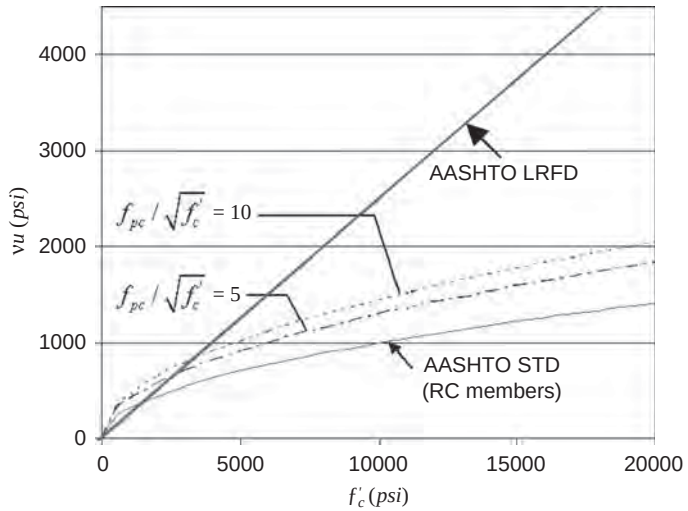

Figure 7. Maximum allowable design shear stress.

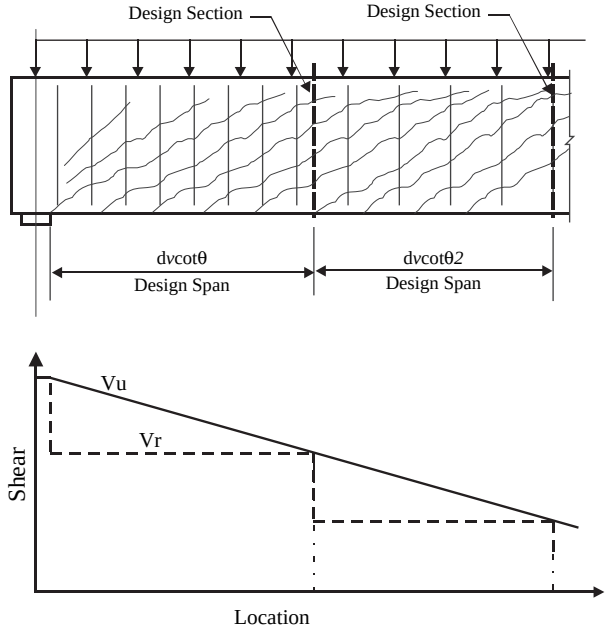

Figure 8. Design regions and shear demand using the Sectional Design Model.

extrapolated to cover the entire length of the member such that the designer only needs to design each shear band for the minimum shear force occurring within the length of that band, as illustrated in Figure 8. While this approach is permitted, it is also considered most likely that the designer will continue with the traditional design approach for the majority of the length of the member. That traditional approach is to design each section to have a capacity greater than the demand of that section except in end regions.

HSC Issues: There is no specific reason why a staggered shear design approach should be less conservative for HSC members than for members with normal-strength concrete. However, given how the staggered shear design concept is coupled with other, potentially less conservative assumptions that become even less conservative when HSC is used, this study also examined the appropriateness of the staggered shear design approach. It was particularly important to examine the behavior of end regions where the compression must funnel into the support and can increase significantly local compressive and shear stresses in the web in the support region.

1.1.8 Design of Longitudinal Reinforcement

One of the significant features in the LRFD Sectional Design Model is that it requires a direct consideration of equilibrium to evaluate the demands on the longitudinal reinforcement at each point over the length of a member. This requirement is expressed in Equation 10 from the LRFD specifications and illustrated in Figure 9.

$$T_{\min} \geq 0.5N_u + 0.5V_u \cot\theta + \mathrm{M}_u / d_v - A_{ps} f_{ps} \qquad (10)$$

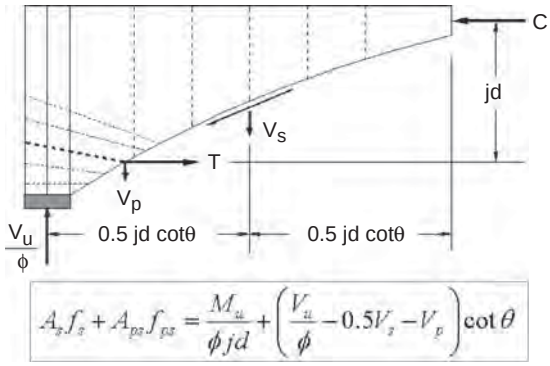

Figure 9. Shear demands on longitudinal reinforcement at end of prestressed girder.

This new requirement has resulted in a significant increase in anchorage demands at the end of prestressed members where the horizontal anchorage demand created by diagonal compression (due to shear) is high and where the force in the strands is not yet fully developed. This demand has required the use of longitudinal deformed bar reinforcement in the end regions of prestressed concrete members designed by the LRFD specifications.

HSC Issues: The HSC issues pertain to the bond performance between strand and HSC. Since the maximum allowable shear stress by the LRFD specifications increases in proportion to cylinder compressive strength, the bond stress demand also increases in proportion to f'_c. Thus, ever larger amounts of longitudinal deformed bar reinforcement are required unless bond strengths increase more than in proportion to f'_c. Although NCHRP Project 12-60, "Transfer, Development, and Splice Length for Strand/Reinforcement in High-Strength Concrete," is addressing bond performance in HSC, it was important in this study to assess bond demand and capacity in the anchorage regions of the test members because there was an opportunity in this program to provide valuable data on this issue.

1.1.9 Summary of the LRFD Sectional Design Model

While many components of the LRFD Sectional Design Model are discussed in the foregoing sections, for completeness a summary of this design procedure is now provided. The LRFD Sectional Design Model is a comprehensive design approach for structural concrete members in which the combined actions of axial load, flexure, and prestressing are taken into account when completing the shear design of any section of any member. The steps in the design are shown in Figure 10. In this approach, the nominal shear capacity is taken as the sum of a concrete component, a shear reinforcement component, and the vertical (or transverse) component of the prestressing:

$$V_n = V_c + V_s + V_p \tag{11}$$

The concrete contribution is controlled by the value of the coefficient β:

$$V_c = 0.0316\beta\sqrt{f'_c}\, b_v d_v \tag{12}$$

where f'_c is in ksi units.

The coefficient of 0.0316 is $1/\sqrt{1000}$ and is used to convert the relationship for V_c from psi to ksi units.

A variable angle truss model is used to calculate the contribution of the shear reinforcement. See Equation 13, where the angle of the field of diagonal compression, θ, is used in calculating how many stirrups, ($d_v$cotθ/s), are included in the transverse tie of the idealized truss.

$$V_s = \frac{A_v f_y d_v \cot\theta}{s} \tag{13}$$

where:

$d_v \geq 0.9d$ or $0.72h$, whichever is greater.

The values for β and θ are obtained from Table 2 for members that contain at least the minimum required amount of shear reinforcement as given by Equation 14, and from Table 1 for members that contain less than that amount.

$$A_{v,\min} \geq 0.0316\sqrt{f'_c}\,\frac{b_v s}{f_y} \tag{14}$$

where f'_c and f_y are in ksi units.

To obtain values for β and θ from Table 2, (A_v $A_{v,\min}$), the designer selects the row in which to enter the table based on the design shear stress ratio (v/f'_c) and the column based on the longitudinal strain ε_x at mid-depth, which may be taken as one-half of the strain in the longitudinal tension reinforcement, ε_t. This strain is equal to the force in the longitudinal tension reinforcement divided by the axial stiffness of the tension reinforcement. As shown in Equation 15 and Figure 9, the effects of all demands on the longitudinal reinforcement are taken into account.

$$\varepsilon_x = \frac{\varepsilon_t}{2} = \frac{M_u/d_v + 0.5N_u + 0.5\left(V_u - V_p\right)\cot\theta - A_{ps}f_{po}}{2\left(E_s A_s + E_p A_{ps}\right)} \tag{15}$$

Equation 15 assumes that the member is cracked and therefore only the axial stiffness of the reinforcement need be

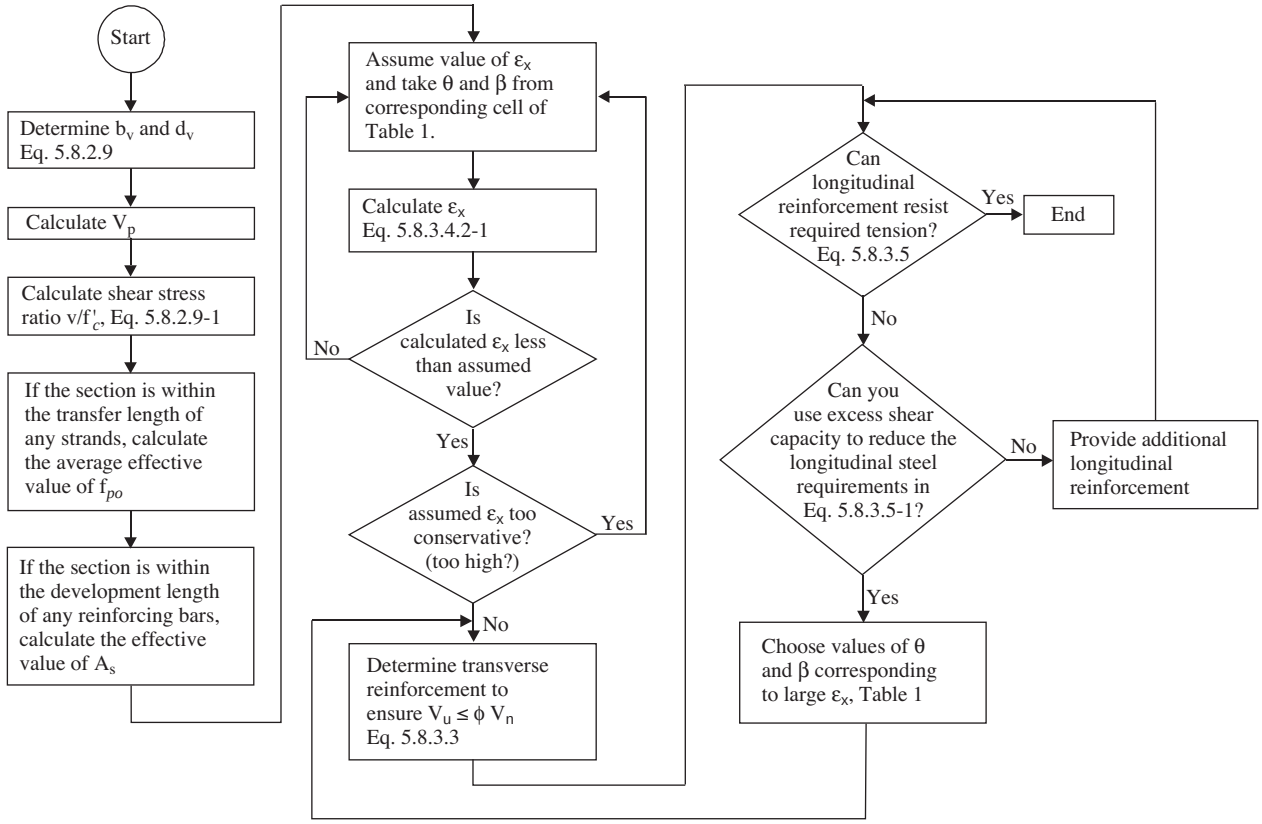

Figure 10. Flowchart for LRFD design procedure.

Table 2. Values of β and θ for members with at least minimum shear reinforcement.

$\frac{v^*}{f_c'}$		Longitudinal Strain, $\varepsilon_x \times 1{,}000$										
		≤ -0.20	≤ -0.10	≤ -0.05	≤ 0	≤ 0.125	≤ 0.25	≤ 0.50	≤ 0.75	≤ 1.00	≤ 1.50	≤ 2.00
≤ 0.075	θ	22.3°	20.4°	21.0°	21.8°	24.3°	26.6°	30.5°	33.7°	36.4°	40.8°	43.9°
	β	6.32	4.75	4.10	3.75	3.24	2.94	2.59	2.38	2.23	1.95	1.67
≤ 0.100	θ	18.1°	20.4°	21.4°	22.5°	24.9°	27.1°	30.8°	34.0°	36.7°	40.8°	43.1°
	β	3.79	3.38	3.24	3.14	2.91	2.75	2.50	2.32	2.18	1.93	1.69
≤ 0.125	θ	19.9°	21.9°	22.8°	23.7°	25.9°	27.9°	31.4°	34.4°	37.0°	41.0°	43.2°
	β	3.18	2.99	2.94	2.87	2.74	2.62	2.42	2.26	2.13	1.90	1.67
≤ 0.150	θ	21.6°	23.3°	24.2°	25.0°	26.9°	28.8°	32.1°	34.9°	37.3°	40.5°	42.8°
	β	2.88	2.79	2.78	2.72	2.60	2.52	2.36	2.21	2.08	1.82	1.61
≤ 0.175	θ	23.2°	24.7°	25.5°	26.2°	28.0°	29.7°	32.7°	35.2°	36.8°	39.7°	42.2°
	β	2.73	2.66	2.65	2.60	2.52	2.44	2.28	2.14	1.96	1.71	1.54
≤ 0.200	θ	24.7°	26.1°	26.7°	27.4°	29.0°	30.6°	32.8°	34.5°	36.1°	39.2°	41.7°
	β	2.63	2.59	2.52	2.51	2.43	2.37	2.14	1.94	1.79	1.61	1.47
≤ 0.225	θ	26.1°	27.3°	27.9°	28.5°	30.0°	30.8°	32.3°	34.0°	35.7°	38.8°	41.4°
	β	2.53	2.45	2.42	2.40	2.34	2.14	1.86	1.73	1.64	1.51	1.39
≤ 0.250	θ	27.5°	28.6°	29.1°	29.7°	30.6°	31.3°	32.8°	34.3°	35.8°	38.6°	41.2°
	β	2.39	2.39	2.33	2.33	2.12	1.93	1.70	1.58	1.50	1.38	1.29

*$v = V_u/b_v d_v$

considered when evaluating ε_t and ε_x. If ε_x is negative, then the member is uncracked and the axial stiffness of the uncracked concrete needs to be considered per Equation 16.

$$\varepsilon_x = \frac{\varepsilon_t}{2} = \frac{M_u/d_v + 0.5N_u + 0.5\left(V_u - V_p\right)\cot\theta - A_{ps}f_{po}}{2\left(E_sA_s + E_pA_{ps} + A_{ct}E_c\right)} \qquad (16)$$

where A_{ct} is the area of the concrete beneath mid-depth.

Alternatively, the designer can conservatively take $\varepsilon_x = 0$ if Equation 15 yields a negative value.

From Table 2, it is seen that, as the longitudinal strain becomes larger, the values for β decrease and the values for θ increase. This means that as the moment and longitudinal strain increase, both the magnitude of the concrete and shear reinforcement contributions to shear resistance decrease.

To obtain values for β and θ when $A_v < A_{v,\min}$, Table 1 is used. For members containing less than minimum shear reinforcement, the column by which the designer enters Table 1 is based on the value of the longitudinal strain at mid-depth, ε_x. To determine the row, the spacing of the layers of crack control reinforcement is used, s_{xe}. See Equation 17 and Figure 2.

$$s_{xe} = \frac{1.38s_x}{0.63 + a_g} \qquad (17)$$

From Table 1, it is seen that as s_{xe} and ε_x increase, the value of β decreases and θ increases. The result is that as the member becomes deeper and the value of the moment increases, the contributions of the concrete and shear reinforcement decrease.

1.1.10 Impact of NCHRP Project 12-61

The LRFD Sectional Design Model presented in Section 1.1.9 provides a comprehensive approach to shear design. Further, because it is derived from a well-tested model for behavior, it is likely to be more applicable for the design of members that have properties that fall outside of the properties of normal test data. This point is important because the characteristics of members tested in laboratories, and from which previous provisions were derived, do not well represent what is designed with shear provisions. Despite these advantages, the LRFD Sectional Design Model is perceived by some designers as being complicated and irrelevant to the parameters that the designer is calculating. For this reason, NCHRP Project 12-61, "Simplified Shear Design of Structural Concrete Members," was conducted with the goal of developing simplified shear design provisions for common design cases. The outcome of Project 12-61 was *NCHRP Report 549*, which contains two proposals. One of the proposals is a simplification of the Sectional Design Model that introduces equations for β and θ to replace the tables. The other is a reinstatement of the AASHTO Standard Specifications approach for shear design, but with some significant changes.

For the proposal to reinstate the use of the V_{ci} and V_{cw} method for calculating the shear capacity of a member, the proposed relationships differ from those of the current AASHTO Standard Specifications in the expression for V_{cw} and in the angle θ of the parallel chord truss model used for evaluating V_s. The expressions for V_{cw} were developed so that they could be applied seamlessly to beams with deformed bar reinforcement only, with prestressed reinforcement only, and all combinations of those reinforcements. The angle θ may be conservatively taken as 45 degrees, or the effects of axial compression on the angle of diagonal cracking may be considered for evaluating the contribution of the shear reinforcement. The new equations offer a more uniform level of safety across a broad range of design cases, a means of assessing the likelihood of cracking under service load levels, and a direct solution for capacity rating.

The other proposal is the introduction of equations that facilitate the direct solution of β and θ for use in the Sectional Design Model. These proposed equations were derived from the MCFT and are now used in the current shear design provisions of the Canadian Standards Association (CSA A23.3-04). A further change is to make the design process noniterative by assuming that θ is equal to 30 degrees for evaluating the demands of shear on longitudinal reinforcement. This was also done in CSA A23.3. It is possible to derive these equations for β and θ in terms of the longitudinal strain at mid-depth (ε_x), as was done in CSA A23.3-04; in terms of the maximum axial strain in the extreme longitudinal reinforcement (ε_t), a quantity that is used in the unified design method of ACI 318-05; or in terms of the stress in the nonprestressed longitudinal tension reinforcement (f_s), a value that some engineers prefer because it is proportional to the strain at mid-depth ($f_s = 2E_s\varepsilon_x = 58{,}000\varepsilon_x$).

Both of these proposed methods are described in Section 2.4, in which the capacity of the members tested in this program is compared with various code provisions.

HSC Issues: The significance of the outcome of NCHRP Project 12-61 is that before either of the foregoing methods can be adopted for use with HSC, they will need to undergo a similar examination as that completed for the current LRFD Sectional Design Model. Each issue for the extension to HSC of these provisions is not discussed at this time. However, each issue is addressed in Section 2.4, which presents the overall experimental strength results of this study.

1.2 Project Objectives

1.2.1 NCHRP Project 12-56 Solicitation

The background and objectives for this project were described in the project solicitation as follows:

The AASHTO LRFD Bridge Design Specifications (Section 5.4.2.1) state: "Concrete strengths above 10.0 ksi shall be used only when physical tests are made to establish the relationships between the concrete strength and other properties." When the LRFD specifications were written, the data was insufficient to demonstrate that the provisions were applicable to concrete compressive strengths above 10.0 ksi (high-strength concrete). However, recent research has started to address design issues with high-strength concrete, and the FHWA Showcase Projects are encouraging the use of high-strength concrete in bridge structures. There is, therefore, a need to expand the LRFD specifications to allow greater use of high-strength concrete.

This project will identify all barriers in the LRFD specifications to the use of high-strength concrete with emphasis on performing the necessary research to remove the barriers related to shear. The specific topics to be addressed in this project include, but are not limited to, the contributions of concrete to shear resistance in high-strength concrete, maximum and minimum transverse reinforcement limits, and bond issues related to shear.

The objective of this research is to develop recommended revisions to the *AASHTO LRFD Bridge Design Specifications* to extend the applicability of shear design provisions for reinforced and prestressed concrete structures to concrete compressive strengths greater than 10 ksi. In addition, other barriers to the use of high-strength concrete will be identified.

1.2.2 Project Objectives

To achieve this objective, it is necessary to address each of the issues associated with the extension of the LRFD Sectional Design Model to HSC that were presented in Section 1.1. A summary of the work items stemming from these issues follows:

- Investigate whether the relationship used in the derivation of the Sectional Design Model for shear slip resistance as presented in Equation 4 is appropriate for use in the design of HSC members.
- Investigate whether the assumption in the LRFD specifications for the spacing of cracks is appropriate for HSC members.
- Investigate whether the equation for calculating the longitudinal strain at mid-depth is sufficiently accurate.
- Evaluate whether the angle of principal compression as given in the design tables is sufficiently accurate. If angles are steeper than given in the tables, the contribution of shear reinforcement will be overestimated by the LRFD Sectional Design Model (which can be more of a problem for members cast with HSC, in which shear design forces can be considerably higher).
- Evaluate whether the staggered shear design concept is safe to employ for the design of end regions as well as over the length of members.
- Investigate the demand and capacity of longitudinal end region reinforcement in member support regions.
- Investigate the overall safety of the extension of the *AASHTO LRFD Bridge Design Specifications* considering the range of possible members to be designed with these provisions and all possible failure mechanisms and modes.
- Investigate the use and extension of minimum shear reinforcement requirements for HSC.
- Evaluate the suitability of the maximum shear stress design limit for use in HSC structures.
- Investigate factors that influence the design and behavior of end regions.
- Assess the performance of structures at serviceability load levels.
- Assess whether computer-based numerical analysis methods can successfully predict the capacity of test members and then subsequently be used for conducting parametric studies.
- Evaluate the ease and reliability of fabricating HSC bridge members by local producers.

1.3 Description of Project Tasks and Research Approach

The project solicitation divided the work into 10 tasks that included identifying barriers to the use of HSC, presenting where provisions can be extended with existing information, conducting any necessary research to extend provisions, and then developing the necessary change proposals to address these issues. The tasks defined in the solicitation to complete the project and the research approach taken on each of these tasks is described in this section.

1.3.1 Task 1: Review HSC Experience and Identify Barriers

Review relevant practice, performance data, research findings, and other information related to the behavior and design of reinforced and prestressed high-strength concrete structures. This information shall be assembled from technical literature and from unpublished experiences of engineers, bridge owners, and others. Information on actual field performance is of particular interest.

In an FHWA Project called "Compilation and Evaluation of Results from High Performance Concrete (HPC) Bridge Projects," led by Henry G. Russell, the available information from 19 HPC bridges was collected and compiled. The assembled information was presented in tables that described the mix design, the design specification, and bridge characteristics, as well as in a detailed individual report for

each bridge structure. The collected information is disseminated in this report, with a summary presented in Section 2.1 of this report, and the individual reports presented on media.

1.3.2 Task 2: Identify Barriers to Use of HSC in Section 5 of AASHTO LRFD Sectional Design Model

Perform a comprehensive article-by-article review of Section 5 of the 1998 LRFD specifications (including interims) and identify all provisions that directly or indirectly have the potential for preventing the extension of the specifications in their current form to high-strength concrete.

A comprehensive article-by-article review of Section 5 of the *AASHTO LRFD Bridge Design Specifications*, Customary U.S. Units, Second Edition 1998, and the 1999, 2000, and 2001 Interim Revisions was performed as part of the FHWA study referenced in Task 1. From this review, the provisions that affect shear design either directly or indirectly by the use of high-strength concrete were extracted and discussed. The results of the work on Task 2 are also presented in Section 2.1, and details are provided in an appendix.

1.3.3 Task 3: Extend Provisions with Existing Information and Determine Research Needs

Use the findings from Tasks 1 and 2 to identify issues (a) where the scope of the specifications can be extended to high-strength concrete based on existing knowledge and (b) where additional research is needed to extend the LRFD specifications to high-strength concrete.

The barriers to the use of HSC that are identified in Task 2 were examined to determine which of them could be overcome using available data and which of them required additional research before they could be overcome. When sufficient information was available, recommended changes to the LRFD specifications were developed. All provisions for which sufficient information is not available are also identified.

To evaluate the extension of the shear provisions, which was the primary focus of this project, a large database of shear test results was developed and then examined to assess the impact of concrete strength on the accuracy of the LRFD Sectional Design Model. Because NCHRP receives funding and input from state DOTs, the expectation for NCHRP Project 12-56 was that sufficient information was not available from previous test reports to enable the extension of provisions to high-strength concrete.

1.3.4 Task 4: Develop Expanded Work Plan for Experimental and Analytical Investigations

Develop an expanded work plan for experimental and analytical investigations of shear resistance in reinforced and prestressed high-strength concrete. The work plan should include all testing needed to provide information that will permit extending the application of the specifications to high-strength concrete and should include estimates of the cost and time to complete each testing component. The project panel will select those portions of the plan that can be accomplished with the funds available for this project.

Tasks 1 through 4 involved identifying LRFD Sectional Design Model provisions for which there was not sufficient information to extend their use to HSC. The database of existing shear test results was then used to develop an experimental testing program that would provide the information necessary to extend the provisions to HSC by addressing the issues discussed in Sections 1.1 and 1.2.2.

1.3.5 Task 5: Submit Interim Report

Submit an interim report, within 10 months of the contract start, to document Tasks 1 through 4 for review by the NCHRP. The contractor will be expected to meet with the NCHRP approximately 1 month later. No work on Tasks 6 through 10 will be performed without project panel approval of the expanded work plan.

The interim report was submitted in February 2002. An experimental research program was proposed to test multiple 63-inch deep bulb-tee, prestressed girders to failure in shear. Design variables included concrete compressive strength, shear design stress ratio (v/f'_c), and end anchorage conditions. The objectives and design details of some girders were left undefined so that results from early tests could be used to determine the most suitable overall test plan.

1.3.6 Task 6: Submit Working Draft Specifications

Submit working draft specifications to NCHRP within 3 months of approval of the expanded work plan. This draft shall include proposed text for all new or revised provisions. It is not anticipated that this draft will contain recommendations for equations or constants.

Proposed changes to the LRFD specifications on items that could be extended with existing information were presented in Task 3. This did not include any shear provisions. For shear, the ideal outcome from this project was to raise the allowable compressive cylinder strength that could be used in shear design provisions from 10 ksi to a value that was at the limit

of concrete strength that can be commercially produced. However, the development of the working draft specifications for shear was complicated by NCHRP Project 12-61, "Simplified Shear Design of Structural Concrete Members," in which significant changes to shear provisions were being proposed. As a result, the submission of the report for this NCHRP Project 12-56 task was more comprehensive than initially envisaged and included changes being considered based on the results of NCHRP Project 12-61.

1.3.7 Task 7: Perform Work Plan

Perform the work plan approved by the NCHRP project panel. Findings from these efforts should be provided in Quarterly Progress Reports as available.

The experimental and analytical work plan was conducted over a 3-year period, with the first experiment being conducted in March 2002 and the last in July of 2005. A total of ten 52-foot long bulb-tee girders were tested to failure in shear under a uniformly distributed load. Each half of each girder was designed differently so that two test results were obtained from each girder. The compressive strength of the concrete used in the girders ranged from 10 ksi to18 ksi, and the shear design stress at the first critical section from the support ranged from 0.7 ksi to 2.5 ksi. Other variables in the testing program included the type of shear reinforcement, anchorage and end region details, and the intended location of failure. This test series was designed to provide an overall assessment of the LRFD specifications and other shear design specifications as well as to generate the detailed test data necessary to address the issues discussed in Section 1.1 and listed in Section 1.2.2. In addition to the experiments on bulb-tee girders, 18 full-scale shear friction experiments were conducted.

1.3.8 Task 8: Revise Working Draft Specifications

Using the results from Tasks 3 and 7, revise the working draft specifications from Task 6 and prepare accompanying commentary for shear provisions in order to extend the application of the LRFD specifications to concrete strengths greater than 10 ksi. Submit this recommended draft for project panel review. Meet with the project panel approximately 1 month later.

As stated in Task 6, the development of the working draft specifications was impacted by NCHRP Project 12-61. Thus, draft specifications were submitted after some information was available from the experiments for their extension. A meeting was held in May 2005 with the project panel to discuss the working draft specifications.

1.3.9 Task 9: Revise Specifications and Commentary

Revise the recommended specifications and commentary in accordance with project panel recommendations.

The proposed specifications and commentary were revised to address the comments of the panel and further revised in response to panel comments on the draft final report.

1.3.10 Task 10: Submit Final Report

Submit a final report documenting the entire research effort.

The final report was submitted approximately 3 months after the submission of a draft final report for panel review and comment.

CHAPTER 2

Findings

This chapter presents the experimental and analytical research program and then summarizes the detailed findings of this work. Because the findings are presented in significant detail in this chapter, it is anticipated that some readers may not wish to review all 10 sections of the chapter. Therefore, they are encouraged to first review the description of the contents of Chapter 2 that is presented in the next few paragraphs before selecting which sections of Chapter 2 to read. The key observations presented in Chapter 2 that pertain to the extension of the LRFD specifications to HSC are summarized in Chapter 3 prior to the presentation in that chapter of the proposed changes to the LRFD specifications.

Section 2.1 summarizes a review of experiences with the use of HSC in design and construction practice, identifies barriers in the LRFD specifications for use of HSC, and then discusses possibilities for extension of provisions with existing data. Section 2.2 presents a large experimental database of shear test results on reinforced and prestressed concrete beams. Measured test strengths are compared with the calculated shear capacity using the LRFD Sectional Design Model to assess the influence of concrete strength on the safety of these provisions and to identify areas of potential concern. This database is also examined to assess where additional experimental research is required for the extension of provisions.

The next several sections of Chapter 2 present the experimental research program and the primary results. Section 2.3 presents a summary of the test program, design details, material properties, and test set-up and instrumentation layout. Section 2.4 presents the measured strengths and compares those strengths with the shear strengths calculated using the LRFD Sectional Design Model Article 5.8.3, the AASHTO Standard Specifications, and several other relevant codes and formulas. Critical mechanisms of resistance and modes of failure are also discussed. Section 2.5 presents the measured cracking strengths, patterns, angles, and widths for all test members. Section 2.6 presents the measured reinforcement strains in the stirrups and longitudinal deformed bars. It also presents measured longitudinal strains at mid-depth and compares these with the development of longitudinal strain at mid-depth, ε_x, as calculated using the LRFD specifications. It also presents the measured shear strains and a formula for predicting shear straining.

The remaining sections in Chapter 2 examine in some depth the measured response of the test girders. In Section 2.7, the detailed test data is used to assess the total force carried by the stirrups and concrete. Section 2.8 presents the results of the interface shear transfer experiments. Section 2.9 examines the behavior of end regions, and Section 2.10 presents the behavior of the girders predicted using nonlinear finite element analyses and compares this behavior with the measured response.

While Chapter 2 presents a topic-by-topic summary of the results, each of the first 10 appendices to this report provide detailed descriptions of the objectives, design, testing, and measured behavior of the experiments on each of the 10 test girders. Appendix 11 presents a discussion on evaluating effective shear depths and on the method that was used for measuring crack patterns.

2.1 Collection, Analysis, and Use of Existing HSC Information

In this section, the work completed in Tasks 1 through 3, which led to defining the objectives and scope of the subsequent large-scale research program, is presented. The description consists of the following three subsections:

2.1.1 Review Experience with Use of HSC;
2.1.2 Identify Barriers to Use of HSC in LRFD Section 5; and
2.1.3 Extend Provisions with Existing Information.

2.1.1 Review Experience with Use of HSC (Results from Task 1)

Task 1 was to review relevant practice, performance data, research findings, and other information related to the

behavior and design of reinforced and prestressed HSC structures. This information was assembled from the technical literature and from the unpublished experiences of engineers, bridge owners, and others. Information on actual field performance was of particular interest.

In November 1999, the FHWA and many state DOTs jointly initiated a 3-year study entitled "Compilation and Evaluation of Results from High Performance Concrete (HPC) Bridge Projects." The study was conducted under Contract DTFH61-00-C-00009 by Henry G. Russell, Inc., with Henry G. Russell as the principal investigator. The HPC bridge program included the construction of demonstration bridges. in each of the FHWA regions and dissemination of the technology and results at showcase workshops. Eighteen bridges in 13 states were included in the national program. Since the program's inception, several states that were not a part of the program at the beginning have implemented the use of HPC in various bridge elements.

All available information was collected and compiled as part of the FHWA study (*22*), and then used on NCHRP Project 12-56. Data from 19 HPC bridges are included in two formats: summary tables and detailed information on individual bridges. The complete information is provided in Section A12.1 of Appendix 12.

2.1.2 Identify Barriers to Use of HSC in LRFD Section 5 (Results from Task 2)

Article 5.4.2.1 of the LRFD specifications limits the applicability of the specifications to concrete compressive strengths of 10 ksi (70 MPa) or less unless physical tests are made to establish the relationship between concrete strength and other properties. With the greater usage of high-strength concrete and its economical and technical advantages, consideration needs to be given to raising the limit above 10 ksi (70 MPa). The objective of work performed in Task 2 was to identify all provisions in Section 5 of the LRFD specifications that directly or indirectly have the potential for preventing the extension of the specifications in their current form to high-strength concrete. Details of the work completed in Task 2 to meet that objective are provided in Section A12.2 of Appendix 12.

2.1.3 Extend Provisions with Existing Information (Results from Task 3)

In Task 2, provisions in Section 5 of the LRFD specifications that are potential barriers to the use of HSC in design practice were also identified. For barriers where sufficient information existed to support a change, proposed revisions were developed and submitted to the AASHTO Committee T-10. Section A12.3 of Appendix 12 provides a summary of the changes with respect to HSC that have been made in the LRFD specifications since the results from the FHWA project, as reported in Task 2, were completed. Revisions through the 2006 Interim Revision are included. Section A12.3 of Appendix 12 also contains an assessment of the articles that cannot be changed based on existing information.

2.2 Development and Analysis of Shear Database

2.2.1 Presentation of Shear Database

A large database was collected from shear tests conducted on reinforced and prestressed concrete members. The database consists of tabularized information on the material, geometry, and test data from each experiment. A total of 1,874 test results were extracted from the literature and used to examine the influence of HSC on the merits and limitations of the Sectional Design Model in the LRFD specifications. A description of the reinforced and prestressed concrete databases is given in Appendix 13.

Based on a review of the characteristics of tested members, the following differences between the types of members tested in laboratories and the types of members designed in practice are noted:

- Members in the field are typically slender ($L/d > 10$) and support distributed loads, while members tested in laboratories are typically stocky and support one or two point loads.
- Members in the field are often large and continuous and contain flanges, while members tested in laboratories are typically small, simply supported, rectangular members.
- Members in the field typically contain shear reinforcement, while the majority of members tested in laboratories do not contain shear reinforcement.
- Members in the field are designed to fail in flexure, while members in laboratories are overreinforced in flexure, often to extreme limits, in the regions of shear failure.
- Members in the field need to be designed for shear over their entire length, while members in laboratories are typically designed to fail in shear near supports.

Despite the very large amount of research that has been conducted to evaluate the shear behavior of members, the significant differences between the characteristics of members designed for the field and members tested in laboratories clearly indicates that the accuracy of code provisions cannot be solely evaluated by their ability to predict the strength of laboratory test structures. Nevertheless, an assessment of the LRFD Sectional Design Model was conducted using existing test data to identify concerns with its extension to HSC and where additional research is required. In these assessments,

no limit was placed on the value of the compressive cylinder strength, f'_c, so as to evaluate where changes were required before this limit could be raised or eliminated.

2.2.2 Influence of Concrete Compressive Strength

Figure 11 plots the ultimate shear stress at failure versus the concrete cylinder strength for the 1,287-member RC database. Different marker types are used to characterize the different levels of shear reinforcement. This figure illustrates that there is very limited data for members designed for high shear stresses, particularly when considering that the LRFD specifications allow members to be designed for shear stresses up to $0.25f'_c$. Figure 12 presents a similar plot for PC members. This plot illustrates that there are few test results for members cast with very high-strength concretes.

To assess whether the limit on f'_c in the LRFD Sectional Design Model can be removed or to what extent it can be raised, the shear strength ratio (V_{test}/V_{LRFD}) was plotted versus the compressive cylinder strength for the 1,287-member RC database, as shown in Figure 13. In calculating the design capacity of members using the LRFD Sectional Design Model, the maximum aggregate size was reduced to zero when f'_c was greater than 10.0 ksi, as has been done in the CSA Code for members cast with concretes that have a compressive strength greater than 10 ksi (70 MPa). The results illustrate that the LRFD specifications are just as accurate and conservative for members cast with concrete strengths above 10.0 ksi as they are for members cast with concrete strengths less than 10.0 ksi. The LRFD specifications typically underestimate the capacity of tested members. While there is significant scatter in the predictive capability of this method for members without shear reinforcement, it should be noted that the LRFD specifications have been found in other comparisons (*23*) to provide more accurate and uniform estimates of the shear capacity of members without shear reinforcement than either the ACI 318-05 or AASHTO Standard Specifications methods. For members with shear reinforcement, the shear strength ratios (V_{test}/V_{LRFD}) range from about 0.70 to 2, with a general upward trend with increasing concrete strength until $f'_c = 10$ ksi.

To assess the impact on calculated strengths of the assumptions made in the derivation of the Sectional Design Model from the MCFT, a similar plot to that of Figure 13 was prepared,

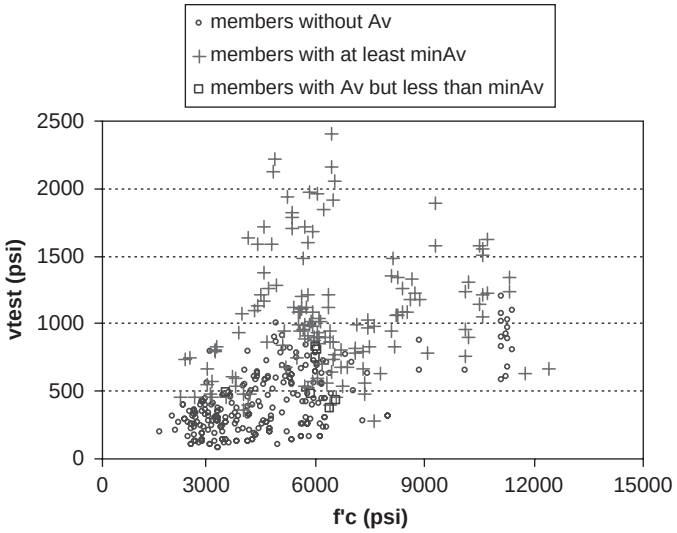

Figure 12. Ultimate shear stress (v_{test}) at failure versus the concrete compressive strength (f'_c) of prestressed concrete members.

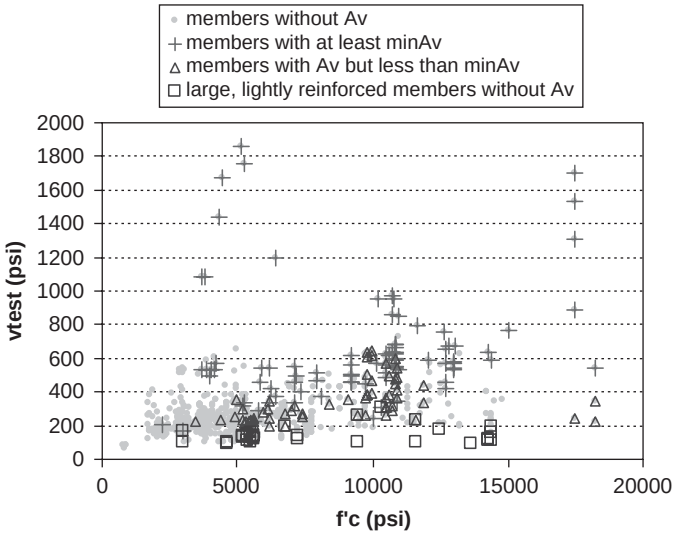

Figure 11. Ultimate shear stress (v_{test}) at failure versus the concrete compressive strength (f'_c) of reinforced concrete members.

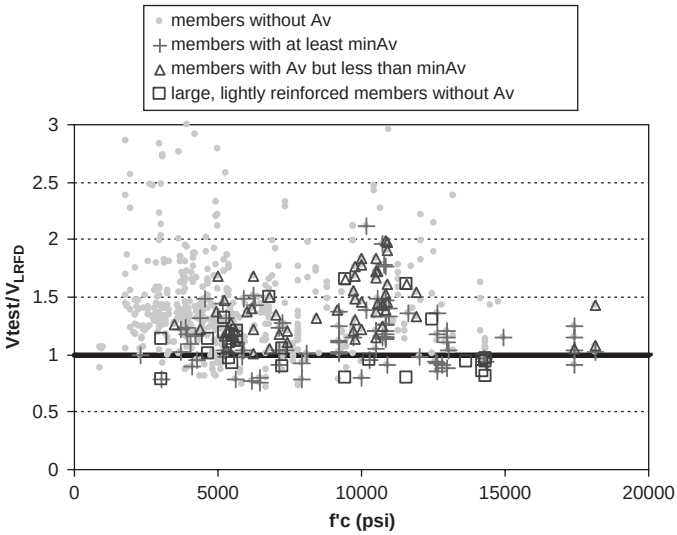

Figure 13. Shear strength ratio (V_{test}/V_{LRFD}) versus the concrete compressive strength (f'_c) of reinforced concrete members.

but the capacity of the members was determined using program Response 2000 (R2K) (*24*). R2K is a computer analysis/design tool based on the MCFT and developed by Dr. Evan Bentz of the University of Toronto. It uses a multilayer analysis approach for determining the distribution of shear stress over the depth of a member, uses more accurate constitutive relationships for the compressive response of HSC, and calculates crack spacing based on the levels of shear and longitudinal reinforcement provided. Figure 14 illustrates that the LRFD Sectional Design Model gives somewhat more conservative estimates of strength than does R2K and that the predictions given by this analysis tool are somewhat less scattered.

A similar set of plots was prepared for examining the influence of concrete compressive strength on the shear strength ratio for members in the PC databank. See Figures 15 and 16. Because there are a very limited number of test results for PC members cast with concrete strengths above 10 ksi, it is difficult to identify a trend from the results of this analysis. The particularly unconservative results that appear in the lower right corner of Figures 15 and 16 are two prestressed I-beam test results reported by J. Jacob and B. Russell at the Transportation Research Board 78th Annual Meeting in 1999. Those beams were cast with a concrete strength of about 12 ksi and used welded wire fabric for shear reinforcement. The authors of this paper reported that substantial strand slip, of up to 0.38 inch, had occurred prior to failure and that this event may have precipitated the failure of these girders. When the shear strength ratio was calculated using R2K, as shown in Figure 16, there was less scatter than when the LRFD specifications were used, as shown in Figure 15. This is particularly true for the PC members that did not contain shear

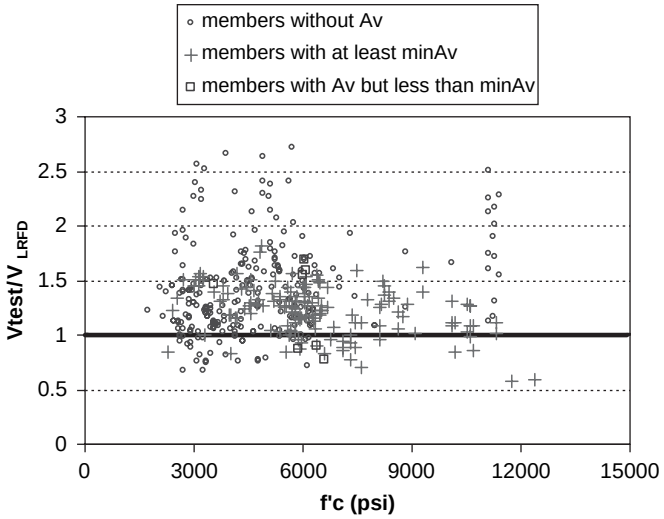

Figure 15. Shear strength ratio (V_{test}/V_{LRFD}) versus the concrete compressive strength (f'_c) of prestressed concrete members.

reinforcement. The HSC PC members with the noticeably different shear stress ratio for the two predictions are part of the "CW series" beams reported by Elzanaty et al. in 1986 (*25*). These 18-inch deep beams did not contain shear reinforcement, and the webs were only 2 inches thick.

Since the majority of the test data is from tests on small members, it is useful to specifically examine the effectiveness of the LRFD specifications for large HSC members. Therefore, Figures 17 and 18 present the shear strength ratio versus beam depth for RC members and versus beam height for PC members, respectively, and different marker types are used to demarcate ranges in concrete strengths.

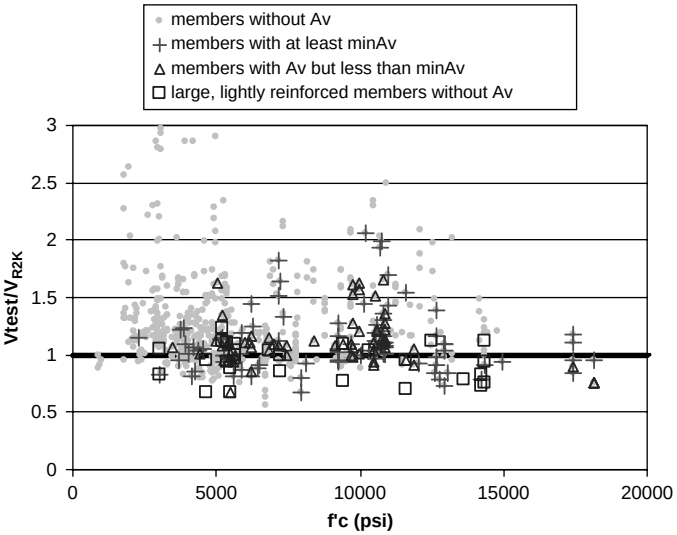

Figure 14. Shear strength ratio (V_{test}/V_{R2K}) versus the concrete compressive strength (f'_c) of reinforced concrete members.

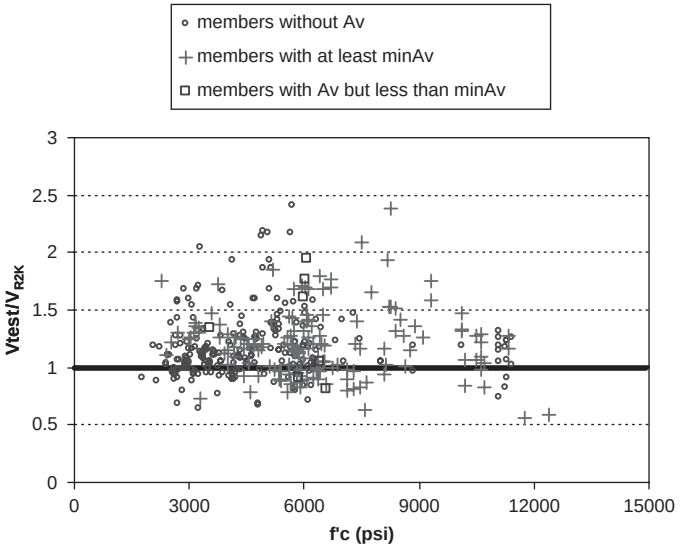

Figure 16. Shear strength ratio (V_{test}/V_{R2K}) versus the concrete compressive strength (f'_c) of prestressed concrete members.

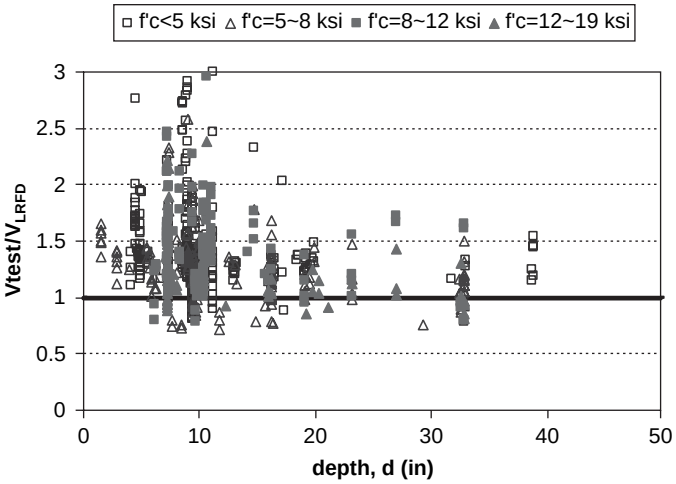

Figure 17. Shear strength ratio (V_{test}/V_{LRFD}) versus the member depth (d) of reinforced concrete members.

2.2.3 Maximum Shear Strength Limitation

The maximum nominal shear resistance permitted in the LRFD specification is $0.25f'_c$ plus the vertical component of inclined prestressing. This is a significant increase over what is permitted in the AASHTO Standard Specifications, and thus it is useful to examine existing test data to assess the safety of this increased limit. Figures 19 and 20 present the distribution of test data as a function of concrete compressive strength. It is apparent from Figure 19 that, for RC members, while there is very little data to evaluate the extreme upper limit, there are a significant number of test results for HSC members that support relatively large shear stresses. For PC members, there is data for members cast with normal- to modestly high-strength concrete that illustrates that shear stresses up to twice the limit used in the LRFD specifications can be supported.

To assess the safety and accuracy of the LRFD specifications and the program R2K for calculating the capacity of members designed for high shear stresses, shear strength ratios are plotted versus f'_c for these members in Figures 21 through 24. For RC members with heavy stirrups, both the LRFD specifications and the R2K predictions give good results. However, the predicted strengths of the PC members were unconservative for some deep members with large amounts of shear reinforcement.

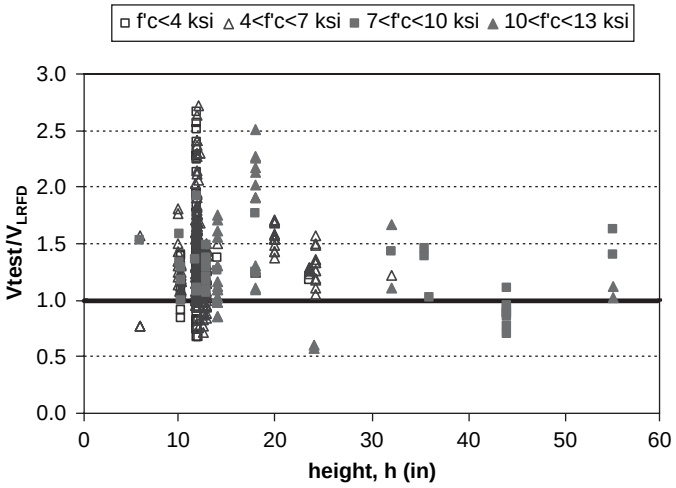

Figure 18. Shear strength ratio (V_{test}/V_{LRFD}) versus the member height (h) of prestressed concrete members.

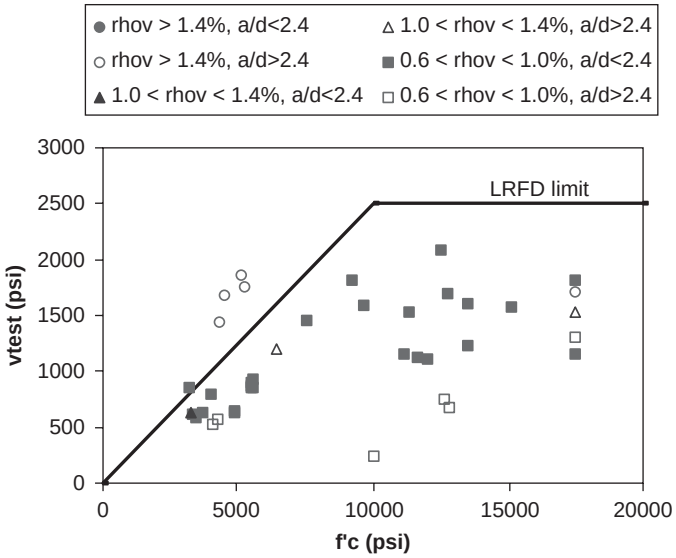

Figure 19. Examination of maximum shear strength limitations for reinforced concrete members.

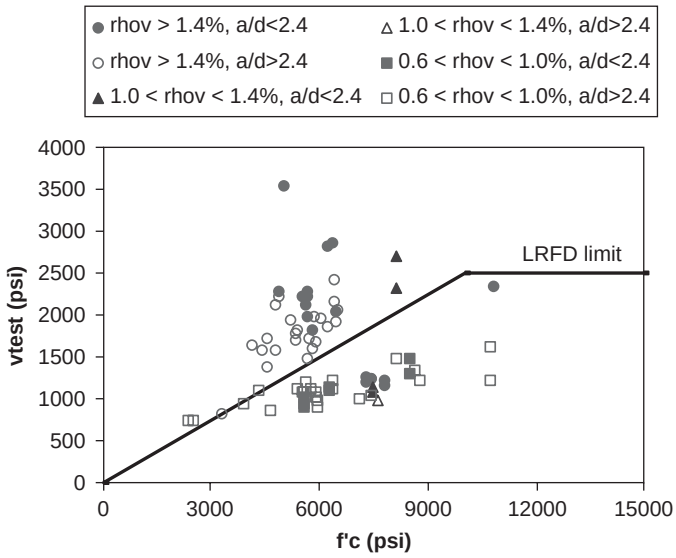

Figure 20. Examination of maximum shear strength limitations for prestressed concrete members.

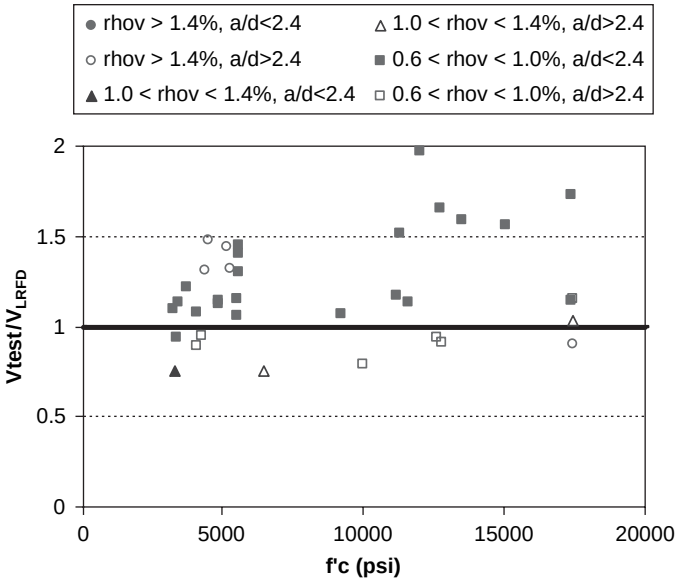

Figure 21. LRFD prediction of reinforced concrete members with heavy amount of shear reinforcement.

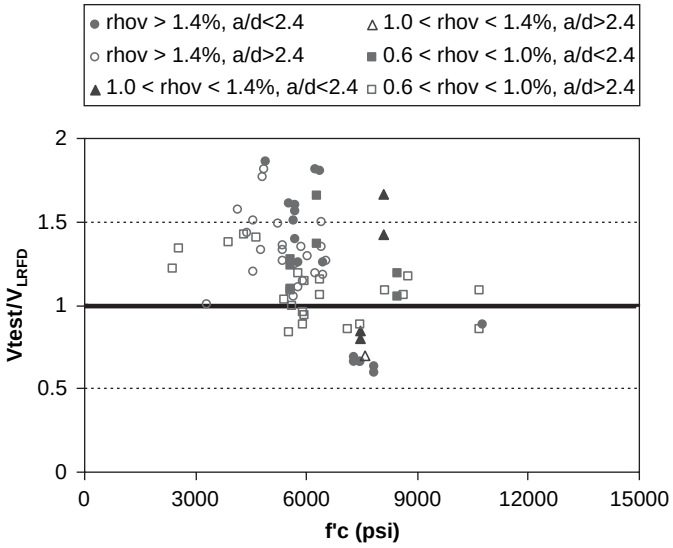

Figure 23. LRFD prediction of prestressed concrete members with heavy amount of shear reinforcement.

2.2.4 Minimum Shear Reinforcement Requirements

The primary roles of minimum reinforcement are to restrain the growth of inclined cracks, to improve ductility, and to ensure that the concrete contribution to shear resistance (V_c) is maintained up until at least yield of the shear reinforcement. In the LRFD specifications, the minimum amount of shear reinforcement is given by Equation 18.

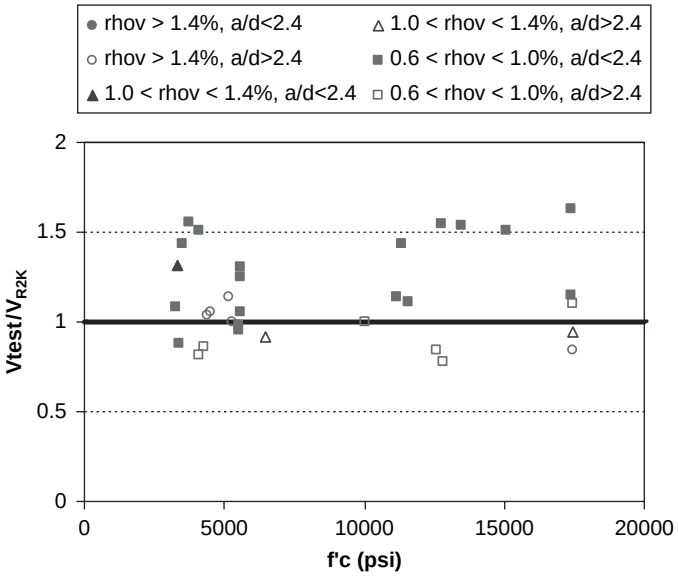

Figure 22. MCFT prediction of reinforced members with heavy amount of shear reinforcement.

$$\frac{A_v f_y}{b_v s} = \rho_v f_y \geq 0.0316\sqrt{f'_c} \text{ (in square inches)} \quad (18)$$

and if v_u ($V_u/b_v d_v$) < 0.125, then $s_{max} = 0.8d_v$ or 24.0 inches, while if $v_u \geq 0.125$, then $s_{max} = 0.4d_v$ or 12.0 inches.

Figure 25 plots the shear strength ratio for a segment of the RC test results with very light amounts of shear reinforcement ($\rho_v f_y$ = 30–150 psi) versus the spacing ratio (stirrup spacing divided by beam depth [s/d]). Different marker types are used to identify the strength ($\rho_v f_y$) of the shear reinforcement that was provided in each test. Furthermore, if the reinforcing details for a test beam did not satisfy code requirements (i.e., less than minimum reinforcement or

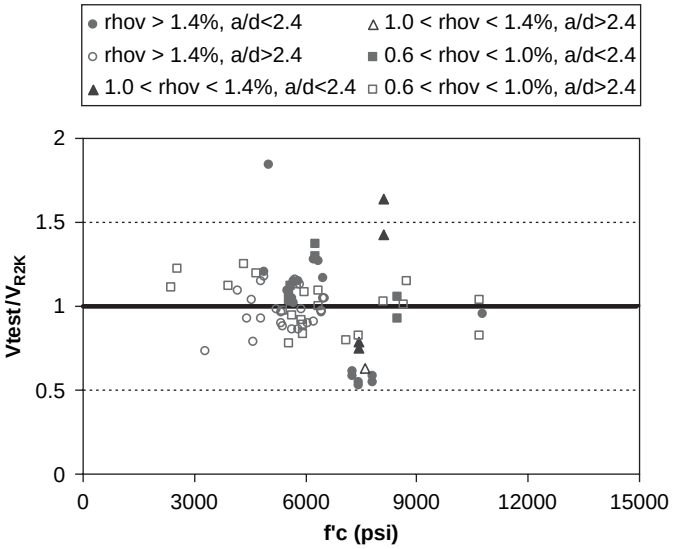

Figure 24. MCFT prediction of prestressed concrete members with heavy amount of shear reinforcement.

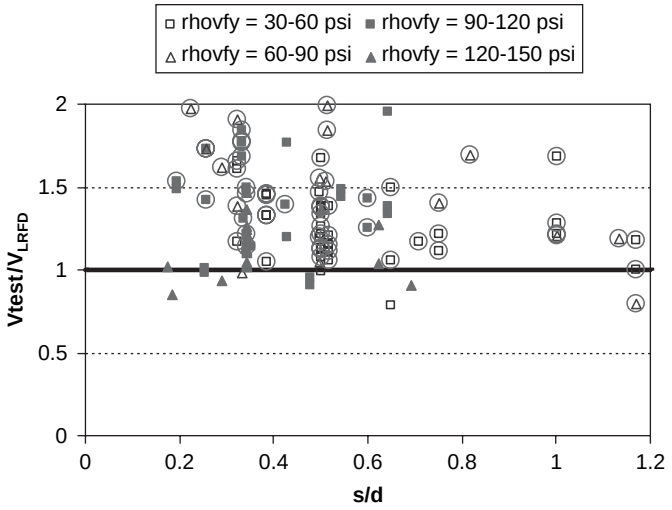

Figure 25. Influence of shear reinforcement details on shear strength ratio (V_{test}/V_{LRFD}) for reinforced concrete members.

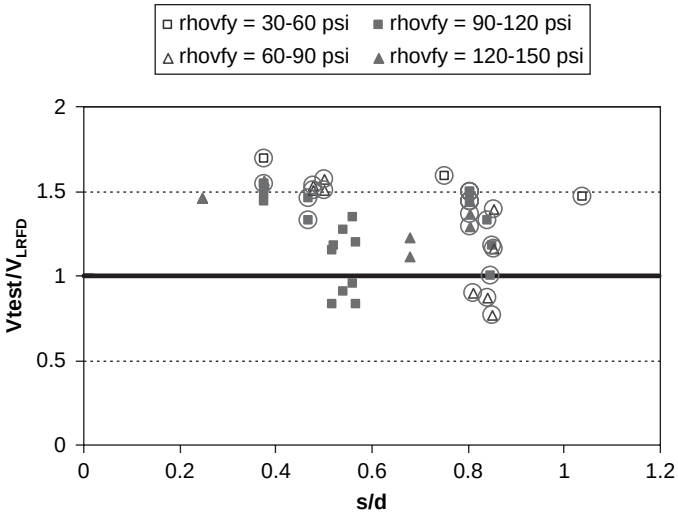

Figure 27. Influence of shear reinforcement details on shear strength ratio (V_{test}/V_{LRFD}) for prestressed concrete members.

too large a spacing of stirrups), then a circle is drawn around the marker for this test result. One measure of assessing the suitability of the minimum shear reinforcement requirement is to count the number of markers without circles below which the shear strength ratio was less than 1.0. The LRFD has seven code-satisfying test results having a ratio of less than 1.0, but most of them are reasonably close to 1.0. In Figure 26, the predictions from R2K are somewhat better because in only three of the members, which satisfied the LRFD specifications, is the shear stress ratio less than 1.0.

Figures 27 and 28 examine the suitability of the minimum shear reinforcement requirements of the LRFD specifications for PC members that are lightly reinforced in shear. As illustrated, in only a few cases was the strength ratio slightly less than 1.0.

Both RC and PC test data in Figures 25 through 28 indicate that the minimum reinforcement requirements used in the LRFD specifications are reasonable and appropriate. They also illustrate that increasing the amounts of minimum shear reinforcement has a marginal influence on the shear strength ratio ($V_{\text{test}}/V_{\text{LRFD}}$). Furthermore, they also result in the rather

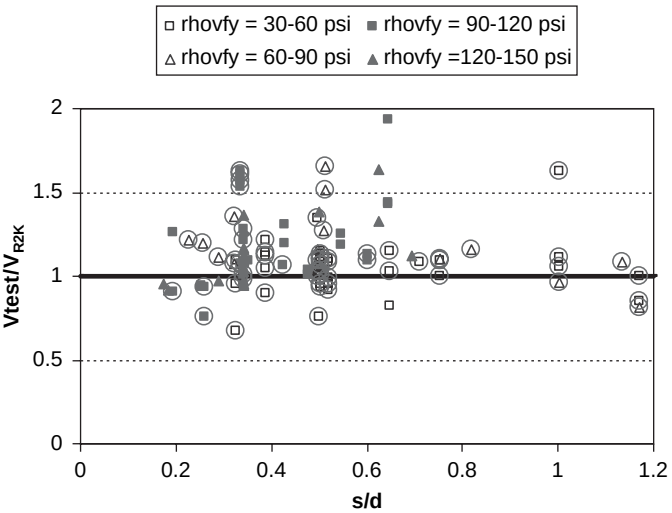

Figure 26. Influence of shear reinforcement details on shear strength ratio (V_{test}/V_{R2K}) for reinforced concrete members.

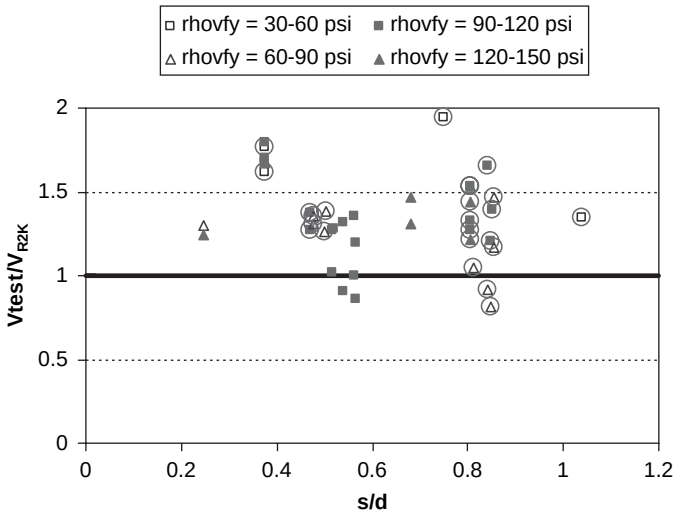

Figure 28. Influence of shear reinforcement details on shear strength ratio (V_{test}/V_{R2K}) for prestressed concrete members.

unexpected observation that the s/d ratio has little to no effect on the shear strength ratio.

2.2.5 Size Effect in Shear

It is now generally accepted that for members without shear reinforcement, the ultimate shear stress decreases as the depth of the member increases. Figure 29 is used to illustrate this effect over the full range in shear design stress levels and concrete strength levels. This depth effect is confirmed by the test data because the strength ratios for the deepest range of members (20 to 40 inches) plot closer to the bottom of the figure, while the strength ratios for the least deep members (less than 10 inches) generally plot toward the top of the figure. It is also interesting to observe that members having more than 2 percent of longitudinal reinforcement generally failed at higher shear stresses than members with lower longitudinal reinforcement levels.

In Figure 30, a similar plot was created to determine whether similar trends would be seen in PC members. The lack of data across a range in depths makes it difficult to identify a trend or lack of a trend. Figure 30 does show that the PC members having more than 2 percent of longitudinal reinforcement have somewhat higher shear failure stress levels than members having less than 2 percent of longitudinal reinforcement.

Many international codes use the depth as a parameter for reducing the limiting shear stress as the depth of the member increases. In the LRFD specifications, a size effect for members without shear reinforcement is made by using the lesser of the overall depth or the distance between layers of longitudinal reinforcement in the tables for selecting the parameter β that

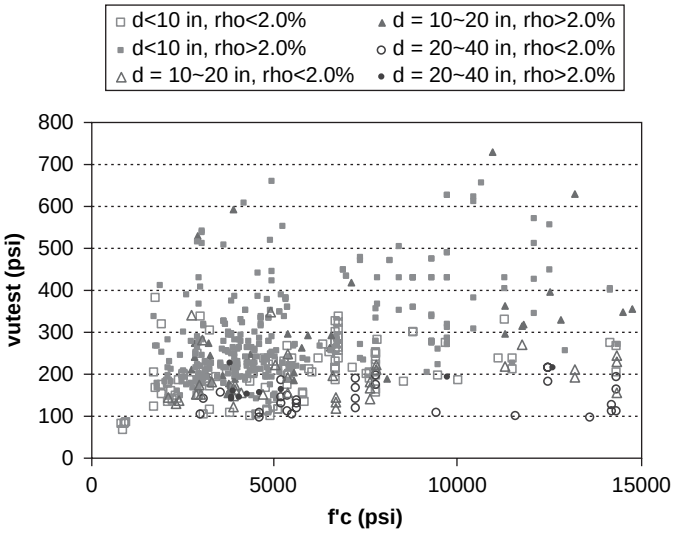

Figure 29. Influence of member size for reinforced concrete members without shear reinforcement.

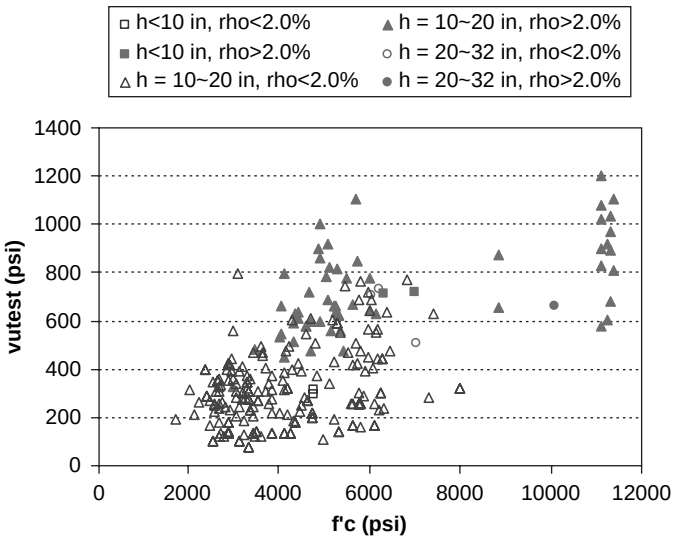

Figure 30. Influence of member size for prestressed concrete members without shear reinforcement.

controls the concrete contribution to shear resistance. The basis for this approach is that (a) crack spacing is proportional to the distance between layers of crack control reinforcement and (b) crack widths, which influence the aggregate interlock mechanism, are roughly in proportion to crack spacing for any given level of longitudinal strain. In members with minimum shear reinforcement, such as the majority of prestressed members, the LRFD method assumes a crack spacing of 12 inches and thereby predicts that there is no size effect in shear.

Figures 31 through 34 show the influence of f'_c, depth, and longitudinal reinforcement ratio on the shear strength ratio. The results reinforce similar trends that have already been identified.

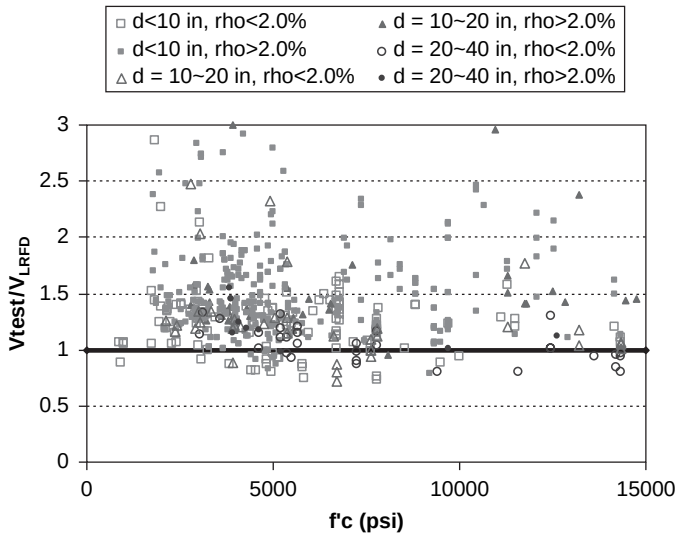

Figure 31. Influence of member size on shear strength ratio (V_{test}/V_{LRFD}) for reinforced concrete members.

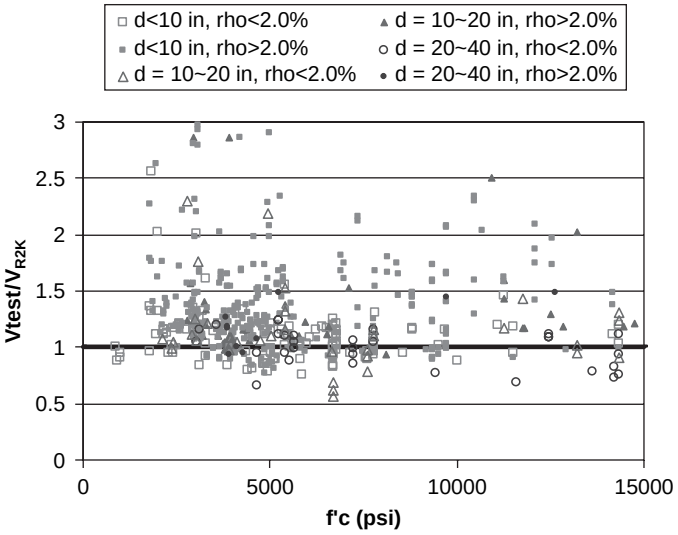

Figure 32. Influence of member size on shear strength ratio (V_{test}/V_{R2K}) for reinforced concrete members.

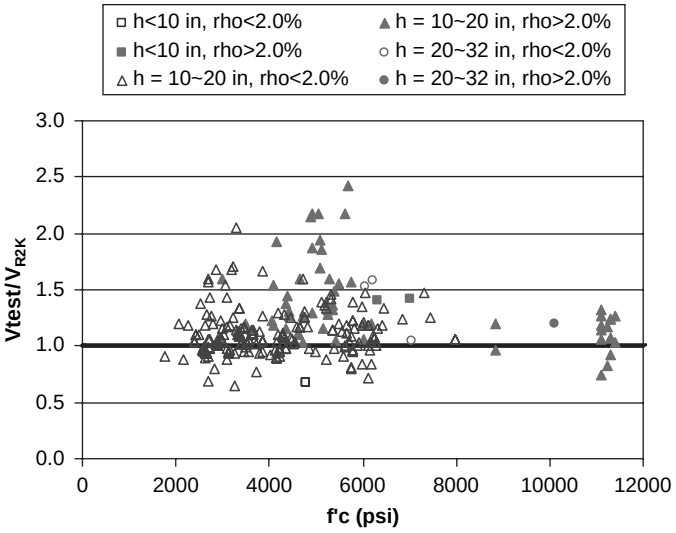

Figure 34. Influence of member size on shear strength ratio (V_{test}/V_{R2K}) for prestressed concrete members.

2.2.6 Influence of Longitudinal Reinforcement Ratio

Figures 35 and 36 illustrate that the LRFD and R2K predictions become more conservative as the amount of longitudinal reinforcement in RC members increases. A similar effect is observed for PC members in Figures 37 and 38.

2.2.7 Summary of Research Needs

The analysis presented in this section illustrates that the LRFD Sectional Design Model and the Response 2000 design/analysis tool provide conservative estimates of capacity in most cases. It further indicates that the LRFD specifications are equally conservative and accurate at predicting the strength of members cast with HSC as those cast with normal strength. However, the considerable scatter in the experimental test results over the entire range of possible concrete compressive strengths indicates that these tools do not accurately account for all influencing factors. This is a concern when coupled with the recognition that members tested in laboratories do not well represent what is built in the field. As summarized at the beginning of this section, there is comparatively little experimental test data on large members, uniformly loaded members,

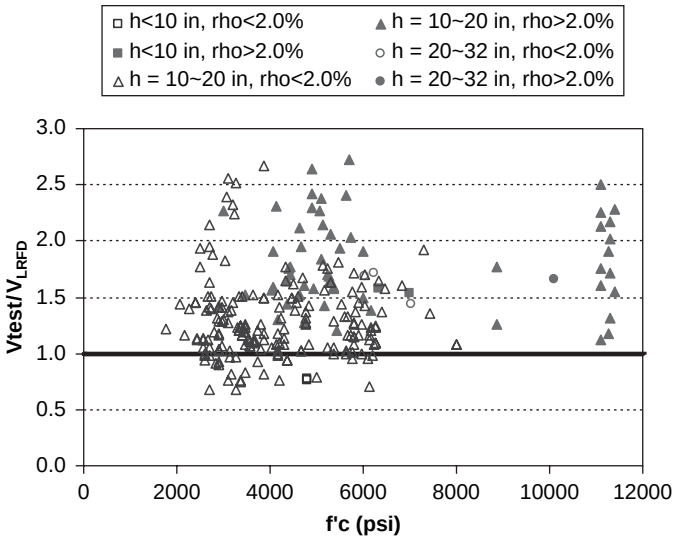

Figure 33. Influence of member size on shear strength ratio (V_{test}/V_{LRFD}) for prestressed concrete members.

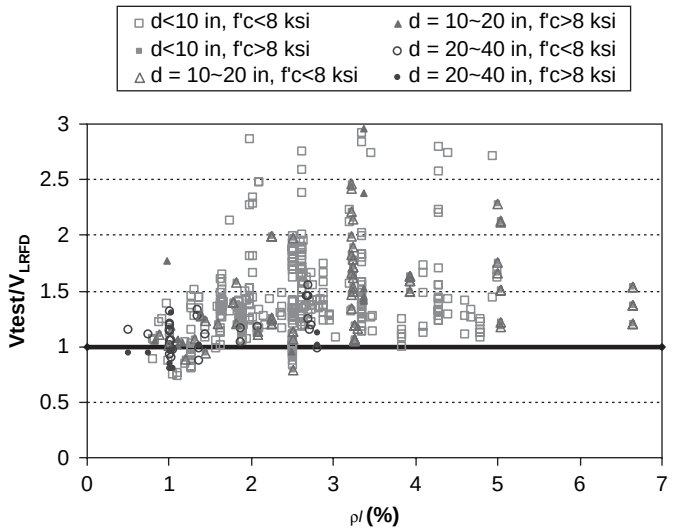

Figure 35. Influence of longitudinal reinforcement ratio on shear strength ratio (V_{test}/V_{LRFD}) of reinforced concrete members without shear reinforcement.

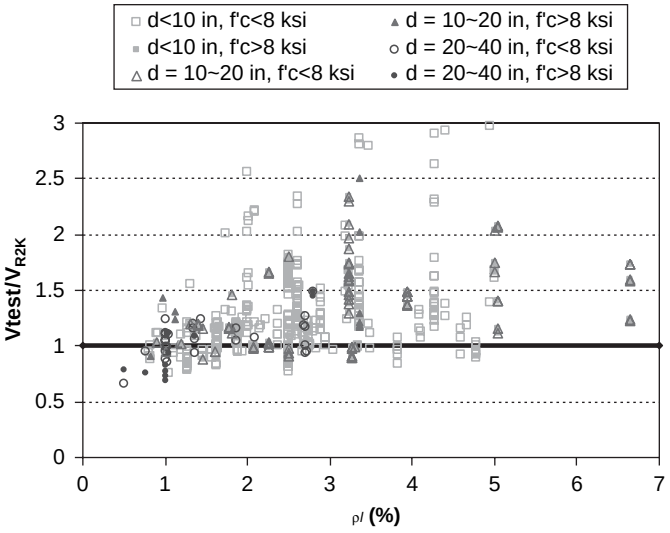

Figure 36. Influence of longitudinal reinforcement ratio on shear strength ratio (V_{test}/V_{R2K}) of reinforced concrete members without shear reinforcement.

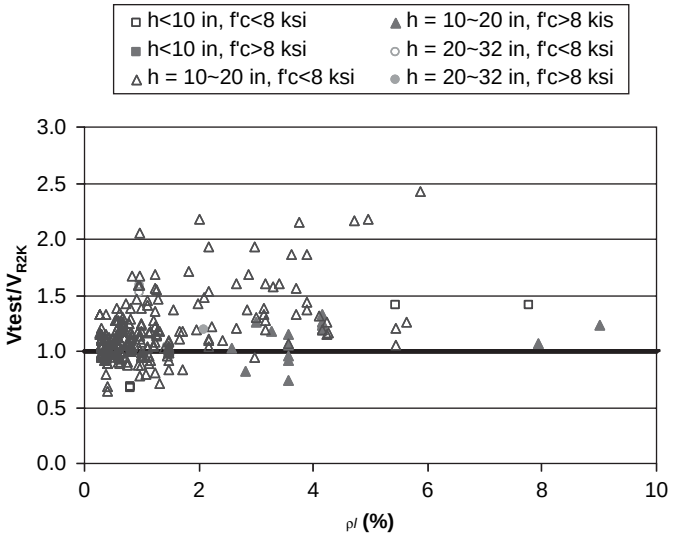

Figure 38. Influence of longitudinal reinforcement ratio on shear strength ratio (V_{test}/V_{R2K}) of prestressed concrete members without shear reinforcement.

continuous members, members for which shear is critical away from the support, and prestressed members cast with HSC.

While the experimental test results did not identify any alarming trends, the new aspects of the LRFD specifications in combination with a lack of specific test data to validate this method for HSC members indicates a significant need for experimental research. As discussed in Chapter 1, the LRFD design issues that are particularly important to validate for HSC members include the upper shear design stress limit, the method for calculating the contribution of shear reinforcement, the design of end regions by the Sectional Design Model, minimum shear reinforcement requirements, and the capacity/demand on longitudinal tension reinforcement in support regions. To evaluate the significance of these design issues, the decision was made to test HSC prestressed bulb-tee girders that were subjected to uniformly distributed loads. This member type and test configuration were selected because HSC is particularly beneficial for this commonly used product and there is very little existing test data for this type of member. The LRFD provisions that were primarily examined by these tests include

- Article 5.8.2.5, Minimum Transverse Reinforcement;
- Article 5.8.4.1, General in Interface Shear Transfer—Shear Friction;
- Article 5.8.3.3 Nominal Shear Resistance; and
- Article 5.8.3.4 Determination of β and θ.

Information relevant for the extension of the following provisions was also collected during NCHRP Project 12-56:

- Article 5.6.3.3.3, Limiting Compressive Stress In Strut;
- Article 5.8.2.8, Design and Detailing Requirements;
- Article 5.4.2.7, Tensile Strength;
- Article 5.9.5.4, Refined Estimates of Time-Dependent Losses; and
- Article 5.11.2, Development of Reinforcement.

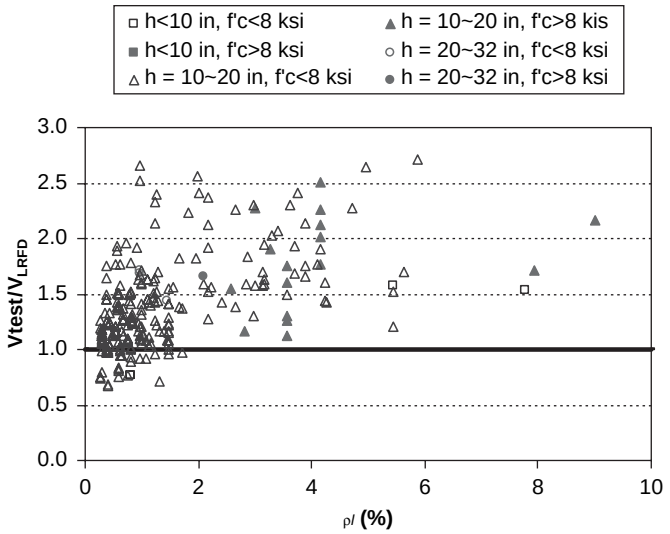

Figure 37. Influence of longitudinal reinforcement ratio on shear strength ratio (V_{test}/V_{LRFD}) of prestressed concrete members without shear reinforcement.

2.3 Description of Experimental Research Program

This section describes the large-scale testing program on 63-inch deep bulb-tee girders. It presents an overview of the test program, material properties, the fabrication process,

the experimental test set-up, and associated shear friction tests.

2.3.1 Overview of Test Program on 63-Inch Deep Bulb-Tee Girders

The overall objective of the experimental testing program was to generate the additional test data necessary to increase the limit on the compressive strength of concrete in the shear provisions of the *AASHTO LRFD Bridge Design Specifications*, specifically including the provisions of the Sectional Design Model (S5.8.3). Based on a review of existing test data, an experimental program was designed to study the overall performance of full-scale bridge members as well as to gather the level of detailed experimental test data on the performance of these members that was considered necessary to assess and validate the individual elements of the Sectional Design Model and other LRFD shear provisions.

Twenty experiments on ten 63-inch deep and 52-foot long bulb-tee girders were planned. Each simply supported member was designed to span 50 feet and to carry a uniformly distributed load over the central 44 feet of its length. A 10-inch deep composite slab was cast on each girder. The overall geometry of the test girders is shown in Figure 39. The primary variables in this study were girder concrete strength (ranging from 10 ksi to 18 ksi), maximum shear design stress (700 psi to 2,500 psi), strand anchorage details (straight, unbonded, and draped), and end reinforcement details (bar size, spacing, and level of confinement). The range of variables in the experiments was selected in part to investigate the limits of resistance associated with different modes of shear failure. These modes included yielding and rupture of the shear reinforcement, localized diagonal crushing with stirrup yield, localized diagonal crushing without stirrup yield, shear failure at the interface between the base of the web and the bottom bulb, distributed diagonal crushing, and failure initiated by strand slip. Each half of each girder (designated as East [E] and West [W]) was designed to be different so as to obtain two test results from each girder. This action was accomplished by reconstructing and strengthening the half of the girder that failed first and then reloading the girder until the second half failed.

Each test girder was designed to satisfy all requirements of the LRFD specifications but with no limit on f'_c used in any of the design calculations. In accordance with the LRFD specifications, the first critical section for shear design was taken to be at $0.5d_v\cot\theta_1$ from the inside face of the bearing plate above the end support. Based on the shear force for this girder

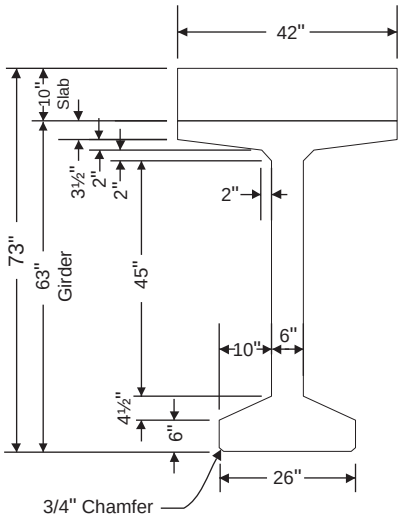

(a) Geometry of test cross sections

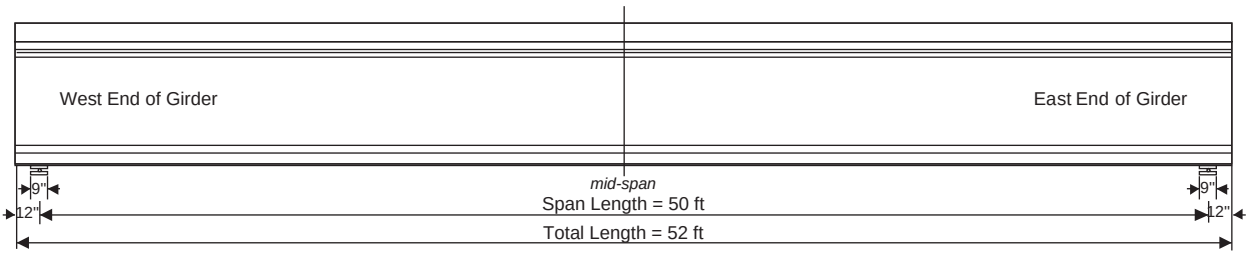

(b) Front elevation view

Figure 39. Geometry of 63-inch bulb-tee girders with slabs.

section, shear reinforcement was selected to provide adequate shear capacity for that section. Then the same quantity of shear reinforcement was used over a length of $d_v\cot\theta_1$ from that section and toward the center of the beam. The next section designed for shear was then taken at $d_v\cot\theta_1 + 0.5d_v\cot\theta_2$ from the inside face of the support, and the shear reinforcement required to provide the necessary resistance at that section was then used over a length $d_v\cot\theta_2$ from that section and towards the center of the beam. This design approach was repeated for subsequent shear regions as necessary. The effect of following this methodology, given in the LRFD specifications, is that these test beams were theoretically just as likely to fail in shear in the regions of lower shear and higher moment away from the support as they were to fail at sections with higher shear and lower moment adjacent to the support. A summary of the design characteristics for each of the girders, including the number of prestressing strands and the amount of shear reinforcement, is shown in Table 3. The reinforcing details for each of the 10 girders are presented in Figures 40 and 41. Note that the factor of safety against flexural failure ranged from 1.1 to 1.4. It was expected that those factors would be high enough to ensure a shear failure but not so high to be unrealistic. A complete summary of the design of each member is presented in the associated appendix for each girder.

Table 3. Summary of experimental research program on 63-inch bulb-tee girders.

Test Specimen	f'_c, (ksi)	b_w, (in)	d_p,[a] (in)	Designed v/f'_c	Number of Strand (ϕ0.6")		ρ_p,[b] (%)	f_{pe}, (ksi)	$\rho_v f_y$,[e] (psi)	Shear Reinforcement		
					bottom	top				Sect.1[c]	Sect.2[c]	Sect.3[c]
G1E	10.0	6	68.50	0.12	32-straight	2	1.70	134.5	389	2-#4 @12"	2-#4 @24"	-
G1W	10.0	6	68.50[a]	0.11	26-straight + 6-draped	2	1.70[b]	134.5	389	2-#4 @12"	2-#4 @24"	-
G2E	10.0	6	67.32	0.18	38-straight	2	2.05	125.9	745	2-#5 @11"	2-#5 @17"	2-#4 @22"
G2W	10.0	6	67.32[a]	0.17	32-straight + 6-draped	2	2.05[b]	125.9	745	2-#5 @11"	2-#5 @17"	2-#4 @22"
G3E	14.0	6	67.67	0.12	42-straight	2	2.26	116.4	565	2-#4 @8"	2-#4 @12"	2-#4 @24"
G3W	14.0	6	67.67	0.12	42-straight	2	2.26	116.4	565	2-#4 @8"	2-#4 @12"	2-#4 @24"
G4E	14.0	6	67.67	0.17	42-straight	2	2.26	116.4	1113	2-#5 @6"	2-#5 @10"	2-#5 @24"
G4W	14.0	6	67.67	0.17	42-straight	2	2.26	116.4	1113	2-#5 @6"	2-#5 @10"	2-#5 @24"
G5E	18.0	6	70.00	0.05	24-straight	-	1.25	141.6	169	2-D11 @20"[d]	-	-
G5W	18.0	6	70.00	0.05	24-straight	-	1.25	141.6	140	2-#3 @20"	-	-
G6E	18.0	6	67.67	0.10	42-straight	2	2.26	123.4	557	2-#5 @12"	2-#5 @20"	2-#3 @24"
G6W	18.0	6	67.67[a]	0.08	42-straight (18 debonded)	2	2.26[b]	123.4	557	2-#5 @12"	2-#5 @20"	2-#3 @24"
G7E	14.0	6	67.67	0.12	42-straight	2	2.26	116.4	577	2-#4 @8	2-#4 @12	2-#4 @24
G7W	14.0	6	67.67	0.04	42-straight	2	2.26	116.4	119	2-#4 @8	2-#3 @23	-
G8E	14.0	6	67.67	0.12	42-straight	2	2.26	116.4	577	2-#4 @8	2-#4 @12	2-#4 @24
G8W	14.0	6	67.67	0.12	42-straight	2	2.26	116.4	577	2-#4 @8	2-#4 @12	2-#4 @24
G9E	8.0	6	66.88	0.25	34-straight	2	1.85	131.4	1040	2-#5 @6.5	2-#4 @7.5	2-#4 @24
G9W	8.0	6	66.88[a]	>0.25	26-straight + 8-draped	2	1.85[b]	131.4	1690	2-#5 @4	2-#4 @7.5	2-#4 @24
G10E	16.0	6	66.88	0.12	34-straight (8-debonded)	2	1.85	138.1	751	2-#5 @9	2-#4 @10	2-#4 @22
G10W	16.0	6	66.88[a]	0.12	26-straight + 8-draped	2	1.85[b]	138.1	751	2-#5 @9	2-#4 @10	2-#4 @22

a) d_p: effective depth at mid-span.
b) ρ_p: longitudinal reinforcement ratio based on effective depth at mid-span.
c) For the location of each section, see drawing of each specimen.
d) Two layers of WWR were used (20×20-D11×D11).
e) $\rho_v f_y$: stirrup strength at the first critical section except G7W (section 2 in flexure-shear region).

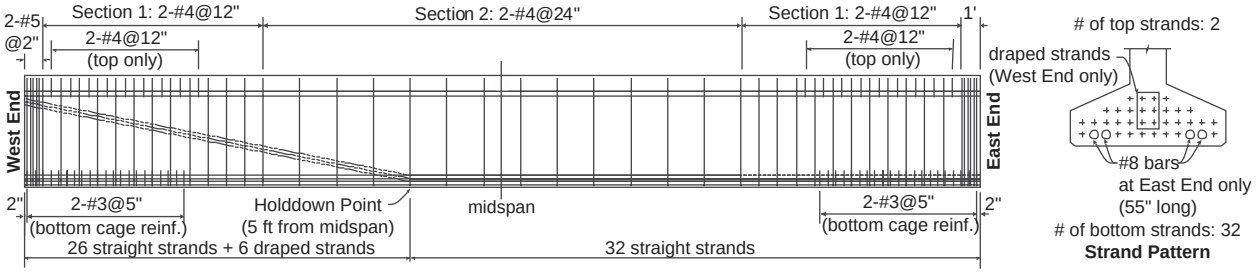

(a) Girder 1

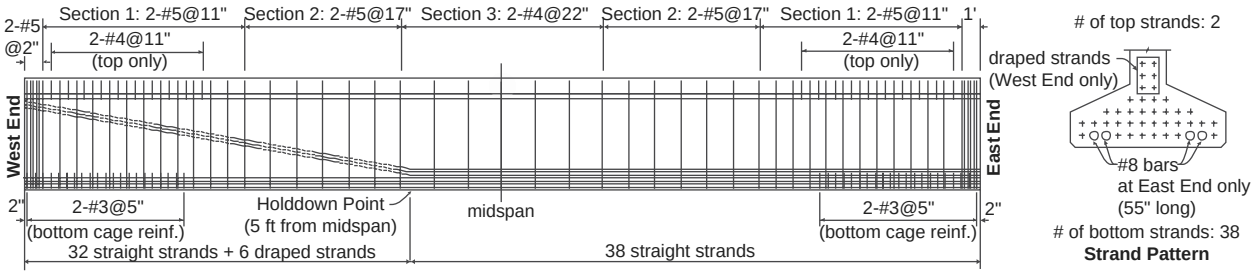

(b) Girder 2

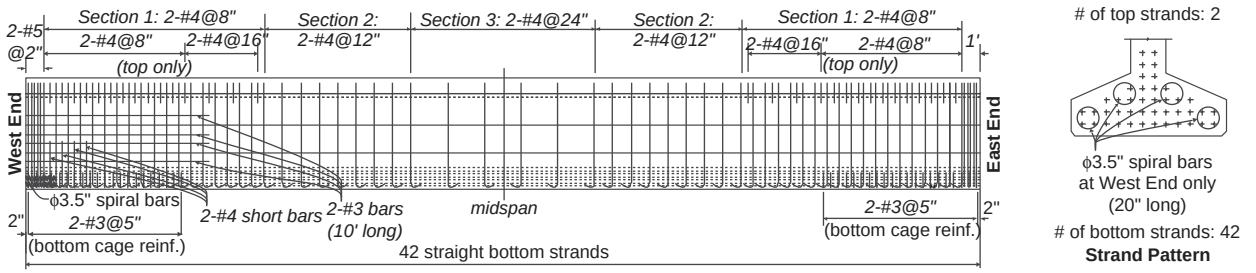

(c) Girder 3

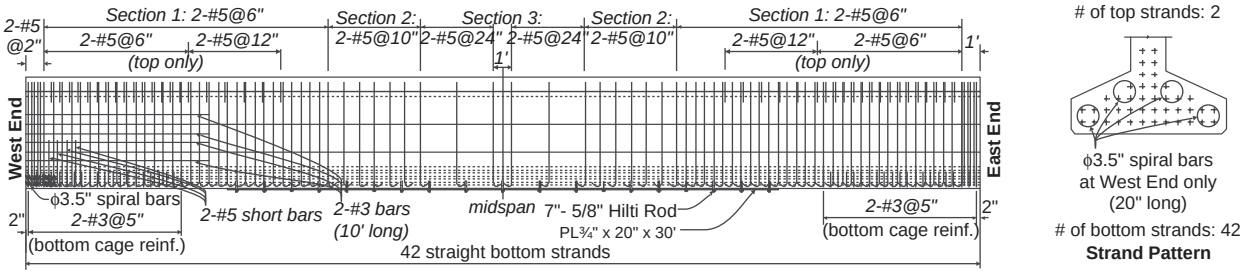

(d) Girder 4

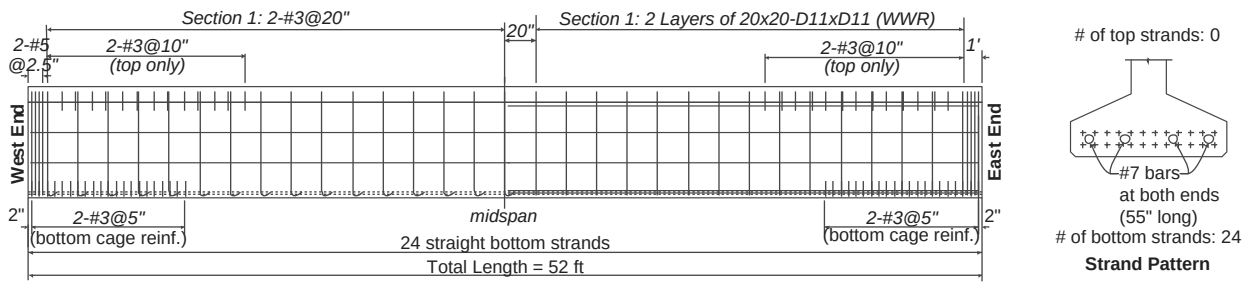

(e) Girder 5

Figure 40. Summary of reinforcing layout in bulb-tee girders.

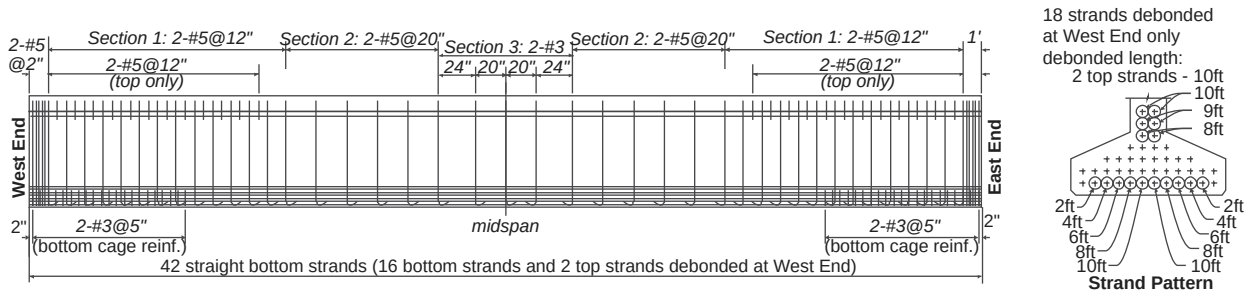

(f) Girder 6

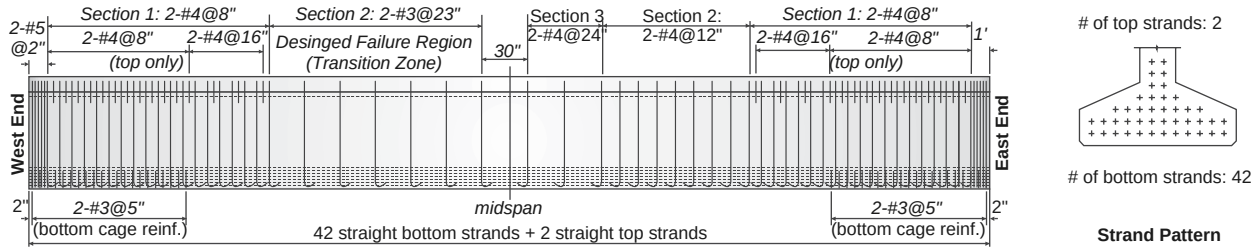

(g) Girder 7

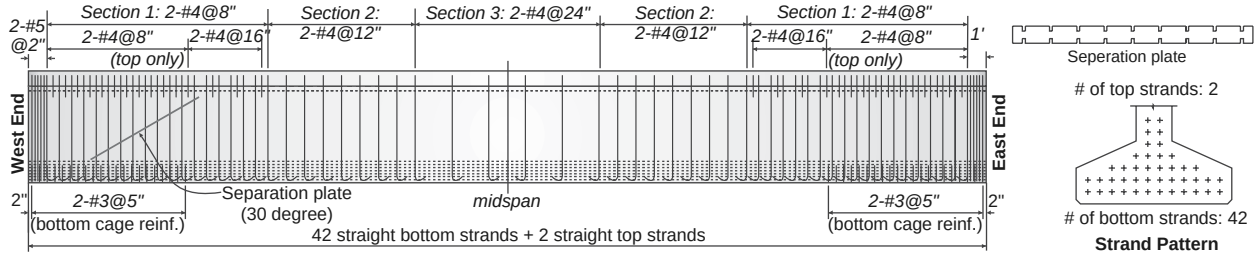

(h) Girder 8

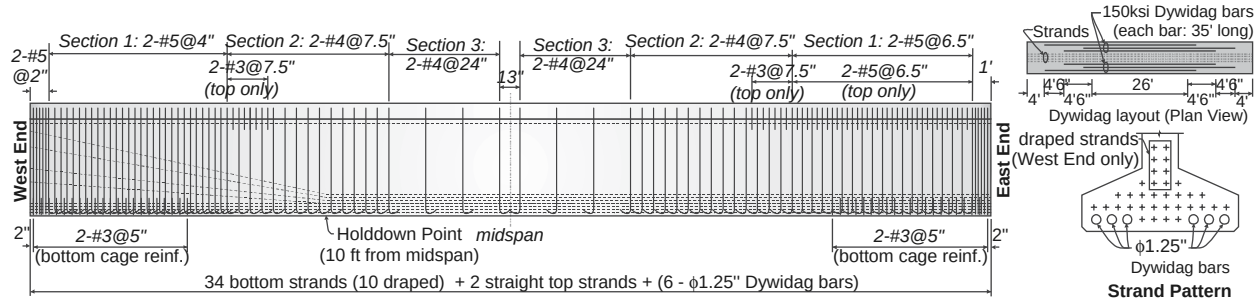

(i) Girder 9

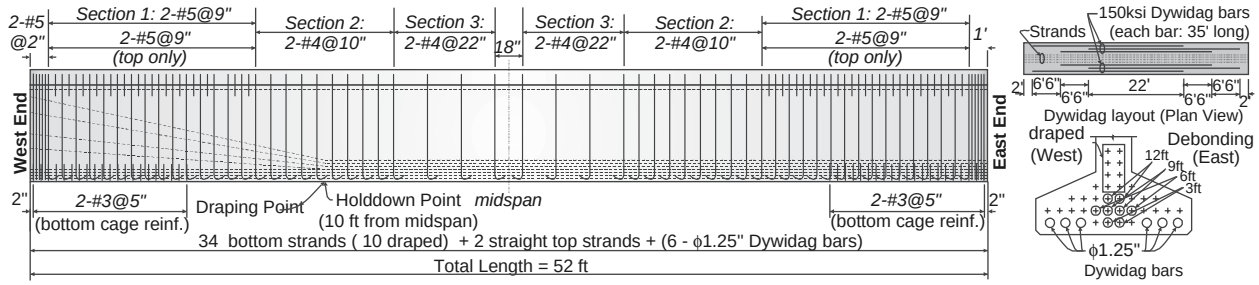

(j) Girder 10

Figure 40. (Continued).

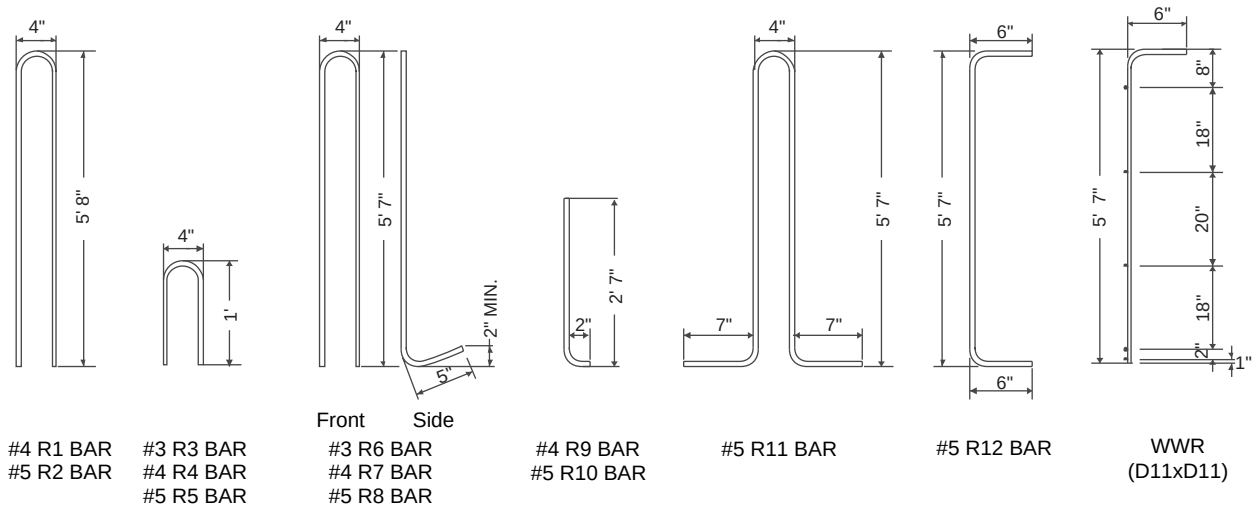

Figure 41. Shapes of stirrup reinforcement.

As described above, the testing program was designed to investigate the design and behavior of HSC prestressed girders that exhibited different modes of resistance and failure. This was accomplished by designing the girders using a range of concrete strengths and shear demand levels, with different end reinforcement details. In the remainder of this section, a brief summary of the design details for each girder is presented.

Girders 1 and 2 were designed using a specified concrete strength of 10 ksi to support shear stresses, v_u, at the first critical section ($0.5d_v\cot\theta_1$ from the inside face of the support) of $0.12f'_c$ (1.2 ksi) and $0.17f'_c$ (1.7 ksi), respectively. From the standpoint of the LRFD shear design provisions, which permit designs with maximum shear stresses of $0.25f'_c$, these girders can be said to have been designed to support moderate and moderately high shear design stress levels, respectively. However, from the perspective of the AASHTO Standard Specifications, the designs corresponded to shear design stresses of $12\sqrt{f'_c}$ and $17\sqrt{f'_c}$, which are near and beyond, respectively, the maximum shear design stress permitted by those specifications. Each end of each girder contained the same quantity of shear reinforcement, but different longitudinal reinforcement details. At the first critical section in Girder 1, double-legged #4 bars at 12-inch centers were used ($\rho_v f_y = 389$ psi). At the first critical section in Girder 2, double-legged #5 bars at 11-inch centers were used ($\rho_v f_y = 745$ psi). Thirty-four 0.6-inch diameter, seven-wire strands were used in Girder 1, and forty 0.6-inch diameter, seven-wire strands were used in Girder 2. At the east end of both of these members, the strands were straight and bonded through to the end of the beam, while at the west end of these members, six strands were draped starting 5 feet from mid-span, as shown in Figures 40(a) and (b). The angle of the six draped strands was about 11 degrees for G1W and about 10 degrees for G2W. Two stressed top strands were provided in each beam to keep the top tensile stresses within the LRFD specified limit. Four #8 deformed bars were placed at the east ends of both girders to provide longitudinal tensile strength at the inside face of the support.

Girders 3 and 4 were designed using a specified concrete strength of 14 ksi and were designed for shear stresses of $0.12f'_c$ (1.68 ksi) and $0.17f'_c$ (2.38 ksi), respectively, at the first critical shear section from the support. These shear stresses were very large relative to the commonly used maximum shear stress level, which is approximately $12\sqrt{f'_c} = 12\sqrt{6{,}000} = 929$ psi, or 0.93 ksi. Each end of each girder contained the same quantity of shear reinforcement, but different end reinforcement details. At the first critical section in Girder 3, double-legged #4 bars at 8-inch centers were used ($\rho_v f_y = 565$ psi). At the first critical section in Girder 4, double-legged #5 bars at 6-inch centers were used ($\rho_v f_y = 1{,}113$ psi). Forty-two straight strands were used in the bottom bulb, and two tensioned prestressing strands were used in the top flange. The west ends of Girder 3 (G3W) and Girder 4 (G4W) were strengthened to reduce the chance of premature failure due to strand slip, diagonal compressive failure, and horizontal shear slip. This strengthening consisted of four 20-inch long spirals wrapped around groups of strands, two #3 horizontal bars on 6-inch centers that extended 10 feet from the end of the member, and four pairs of vertical bars (#4 in Girder 3, #5 in Girder 4) at the inside face of the support. See Figures 40(c) and (d). In Girder 4, a 0.75-inch thick, 20-inch wide, and 30-feet long plate was added under the bottom flange to provide the additional flexural reinforcement that was calculated to be necessary to avoid a flexural failure.

Girder 5 was designed with a specified concrete strength of 18 ksi and was reinforced with only slightly more than the minimum required amount of shear reinforcement.

By the LRFD specifications, the minimum required amount of shear reinforcement is $\rho_v f_y \geq 0.0316\sqrt{f'_c} = 134$ psi. On the east half of Girder 5 (G5E), welded wire reinforcement (WWR) was used. The reinforcement consisted of a grid of D11 × D11 bars (area = #3 bar) on 20-inch centers ($\rho_v f_y$ = 169 psi). On the west half of Girder 5 (G5W), deformed bar reinforcement was used that consisted of double-legged #3 bars on 20-inch centers ($\rho_v f_y$ = 140 psi). See Figure 40(e). Twenty-four strands were located in the bottom bulb, and no prestressing strands were used in the top flange. Four #7 deformed bars (55 inches long) were placed at both ends of Girder 5 to provide longitudinal tensile strength at the inside face of the support.

Girder 6 was designed using a specified concrete strength of 18 ksi. While each half of the girder was designed using the same pattern of shear reinforcement, the halves differed in how strands were anchored. The shear reinforcement at the first critical section from either support consisted of double-legged #5 bars on 12-inch centers ($\rho_v f_y$ = 557 psi). At the east end of the girder, all strands were bonded, while in the west end, 18 of the 44 strands were debonded. Figure 40(f) shows the reinforcement details and the debonding pattern. The level of debonding slightly exceeded what would be permitted by the LRFD specifications (S5.11.4.3), but this was considered useful to experimentally evaluate performance at this higher level of debonding. Both ends of Girder 6 failed to meet the requirements for longitudinal reinforcement specified in Section 5.8.3.5 of the LRFD specifications.

Girder 7 was designed using a specified concrete strength of 14 ksi. The east end was designed to contain the same shear reinforcement as used in Girder 3. At the west end of the member, only the minimum shear reinforcement was included in Section 2 in an effort to induce a failure away from the end region. See Figure 40(g). This region is designated as a "transition" zone because its behavior is somewhere between that of "web-shear" and "flexure-shear." In the west transition zone, the shear reinforcement consisted of double-legged #3 bars at 23-inch centers ($\rho_v f_y$ = 119 psi), while in the equivalent region on the east side of the member, double-legged #4 bars at 12-inch centers ($\rho_v f_y$ = 384 psi) were provided. Thus, only 31 percent (119 out of 384 psi) of the required strength of shear reinforcement was provided in the west transition region. The member contained 42 bottom and 2 top straight, fully bonded, and stressed 0.6-inch diameter seven-wire strands.

Girder 8 was designed on both halves to contain the same amount and distribution of longitudinal and shear reinforcement as used in the east halves of Girders 3 and 7. Girder 8 was also designed using a specified concrete strength of 14 ksi. Girder 8 differed from Girders 3 and 7 in the use of a diagonal slip plane and side diaphragms. The diagonal slip plane was inserted near the first critical section at the west end of the girder and was to eliminate, or at least minimize, the shear stress that could be transferred in the web by "interface shear transfer." This slip plane was created by inserting into the web two aluminum sheets pressed against each other, as shown in Figure 40(h). At the east end of Girder 8, side diaphragms were cast and posttensioned against the web so as to prevent an end region failure and force the failure into a region where there was a uniform field of diagonal compression. The member contained 42 bottom and two top straight, fully bonded, and stressed 0.6-inch diameter seven-wire strands.

Girder 9 was designed using a specified concrete strength of 8 ksi. The east end was designed for a shear stress equal to the maximum LRFD limit of $0.25f'_c$. The corresponding shear reinforcement consisted of double-legged #5 bars at 6.5-inch centers ($\rho_v f_y$ = 1,040 psi). The design of the west end region differed from that in the east in two ways. Approximately 60 percent more shear reinforcement was provided at the first critical section by using double-legged #5 bars at 4-inch centers ($\rho_v f_y$ = 1,690 psi) and by draping eight of the strands in a splayed manner such that they were close to uniformly distributed over the height of the web at the west end of the member. See Figure 40(i). Girder 9 contained 34 bottom and two top straight and fully bonded 0.6-inch diameter strands. Additionally, six 1.25-inch diameter, high-strength (150 ksi) unstressed posttensioning bars were placed over the majority of the length of the member to provide the additional flexural capacity calculated as necessary to produce a shear failure.

Girder 10 was designed using a specified concrete strength of 16 ksi. It was designed for a shear stress ratio (v/f'_c) of 0.12. It contained the same quantity of shear reinforcement in both halves of the member. At the first critical section, this reinforcement consisted of double-legged #5 bars on 9-inch centers ($\rho_v f_y$ = 751 psi). Thirty-four bottom and two top 0.6-inch diameter strands were used. At the east end, eight strands were debonded, while at the west end, eight strands were draped and splayed out over the depth of the web, as was done at the west end of Girder 9. See Figure 40(j). Six 1.25-inch diameter high-strength (150-ksi) unstressed bars were also placed in the bottom flange.

2.3.2 Material Properties

A variety of material tests were conducted to measure the mechanical properties of the concrete and the steel reinforcement. This section provides a summary of these properties. The concrete mix designs are presented in Table 4, the measured concrete strength properties at the time of the test are listed in Table 5, the concrete compressive stress-strain responses are plotted in Figure 42, and the strength

Table 4. Summary of concrete mix designs.

Property	G1 & G2	G3 & G4	G5 & G6	G7 & G8	G9	G10
Type I Cement Weight (lbs/yd^3)	-	-	1,050			1,050
Type III Cement Weight (lbs/yd^3)	750	1,030	-	1,030	700	
Fly Ash Weight (lbs/yd^3)	-	-	-			
Silica Fume Weight (lbs/yd^3)	-	125	150	125		150
Water Weight (lbs/yd^3)	210	300	264	300	280	264
Sand Weight (lbs/yd^3)	1,328	777	858	777	1,180	858
Coarse Aggregate (3/4" max) Weight (lbs/yd^3)	1,880	-	-	-	1,786	
Coarse Aggregate (1/2" max) Weight (lbs/yd^3)	-	1,820	-	1,820		
Coarse Aggregate (3/8" max) Weight (lbs/yd^3)	-	-	1,820	-		1,820
Retarder (100XR) Weight	-	-	4 oz/ 100 lbs	20 oz/ yard		4 oz/100 lbs
Super Plasticizer (MB 300FC) Weight	-	as needed	15-18 oz/ 100 lbs	as needed	175 oz/yard	15-18 oz/ 100 lbs
water/cementitious mat. ratio	0.28	0.24	0.25	0.24	0.40	0.25

Note: 1 in = 25.4 mm, 1 ksi = 6.895 MPa, 1 lb/yd^3 = 432 kg/m^3.

properties of the reinforcement are summarized in Table 6. Additional information about the materials used in this study follows.

Concrete

The concrete mix designs, as presented in Table 4, were developed at Wiss, Janney, Elstner Associates, Inc. (WJE), using aggregate supplies available from the precaster, Prestress Engineering Cooperation (PEC), and a Traprock aggregate imported from Wisconsin. After several batch plant trials, the mix designs were adjusted to obtain the target concrete strengths. Target strengths were as listed in Table 3. With the exception of Girders 6 and 10, the concrete strengths achieved were close to or in excess of the target strengths. The shortfalls in strengths were considered to be associated with difficulties in very accurately measuring the moisture content in the aggregates. With these very dry mixes, a small error in moisture content can have a significant effect on the water-cement ratio and thus the final compressive strength.

Table 5. Summary of concrete strength properties.

Specimen	Girder				Deck
	Strength (ksi)	Strain* ($\times 10^{-6}$)	Split Tensile (psi)	Modulus of Rupture (psi)	Strength (ksi)
Girder 1	12.1	3,000	867	991	4.5
Girder 2	12.6	2,600	811	991	8.6
Girder 3	15.9	3,300	766	1,090	3.6
Girder 4	16.3	3,400	766	1,090	6.3
Girder 5	17.8	3,500	894	1,190	6.1
Girder 6	12.7	2,800	823	1,190	9.2
Girder 7	12.5	3,200	706	720	4.5
Girder 8	13.3	3,200	706	720	7.0
Girder 9	9.6	2,400	686	1,080	6.0
Girder 10	10.6	2,600	765	1,180	5.4

*Strain value at peak stress.

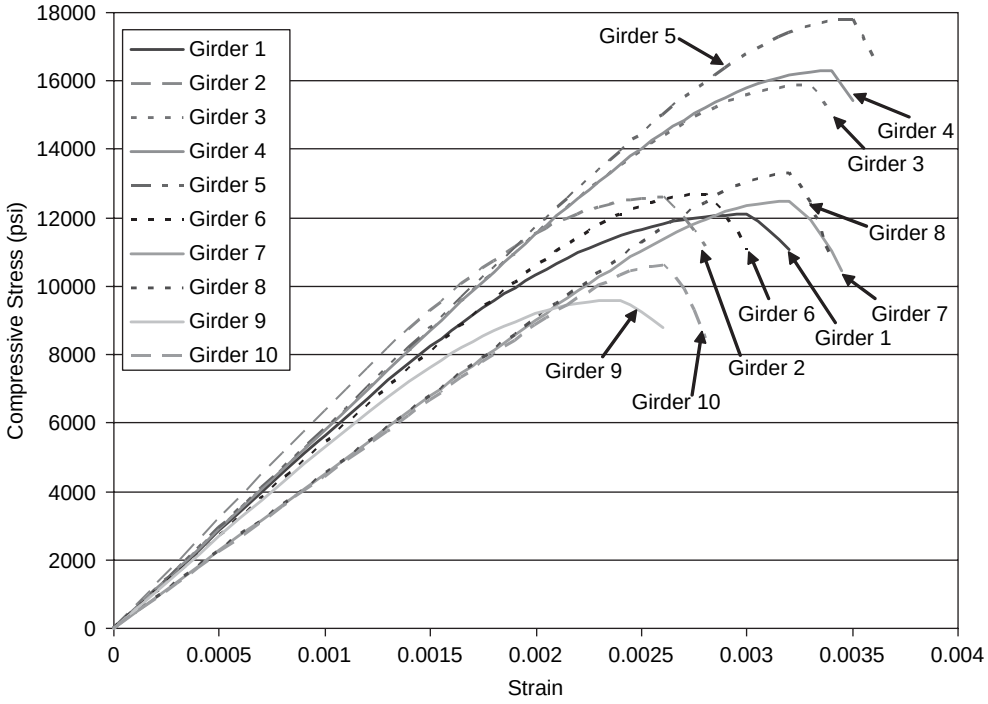

Figure 42. Concrete compressive stress-strain relationships.

The concrete compressive strengths finally achieved are shown in Table 5. These strength values are used in all subsequent calculations, including the evaluation of the LRFD-calculated shear design strength of the girders. This distribution of delivered strengths, coupled with the experimental measurements presented in the remaining subsections of Chapter 2 and other available test data, were considered to be sufficient to support the proposed changes to design specifications that are presented in Chapter 3.

The volume of concrete in each girder was approximately 10 cubic yards. Because the precaster, PEC, used a 2-cubic-yard pan mixer, six batches were required to cast each girder and the associated material test samples. Two girders were often cast one after another using the same mix design. Deck slabs were cast after the girders were delivered to the Newmark Laboratory at the University of Illinois using concrete with a 5-ksi design strength. As shown in Table 5, with the exception of Girders 1, 3, and 7, this strength was also

Table 6. Summary of steel reinforcement properties.

(a) Transverse Reinforcement										
Specimen	G1		G2		G3		G4		G5	
Bar	#4	#5	#4	#5	#4	#5	#4	#5	#3	WWR
Nominal Area (in^2)	0.20	0.31	0.20	0.31	0.20	0.31	0.20	0.31	0.11	0.11
Yield Strength, f_y (ksi)	70.0	79.3	70.0	79.3	67.8	64.6	67.8	64.6	76.5	92.2
Tensile Strength, f_u (ksi)	109.0	119.0	109.0	119.0	106.1	101.8	106.1	101.8	112.5	106.1
Specimen	G6		G7		G8		G9		G10	
Bar	#5		#3	#4	#4	#5	#4	#5	#4	#5
Nominal Area (in^2)	0.31		0.11	0.20	0.20	0.31	0.20	0.31	0.20	0.31
Yield Strength, f_y (ksi)	64.7		74.5	69.2	69.2	68.4	67.9	65.4	67.9	65.4
Tensile Strength, f_u (ksi)	102.0		109.5	107.8	107.8	107.4				

(b) Prestressing Strands					
Beam	Girder 1	Girder 2	Girder 3	Girder 4	Girder 5
Effective Stress, f_{pe} (ksi)	159.7	150.2	154.9	153.7	174.7
Prestressing Loss* (%)	21.1	25.8	23.5	24.1	13.7
Beam	Girder 6	Girder 7	Girder 8	Girder 9	Girder 10
Effective Stress, f_{pe} (ksi)	167.6	167.0	158.5	166.5	173.7
Prestressing Loss* (%)	17.2	17.5	21.7	17.8	14.2

*The prestressing loss was calculated based on measurements at the time of testing.

achieved. Since these girders failed well before their flexural capacity was reached, the lower-than-specified strength for the deck slabs was considered to have no significant effect on the project outcome.

Compression Strength Tests: From each of the six concrete batches used in casting a single girder, seven 4-inch diameter cylinders were cast. The initial cylinder tests were conducted using cylinder testing machines available at WJE and the University of Illinois and were made in accordance with ASTM C 39. However, there were larger-than-expected variations in the cylinder strengths, and some of the cylinders for the very high-strength mix failed under lower stresses than seemed to be realistic. The variations were considered to be due to the sensitivity of the test results to the cylinder end preparation methods, as has been the experience of producers of very high-strength concretes. To address this difficulty, Prairie Materials Group out of Chicago was retained to prepare the cylinder ends and test many of the very high-strength concretes. In parallel, end preparation techniques were improved at the University of Illinois by using a rock saw to cut thin, (3/16-inch thick) strips off the ends of cylinders perpendicular to their axes. This enabled the measuring of cylinder strengths in excess of 16 ksi in the University of Illinois testing machines.

Tensile Strength Tests: The results of the split cylinder and modulus of rupture (MOR) tests are also reported in Table 5. The MOR tests were made under third-point loading and using an 18-inch span. As shown in Figure 43, failure cracks in the MOR tests passed through the aggregates, and the resultant surfaces were relatively smooth.

Reinforcement

Seven-wire, low-relaxation prestressing strands with a diameter of 0.6 inch, an area of 0.218 square inch, and a specified ultimate tensile strength of 270 ksi were used for all girders. The number of strands and the strand pattern for each beam is presented in Figure 40. In the original designs, the anticipated prestressing loss was calculated in accordance with the provisions of the LRFD specifications. Anticipated losses ranged from 39 percent to 42 percent depending on the number of strands and the concrete compressive strength. The actual prestressing loss at the time of testing was determined from displacement measurements of the change in distance between targets mounted on the bottom bulb of the girder at the level of the centroid of the prestressing steel. The measured prestressing losses ranged from about 15 percent to 25 percent, and these measured values were used in calculating nominal capacities of the girders. The displacement targets also permitted determination of the transfer lengths for the strands. Detailed results are presented in the Appendices.

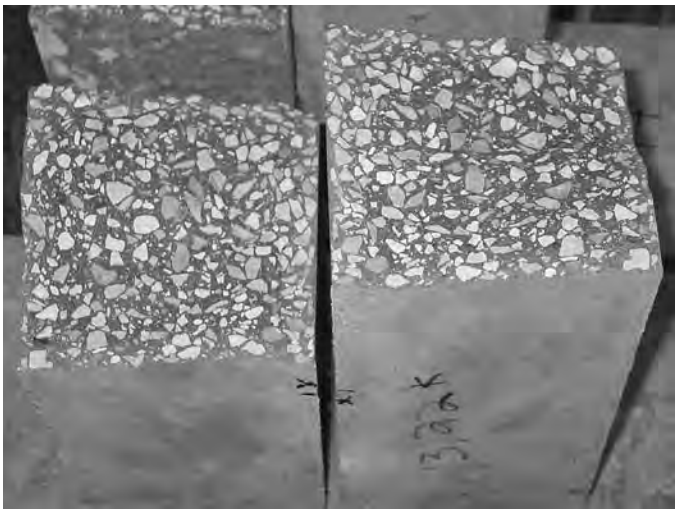

Figure 43. Tested specimens.

All transverse reinforcements were ASTM A 615 Grade 60 deformed steel bars except for the deformed welded wire fabric used as shear reinforcement in the east end of Girder 5. The welded wire reinforcement conformed to ASTM A 496. The structural properties of the transverse reinforcement are listed in Table 6, and the shapes of the various transverse reinforcements used in the girders are shown in Figure 41. The yield strength of the welded wire reinforcement was determined in accordance with ASTM A 497 requirements where the yield strength is measured at a strain of 0.5 percent. All shear reinforcements were double legged, with a loop extending out of the top flange of the girder to provide horizontal shear resistance between the girder and the deck slab. Additional short double-legged stirrups were placed in the end zone of each girder to provide the additional horizontal shear resistance required by LRFD specifications for end regions of the girder-to-slab interface. All girders also had between four and six No. 5 stirrups at each end to control spalling stresses caused by release of the prestressing strands and to provide confinement for the concrete over the support per LRFD requirements.

Deformed longitudinal bars were used in the top flange of the girders and deck slab. No. 7, No. 8, or No. 9 bars were used in the top flange of the girders to control tension cracks due to prestressing. No. 6 bars were used as compression reinforcement in the deck slab. In all girders, confinement reinforcement was also placed around the prestressing steel in the bottom flange for a distance of 100 inches from each end of each girder. This confinement reinforcement consisted of No. 3 bars placed at 6-inch spacing. In Girders 9 and 10, large 1.25-inch diameter high-strength deformed bars were used to provide additional flexural capacity.

The locations for all reinforcements are shown in Figure 40.

2.3.3 Fabrication of Test Girders

All test beams were fabricated at Prestress Engineering Cooperation (PEC) in Blackstone, Illinois. That plant was located about 100 miles from the University of Illinois. After the stirrup and confinement cage reinforcements were fabricated at PEC, selected bars were brought to the University of Illinois laboratory, electrical resistance strain gages were attached to the cages, and then the reinforcements were delivered back to PEC for insertion into the girders. In the prestressing operation, a load cell was used to measure the prestressing force in the strands. After the strands were pulled, University of Illinois researchers attached electrical resistance strain gages onto selected strands near the ends of the girders. The reinforcement cage and one side of the form were then placed in their final position. Preparation of the reinforcement cage was completed outside the stressing bed, and then, once completed and checked, the reinforcement cage was moved into the bed and anchored to one side of the form. See Figure 44. After a final check for all reinforcement details, pictures were taken and the other side of the steel form was put into place.

Each girder required approximately 10 cubic yards of concrete that was prepared into 6 batches. Four vibrators (two form vibrators and two immersion vibrators) were used to consolidate the concrete as it was placed. After casting, the top surface was intentionally roughened to satisfy the requirements of the LRFD specifications. See Figure 45. After casting and the initial set, a soaker hose was placed on top of the girder and a tarp was placed over the girder to prevent excess drying of the concrete. After removal of the formwork and before release of the strands, aluminum targets were placed on the end anchorage zone and in the middle of each girder for the measurement of the effects of strand release using a Whittemore gage.

Figure 44. Placement of reinforcement.

Figure 45. Roughening of surface of top flanges.

The strands were released a few days after casting the girders and when the measured concrete compressive strengths were at about the required level for strand release. The strain in the end reinforcement, strands, and the surface deformation of the bottom flange at release were measured. The 4-inch by 8-inch cylinders, the modulus of rupture beams, the fracture beams, and the shear friction specimens were cast alongside the girders, as shown in Figure 46. These specimens were kept with the test girders to ensure similar conditions for curing.

The girders were transported by truck from PEC to Newmark Laboratory, as shown in Figure 47. All material test

Figure 46. Material test specimens.

Figure 47. Transportation of test girders to Newmark Laboratory.

specimens were delivered to the Newmark Laboratory at the same time. As shown in Figure 48, a 10-inch deep and 42-inch wide deck slab with a design concrete compressive strength of 5,000 psi was then cast on the top of the girder. A detachable and reusable formwork were created and used for casting the deck slab.

2.3.4 Test Set-Up

A reaction structure, shown in Figures 49 and 50, was created to support the ends of the girders, and a loading from the jacks was placed on top of the girder of up to 60 kips per linear foot. The reaction structure consisted of six W12 × 65 steel columns fastened to the Newmark Laboratory strong floor at regular 9-foot intervals along the length of each side of the test specimen. The overall height of the columns was 15 feet 4 inches. Six pairs of W18 × 119 steel sections were used as transverse beams to span across the test specimen between each pair of columns. A W27 × 146 section 50 feet long served as a longitudinal reaction beam that resisted the loading from the individual hydraulic jacks. To avoid possible cracking of the strong floor in the Newmark Laboratory due to the end reaction forces that could exceed 1 million pounds, abutments at either end of the test specimen were designed as simply supported beams that distributed the loading directly to the top of the web walls located under the top flange of the strong floor.

Each abutment was made from two W27 × 146 steel sections 14 feet long. The steel sections of the abutments were

Figure 48. Casting of top deck.

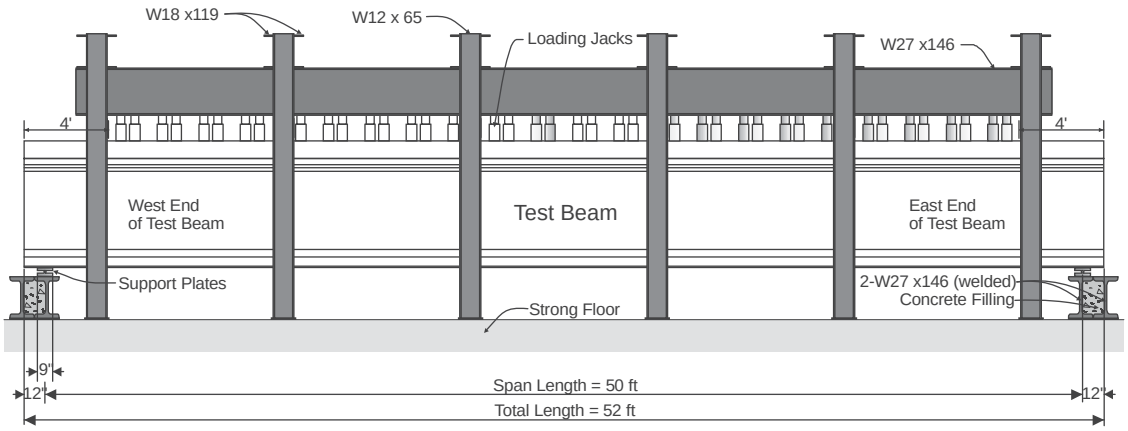

Figure 49. Front elevation view of reaction structure.

welded together at the flanges to make a box section. An additional 1-inch thick steel plate was added to the top and bottom flange in the middle portion of the section to increase the moment capacity near mid-span. The insides of the box sections were reinforced in flexure and shear and then filled with concrete to increase shear capacity and provide lateral and torsional rigidity. The abutments were designed to support a 1,500-kip load at mid-span that caused a 4,500 kip-ft bending moment. The transverse beams spanning between the columns across the test specimen were 9 feet long and designed as simply supported to resist 550 kips of load and a 1,200 kip-ft bending moment at mid-span.

A combination of twenty-two 100-ton, single-acting hydraulic jacks and twenty-two 60-ton, double-acting hydraulic jacks were used for imposing the uniformly distributed load, as shown in Figure 51. A linear variable displacement transducer (LVDT) was attached to the centermost double-acting jack to measure the extension of its piston. During the test, a servo controller was used to regulate the pressures that controlled the movement of this center point jack as measured by the LVDT. Through a series of 12 manifolds, the same high and low pressures that were used to control the force in the centermost double-acting jack were then distributed to all double-acting jacks. The actions of the single-acting jacks were controlled by a single pressure value that was regulated by hand so as to keep the force in those jacks close to a selected fixed proportion of the total load. With this system, a center point displacement controlled test was conducted in which a uniformly distributed load was achieved by having each pair of alternating single- and double-acting jacks apply the same force.

The average jack spacing was one jack per foot, with 22 jacks on each side of mid-span. For the majority of the tests, this meant that a uniformly distributed load was applied over the central 44 feet of the length of the girder. For a

Figure 50. Test set-up.

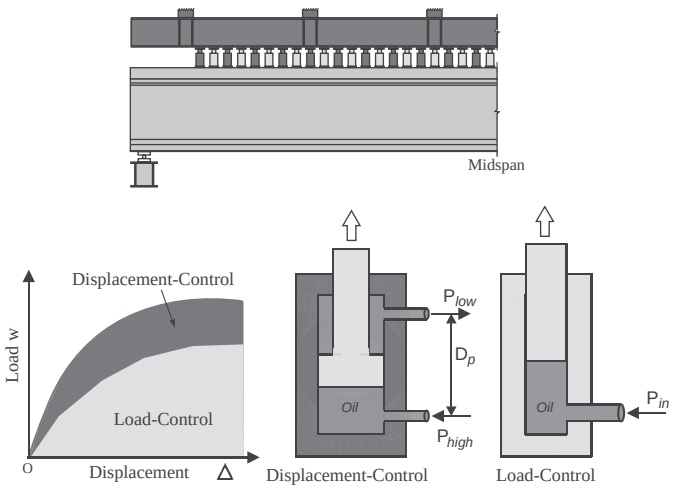

Figure 51. Load control system.

variety of different reasons, ranging from concern over the effectiveness of the repair to the first failed region of the girder, to concern over the possibility of a flexural failure, the pattern of loading was modified on a several occasions. Figure 52 summarizes the actual patterns of distributed loading used for each girder.

2.3.5 Instrumentation

Traditional and advanced measurement systems were used to gather detailed data on the displacement, straining, and cracking of the test girders. This data was subsequently used to assess the overall stiffness of the test girders, the contribution of the stirrups to shear resistance, and the behavior of the complicated end regions of the test girders. The types of measurement systems used during the experiments and the location of these measurements are now described.

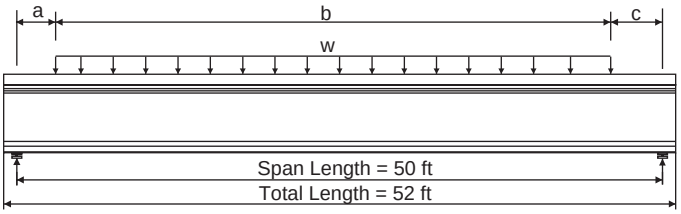

Specimen	Loading Pattern			Load
	a (ft)	b (ft)	c (ft)	w (kips/ft)
G1E	3.0	44.0	3.0	26.03
G1W	3.0	44.0	3.0	30.09
G2E	3.0	44.0	3.0	33.79
G2W	3.0	44.0	3.0	38.74
G3E	3.0	44.0	3.0	35.68
G3W	3.0	44.0	3.0	38.82
G4E	3.0	44.0	3.0	42.74
G4W	3.0	44.0	3.0	42.74
G5E	3.0	44.0	3.0	23.70
G5W	3.0	44.0	3.0	19.90
G6E	15.0	32.0	3.0	38.32
G6W	3.0	44.0	3.0	27.85
G7E	3.0	44.0	3.0	33.47
G7W	11.0	28.0	11.0	44.76
G8E	13.0	28.0	9.0	43.73
G8W	3.0	34.0	13.0	32.70
G9E	3.0	44.0	3.0	32.80
G9W	3.0 4.0	26.0 10.0	21.0 36.0	37.19 22.32
G10E	3.0	44.0	3.0	33.93
G10W	3.0	43.0	4.0	42.85

Figure 52. Typical loading pattern.

Linear Variable Displacement Transducer (LVDT) Measurements

Vertical deflections were measured using LVDTs at five locations, including mid-span, quarter points, and immediately inside of the face of the supports. These locations are labeled as V1 through V5 in Figure 53. Longitudinal deformations of the top flange and bottom flange at mid-span, and of the bottom bulb at both ends of girder, were measured. Those locations are shown as H1 through H4 in Figure 53. These measurements were taken to calculate the curvature at mid-span, the development of flexural cracking, and the loss in prestressing or the development of cracking at member ends. Web-shear strains were measured at multiple locations using displacement transducers, as also shown in Figure 53. In most cases, three LVDTs (ED1, 2, 3 or WD1, 2, 3) were located at 3 feet from the support, and another three LVDTs (ED4, 5, 6 or WD4, 5, 6) were located at 6 feet from the support. Initial shear cracking was expected at approximately 3 feet from the support, and the critical section for shear design was about 6 feet from the support. Finally, LVDTs were mounted on end strands to monitor the slip between individual strands and the end of the test girder. See S1 and S2 in Figure 53.

Strain Gages on Reinforcement

Electrical resistance strain gages were used to measure strains in the shear reinforcement, in the end bursting reinforcement, and in the reinforcement of the bottom bulb confinement cages and a few selected prestressing strands. Because the test beams were designed so that they were as likely to fail in shear in regions of low shear and high moment as they were to fail in regions of high shear and low moment, a large number of stirrups were gauged over the entire length of the girder. In each girder, four strain gages were placed on each of 16 to 20 stirrups. The density of this grid of gages was selected deliberately so that a reasonably accurate measurement was made of the contribution of the shear reinforcement to the shear capacity over the entire length of the member. Strain gages were also placed on the bursting reinforcement located at the ends of the girders to assess the demands placed on this special purpose reinforcement. The locations of the strain gages on the vertical transverse reinforcement for each girder are given in Figure 54.

Strain gages were also placed on deformed bar longitudinal reinforcement that was used at the end of the members to satisfy

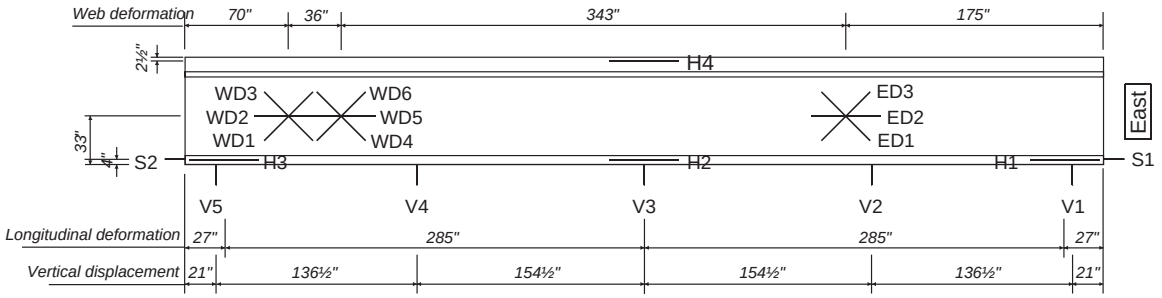

(a) Girder 1

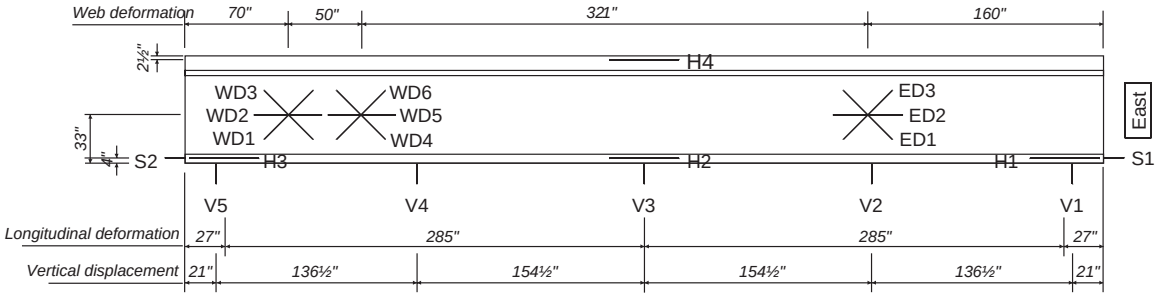

(b) Girder 2

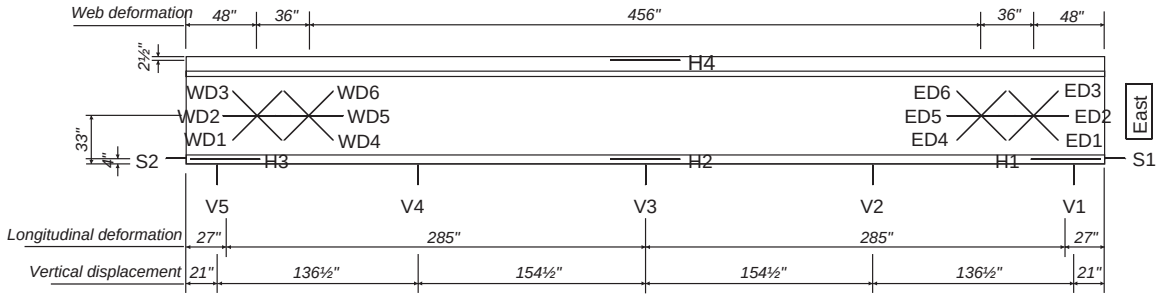

(c) Girder 3, Girder 4, Girder 5, and Girder 6, Girder 9 and Girder 10

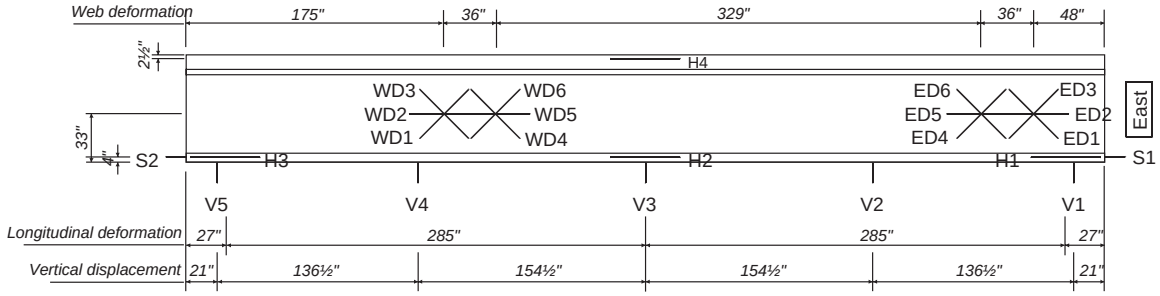

(d) Girder 7

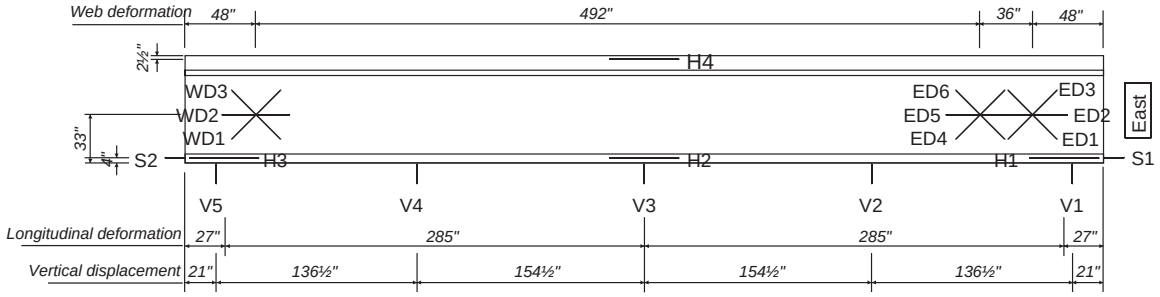

(e) Girder 8

Figure 53. Displacement transducers (LVDTs).

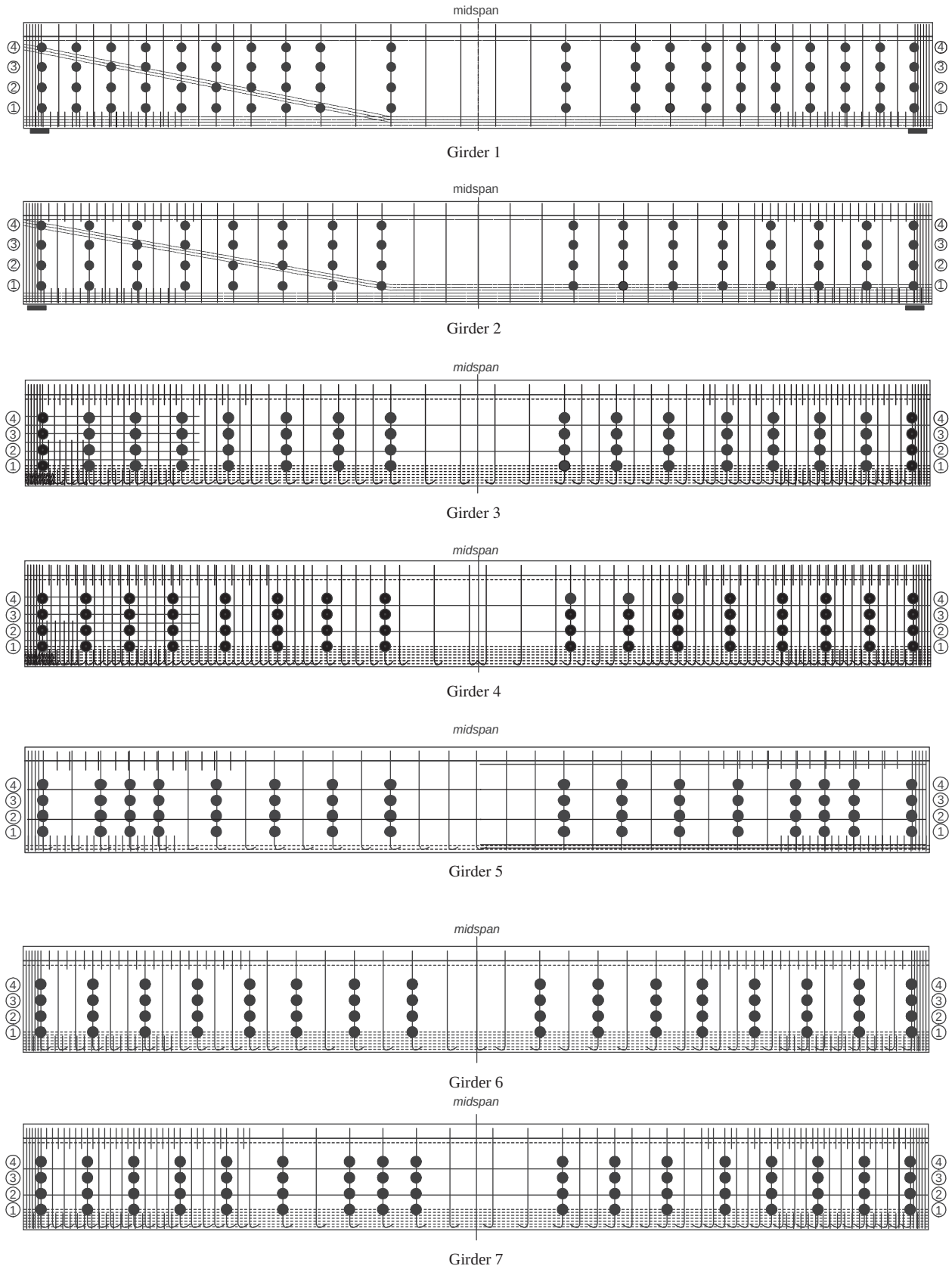

Figure 54. Stirrup strain gages.

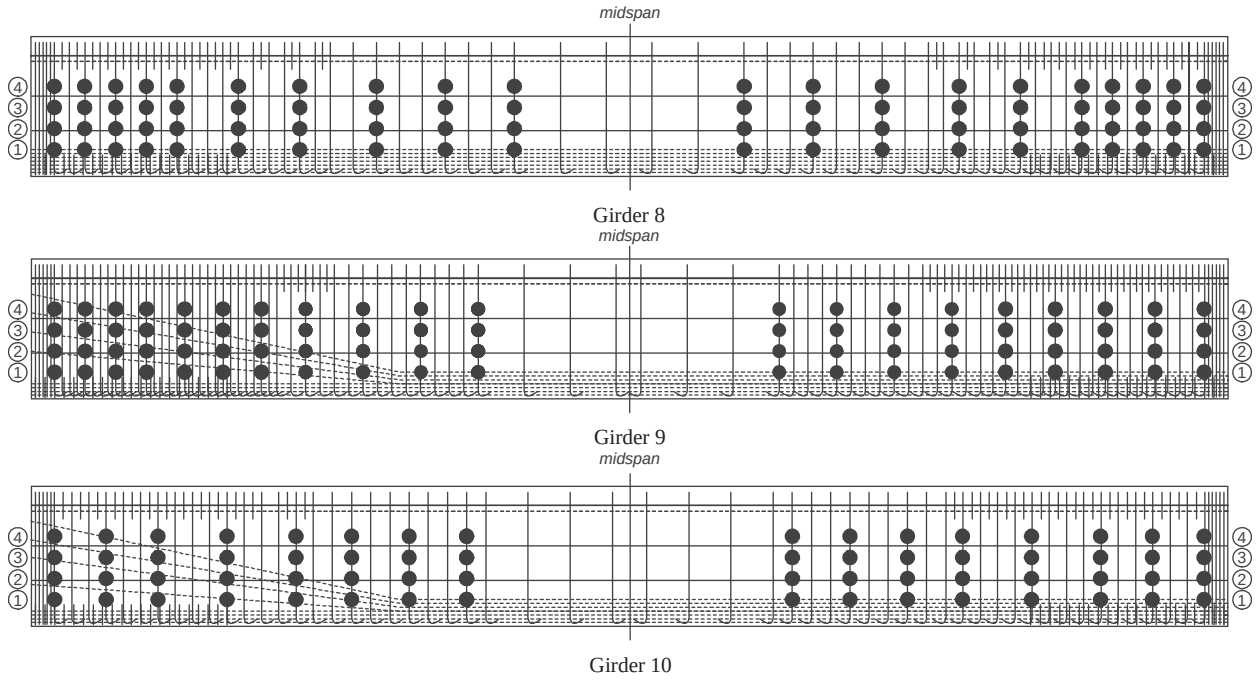

Figure 54. (Continued).

the longitudinal reinforcement capacity requirements of the LRFD specifications. Four strain gages were used at the east ends of Girders 1 and 2, in which four No. 8 deformed bars were required. Six strain gages were used at the west end of Girders 3 and 4, while four strain gages were used on the deformed bar longitudinal reinforcement used in Girder 5. The locations for all longitudinal gages are provided in the appendices.

Confinement reinforcement was used, as required by the LRFD specifications, around the prestressing steel in the bottom flange for 100 inches from the end of each girder. The locations of the strain gages on the confinement reinforcement are shown in Figure 55. Four strain gages (Gages 1 through 4) were attached to longitudinal bars, and six strain gages (Gages 5 through 10) were placed on transverse bars. The change in strain in the longitudinal reinforcement was used to assess the loss in prestressing force due to the demands of shear and flexure, while the strain in the transverse reinforcement was used to evaluate the magnitude of the confinement pressure on the prestressing strands.

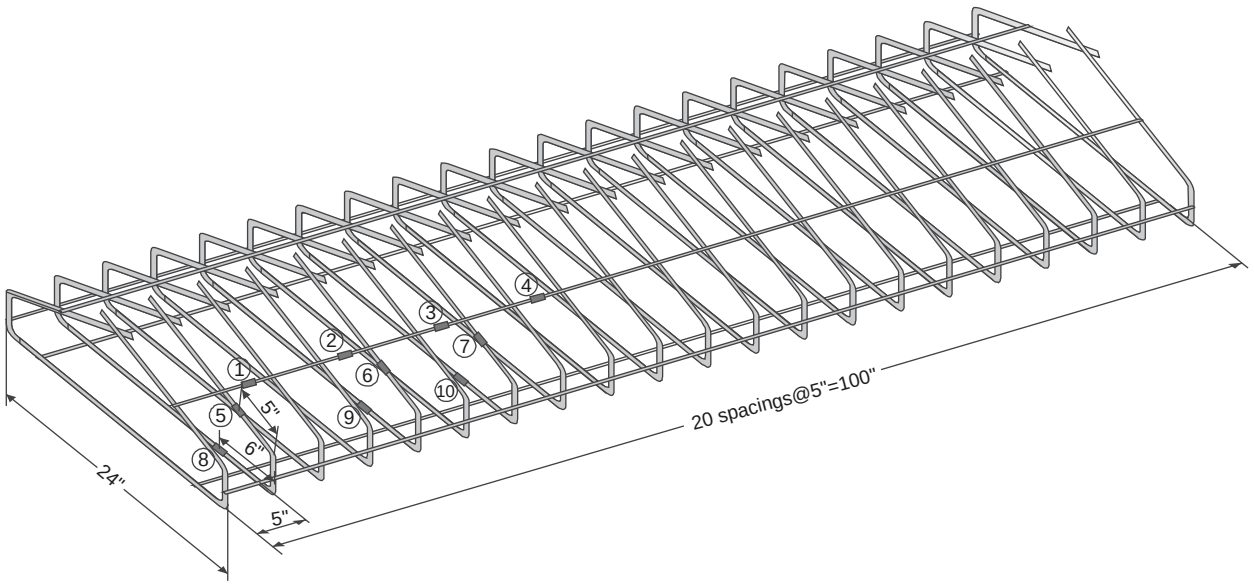

Figure 55. Strain gages on confinement reinforcement.

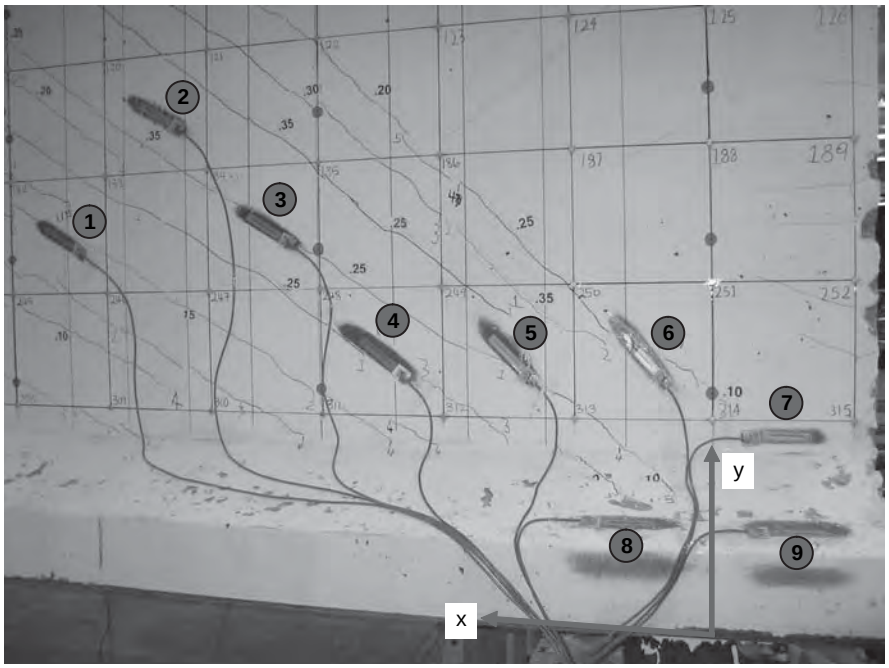

Figure 56. Concrete surface strain gages.

Strain Gages on Concrete

Beginning with Girder 5, 2-inch long concrete surface strain gages were used on the ends of the girders to measure the diagonal compressive strain in the web and the loss in precompression strain in the bottom bulb. The number of gages used on Girders 5 to 10 ranged from 22 to 58. Figure 56 shows the location of the strain gages used on the ends of Girder 4. The locations of the concrete strain gages for each girder are presented in the appendices. The strain gage locations were selected based on the crack patterns of previously tested girders. However, because crack patterns were not exactly the same from girder to girder, it was occasionally necessary to attach additional strain gages in better positions relative to the shear cracking when crack patterns were determined. It should be noted that the concrete strains obtained from these gages did not include initial strains due to prestressing.

Whittemore Gage Readings

A portable displacement measurement system known as a Whittemore gage was used to measure changes in deformation along the length of the bottom bulb. See Figure 57.

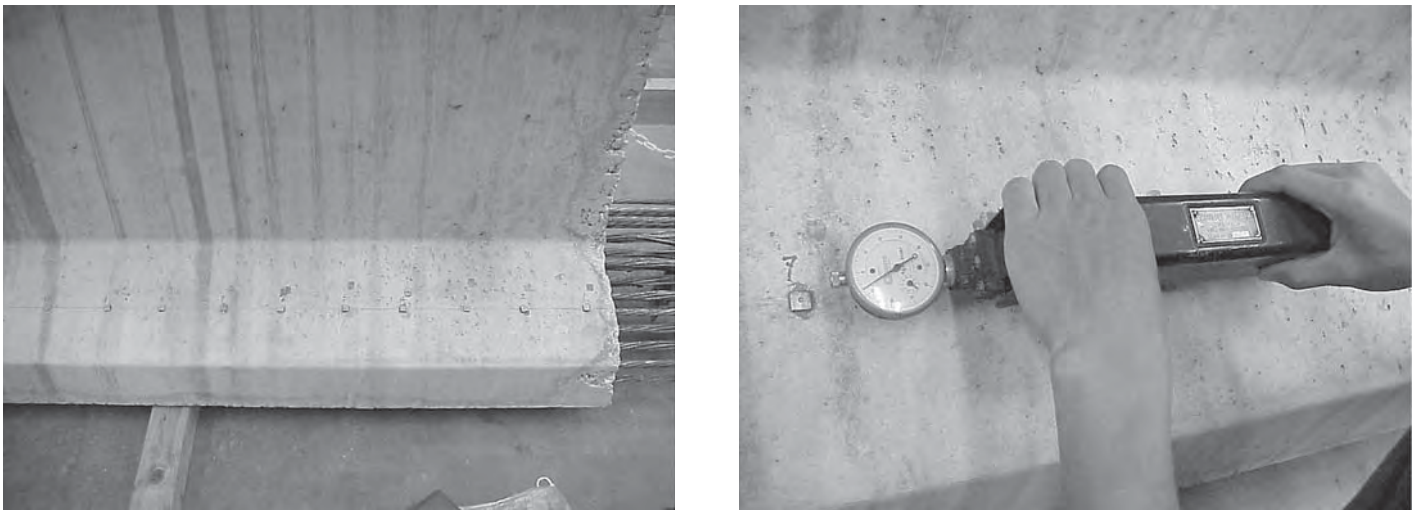

(a) Whittemore gage targets

(b) Whittemore gage reading

Figure 57. Whittemore gage and transfer length measurements.

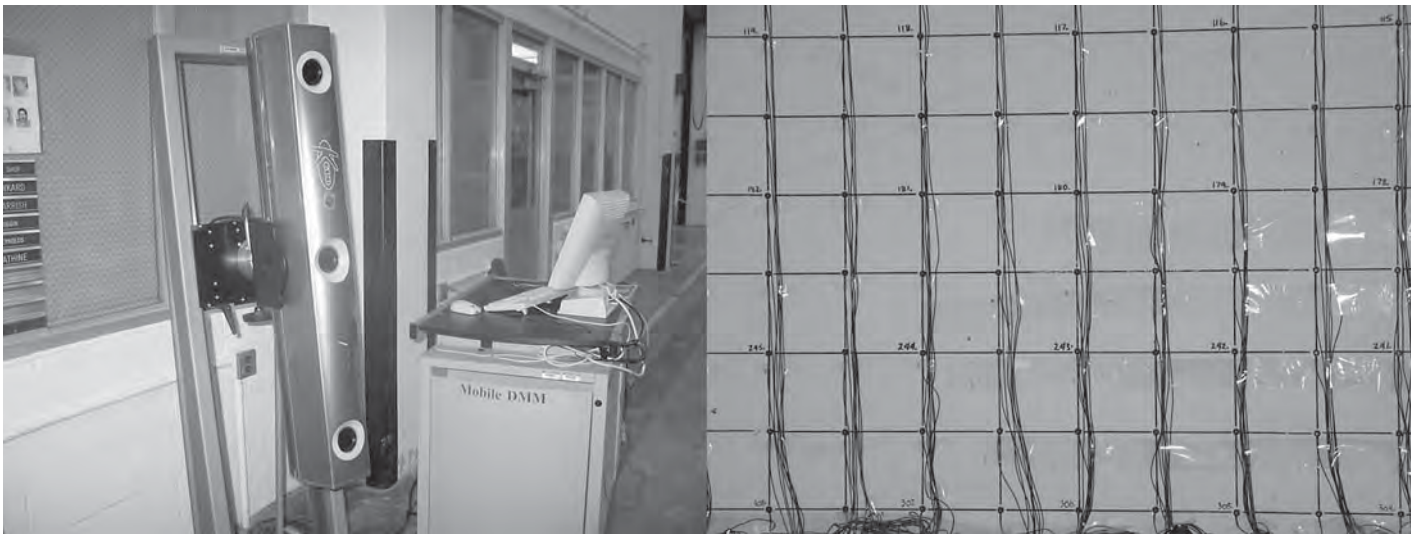

(a) Krypton camera (b) Krypton LED markers

Figure 58. Krypton K-600 Dynamic Measurement Machine.

Displacement measurements over 10-inch gage lengths were determined using targets glued to the girder at 5-inch centers along the bottom bulb at both ends and in the middle of the girder. These targets were attached after the forms were removed and before strands were detensioned. Measurements were taken before strand release, after strand release, at periodic intervals, and before testing to assess transfer length, prestressing loss, and the distribution of strains prior to testing.

Krypton's RODYM and K-600 Dynamic Measurement Machine

The Krypton Dynamic Measurement Machine is able to measure the position of up to 256 small (8-gram and 5/16-inch diameter) light emitting diode (LED) markers in three-dimensional space to an accuracy of ±0.0008 inch (±0.02 millimeter) at a sampling rate of up to 3,000 individual readings per second. The Krypton system consists of a portable housing containing three 2,048-CCD (charge-coupled device) line-element cameras. The camera system has an effective measurement volume of 600 cubic feet. Figure 58 shows a grid of LED targets on the surface of the test beam and the K-600 camera system. The data acquisition system reports the time-stamped position of each marker in three-dimensional space to a resolution of 0.00004 inch (0.001 millimeter). Measurements were made using the Krypton system to assess the directions of principal straining in the members, the contributions of shear reinforcement, the magnitude of the diagonal compressive straining in the web, and the overall distribution of straining and deformations in the complex end regions of the girders.

Zurich Gage Measurement System

The Zurich gage measurement system is analogous to an electronic Whittemore or Demac gage. As illustrated in Figures 59 and 60, the Zurich gage system consists of an LVDT rigidly clamped to, and within, an aluminum channel. The LVDT plunger is attached to a linear bearing. There are two measurement legs that terminate with tapered ends into which a spherical ball is mounted. One leg extends from the aluminum channel and the other leg extends from the linear bearing. The distance between these legs when the linear bearing is at mid-stroke is 10 inches, and the LVDT has a range of ±0.5 inch. There is a second Zurich gage measurement device in which the legs are spaced at $14.14(10\sqrt{2})$ inches when the linear bearing is at mid-stroke. These two devices were used to measure the horizontal, vertical, and diagonal distances between targets on a 10-inch grid over the surface of the web of the test girder at selected load stages. See Figure 61. Because the resolution of this system was not sufficient to measure small strains and because it took about

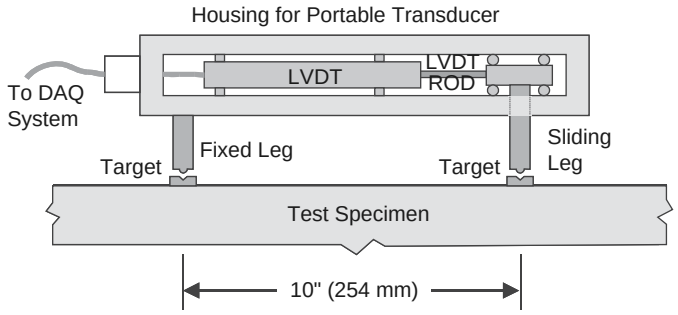

DAQ = data acquisition system.

Figure 59. Components of a Zurich gage.

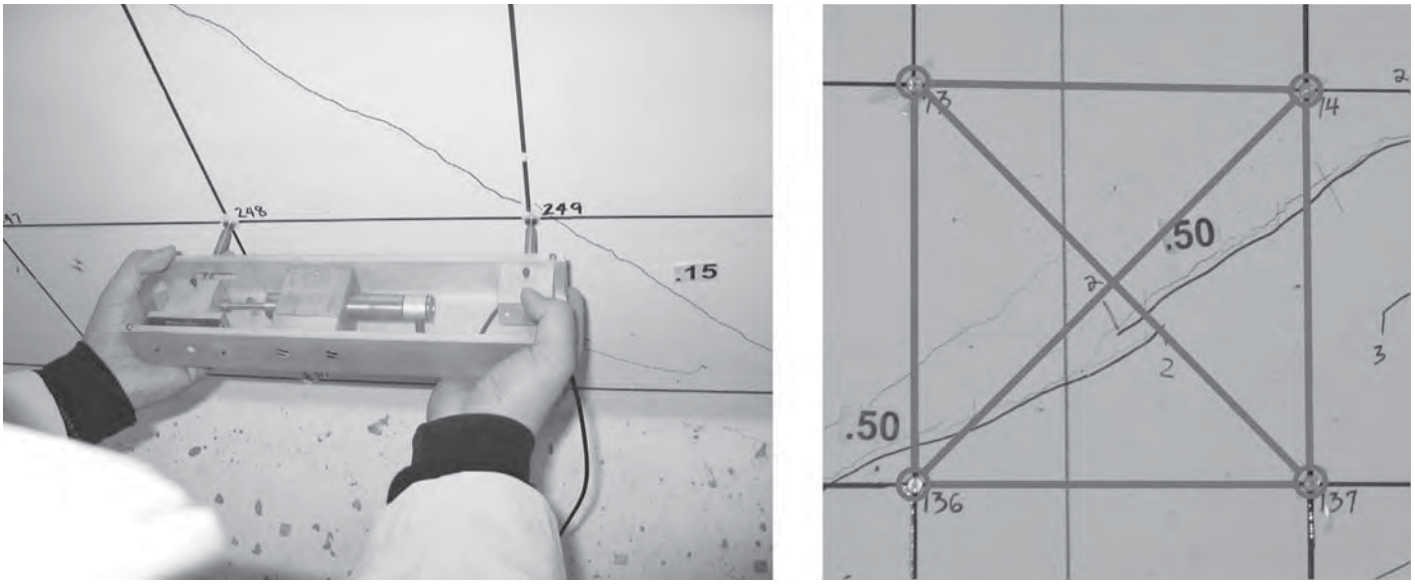

Figure 60. Zurich gage measurements.

90 minutes for a full set of readings, at some load stages only a partial set of readings was taken.

2.3.6 Test Procedure

A combination of twenty-two 100-ton, single-acting hydraulic jacks and twenty-two 60-ton, double-acting hydraulic jacks were used for imposing the uniformly distributed load. Using the laboratory's 3,000-psi pump, the twenty-two 100-ton jacks could exert a total loading of 1,320 kips, which corresponded to a shear stress of 1,884 psi at the inside face of the support. Using the same pump, the twenty-two 60-ton jacks could be used to exert a total loading of 792 kips, which corresponded to a shear stress of 1,130 psi. In combination, a total shear stress of 3,014 psi could be applied to the girder at the inside face of the support. This corresponds to a maximum load of 48 kips per foot over the 44-foot length of the distributed loading.

After the girder was positioned underneath the reaction frame and the deck was cast, a series of loading plates were placed on top of the girder. The hydraulic jacks were lowered into position, and a 60-ton load cell was placed between the piston of each jack and the steel reaction beam. Next, the girder was painted using a whitewash, and a 10-inch square grid was drawn on the web. The instrumentation was then attached, including concrete surface strain gages, LVDTs,

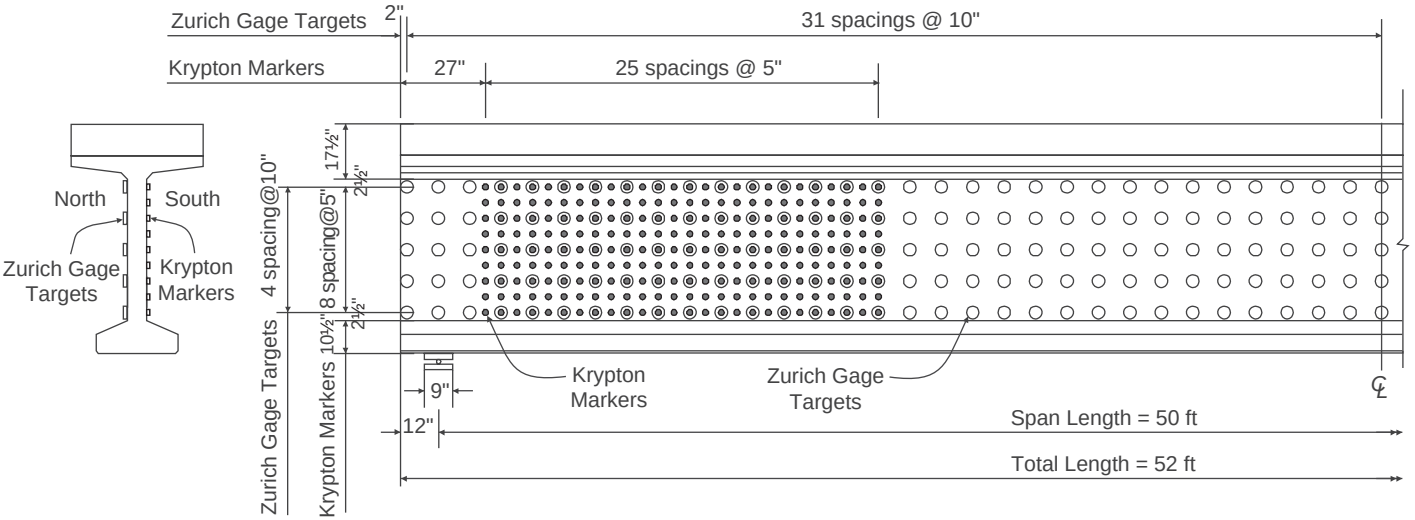

Figure 61. Location of LED markers and Zurich gage targets.

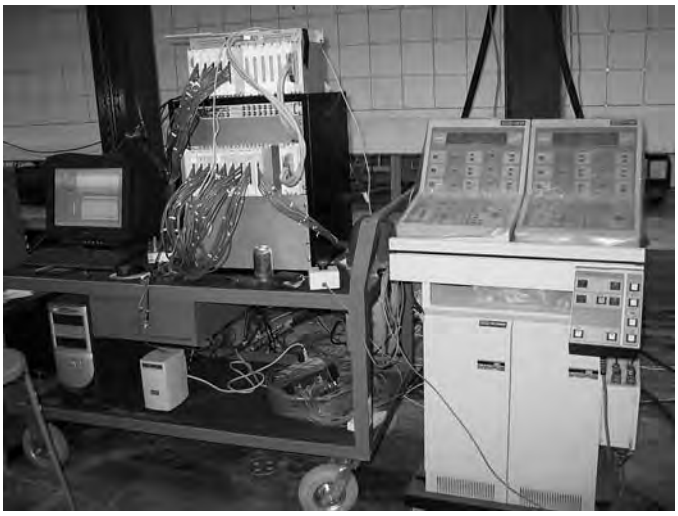

Figure 62. Data acquisition system.

Krypton's LED markers, and Zurich gage targets. All instrumentation devices and strain gage wires were then connected to the signal conditioning equipment.

Four different data acquisition systems were used in the experiments. One National Instruments (NI) signal conditioning and data acquisition system was used to record the data from the strain gages on the reinforcement, the data from the LVDTs, and the data from the load cells. With that system, a complete set of readings was taken every second during testing. A second NI system was used to record the concrete surface strain gage measurements in which readings were taken as quickly as 100 times per second as failure approached. A third NI system was used to record the Zurich gage readings. One of these three NI data acquisition systems and a load controller is shown in Figure 62. The Krypton camera measurements were recorded by dedicated software and data acquisition programs.

A pretest was completed 1 or 2 days ahead of the actual loading to check for hydraulic leaks in the loading system. This check was critical because the system had more than 200 points where leakage was possible. Prior to the first day of testing, all initial measurement readings were zeroed, and shunt-calibrations were performed on the strain gages. In addition, two full sets of Zurich readings were taken, with each involving the taking and recording of 1,058 individual readings. This activity required a three-person crew, with one person at the data acquisition computer and each of the other two holding one of the two Zurich gages (10 and 14.14 inches). All three people were connected on wireless headsets.

On the day of testing, the loading was increased until first the diagonal cracking, "load stage 1," occurred. At that point, the displacement at mid-span was held constant, cracks were marked, and a complete set of measurements was taken. Subsequent "load stages" were taken at points of significant additional cracking, when local damage was observed, or after there had been a significant increase in applied load or deformation. During each of these load stages, Zurich gage readings were taken, cracks were marked, crack widths were measured, and pictures were taken. After one end of the girder failed, the loading was removed. The failed regions were then repaired by removing all loose concrete from the failed region, adding reinforcement on either side of the web, casting a 10- to 15-foot long repair on either side of the web using self-compacting concrete, and then vertically posttensioning this region of the girder using posttensioning bars placed 2 feet apart on centers. See Figure 63. After the girder was repaired, it could be reloaded until failure occurred at the other end.

(a) Failed end region before repair

(b) Failed end region after repair

Figure 63. Repair of failed end region.

2.3.7 Data Processing and Reduction

After testing on an individual girder was completed, the data was postprocessed and reduced using a combination of commercial and locally written tools.

The volume of test data was very large. Over 300 MB of numerical data and 700 MB of pictures and video were acquired for each girder. The multiplicity of measurement sources increased the difficulty of data reduction, synchronization, and review. To better understand the test data, an integral visualization system named GrdVis was developed that enabled the results from multiple data sources to be displayed simultaneously and provided a convenient and complete environment for data analysis. Figure 64 shows a screen shot of the user interface. GrdVis has three windows: a visualization window, a data window, and an output window. The visualization window displays the structural elements and instrumentation, the data window displays data curves, and the output window shows numerical results. GrdVis also provides many operations for exploring, manipulating, and analyzing the mixed data.

Data collected from the Krypton system was reported as three-dimensional position data versus time for each LED target placed on the specimen. This information was also very dense, with files consisting up to 298 columns of data with more than 40,000 rows. A program called DIAdem, developed by NI, was used to extract useful information from the raw Krypton displacement data. Scripts were created in DIAdem to calculate the strain between targets and to present various strain distributions along the length or height of the girder. These strain distributions were then imported into the GrdVis software.

In this data processing and reduction, it was necessary to synchronize the time of acquisition of the data from the multiple measurement sources as well as develop a protocol for what assumptions to employ in merging together data from multiple days of testing. The latter issue was important because there was likely some shift in the strains and deformations of the girder from the time that failure occurred at one end of the girder to after the repair was completed and the girder was reloaded. The procedure used in data merging is described below.

The first step of data merging was to establish a point of zero deformation and strain at the start of a test. When a test spanned over multiple days, values were checked and adjusted as necessary so that the original values from the start of testing were

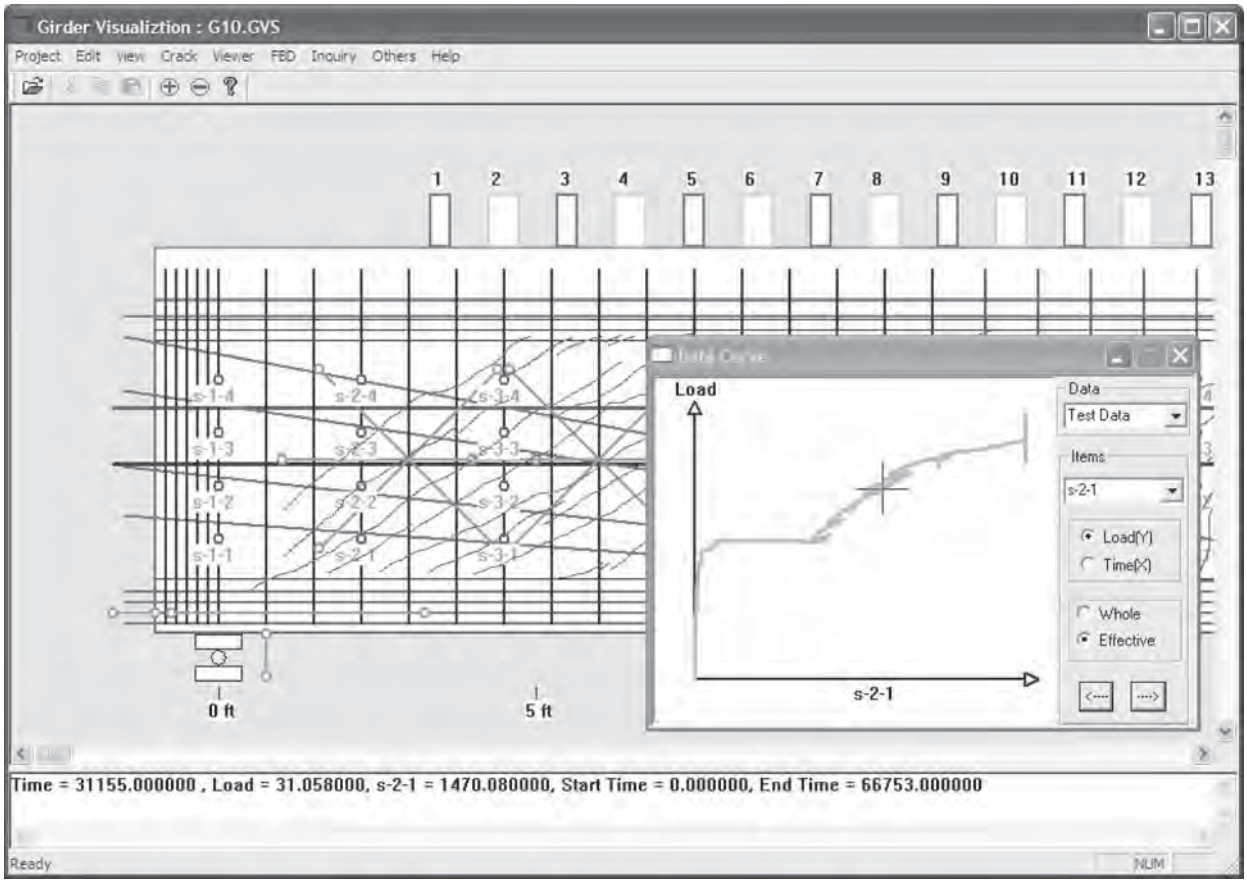

Figure 64. Girder visualization program.

used. After data merging, a data cleaning operation was applied to improve the quality of data, such as detecting and removing errors and inconsistencies. Data reduction was the last step, in which the number of data points in the array was reduced to around 2,000 per channel. This number was sufficient to produce an accurate and detailed envelope (unloading and reloading parts removed) for each instrument reading. A semi-automatic approach was taken to ensure that the reduced data sufficiently captured all relevant aspects of girder behavior.

The procedures employed above are considered to provide the best possible documentation of the response of the test girders.

2.3.8 Shear Friction Experiments

As discussed in Chapter 1, one of the primary motivations for this project was a concern that the smooth cracks that occur in HSC could lead to a breakdown in the aggregate interlock, or interface shear transfer mechanism, and subsequently lower shear strengths. This was considered to be of particular concern for shear design provisions derived from the MCFT, because that procedure assumes that interface shear transfer is the primary source of the concrete contribution to shear resistance. While the large-scale girder tests provided an overall evaluation of the performance of the LRFD specifications, it was also considered useful to directly evaluate the interface shear transfer mechanisms for the materials and reinforcement arrangements used in the experimental testing program. Figure 65 illustrates the idealized segment of the girder for which the interface shear friction resistance was evaluated and the reinforcement details for a typical test specimen used to represent that segment. The complete interface shear transfer testing program and results are presented in Section 2.9.

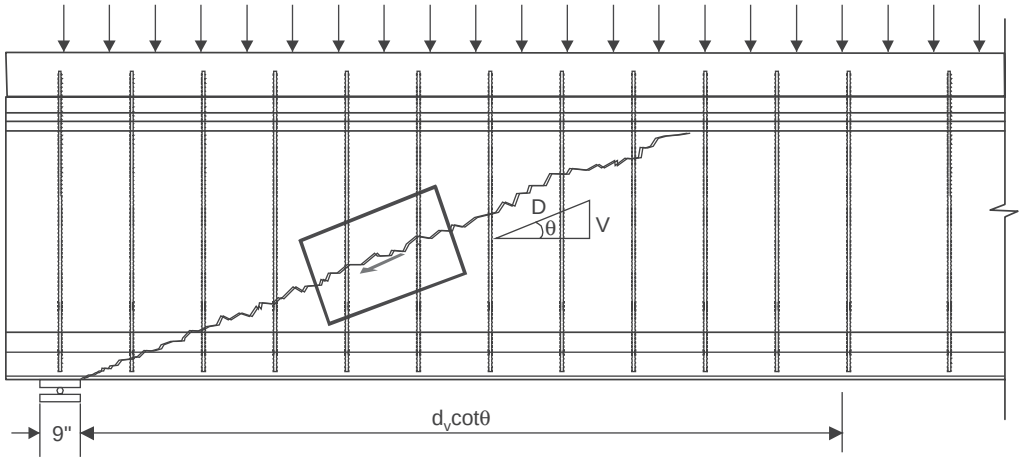

(a) Segment of web idealized in shear friction experiments

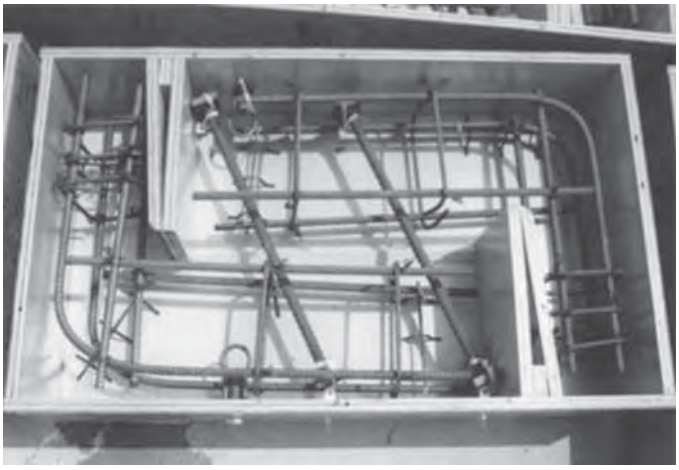

(b) Reinforcement in a shear friction experiment

Figure 65. Shear friction test.

2.4 Measured and Code-Calculated Strengths Plus Modes of Failure

Section 2.4.1 presents the measured capacities of the test girders and compares these capacities with the shear capacities calculated using the LRFD Sectional Design Model. From this comparison, observations are drawn about the extension of these provisions to high-strength structural concrete. Section 2.4.2 compares the measured capacities with those calculated by other codes of practice, including the AASHTO Standard Specifications, the new provisions in the Canadian Standards Association, and the proposed LRFD Simplified Design Provisions that were developed in NCHRP Project 12-61 and that are described in *NCHRP Report 549*. Section 2.4.3 examines the impact of using the staggered shear design methods on the safety of the Sectional Design Model. Section 2.4.4 discusses the modes of failure and conditions at the point of failure for the test girders and examines the significance of these observations for use of the Sectional Design Model. Finally, Section 2.4.5 presents the overall load-deformation response of the test girders.

2.4.1 Measured Strengths and Comparisons with LRFD Sectional Design Model

As discussed in Section 2.3, the objective of the test series was to evaluate the shear performance of girders made with concrete design strengths ranging from 10 ksi to 18 ksi, designed for different shear stress levels (from a minimum shear stress to a shear stress greater than or equal to $0.25f'_c$) and with different end reinforcement conditions (straight strands, draped strands, bonded and debonded strands, and different amounts of deformed bar reinforcement). The objective was to test girders that would demonstrate a range of different types of behavior and failure mechanisms, including yielding of the shear reinforcement, local diagonal crushing, distributed diagonal crushing, shear slip at interfaces, and strand slip. Section 2.3.1, Table 3, and Figure 40 present the shear design procedures and reinforcement used in each of the 10 girders. The following list provides a brief summary of some of the key characteristics and objectives of each test. The abbreviations used in this description are as follows: S = straight strands; Dr = some draped strands; B = bonded strands; Db = some debonded strands; and E = Enhanced end region reinforcement consisting of distributed vertical and horizontal reinforcement.

- Girder 1: f'_c = 12.1 ksi; v_u =1.21 ksi = $0.10f'_c$; east (S,B); west (Dr,B); examine behavior of HSC girder designed for moderately high shear stresses and having draped strands.
- Girder 2: f'_c = 12.6 ksi; v_u = 1.89 ksi = $0.15f'_c$; east (S,B); west (Dr,B); examine behavior of HSC girder designed for high shear stresses and having draped strands.
- Girder 3: f'_c = 15.9 ksi; v_u = 1.59 ksi = $0.10f'_c$; east (S); west (S,E); examine behavior of very high-strength concrete girder designed for moderately high shear stresses and having added distributed reinforcement and improved strand anchorage in end regions.
- Girder 4: f'_c = 16.3 ksi; v_u = 2.45 ksi = $0.15f'_c$; east (S); west (S,E); examine behavior of very high-strength concrete girder designed for high shear stresses and using distributed reinforcement and improved strand anchorage in end regions.
- Girder 5: f'_c = 17.8 ksi; v_u = 0.89 ksi = $0.05f'_c$; east (S); west (S); examine behavior of very high-strength concrete girder, with minimum shear reinforcement throughout its length, with welded wire reinforcement used on the east half and regular deformed bars used in the west half of the girder.
- Girder 6: f'_c = 12.7 ksi; v_u = 1.65 ksi = $0.13f'_c$; east (S); west (S,Db); examine behavior of girder with a large number of debonded strands.
- Girder 7: f'_c = 12.5 ksi; v_u = 1.63 ksi = $0.13f'_c$; east (S); west (S); at east end examine behavior of a girder with shear reinforcement the same as for Girder 3E, providing for duplicate test; and at west end examine behavior of a transition region by underdesigning this region for shear in comparison with the shear design for rest of girder.
- Girder 8: f'_c = 13.3 ksi; v_u = 1.60 ksi = $0.12f'_c$; east (S); west (S); at east end examine behavior of girder with externally strengthened end region that forces failure in beam region away from support; and at west end examine behavior when interface shear transfer is minimal as a result of inserting two aluminum plates in the web to form a slip plane.
- Girder 9: f'_c = 9.6 ksi; v_u = 2.40 ksi = $0.25f'_c$; east (S); west (Dr); east end examine behavior of girder designed for close to maximum permissible shear design stress of $0.25f'_c$; west end examine behavior of girder heavily overdesigned for shear with eight draped strands uniformly distributed over height of the web at member end.
- Girder 10: f'_c = 10.6 ksi; v_u = 1.70 ksi = $0.16f'_c$; east (S); west (Dr); east end examine behavior of girder with eight strands debonded; west end examine behavior of girder with eight draped strands distributed over the height of the web at the member end.

The calculated strength of the test girders by the LRFD Sectional Design Model is presented in Table 7. No limit on the compressive strength of the concrete was used in calculating nominal capacities. In making these calculations, measured material properties and prestressing losses were used. Column 3 lists the distance, x, from the center of the support to the critical design section for shear in the first design region ($d_v \cot\theta$). Column 4 lists the shear design

Table 7. Measured and calculated shear strength for LRFD procedure.

Girder End	w_n (kips/ft)	x (ft)	v/f'_c	d_v (in)	ε_x ($\times 10^{-3}$)	β	θ	f_{yv} (kips)	A_v/s (in)	V_c (kips)	V_s (kips)	V_p (kips)	V_n (kips)	Test / LRFD	Test / LRFD
G1E	24.47	6.36	0.102	61.7	-0.046	2.98	23.2	70.0	0.40/12	121.0	335.2	0	456.2	1.06	1.06
G1W	24.70	5.94	0.096	62.0	0.005	2.91	24.9	70.0	0.40/12	118.9	311.5	40.5	470.9	1.22	1.22
G2E	35.08	5.68	0.148	60.6	0.000	2.67	25.5	79.3	0.62/11	109.0	568.8	0	677.8	0.96	0.96
G2W	33.56	5.25	0.135	61.7	0.067	2.56	27.8	79.3	0.62/11	106.3	523.0	33.6	662.9	1.15	1.15
G3E	31.98	6.16	0.104	60.9	0.043	2.87	23.7	67.8	0.40/8	132.1	470.3	0	602.4	1.12	1.12
G3W	31.98	6.16	0.104	60.9	0.043	2.87	23.7	67.8	0.40/8	132.1	470.3	0	602.4	1.21	1.21
G4E	43.43	5.05	0.146	60.9	0.018	2.53	28.5	64.6	0.62/6	118.0	748.4	0	866.5	0.98#	0.98#
G4W	43.43	5.05	0.146	60.9	0.018	2.53	28.5	64.6	0.62/6	118.0	748.4	0	866.5	0.98#	0.98#
G5E	19.31	6.94	0.052	63.0	-0.003	3.75	21.8	92.2	0.22/20	189.0	159.7	0	348.7	1.23	1.23
G5W	17.80	6.94	0.048	63.0	-0.019	3.75	21.8	76.5	0.22/20	189.0	132.5	0	321.5	1.12	1.12
G6E	34.88	6.16	0.125	60.9	-0.044	2.87	23.7	64.7	0.62/12	118.1	463.8	0	581.9	1.10	0.97**
G6W	27.67	5.64	0.113	61.3	0.126	2.74	25.9	64.7	0.62/12	113.5	422.2	0	535.7	1.01	0.99**
G7E	30.69	6.02	0.128	60.9	-0.075	2.78	24.2	69.2	0.40/8	113.5	468.9	0	582.4	1.09	1.05**
G7W	41.60	6.02	0.128	60.9	-0.096	2.78	24.2	69.2	0.40/8	113.5	468.9	0	582.4	1.08	1.04**
G8EB†	37.39	9.78	0.110	60.9	-0.006	2.87	23.7	69.2	0.40/8,12	120.9	415.2	0	536.1	1.17	1.16**
G8W	34.85	6.16	0.124	60.9	-0.050	2.87	23.7	69.2	0.40/8	120.9	480.0	0	600.9	0.94	0.93**
G9E	36.15	4.72	0.211	60.2	-0.004	2.34	30.0	65.4	0.62/6.5	82.7	650.4	0	733.1	0.91	0.91
G9W	40.97	4.13	0.250	58.0	0.499	1.70	32.8	65.4	0.62/4	58.0	912.9	40.4	876.6*	0.91#	0.91#
G10E	28.90	4.89	0.153	59.6	0.234	2.52	28.8	65.4	0.62/9	92.7	488.5	0	581.2	1.17	1.16**
G10W	31.89	5.02	0.160	58.3	-0.007	2.54	27.6	65.4	0.62/9	91.2	501.5	42.2	634.9	1.34	1.27**
													Average	1.11	1.09
													COV	0.10	0.10

† B = beam or Bernoulli region.

* Controlled by $V_n = 0.25 f'_c b_w d_v + V_p$.

\# No shear failure in this region; strength ratio not used in statistical calculations.

** Specified f'_c used when measured strength less than the specified f'_c.

stress ratio (v/f'_c) at section x. Column 5 lists the effective depth at the critical section (d_v). Column 6 lists the longitudinal strain at mid-depth (ε_x), as calculated using Equations 15 or 16. Columns 7 and 8 list the values of β and θ, respectively, as derived from Table 5.8.3.4.2-1 of the LRFD specifications. Columns 9 through 14 list the stirrup yield strength (f_{yv}), the shear reinforcement ratio (A_v/s), and the contributions to shear resistance of the concrete (V_c), the shear reinforcement (V_s), the prestressing (V_p), and the sum of those resistances which is the nominal shear resistance (V_n), respectively. In Column 2, the distributed loading (w_n) that would produce this V_n at the critical section is listed as the calculated LRFD shear capacity of the member. That capacity is expressed in terms of a uniformly distributed load. All girders except 7 and 8 have listed only one calculated capacity for failure of the east (E) end and only one for failure of the west (W) end. For the west end of Girder 7, the LRFD shear capacity is listed at the location $0.5d_v\cot\theta$ from the center of the support (G7W). For the east end of Girder 8, a 5-foot long diaphragm was cast against the very end of the member on both sides of the web and laterally posttensioned to the web in order to ensure a failure away from this region and in a part of the member where essentially flexural behavior only was expected. Therefore, the shear capacity is also listed for the location $0.5d_v\cot\theta$ from the inner face of the diaphragm (G8EB).

In the second-to-last column of Table 7, the ratio of the measured-to-calculated capacity for each girder is given. The mean of these ratios is 1.11 with a coefficient of variation of 0.10. It should be noted that the results from Girder 4 and 9W are not failure loads. Girder 4 failed in flexure at a load that was considered to be within 10 percent of the shear failure load, while Girder 9W was considered, from its behavior, to be within a few percentage points of its failure load. Justification for this conclusion is provided later. From a review of these strength ratios, and considering the range of experiments that were conducted in this study, the following observations can be made about the LRFD specifications:

- The LRFD Sectional Design Model provides relatively accurate estimates for the shear capacity of members cast with concrete strengths ranging from 10 ksi through 18 ksi, regardless of whether draped or debonded strands are used.
- A slight exception to the foregoing observation is that the LRFD specifications become slightly unconservative for members designed to resist shear stresses exceeding $v = 0.2f'_c$. This unconservatism is due to the funneling into the support of the diagonal compressive stresses above the support. That funneling leads to local diagonal crushing and very high shear stresses at the interface between the bottom bulb and the base of the web. Failure was observed to occur

in these situations before yielding occurred in a band of reinforcement that formed the critical shear plane. This local crushing effect in the web above a support is somewhat analogous to the web crippling effect that has long been a design consideration for the same location in steel beams.

- Design of the end regions of a beam—including consideration of the consequences of using draped strands, debonded strands, and added deformed bar longitudinal reinforcement—has a significant effect on the overall shear strength of girders. The use of draped strands, particularly strands that are draped over the depth of the web of the girder in its end region, can significantly improve the shear capacity of the end region.

The sensitivity of the strength ratios to the concrete cylinder compressive strength was evaluated by adding a final column, Column 16, to Table 7. Column 16 lists the calculated LRFD capacity when that capacity is evaluated using the specified compressive strength of the concrete for those girders where the measured concrete strength was less than that specified. As illustrated by a comparison of the last two columns, because V_c is typically much less than V_s for shear designs in accordance with the LRFD specifications, the strength ratios are only slightly affected. The overall mean of these new strength ratios is 1.09, with a coefficient of variation of 0.10. Thus, if the measured strength of the concrete would have always been at least equal to that specified, then the overall conclusions about the accuracy and safety of the shear design provisions of the LRFD specifications for HSC remain unaltered.

2.4.2 Evaluation of Other Shear Design Provisions

The measured strength of each test girder was also compared with its nominal capacity calculated using the AASHTO Standard Specifications, the computer program Response 2000 (*24*), the Canadian Standard Association A23.3-04 provisions, and the proposed simplified design provisions that were developed as part of NCHRP Project 12-61. The basis, and the governing shear equations, for each of these four procedures are briefly summarized below. The measured strengths and the strengths predicted by those four procedures, together with the LRFD predictions, are listed in Table 8.

AASHTO Standard Specifications

The AASHTO Standard Specifications method for calculating the shear strength of prestressed concrete members is essentially the same as the detailed method of ACI 318 (*26*). The components of resistance are from the contribution of the concrete, the shear reinforcement, and the vertical

Table 8. Measured and calculated shear strengths for differing evaluation methods.

Girder End	Test (kips/ft)	Calculated Load (kips/ft)					Test/Calculation Ratio				
		LRFD	STD	R2K	CSA	PROP	LRFD	STD	R2K	CSA	PROP
G1E	26.03	24.47	19.92	23.14	24.18	21.84	1.06	1.31	1.12	1.08	1.19
G1W	30.09	24.70	23.17	23.71	25.24	25.19	1.22	1.30	1.27	1.19	1.19
G2E	33.79	35.08	26.34	36.90	34.65	32.57	0.96	1.28	0.92	0.98	1.04
G2W	38.74	33.56	29.58	37.57	34.22	36.55	1.15	1.31	1.03	1.13	1.06
G3E	35.68	31.98	25.81	29.68	31.73	29.61	1.12	1.38	1.20	1.12	1.21
G3W	38.82	31.98	25.81	29.68	31.73	29.61	1.21	1.50	1.31	1.22	1.31
G4E[#]	42.74	43.43	33.41	43.28	44.07	45.81	0.98	1.28	0.99	0.97	0.93
G4W[#]	42.74	43.43	33.41	43.28	44.07	45.81	0.98	1.28	0.99	0.97	0.93
G5E	23.70	19.31	15.47	21.86	18.95	11.63	1.23	1.53	1.08	1.25	2.04
G5W	19.91	17.80	14.90	21.70	18.11	10.92	1.12	1.34	0.92	1.10	1.82
G6E	38.32	34.88	25.59	34.29	34.27	30.15	1.10	1.50	1.12	1.12	1.27
G6W	27.85	27.67	20.59	29.95	28.07	20.13	1.01	1.35	0.93	0.99	1.38
G7E	33.47	30.69	24.12	28.41	31.38	28.57	1.09	1.39	1.18	1.07	1.17
G7W	44.76	41.60	37.18	37.51	45.01	40.94	1.08	1.20	1.19	0.99	1.09
G8EB[†]	43.73	37.39	33.29	37.86	36.70	32.41	1.17	1.31	1.16	1.19	1.35
G8W	32.70	34.85	24.96	31.46	34.38	28.22	0.94	1.31	1.04	0.95	1.16
G9E	32.80	36.15	26.14	37.83	36.82	31.03	0.91	1.25	0.87	0.89	1.06
G9W[#]	37.19 (22.32)	40.97 (24.59)	27.19 (16.32)	48.14 (28.89)	39.94 (23.97)	31.53 (18.92)	0.91	1.37	0.77	0.93	1.18
G10E	33.93	28.90	24.59	31.56	28.15	29.79	1.17	1.38	1.08	1.21	1.14
G10W	42.85	31.89	27.73	34.85	33.27	34.41	1.34	1.55	1.23	1.29	1.25
						Average	1.11	1.36	1.10	1.10	1.28
						COV	0.10	0.07	0.12	0.10	0.21

No shear failure in this region; strength ratio not used in statistical calculations.
[†] B = beam or Bernoulli region.
STD = AASHTO Standard Specifications.
PROP = proposed provisions.

component of the prestressing force—V_c, V_s, and V_p, respectively. The V_c term is the lesser of the shear forces estimated to cause web-shear cracking (as calculated in Equation 19) and those estimated to cause flexure-shear cracking (as calculated in Equation 20).

$$V_{cw} = \left(3.5\sqrt{f'_c} + 0.3 f_{pc}\right) b_w d + V_p \quad \text{(in inches and psi)} \tag{19}$$

$$V_{ci} = 0.6\sqrt{f'_c}\, b_w d + V_d + \frac{V_i M_{cr}}{M_{\max}} \quad \text{(in inches and psi)} \tag{20}$$

The contribution of shear reinforcement to capacity, V_s, is calculated using the 45-degree truss analogy (as calculated in Equation 21), with a limitation of $V_s \le 8\sqrt{f'_c}\, b_w d$ (in inches and psi). In the calculated strengths for AASHTO Standard Specifications presented in Table 8, no limitation on V_s is imposed.

$$V_s = \frac{A_v f_y d}{s} \tag{21}$$

where:

$V_{ci} \ge 1.7\sqrt{f'_c}\, b_w d$ (in inches and psi) and
$d \ge 0.8h$;

d = distance from extreme compressive fiber to centroid of the prestressing force, or to centroid of negative moment reinforcement for precast girder bridges made continuous;

V_d = shear force at section due to unfactored dead load;

V_i = factored shear force at section due to externally applied loads occurring simultaneously with $M_{\max}$;

$M_{cr} = \frac{I}{y_t}(6\sqrt{f'_c} + f_{pe} - f_d)$ (in inches and psi): moment causing flexural cracking at section due to externally applied loads;

$M_{\max}$ = maximum factored moment at section due to externally applied loads; and

f_{pc} = compressive stress in concrete (after allowance for all prestress losses) at the centroid of the cross section resisting externally applied loads or at the junction of web and flange when the centroid lies within the flange. (In a composite member, f_{ps} is the resultant compressive stress at the centroid of the composite section, or at the junction of web and flange when the centroid lies within the flange, due to both prestress and moments resisted by the precast member acting alone.)

Computer Program Response 2000 (24)

The computer program Response 2000 (R2K) is a sectional design and analysis tool for predicting the response of a reinforced or prestressed concrete section to the actions of shear, moment, and axial load, including the effects of prestressing. The calculations assume that plane sections remain plane and use an equivalent dual-section analysis method in conjunction with the modified compression field theory for evaluating the distribution of shear stresses over the depth of a member. The program is as complete an implementation of the MCFT as is possible for a member in which a linear variation in longitudinal strains is assumed over the depth of a member. The program was used to predict the capacities for the girders at each of the critical sections identified in Table 7. The calculation required inputting into the R2K program the appropriate material properties, level of prestressing (including accounting for losses), and the moment-to-shear ratio at the critical shear section, and then solving for the complete shear versus shear strain response. In using this program, the ultimate strength of the stirrups was taken as the yield strength of the stirrups.

Canadian Standards Association (CSA A23.3-04) Design of Concrete Structures

The MCFT is the basis for the general shear provisions of the both the CSA and the LRFD specifications. In previous versions of the CSA code, values for β and θ were selected from tables, as is presently done in the LRFD Sectional Design Model. In order to simplify the CSA shear design procedure, equations were introduced for β and θ in the 2004 CSA specifications in which these parameters were made, for members with minimum or more shear reinforcement, a function of the longitudinal strain at mid-depth, ε_x, only. In addition, the equation for evaluating ε_x was simplified by taking θ equal to 30 degrees for evaluations of the demand of shear on the longitudinal reinforcement requirements. These simplifications eliminated the need for iteration in shear design. In this approach, the nominal strength is calculated by Equation 22 and the concrete contribution and transverse reinforcement contributions calculated by Equations 23 and 24, respectively.

$$V_n = V_c + V_s + \phi_p V_p \le 0.25 f'_c\, b_w d_v + \phi_p V_p \tag{22}$$

where:

ϕ_p = strength reduction factor for prestress and

$$V_c = \beta\sqrt{f'_c}\, b_w d_v \tag{23}$$

in inches and psi.

$$V_s = \frac{A_v f_y d_v (\cot\theta)}{s} \tag{24}$$

The values of β and θ are directly determined from the longitudinal strain, at mid-depth, as computed from Equations 25 or 26.

$$\varepsilon_x = \frac{M_f / d_v + 0.5N_f + V_f - \phi_p V_p - A_p f_{po}}{2\left(E_s A_s + E_p A_p\right)} \quad (25)$$

where:

M_f = ultimate moment = factored moment at the section,
N_f = factored axial force, and
V_f = factored shear force.

When ε_x is negative, it is either taken as zero or recalculated by changing he denominator of Equation 25 such that the equation becomes:

$$\varepsilon_x = \frac{M_f / d_v + 0.5N_f + V_f - \phi_p V_p - A_p f_{po}}{2\left(E_s A_s + E_p A_p + E_c A_{ct}\right)} \quad (26)$$

However, ε_x shall not be taken as less than 0.2×10^{-3}. For members having at least minimum transverse reinforcement, with the longitudinal strain, ε_x, computed from Equation 25 or 26, the angle of the diagonal compression field, θ, is calculated as:

$$\theta = 29 + 7{,}000\varepsilon_x \quad (27)$$

and the coefficient, β, is obtained from Equation 28.

$$\beta = \frac{4.8}{\left(1 + 1{,}500\varepsilon_x\right)} \quad (28)$$

NCHRP Report 549 (*7*) recommended that Table 5.8.3.4.2-1 of the LRFD specifications be replaced with equations similar to the foregoing for β and θ. The iteration procedure is then completely removed in this method, and there are trade-offs made between simplicity, generality, and accuracy. Collins and Rahal (*23*) reported that this approach had been checked against a database of 413 large reinforced and prestressed concrete beams. The average shear capacity ratio was $V_{test}/V_{prediction}$ 1.16, with a coefficient of variation of 0.169 and a 1-percent fractile value of $V_{test}/V_{prediction}$ of 0.77.

AASHTO Simplified Shear Design Provisions

The second recommendation from *NCHRP Report 549* was the addition of an alternative or simplified set of shear design relationships that would be applicable to both reinforced and prestressed concrete members containing at least the minimum required amount of shear reinforcement and not subjected to a net axial tension. The recommendation has been incorporated into the fourth edition of the LRFD specifications. These recommendations are a modified version of the AASHTO Standard Specifications. The expression for web-shear cracking strength was modified so that it was applicable to both nonprestressed and prestressed members. Thus, when the decompression stress f_{pc} is equal to zero, then the web-shear cracking stress is equal to $2\sqrt{f'_c}$ (in psi units). The expression for flexure-shear cracking was kept virtually unchanged, while the contribution of the shear reinforcement was evaluated using a variable angle truss model. The angle used for calculating the contribution of the transverse reinforcement to shear resistance was evaluated from Mohr's circle of stress considering the effect of the decompression stress, f_{pc}. When there was no decompression stress, as in nonprestressed members, the angle of cracking is 45 degrees and cotθ equals unity. With increasing levels of decompression stress, the angle of cracking becomes flatter, cotθ increases, and the contributions of the shear reinforcement to shear capacity increase. A limit of 1.8 was imposed on cotθ, which is equivalent to limiting θ to 29 degrees. The other differences from the AASHTO Standard Specifications were that d_v rather than d was used for the shear depth, the LRFD required that minimum shear reinforcement limit be applied, and the limit on V_s was replaced with the LRFD maximum allowable design shear stress. These provisions are shown below in both ksi and psi units. Note that coefficients were selected so that they would be simpler in the LRFD ksi unit system.

$$V_{cw} = (0.06\sqrt{f'_c} + 0.30 f_{pc}) b_v d_v + V_p \quad (29)$$

where stress is in ksi units, which is equivalent to

$$V_{cw} = (1.9\sqrt{f'_c} + 0.30 f_{pc}) b_v d_v + V_p \quad (30)$$

where stress is in psi units.

$$V_{ci} = 0.02\sqrt{f'_c}\, b_v d_v + V_d + \frac{V_i M_{cr}}{M_{max}} \geq 0.06\sqrt{f'_c}\, b_v d_v \quad (31)$$

where stress is in ksi units, which is equivalent to

$$V_{ci} = 0.632\sqrt{f'_c}\, b_v d_v + V_d + \frac{V_i M_{cr}}{M_{max}} \geq 1.9\sqrt{f'_c}\, b_v d_v \quad (32)$$

where stress is in psi units.

The 0.06 coefficient establishes a uniform minimum V_c contribution over the length of the member independent of whether a web-shear or flexure-shear region is being designed. The coefficient of 0.06 (in ksi units) is also very close to the traditional coefficient of 1.7 (in psi units) when it is considered that $d_v = 0.9d$.

$$\cot\theta = 1.0 + 3\frac{f_{pc}}{\sqrt{f'_c}} \leq 1.8 \quad (33)$$

when

$V_{cw} < V_{ci}$

where stress is in ksi units, which is equivalent to:

$$\cot\theta = 1.0 + 0.095\frac{f_{pc}}{\sqrt{f'_c}} \leq 1.8 \quad (34)$$

where stress is in psi units.

Comparison of Measured Strengths with Shear Design Provisions

The measured strengths of the test girders are compared with the calculated capacities of the LRFD specifications and the four methods described above (AASHTO Standard Specifications, the computer program Response 2000, CSA A23.3-04, and Simplified Proposed Specifications), plus the LRFD Sectional Design Model in Table 8. In these calculations, no limit was placed on the value of f'_c, and the LRFD maximum shear strength limitation was imposed. The shear strength limitation was not imposed upon the R2K prediction because it directly evaluates the diagonal compression stress and checks against available compressive capacity. Table 8 shows the measured distributed loading in kips per foot at failure and the distributed loading at nominal capacity as calculated by the five methods. That listing is followed by the strength ratios for each of the five methods expressed as the measured strength divided by the calculated nominal capacity. At the bottom of the columns for these strength ratios, the mean strength ratio and the coefficient of variation for these ratios are given. In these calculations, the results from tests G4E, G4W, and G9W were not included because these members did not fail in shear. From an examination of these strength ratios, the following observations are drawn:

- All five methods predicted the capacity of the test girders to an acceptable level of accuracy.
- The strength ratios from the LRFD and CSA methods produced very similar results, as was expected given that they are both derived from the MCFT and use the longitudinal strain at mid-depth to characterize the condition of the member in shear.
- The AASHTO Standard Specifications method was the most conservative and had the lowest coefficient of variation. The ratios of the measured to code-calculated nominal strengths ranged from 1.20 to 1.55.
- The program Response 2000 (R2K) had the lowest average strength ratio. Higher strength estimates of Girder 9 were to be expected because R2K assumes that there is a uniform field of diagonal compression, that there is no local crushing due to funneling of compressive stresses, and that for Girder 9 the stirrups yielded prior to failure.
- The proposed simplified provisions provided a safe estimate of the capacity of all test girders that failed in shear. The proposed provisions were particularly conservative at predicting the capacity of Girder 5, which contained minimum shear reinforcement only. These provisions are intentionally more conservative for lightly reinforced members to guard against serviceability and fatigue problems.

The results presented in Table 8 are useful for evaluating whether these other shear design provisions and methods can be used with HSC. However, it should be recognized that this is only one set of comparisons. Extension of the LRFD and other specifications to HSC for all member types requires consideration of all available test results, including those presented in Section 2.2. Caution is urged in drawing too strong a conclusion about the relative accuracy and conservatism of these five methods from the range of tests in this program and those in the experimental databases presented in Section 2.2 because that range is limited. This matter is further discussed in Chapter 4. Additional observations from these girder tests, and of the success of the different methods for calculating nominal capacity, are presented in, and discussed throughout, the remaining sections of Chapter 2.

2.4.3 Impact of Method Selected for Staggered Shear Design on Strength Evaluations

The LRFD Sectional Design Model (S5.8.2.3) permits the use of a staggered shear design approach over the entire length of a member. The shear design force permitted in a region is taken as the lowest shear force at the edge of that region. This concept and its consequences are illustrated in Figure 66. The justification for the LRFD approach is that the design force for a region should only consider the force that needs to be carried across the diagonal crack that spans that region, as illustrated in Figure 66(b).

One difficulty with using the staggered shear design approach of LRFD is that the designer needs to evaluate the angle θ before determining the location of the shear design force, V_u, to be used in the design. Since θ is a function of ε_x and ε_x is a function of V_u, the design becomes awkwardly iterative. Consequently, the contractor used the approach shown in Figure 66(a) when designing the test girders.

In order to evaluate the safety of using a staggered shear design method over the entire length of the girder, it is useful to reevaluate the capacity of the test girders using only the load that occurs to the right of section (2), as shown in Figure 67. The revised strength ratios are presented in Table 9, where the shear force under the test load w_u was computed at section (2) and then was compared with the calculated shear strength from above evaluation methods. Note that the locations of section (2) were different in these methods and that the test load w_u is shown in the second column of Table 8. From Table 9, the following observations are made about the staggered shear design approach:

- The use of a staggered shear design method over the length of the girder leads to a lower ratio of the measured capacity to calculated capacity than when a region is designed for the shear force at the center of that region.
- The strength ratios calculated using the LRFD, R2K, CSA and proposed methods had very similar mean values of

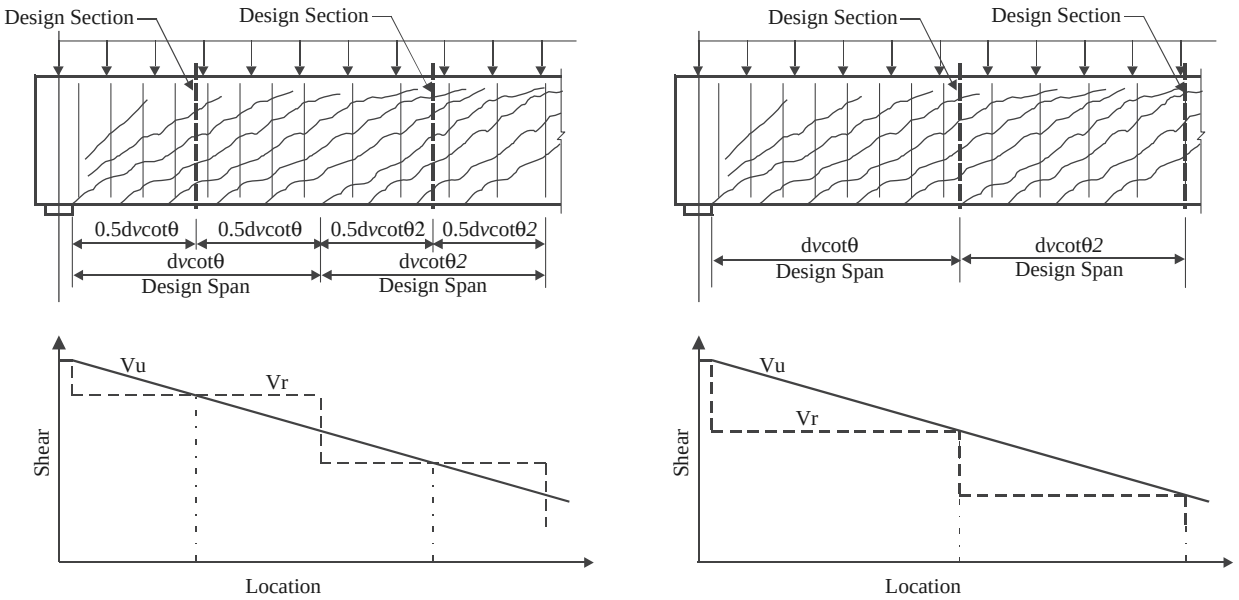

(a) Designing a region for shear at center of region

(b) Staggered shear design for calculating shear design force

Figure 66. Staggered shear design concept.

around 0.78. That the mean value is less than 1.0 suggests that the use of the staggered shear design method over the entire length of a member leads to unconservative results.

- The strength ratio from the AASHTO Standard Specifications was still conservative at 1.19. The lesser impact of the staggered shear design concept for the AASHTO Standard Specifications is in large part due to the much shorter length of the shear design region when the angle of diagonal compression is taken as 45 degrees and due to the stocky aspect ratio of the test girders.

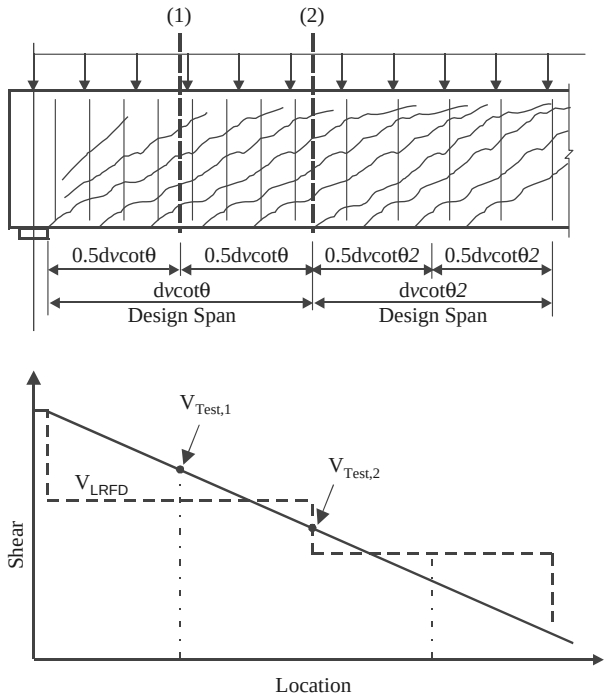

Figure 67. Locations for evaluating design shear force in test girders.

Table 9. Shear strength ratios for critical section at $d_v \cot\Theta$ from face of support.

Girder End	Test/Calculation Ratio				
	LRFD	STD	R2K	CSA	PROP
G1E	0.72	1.12	0.76	0.68	0.75
G1W	0.86	1.12	0.90	0.81	0.81
G2E	0.70	1.10	0.67	0.68	0.72
G2W	0.87	1.13	0.78	0.84	0.79
G3E	0.77	1.19	0.83	0.74	0.78
G3W	0.84	1.29	0.91	0.80	0.85
G4E#	0.75	1.10	0.76	0.73	0.71
G4W#	0.75	1.10	0.76	0.73	0.71
G5E	0.78	1.32	0.69	0.73	1.12
G5W	0.71	1.15	0.58	0.64	1.00
G6E	0.72	1.26	0.73	0.69	0.77
G6W	0.73	1.16	0.67	0.70	0.93
G7E	0.77	1.19	0.83	0.71	0.78
G7W	1.02	1.20	1.14	0.95	1.04
G8EB	0.70	1.22	0.69	0.67	0.76
G8W	0.62	1.11	0.69	0.60	0.71
G9E	0.71	1.08	0.68	0.70	0.84
G9W#	0.65	1.09	0.55	0.71	0.78
G10E	0.91	1.19	0.83	0.92	0.87
G10W	1.03	1.33	0.94	0.97	0.94
Average	0.79	1.19	0.78	0.75	0.85
COV	0.15	0.06	0.17	0.15	0.14

# No shear failure in this region; strength ratio not used in statistical calculations.
STD = AASHTO Standard Specifications.
PROP = proposed provisions.

2.4.4 Modes of Failure and Condition of Members at Ultimate Limit State

The values of the design parameters selected for the tests were intended to facilitate the evaluation of different mechanisms of shear resistance. The events that could precipitate shear failure included stirrup yielding, stirrup rupturing, strands slipping, local crushing of concrete along the line of diagonal compression as it funnels to the support, distributed crushing across a band of diagonal compression, or shear slip along a crack or between the web and bottom bulb. Each of these events was exhibited in this experimental research program, as illustrated in Figure 68.

The modes of failure for all of the test girders are described in Figures 69(a) through 69(t). Each of these figures consists of two text boxes and selected photographs. In the left text box

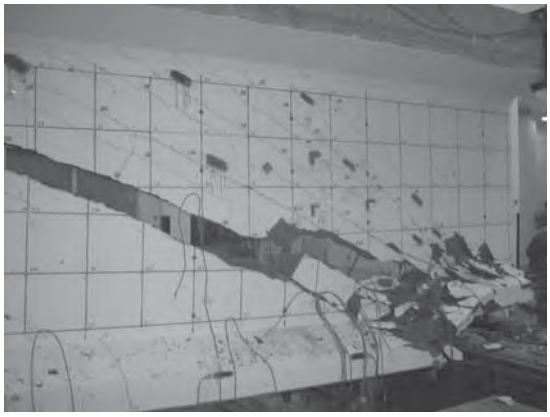

(a) Low v/f'_c, stirrups yield and rupture

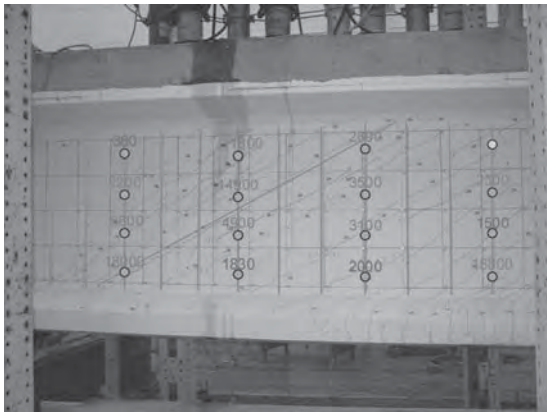

(b) Moderate v/f'_c, stirrups yielding

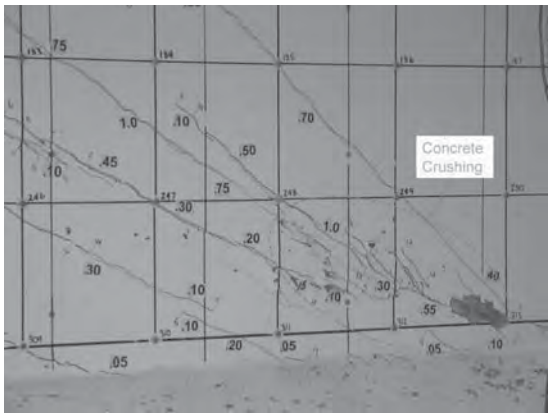

(c) Moderate v/f'_c, local crushing

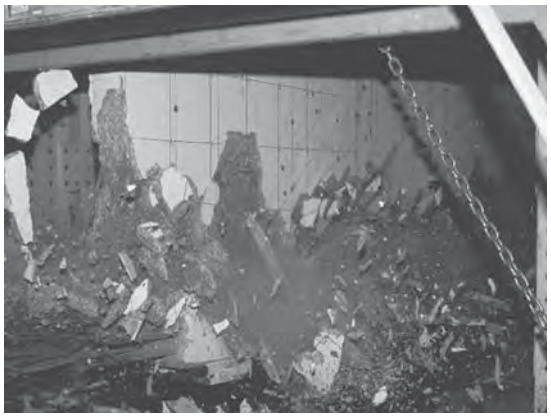

(d) Moderate to high v/f'_c, brittle compression/shear failure

(e) Horizontal shear slip

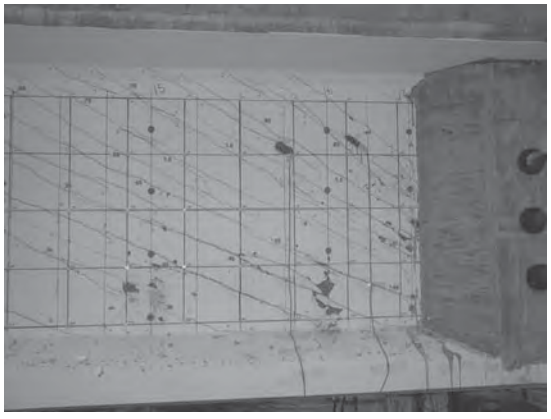

(f) Crushing of diagonal compression field

Figure 68. Typical failure modes.

G1E

Concrete: f'_c = 12.1 ksi, $f'_{c,deck}$ = 4.5 ksi
Stirrup: 2-#4@12, $\rho_v f_y$ = 389 psi
Strand: 32-straight on bottom, 2-straight on top

Failure Load: 26.03 kips/ft
Loading pattern: (3,44,3)ft
Support Reaction R: 573 kips

R(first crack)/R(failure) = 57%
R(first stirrup yield)/R(failure) = 65%
average stirrup strain at failure = $2.0\varepsilon_y$
strand slip prior to failure: minor
shear slip along cracks: significant
localized crushing: significant
Test/LRFD = 1.06
failure manner: explosive

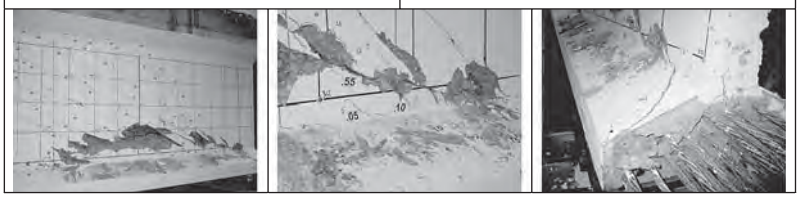

(a) Failure Mode of G1E

G1W

Concrete: f'_c = 12.1 ksi, $f'_{c,deck}$ = 4.5 ksi
Stirrup: 2-#4@12, $\rho_v f_y$ = 389 psi
Strand: 26-straight and 6-draped on the bottom half; 2-straight on top

Failure Load: 30.09 kips/ft
Loading pattern: (3,44,3)ft
Support Reaction R: 662 kips

R(first crack)/R(failure) = 60%
R(first stirrup yield)/R(failure) = 71%
average stirrup strain at failure = $2.3\varepsilon_y$
strand slip prior to failure: 0.08 inch
shear slip along cracks: significant
localized crushing: significant
Test/LRFD = 1.22
failure manner: explosive

(b) Failure Mode of G1W

G2E

Concrete: f'_c = 12.6 ksi, $f'_{c,deck}$ = 8.6 ksi
Stirrup: 2-#5@11, $\rho_v f_y$ = 745 psi
Strand: 38-straight on the bottom half; 2-straight on the top

Failure Load: 33.79 kips/ft
Loading pattern: (3,44,3)ft
Support Reaction R: 743 kips

R(first crack)/R(failure) = 55%
R(first stirrup yield)/R(failure) = 82%
average stirrup strain at failure = $1.1\varepsilon_y$
strand slip prior to failure: 0.02 inch
shear slip along cracks: significant
localized crushing: significant
horizontal sliding after failure: 2.5 inches
Test/LRFD = 0.96
failure manner: explosive

(c) Failure Mode of G2E

Figure 69. Failure Modes.

G2W

Concrete: f'_c = 12.6 ksi, $f'_{c,deck}$ = 8.6 ksi
Stirrup: 2-#5@11, $\rho_v f_y$ = 745 psi
Strand: 32-straight and 6-draped on the bottom half; 2-straight on the top

Failure Load: 38.73 kips/ft
Loading pattern: (3,44,3)ft
Support Reaction R: 852 kips

R(first crack)/R(failure) = 56%
R(first stirrup yield)/R(failure) = 61%
average stirrup strain at failure = 2.1ε_y
strand slip prior to failure: 0.025 inch
shear slip: minor
localized crushing: significant
Test/LRFD = 1.15
failure manner: very explosive with 10-inch high web segment totally crushed.

(d) Failure Mode of G2W

G3E

Concrete: f'_c = 15.9 ksi, $f'_{c,deck}$ = 3.6 ksi
Stirrup: 2-#4@8, $\rho_v f_y$ = 565 psi
Strand: 42-straight on the bottom; 2-straight on the top

Failure Load: 35.68 kips/ft
Loading pattern: (3,44,3)ft
Support Reaction R: 785 kips

R(first crack)/R(failure) = 45%
R(first stirrup yield)/R(failure) = 50%
average stirrup strain at failure = 2.3ε_y
strand slip prior to failure: none
shear slip along cracks: significant
localized crushing: significant
horizontal sliding after failure: 4 inches
Test/LRFD = 1.12
failure manner: very explosive

(e) Failure Mode of G3E

G3W

Concrete: f'_c = 15.9 ksi, $f'_{c,deck}$ = 3.6 ksi
Stirrup: 2-#4@8, $\rho_v f_y$ = 565 psi
Strand: 42-straight on the bottom; 2-straight on the top
Enhancement: Additional 10-foot long #3 horizontal skin bars;
Four pairs of #4 vertical bars in the bottom web near support;
Four 20-inch long spirals wrapped around groups of strands;
Failure Load: 38.82 kips/ft
Loading pattern: (3,44,3)ft
Support Reaction R: 854 kips

R(first crack)/R(failure) = 39%
R(first stirrup yield)/R(failure) = 41%
average stirrup strain at failure = 2.7ε_y
strand slip prior to failure: none
shear slip along cracks: significant
localized crushing: significant
horizontal sliding after failure: minor
Test/LRFD = 1.21
failure manner: very explosive

(f) Failure Mode of G3W

Figure 69. (Continued).

G4E	
Concrete: f'_c = 16.3 ksi, $f'_{c,deck}$ = 6.3 ksi Stirrup: 2-#5@6, $\rho_v f_y$ = 1,113 psi Strand: 42-straight on the bottom; 2-straight on the top Failure Load: 42.73 kips/ft Loading pattern: (3,44,3)ft Support Reaction R: 940 kips	R(first crack)/R(failure) = 33% R(first stirrup yield)/R(failure) = 100% average stirrup strain at failure = 0.9ε_y strand slip prior to failure: none shear slip along cracks: small localized crushing: none Test/LRFD = 0.98 failure manner: No shear failure
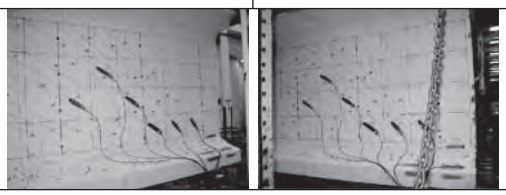	

(g) Failure Mode of G4E

G4W	
Concrete: f'_c = 16.3 ksi, $f'_{c,deck}$ = 6.3 ksi Stirrup: 2-#5@6, $\rho_v f_y$ = 1113 psi Strand: 42-straight on the bottom; 2-straight on the top Enhancement: Additional 10-foot long #3 horizontal skin bars; Four pairs of #5 vertical bars in the bottom web near support; Four 20-inch long spirals wrapped around groups of strands; Test Load: 42.73 kips/ft Loading pattern: (3,44,3)ft Support Reaction R: 940 kips	R(first crack)/R(failure) = 36% R(first stirrup yield)/R(failure) = 100% average stirrup strain at failure = 0.9ε_y strand slip prior to failure: none shear slip along cracks: small localized crushing: none Test/LRFD = 0.98 failure manner: No shear failure
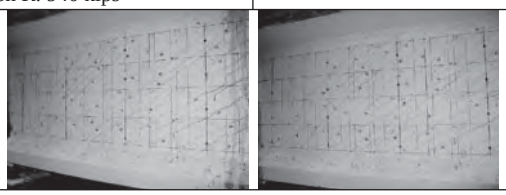	

(h) Failure Mode of G4W

G5E	
Concrete: f'_c = 17.8 ksi, $f'_{c,deck}$ = 6.1 ksi Stirrup: 2-#3@20, $\rho_v f_y$ = 169 psi, Welded-wire reinforcement were used Strand: 24-straight on the bottom Test Load: 23.70 kips/ft Loading pattern: (3,44,3)ft Support Reaction R: 521 kips	R(first crack)/R(failure) = 71% R(first stirrup yield)/R(failure) = 71% average stirrup strain at failure = 3ε_y stirrups fractured strand slip prior to failure: 0.02 inch shear slip along cracks: significant the bottom bulb flange: broken horizontal sliding after failure: 4.5 inches Test/LRFD = 1.23 failure manner: very explosive
	

(i) Failure Mode of G5E

Figure 69. (Continued).

G5W

Concrete: f'_c = 17.8 ksi, $f'_{c,deck}$ = 6.1 ksi
Stirrup: 2-#3@20, $\rho_v f_y$ = 140 psi
Strand: 24-straight on the bottom

Test Load: 19.91 kips/ft
Loading pattern: (3,44,3)ft
Support Reaction R: 438 kips

R(first crack)/R(failure) = 61%
R(first stirrup yield)/R(failure) = 73%
average stirrup strain at failure = $2\varepsilon_y$
strand slip prior to failure: none.
Local crushing: significant
horizontal sliding found along a preexisting crack.
Test/LRFD = 1.12
failure manner: brittle

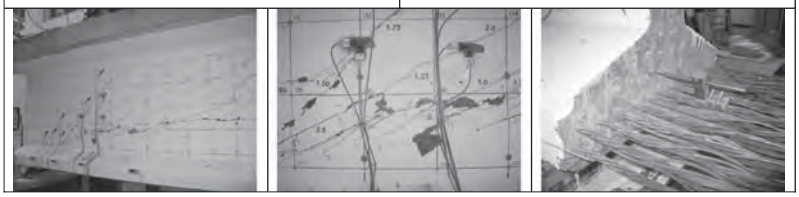

(j) Failure Mode of G5W

G6E

Concrete: f'_c = 12.7 ksi, $f'_{c,deck}$ = 9.2 ksi
Stirrup: 2-#5@12, $\rho_v f_y$ = 557 psi
Strand: 42-straight on the bottom, 2-straight on the top

Test Load: 38.32 kips/ft
Loading pattern: (15,32,3)ft
Support Reaction R: 760 kips

R(first crack)/R(failure) = 47%
R(first stirrup yield)/R(failure) = 77%
average stirrup strain at failure = $1.7\varepsilon_y$
strand slip prior to failure: none
shear slip along cracks: significant
localized crushing: significant
horizontal sliding after failure: 2.0 inches
Test/LRFD = 1.1
failure manner: explosive

(k) Failure Mode of G6E

G6W

Concrete: f'_c = 12.7 ksi, $f'_{c,deck}$ = 9.2 ksi
Stirrup: 2-#5@12, $\rho_v f_y$ = 557 psi
Strand: 42-straight (16-debonded) on the bottom, 2-straight on the top (2 debonded)

Failure Load: 27.85 kips/ft
Loading pattern: (3,44,3)ft
Support Reaction: 613 kips

R(first crack)/R(failure) = 60%
R(first stirrup yield)/R(failure) = 100%
average stirrup strain at failure = $1.6\varepsilon_y$
strand slip prior to failure: 0.5 inch
shear slip along cracks: significant
localized crushing: significant
horizontal sliding after failure: 1.0 inch
Test/LRFD = 1.01
failure manner: brittle

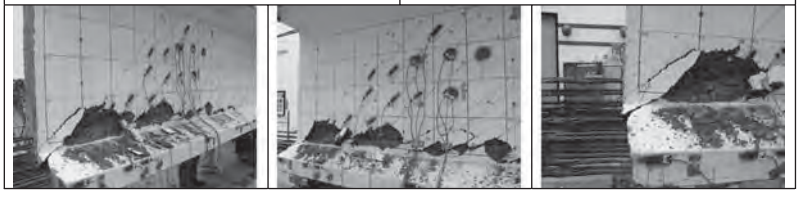

(l) Failure Mode of G6W

Figure 69. (Continued).

G7E	
Concrete: f'_c = 12.5 ksi, $f'_{c,deck}$ = 4.5 ksi Stirrup: 2-#4@8, $\rho_v f_y$ = 557 psi Strand: 42-straight on the bottom, 2-straight on the top Test Load: 33.47 kips/ft Loading pattern: (3,44,3)ft Support Reaction: 736 kips	R(first crack)/R(failure) = 54% R(first stirrup yield)/R(failure) = 93% average stirrup strain at failure = 1.2ε_y strand slip prior to failure: none shear slip along cracks: minor localized crushing: minor Test/LRFD = 1.09 failure manner: loading stopped before explosive failure formed.
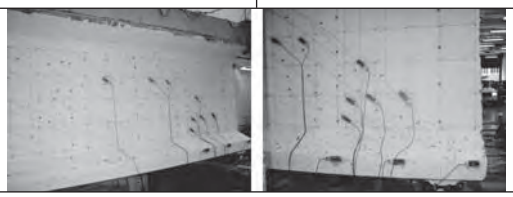	

(m) Failure Mode of G7E

G7W	
Concrete: f'_c = 12.5 ksi, $f'_{c,deck}$ = 4.5 ksi Stirrup: 2-#4@8, $\rho_v f_y$ = 557 psi (end) 2-#3@23, $\rho_v f_y$ = 119 psi (transition) Strand: 42-straight on the bottom, 2-straight on the top Enhancement: all strands were anchored to a steel plate; A 5-foot long diaphragm was cast Test Load: 44.75 kips/ft Loading pattern: (11,28,11)ft Support Reaction R: 627 kips	R(first crack)/R(failure) = 66% R(first stirrup yield)/R(failure) = 95% average stirrup strain at failure = 2.6ε_y strand slip prior to failure: none shear slip along cracks: significant localized crushing: significant horizontal sliding after failure: minor Test/LRFD = 1.08 failure manner: brittle
	

(n) Failure Mode of G7W

G8E	
Concrete: f'_c = 13.3 ksi, $f'_{c,deck}$ = 7.0 ksi Stirrup: 2-#4@8, $\rho_v f_y$ = 557 psi Strand: 42-straight on the bottom, 2-straight on the top; Enhancement: all strands were anchored; 5-foot long diaphragms were cast on either side with lateral post-tensioning. Failure Load: 43.72 kips/ft Loading pattern: (13,28,9)ft Support Reaction R: 661 kips	R(first crack)/R(failure) = 48% R(first stirrup yield)/R(failure) = 62% average stirrup strain at failure = 1.8ε_y strand slip prior to failure: none shear slip along cracks: small localized crushing: significant Test/LRFD = 1.17 failure manner: brittle, distributed crushing across a bond of diagonal compression before the diaphragms
	

(o) Failure Mode of G8E

Figure 69. (Continued).

G8W	
Concrete: f'_c = 13.3 ksi, $f'_{c,deck}$ = 7.0 ksi Stirrup: 2-#4@8, $\rho_v f_y$ = 557 psi Strand: 42-straight on the bottom, 2-straight on the top; Enhancement: two aluminum plates were installed Failure Load: 32.70 kips/ft Loading pattern: (3,34,13)ft Support Reaction: 667.1 kips	R(first crack)/R(failure) = 52% R(first stirrup yield)/R(failure) = 82% average stirrup strain at failure = 0.95ε_y strand slip prior to failure: none shear slip along cracks: significant along plates localized crushing: significant Test/LRFD = 0.94 failure manner: the loading was halted after failure was deemed imminent.

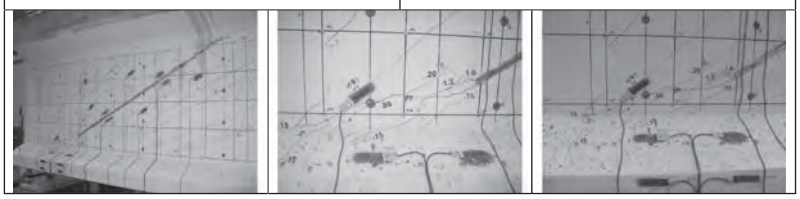

(p) Failure Mode of G8W

G9E	
Concrete: f'_c = 9.6 ksi, $f'_{c,deck}$ = 6.0 ksi Stirrup: 2-#5@6.5, $\rho_v f_y$ = 1040 psi Strand: 34-straight on the bottom, 2-straight on the top Failure Load: 32.80 kips/ft Loading pattern: (3,44,3)ft Support Reaction: 722 kips	R(first crack)/R(failure) = 49% Stirrup didn't yield at failure; average stirrup strain at failure = 0.7ε_y strand slip prior to failure: 0.013 inch shear slip along cracks: none localized crushing: significant horizontal sliding after failure: 4.0 inches Test/LRFD = 0.91 failure manner: explosive, concrete crushed along the interface of web and bottom bulb.

(q) Failure Mode of G9E

G9W	
Concrete: f'_c = 9.6 ksi, $f'_{c,deck}$ = 6.0 ksi Stirrup: 2-#5@4, $\rho_v f_y$ = 1690 psi Strand: 24-straight and 10-draped on the bottom, 2-straight on the top Test Load: 37.20 kips/ft, 22.32 kips/ft Loading pattern: (3,26,21)ft /(4, 10,36)ft Support Reaction: 840.7 kips	R(first crack)/R(failure) = 57% Stirrup didn't yield at failure; average stirrup strain at failure = 0.5ε_y strand slip prior to failure: none shear slip along cracks: none localized crushing: significant Test/LRFD = 0.91 failure manner: test load was stopped when local crushed was observed, which suggested the loading was within a few percent of the failure.

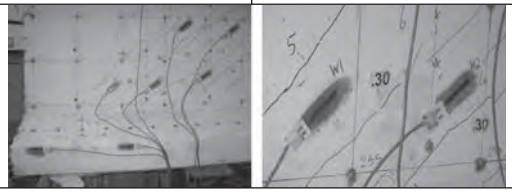

(r) Failure Mode of G9W

Figure 69. (Continued).

G10E	
Concrete: f'_c = 10.6 ksi, $f'_{c,deck}$ = 5.4 ksi Stirrup: 2-#5@9, $\rho_v f_y$ = 751 psi Strand: 34-straight (8-debonded) on the bottom, 2-straight on the top Test Load: 33.93 kips/ft Loading pattern: (3,44,3)ft Support Reaction: 747 kips	R(first crack)/R(failure) = 46% R(first stirrup yield)/R(failure) = 92%; average stirrup strain at failure = 1.3ε_y strand slip prior to failure: 0.01 inch shear slip along cracks: significant localized crushing: significant Test/LRFD = 1.17 failure manner: test load was halted to prevent a brittle failure when local crushing was observed near the support; failure was considered imminent
	

(s) Failure Mode of G10E

G10W	
Concrete: f'_c = 10.6 ksi, $f'_{c,deck}$ = 5.4 ksi Stirrup: 2-#5@9, $\rho_v f_y$ = 751 psi Strand: 24-straight and 10-draped on the bottom, 2-straight on the top Test Load: 42.85 kips/ft Loading pattern: (3,43,4)ft Support Reaction: 940 kips	R(first crack)/R(failure) = 46% R(first stirrup yield)/R(failure) = 87%; average stirrup strain at failure = 1.7ε_y strand slip prior to failure: none shear slip along cracks: minor localized crushing: significant horizontal sliding after failure: minor Test/LRFD = 1.34 failure manner: very explosive, with concrete in the bottom web near support totally crushed over 10 inches height.
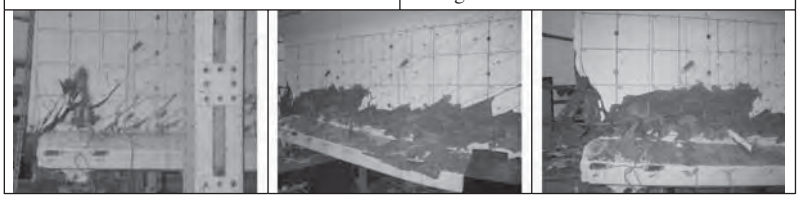	

(t) Failure Mode of G10W

Figure 69. (Continued).

is presented material strengths, reinforcement details, and whether the loads are failure or ultimate loads. In the right text box, the condition of the structure just prior to failure and the mode of failure are described. This description includes

- The ratio of the support reaction force at first shear cracking to the support reaction force at failure/ultimate—R(first crack)/R(failure);
- The equivalent reaction ratio for first stirrup yield—R(first stirrup yield)/R(failure);
- The average stirrup strain at peak loading;
- Whether or not slip had occurred of strands or along shear cracks; and
- A brief description of the type of failure.

At the bottom of each summary, several images are used to describe the condition of the structure immediately before and/or just after failure. Table 10 is then used to summarize and compare the conditions at the end of each girder immediately prior to failure or at the ultimate sustained load. Table 10 lists in turn: (1) the reaction force at ultimate load; (2) the compressive state in the web above the reaction; (3) whether or not the stirrups yielded and the extent of the yielding; (4) the magnitude of strand slip; (5) the web-shear crack spacing, maximum web-shear crack width, and the shear-slip condition along shear cracks; and (6) the magnitude of the slip between the bottom bulb and the web of the member after failure. From the description and summary provided in Figure 69 and Table 10, the following should be noted:

Table 10. Conditions at failure of girders.

End	Reaction Force (kips)	Condition of Web Concrete Above Support	Max. Stirrup Strain	Strand Slip (in)	Web-Shear Cracks			Bulb-Web Interface Sliding (in)
					Spacing (in)	Width (mm)	Shear Slip	
G1E	572.7	Web base crush	$3.2\varepsilon_y$	0.08	5.8	1.0	Large	Yes
G1W	662.0	Web base crush	$3.7\varepsilon_y$	0.07	3.7	1.0	Small	Yes
G2E	743.4	Web base crush	$2.0\varepsilon_y$	0.02	5.1	0.60	Yes	2.5
G2W	852.1	Web base crush	$3.5\varepsilon_y$	0.025	4.2	0.80	No	Yes
G3E	785.0	Web base crush	$4.0\varepsilon_y$	No	4.7	0.55	Yes	4.0
G3W	854.0	Web base crush	$4.0\varepsilon_y$	No	4.3	0.50	Yes	Yes
G4E	940.1	Good	$1.0\varepsilon_y$	No	3.5	0.55	Small	No
G4W	940.1	Good	$1.0\varepsilon_y$	No	3.1	0.30	Small	No
G5E	521.4	Bulb broken	Fracture	0.02	5.7	>5.0	Yes	4.5
G5W	438.0	Sign	$5.0\varepsilon_y$	No	6.1	2.5	Yes	No
G6E	760.3	Web base crush	$3.1\varepsilon_y$	No	5.0	1.0	Yes	2.0
G6W	612.7	Web base crush	$3.7\varepsilon_y$	0.5	5.8	0.70	Yes	1.0
G7E	736.3	Sign	$1.7\varepsilon_y$	No	4.6	0.90	Yes	No
G7W	626.5	Web base crush	$3.7\varepsilon_y$	No	3.8	1.2	Yes	Yes
G8E	661.0	Field crushing	$2.5\varepsilon_y$	No	4.0	1.5	Yes	No
G8W	667.1	Sign	$1.7\varepsilon_y$	No	4.8	1.2	Yes	No
G9E	721.6	Web base crush	$0.8\varepsilon_y$	0.013	4.1	0.50	No	4.0
G9W	840.7	Sign	$0.6\varepsilon_y$	No	3.1	0.30	No	No
G10E	746.5	Sign	$1.7\varepsilon_y$	0.01	3.9	1.0	Yes	No
G10W	939.7	Web base crush	$2.4\varepsilon_y$	No	4.3	0.55	Yes	Yes

Sign: Modest local crushing or significant cracking in web or bottom bulb that typifies the initiation of failure.

- The top flange was never damaged in any test.
- The bottom bulb remained intact in all girders except for G5E, where the bottom bulb failed in shear after rupture of the shear reinforcement. For most girders, the bottom bulb looked completely unharmed at failure, except for narrow flexural cracks.
- In most cases, the girders failed after significant local crushing was observed in the web just above and inside of the support. Associated with this local crushing were also significant shear stresses between the bottom bulb and web. These led to flatter cracks as well as localized crushing and slip along shear cracks.
- In many cases, the girders supported considerable additional load after stirrup yielding and before failure.
- In about one-third of the tests, some strand slip was observed prior to failure.
- The direction of shear slip along diagonal cracks in the web-shear zone was almost always in the direction opposite to what would be expected if interface shear transfer contributes to the concrete contribution to shear resistance. Figure 70(a) illustrates the typical shear slip that was observed, and it is opposite to what is needed to produce the shear stress on the crack, shown in Figure 70(b).
- The different events that led to failure in this testing program included the following:
  - Stirrup yield and rupture,
  - Stirrup yield and localized crushing near support,
  - Stirrup yield and distributed diagonal crushing over wide band of the web,
  - Stirrups that did not yield before localized crushing above the support, and
  - Stirrup yield followed by strand slip and localized crushing near support.

  The localized crushing that is observed near the support occurs in a region that also has very large shear stresses.

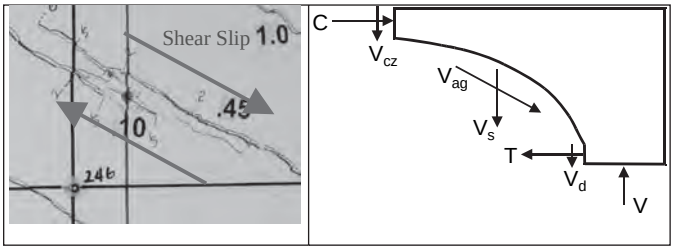

(a) Shear slip in experimental test (b) Shear resistance components

Figure 70. Typical shear slip in girder test.

This was evident in the direction of cracking and level of damage. Therefore, in many cases, it is appropriate to consider that the localized crushing failure was actually a failure induced by a combination of both high local compressive and shear stresses. This is discussed further in Appendix 11. Also presented in Appendix 11 is a discussion the definition of the effective depth *d*.

- The types of failures ranged from relatively ductile shear failures to very brittle and explosive shear failures. The most brittle and explosive failures were observed in members that failed due to local crushing and concrete compression shear failures between the bottom bulb and the girder web. In these members, the sudden loss of compressive and horizontal shear capacity resulted in an explosive failure of the web coupled with a large horizontal shearing between the bottom bulb and the web, as described for many of the failures presented in Figure 69. The more ductile shear failures were observed in members with light shear reinforcement (G5E), in which large numbers of strands were debonded (G6W), and in which failure occurred away from end regions (G8E).

2.4.5 Load-Deformation Response of Test Girders

To complete this presentation of the overall strength and mode of failure of the test girders, it is also useful to present the measured load versus center point displacement relationships for all of the test girders. These results are given in Figure 71, in which the plots from 10 girders have been organized into two groups in accordance with the number of strands used in the girders. Girders 1, 2, 5, 9 and 10 are grouped in Figure 71(a), and their strands numbers are 32(G1), 38(G2), 24(G5), 34(G9) and 34(G10). The load-versus-displacement response of Girders 3, 4, 6, 7, and 8 are shown in Figure 71(b), and all of these girders contained 42 strands that are each 0.6 inch in diameter. From these plots, the following observations can be made:

- The load-deformation response was linear until first shear cracking.
- After first shear cracking, there was a very small and almost imperceptible change in overall member stiffness.
- The significant change in stiffness occurred at the onset of flexural cracking, and the response became progressively softer as the extent of flexural cracking increased.
- The onset of yield of the shear reinforcement had little to no influence on the overall load-deformation response.
- All plots have a similar initial elastic slope prior to cracking except Girder 4. A steel plate was attached on the bottom of Girder 4 before the test. That plate increased its elastic modulus, and as a result the girder had a higher initial elastic stiffness than the other nine girders.

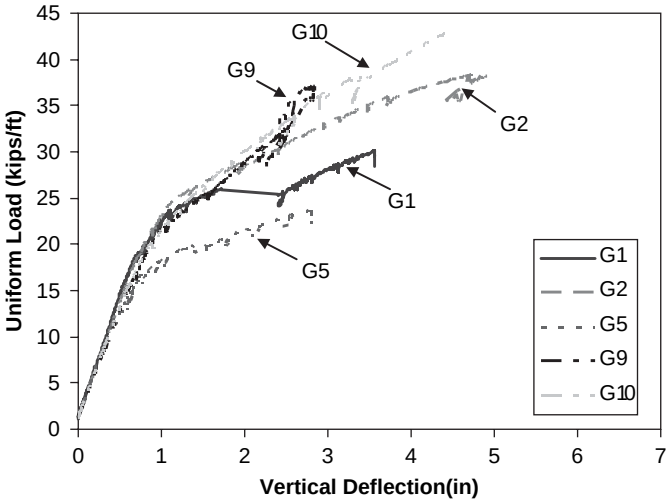

(a) Vertical displacements at middle span point for Girders 1, 2, 5, 9, and 10

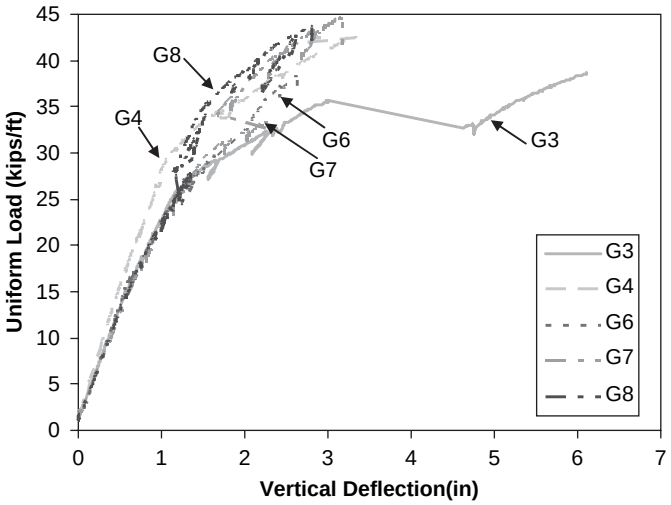

(b) Vertical displacements at middle span point for Girders 3, 4, 6, 7, and 8.

Figure 71. Load-deformation response of test girders.

- The number of strands had the most influence on the load for flexural cracking and the subsequent drop in stiffness.

2.5 Cracking

This section presents a summary of the measured cracking of the test girders and discusses the significance of these results. It is divided into several subsections, beginning with an introduction in Section 2.5.1 on the relevance of the measured cracking behavior and the methods that were employed to measure and document cracking. Section 2.5.2 describes the development of cracking in a typical girder, and Section 2.5.3 summarizes the measured crack angles and crack spacing for all girders. Section 2.5.4 compares measured and predicted web-shear cracking loads and angles, while Sections 2.5.5 and 2.5.6 compare measured and predicted

flexure-shear and flexural cracking loads, respectively. Section 2.5.7 summarizes the crack widths and their development, and Section 2.5.8 presents the most significant observations on cracking.

2.5.1 Introduction

The loads at which cracks occur, the angle of cracking, and the width and spacing of cracks are all important aspects of the behavior of prestressed concrete members. The load at shear cracking is important because this cracking can lead to serviceability problems due to corrosion or fatigue of transverse reinforcement. The angle of shear cracking is important for calculating the contribution of shear reinforcement to capacity because this angle is a good indicator of how many stirrups participated in lifting the diagonal compressive force above an inclined crack. The rate of growth of crack widths is important for evaluating the durability of structures in different environments.

In reviewing the results that are presented in the reminder of Section 2.5, it is useful to consider the following:

- In the LRFD Sectional Design Model, the effectiveness of shear reinforcement is proportional to the cotangent of the angle of diagonal compression. Although the angle of diagonal cracking is not necessarily equivalent to the angle of diagonal compression, it is still an important indicator for assessing the accuracy of the LRFD variable angle truss model.
- With the LRFD Sectional Design Model, members can be designed for much higher shear stresses than permitted by the AASHTO Standard Specifications. If members are designed for these higher shear stresses, then shear cracking will occur at a lower fraction of the design shear strength. With the phasing out of the AASHTO Standard Specifications shear design provisions, the relationships for evaluating web-shear and flexure-shear cracking strengths will be lost. To evaluate whether these relationships are useful for assessing the state of cracking at service loads and whether they should continue to be used for serviceability design considerations, it is useful to examine whether the AASHTO Standard Specifications relationships are effective at predicting the web-shear and flexure-shear cracking strengths for the test girders.
- An outcome of NCHRP Project 12-61 was the development of simplified shear design provisions for structural concrete members that are applicable to members containing the minimum required amount of shear reinforcement and are not subjected to a net-axial tension. In this method, a variable angle truss model was introduced that uses the calculated angle of diagonal cracking from Mohr's circle of stress for evaluating cotθ and the contribution of shear reinforcement. The measured crack angles for the test girders are also useful for evaluating the realism of this variable angle truss model.

During each test, the loading was paused at several "load stages" so that discrete measurements could be taken, cracks could be marked and measured, and pictures could be taken. Cracks occurred and propagated with increasing load. Pictures for each loading stage were taken to record crack development. Each girder test was divided into many load stages, and hence there were several hundreds of pictures taken per test. It was necessary to find a way to extract the crack information stored in those pictures in an automated manner in order to produce crack drawings in an efficient and accurate manner. A crack recording method based on digital close-range photogrammetry was developed to track the development of cracking in the girders. Crack patterns were created, and then crack angles and spacing were computed for each girder test. This method is fully described in Appendix 11.

2.5.2 Crack Development and Patterns

The development of cracking, as measured during the 13 load stages in Girder 1, is presented in Figure 72. This pattern of development is quite similar to what was recorded for each of the test girders; full crack patterns for each test girder are presented in the appendices. Prior to loading, and when the girders were delivered to the testing laboratory, diagonal cracks were present in the ends of most members, as shown for the extreme ends of Girder 1 in Figure 72(a). These initial cracks were predicted by the finite element analyses that are reported in Section 2.10 and are due to the tensile stresses caused by anchoring of the strands in the bottom bulb. These initial cracks did not propagate further during the loading, typically decreased in width with loading, and should be ignored as far as NCHRP Project 12-56 objectives are concerned.

The first cracks to occur in all members were web-shear cracks in the end region of the members, as shown for the east and west ends of Girder 1 in Figures 72(a) and 72(b). Nearly all these first cracks, and most other web-shear cracks, occurred with a significantly loud popping sound. Thus, it was possible to pause the loading immediately after first cracking and after other significant cracking developments. Under increasing load, additional web-shear cracks occurred, typically further from the support, as shown at the east end of Girder 1 in Figures 72(a) through 72(f). It was unusual to first have the first web-shear crack occur some distance from the support and then have subsequent cracks form closer to the support, as apparent for the west end of Girder 1 in Figures 72(c) through 72(e). In this case, the development of

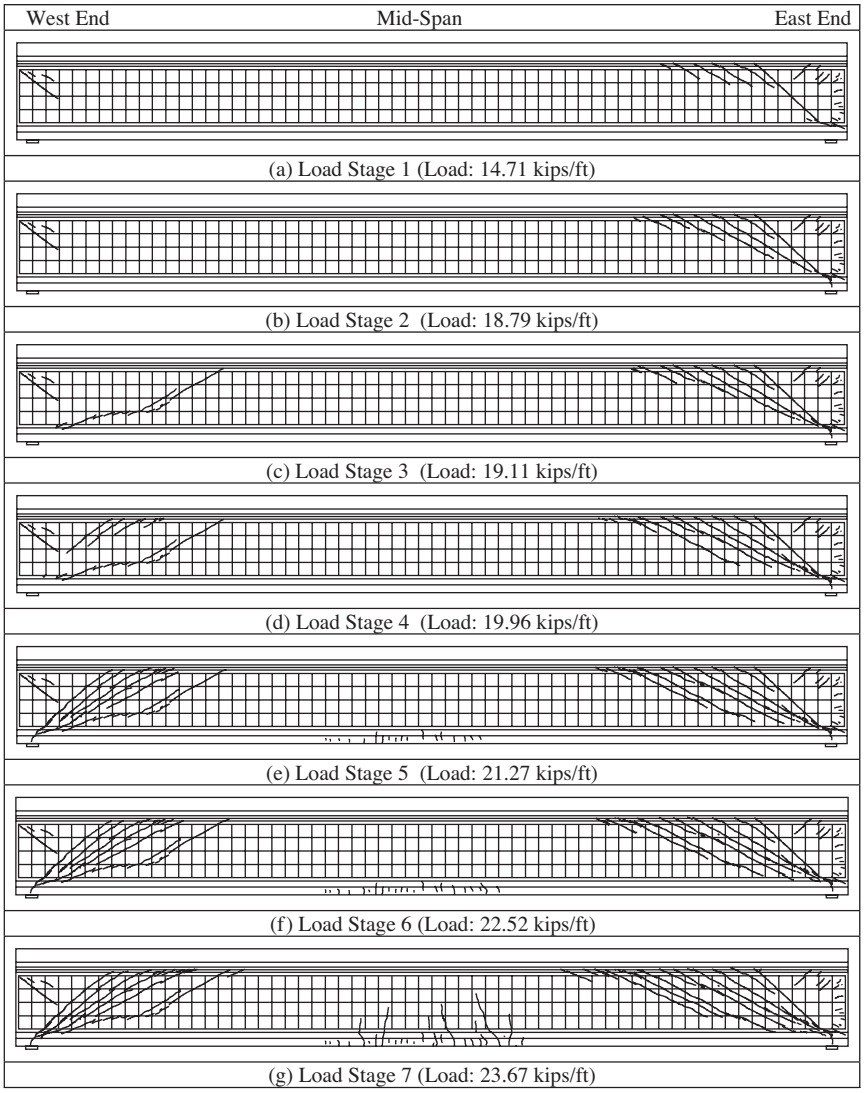

Figure 72. Crack pattern of Girder 1.

cracking close to the support was undoubtedly suppressed by the six draped strands that ran from 0.4L from the west support to the top of the web.

The onset of flexural cracking at mid-span is shown in Figure 72(e). As the loading continued beyond this point, shown in Figures 72(e) through 72(h), existing flexural cracks propagated upward while new flexural and shear cracks developed. In the flexural region farther from mid-span, the effect of the shear caused what were initially flexural cracks to grow into flexure-shear cracks. Also during these load increases, the widths of existing cracks increased. The extent of shear cracking over the length of the girder was influenced by the level of prestressing and the magnitude of the design shear stress. For members designed for higher design shear stresses than those for Girder 1, the webs of the girders became heavily cracked over their entire length and the bottom bulbs became cracked to within a few feet of the support. In some of the girders designed for large shear stresses, a close to stable crack pattern developed, after which cracks only widened with increasing load.

The majority of the web-shear cracks developed over the full height of the girder at one time and with a very audible sound. By contrast, the development of the flexure and flexure-shear cracks was more progressive and quieter.

2.5.3 Crack Angles and Spacing

In this section, the crack angles and the spacing of cracks are summarized for all test girders. As illustrated in Figure 72, it is reasonable to characterize shear cracks as straight lines with one slope (or angle). Using the image analysis methods described in Appendix 11, a least squares procedure was used to find the average angle for each crack. Only the crack profiles within the web were considered when assessments were made of the angle of best fit for each crack.

An example of the making of this crack angle assessment is illustrated in Figure 73 for the east half of Girder 1 (G1E). The longitudinal position of each crack was taken as the point where each crack crossed the centroid line of the composite

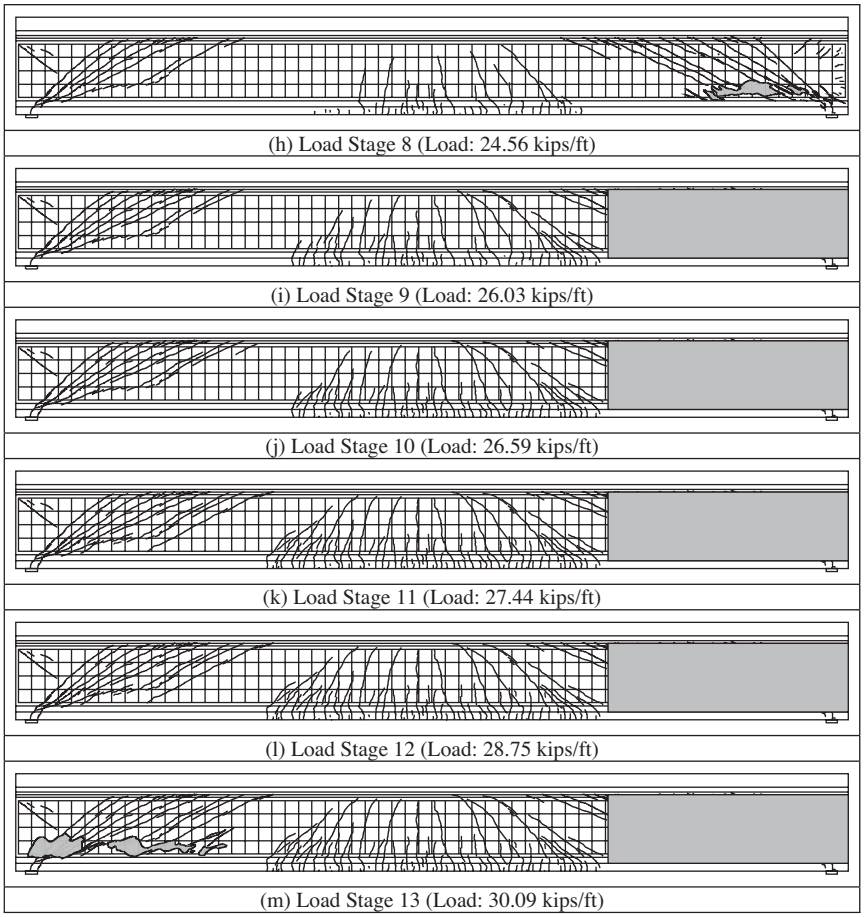

Figure 72. (Continued).

section. The shape of the curve for the distribution of angles with distance from the support is close to a parabolic curve. For G1E, the crack angle was approximately 45 degrees near the support. It then decreased to 25 degrees in the first shear design region, went back up to 45 degrees in the flexure-shear cracking zone, and then increased to the finally expected 90 degrees near mid-span, where only flexural cracking occurred. Observations from the other girder tests were similar, as apparent from the crack angle diagrams shown for each girder in Figure 74. In girders designed for higher shear stresses, such as Girders 4 and 9, the cracking was very extensive and the many crack angle data points illustrated a clear parabolic pattern; see Figures 74[4(a), 4(b), 9(a), and 9(b)].

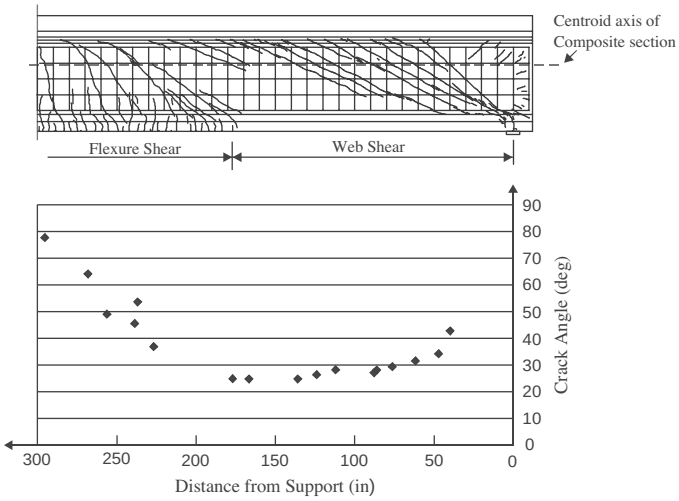

Figure 73. Crack angle distribution of G1E.

The pattern of cracking was also used to assess the average spacing of cracks. The horizontal spacing S_x, or the horizontal distance between any two adjacent cracks, can be computed from their positions. Furthermore, the spacing of any two adjacent cracks S can be computed from S_x and from the crack angle θ as $S = S_x \sin\theta$. Table 11 lists the average spacing of web-shear and flexure-shear cracks for all the tests. The horizontal spacing of the web-shear cracks was computed for the centroidal axis of the composite section, while for flexure-shear cracks the spacing was computed along a line at a height of 23 inches (584 millimeters) from the bottom. Table 11 also shows the details of the stirrup layouts. As apparent from the values in the table, there is some, but not

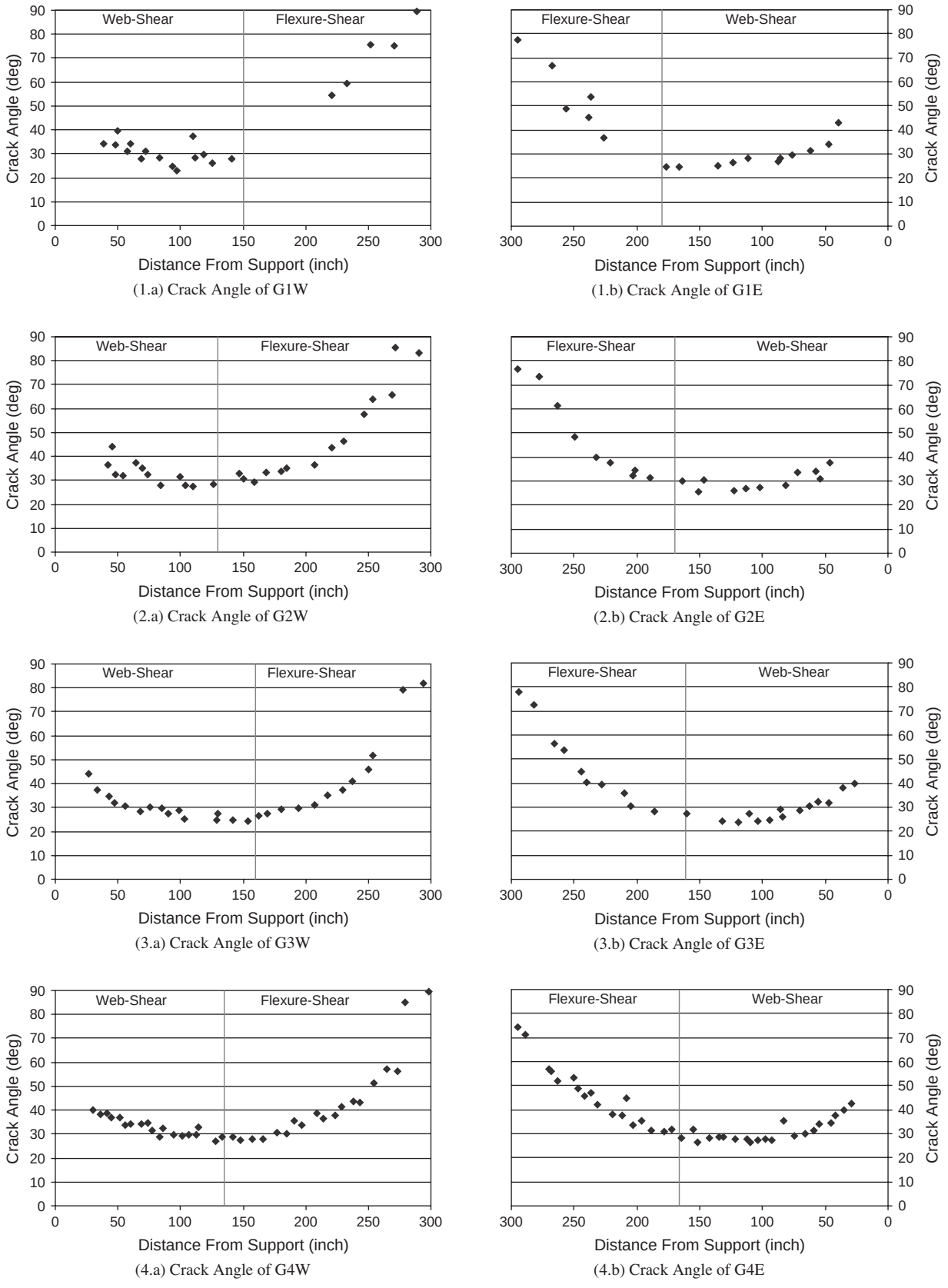

(1.a) Crack Angle of G1W

(1.b) Crack Angle of G1E

(2.a) Crack Angle of G2W

(2.b) Crack Angle of G2E

(3.a) Crack Angle of G3W

(3.b) Crack Angle of G3E

(4.a) Crack Angle of G4W

(4.b) Crack Angle of G4E

Figure 74. Crack angle distribution along centroid axis of composite section.

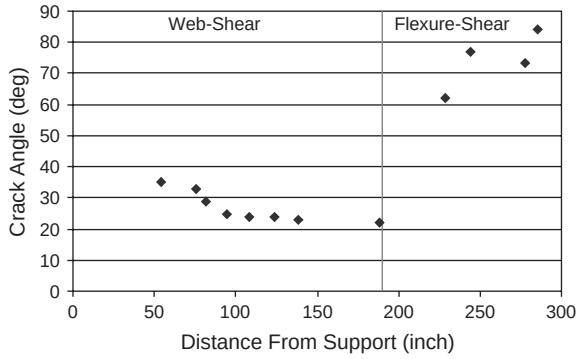

(5.a) Crack Angle of G5W

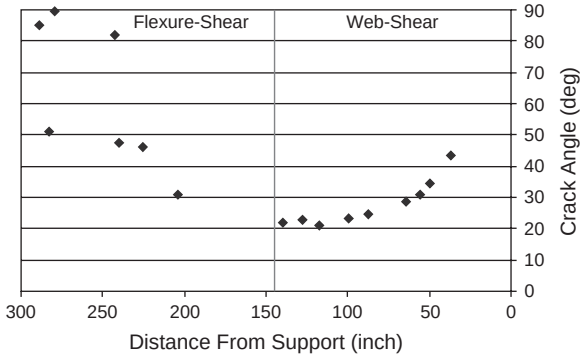

(5.b) Crack Angle of G5E

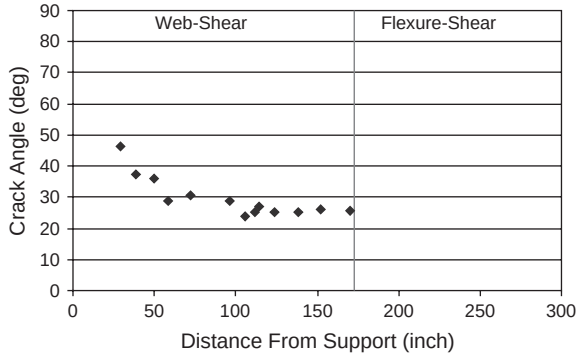

(6.a) Crack Angle of G6W

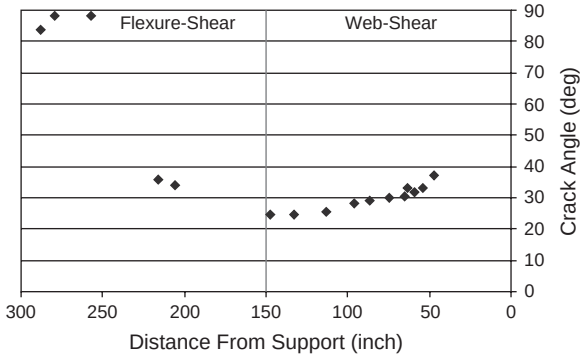

(6.b) Crack Angle of G6E

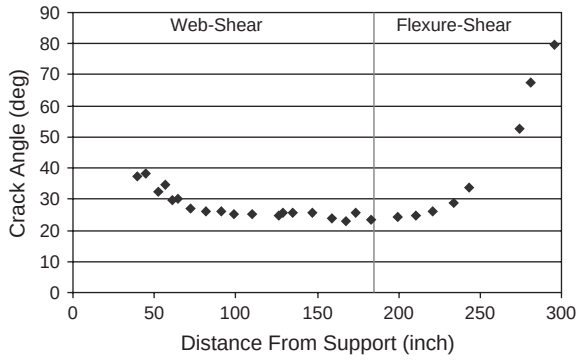

(7.a) Crack Angle of G7W

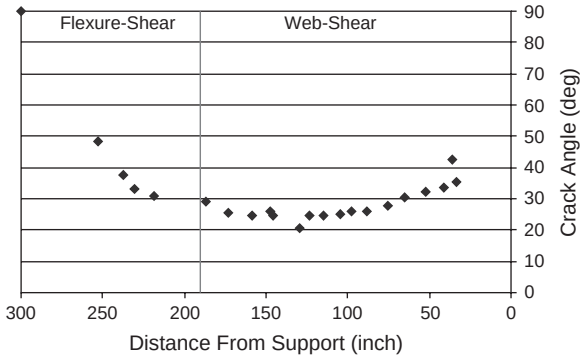

(7.b) Crack Angle of G7E

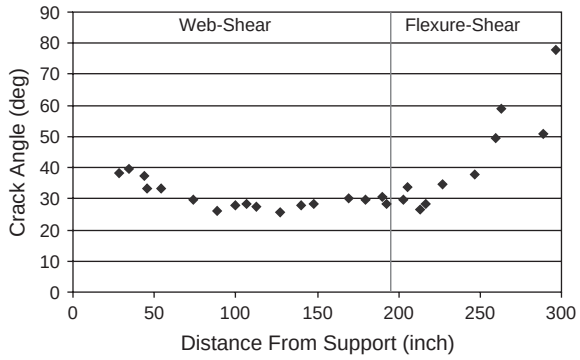

(8.a) Crack Angle of G8W

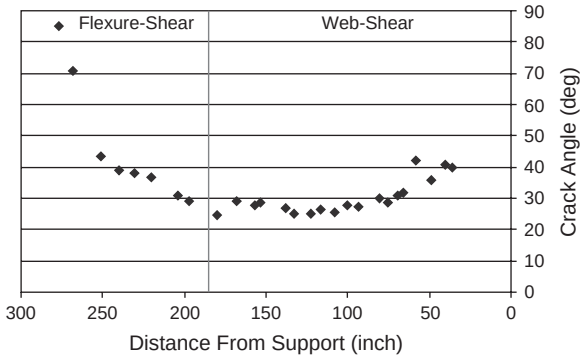

(8.b) Crack Angle of G8E

Figure 74. (Continued).

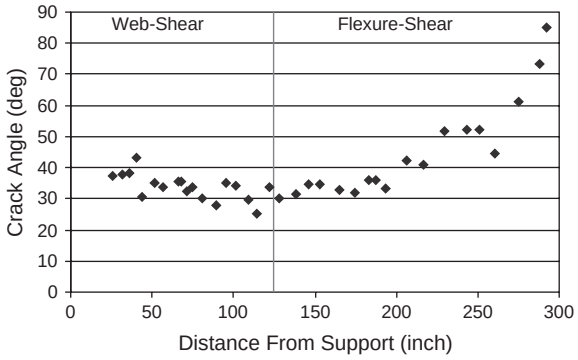

(9.a) Crack Angle of G9W

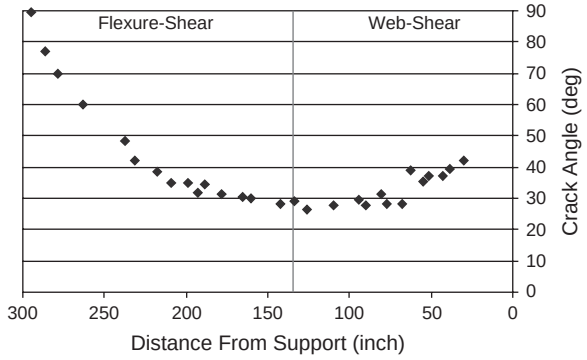

(9.b) Crack Angle of G9E

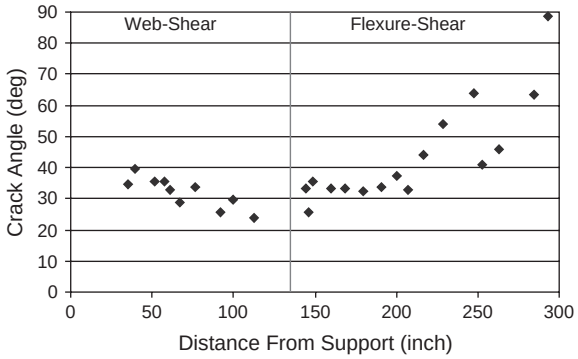

(10.a) Crack Angle of G10W

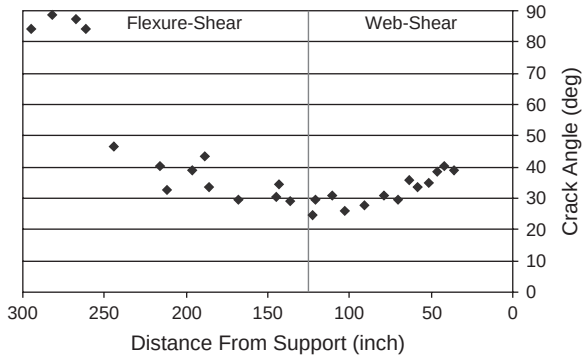

(10.b) Crack Angle of G10E

Figure 74. (Continued).

Table 11. Average spacing of shear cracks.

Girder End	Web-Shear Cracking			Flexure-Shear Cracking		
	Stirrup Layout	Average Spacing		Stirrup Layout	Average Spacing	
		Test (in)	CEB-FIP (in)		Test (in)	CEB-FIP (in)
G1E	#4@12	5.82	12.76	#4@24	7.53	17.04
G1W	#4@12	3.71	12.71	#4@24	7.26	17.08
G2E	#5@11	5.13	11.09	#5@17/#4@22	5.56	13.80
G2W	#5@11	4.18	11.09	#5@17/#4@22	4.34	13.76
G3E	#4@8	4.70	10.28	#4@12/#4@24	5.40	12.68
G3W	#4@8	4.24	8.17	#4@12/#4@24	4.70	12.76
G4E	#5@6	3.52	8.26	#5@10/#@24	3.46	10.59
G4W	#5@6	3.08	6.73	#5@10/#@24	3.73	10.58
G5E	#3@20	5.66	20.69	#3@20	7.17	18.98
G5W	#3@20	6.06	20.38	#3@20	7.97	18.03
G6E	#5@12	4.95	11.64	#5@20/#3@24	9.21	14.97
G6W	#5@12	5.80	11.74	#5@20/#3@24	8.30	14.89
G7E	#4@8	4.60	10.28	#4@12/#4@24	5.62	12.66
G7W	#4@8	3.78	10.28	#3@23	6.36	19.20
G8E	#4@8	3.98	10.27	#4@12/#4@24	7.50	12.69
G8W	#4@8	4.81	10.27	#4@12/#4@24	5.47	12.64
G9E	#5@6.5	4.09	8.58	#4@7.5/#4@24	4.92	10.08
G9W	#5@4	3.08	7.09	#4@7.5/#4@24	4.40	10.31
G10E	#5@9	3.90	10.09	#4@10/#4@22	6.36	11.98
G10W	#5@9	4.35	10.05	#4@10/#4@22	4.61	13.31

CEB-FIP = Comité Européen du Béton (European Committee for Concrete)–Fédération Internationale de la Précontrainte (International Federation for Prestressing).

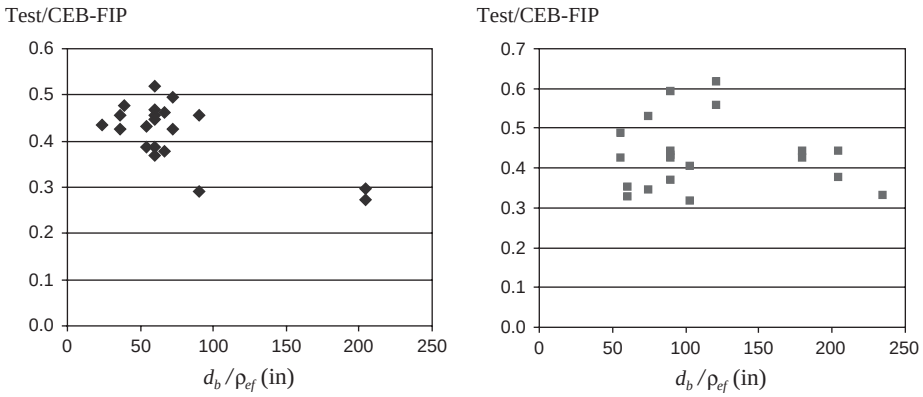

(a) Comparison of average spacing for web-shear cracks

(b) Comparison of average spacing for flexure-shear cracks

Figure 75. Ratio of the measured and CEB-FIP predicted average shear crack spacing.

a strong, correlation between crack spacing and the amount and spacing of shear reinforcement. The same effect is predicted by the CEB-FIP (Comité Européen du Béton [European Committee for Concrete]–Fédération Internationale de la Précontrainte FIP [International Federation for Prestressing]) model for crack spacing as described below.

The CEB-FIB Code (*27*) expression for the average crack spacing accounts for the influence of several variables in the following manner:

$$s_m = 2(c + \frac{s}{10}) + k_1 k_2 \frac{d_b}{\rho_{ef}} \quad (35)$$

where:

c = concrete cover,
s = maximum spacing between reinforcing bars,
d_b = bar diameter,
ρ_{ef} = effective reinforcement ratio,
k_1 = coefficient for the bond properties of the bar, and
k_2 = coefficient to account for the strain gradient.

It is suggested that the spacing of the inclined cracks, $s_{m\theta}$, be taken as

$$s_{m\theta} = 1 \Big/ \left(\frac{\sin\theta}{s_{mx}} + \frac{\cos\theta}{s_{mv}} \right) \quad (36)$$

where:

s_{mx} and s_{mv} = spacing of the longitudinal and transverse reinforcement, respectively, and
θ = angle of the inclined crack.

Table 11 also gives the crack spacing predicted by the CEB-FIP model. The measured and predicted crack spacings are compared in Figure 75. These comparisons illustrate that the average measured spacing was about half of the value predicted by the CEB-FIP procedure.

The length over which flexural cracks occurred and the average spacing for those cracks are listed in Table 12. In this table, L_w and L_e are the lengths of the distances from mid-span to the flexural crack that was closest to the west and east supports, respectively; L is the total length of the flexural cracking region; and N is the total number of flexural cracks. The average spacing of the flexural cracks, S, and the coefficient of variation are also presented. The mean of the average spacing is 5.56 inches (141 millimeters), with an average COV of 0.44. The average spacing of flexural cracks depends on the bond properties of the prestressing strands, which were reasonably constant throughout the tests. The largest average crack spacing was in Girder 6 (S = 7.80 inches), for which 10 strands were debonded on the west end of the girder. The girders that were loaded close to their flexural capacity, such as Girder 4, had the smallest average crack spacing, at 4.51 inches. The bottom bulb of Girder 10 was

Table 12. Average spacing of flexural cracks.

Girder End	L_w (in)	L_e (in)	L (in)	Crack Numbers N	Average Spacing S (in)	COV
G1	123.2	125.7	248.9	51	4.98	0.34
G2	220.1	200.3	420.4	93	4.57	0.40
G3	160.5	161.3	321.9	71	4.60	0.40
G4	209.7	232.3	442.0	99	4.51	0.45
G5	122.0	183.3	305.3	56	5.55	0.53
G6	130.0	127.4	257.4	34	7.80	0.52
G7	85.6	151.7	237.3	32	7.65	0.41
G8	135.3	157.8	293.1	59	5.05	0.50
G9	226.5	218.6	445.1	85	5.30	0.39
G10	246.8	245.6	248.9	-	-	-
				Average	5.56	0.44

- Not available.
L_w and L_e = lengths of the distances from mid-span to the flexural crack that was closest to the west and east supports, respectively.
L = total length of the flexural cracking region.
N = total number of flexural cracks.

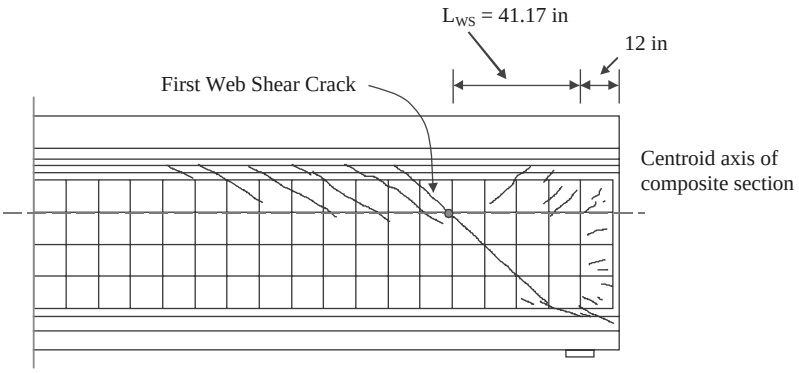

Figure 76. Location of first web-shear cracking at east end of Girder 1.

covered by a fiber-reinforced plastic sheet, so no flexure cracks were marked during the test.

2.5.4 Web-Shear Cracking

This section compares the loads and the angles of first diagonal cracking, as well as the angles for the primary web-shear cracks, with the web-shear cracking loads predicted using the AASHTO Standard Specifications and the angles of diagonal compression calculated from the LRFD Sectional Design Model.

The occurrence of the first diagonal crack is a significant event in the life of a structure because it signifies the point at which stirrups begin to significantly participate in the response and fatigue concerns must be evaluated. That cracking is also significant because it is often desirable, and sometimes required, that members remain uncracked under service loads in order to ensure durability of the structure. The first load stage was terminated when the first, very audible, web-shear crack occurred. It was also possible to verify the first cracking load by the sudden increased in stirrup strains that occurred. The first diagonal cracking often consisted of two or three diagonal cracks that appeared simultaneously. Figure 76 shows an example of first cracking for the east end of Girder 1(G1E). In this example, the first crack crossed the centroid of the composite section at an angle of 43 degrees. The intersection point was located at L_{ws} = 41.17 inches (1,046 millimeters) from the center of the east support.

Table 13 summarizes the measured web-shear cracking loads and the locations of the first web-shear crack from the center of the support for all girder tests. It can be seen that first

Table 13. First web-shear cracks.

Ends	Location L_{ws} (in)	Test		STD		$\frac{V_{test}}{V_{cw}}$
		Load (kips/ft)	V_{test} (kips)	f_{pc} (psi)	V_{cw} (kips)	
G1E	41.17	14.71	317.3	907.4	270.1	1.17
G1W	120.93	18.09	269.9	1086.6	313.8	0.86
G2E	47.03	18.51	390.2	903.8	268.2	1.45
G2W	64.66	21.74	426.4	1103.8	331.2	1.29
G3E	50.05	16.11	335.5	1224.0	328.3	1.02
G3W	71.44	14.96	284.9	1236.4	329.8	0.86
G4E	57.09	14.26	288.6	1036.7	307.7	0.94
G4W	63.33	15.44	304.5	1041.1	308.2	0.99
G5E	40.33	16.80	363.5	528.2	262.7	1.38
G5W	55.60	12.20	248.5	539.3	264.1	0.94
G6E	66.40	16.19	315.1	930.3	273.4	1.15
G6W	31.29	16.70	367.4	452.6	216.1	1.70
G7E	55.55	17.93	365.3	1058.2	287.8	1.27
G7W	48.66	18.90	395.9	1052.8	287.1	1.38
G8E	53.63	14.50	297.7	838.8	266.0	1.12
G8W	59.71	15.71	314.5	844.1	266.7	1.18
G9E	56.03	16.00	325.3	940.7	250.9	1.30
G9W	52.67	21.60	445.2	1100.5	301.2	1.48
G10E	55.34	15.57	317.5	759.3	233.7	1.36
G10W	40.05	19.30	418.0	1091.6	311.4	1.34
					Average	1.21
					COV	0.19

STD = AASHTO Standard Specifications.

cracking occurred within less than one girder depth (73 inches, or 1,854 millimeters) from the center of the support for all tests except G1W. In Table 13, the AASHTO Standard Specifications web-shear cracking load is given for each end of each girder, and a comparison is made with the measured cracking load. The mean of the shear strength ratio $V_{test}/V_{cw,STD}$ is 1.21, with COV of 0.19. It is apparent that the AASHTO Standard Specifications expression for V_{cw} provides a usually conservative and reasonably accurate prediction of the first web-shear cracking strength. Figure 77 shows the ratio of the measured web-shear cracking load to the design shear strength for all the test girders. Ratios range from 0.33 (for G4E) to 0.87 (for G5E). This is useful for assessing whether the member is likely to be cracked in shear under service load levels.

To assess the significance or lack of significance of this observation, it is useful to examine the derivation of the AASHTO Standard Specifications expression for web-shear cracking strength, V_{cw}.

$$V_{cw} = (3.5\sqrt{f'_c} + 0.30 f_{pc}) b_w d + V_p \quad (37)$$

Equation 37 was derived from the Mohr's circle of stress, with the state of stress taken as that at the centroidal axis of the girder and the tensile cracking strength of the concrete taken as approximately $4\sqrt{f'_c}$ where f'_c is in psi units. In this relationship, the cracking stress increases as a linear function of the applied precompression stress f_{pc}. For the calculated value of V_{cw} presented in Table 13, the full effective prestress force in the given location was used to compute f_{pc}, and d was taken as the distance from the top of the deck to the centroid of the strands in the bottom half of the girder. The value of d was usually larger than 63 inches. Because the first crack occurred close to the support and the prestressing was anchored in the bottom of the member, the actual f_{pc} at mid-depth is expected to be less than that used in the calculations, and yet the expression for V_{cw} was typically conservative. The apparent contradiction suggests that either the principal tensile stress is higher than $4\sqrt{f'_c}$ or the shear forces carried by the top flange and the bottom bulb are not negligible, or both.

Table 14 presents the measured and calculated angles of diagonal cracking. The predicted angle of diagonal cracking was calculated using Mohr's circle of stress, the full magnitude of f_{pc}, and Equation 38.

$$\cot\theta = \sqrt{1 + \frac{f_{pc}}{f_t}} \quad (38)$$

where:

$$f_t = 4\sqrt{f'_c}$$

The predicted angle of diagonal cracking was also calculated from a nonlinear finite element analysis Vector2 (*28*), as explained in Section 2.10.

The mean ratio of $\theta_{test}/\theta_{Mohr}$ is 1.21, with a COV of 0.10. The high mean value of 1.29 is to be expected given the likely overestimation of f_{pc}. The mean ratio of $\theta_{test}/\theta_{Vector2}$ is 1.21, with a COV of 0.09. There is a relatively close correlation between the angles of cracking predicted by the two procedures.

For a member with shear reinforcement, the more important angle of web-shear cracking is not at the end of the girder but at the first shear design span, because it is this latter angle that determines the effectiveness of the shear reinforcement. Figure 78 illustrates that the angle of diagonal cracking for much of this design shear span was reasonably constant. This first design shear span can be said to typically extend from about d distance away from the support to the point where web-shear cracking ends and flexure-shear cracking begins. The average angle for that crack average region was computed

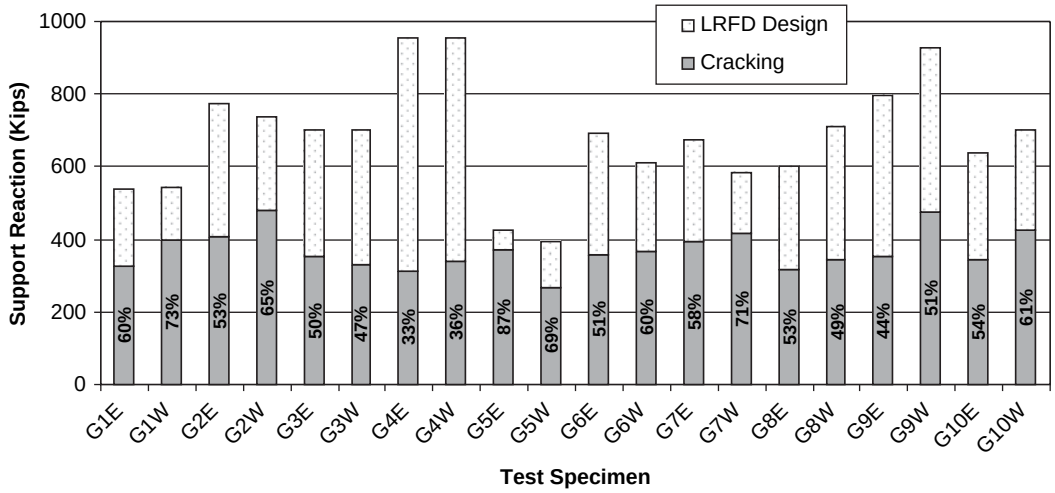

Figure 77. Ratio of the web-shear cracking load to the design shear strength.

Table 14. Crack angles of first web-shear cracks.

Girder End	f'_c (ksi)	θ_{test} (deg)	Mohr Circle			Vector2		
			f_{pc} (psi)	θ_{Mohr} (deg)	$\frac{\theta_{test}}{\theta_{Mohr}}$	f_{pc} (psi)	$\theta_{Vector2}$ (deg)	$\frac{\theta_{test}}{\theta_{Vector2}}$
G1E	12.1	43.0	907.4	29.7	1.45	622	32.8	1.31
G1W	12.1	30.0	1,086.6	28.2	1.06	1,108	28.1	1.07
G2E	12.6	38.0	903.8	29.9	1.27	880	30.2	1.26
G2W	12.6	37.0	1,103.8	28.3	1.31	1,194	27.6	1.34
G3E	15.9	38.0	1,224.0	28.4	1.34	950	30.5	1.25
G3W	15.9	28.0	1,236.4	28.3	0.99	1,143	29.0	0.97
G4E	16.3	35.0	1,036.7	29.9	1.17	1,034	29.9	1.17
G4W	16.3	34.0	1,041.1	29.8	1.14	1,109	29.3	1.16
G5E	17.8	43.0	528.2	35.3	1.22	348	37.9	1.14
G5W	17.8	35.0	539.3	35.2	0.99	531	35.3	0.99
G6E	12.7	38.0	930.3	29.7	1.28	1,252	27.2	1.40
G6W	12.7	46.0	452.6	35.2	1.31	397	36.1	1.27
G7E	12.5	32.0	1,058.2	28.6	1.12	1,069	28.5	1.12
G7W	12.5	38.0	1,052.8	28.6	1.33	920	29.8	1.28
G8E	13.3	36.0	838.8	30.8	1.17	1,186	27.9	1.29
G8W	13.3	33.0	844.1	30.7	1.07	1,186	27.9	1.18
G9E	9.6	35.0	940.7	28.5	1.23	982	28.1	1.25
G9W	9.6	35.0	1,100.5	27.1	1.29	1,153	26.7	1.31
G10E	10.6	35.0	759.3	30.7	1.14	883	29.4	1.19
G10W	10.6	35.0	1,091.6	27.6	1.27	1,072	27.8	1.26
				Average	1.21		Average	1.21
				COV	0.10		COV	0.09

for each girder end, and results are presented in Table 15. Equation 38 was also used for predicting the cracking angle in the same region. In this case, the use of that equation is more appropriate than for the end region because the full prestressing force must be effective. The mean ratio of $\cot\theta_{test}/\cot\theta_{Mohr}$ for this first shear design span was 1.06, with a COV of 0.16. The predicted angle matches reasonably well and slightly conservatively with that measured except for Girders 5 and 6.

It is also useful to compare the measured cracking angles with the LRFD Sectional Design Model's angle of diagonal compression, as presented in Table 5.8.3.4.2-1 of the second edition (1994) of the LRFD specifications. The mean ratio of $\cot\theta_{test}/\cot\theta_{LRFD}$ is 0.91, with a COV of 0.08. The average ratio

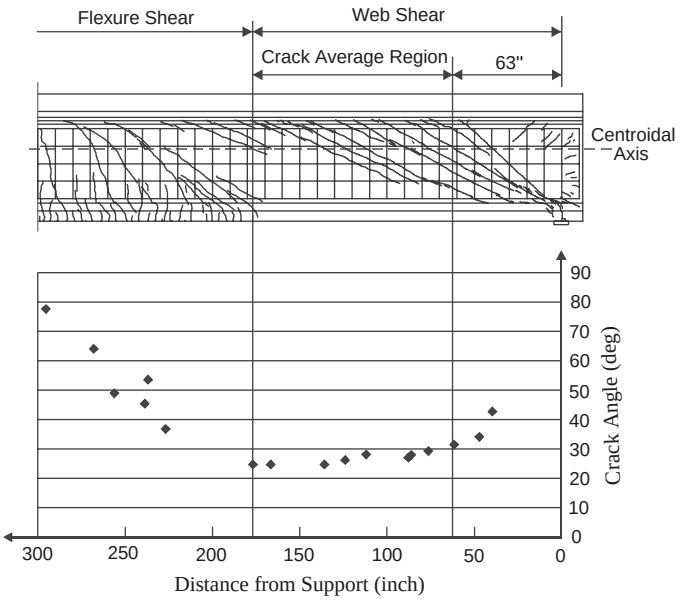

Figure 78. Average crack angle of web-shear cracks for G1E.

Table 15. Average crack angle for web-shear cracks.

Girder End	f'_c (ksi)	θ_{test} (deg)	Mohr Circle		LRFD	
			θ_{Mohr} (deg)	$\frac{\cot\theta_{test}}{\cot\theta_{Mohr}}$	θ_{LRFD} (deg)	$\frac{\cot\theta_{test}}{\cot\theta_{LRFD}}$
G1E	12.1	26.7	29.2	1.11	23.2	0.85
G1W	12.1	28.4	27.8	0.98	24.9	0.86
G2E	12.6	28.5	29.8	1.05	25.5	0.88
G2W	12.6	30.9	28.2	0.90	27.8	0.88
G3E	15.9	26.1	27.5	1.06	23.7	0.90
G3W	15.9	27.1	27.5	1.02	23.7	0.86
G4E	16.3	28.7	28.8	1.00	28.5	0.99
G4W	16.3	30.7	28.8	0.93	28.5	0.91
G5E	17.8	23.7	33.9	1.53	21.8	0.91
G5W	17.8	25.6	33.9	1.40	21.8	0.83
G6E	12.7	28.2	28.7	1.02	23.7	0.82
G6W	12.7	26.4	32.3	1.27	25.9	0.98
G7E	12.5	25.8	26.8	1.04	24.2	0.93
G7W	12.5	25.5	26.8	1.06	24.2	0.94
G8E	13.3	27.7	28.4	1.03	23.7	0.84
G8W	13.3	28.3	28.4	1.00	23.7	0.82
G9E	9.6	28.5	28.3	0.99	32.8	1.19
G9W	9.6	32.2	27.1	0.81	30.0	0.92
G10E	10.6	29.4	29.2	0.99	28.8	0.98
G10W	10.6	28.3	26.8	0.94	27.6	0.97
			Average	1.06	Average	0.91
			COV	0.16	COV	0.08

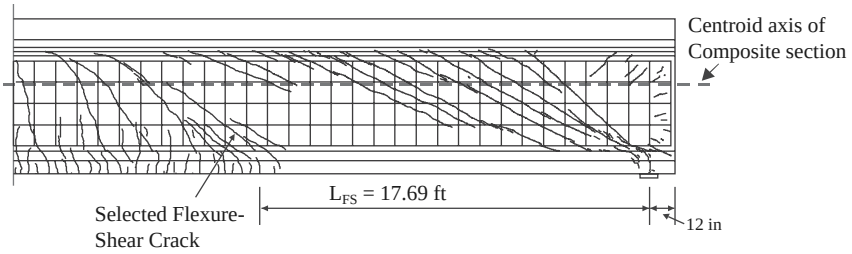

Figure 79. Location of selected flexure-shear crack for evaluation at G1E.

of 0.91 suggests that the LRFD specifications are unconservative for estimating the angle of diagonal compression, and therefore for evaluating the contribution of the shear reinforcement, if the angle of diagonal compression and that of cracking are equivalent.

These comparisons of the angles of cracking in the end region of the girder and in the first shear design region beyond that end region demonstrate the appropriateness of the LRFD specifications Article 5.8.1, which require the designer to differentiate between shear design for flexural regions (the first shear design region) and regions near discontinuities. The latter region can be defined as the portion of the girder within one overall girder depth from the centerline of the support, as shown in Figure 78.

2.5.5 Flexure-Shear Cracking

This section examines the measured loads for flexure-shear cracking and the angles of those cracks. Consistent with their name, flexure-shear cracks develop from the extension of flexural cracks in regions of high flexure and significant shear. They extended in the region from the end of the web-shear cracking region to near mid-span. The occurrence of flexure-shear cracking is indicated by a rapid change in stirrup strain gage readings. For each half of the girder, the flexure-shear crack that was farthest from mid-span was selected for examination. Figure 79 shows the selected flexure-shear crack for the east end of Girder 1, in which the crack location is reported as the distance, L_{FS}, from the center of the support to the location of the flexural crack from which the flexure-shear crack formed. Table 16 lists the selected flexure-shear crack's position, its angle, the distributed load at cracking, and the moment and shear forces at the location of the flexural crack from which that selected flexure-shear crack originated. The measured angles for flexure-shear cracking range from 30.2 degrees to 60.8 degrees. The occurrence of very steep shear cracks may be of concern if the member is limited by its shear capacity in this region

Table 16. Flexure-shear cracks.

Girder End	Position L_{FS} (ft)	Test				STD		M/M_{cr}	V/V_{ci}
		Angle (deg)	Load (kips/ft)	M (k-ft)	V (kips)	M_{cr} (k-ft)	V_{ci} (kips)		
G1E	17.68	51.3	24.13	6,785.9	176.6	5,628.0	182.2	1.21	0.97
G1W	14.71	46.4	26.34	6,718.2	271.0	5,388.9	255.7	1.25	1.06
G2E	12.46	34.6	26.82	6,151.8	336.3	6,340.3	388.6	0.97	0.87
G2W	12.16	39.0	26.82	6,049.7	344.4	5,996.2	382.6	1.01	0.90
G3E	15.18	39.4	28.634	7,439.4	281.1	6,996.6	306.7	1.06	0.92
G3W	15.96	42.8	28.634	7,649.3	258.9	6,985.8	277.8	1.09	0.93
G4E	10.70	31.3	31.8	6,544.4	454.6	7,270.2	553.0	0.90	0.82
G4W	11.08	30.2	31.04	6,552.6	432.1	7,262.1	526.4	0.90	0.82
G5E	13.39	31.1	16.59	3,991	192.7	5,222.7	299.4	0.76	0.64
G5W	18.57	59.8	19.97	5,737.9	128.4	5,151.2	156.5	1.11	0.82
G6E	14.36	35.8	34.08	6,255.3	288.9	7,892.4	557.9	0.79	0.74
G6W	15.09	39.6	34.09	6,257.1	411.2	5,614.9	413.5	1.11	0.99
G7E	16.06	38.0	31.85	8,537.7	284.8	7,690.8	294.3	1.11	0.97
G7W	13.11	37.0	32.24	7,650.2	383.3	7,738.3	429.0	0.99	0.89
G8E	16.01	39.9	35.5	7,720.8	288	7,535.1	319.7	1.02	0.90
G8W	16.82	36.2	35.5	8,791.6	233.5	7,524.0	237.6	1.17	0.98
G9E	12.05	35.0	23.49	5,265.3	304.2	6,116.3	392.7	0.86	0.77
G9W	13.06	41.4	24.3	5,752.3	290.1	5,992.9	340.2	0.96	0.85
G10E	14.64	46.2	22.87	5,815.6	236.8	5,337.7	254.7	1.09	0.93
G10W	17.38	60.8	22.01	6,139.4	167.7	6,412.8	209.6	0.96	0.80
							Average	1.02	0.88
							COV	0.13	0.11

because there will then be fewer stirrups carrying the load than would be calculated by either the AASHTO Standard Specifications or the LRFD specifications.

In Table 16, the flexure-shear cracking loads calculated by the AASHTO Standard Specifications are also presented and compared with the measured values. In the AASHTO Standard Specifications, the flexure-shear cracking strength, V_{ci}, is calculated by Equation 39.

$$V_{ci} = 0.6\sqrt{f'_c}\, b_w d + V_d + \frac{V_i M_{cr}}{M_{\max}} \tag{39}$$

where:

$$M_{cr} = (I / y_t)(6\sqrt{f'_c} + f_{pe} - f_d) \tag{40}$$

where:

I = moment of inertia of the section resisting externally applied factored loads.

In this relationship, V_{ci} consists of three terms. The sum of the latter two is the shear force corresponding to flexural cracking, and the first term is the increment in shear force that is expected to lead to the formation of a shear crack from the flexure crack. When computing the flexure-shear strength, the flexural cracking stress is taken as $6\sqrt{f'_c}$ (in psi units).

The shear force V_{test} for the crack selected for evaluations of the flexure-shear cracking load was computed at the section L_{FS} from the centerline of the adjacent support. (L_{FS} is the distance from the center of the support to the location of the flexural crack.) The mean ratio of the test shear force V_{test} to the predicted shear cracking strength V_{ci} is 0.88, with a COV of 0.11. Therefore, the AASHTO Standard Specifications are somewhat unconservative for most of the test results. In the second-to-last column of Table 16, the ratio of the moment at the location of the selected flexure-shear crack (M) to the calculated cracking moment (M_{cr}) for the same location is given. The mean ratio is 1.02, with a COV of 0.13. Since the flexure-shear crack typically formed as the extension of a flexural crack, the flexural cracking strength is reasonably well predicted by using a cracking stress of $6\sqrt{f'_c}$ (in psi units). This result also implies that the unconservatism of the V_{ci} expression of the AASHTO Standard Specifications is the result of an unconservatism in the first term of Equation 39 for beams with depths like those of the test girders.

2.5.6 Flexural Cracking

Table 17 compares measured and computed flexural cracking loads. To assess when flexural cracking occurred, a linear variable displacement transducer (LVDT) was attached to the bottom bulb at mid-span to measure the change in displacement over the central 48 inches of the span. Columns 2 through 4 in this table list the distributed load at first cracking, the average strain measured by the bottom LVDT, and the corresponding cracking moment.

Table 17. Flexure cracks and flexural cracking moment.

Girder End	Test			AASHTO Standard Specifications		$\frac{\varepsilon_{Test}}{\varepsilon_{STD}}$	$\frac{M_{cr,Test}}{M_{cr,STD}}$
	Load (kips/ft)	Strain ε (10^{-6})	M_{cr} (k-ft)	Strain ε (10^{-6})	M_{cr} (k-ft)		
G1	19.56	661.1	6,024.5	782.6	6,385.8	0.84	0.94
G2	21.56	683.1	6,641.5	757.0	7,157.6	0.90	0.93
G3	23.14	724.9	7,127.1	961.6	7,984.3	0.75	0.89
G4	26.28	667.6	8,094.2	956.9	10,081.0	0.73	0.83
G5	16.75	508.7	5,159.0	696.4	5,734.2	0.73	0.90
G6	23.70	703.4	7,298.5	1,089.6	8,878.4	0.65	0.82
G7	23.27	808.3	7,167.2	1,299.2	8,795.1	0.62	0.81
G8	25.70	802.7	7,915.6	1,244.3	8,662.2	0.65	0.91
G9	20.21	634.3	6,224.7	865.5	6,770.9	0.73	0.92
G10	20.01	777.3	6,163.1	1,094.3	7,307.5	0.71	0.84
					Average	0.73	0.88
					COV	0.12	0.06

Both AASHTO Standard Specifications and LRFD specifications take the modulus of rupture f_r as $7.5\sqrt{f'_c}$ in computing the cracking moment. Table 17 also lists the predicted cracking moment and the predicted horizontal strain increase for calculations using the AASHTO Standard Specifications. The predictions were based on the prestressing strains measured before testing and take into account the strain changes in the strands due to the external loading. The average ratio of the measured to predicted cracking strain is 0.73, with a COV of 0.12, and the average ratio of the measured to predicted cracking moment is 0.88, with a COV of 0.06. The comparison shows that the cracking moment prediction fits the test result well, but it also suggests that a better fit would be obtained if the modulus of rupture f_r were taken as less than $7.5\sqrt{f'_c}$.

2.5.7 Crack Widths

This section summarizes measured crack widths. The growth in crack widths is important for a number of reasons. In the LRFD model, the concrete contribution to shear resistance is limited by the slip resistance along cracks. This interface shear transfer resistance, also referred to as "aggregate interlock," is a function of the width and smoothness of shear cracks. The expression used in the derivation of the LRFD specifications is shown as Equation 41 (*29*).

$$v_{ci} = \frac{2.16\sqrt{f'_c}}{0.31 + \frac{24w}{a + 0.63}} \text{ (in inches and psi)} \tag{41}$$

According to this expression, the interface transfer resistances for crack widths of 0.012, 0.024, and 0.04 inch (0.3, 0.6, and 1.0 millimeter) are 63 percent, 43 percent, and 31 percent, respectively, of the shear slip resistance of a hairline crack of width 0.002 inch (0.05 millimeter). These values were

calculated using a maximum aggregate size of 0.50 inch. It has been suggested that for very high-strength concrete, cracks are so smooth that the aggregate size should be taken as zero in the use of Equation 39. If this is done, then the drop in shear resistance is even more sensitive to crack width, with only 51 percent, 32 percent, and 21 percent of the resistances being available at crack widths 0.012, 0.024, and 0.04 inch (0.3, 0.6, and 1.0 millimeter), respectively, as was available along a hairline crack of width 0.002 inch (0.05 millimeter). Crack width is also important for evaluating the durability of a member. The PCI Bridge Committee guidelines suggested that cracks of up to 0.006 inch (0.15 millimeter) are generally considered acceptable, while once a crack exceeds 0.0012 inch (0.3 millimeter), repair using epoxy grouting techniques are warranted to protect the reinforcement from salt water penetration and corrosion. In heavily cracked members, the combination of average crack width and crack spacing can be used for assessing the principal tensile strain in the member because the elastic tensile strain in concrete at cracking is very small.

During the experiments, crack widths were measured using a crack comparator gage at each load stage. Prefabricated crack width markings were then taped beside the associated cracks, and this information was recorded in pictures. The crack widths were measured in millimeters because of the ready availability of crack comparator gages. This process is illustrated in Figure 80.

Table 18 summarizes the development of crack widths with increasing load. At each load stage for each girder, the maximum crack width in the web-shear zone, the flexure-shear zone, and the flexural zone was recorded. Crack widths are given in millimeters. Figure 81 shows the growth of the web-shear cracks with loading. The maximum measured crack width is plotted on the x-axis, while the external test load is plotted on the y-axis. The results from the 20 web-shear regions were classified into five groups according to the different effective stirrup strengths, $\rho_v f_{yv}$. The first group (Girders 1 and 5) had low $\rho_v f_{yv}$ values that ranged from 140 psi to 389 psi, the second group (Girders 3 and 6) and the third group (Girders 7 and 8) had average $\rho_v f_{yv}$ ranging from 557 to 577 psi. The fourth group (Girders 2 and 10) had moderately high $\rho_v f_{yv}$ values ranging from 745 to 751 psi. The last group (Girders 4 and 9) had the highest $\rho_v f_{yv}$ values ranging from 1,040 to 1,113 psi. It can be seen from Figure 81 that once cracking occurred, the maximum crack width reached between 0.3 millimeters and 0.5 millimeters. The low $\rho_v f_{yv}$ values were associated with the higher maximum crack width values.

The measured maximum flexure-shear crack widths are shown in Figure 82. Compared with web-shear crack plots of Figure 81, the plots of Figure 82 show that the flexure-shear cracks opened faster with increasing load once flexure-shear cracking had occurred. The maximum crack width for the flexure-shear region of G7W was larger than the maximum flexure-shear crack widths for other girders because of the low amount of stirrup reinforcement in G7W (119 psi).

The maximum flexural cracks measured are plotted in Figure 83, with the vertical axis being M for Figure 83(a) and M/M_{cr} for Figure 83(b), where M_{cr} was calculated using a tensile fiber cracking stress of $7.5\sqrt{f'_c}$ (in psi units). As discussed previously, flexural cracking occurred a little earlier than predicted, as apparent from the initial M/M_{cr} values plotted in Figure 83(b). The plots of Figure 83 show that after flexural cracking occurred, the maximum crack width increased linearly with increasing external moment.

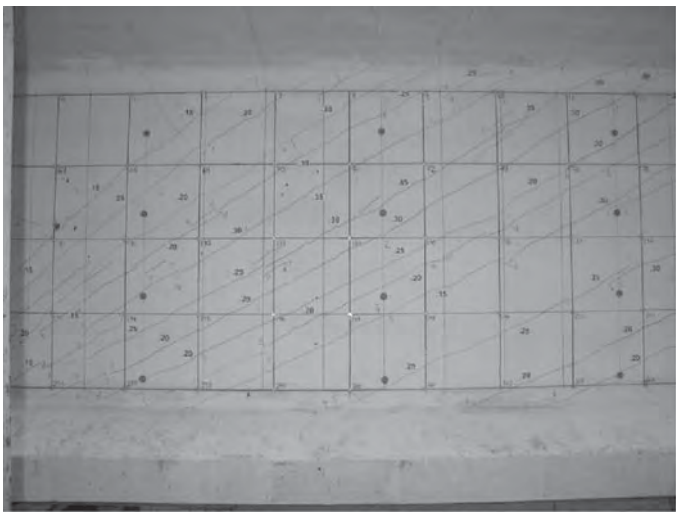

Figure 80. Crack measurement.

2.5.8 Summary of Primary Observations

From the comparison of measured values with (a) cracking loads calculated using the AASHTO Standard Specifications, (b) crack angles calculated using Mohr's circle of stress and angles of diagonal compression calculated using the LRFD specifications, and (c) crack spacings predicted using the CEB-FIP model, some of the key observations are as follows:

- Typically, web-shear cracks occurred very suddenly, along straight lines, and with a significantly loud "pop."
- The first web-shear crack usually occurred within a longitudinal distance equal to the overall height of the member from the center of the support. This shear cracking was within a region of discontinuity, as defined by Article 5.8.1.2 of the LRFD specifications. These web-shear cracks had angles ranging from 28 degrees to 46 degrees, with an

Table 18. Maximum crack width at each load stage for each girder.

Girder 1

Load (kips/ft)	West		Mid	East	
	WS (mm)	FS (mm)	F (mm)	FS (mm)	WS (mm)
14.71	0.00	0.00	0.00	0.00	0.25
18.79	0.00	0.00	0.00	0.00	0.35
19.11	0.35	0.00	0.00	0.00	0.40
19.96	0.40	0.00	0.00	0.00	0.40
21.17	0.40	0.00	0.05	0.00	0.50
22.52	0.40	0.00	0.05	0.00	0.55
23.67	0.40	0.05	0.10	0.10	0.80
24.56	0.40	0.15	0.15	0.30	1.0
26.03	>0.40	>0.15	>0.15	>0.30	>1.0
26.59	0.50	0.30	0.25		
27.44	0.75	0.50	0.25		
28.75	1.00	0.55	0.30		
30.09	>1.00	>0.55	>0.30		

Girder 2

Load (kips/ft)	West		Mid	East	
	WS (mm)	FS (mm)	F (mm)	FS (mm)	WS (mm)
18.79	0.00	0.00	0.00	0.00	0.40
21.74	0.30	0.00	0.00	0.00	0.40
25.94	0.40	0.10	0.05	0.10	0.45
28.94	0.40	0.15	0.10	0.20	0.45
30.36	0.50	0.75	0.20	0.60	0.60
33.79	>0.50	>0.75	>0.20	>0.60	>0.60
38.34	0.80	0.85	0.40		
38.74	>0.80	>0.85	>0.40		

Girder 3

Load (kips/ft)	West		Mid	East	
	WS (mm)	FS (mm)	F (mm)	FS (mm)	WS (mm)
14.96	0.20	0.00	0.00	0.00	0.00
16.17	0.30	0.00	0.00	0.00	0.20
18.83	0.30	0.00	0.00	0.00	0.30
22.79	0.30	0.00	0.00	0.00	0.35
26.05	0.30	0.00	0.05	0.00	0.35
29.29	0.35	0.25	0.10	0.25	0.50
32.4	0.45	0.40	0.15	0.40	0.55
35.68	0.45	0.40	0.15	0.40	>0.55
33.23	0.45	0.40	0.15		
38.82	0.50	0.45	0.20		

Girder 4

Load (kips/ft)	West		Mid	East	
	WS (mm)	FS (mm)	F (mm)	FS (mm)	WS (mm)
17.63	0.15	0.00	0.00	0.00	0.15
21.61	0.15	0.00	0.00	0.00	0.25
26.90	0.20	0.00	0.00	0.00	0.30
30.61	0.25	0.05	0.10	0.15	0.30
34.73	0.25	0.25	0.15	0.25	0.35
42.65	0.30	0.80	0.35	0.80	0.55
42.74	0.30	0.80	0.35	0.80	0.55

Girder 5

Load (kips/ft)	West		Mid	East	
	WS (mm)	FS (mm)	F (mm)	FS (mm)	WS (mm)
12.20	0.50	0.00	0.00	0.00	0.00
13.10	0.75	0.00	0.00	0.00	0.00
15.40	1.50	0.00	0.00	0.00	0.00
16.80	1.50	0.00	0.00	0.00	0.75
18.20	1.75	0.10	0.15	0.10	1.00
18.70	2.50	0.20	0.15	0.20	1.50
19.90	>2.50	>0.20	>0.15	>0.20	>1.50
20.95			0.30	0.40	2.00
22.07			0.35	0.60	2.50
23.24			0.40	0.70	3.00
23.70			>0.40	>0.70	>5.00

Girder 6

Load (kips/ft)	West		Mid	East	
	WS (mm)	FS (mm)	F (mm)	FS (mm)	WS (mm)
17.27	-	0.00	0.00	0.00	-
19.80	0.40	0.00	0.00	0.00	0.40
23.90	-	0.00	0.00	0.00	-
27.40	0.70	0.10	10.00	0.05	0.60
27.85	-	-	-	-	-
27.67	>0.70	>0.10	-	-	-
30.00			0.10	0.10	0.70
29.72			-	-	0.70
37.30			0.15	0.15	10
38.32			>0.15	>0.15	>1.0

Girder 7

Load (kips/ft)	West		Mid	East	
	WS (mm)	FS (mm)	F (mm)	FS (mm)	WS (mm)
18.10	0.00	0.00	0.00	0.00	0.30
18.90	0.30	0.00	0.00	0.00	0.30
24.40	0.35	0.00	0.00	0.00	0.40
31.23	0.50	0.10	0.15	0.10	0.75
32.27	0.75	0.15	0.15	0.20	0.90
33.47	>0.75	>0.15	>0.15	>0.20	>0.90
36.20	0.75	0.70	0.15		
40.57	1.00	1.00	0.15		
43.40	1.20	1.00	0.25		
44.75	>1.20	>1.00	>0.25		

Girder 8

Load (kips/ft)	West		Mid	East	
	WS (mm)	FS (mm)	F (mm)	FS (mm)	WS (mm)
14.71	0.00	0.00	0.00	0.00	0.20
18.20	0.30	0.00	0.00	0.00	0.35
21.50	0.35	0.00	0.00	0.00	0.35
23.65	0.40	0.00	0.00	0.00	0.35
26.44	0.60	0.00	0.00	0.00	0.40
27.90	0.70	0.00	0.05	0.00	0.40
32.70	1.20	0.05	0.05	0.00	0.50
35.50			0.15	0.10	0.75
38.60			0.20	0.30	0.75
40.20			0.20	0.40	1.00
43.00			>0.20	0.40	1.50
43.73			>0.20	>0.40	>1.50

Table 18. (Continued).

Girder 9

Load (kips/ft)	West		Mid	East	
	WS (mm)	FS (mm)	F (mm)	FS (mm)	WS (mm)
17.90	0.00	0.00	0.00	0.00	0.30
22.12	0.10	0.10	0.10	0.15	0.30
25.80	0.15	0.30	0.15	0.30	0.30
30.80	0.20	0.40	0.20	0.45	0.30
32.80	0.20	0.40	0.30	0.45	0.50
37.19	0.30	0.40	>0.30		

Girder 10

Load (kips/ft)	West		Mid	East	
	WS (mm)	FS (mm)	F (mm)	FS (mm)	WS (mm)
15.84	0.00	0.00	0.00	0.00	0.30
20.21	0.20	0.00	0.00	0.00	0.40
22.54	0.30	0.15	N/A	0.20	0.45
23.91	0.30	0.15	N/A	0.20	0.45
26.43	0.30	0.30	N/A	0.25	0.50
29.12	0.30	0.30	N/A	0.30	0.50
31.59	0.30	0.30	N/A	0.40	0.75
33.93	0.30	0.30	N/A	0.40	1.00
33.68	0.40	0.75	N/A		
36.46	0.50	0.80	N/A		
38.56	0.55	1.00	N/A		
42.85	>0.55	>1.00	N/A		

Note: A blank cell indicates that no information was possible at that load level because the associated end of the girder had already failed. A dash indicates that the researchers did not take the measurement at that load stage. "N/A" indicates that the information was not available to be taken.

average angle of 36.2 degrees. The closer the crack was to the end of the member, the steeper was the crack angle.

- The angle of web-shear diagonal cracking in the first shear design region (a flexural region in the terms of Article 5.8.1.1 of the LRFD specifications) was reasonably constant and substantially flatter than the first web-shear crack. The crack angles ranged from 23 degrees to 32 degrees, with an average angle of 27.8 degrees.
- The angle of shear cracking over the length of the member went from close to 45 degrees near the support, to a

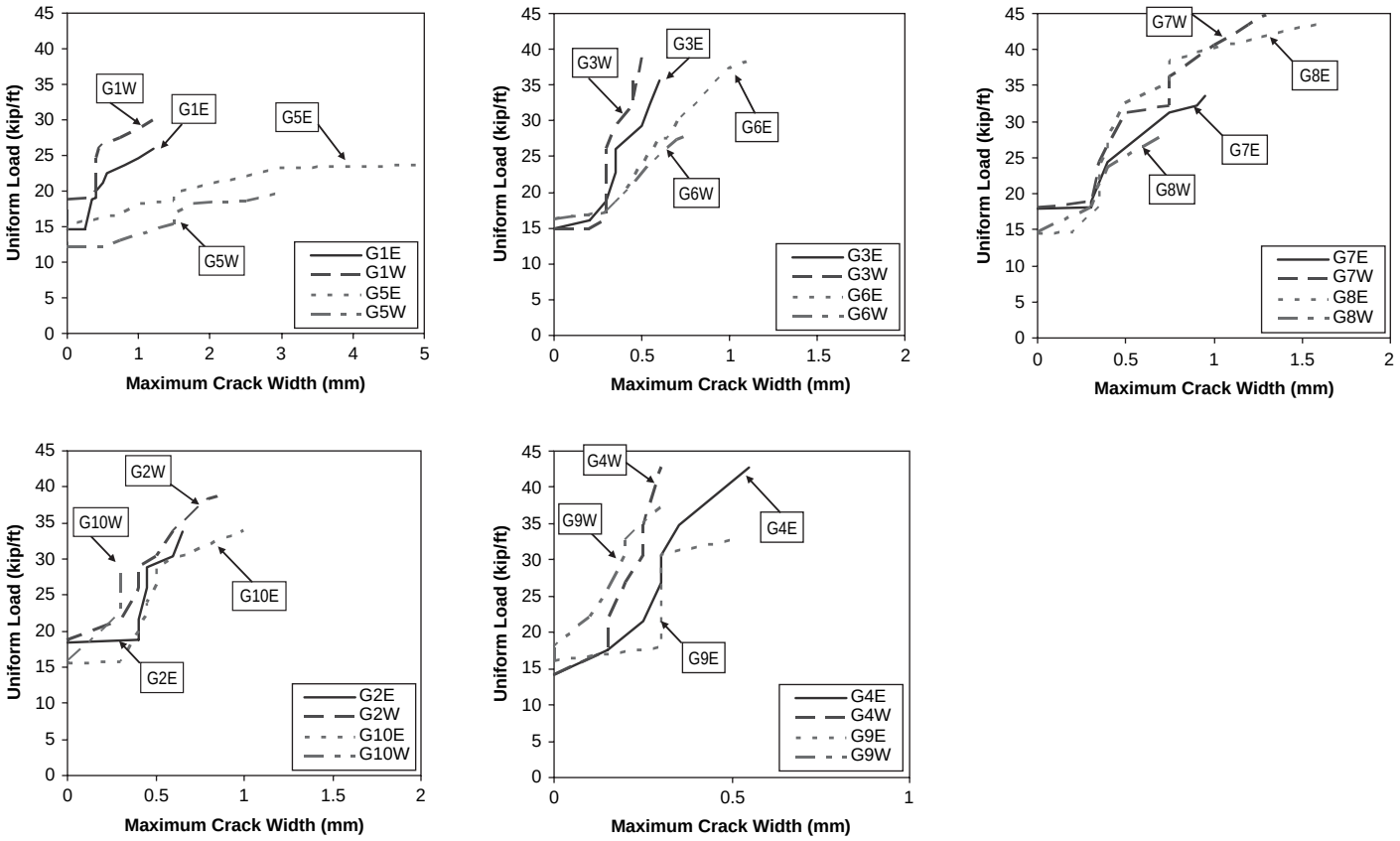

Figure 81. Maximum crack width of the web-shear cracks.

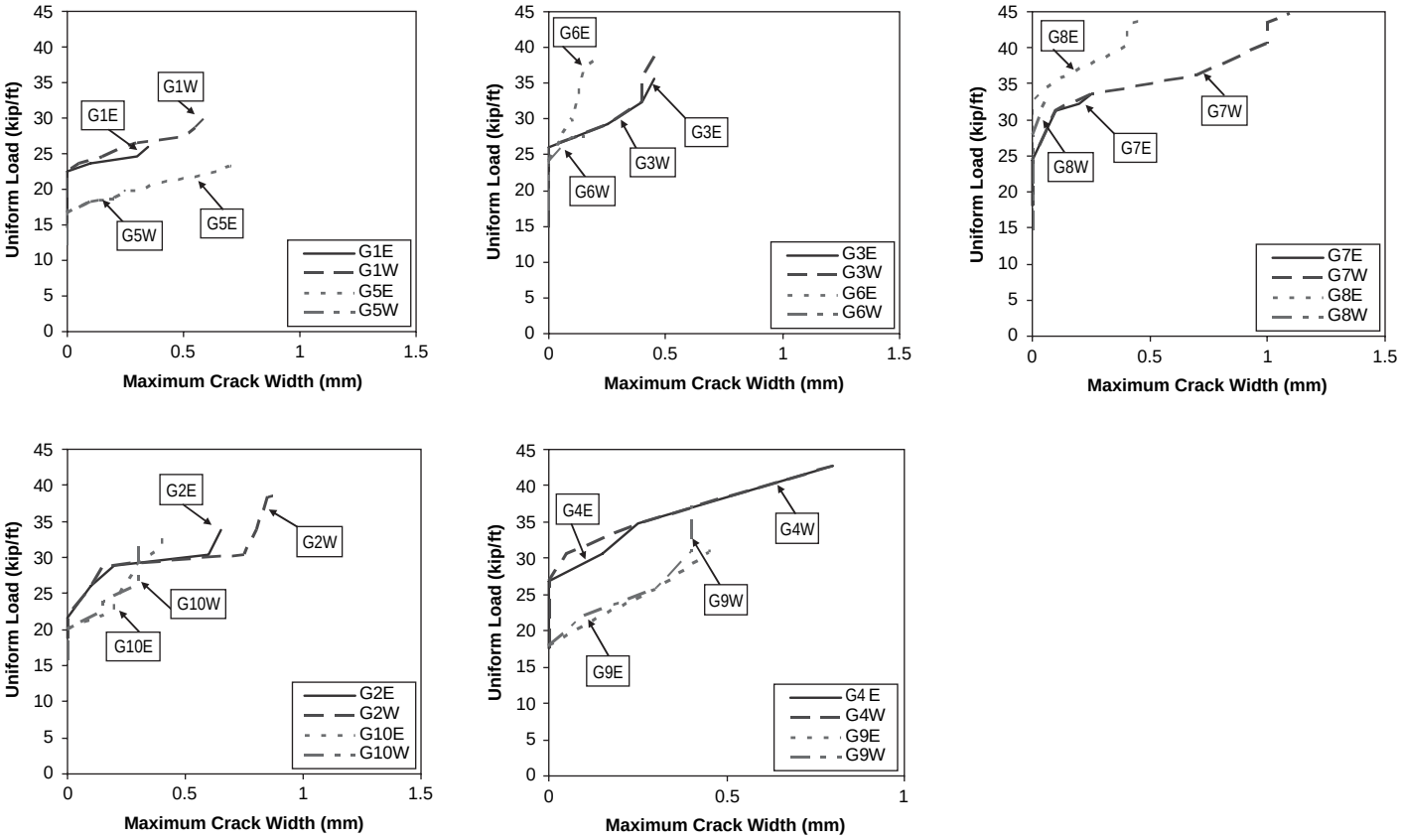

Figure 82. Maximum crack width of the flexure-shear cracks.

constant value in the web-shear region, to an increasing quadratic curve relationship in the flexure-shear region, and to almost 90 degrees at mid-span.

- The angle of diagonal cracking could be accurately predicted using Mohr's circle of stress.
- The angle of diagonal cracking in the first shear design region was typically a little steeper than the angle of diagonal compression calculated from Table 5.8.3.4.2-1 of the LRFD Sectional Design Model. Consequently, the LRFD method may overestimate the contribution of shear reinforcement unless there are significant shear stresses acting on the faces of the cracks.
- The angle of potentially critical flexure-shear cracks can be up to 60 degrees, which suggests that the contribution of

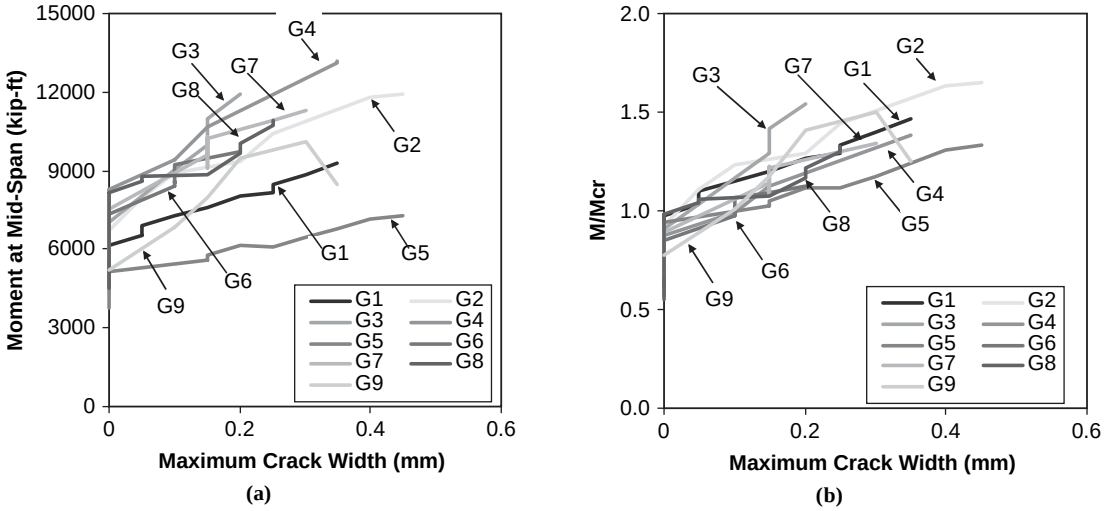

Figure 83. Maximum crack width of flexure cracks.

shear reinforcement by most codes of practice is likely to be overestimated in these regions.
- The spacing of shear cracks in the web was on average about half of the values predicted using the CEB-FIP expression for crack spacing.
- The AASHTO Standard Specifications provided a reasonably accurate and somewhat conservative estimate of the web-shear cracking load, V_{cw}, even when the full value of f_{pc} was used in the calculations. It is to be expected that the longitudinal stress in the concrete at the centroidal axis will be less than f_{pc} because the axial compressive force takes up to the last 30 inches in length of the bottom bulb to be fully transferred into the girder.
- First web-shear cracking was observed to occur at between 33 percent and 87 percent of the LRFD shear design stress. Values can be a much lower percentage of the shear design stress than would have been possible with the use of the AASHTO Standard Specifications. The low percentages are possible because the LRFD specifications permit members to be designed for shear stresses up to $0.25f'_c$.
- The AASHTO Standard Specifications marginally overestimated the flexure-shear cracking loads V_{ci}.
- The flexural cracking loads were reasonably well predicted by M_{cr} when the tensile cracking stress was taken as $7.5\sqrt{f'_c}$ (in psi units).
- Upon initiation of web-shear cracking, the first measured web-shear crack width ranged from 0.3 millimeter to 0.5 millimeter. The initial crack widths were larger for members with less shear reinforcement. Flexure-shear cracks opened faster than web-shear cracks once flexure-shear cracking occurred. After flexural cracking occurred, the maximum crack width increased linearly with increasing external moment.

2.6 Reinforcement and Other Strains

This section summarizes the measured strains in the reinforcing steel, as well as the longitudinal strains in the concrete at mid-depth and the shear strains. Section 2.6.1 introduces the value and challenge of measuring reinforcement strains. Section 2.6.2 describes the development of stirrup strains in the west half of Girder 3. Sections 2.6.3 and 2.6.4 summarize the measured strains in the web-shear regions and flexure-shear regions, respectively, for all girder tests. Section 2.6.5 presents longitudinal reinforcement strains, and Section 2.6.6 presents strains in the confinement reinforcement. Section 2.6.7 presents the measured longitudinal strains at mid-depth, ε_x, and compares these values with the development of longitudinal strains as calculated by the general method of the LRFD specifications. Section 2.6.8 presents the shear stress versus shear strain response of the test girders and provides a relationship for predicting shear stiffness that is derived from the test data. Section 2.6.9 compares measured and LRFD-predicted time-dependent losses, and Section 2.6.10 compares measured and LRFD-predicted transfer lengths.

2.6.1 Introduction

Measuring stirrup strains is useful for identifying when cracking first occurs, for evaluating the contribution of stirrup reinforcement to capacity, for determining when cracks are rapidly opening, for assessing the strength of the bond between concrete and reinforcement, for evaluating fatigue concerns, and for measuring the magnitude of fracture energy release. One of the challenges to assessing stirrup strains is that these reinforcement strains at crack locations are usually much larger than reinforcement strains between cracks because between cracks, particularly in HSC members, the concrete has the capacity to carry significant tensile stress. Consequently, to accurately assess the strain in an individual stirrup, it is necessary to measure the strain at multiple points over the height of a stirrup. In this research program, strain gages were attached to the stirrups at 6, 17, 28, and 39 inches from the bottom of the 45-inch deep web. The girders were designed for shear by the LRFD specifications so that they were, according to the LRFD design philosophy, just as likely to fail in a region of low shear and high moment as they were in a region of high shear and low moment. Thus, as shown in Figure 54, selected stirrups were gauged over the entire length of the test girder, with between 14 and 20 stirrups being gauged on each girder.

Measuring the strains in the longitudinal reinforcement before testing is useful for assessing the level of precompression due to prestressing and for measuring prestressing losses due to shrinkage and creep. During a test, this measuring is also useful for assessing the demands placed on the longitudinal tension reinforcement due to flexure and shear. In this program, strains were measured on the longitudinal reinforcement in the confinement cages and on larger deformed bar reinforcement that was required by the LRFD specifications for some girder designs in order to provide the necessary longitudinal tensile capacity. The locations for these gages are shown in Figure 55 and in the appendices.

Measuring strains on confinement reinforcement prior to loading is useful for assessing the level of confinement developed following strand release and for determining the confinement available to help anchor the strands. Measuring strains during testing is useful for helping to identify whether slip is occurring and for correlating behavior with the demands placed on longitudinal tensile reinforcement and other effects. In this research program, 20 gages, 10 on each end, were attached to the confinement reinforcement. The locations for these gages are shown in Figure 55 and in the appendices.

2.6.2 Stirrup Reinforcement Strains in the West Half of Girder 3

Figure 84 summarizes the development of strains in the west end of Girder 3. Figure 84(a) shows the locations of the strain gages on Stirrups S2, S3, and so forth through S8, with the four gages on each stirrup numbered sequentially from the bottom to the top of the stirrup. The web-shear and flexure-shear regions for each girder were defined from the measured pattern of cracking. If a given stirrup extended across both web-shear and flexure-shear cracks, then only those gages crossing each pattern or crack were counted as part of that region. The development of the strains in each stirrup in the web-shear region, Stirrups S2 through S5, is shown in Figure 84(b). From Figures 84(a) and 84(b), the following observations can be made:

- Prior to first cracking, the strains in the stirrups were small, less than 30 microstrain, which corresponds to a stress of less than 1 ksi. A large portion of this strain must be due to a Poisson's effect from the significant diagonal compression in the web of the girder. The strain expected to lead to first cracking, not including strains due to Poisson's effect, was 60–100 microstrain.
- Immediately after occurrence of web-shear cracking, the first web-shear crack was at 14.96 kips/ft, and strains in some gages jumped to very close to the yield strain.
- With the development of additional web-shear cracks, similarly large jumps in stirrup strains were observed.
- There was a dramatic variation in strain in some stirrups, with a gage near a crack measuring the yield strain while a gage farther from the same crack measured very little strain. For example, for the gages on Stirrup 3, shortly after first diagonal cracking, one gage measured about 3,500 microstrain (well above yield), while the other three gages were all less than 100 microstrain (less than 5 percent of the yield).
- As the magnitude of the strains increased, particularly beyond yield, the ratio of the maximum to minimum strain in a stirrup decreased.
- Along a given critical crack line in a field of diagonal cracking, where cracks are close to parallel and of similar widths, it is to be expected that the strain in the stirrups across this

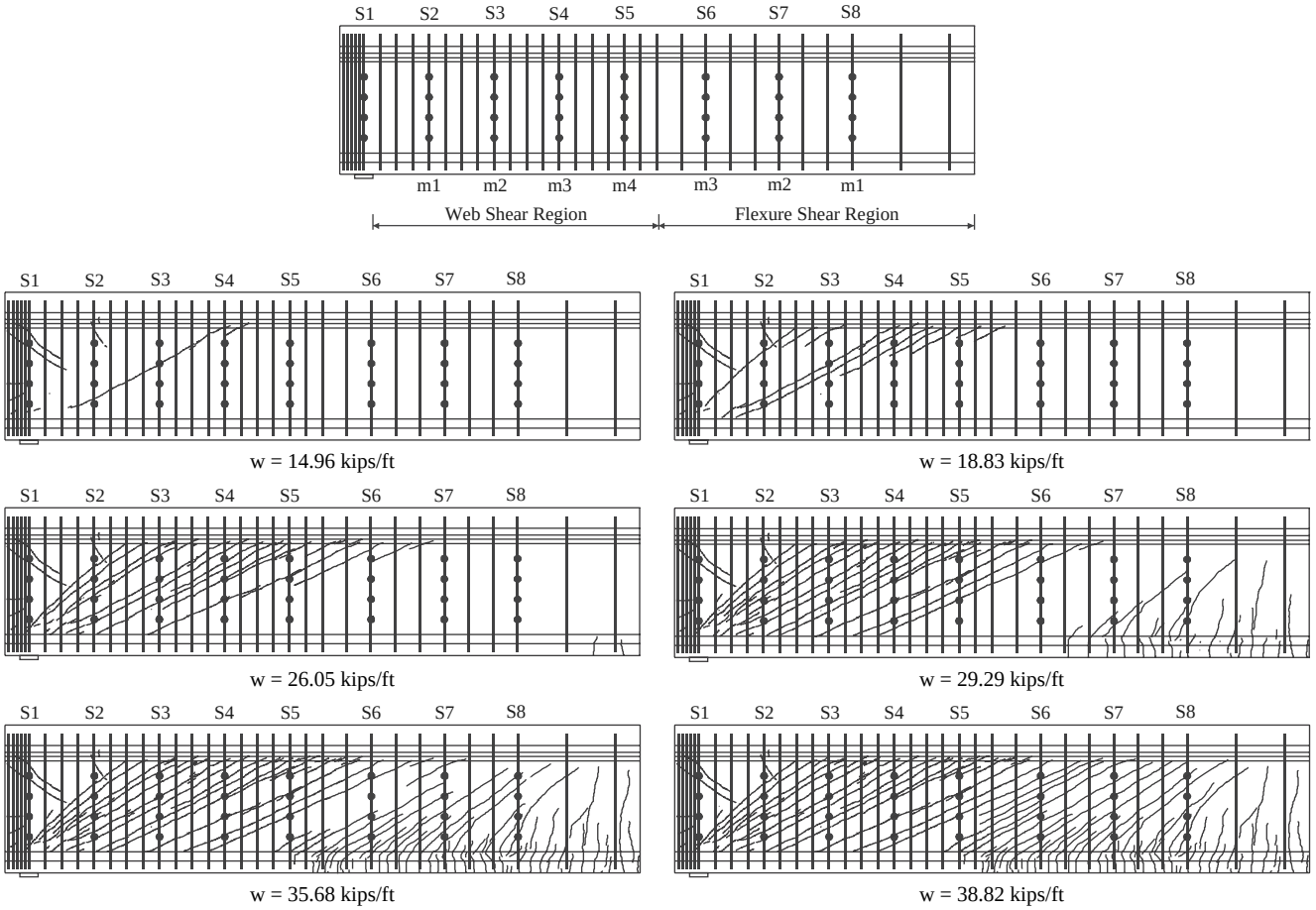

(a) Development of Shear Cracking in West End of Girder 3 (G3W)

Figure 84. Stirrup reinforcement strain in west end of Girder 3 (G3W).

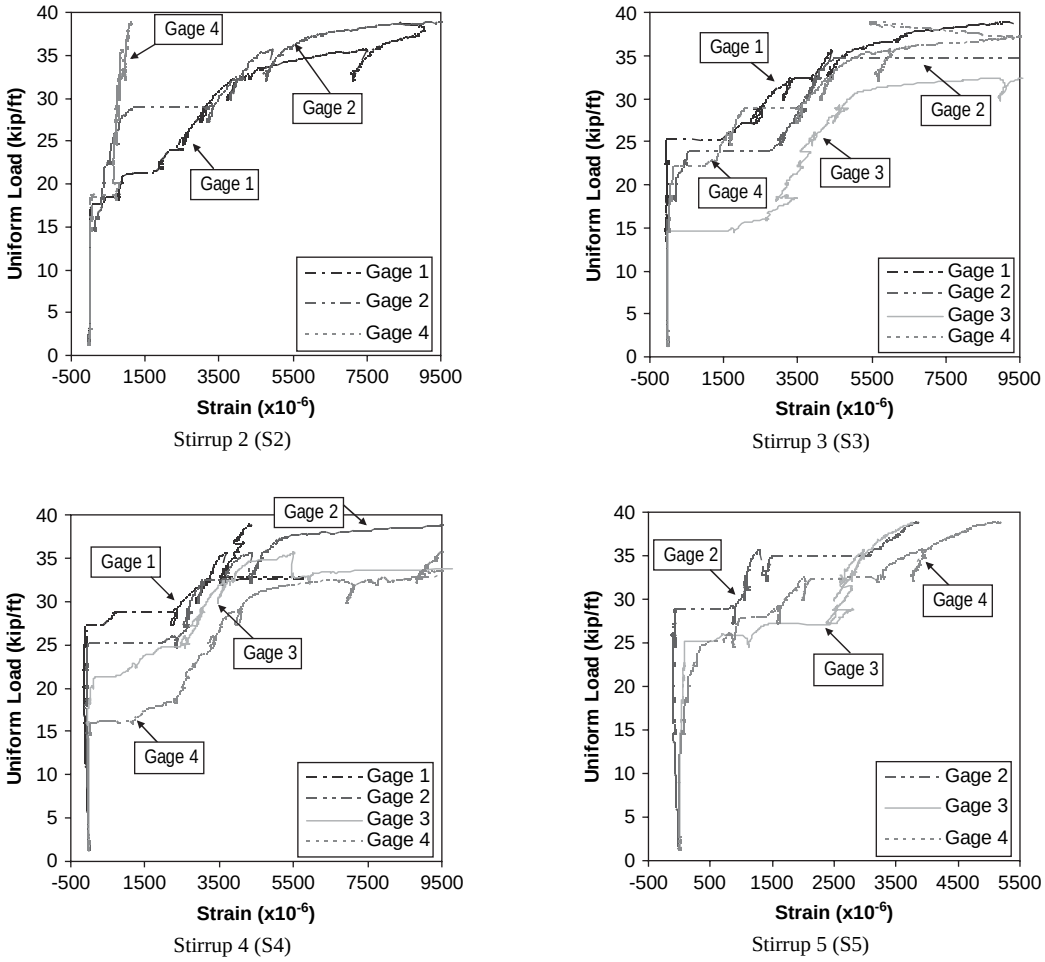

(b) Stirrup Reinforcement Strain in Web-Shear Region of G3W

Figure 84. (Continued).

band of cracks should be similar. However, the measurements show that this was not always the case, and this result is probably due to differences in the distance from the crack to the closest gage for each of the stirrups that crossed the same crack.

- Prior to failure, yielding progressed until it extended over the height of the stirrups in the field of web-shear cracking.

Figure 84(c) shows the development of straining in each stirrup in the flexure-shear region. Note that Gage 4 of Stirrup 6 was not considered part of the flexure-shear region. From these figures, the following observations can be made:

- Because flexure-shear cracking did not occur until considerably later than web-shear cracking in the loading history of the test specimens, the straining of stirrups in the flexure-shear regions occurred much later than in the web-shear regions. For example, in test G3W, flexure-shear cracking did not occur until 28 kips/ft was uniformly distributed. In comparison, web-shear cracking occurred initially at a load of 15 kips/ft.
- Prior to flexure-shear cracking, significant compressive strains developed in the flexure-shear reinforcement. The compressive strains were largest in the stirrups that were closest to mid-span, but even some compressive strains were observed in web-shear regions. See Stirrups S4 and S5 in Figure 84(b). The compressive strains were largest in the lower strain gages of a stirrup, with strains ranging from around 100 microstrain to 300 microstrain. This compressive straining must have been the result of a release of tensile strains caused by Poisson's effect during prestressing. As the loading increased, the positive bending moment increased and the magnitude of decompression stress decreased with a corresponding decrease in the vertical tensile strain. Because the magnitudes of the strains in the gages were set to zero at the beginning of each test, this reduction in tensile strain is measured as compressive strain. For the purpose of assessing the tensile stress in a given stirrup, it is appropriate to use a strain equal to the total tensile strain due to loading less the maximum compressive strain that occurred as the strains caused by prestressing were released. Since the magnitudes of these

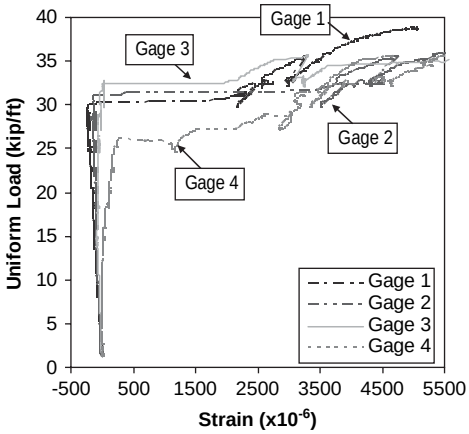

Stirrup 6 (S6)

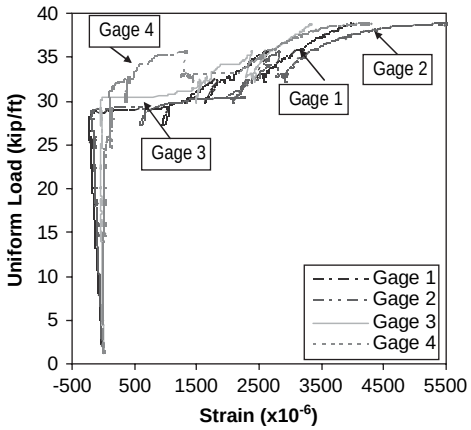

Stirrup 7 (S7)

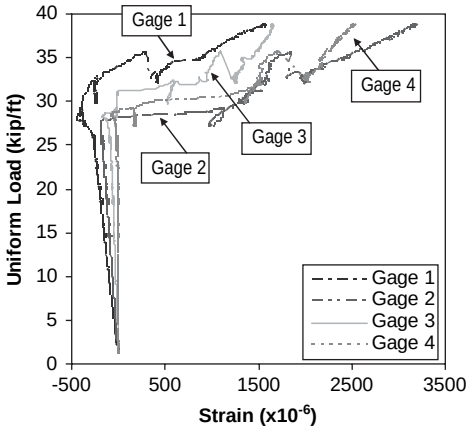

Stirrup 8 (S8)

(c) Stirrup Reinforcement Strain in Flexure-Shear Region of G3W

Figure 84. (Continued).

compressive strains are typically small, they were ignored in calculating the stresses in stirrups.

- As with the development of web-shear cracking, there was a rapid increase in stirrup strains following the formation of flexure-shear cracking, with strain values approaching the yield strain being measured immediately upon cracking. Unlike the situation for web-shear cracking, the development of a complete pattern of flexure-shear cracks occurred rapidly over a very narrow loading range. Consequently, the measured strains in all gages crossing flexure-shear cracks went from close to zero strain to almost all being close to the yield strain, with an increase in loading of around 10 to15 percent.
- Within the flexure-shear region, the farther a stirrup was from mid-span, the larger the shear was, the flatter the flexure-shear crack was, and the larger the magnitude of the stirrup strains was. As shown in Figure 84(c), the strains in Stirrup S6 were much larger than those in Stirrup S8.
- While the strains in Stirrup S6 were well beyond the yield strain and cracks were quite large in this region, there were no other significant signs of an impending shear failure.

The foregoing observations concerning the behavior of the west half of Girder 3 were reasonably typical of the behavior in many, but not all, of the girder tests. The next two sections present a summary and a discussion of the measured stirrup strains in each of the test girders.

2.6.3 Stirrup Reinforcement Strains in Web-Shear Regions

Table 19 and Figure 85 summarize the measured stirrup strains in all 20 web-shear regions. The locations of these gages were shown in Figure 54. Table 19 lists, for each girder and for eight characteristic load levels, the maximum strain in each of the first four gauged stirrups from the inside face of the support (labeled $\varepsilon_{m1}, \varepsilon_{m2}, \varepsilon_{m3}, \varepsilon_{m4}$ in relation to their proximity to the support) the overall maximum strain ($\varepsilon_m = \max(\varepsilon_{m1}, \varepsilon_{m2}, \varepsilon_{m3}, \varepsilon_{m4})$), and the average maximum strain ($\varepsilon_{ma} = \text{ave}(\varepsilon_{m1}, \varepsilon_{m2}, \varepsilon_{m3}, \varepsilon_{m4})$). The eight characteristic load levels provide measured strains immediately before cracking (Crk), at selected load stages for which cracking was measured (CS1 through CS5), 2 minutes

Table 19. Maximum stirrup strains in web-shear regions.

G1W	w	ε_{m1}	ε_{m2}	ε_{m3}	ε_{m4}	ε_{m}	ε_{ma}
<Crk	9.00	-44	-4	27	-12	27	-8
CS1	14.71	-61	12	59	-19	59	-2
CS2	19.11	438	1,161	914	1,988	1,988	1,125
CS3	21.17	1,752	2,240	2,294	1,956	2,294	2,060
CS4	24.56	2,424	3,328	3,465	2,861	3,465	3,019
CS5	26.59	3,878	5,537	8,894	4,011	8,894	5,580
2<F	29.83	11,459	11,074	17,126	7,431	17,126	11,773
<Fail	30.09	11,459	11,256	17,654	9,152	17,654	12,380

G1E	w	ε_{m1}	ε_{m2}	ε_{m3}	ε_{m4}	ε_{m}	ε_{ma}
<Crk	9.00	-9	37	-11	0	37	4
CS1	14.71	1,630	901	162	64	1,630	689
CS2	18.79	1,398	1,302	595	764	1,398	1,015
CS3	19.96	1,696	2,058	1,411	1,768	2,058	1,734
CS4	21.17	1,959	2,130	1,456	2,183	2,183	1,932
CS5	23.67	2,141	3,462	1,490	2,172	3,462	2,316
2<F	25.90	2,418	5,071	1,629	2,680	5,071	2,949
<Fail	26.03	2,418	5,071	1,657	2,717	5,071	2,966

G2W	w	ε_{m1}	ε_{m2}	ε_{m3}	ε_{m4}	ε_{m}	ε_{ma}
<Crk	14.02	61	-20	22	-62	61	0
CS1	18.79	100	-15	64	-75	100	18
CS2	25.94	3,684	2,719	1,873	-61	3,684	2,053
CS3	30.36	4,102	2,969	2,442	2,398	4,102	2,978
CS4	33.79	4,928	3,432	3,529	2,961	4,928	3,713
CS5	38.34	7,953	4,378	4,378	3,579	7,953	5,072
2<F	38.63	9,586	4,783	4,198	4,524	9,586	5,773
<Fail	38.74	12,365	15,317	4,464	3,694	15,317	8,960

G2E	w	ε_{m1}	ε_{m2}	ε_{m3}	ε_{m4}	ε_{m}	ε_{ma}
<Crk	14.02	-9	37	-11	0	37	4
CS1	18.79	1,630	901	162	64	1,630	689
CS2	21.74	1,398	1,302	595	764	1,398	1,015
CS3	25.94	1,696	2,058	1,411	1,768	2,058	1,734
CS4	28.94	1,959	2,130	1,456	2,183	2,183	1,932
CS5	30.36	2,141	3,462	1,490	2,172	3,462	2,316
2<F	33.57	2,418	5,071	1,629	2,680	5,071	2,949
<Fail	33.79	2,418	5,071	1,657	2,717	5,071	2,966

G3W	w	ε_{m1}	ε_{m2}	ε_{m3}	ε_{m4}	ε_{m}	ε_{ma}
<Crk	6.72	22	5	-10	8	22	6
CS1	14.96	139	1,779	39	66	1,779	506
CS2	18.83	818	3,395	2,323	140	3,395	1,669
CS3	29.29	3,315	4,857	4,077	2,803	4,857	3,763
CS4	32.40	3,983	9,098	7,104	2,798	9,098	5,746
CS5	35.68	7,511	10,039	7,935	3,920	10,039	7,351
2<F	38.63	9,319	10,039	12,457	5,073	12,457	9,222
<Fail	38.82	10,013	9,924	12,648	5,172	12,648	9,439

G3E	w	ε_{m1}	ε_{m2}	ε_{m3}	ε_{m4}	ε_{m}	ε_{ma}
<Crk	14.96	36	80	95	32	95	61
CS1	16.17	85	2,207	362	98	2,207	688
CS2	22.79	3,153	2,632	3,210	1,418	3,210	2,603
CS3	26.05	3,919	2,974	3,822	2,205	3,919	3,230
CS4	29.29	4,445	3,474	4,588	2,501	4,588	3,752
CS5	32.40	9,138	4,078	5,513	2,649	9,138	5,345
2<F	35.49	15,006	4,916	7,657	3,332	15,006	7,728
<Fail	35.68	15,173	4,992	8,222	3,407	15,173	7,948

G4W	w	ε_{m1}	ε_{m2}	ε_{m3}	ε_{m4}	ε_{m}	ε_{ma}
<Crk	13.25	11	30	2	22	30	16
CS1	17.63	394	610	15	58	610	269
CS2	21.61	690	936	178	415	936	555
CS3	26.90	800	1,078	536	671	1,078	771
CS4	30.61	1,005	1,289	1,161	878	1,289	1,083
CS5	34.73	1,307	1,512	1,327	997	1,512	1,286
2<F	42.04	1,860	1,802	1,666	1,363	1,860	1,673
<Fail	42.65	2,397	2,056	1,877	1,484	2,397	1,953

G4E	w	ε_{m1}	ε_{m2}	ε_{m3}	ε_{m4}	ε_{m}	ε_{ma}
<Crk	13.25	-4	54	0	26	54	19
CS1	17.63	878	704	15	64	878	415
CS2	21.61	902	832	203	322	902	565
CS3	26.90	1,121	1,158	654	810	1,158	936
CS4	30.61	1,372	1,401	679	1,277	1,401	1,182
CS5	34.73	1,609	1,617	1,121	1,349	1,617	1,424
2<F	42.04	2,055	1,933	1,473	1,736	2,055	1,799
<Fail	42.65	2,362	2,097	1,556	1,844	2,362	1,965

G5W	w	ε_{m1}	ε_{m2}	ε_{m3}	ε_{m4}	ε_{m}	ε_{ma}
<Crk	9.95	32	56	72	24	72	46
CS1	12.20	81	867	336	519	867	451
CS2	13.10	86	911	2,657	407	2,657	1,015
CS3	15.40	90	1,821	10,625	470	10,625	3,252
CS4	16.80	92	3,609	14,021	843	14,021	4,641
CS5	18.20	91	3,609	14,021	1,443	14,021	4,791
2<F	19.66	96	13,997	14,021	14,047	14,047	10,540
<Fail	19.90	99	3,679	14,021	14,032	14,032	7,958

G5E	w	ε_{m1}	ε_{m2}	ε_{m3}	ε_{m4}	ε_{m}	ε_{ma}
<Crk	12.20	58	9	0	-3	58	16
CS1	15.40	73	16	0	5	73	23
CS2	16.80	2,513	2,708	24	1,029	2,708	1,569
CS3	18.70	2,393	6,088	7,457	2,473	7,457	4,603
CS4	20.95	2,568	8,412	17,569	3,105	17,569	7,914
CS5	22.07	2,632	8,412	17,574	3,326	17,574	7,986
2<F	23.57	2,950	8,412	17,574	14,133	17,574	10,767
<Fail	23.70	2,950	8,412	17,574	14,037	17,574	10,743

Table 19. (Continued).

G6W	w	ε_{m1}	ε_{m2}	ε_{m3}	ε_{m4}	ε_{m}	ε_{ma}
<Crk	7.35	79	16	12	8	79	29
CS1	17.27	587	527	61	38	587	303
CS2	19.80	591	1,012	61	47	1,012	428
CS3	23.90	933	1,399	938	380	1,399	912
CS4	27.40	1,885	2,091	1,381	1,494	2,091	1,713
CS5	27.85	2,763	2,204	1,472	1,572	2,763	2,003
2<F	27.48	3,056	2,147	1,431	1,543	3,056	2,044
<Fail	27.67	8,232	3,218	1,585	1,592	8,232	3,657

G6E	w	ε_{m1}	ε_{m2}	ε_{m3}	ε_{m4}	ε_{m}	ε_{ma}
<Crk	7.35	4	7	7	0	7	4
CS1	17.27	929	542	292	39	929	451
CS2	23.90	1,331	980	871	1,012	1,331	1,048
CS3	27.40	1,839	1,175	1,073	1,553	1,839	1,410
CS4	30.00	4,784	1,581	1,369	1,668	4,784	2,351
CS5	37.30	6,664	1,902	1,656	1,834	6,664	3,014
2<F	38.00	7,010	2,031	1,646	1,850	7,010	3,134
<Fail	38.32	7,025	4,785	1,718	1,880	7,025	3,852

G7W	w	ε_{m1}	ε_{m2}	ε_{m3}	ε_{m4}	ε_{m}	ε_{ma}
<Crk	18.10	86	83	75	32	86	69
CS1	24.40	1,207	1,020	1,220	598	1,220	1,011
CS2	32.27	3,306	1,917	2,975	1,615	3,306	2,453
CS3	36.20	4,725	2,201	3,975	1,978	4,725	3,220
CS4	40.57	6,152	3,627	6,451	2,855	6,451	4,771
CS5	43.40	6,152	2,452	6,451	6,571	6,571	5,406
2<F	44.50	6,152	4,006	6,451	6,571	6,571	5,795
<Fail	44.76	6,152	2,933	8,824	6,571	8,824	6,120

G7E	w	ε_{m1}	ε_{m2}	ε_{m3}	ε_{m4}	ε_{m}	ε_{ma}
<Crk	8.70	6	16	3	8	16	8
CS1	18.10	641	677	426	71	677	454
CS2	18.90	691	573	501	47	691	453
CS3	24.40	1,140	1,319	1,047	1,235	1,319	1,185
CS4	31.23	3,381	2,495	1,461	1,774	3,381	2,278
CS5	32.27	4,165	2,978	1,565	1,864	4,165	2,643
2<F	32.93	4,165	3,429	1,660	1,932	4,165	2,796
<Fail	33.47	4,165	3,583	1,739	1,989	4,165	2,869

G8W	w	ε_{m1}	ε_{m2}	ε_{m3}	ε_{m4}	ε_{m}	ε_{ma}
<Crk	6.05	-23	-3	11	20	20	1
CS1	14.71	-62	149	100	896	896	271
CS2	18.20	234	470	1,019	1,763	1,763	872
CS3	21.50	342	763	1,345	1,790	1,790	1,060
CS4	26.44	799	1,046	1,534	4,134	4,134	1,878
CS5	27.90	916	1,138	1,662	4,134	4,134	1,962
2<F	32.36	1,670	1,310	1,810	4,134	4,134	2,231
<Fail	32.70	1,823	1,325	1,825	4,134	4,134	2,277

G8E	w	ε_{m1}	ε_{m2}	ε_{m3}	ε_{m4}	ε_{m}	ε_{ma}
<Crk	18.20	851	851	670	691	851	766
CS1	23.65	1,192	1,112	1,015	1,034	1,192	1,088
CS2	27.90	1,538	1,451	1,778	1,599	1,778	1,592
CS3	35.50	5,860	2,184	2,303	2,969	5,860	3,329
CS4	38.60	5,860	4,860	2,523	3,203	5,860	4,112
CS5	40.20	5,860	4,502	3,204	3,290	5,860	4,214
2<F	43.30	5,860	6,853	14,562	4,956	14,562	8,058
<Fail	43.73	5,860	6,853	14,562	6,793	14,562	8,517

G9W	w	ε_{m1}	ε_{m2}	ε_{m3}	ε_{m4}	ε_{m}	ε_{ma}
<Crk	8.76	-16	17	10	10	17	5
CS1	17.00	-32	99	28	61	99	39
CS2	22.12	193	533	362	296	533	346
CS3	25.80	739	678	547	490	739	614
CS4	30.80	930	929	692	699	930	812
CS5	32.80	1,026	1,004	761	735	1,026	882
2<F	36.45	1,225	1,116	816	792	1,225	987
<Fail	37.19	1,384	1,239	899	888	1,384	1,102

G9E	w	ε_{m1}	ε_{m2}	ε_{m3}	ε_{m4}	ε_{m}	ε_{ma}
<Crk	8.76	6	7	11	5	11	7
CS1	17.00	820	398	183	126	820	382
CS2	22.12	1,061	962	419	701	1,061	786
CS3	25.80	1,151	1,213	554	803	1,213	930
CS4	30.80	1,379	1,559	1,355	1,069	1,559	1,340
CS5	31.80	1,474	1,612	1,478	1,160	1,612	1,431
2<F	32.28	1,489	1,658	1,501	1,195	1,658	1,460
<Fail	32.80	1,657	1,909	1,549	1,239	1,909	1,588

G10W	w	ε_{m1}	ε_{m2}	ε_{m3}	ε_{m4}	ε_{m}	ε_{ma}
<Crk	15.84	22	41	102	8	102	43
CS1	22.54	538	1,120	1,273	83	1,273	753
CS2	26.43	1,157	1,139	1,536	1,057	1,536	1,222
CS3	29.12	1,272	1,319	1,519	1,126	1,519	1,309
CS4	33.68	1,674	1,632	1,789	1,501	1,789	1,649
CS5	38.56	2,573	2,260	2,246	1,726	2,573	2,201
2<F	42.51	2,573	5,319	4,589	2,549	5,319	3,757
<Fail	42.85	2,573	5,520	4,723	2,658	5,520	3,868

G10E	w	ε_{m1}	ε_{m2}	ε_{m3}	ε_{m4}	ε_{m}	ε_{ma}
<Crk	9.65	-14	44	12	2	44	11
CS1	15.84	400	994	832	41	994	567
CS2	20.21	958	1,159	1,325	769	1,325	1,053
CS3	23.91	1,354	1,347	1,317	1,192	1,354	1,303
CS4	29.12	1,659	1,844	1,890	1,387	1,890	1,695
CS5	31.59	1,871	2,482	2,496	1,606	2,496	2,114
2<F	33.61	2,145	3,467	3,639	1,775	3,639	2,757
<Fail	33.93	2,279	3,639	3,871	1,805	3,871	2,898

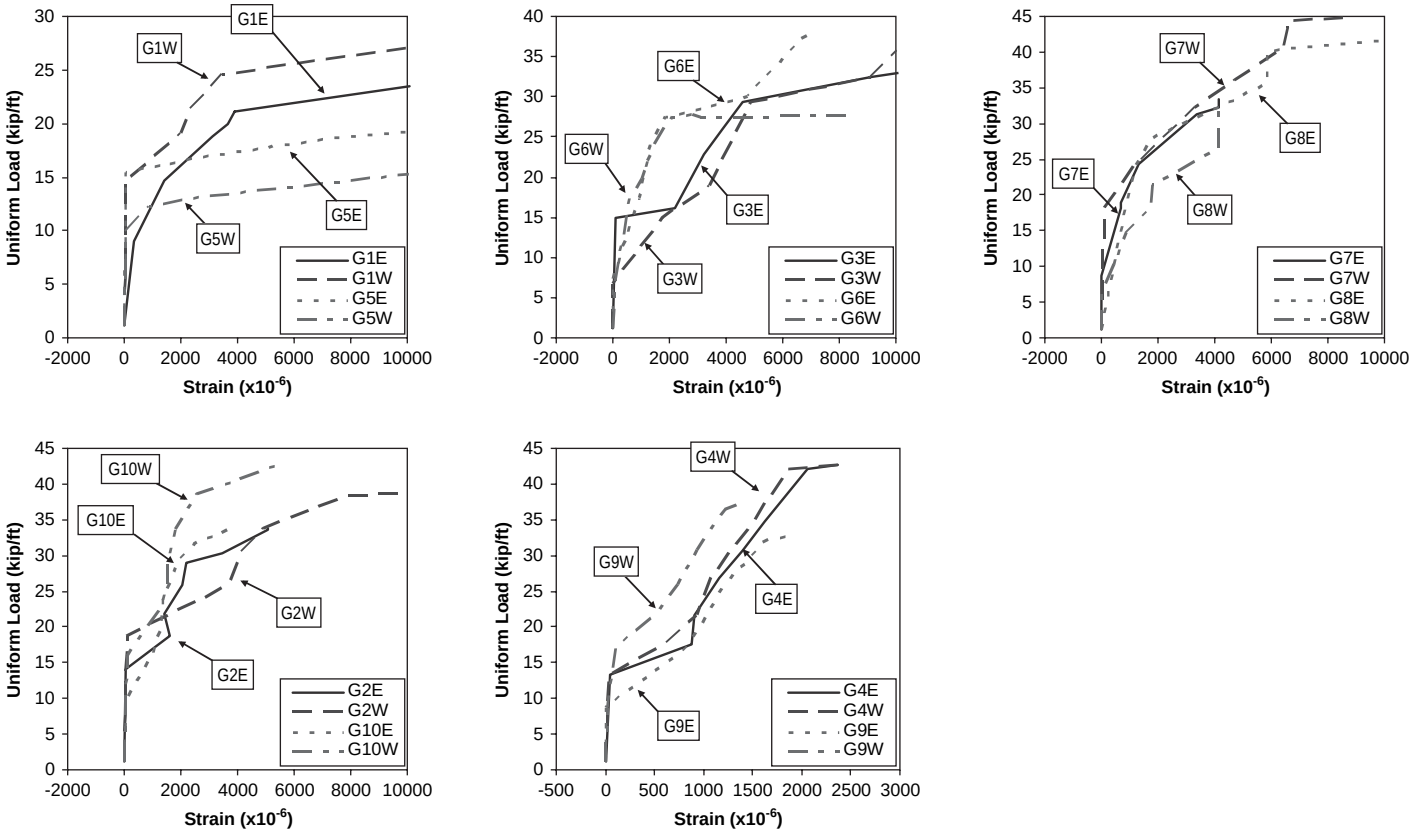

(a) Overall Maximum Strain of Stirrups in Web-Shear Region of Each End

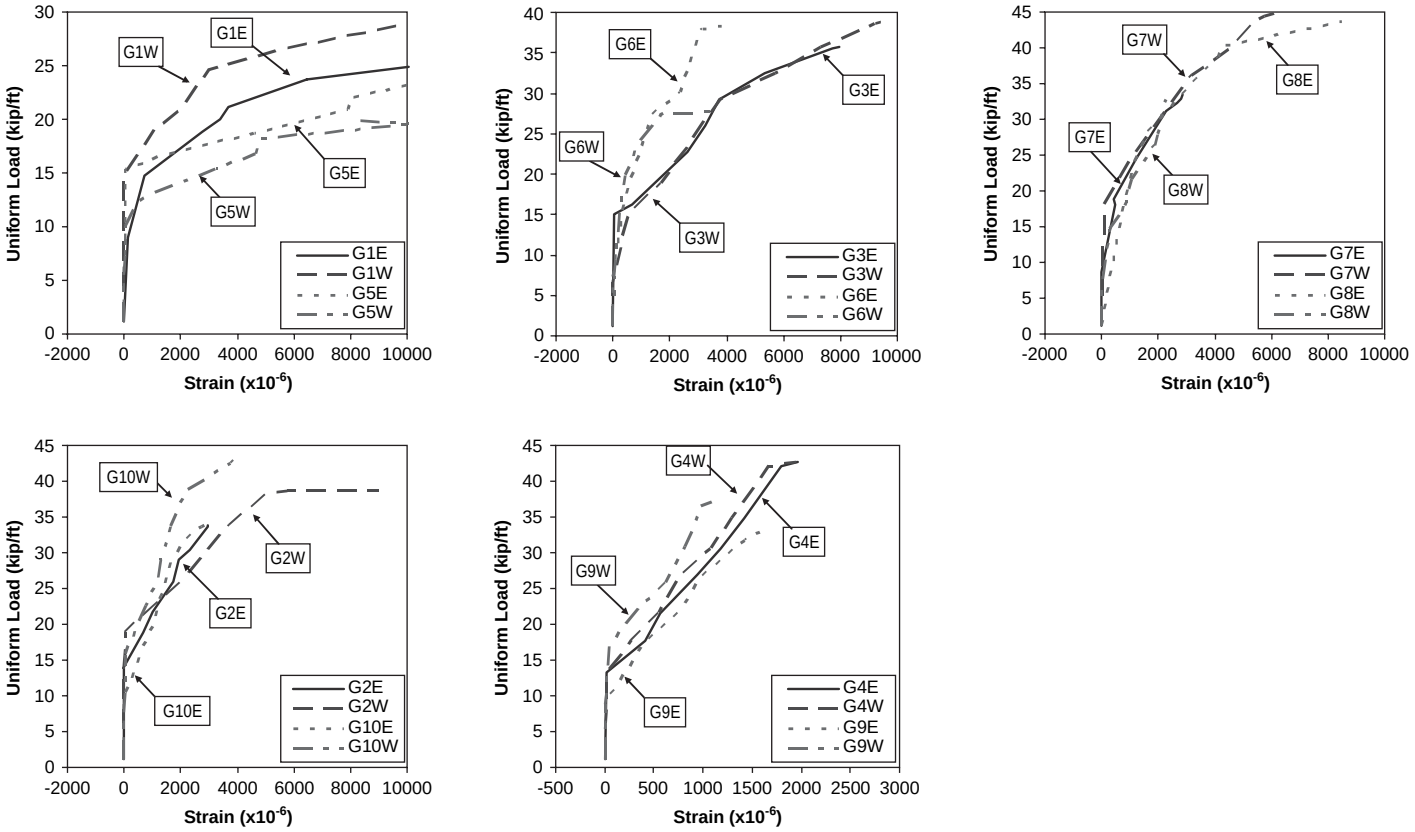

(b) Average Maximum Strain of Stirrups in Web-Shear Region of Each End

Figure 85. Maximum stirrup strain in web-shear region.

before failure (2<F), and for the last measured dataset before failure or peak load (<Fail). Using these selected strain levels, load versus strain envelopes were developed for the overall maximum strain (ε_m) and the average maximum strain (ε_{ma}). These envelopes are presented in Figures 85(a) and 85(b), in which the results from the 20 girder tests have been organized into five groups based on the strength of the shear reinforcement provided in the first critical shear design region from the end:

Group 1: G1E, G1W, G5E, and G5W; $\rho_v f_y$ = 140 – 389 psi

Group 2: G3 and G6; $\rho_v f_y$ = 557 – 577 psi

Group 3: G7 and G8; $\rho_v f_y$ = 557 – 577 psi

Group 4: G2 and G10; $\rho_v f_y$ = 745 – 751 psi

Group 5: G4E(1,113 psi), G4W (1,113 psi), G9E (1,040 psi) and G9W (1,690 psi)

Section 2.6.1 presented the primary observations concerning the development of strains in the stirrups crossing web-shear cracks. From Table 19 and Figure 85, the following additional observations are made:

- For members with the least amount of shear reinforcement, $\rho_v f_y$, the increases in stirrup strains at the onset of web-shear cracking are the largest. Girder 5 contained the least amount of shear reinforcement, and its stirrups yielded at cracking. The east end of Girder 5 failed due to fracture of the stirrups, while the remainder of the member was in good condition. By contrast, the members with the largest amount of shear reinforcement failed when the maximum stirrup strains were only slightly beyond yield or somewhat less than yield.
- The maximum (ε_m) and the average maximum (ε_{ma}) web-shear stirrup strain for all girders in the first four groups ($\rho_v f_y$ <1,000 psi) exceeded the yield strain, with many of the strains being several times the yield strain.
- The maximum (ε_m) and the average maximum (ε_{ma}) web-shear stirrup strains in both ends of Girder 4 ($\rho_v f_y$ = 1,113 psi) were just a little less than the yield strain when this member failed in flexure.
- In the east web-shear region of Girder 9 ($\rho_v f_y$ = 1,040 psi), the strains were less than yield when the member failed in diagonal compression.
- In the west web-shear region of Girder 9 ($\rho_v f_y$ = 1,690 psi), the maximum stirrup strain was only two-thirds of the yield strain and the average maximum stirrup strain was only one-half of the yield strain when the member was unloaded due to an impending failure of the east end repair. At this time, local crushing was observed, with long diagonal cracks above the west end support.
- The maximum web-shear stirrup strains in the ends with draped strands—G1W, G2W, G9W, and G10W—were lower, at the same magnitude of loading, than the maximum web-shear stirrup strains in the east ends of the same girders where the strands were straight.

2.6.4 Stirrup Reinforcement Strains in Flexure-Shear Regions

This section discusses the measured stirrup reinforcement strains in the flexure-shear regions. Table 20 shows the maximum strain for each girder and for several selected load levels for each of the first three to four gauged stirrups toward the end from mid-span (labeled ε_{m1}, ε_{m2}, ε_{m3}, and ε_{m4} in relation to their proximity to mid-span), the overall maximum strain ($\varepsilon_m = \max(\varepsilon_{m1}, \varepsilon_{m2}, \varepsilon_{m3}, \varepsilon_{m4})$), and the average maximum strain ($\varepsilon_{ma} = \text{ave}(\varepsilon_{m1}, \varepsilon_{m2}, \varepsilon_{m3}, \varepsilon_{m4})$). The six load stages provide the measured strains immediately before cracking (Crk), at selected load stages in which flexure-shear cracking was measured (CS1 through CS3), 2 minutes before failure (2<F), and for the last measured dataset before failure or peak load (<Fail). Using these selected strain levels, load versus strain envelopes were developed for the overall maximum strain (ε_m) and the average maximum strain (ε_{ma}). These envelopes are presented in Figures 86(a) and 86(b), in which the results from the 20 girder tests have been organized into five groups based on the strength of the shear reinforcement provided in the flexure-shear region:

Group 1: G1E, G1W, G5E, G5W, and G7W; $\rho_v f_y$ < 200 psi (119 psi ~ 194 psi)

Group 2: G3 and G6; $\rho_v f_y$ = 334 – 384 psi

Group 3: G7E and G8; $\rho_v f_y$ = 453 – 482 psi

Group 4: G2 and G10; $\rho_v f_y$ = 745 – 751 psi

Group 5: G4E (668 psi), G4W (668 psi), G9E (604 psi), and G9W (604 psi)

Section 2.6.1 presented the primary observations concerning the development of strains in the stirrups crossing flexure-shear cracks. From Table 20 and Figure 86, the following additional observations are made:

- In general, the strains in the flexure-shear regions were less than the maximum strains in the web-shear regions even though the members were designed to be equally as likely to fail in a web-shear region as they were to fail in a flexure-shear region.
- Sometimes, the differences between the states of strain in the web-shear and flexure-shear regions were modest. For example, the development of straining in the web-shear and flexure-shear regions of the west end of Girder 2 was

Table 20. Maximum stirrup strains in flexure-shear regions.

G1W	*w*	ε_{m1}	ε_{m2}	ε_{m3}	ε_{m4}	ε_{m}	ε_{ma}
<Crk	19.96	-14	3	27	21	27	9
CS1	26.59	-69	84	139	272	272	106
CS2	27.44	177	1,597	1,122	303	1,597	800
CS3	28.75	433	2,286	2,529	357	2,529	1,401
2<F	29.83	718	2,863	4,101	3,136	4,101	2,704
<Fail	30.09	803	4,180	4,409	3,489	4,409	3,220

G1E	*w*	ε_{m1}	ε_{m2}	ε_{m3}	ε_{m4}	ε_{m}	ε_{ma}
<Crk	14.71	-10	-13	3	-32	3	-13
CS1	19.96	-5	31	126	-39	126	28
CS2	22.52	-18	75	166	-8	166	54
CS3	24.56	481	199	610	193	610	371
2<F	25.90	1,593	2,606	1,807	4,908	4,908	2,729
<Fail	26.03	1,637	2,631	1,870	295	2,631	1,608

G2W	*w*	ε_{m1}	ε_{m2}	ε_{m3}	ε_{m4}	ε_{m}	ε_{ma}
<Crk	21.74	-30	199	55	0	199	56
CS1	25.94	-111	279	388	0	388	139
CS2	30.36	1,366	1,892	2,463	2,398	2,463	2,030
CS3	33.79	1,667	4,288	3,110	2,961	4,288	3,006
2<F	38.63	2,290	10,849	4,676	4,524	10,849	5,585
<Fail	38.74	2,290	10,849	4,707	3,694	10,849	5,385

G2E	*w*	ε_{m1}	ε_{m2}	ε_{m3}	ε_{m4}	ε_{m}	ε_{ma}
<Crk	18.79	8	-23	-11	64	64	10
CS1	21.74	8	-27	57	764	764	200
CS2	25.94	-33	113	652	1,768	1,768	625
CS3	28.94	2,865	1,608	751	2,183	2,865	1,852
2<F	33.57	3,232	3,160	1,736	2,680	3,232	2,702
<Fail	33.79	3,251	3,180	1,754	2,717	3,251	2,725

G3W	*w*	ε_{m1}	ε_{m2}	ε_{m3}	ε_{m}	ε_{ma}
<Crk	1.18	0	0	0	0	0
CS1	26.05	-13	119	-66	119	13
CS2	29.29	1,121	1,030	-67	1,121	695
CS3	32.40	1,534	2,311	3,873	3,873	2,573
2<F	35.68	1,853	2,824	4,756	4,756	3,145
<Fail	38.63	3,146	5,251	11,722	11,722	6,706

G3E	*w*	ε_{m1}	ε_{m2}	ε_{m3}	ε_{m}	ε_{ma}
<Crk	14.96	-13	33	0	33	7
CS1	26.05	-29	77	0	77	16
CS2	29.29	506	1,223	0	1,223	576
CS3	32.40	1,852	3,899	2,744	3,899	2,831
2<F	35.49	2,454	3,802	3,221	3,802	3,159
<Fail	35.68	2,501	4,090	3,265	4,090	3,285

G4W	*w*	ε_{m1}	ε_{m2}	ε_{m3}	ε_{m4}	ε_{m}	ε_{ma}
<Crk	17.63	-3	14	4	24	24	10
CS1	26.90	-3	36	54	139	139	57
CS2	30.61	-7	57	71	878	878	250
CS3	34.73	783	1,004	461	997	1,004	811
2<F	42.04	888	1,333	551	1,363	1,363	1,034
<Fail	42.65	1,094	1,700	569	1,484	1,700	1,212

G4E	*w*	ε_{m1}	ε_{m2}	ε_{m3}	ε_{m4}	ε_{m}	ε_{ma}
<Crk	17.63	-5	-4	0	-21	0	-7
CS1	26.90	-8	3	76	-13	76	14
CS2	30.61	359	35	569	286	569	312
CS3	34.73	821	1,054	695	762	1,054	833
2<F	42.04	934	1,317	1,231	1,736	1,736	1,305
<Fail	42.65	1,245	1,641	1,409	1,611	1,641	1,477

G5W	*w*	ε_{m1}	ε_{m2}	ε_{m3}	ε_{m}	ε_{ma}
<Crk	12.20	0	-13	20	20	2
CS1	16.80	25	32	275	275	111
CS2	18.20	131	46	1,307	1,307	495
CS3	18.70	162	17	1,557	1,557	579
2<F	19.66	183	27	1,772	1,772	661
<Fail	19.90	230	40	1,896	1,896	722

G5E	*w*	ε_{m1}	ε_{m2}	ε_{m3}	ε_{m}	ε_{ma}
<Crk	16.80	-26	57	64	64	32
CS1	18.20	-27	774	73	774	273
CS2	20.95	532	1,965	67	1,965	855
CS3	22.07	1,067	2,450	1,030	2,450	1,516
2<F	23.57	1,810	5,621	4,395	5,621	3,942
<Fail	23.70	1,867	6,852	4,395	6,852	4,371

G6W	*w*	ε_{m1}	ε_{m2}	ε_{m3}	ε_{m}	ε_{ma}
<Crk	17.27	0	-3	0	0	-1
CS1	19.80	0	-14	0	0	-5
CS2	23.90	0	-20	0	0	-7
CS3	27.40	0	22	0	22	7
2<F	27.48	0	23	0	23	8
<Fail	27.85	0	25	0	25	8

G6E	*w*	ε_{m1}	ε_{m2}	ε_{m3}	ε_{m}	ε_{ma}
<Crk	17.27	-7	0	16	16	3
CS1	23.90	-21	0	72	72	17
CS2	30.00	-33	0	111	111	26
CS3	37.30	23	556	1,020	1,020	533
2<F	38.00	37	680	1,175	1,175	630
<Fail	38.32	60	706	1,221	1,221	662

Table 20. (Continued).

G7W	*w*	ε_{m1}	ε_{m2}	ε_{m3}	ε_{m}	ε_{ma}
<Crk	24.40	11	8	-13	11	2
CS1	31.23	11	27	71	71	36
CS2	33.47	700	171	1600	1,600	824
CS3	40.57	978	440	2,357	2,357	1,258
2<F	44.50	1,211	2,483	2,357	2,483	2,017
<Fail	44.76	1,262	2,484	2,357	2,484	2,034

G7E	*w*	ε_{m1}	ε_{m2}	ε_{m3}	ε_{m}	ε_{ma}
<Crk	18.90	0	-3	-19	0	0
CS1	24.40	0	22	-19	22	1
CS2	31.23	0	213	965	965	392
CS3	32.27	0	328	1,085	1,085	471
2<F	32.93	37	1,103	1,349	1,349	830
<Fail	33.47	72	1,217	1,098	1,217	796

G8W	*w*	ε_{m1}	ε_{m2}	ε_{m3}	ε_{m}	ε_{ma}
<Crk	18.20	-11	2	21	21	4
CS1	21.50	-12	21	103	103	37
CS2	23.65	-11	36	162	162	62
CS3	26.44	-8	61	522	522	192
2<F	32.36	2	187	662	662	284
<Fail	32.70	8	198	675	675	293

G8E	*w*	ε_{m1}	ε_{m2}	ε_{m3}	ε_{m}	ε_{ma}
<Crk	21.50	-9	8	13	13	4
CS1	27.90	12	0	55	55	22
CS2	32.70	179	399	1,590	1,590	723
CS3	38.60	418	257	1,715	1,715	797
2<F	43.30	753	560	4,000	4,000	1,771
<Fail	43.73	763	579	1,888	1,888	1,077

G9W	*w*	ε_{m1}	ε_{m2}	ε_{m3}	ε_{m4}	ε_{m}	ε_{ma}
<Crk	22.12	-14	3	-3	-14	3	-7
CS1	25.80	166	134	765	152	765	304
CS2	30.80	540	170	1,193	882	1,193	696
CS3	32.80	525	210	1,486	1,130	1,486	838
2<F	36.45	266	88	618	654	654	407
<Fail	37.19	0	102	660	717	717	370

G9E	*w*	ε_{m1}	ε_{m2}	ε_{m3}	ε_{m4}	ε_{m}	ε_{ma}
<Crk	17.00	-19	8	16	-36	16	-8
CS1	22.12	125	32	104	-45	125	54
CS2	25.80	153	712	375	857	857	525
CS3	30.80	534	1,032	875	1,400	1,400	960
2<F	32.28	606	1,044	997	1,625	1,625	1,068
<Fail	32.80	613	803	1,020	1,680	1,680	1,029

G10W	*w*	ε_{m1}	ε_{m2}	ε_{m3}	ε_{m}	ε_{ma}
<Crk	23.91	0	19	0	19	6
CS1	29.12	91	1,028	212	1,028	444
CS2	33.68	621	1,513	1,277	1,513	1,137
CS3	38.56	939	1,890	1,628	1,890	1,486
2<F	42.51	1,547	2,504	2,143	2,504	2,065
<Fail	42.85	1,567	2,545	2,172	2,545	2,094

G10E	*w*	ε_{m1}	ε_{m2}	ε_{m3}	ε_{m}	ε_{ma}
<Crk	15.84	0	76	0	76	25
CS1	20.21	0	373	187	373	187
CS2	23.91	0	822	1,112	1,112	645
CS3	29.12	1,039	1,293	1,252	1,293	1,195
2<F	33.61	5,518	1,741	1,860	5,518	3,040
<Fail	33.93	1,314	1,776	1,908	1,908	1,666

quite similar with the average maximum strain 2 minutes before failure being between 5,000 and 6,000 microstrain.

- After diagonal cracking, strains in the flexure-shear regions increased more rapidly with increasing load than strains in the web-shear region.
- The strains in Girder 6 were low; this member failed in the web-shear region before the development of significant flexure-shear cracking and thus significant flexure-shear stirrup strains. This observation was particularly true for the west end of Girder 6, which had a lower shear capacity than the east end due to the debonding of some strands.
- Due to a dramatic change in the loading pattern in a final attempt to fail the west part of Girder 9, the shear force in the flexure-shear region was reduced, and that reduction is responsible for the apparent decrease in strain for that test with increasing load. It is interesting to note that before this change in loading pattern, and at a uniformly distributed loading of 32.8 kips/ft, the maximum measured flexure-shear strain was 1,486 microstrain, and that value was larger than the maximum measured web-shear strain of 1,026 microstrain.

2.6.5 Longitudinal Reinforcement Strains

This section reports the measured strains in the longitudinal reinforcement. These strains include the longitudinal strains in the confinement cages, the longitudinal strains on some deformed bars that were connected to bearing plates at the east ends of Girders 1 and 2, and the longitudinal strains in the additional web skin reinforcements in the west ends of Girders 3 and 4. The locations of the gages on the confinement reinforcement are shown in Figure 55, and the locations on other bars are reported in the appendices. The changes in strain during the tests can be used to examine the demands placed on the longitudinal reinforcement. When interpreting the results from these measurements, it

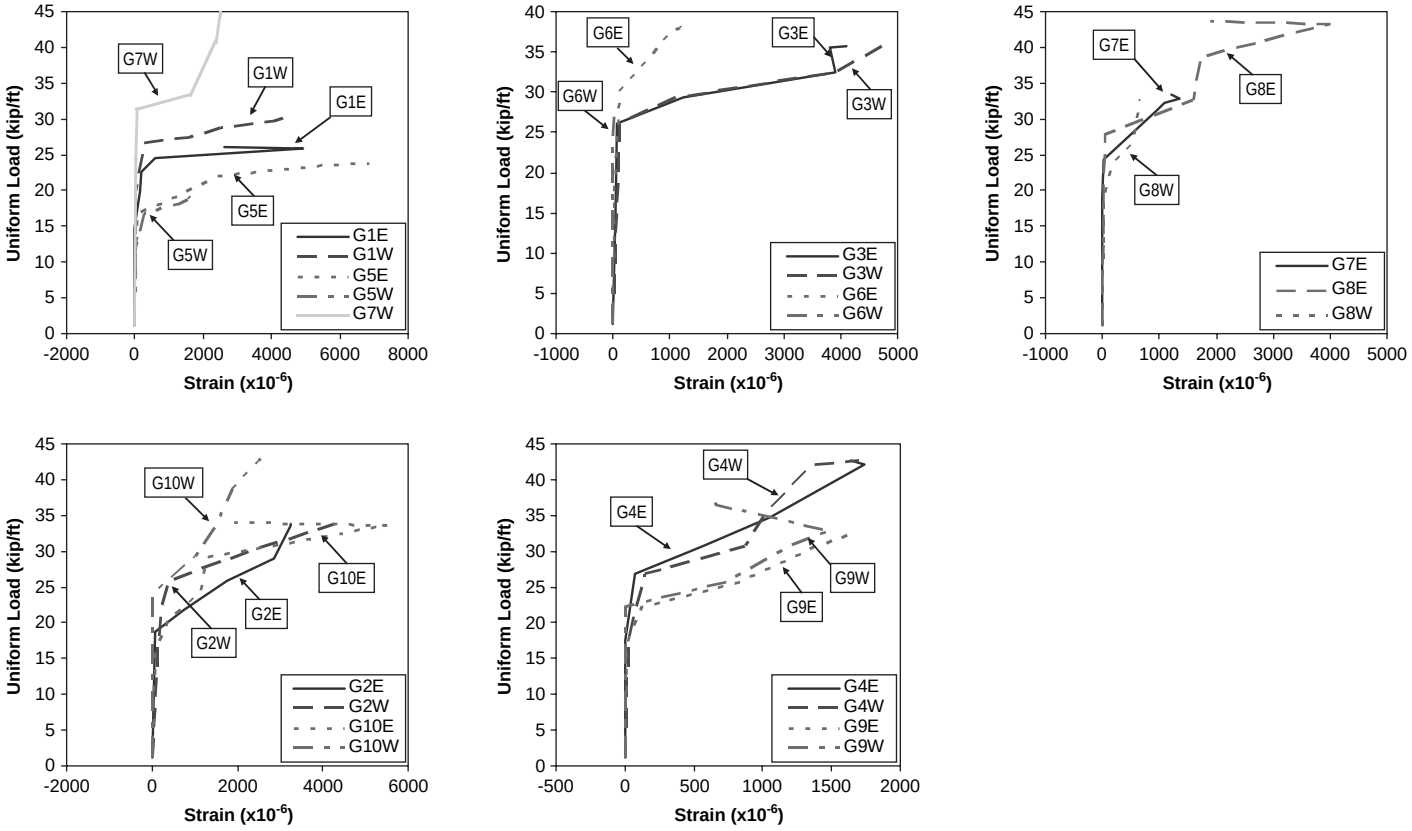

(a) Overall Maximum Strain of Stirrups in Flexure-Shear Region of Each End

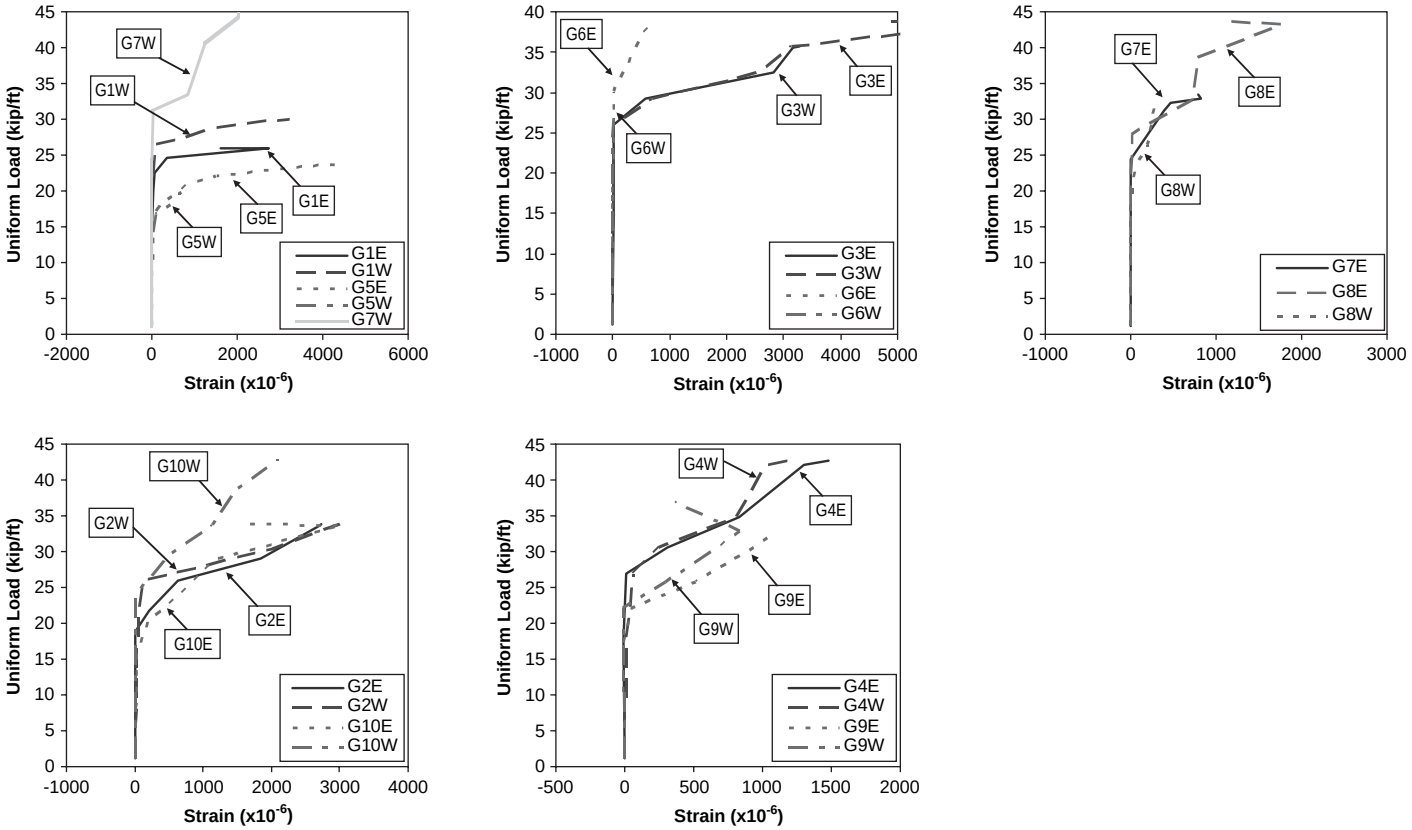

(b) Average Maximum Strain of Stirrups in Flexure-Shear Region of Each End

Figure 86. Maximum stirrup strain in flexure-shear region.

is useful to note that the strain in the bottom bulb due to the effects of prestressing typically changed linearly from 0 microstrain at the very end of the member to between –700 and –1,500 microstrain at 30 inches from the end of the member depending on the amounts of prestressing, debonding, and draping of tendons.

Figure 87 shows the longitudinal strains as measured by Gages 1, 2, 3, and 4 in the bottom cages for all girders. Those gages were located at longitudinal distances of 10, 20, 30 and 40 inches from the actual end of the girder. Figure 87 shows that strains in Gages 1 and 2 typically increased more rapidly than those in Gages 3 and 4. Most strains in Gage 1 and/or Gage 2 were larger than 1,200 microstrain at maximum load, and some reached very high values due to cracks that extended from the web and into the bottom bulb near the support. Usually Gage 4, located 40 inches from the very end, had strain increases that were small and less than 200 microstrain.

Figures 88(a) and 88(b) show the longitudinal strains in the bottom bars (No.8 deformed bars) of G1E and G2E, respectively. Gages 1, 2, and 3 were located at 46, 27, and 19 inches from the actual end of the girder, respectively. Figures 88(c) through 88(f) show the longitudinal strains in the skin bars in the west webs of Girders 3 and 4. As discussed in Section 2.3, two No. 3 horizontal bars at 6-inch centers were distributed over the depth of the webs of Girders 3 and 4. Those bars extended to 10 feet from the west ends of the girders. Six gages were attached to the two skin bars at heights of 18 and 30 inches from the bottom of the girders. Those results are labeled as h18 and h30 in Figure 88. Gages 1, 2, and 3 on bar h18 were located at 6, 21, and 45 inches, respectively, from the actual end of the girder, while Gages 1, 2, and 3 on bar h30 were at 21, 45, and 75 inches, respectively, from the actual end. Rapid increases in the longitudinal strains occurred with web-shear cracking. In G3W, the distributed horizontal bars yielded, while in G4W the maximum measured strains were less than yield.

The very large longitudinal reinforcement strains that were measured near the support indicate that the tensile force demands specified in the LRFD specifications section S5.8.3.5 are very real and need to be resisted by appropriately detailed longitudinal reinforcement. Some of these strains were in excess of the yield strain well before the design strength of the member was realized. This result suggests that adding additional longitudinal reinforcement would have improved the response of the girders and that to accommodate the absence of such reinforcement some internal redistribution of the shear force resisting mechanisms must have occurred.

2.6.6 Confinement Reinforcement Strains

In accordance with LRFD specifications, confinement cages were used to enclose the strands in the bottom bulb of the test girders over a distance of 100 inches from the ends of each girder. The purpose of this reinforcement was to aid in preventing splitting cracks in the end anchorage region and to enhance prestress transfer between the steel and concrete through bond. This reinforcement consisted of twenty-one No. 3 hoops arranged at a spacing of 5 inches on centers. Six strain gages, numbered 5 through 10 in Figure 55, were used to measure the strains in this reinforcement. Gages 5 through 7 were on the inclined reinforcement near the top of the bottom bulb, while Gages 8 through 10 were located on the reinforcement crossing the bottom of the bottom bulb.

Figure 89 shows the strains measured by the gages on the cages. Compressive strains developed in Gages 5, 6, and 7 over the first segment of the loading history. This increase in compressive strain is probably due to the vertical components of the diagonal compression in the member. The only other possibility would seem to be a decrease in the Poisson's effect–induced tensile strain, which would have produced a similar decrease in Gages 8, 9 and 10. However, a similar decrease was not seen in these gages. Most gages reached strain values less than 500 microstrain at failure of the girder. Gages 6 and 7 typically developed the largest strains. Those strains reached values as large as 2,000 millistrain and occurred in regions where shear cracking progressed into the bottom bulb. The significant levels of straining measured in the cages indicate that those cages provided significant confinement for the anchorage of the prestressing strands.

2.6.7 Longitudinal Strain of Web at Mid-Depth (ε_x)

In the LRFD Sectional Design Model, the longitudinal strain at mid-depth, e_x, is used in conjunction with the design shear stress ratio (v/f'_c) to characterize the condition of the web of a member in shear for members with shear reinforcement. From these characterizing values of ε_x and (v/f'_c), the contributions of the concrete and reinforcement are determined from the MCFT, as reflected in the values for β and θ in Table 5.8.3.4.2-1 of the LRFD specifications. To monitor the development of longitudinal strain, two LVDTs were attached to the web of each end of each girder. One of these LVDTs was located in the first critical design region, as shown in Figure 53. The center position of this transducer was within a few inches of $d_v\cot\theta/2$ from the support. The gage length of the LVDT was 48 inches; hence, by dividing the measured change in distance by 48 inches, the average strain over this length can be calculated. The LVDT recorded the deformation due to externally applied load only and therefore did not include the deformation caused by the prestressing force

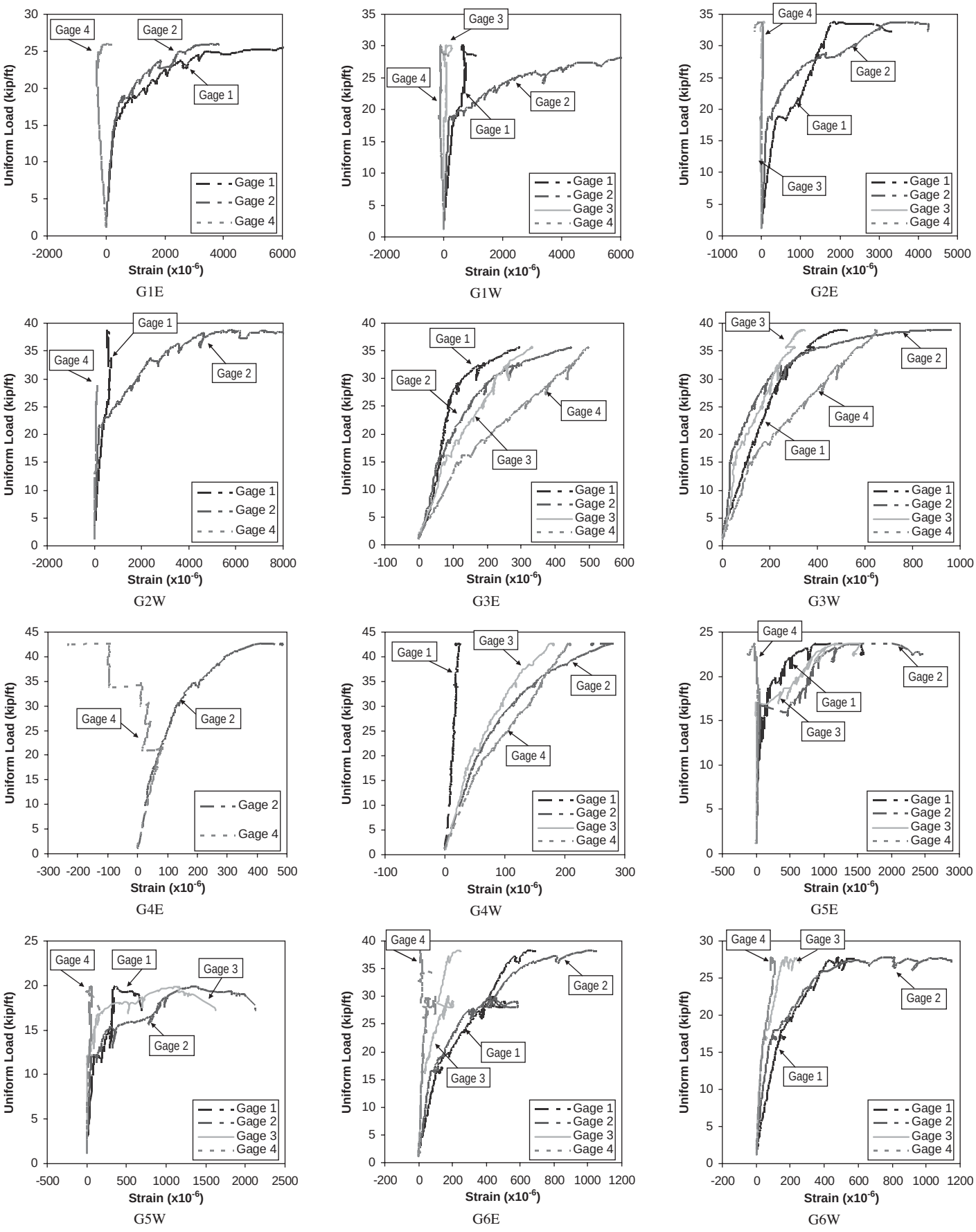

Figure 87. Longitudinal strains in the confinement cages.

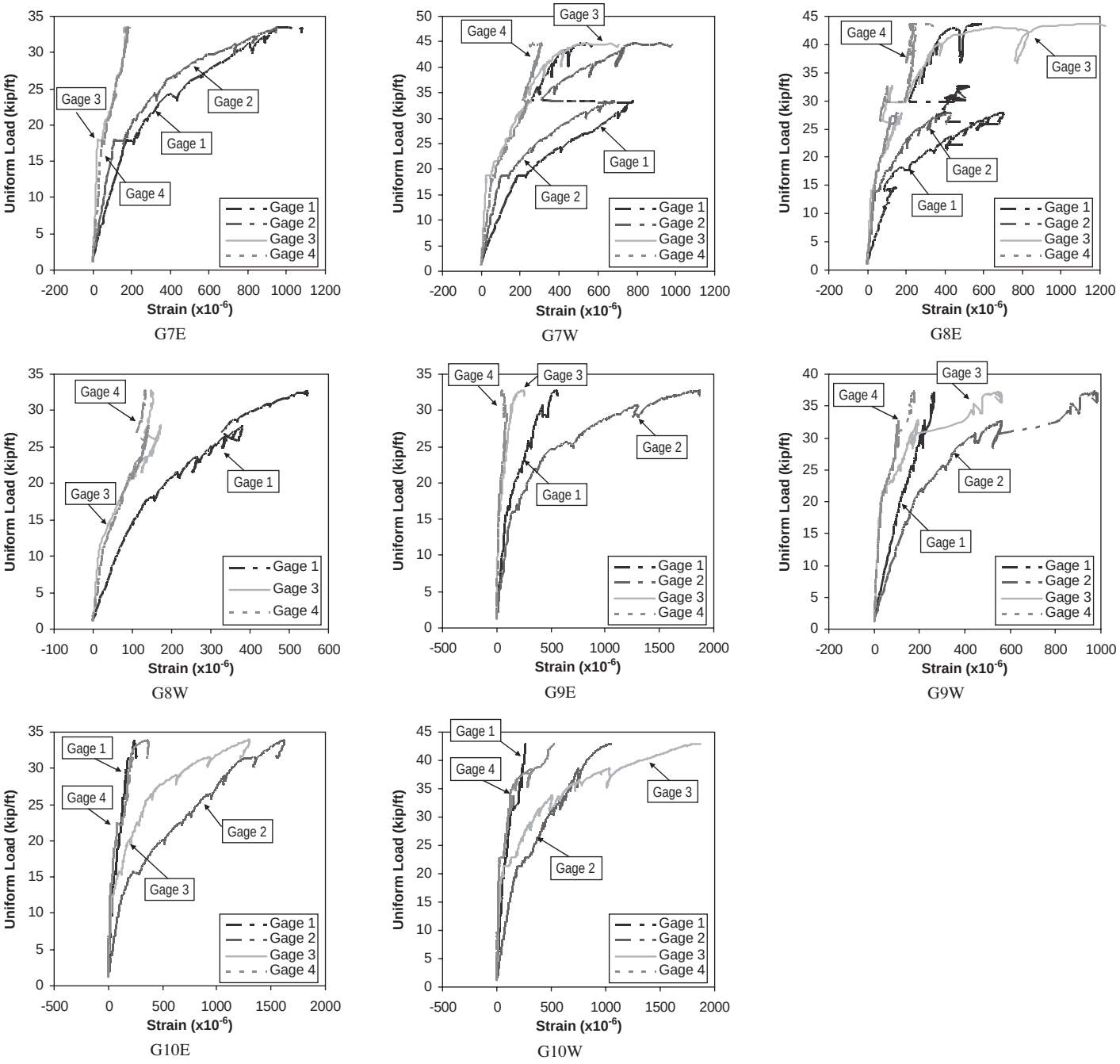

Figure 87. (Continued).

prior to testing. To obtain the total strain in the web, the strains prior to testing were computed using the finite element program Vector2, and then those values were added to the measured values. Those total strains were compared with the calculated values for the same location based on the corresponding equations and the overall strain distribution for the section provided by the LRFD expression for ε_x. The comparison of the measured and calculated values is presented in Figure 90, from which the following observations can be made:

- There was reasonably good agreement between the LRFD-calculated strain at mid-depth due to the effects of prestressing and the strain calculated from Vector2. This result was to be expected, for the girders behave as linear elastic structures prior to the application of the distributed loading.
- The kink in some of the LRFD-calculated relationships for ε_x is because the LRFD specifications use two different equations to compute the longitudinal strain. One relationship is used when the axial straining is all expected to be compressive, and the other is used when the member is

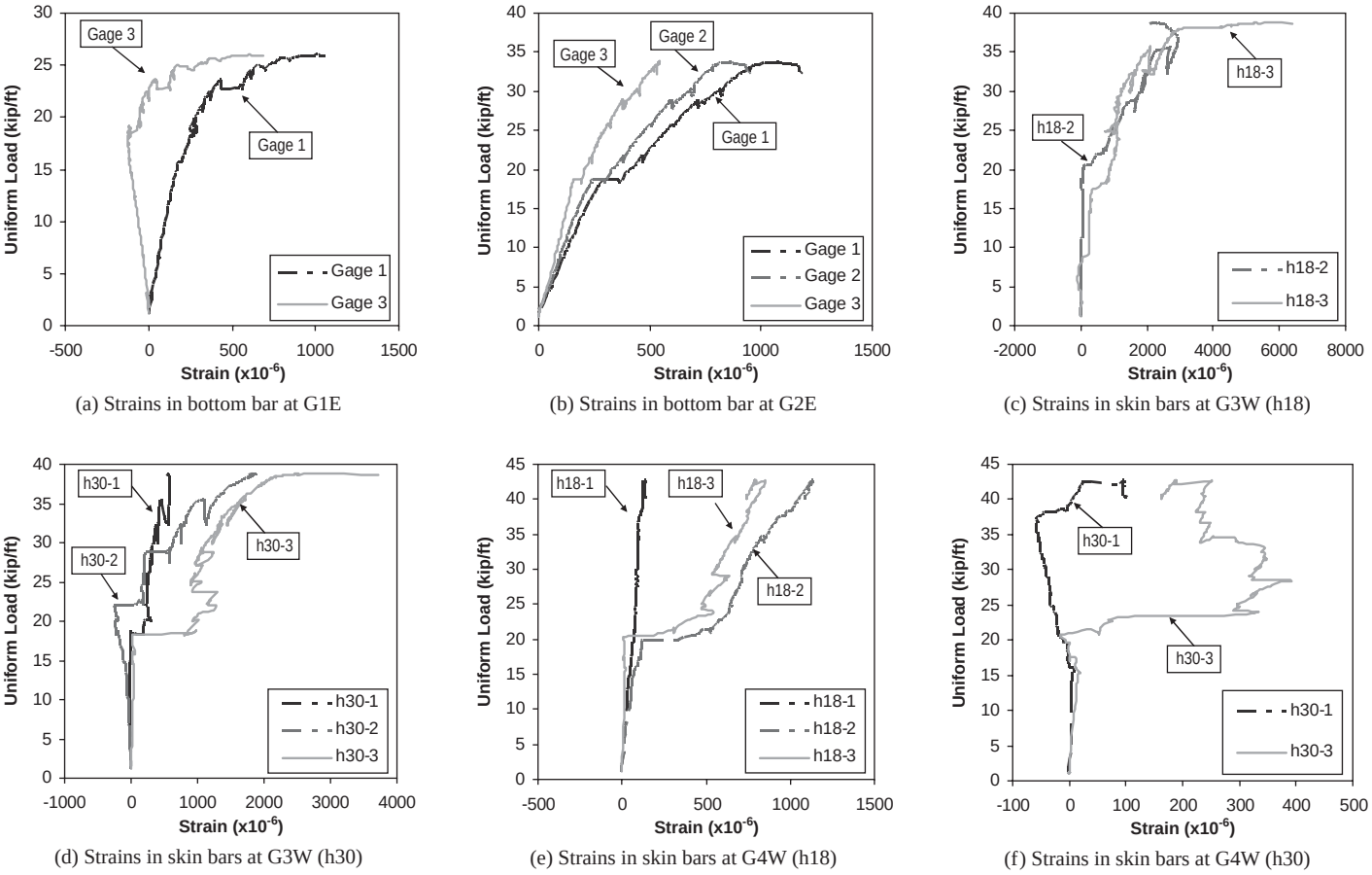

(a) Strains in bottom bar at G1E

(b) Strains in bottom bar at G2E

(c) Strains in skin bars at G3W (h18)

(d) Strains in skin bars at G3W (h30)

(e) Strains in skin bars at G4W (h18)

(f) Strains in skin bars at G4W (h30)

Figure 88. Longitudinal strains in bottom bars (G1E, G2E) and web skin bars (G3W, G4W).

predicted to be cracked in flexure. The LRFD equation for ε_x was successful in about 50 percent of the cases in providing a reasonable estimate for the development of longitudinal strain at mid-depth. In the worst cases, the calculated values and measured values differed by up to 1 millistrain at the design load level, which translates to a difference in β of up to 0.8 and in θ of up to 10 degrees.

- The plane section assumption was adopted in the LRFD equation for calculating the longitudinal strain at mid-depth. However, the experimental results showed that the longitudinal strain in the web could be tensile due to web-shear cracking, even while the bottom bulb and top flange remain uncracked. This may be a source of the significant differences in predicted and measured levels of longitudinal straining at mid-depth.

2.6.8 Web-Shear Strains

LVDTs were installed on the surface of the web to measure the web strains, as shown in Figure 53. In most cases, 12 LVDTs were used, and they were grouped in four rosettes. Each rosette contained two diagonal LVDTs on an inclination of ±45 degrees and one LVDT that measured horizontal deformation. Those rosettes were normally located in the critical shear design regions. There were typically two rosettes at one end, and they were located at 3 feet and 6 feet from the support, respectively. The gage lengths of the LVDTs were all 48 inches. Thus, the strains computed from the LVDTs are average strains over a distance of 48 inches. Note that the measured values from the LVDTs were the deformations due to externally applied load only and therefore did not include the deformations due to the effects of prestressing prior to testing.

From the two diagonal LVDTs, the change in shear strain due to the externally applied load can be computed for each rosette. Because the shear strain in the web due to effects of prestressing is very small, the measured shear strain change can be treated as the actual shear strain in the web. Thus, the measured shear strain can be obtained by $\gamma = \varepsilon(\text{diagonal 1}) - \varepsilon(\text{diagonal 2})$. Figure 91 presents plots of the measured shear strain versus the shear force for each end of each girder. Note that the shear force was computed for the section located at the center point of the rosette. From these plots, the following observations can be made:

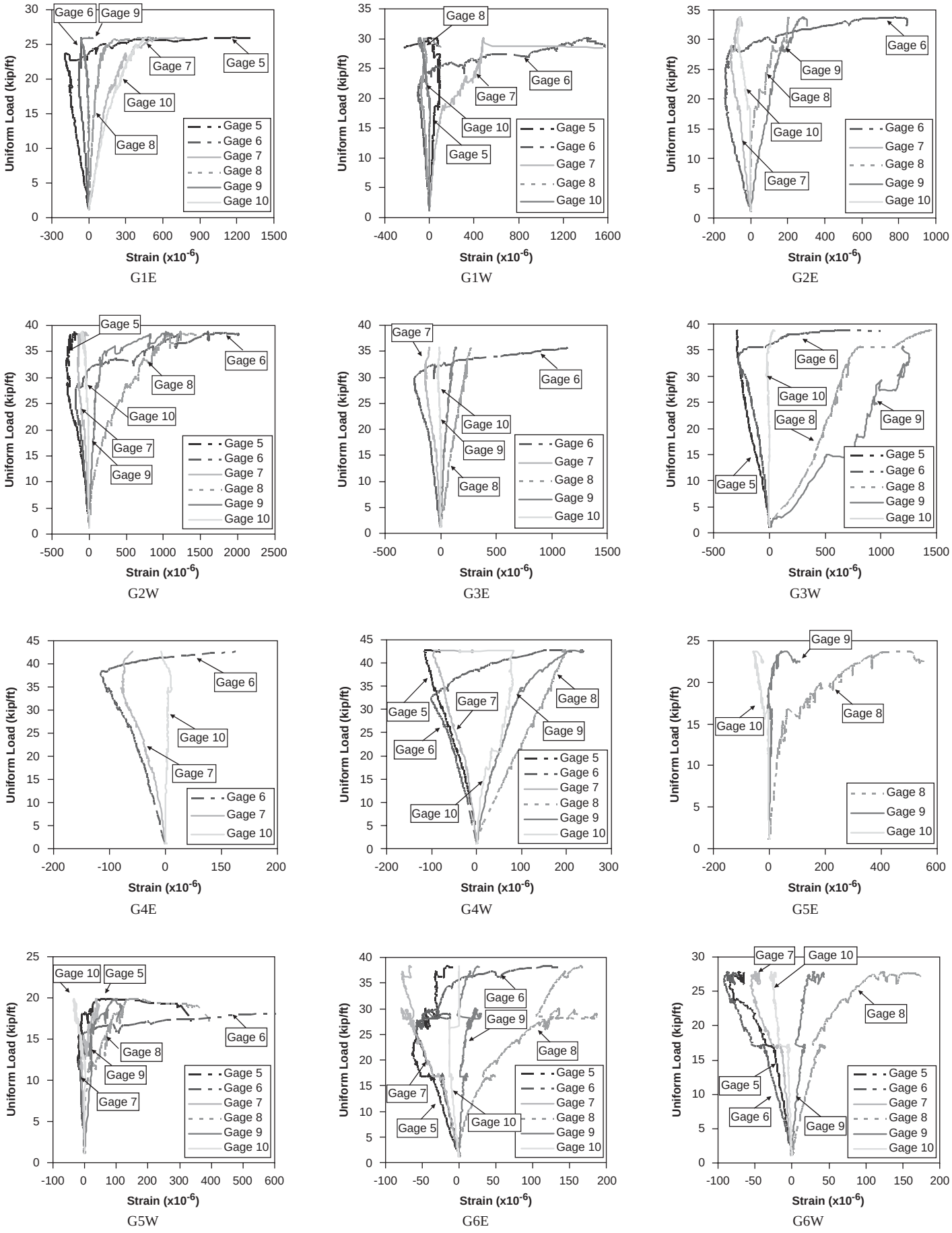

Figure 89. Transverse strains in confinement cages.

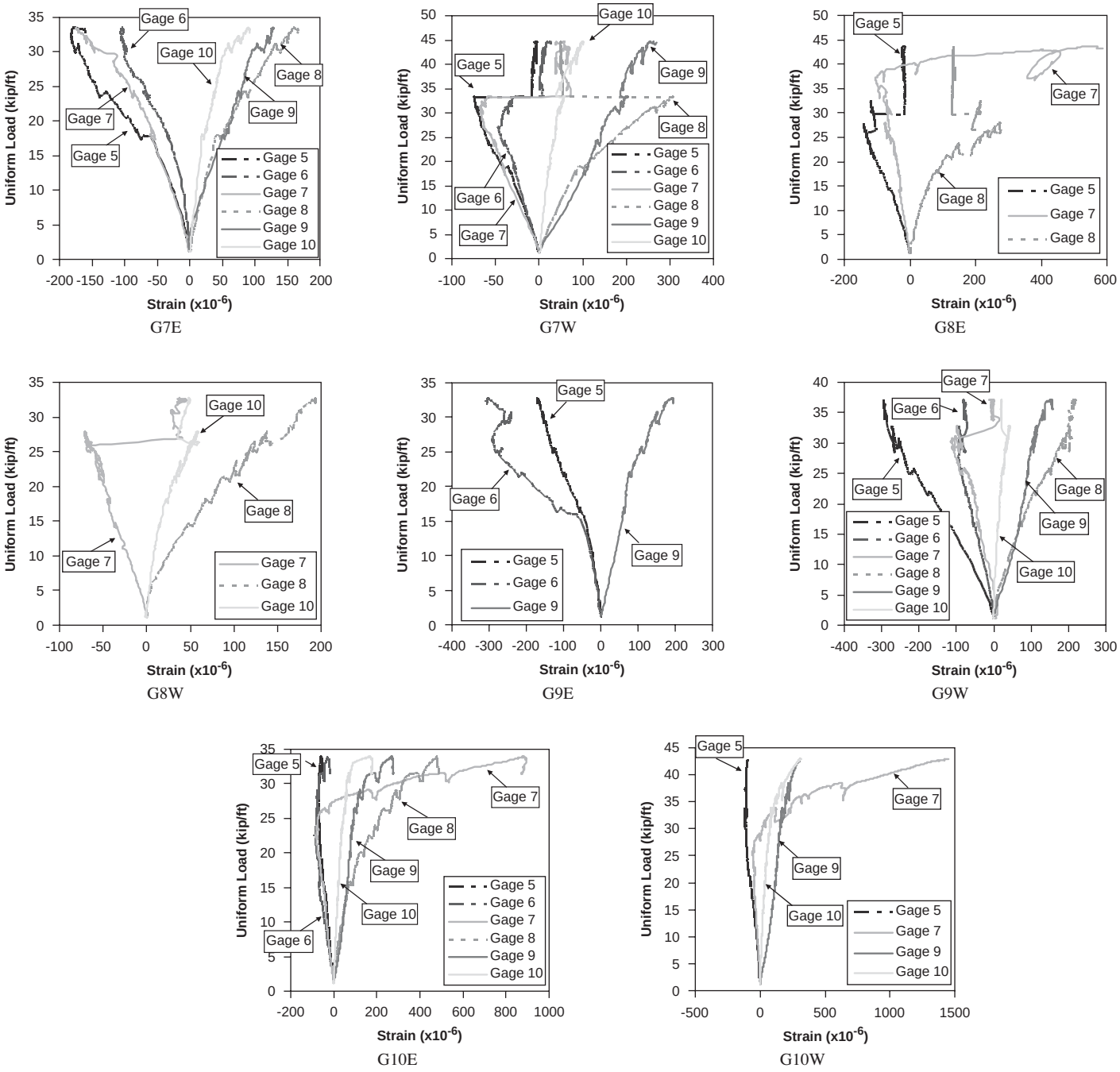

Figure 89. (Continued).

- Prior to cracking, the behavior was essentially linear elastic. After cracking, there was an abrupt change in stiffness followed by another region of essentially elastic behavior before shear strains began to develop rapidly with large increases in strain for only small increases in shear once shear strains reached 3,000 microstrain and above.
- Rosettes in the same girder yielded similar elastic slopes or stiffness prior to cracking. The shear strain at cracking was small, ranging from 200 to 600 microstrain.
- Immediately after cracking, there was often a sudden jump in shear strain without any increase in load (a plateau) of the shear strain. The length of the plateau depended on the stirrup reinforcement ratio. Members with low stirrup reinforcement ratios had longer plateaus than members with higher stirrup reinforcement ratios. For example, the longest plateau, 1,200 microstrain, occurred in G5E, where the stirrup reinforcement was only $\rho_v f_y = 169$ psi.
- Within the inelastic portion of the response, the initiation of stirrup yielding had a significant influence on the slope of the curve. Before stirrup yielding, the response was almost linear, as exhibited in G4E, G4W, G9E, and G9W, in which little or no stirrup yielding occurred. When more

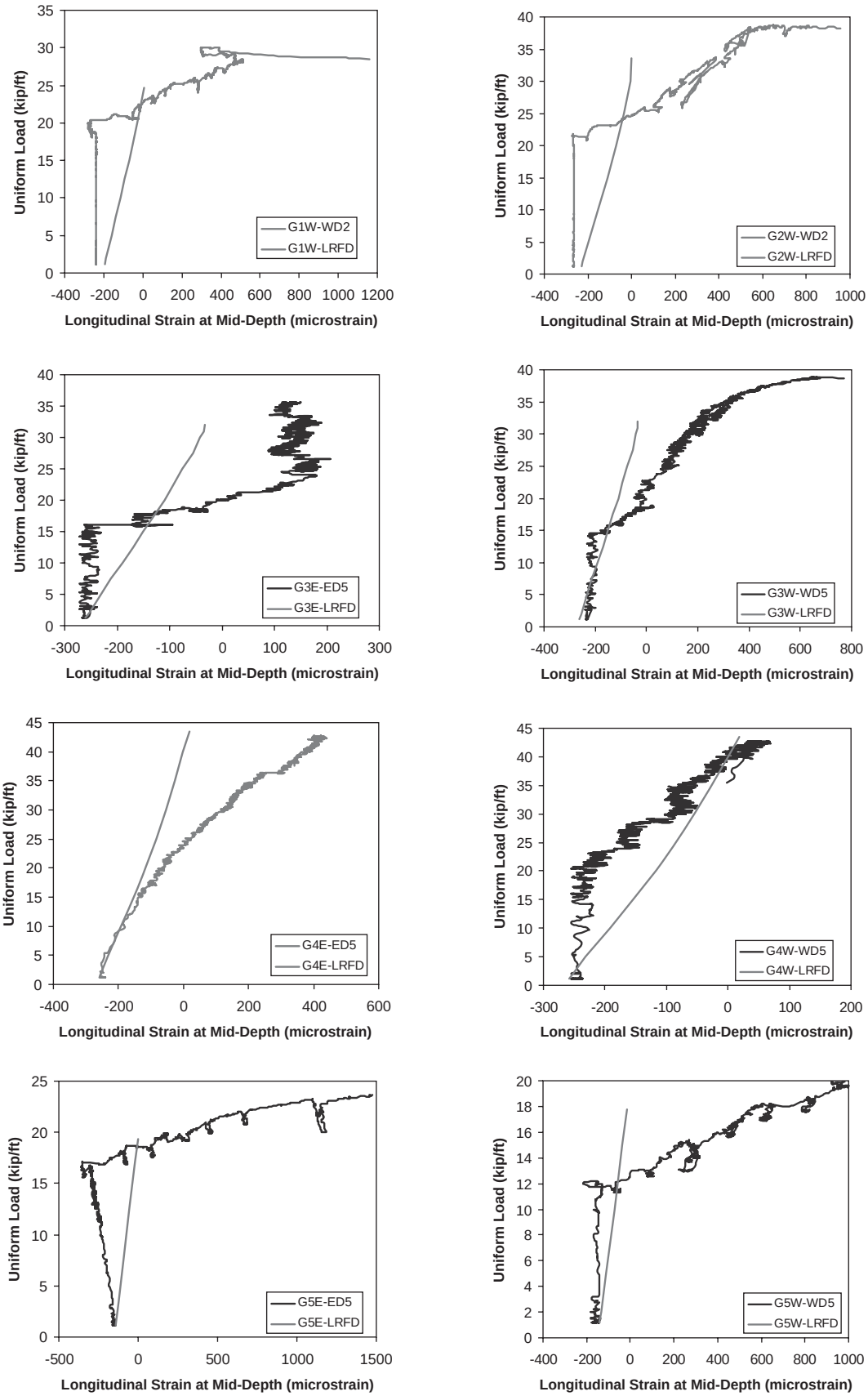

Figure 90. Longitudinal strain at web.

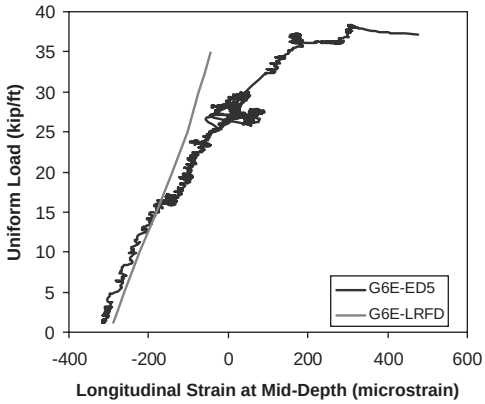

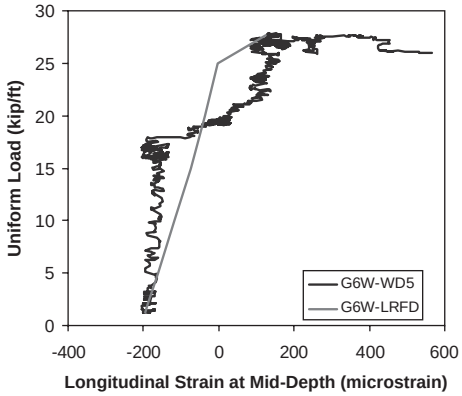

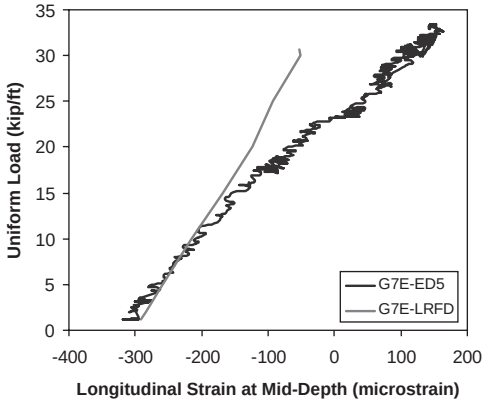

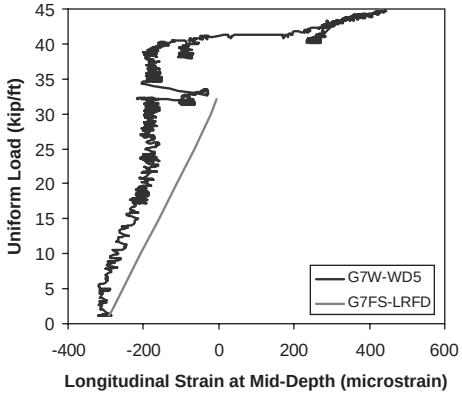

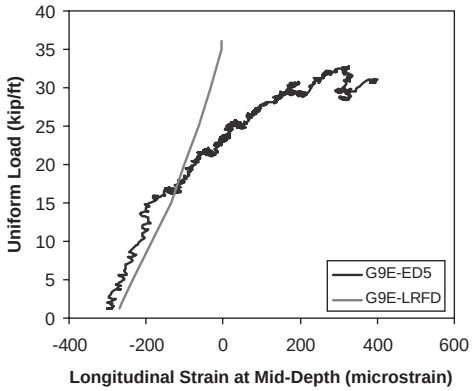

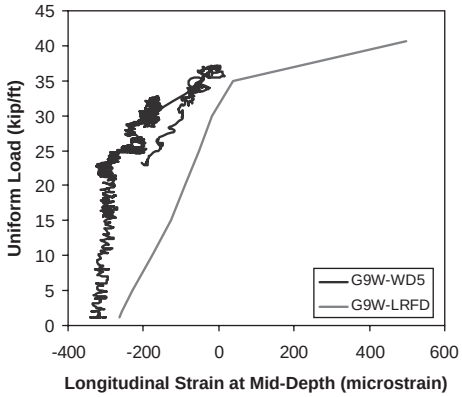

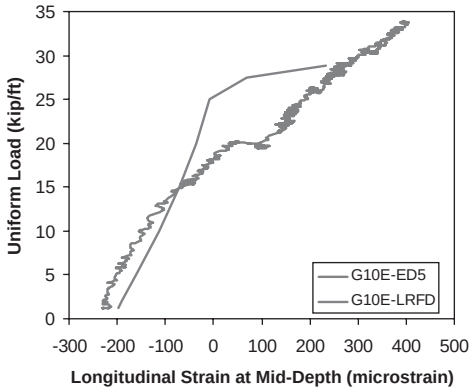

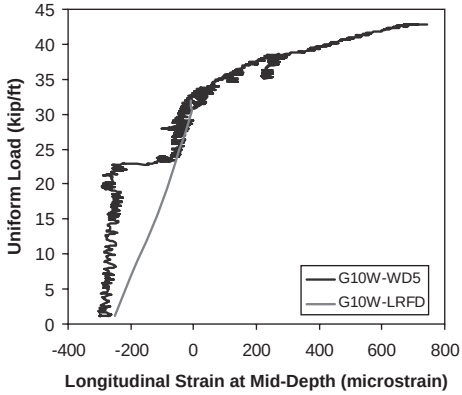

Figure 90. (Continued).

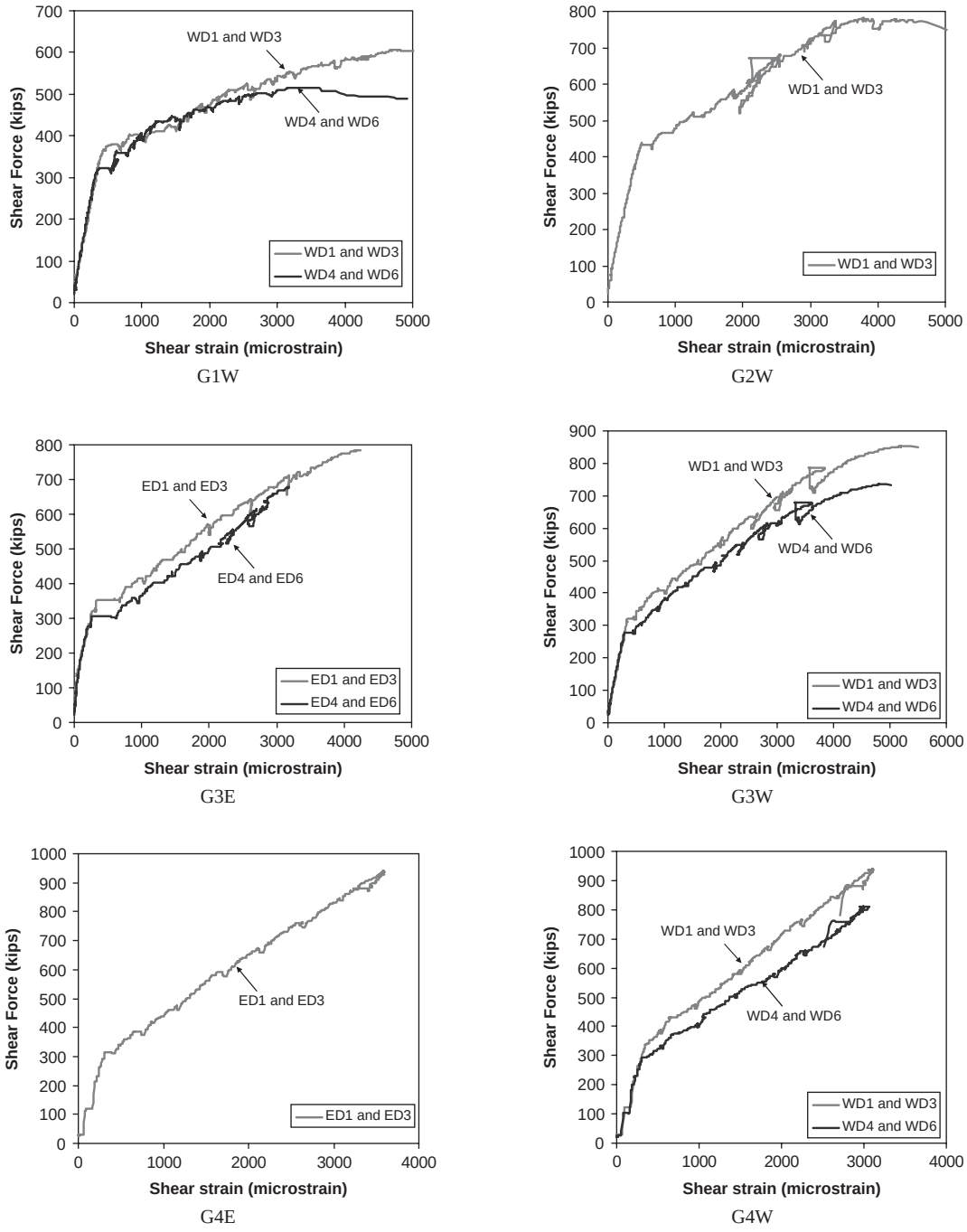

Figure 91. Web-shear strain versus sectional shear force.

significant yielding of the stirrups occurred, there was a marked change in shear stiffness.

- As is expected, the rosette close to the actual end measured higher shear strains than the rosette farther from the end. The shear strain under the peak or failure load ranged from 4,000 microstrain to 6,000 microstrain for the rosette close to the actual end.

Based on the above observations, a simplified tri-linear curve can be used to model the relationship of the sectional shear force versus shear strain, as shown in Figure 92. The idealized response consists of three line segments defined by four points: A, B, C, and D. Line segment AB represents the elastic range of behavior, while the inelastic range is divided into two straight segments defined by BC and CD. C is the characteristic point where the stirrups start to yield. The girder failed or the maximum load was reached at point D. The slopes of these three segments are designated in the figure as S_e, S_{t1} and S_{t2}, with $S_e > S_{t1} > S_{t2}$.

Table 21 presents the characteristic points of the tri-linear model for the plots in Figure 91. In the second column

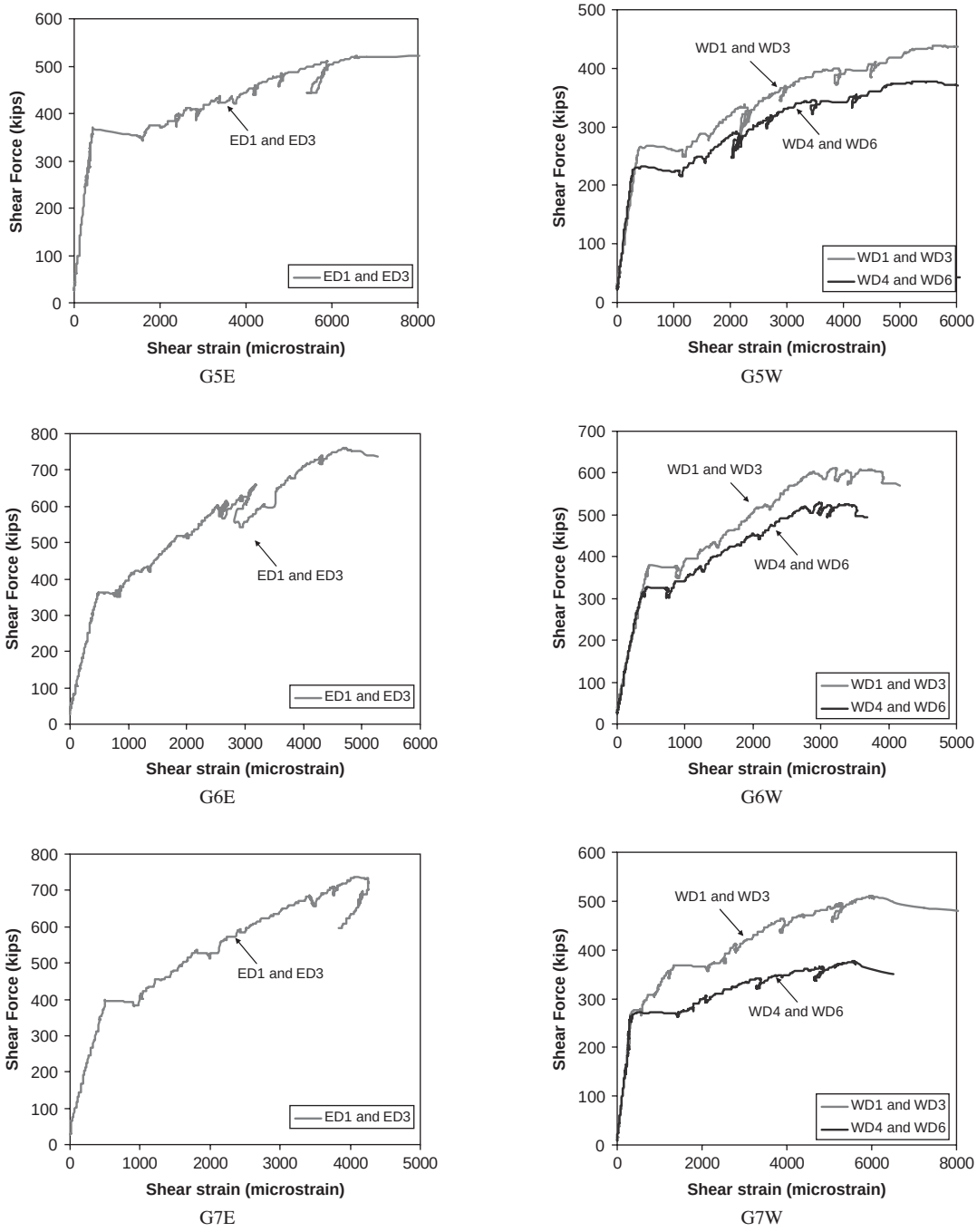

Figure 91. (Continued).

of the table, x is the location of the center of the rosette measured from the actual end of the girder. The measured shear force, V, and the measured shear strain, γ, are listed in turn in each of the subsequent columns for each point A, B, C, and D. The elastic stiffness S_e and tangent stiffnesses S_{t1} and S_{t2} are listed in the last three columns of the table.

The following subsections discuss findings concerning the elastic behavior and the inelastic behavior in detail. For the elastic stage, the shear stress distribution was computed using elastic theory, and the calculated elastic stiffness was compared with the measured values. For the inelastic stages, equations for computing the tangent stiffnesses S_{t1} and S_{t2} are proposed based on analysis of the test data.

Elastic Stage

By the traditional theory for homogeneous and elastic beams, the shear stress v on any section can be computed using Equation 42:

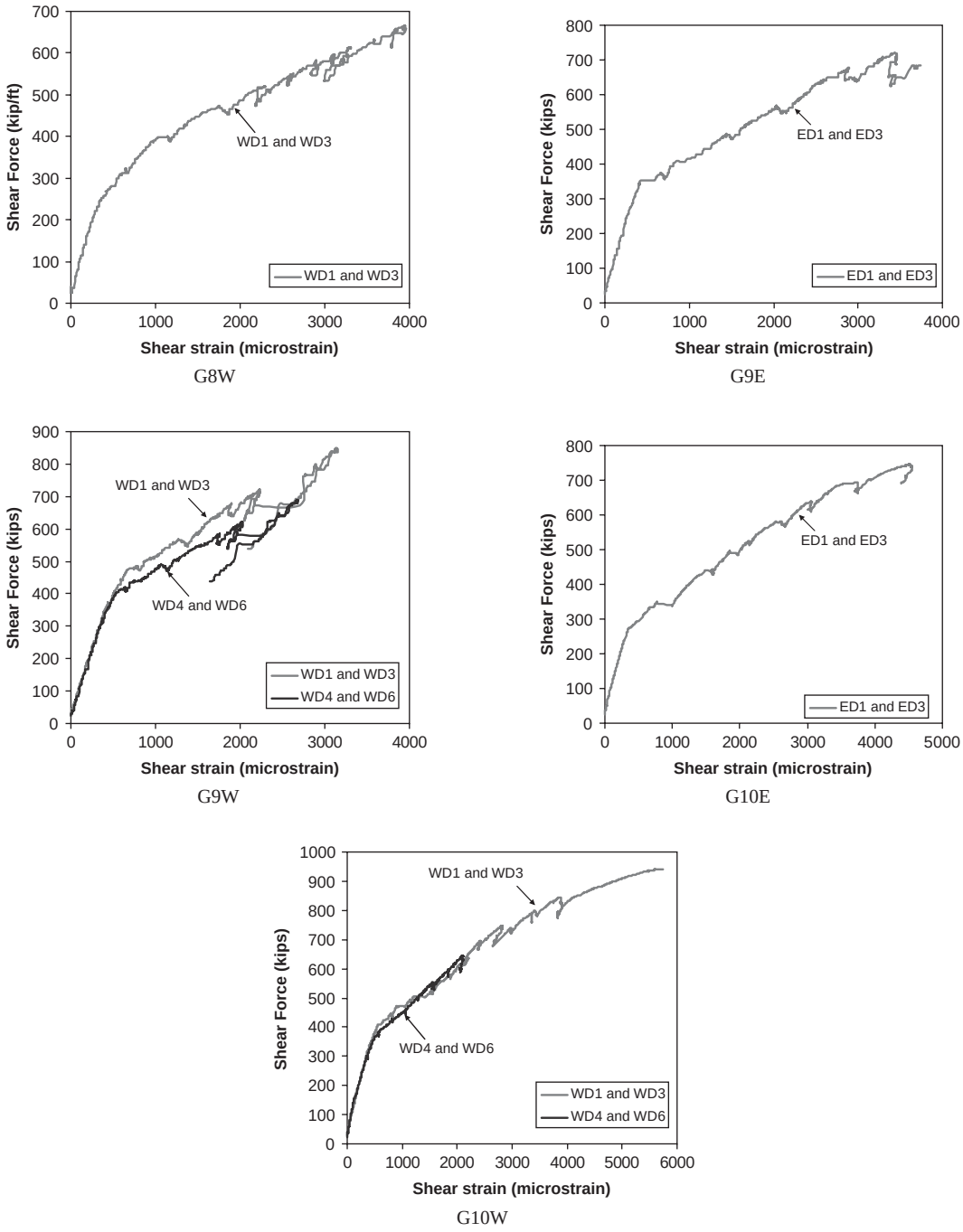

Figure 91. (Continued).

$$v = \frac{VQ}{Ib} \tag{42}$$

where:

V = shear force on the cross section,
I = moment of inertia of the cross section,
Q = first moment about the neutral axis of the part of the section lying between the bottom or top edge and the point where the shear stress is being calculated, and
b = width of the member where the stress is being calculated.

Figure 93 shows the typical shear stress distribution calculated by the foregoing equation for the composite section of the test girders. Note that the composite section properties were calculated based on the transformed slab width and the calculated modulus of the precast girder. The shear stress on the web is much higher than that on the top flange and bottom bulb. The maximum stress occurred at the location of the neutral axis. The average stress within the web region (45 inches deep) was also computed, and that stress is indicated in Figure 93.

Following the above procedure, the shear stress distribution on the girder section under a shear force of $V = 100$ kips

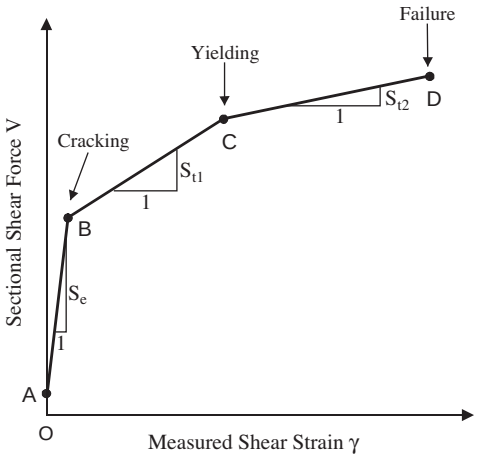

Figure 92. Idealized tri-linear curve of shear strain versus shear force.

was computed for each girder. Table 22 lists the calculated results. The shear force resistance is provided by three parts: V_{top}, the shear force in the top flange and deck; V_{web}, the shear force in the web; and V_{bot}, the shear force in the bottom bulb. It is seen that the web provides about 75 percent of the total shear force resistance. The remaining 25 percent is provided by the top flange and deck (17 percent) and by the bottom bulb (8 percent). The ratio between the maximum shear stress τ_{max} and the average stress within the web τ_{avg} is 1.070, with values ranging from 1.065 to 1.077.

The last column of Table 22 provides the calculated elastic stiffness $S_{e,cal}$ which is computed as

$$S_{e,cal} = \frac{V}{\tau_{avg} / G} \tag{43}$$

where:

τ_{avg} = average sheer stress over the web region,

G = shear modulus of the girder computed from the measured concrete elastic modulus,

$$G = \frac{E}{2(1+\nu)}, \text{ and}$$

ν = Poisson ratio = 0.2.

To evaluate the accuracy of elastic theory in predicting the measured stiffness, Table 23 compares the average value of the measured stiffness for each girder with the value calculated by the foregoing equation. The ratio of the average measured stiffness to the calculated stiffness ranges from 0.80 to 1.18, with a mean value of 0.96 and a COV of 0.12. Note that no comparison was made for G8W because of the two strengthening plates that were placed on the west end of that girder.

Table 21. Characteristic points of the tri-linear model for measured web strains.

Girder	x (in)	A		B		C		D		Stiffness		
		V (kips)	γ (ms)	V (kips)	γ (ms)	V (kips)	γ (ms)	V (kips)	γ (ms)	S_e (kips)	S_{t1} (kips)	S_{t2} (kips)
G1WD13	70	23.8	0	362.8	414	522.5	2,569	606.8	4,671	818,841	74,107	40,105
G1WD46	106	20.3	0	318.4	340	462.7	1,770	516.5	3,161	876,765	100,909	38,677
G2WD13	70	23.8	0.0	431.4	478	755.5	3,349.0	781.3	3,777	852,727	112,887	60,280
G3ED13	48	26.0	0	312.0	244	707.0	3,168	785.0	4,201	1,172,295	135,089	75,508
G3ED46	84	22.4	0	277.4	207	677.9	3,175	677.9	3,175	1,231,787	134,939	N/A
G3WD13	48	26.0	0	321.2	343	774.7	3,752	854.0	5,184	860,758	133,030	55,377
G3WD46	84	22.4	0	277.4	298	611.6	2,864	737.6	4,824	855,638	130,242	64,286
G4ED13	48	26.0	0	313.7	308	938.3	3,591	N/A	N/A	934,221	190,253	N/A
G4WD13	48	26.0	0	339.7	343	938.3	3,117	N/A	N/A	914,694	215,789	N/A
G4WD46	84	22.4	0	293.4	307	810.4	3,061	N/A	N/A	882,671	187,727	N/A
G5ED13	48	26.0	0	369.6	438	521.4	6,569	N/A	N/A	784,566	24,759	N/A
G5WD13	48	26.0	0	266.2	402	394.8	3,520	437.8	5,575	597,612	41,244	20,925
G5WD46	84	22.4	0	226.1	278	340.9	3,180	378.1	5,210	732,662	39,559	18,325
G6ED13	48	26.0	0	363.7	483	654.5	3,168	760.3	4,735	699,255	108,305	67,518
G6WD13	48	26.0	0	379.9	466	599.6	2,914	612.7	3,210	759,528	89,747	44,257
G6WD46	84	22.4	0	328.1	431	517.9	2,786	529.2	3,004	709,234	80,594	51,835
G7ED13	48	26.0	0	398.2	502	736.3	4,054	N/A	N/A	741,514	95,186	N/A
G7WD13	175	13.5	0	273.4	354	463.1	3,912	511.0	5,968	734,261	53,316	23,298
G7WD46	211	9.9	0	268.1	364	376.7	5,580	N/A	N/A	709,254	20,821	N/A
G8WD13*	48	26.0	0	252.3	363	399.4	1,038	667.1	3,952	623,526	217,926	91,867
G9ED13	48	26.0	0	352.0	422	721.6	3,439	N/A	N/A	772,607	122,506	N/A
G9WD13	48	26.0	0	475.2	675	840.5	3,119	N/A	N/A	665,541	149,468	N/A
G9WD46	84	22.4	0	400.7	525	684.3	2,658	N/A	N/A	720,533	132,958	N/A
G10ED13	48	26.0	0	273.5	359	690.5	3,542	746.5	4,521	689,526	131,008	57,201
G10WD13	48	26.0	0	407.4	556	837.1	3,886	939.7	5,644	686,043	129,039	58,362
G10WD46	84	22.4	0	363.3	490	641.3	2,102	N/A	N/A	695,673	172,457	N/A

*Aluminum plates were plated at the west end of Girder 8.

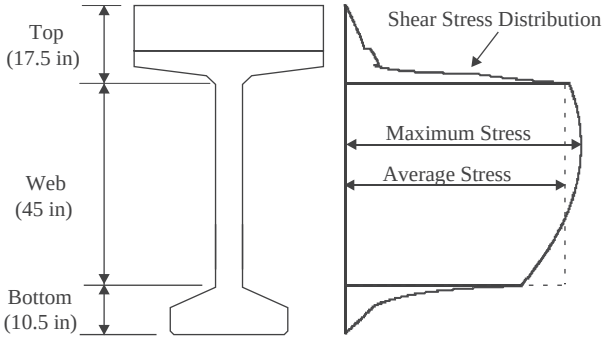

Figure 93. Shear stress distribution in girder section.

Table 22. Shear force and stress distribution under shear force *V* = 100 kips

Girder	V_{top} (kips)	V_{web} (kips)	V_{bot} (kips)	τ_{max} (ksi)	τ_{avg} (ksi)	$S_{e,cal}$ (kips)
Girder 1	18.2	73.8	8.0	0.296	0.276	860,807
Girder 2	19.0	73.1	7.8	0.294	0.273	973,675
Girder 3	17.7	74.2	8.1	0.297	0.278	873,554
Girder 4	18.8	73.3	7.9	0.295	0.274	884,561
Girder 5	18.7	73.4	7.9	0.295	0.275	889,735
Girder 6	19.7	72.6	7.7	0.294	0.271	833,250
Girder 7	19.1	73.1	7.8	0.294	0.273	690,471
Girder 8	19.9	72.4	7.7	0.294	0.271	697,005
Girder 9	19.0	73.2	7.8	0.295	0.274	817,476
Girder 10	19.5	72.8	7.7	0.294	0.272	681,468

Inelastic Stage

After web cracking occurred, the shear behavior exhibited an inelastic response. Shear strains in a cracked web result from three primary components: deformations of the uncracked concrete, opening of the diagonal cracks, and relative slip between crack faces along the crack surface. Compared with the latter two components, the deformation of the uncracked concrete is small. Hence, the total shear strain depends on the crack width and crack slip. Because the crack width and crack slip are strongly influenced by the stirrup reinforcement ratio, the test results were used to develop a relationship for shear stiffness that depended on the stirrup reinforcement ratio.

Table 24 lists relative stirrup reinforcement ratios and relative stiffness ratios S_{t1}/S_e and S_{t2}/S_{t1}, respectively, for each of the test girders. Values for S_e, S_{t1}, and S_{t2} were presented in Table 21. Table 24 introduces a nondimensional parameter $n\rho_v$, where $n = (E_s/E_c)$ and $\rho_v = A_v/(bs)$. This parameter takes into account the influences of both the stirrup reinforcement ratio and its stiffness. The ratio of S_{t1}/S_e ranges from 0.07 to 0.25, while the ratio of S_{t2}/S_{t1} ranges from 0.38 to 0.64 and averages 0.50.

Figure 94 presents the stiffness ratio S_{t1}/S_e versus the nondimensional parameter $n\rho_v$. It is seen that when $n\rho_v$ is less than around 0.06, there exists a good correlation between S_{t1}/S_e and $n\rho_v$. However, for values of $n\rho_v$ greater than 0.06, the S_{t1}/S_e values tend to be constant at values between 0.18 and 0.25. Regression analysis was used on the results to obtain the following equations:

$$\frac{S_{t1}}{S_e} = 2.45(n\rho_v) + 0.05 \qquad (44a)$$

when

$$n\rho_v \le 0.065$$

$$\frac{S_{t1}}{S_e} = 0.21 \qquad (44b)$$

when

$$n\rho_v > 0.065$$

Figure 95 shows the stiffness ratio S_{t2}/S_{t1} versus the same nondimensional parameter $n\rho_v$. It can be seen that ratios oscillate around a value of 0.5 and depend little on $n\rho_v$. For simplicity, the following relationship is suggested:

$$\frac{S_{t2}}{S_{t1}} = 0.5 \qquad (45)$$

Table 23. Measured and calculated shear stiffness.

Girder	Measured Stiffness $S_{e,test}$ (kips)					$S_{e,cal}$ (kips)	$\frac{S_{e,test}}{S_{e,cal}}$
	ED13	ED46	WD13	WD46	Average		
Girder 1	N/A	N/A	818,841	876,765	847,803	860,807	0.98
Girder 2	N/A	N/A	852,727	N/A	852,727	973,675	0.88
Girder 3	1,172,295	1,231,787	860,758	855,638	1,030,120	873,554	1.18
Girder 4	934,221	N/A	914,694	882,671	910,528	884,561	1.03
Girder 5	784,566	N/A	597,612	732,662	704,946	889,735	0.79
Girder 6	699,255	N/A	759,528	709,234	722,672	833,250	0.87
Girder 7	741,514	N/A	734,261	709,254	728,343	690,471	1.05
Girder 8	N/A	N/A	623,526	N/A	N/A	697,005	N/A
Girder 9	772,607	N/A	665,541	720,533	719,560	817,476	0.88
Girder 10	689,526	N/A	686,043	695,673	690,414	681,468	1.01
						Average	0.96
						COV	0.12

Table 24. Ratios between measured stiffness.

Girder	$n\rho_v$ 100	S_{t1}/S_e	S_{t2}/S_{t1}
G1WD13	0.56	0.09	0.54
G1WD46	2.42	0.12	0.38
G2WD13	4.00	0.13	0.53
G3ED13	3.16	0.12	0.56
G3ED46	3.16	0.11	N/A
G3WD13	3.16	0.15	0.42
G3WD46	3.16	0.15	0.49
G4ED13	6.45	0.20	N/A
G4WD13	6.45	0.24	N/A
G4WD46	6.45	0.21	N/A
G5ED13	0.66	0.03	N/A
G5WD13	0.66	0.07	0.51
G5WD46	0.66	0.05	0.46
G6ED13	3.66	0.15	0.62
G6WD13	3.66	0.12	0.49
G6WD46	3.66	0.11	0.64
G7ED13	3.57	0.13	N/A
G7WD13	0.68	0.07	0.44
G7WD46	0.68	0.03	N/A
G9ED13	7.76	0.16	N/A
G9WD13	12.61	0.22	N/A
G9WD46	12.61	0.18	N/A
G10ED13	5.33	0.19	0.44
G10WD13	5.33	0.19	0.45
G10WD46	5.33	0.25	N/A

2.6.9 Time-Dependent Losses

As mentioned in Section 2.3, a Whittemore gage was used to measure changes in deformation along the length of the bottom bulb of the girders. Measurements were usually taken before strand release, after strand release, at periodic intervals between strand release and testing, and shortly before testing to assess the transfer length, the prestressing loss, and the development of strains prior to testing. Those measurements also provided experimental data for the evaluation of the time-dependent prestress losses due to concrete shrinkage and creep, as well as strand relaxation. The detailed measurements for each girder are presented in the associated appendices.

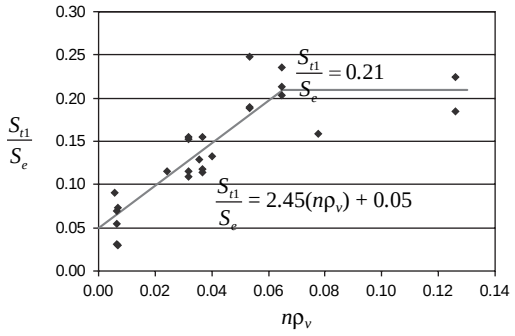

Figure 94. **$n\rho_v$ *versus stiffness ratio* S_{t1}/S_e.**

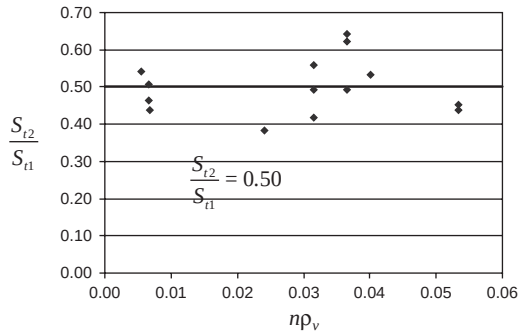

Figure 95. **$n\rho_v$ *versus stiffness ratio* S_{t2}/S_{t1}.**

In Article 5.8.5.4, the LRFD specifications present a refined method for computing time-dependent losses. The refined method, based on the measured material properties and measured elastic shortening, was used to compute the calculated time-dependent losses. Figure 96 compares the calculated total losses with the measured values for each girder. The calculated total prestress loss was computed by adding the measured elastic loss to the calculated time-dependent loss. The comparisons show that, for the data as a whole, the refined estimates of time-dependent losses agree reasonably well with the experimental data.

2.6.10 Transfer Length

Elastic shortening due to strand release was obtained from the two sets of Whittemore readings, with one reading taken immediately before strand release and one reading taken immediately after strand release. From the strain profile of the elastic shortening, the transfer length was measured for each end of each girder. Table 25 lists the measured transfer lengths for the two ends for each girder. Transfer lengths range from 18 to 28 inches and average 23 inches. The LRFD specifications suggest that the transfer length is 60 times the strand diameter, or 36 inches for the test girders. The measured transfer length is only about two-thirds of the LRFD value. ACI Code 318-05 specifies a transfer length equal to effective prestress divided by three, in ksi units, times the strand diameter. For the typical effective prestress for these girders of 160 ksi, the corresponding transfer length is 53 times the strand diameter, or 32 inches.

2.7 Components of Shear Resistance

2.7.1 Introduction

As discussed in Chapter 1, there are substantial differences in how codes of practice evaluate the contributions of transverse reinforcement, V_s, and concrete, V_c, to shear

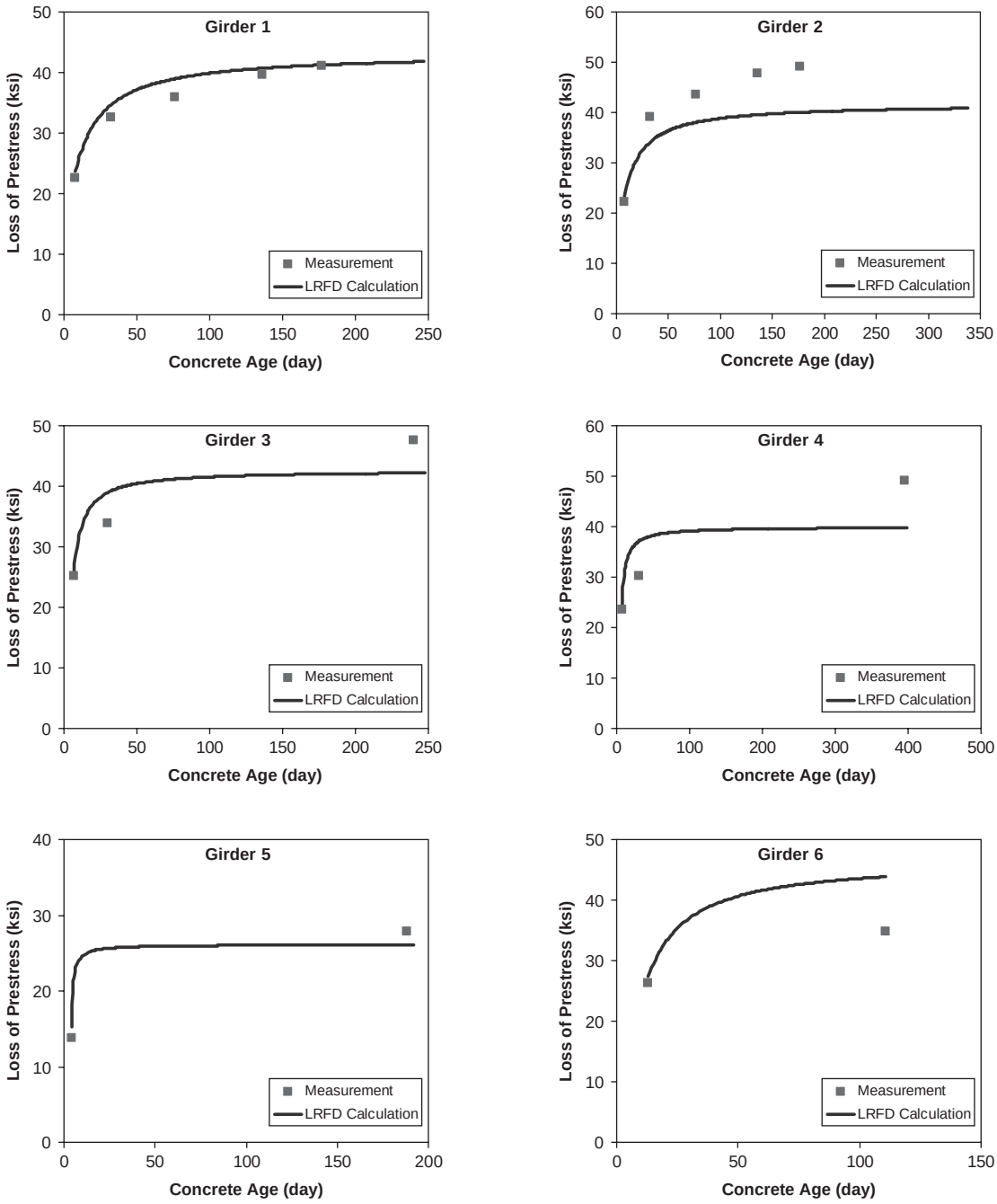

Figure 96. Comparison between the measured and calculated prestress losses.

resistance. For example, the AASHTO Standard Specifications evaluate V_s based on a 45-degree truss model, whereas the LRFD specifications use a variable angle truss model in which the angle of diagonal compression can be as low as 18 degrees. The effect of this difference is that the calculated V_s contribution to shear resistance according to the LRFD specifications can be two to three times larger than that calculated by the AASHTO Standard Specifications for the same member with the same quantity of shear reinforcement. There are similarly large differences in the magnitude of the calculated concrete contribution to shear resistance with the additional complication of different explanations for the source of this resistance. In the AASHTO Standard Specifications, V_c is taken as the calculated diagonal cracking strength, while in the LRFD specifications, V_c is calculated from the average principal postcracking tensile stress that can be carried in the web of a member and is limited by the shear slip resistance along a crack face. Other codes and shear design methods provide different explanations for the concrete contribution to resistance.

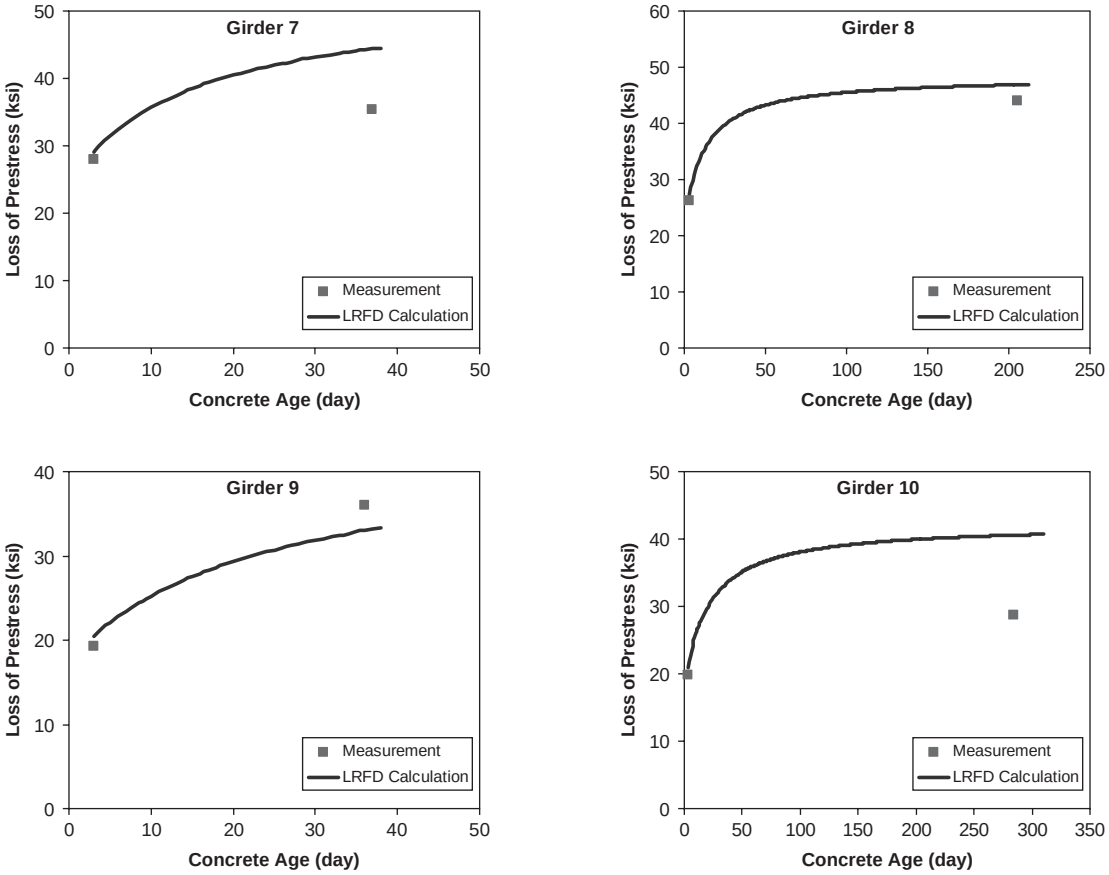

Figure 96. (Continued).

In this section, the contributions of the transverse reinforcement and the concrete to the shear resistance are evaluated over the loading history of each girder, with V_s evaluated from free-body diagrams and from measured values for stirrup strains from strain gauge readings. The results are used to investigate influencing factors and the safety of the LRFD specifications. Section 2.7.2 describes the method used to evaluate the components of resistance, and Section 2.7.3 describes the method used to evaluate the components' contributions over the loading history for all girder ends. Section 2.7.4 introduces a new term, called the "characteristic angle," for evaluation of postcracking behavior, and Section 2.7.5 evaluates the LRFD method for calculating the components of resistance.

Table 25. Measured transfer length.

Girder	Transfer Length (in)	
	West	East
Girder 1	28	28
Girder 2	23	23
Girder 3	NA	18
Girder 4	23	23
Girder 5	23	25
Girder 6	N/A	23
Girder 7	23	23
Girder 8	23	23
Girder 9	20	23
Girder 10	23	N/A

2.7.2 Method for Evaluating V_s and V_c

Crack-Based Free Body Diagram

As reported in Section 2.5, the loading of each girder was paused at several load stages in the testing of each girder to mark cracks and to make other key measurements. The locations of these cracks were recorded by photographs, and then an image analysis method was used to produce a complete cracking history for each girder, as described in Appendix 11. For every diagonal crack at the ultimate crack pattern, a free body between the end of the girder and this crack was produced. In this evaluation, that free body is termed a "crack-based free body diagram" (CFBD). Figure 97 gives an example of the selection of crack-based free body for the west end of Girder 1. Figure 97(a) shows the crack pattern of the west end of Girder 1 (G1W), and Figure 97(b) shows the dimensions for the CFBD of a selected diagonal

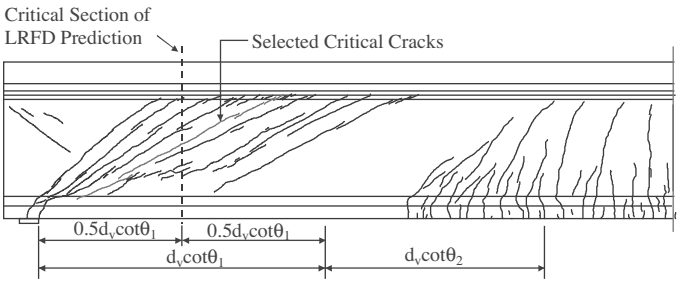

(a) Selected Crack for Free Body Diagram Analysis

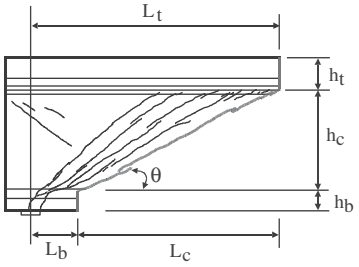

(b) Dimensions of Selected Free Body Diagram

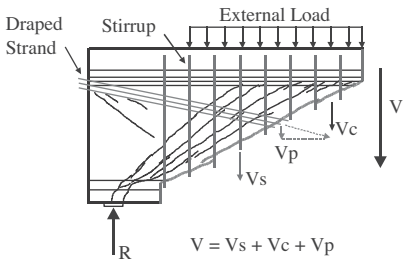

(c) Shear Resistance in the Crack Section

Figure 97. Free body diagram for components of shear resistance.

crack. Figure 97(c) shows the vertical forces acting on the free body. These forces consist of the reaction force "R" at the end support, the external distributed load on the top of the girder, the forces in the stirrups, the vertical component of the prestress, and the concrete contribution V_c to shear resistance. The individual components of V_c are not shown, but they are recognized to consist of interface shear transfer, shear in the uncracked compression zone at the top of the member, shear in the typically uncracked bottom bulb, dowel action, and stress transmitted directly across a crack.

While there are several potential free body diagrams at the end of each girder, each corresponding to a different diagonal crack, one CFBD was selected for each end to be used for presenting the measured components of resistance. The exceptions were the west end of Girder 7 and the east end of Girder 8, in which two CFBDs were selected. Table 26 presents the geometric and reinforcement details for each of these selected CFBDs. The dimensional parameters used in Table 26 are defined in Figure 97(b). L_b and L_t are longitudinal distances from the center of the support to the very bottom and very top points of the cracks, respectively. L_c is the horizontal projection of the crack; h_b and h_t are the uncracked concrete depths of the bottom bulb and the top flange, respectively; and h_c is the overall depth of the crack. For the test girders, h_c ranges from 38.95 to 51.73 inches and averages 46.3 inches, which is very close to the web depth of 47 inches. Also listed in the table are the measured crack angle θ and the numbers and yield strength of the stirrups that cross the selected cracks. The last two columns of Table 26 list the sum of the yield force of those stirrups, V_y, and the effective stirrup strength, $\rho_v f_{yv}$, for the stirrups that crossed the boundary crack of the free body.

Two considerations controlled the selection of the critical crack. The first was that it should be in the region of the widest cracks, the largest stirrup strains, and the location where the failure was observed. Second, if there were two or more cracks in this failure region, the crack whose midpoint was closest to the LRFD-specified critical section ($0.5d_v\cot\theta$ from the inside face of the support) was selected, as illustrated in Figure 97.

Method for Evaluating V_s and V_c

As shown in Figure 97(c), the total shear force V in the inclined section was computed from the reaction force and the external test load. The vertical component of the prestress force V_p was calculated from geometry and neglected the increment in prestress force due to the external load. The contribution of the stirrup reinforcement was evaluated from strain gage readings, and then V_c was directly calculated from equilibrium of the vertical forces.

Evaluation of V_s

The transverse reinforcement was extensively instrumented, with four gages on 10-inch centers applied over the depth of between 14 and 18 transverse bars. The measured strain gage readings were used to compute the stirrup stresses and their forces. To compute the shear contribution of the stirrups, V_s, the strains at crack locations along every stirrup should be measured. Because this was not practical, an approach was adopted for making the best possible estimate of stirrup strains. This method can effectively use the strain gage readings and deals with both gauged and ungauged stirrups using different approaches. For gauged stirrups, if cracking was located between two consecutive gages, then the strain at the boundary crack was obtained from the gage with the higher reading. If the boundary crack point was located outside any two consecutive gages, then the strain at the boundary crack point was taken as that at the nearest gage. For stirrups without gages, the strain at the boundary crack point was interpolated from the "crack strains" of the two gauged stirrups on either side of the ungauged stirrup or was

Table 26. Dimensions and transverse reinforcement in selected free body diagrams.

Girder	Dimensions for Free Body Diagrams							Stirrup Layout			
	L_b (in)	L_c (in)	L_t (in)	h_b (in)	h_c (in)	h_t (in)	θ (deg)	A_v	f_{yv} (ksi)	V_y* (kips)	$\rho_v f_{yv}$* (psi)
G1E	27.67	91.41	119.08	10.62	47.39	14.99	27.2	7-2#4	70.0	196.0	357
G1W	22.48	92.48	114.96	9.20	47.68	16.12	28.2	8-2#4	70.0	224.0	404
G2E	34.99	92.28	127.28	11.58	45.53	15.89	26.4	8-2#5	79.3	393.3	710
G2W	26.70	87.46	114.16	10.47	47.20	15.33	29.8	8-2#5	79.3	393.3	750
G3E	23.59	97.94	121.53	10.55	47.02	15.43	26.0	13-2#4	67.8	352.6	600
G3W	33.43	89.96	123.39	10.89	46.26	15.85	27.3	11-2#4	67.8	298.3	553
G4E	24.26	82.46	106.72	10.66	47.41	14.93	28.4	13-2#5	64.6	520.7	1,052
G4W	17.48	92.35	109.83	9.03	48.74	15.23	28.4	16-2#5	64.6	640.8	1,157
G5E	31.29	125.93	157.22	9.70	49.23	14.07	21.1	6-2#3	82.2	121.7	161
G5W	12.30	120.13	132.43	7.60	51.73	13.67	23.7	6-2#3	76.5	101.0	140
G6E	16.73	79.93	96.66	11.47	46.25	15.28	30.1	7-2#5	64.7	280.8	585
G6W	38.15	73.06	111.21	13.94	41.33	17.73	29.9	6-2#5	64.7	240.7	549
G7E	21.79	94.40	116.19	10.81	45.03	17.17	25.9	12-2#4	69.2	332.2	586
G7W	81.52	103.82	185.34	13.01	45.09	14.90	23.6	8-2#4/1-2#3	69.2/74.5	237.8	382
G7FS	161.04	91.89	252.93	10.64	46.31	16.06	25.9	4-2#3	74.5	65.6	119
G8E	24.22	80.79	105.01	11.30	46.74	14.96	30.1	10-2#4	69.2	276.8	571
G8EB	49.48	99.79	149.26	10.54	47.62	14.83	25.1	12-2#4	69.2	332.2	555
G8WP	21.84	80.16	101.99	10.96	47.65	14.39	30.0	10-2#4	69.2	276.8	576
G9E	19.34	85.16	104.50	13.22	43.42	16.36	27.8	14-2#5	65.4	567.7	1,111
G9W	28.51	55.73	84.24	15.12	38.95	18.93	35.7	14-2#5	65.4	567.7	1,698
G10E	10.84	73.94	84.78	7.46	42.54	23.01	30.8	8-2#5	65.4	324.4	731
G10W	9.91	90.64	100.54	6.76	49.42	16.82	29.2	10-2#5	65.4	405.5	746

*$V_y = \sum f_{yv} A_v$, $\rho_v f_{yv} = V_y / (b_w L_c)$, and $b_w = 6$ inches.

taken from the nearest gauged stirrup if there were only one gauged stirrup available on one side of the boundary crack. By using this method, all stirrups in the free body were assigned a strain considered to be the best possible estimate of the strain along the line of cracking.

Once the strains at cracks had been calculated, the reinforcement stresses were computed using the measured material properties of the reinforcement. When the measured strain was above the yield strain, then the yield stress was used. This approach is considered appropriate for all of the girder tests except for the east side of Girder 5, in which the welded wire fabric would be expected to exhibit a cold-rolled stress-strain response. Thus, V_s may be underestimated and V_c overestimated for the east end of Girder 5. The contribution of the stirrups V_s was then obtained by summing the forces in all the stirrups crossing the boundary crack.

Evaluation of V_c

It was impractical to attempt to directly measure the concrete contribution to shear resistance. Therefore, it was computed from equilibrium by subtracting V_s and V_p from the total shear force V acting on the section.

2.7.3 Shear Resistance Components

By using the above procedure, the shear components for all selected CFBDs shown in Table 26 were computed. The results are presented in the 22 plots shown in Figure 98, where V_p is considered to be part of V_s for ends with draped strands. The difference between the sectional shear force V and the contribution of the shear reinforcement V_s is the concrete contribution V_c. The calculated yield strength of the stirrups V_y is also shown in these figures and is useful for assessing when in the history of loading, if at all, the maximum potential contribution of the shear reinforcement was realized.

The plots of sectional shear force versus shear components, as shown in Figure 98, can be idealized as four linear segments defined by five points OABCD, as shown in Figure 99. Segment OA is the response before cracking. In this stage, the contribution of the stirrups to resistance is very small and nearly all of the shear force is carried by the uncracked concrete in tension. Cracking occurs at point A. Segment AB is straight and vertical, which means that part of the shear force previously carried by the uncracked concrete is transferred to the stirrups, with a sharp increment in stirrup force. Segment BC is effectively a serviceability behavioral stage where the stirrup force increases linearly with increase in the external test load. The characteristic angle a for this stage reflects directly the concrete contribution V_c. Yielding of the stirrups occurs at point C. In segment CD, with the stirrups yielding, any further shear force increment must be carried by the concrete. In this idealization, the possible contribution from strain hardening of the stirrups is ignored.

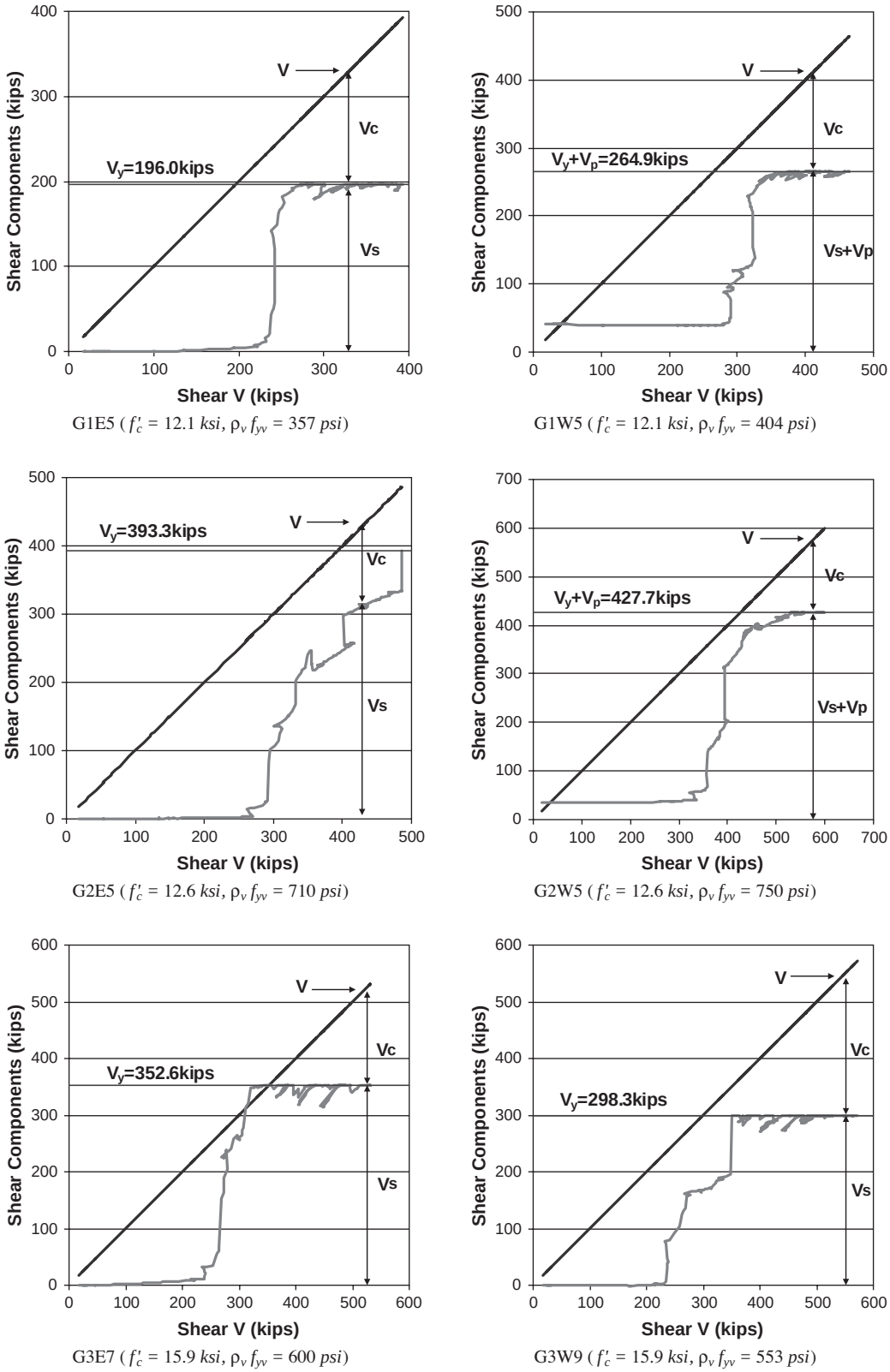

G1E5 (f'_c = 12.1 *ksi*, $\rho_v f_{yv}$ = 357 *psi*)

G1W5 (f'_c = 12.1 *ksi*, $\rho_v f_{yv}$ = 404 *psi*)

G2E5 (f'_c = 12.6 *ksi*, $\rho_v f_{yv}$ = 710 *psi*)

G2W5 (f'_c = 12.6 *ksi*, $\rho_v f_{yv}$ = 750 *psi*)

G3E7 (f'_c = 15.9 *ksi*, $\rho_v f_{yv}$ = 600 *psi*)

G3W9 (f'_c = 15.9 *ksi*, $\rho_v f_{yv}$ = 553 *psi*)

Figure 98. Components of resistance over loading history.

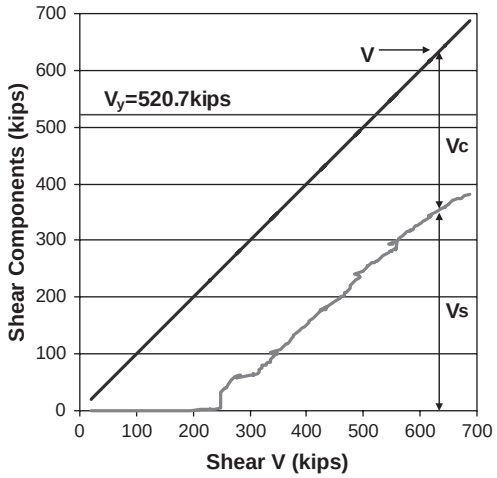

G4E7 (f'_c = 16.3 *ksi*, $\rho_v f_{yv}$ = 1052 *psi*)

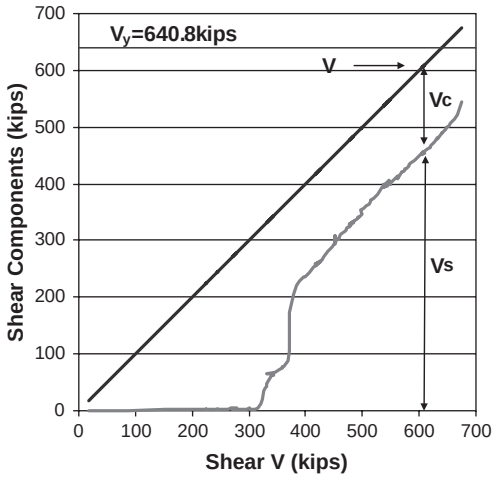

G4W8 (f'_c = 16.3 *ksi*, $\rho_v f_{yv}$ = 1157 *psi*)

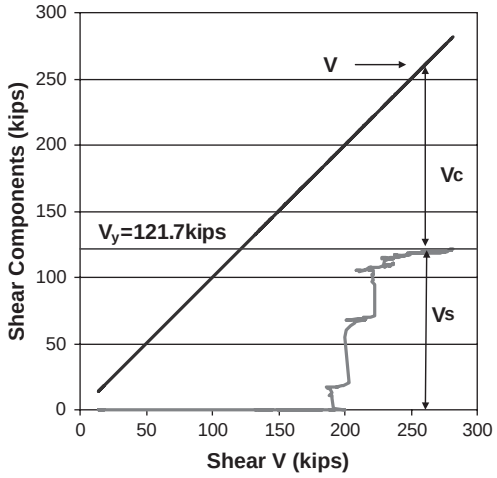

G5E8 (f'_c = 17.8 *ksi*, $\rho_v f_{yv}$ = 161 *psi*)

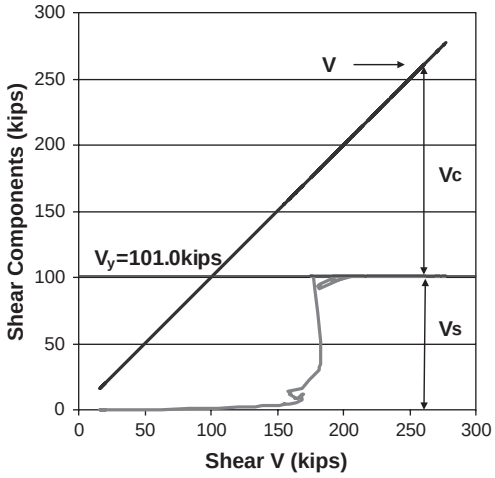

G5W4 (f'_c = 17.8 *ksi*, $\rho_v f_{yv}$ = 140 *psi*)

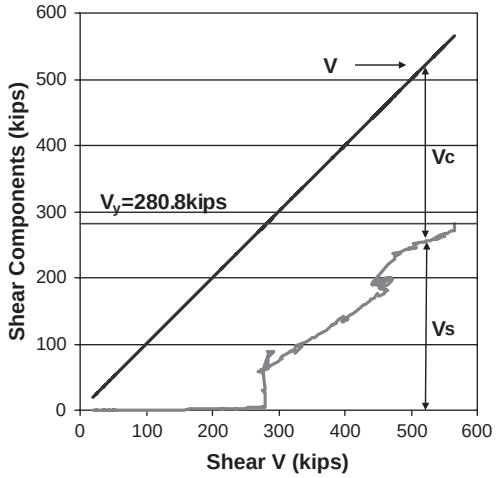

G6E4 (f'_c = 12.7 *ksi*, $\rho_v f_{yv}$ = 585 *psi*)

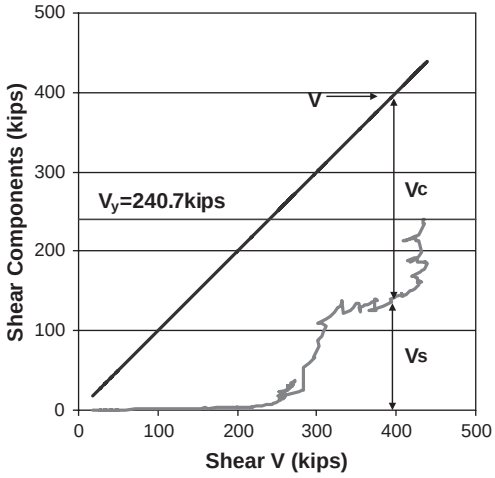

G6W6 (f'_c = 12.7 *ksi*, $\rho_v f_{yv}$ = 549 *psi*)

Figure 98. (Continued).

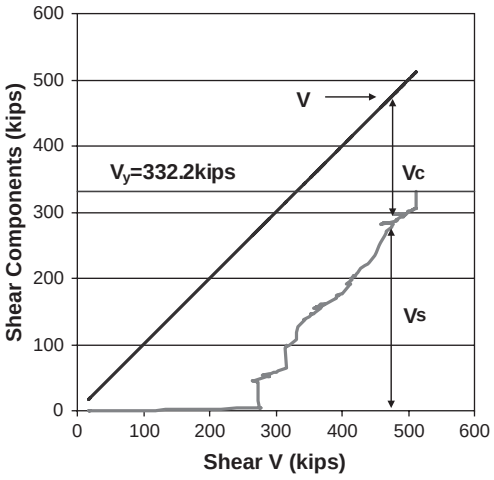

G7E7 (f'_c = 12.5 *ksi*, $\rho_v f_{yv}$ = 586 *psi*)

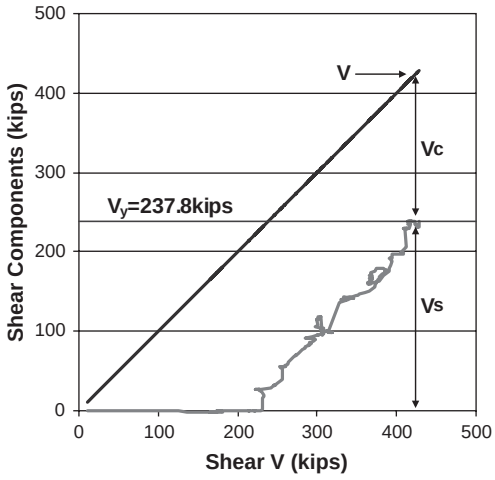

G7W13 (f'_c = 12.5 *ksi*, $\rho_v f_{yv}$ = 382 *psi*)

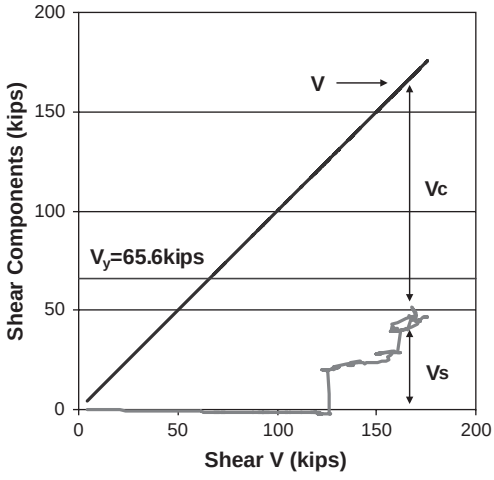

G7W20 (f'_c = 12.5 *ksi*, $\rho_v f_{yv}$ = 119 *psi*)

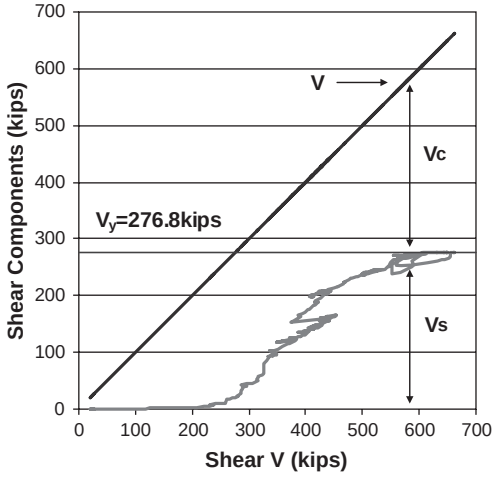

G8E5 (f'_c = 13.3 *ksi*, $\rho_v f_{yv}$ = 571 *psi*)

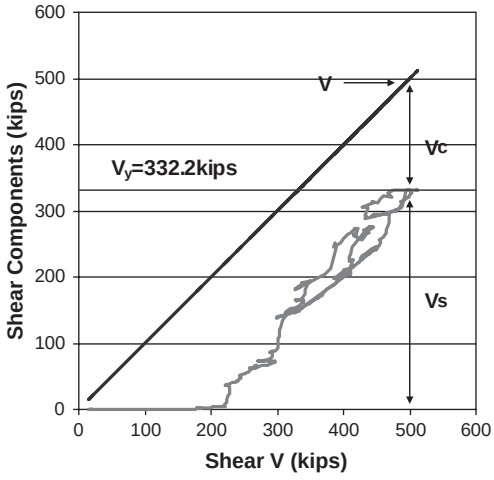

G8E8 (f'_c = 13.3 *ksi*, $\rho_v f_{yv}$ = 555 *psi*)

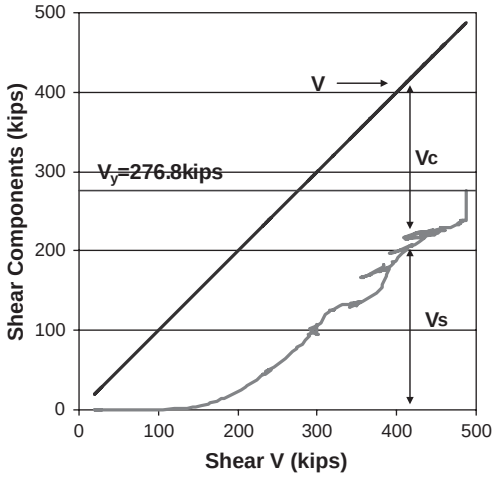

G8W4P (f'_c = 13.3 *ksi*, $\rho_v f_{yv}$ = 576 *psi*)

Figure 98. (Continued).

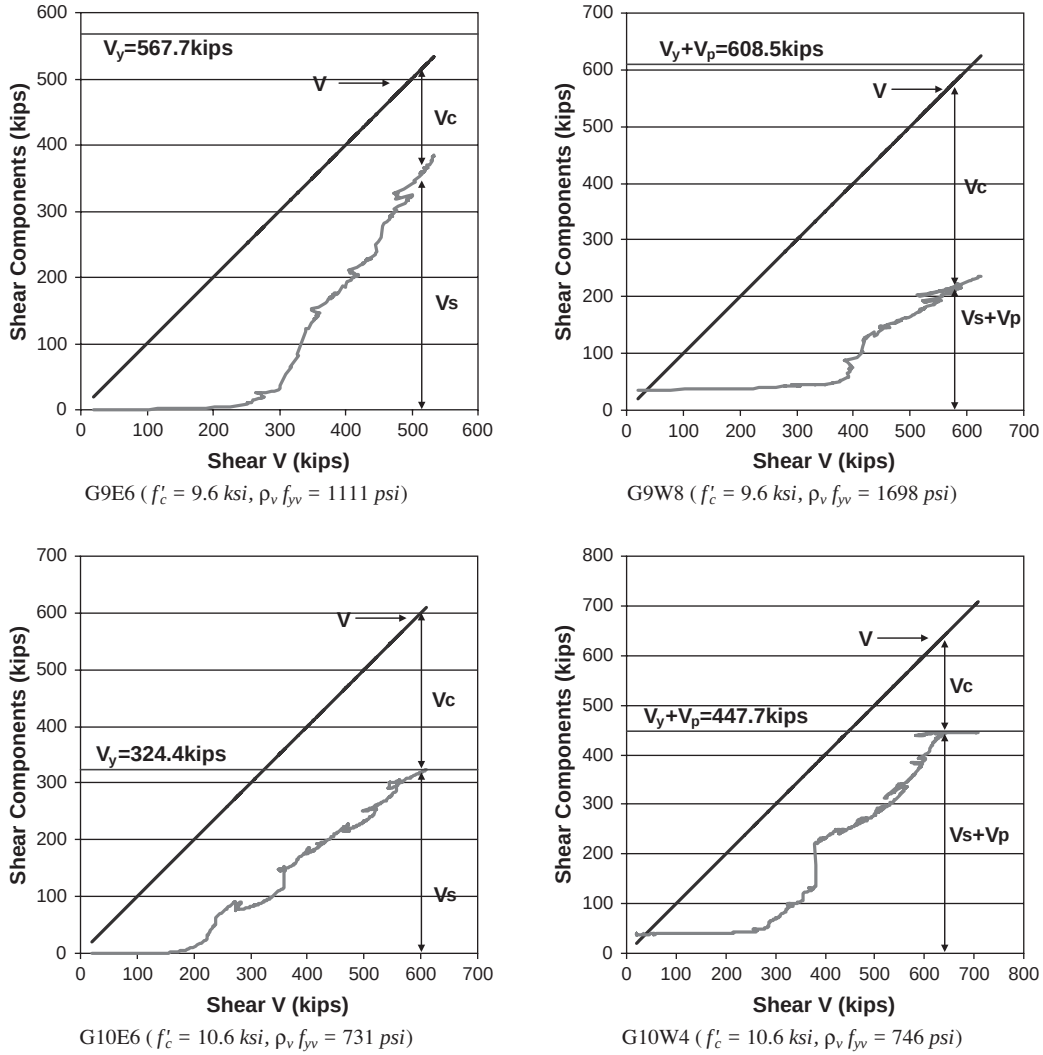

G9E6 (f'_c = 9.6 *ksi*, $\rho_v f_{yv}$ = 1111 *psi*)

G9W8 (f'_c = 9.6 *ksi*, $\rho_v f_{yv}$ = 1698 *psi*)

G10E6 (f'_c = 10.6 *ksi*, $\rho_v f_{yv}$ = 731 *psi*)

G10W4 (f'_c = 10.6 *ksi*, $\rho_v f_{yv}$ = 746 *psi*)

Figure 98. (Continued).

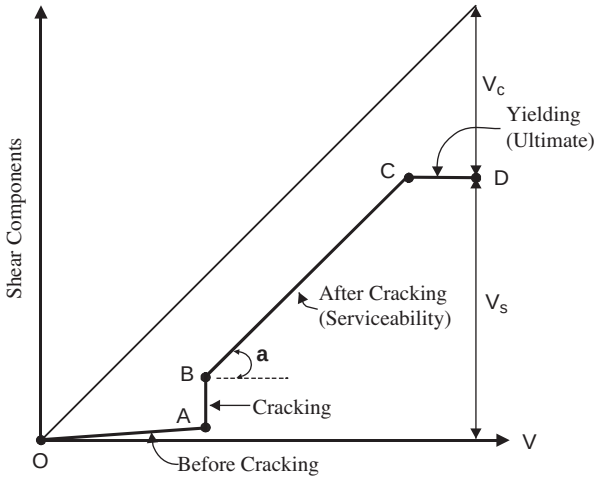

Figure 99. Idealized components of shear resistance.

Each plot in Figure 98 was used to derive characteristic values for the points OABCD and angle a. The resultant values are listed in Table 27 for each CFBD. From these tables and plots, the following observations are made.

- With first diagonal cracking, the stirrups in both G1E ($\rho_v f_{yv}$ = 357 psi) and G1W ($\rho_v f_{yv}$ = 404 psi) quickly yielded and the contribution of the concrete decreased to a very small fraction of what the concrete had provided before cracking. After the stirrups yielded, the member supported an additional 60 to 80 percent of the stirrup yield load. All that contribution was provided by the contribution of the concrete.
- After first diagonal cracking, the stirrups strains in G2E ($\rho_v f_{yv}$ = 710 psi) and G2W ($\rho_v f_{yv}$ = 750 psi) increased rapidly with increasing load but at a rate less than that for Girder 1. G2E failed when the stirrups yielded, while G2W failed shortly after

Table 27. Characteristic shear force points for selected free bodies.

Free Body Diagram	V_p (kips)	A			B			C			D			Characteristics		
		V (kips)	V_s (kips)	V_c (kips)	V (kips)	V_s (kips)	V_c (kips)	V (kips)	V_s (kips)	V_c (kips)	V (kips)	V_s (kips)	V_c (kips)	α	Type	Stirrup
G1E5	0.0	242.5	8.6	233.9	242.5	196.0	46.5	242.5	196.0	46.5	392.4	196.0	196.4	90°	I	Yield
G1W5	40.9	307.5	0.0	266.6	307.5	224.0	42.6	307.5	224.0	42.6	464.0	224.0	199.1	90°	I	Yield
G2E5	0.0	293.3	8.5	284.8	293.3	101.4	191.9	486.3	393.3	93.0	486.3	393.3	93.0	57°	II	Yield
G2W5	34.4	357.0	13.6	309.0	357.0	110.2	212.4	529.0	393.3	101.3	600.0	393.3	172.3	59°	II	Yield
G3E7	0.0	269.5	15.0	254.5	269.5	203.5	66.0	391.0	352.6	38.4	530.6	352.6	178.0	51°	II	Yield
G3W9	0.0	235.9	7.0	228.9	235.9	80.0	155.9	350.4	298.3	52.1	571.3	298.3	273.0	62°	II	Yield
G4E7	0.0	248.6	5.0	243.6	248.6	35.3	213.3	688.4	382.4	306.0	688.4	382.4	306.0	38°	IV	No
G4W8	0.0	371.4	5.0	366.4	371.4	236.0	135.4	676.0	544.6	131.4	676.0	544.6	131.4	45°	III	No
G5E8	0.0	200.0	1.0	199.0	200.0	121.7	78.3	200.0	121.7	78.3	282.0	121.7	160.3	90°	I	Yield
G5W4	0.0	183.0	5.0	178.0	183.0	101.0	82.0	200.0	101.0	99.0	277.9	101.0	176.9	90°	I	Yield
G6E4	0.0	280.0	5.0	275.0	280.0	65.0	215.0	566.6	280.8	285.8	566.6	280.8	285.8	37°	II	Yield
G6W6	0.0	282.0	5.0	277.0	282.0	54.0	228.0	435.2	240.7	194.5	435.2	240.7	194.5	51°	II	Yield
G7E7	0.0	274.0	5.0	269.0	274.0	50.0	224.0	512.7	332.2	180.5	512.7	332.2	180.5	50°	II	Yield
G7W	0.0	231.4	0.0	231.4	231.4	27.0	204.4	427.6	237.8	189.8	427.6	237.8	189.8	47°	II	Yield
G7W20	0.0	125.0	0.0	125.0	125.0	20.0	105.0	167.8	51.5	116.3	167.8	51.5	116.3	37°	II	No
G8E5	0.0	261.4	5.0	256.4	261.4	15.0	246.4	563.9	276.8	287.1	661.2	276.8	384.4	40°	II	Yield
G8E8	0.0	222.0	5.0	217.0	222.0	40.0	182.0	510.8	332.2	178.6	510.8	332.2	178.6	45°	III	Yield
G8W4P	0.0	210.5	0.0	210.5	210.5	0.0	210.5	487.3	276.8	210.5	487.3	276.8	210.5	45°	III	Yield
G9E6	0.0	257.8	12.0	245.8	257.8	12.0	245.8	534.4	384.7	149.7	534.4	384.7	149.7	53°	IV	No
G9W8	40.8	392.0	9.2	342.0	392.0	79.2	272.0	623.6	195.0	387.8	623.6	195.0	387.8	27°	II	No
G10E6	0.0	220.0	0.0	220.0	220.0	31.0	189.0	608.5	324.4	284.1	608.5	324.4	284.1	57°	IV	Yield
G10W4	42.2	285.0	0.0	246.4	285.0	0.0	246.4	620.0	405.5	172.3	709.2	405.5	261.5	50°	IV	Yield

the stirrups yielded. After shear cracking, the concrete contribution decreased with increasing load but then increased again with increasing load after the stirrups yielded.

- The results for G3E ($\rho_v f_{yv} = 600$ psi) illustrate that there are some inaccuracies in the calculation method, as the calculated contribution of the stirrups in G3E to the shear capacity exceeds the total shear V. This probably occurred because some ungauged stirrups that may not have yielded were assigned yield strains and therefore higher strengths than their real values because the adjacent gauged stirrups had yielded. Both G3E and G3W ($\rho_v f_{yv} = 553$ psi) supported considerable additional load after stirrup yielding and with all this additional load being supported by the concrete.
- Girder 4 was very heavily reinforced in shear (in G4E, $\rho_v f_{yv} = 1{,}052$ psi; in G4W, $\rho_v f_{yv} = 1{,}157$ psi). While the member failed in flexure before failing in shear, it is still very useful to examine the contributions of the stirrups and the concrete up to the failure load, particularly because of how different the pattern of those contributions is from that measured in the tests on the first three girders. After diagonal cracking, there was only a gradual increase in stirrup strain with increasing load. In G4E, the concrete contribution remained relatively constant with increasing load. In G4W, there was a somewhat more rapid increase in stirrup strain with increasing load before V_c began to remain relatively constant.
- Girder 5 contained the minimum required amount of shear reinforcement. The plots for G5E ($\rho_v f_{yv} = 161$ psi) and G5W ($\rho_v f_{yv} = 140$ psi) illustrate that the stirrups yielded very shortly after diagonal cracking occurred. There was considerable increase in the calculated concrete contribution to shear resistance after the stirrups yielded. This was especially evident in G5W.
- In both G6E ($\rho_v f_{yv} = 585$ psi) and G6W ($\rho_v f_{yv} = 549$ psi), there was only a modest increase in the straining in the stirrups following initial shear cracking. These stirrup strains increased roughly in proportion to the increase in loading, and both ends of the girder failed soon after the stirrups first yielded.
- In both G7E ($\rho_v f_{yv} = 586$ psi) and G7W ($\rho_v f_{yv} = 382$ psi), after initial shear cracking, there were only modest increases in strain in the stirrups with increases in load. The strain in the stirrups increased gradually with increasing load, while the concrete contribution remained relatively constant. The girder failed when the stirrups reached yield. An additional free body diagram was prepared for Girder 7 at a location farther from the support than the location for the first diagram and in a transition region between web-shear and flexure-shear behavior, G7W20 ($\rho_v f_{yv} = 119$ psi). The stirrups in this region came close to yielding, but did not yield, and the member did not fail in this region. This plot is shown because the member was designed to fail in shear in Region 2 but did not due to the stronger than anticipated contribution of the concrete to shear resistance. Note that the contribution of the concrete to shear resistance for that region is the largest for any of the regions studied and for all of the girders.

- The plots for G8E ($\rho_v f_{yv}$ = 571 psi) and G8E8 ($\rho_v f_{yv}$ = 555 psi) show that G8E failed shortly after the stirrups yielded. Two different sections are also shown for G8E. On the west end of Girder 8, two aluminum plates were placed back to back along the expected shear critical plane to minimize interface shear transfer over the height of the web. The plot of G8W4P ($\rho_v f_{yv}$ = 576 psi) illustrates that there was a much more gradual increase in stirrup strain with increasing load than for the other tests. That gradual increase is likely due to the shear plane of weakness, and consequently the concrete contribution remained relatively constant from when the stirrups first began to carry load up until the time of stirrup yielding. Then, once the stirrups yielded, the member failed. Because of the plane of weakness, the concrete contribution must have been due principally to shear transfer through the top and bottom flanges.
- Both G9E ($\rho_v f_{yv}$ = 1,111 psi) and G9W ($\rho_v f_{yv}$ = 1,698 psi) were designed to contain particularly heavy amounts of shear reinforcement. G9E failed by concrete crushing along the main diagonal when the maximum strain in an individual stirrup was 80 percent of the yield strain. G9W contained a particularly heavy amount of shear reinforcement. Yet there was still a very significant contribution of V_c to the total shear resistance.
- Upon first cracking in G10E ($\rho_v f_{yv}$ = 731 psi) and G10W ($\rho_v f_{yv}$ = 746 psi), the stirrups strains increased gradually in response to additional loading and the contribution of the concrete remained relatively constant or increased slightly with increasing load.

2.7.4 Characteristic angle α and its classification

This section introduces the concept of a parameter, designated as the characteristic angle, α, that is used in describing the concrete contribution V_c to the capacity between the load for diagonal cracking and the load for yield of the shear reinforcement. With this parameter, the patterns of the different contributions to the shear component can then be classified into four types, with an angle value as shown in Figure 100:

- Type I: α = 90 degrees, stirrup yielded immediately after cracking.
- Type II: 45 degrees < α < 90 degrees, stirrup contribution increases and concrete contribution decreases with increasing applied load.
- Type III: α = 45 degrees, concrete contribution constant between cracking and stirrup yielding.

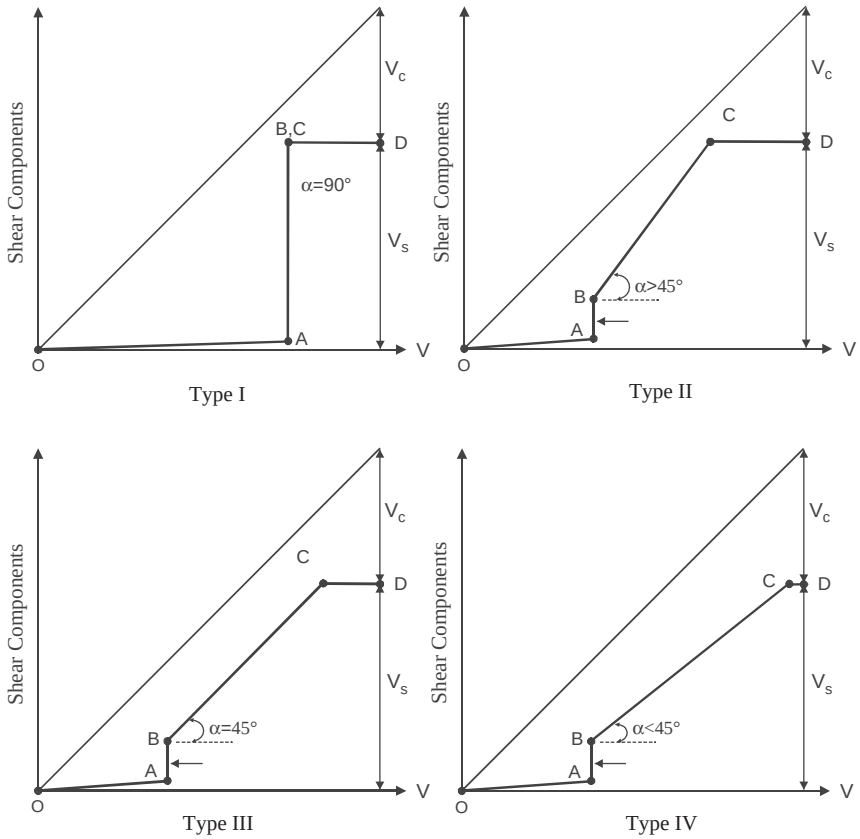

Figure 100. Shear component resistance patterns.

- Type IV: 0 degrees < α < 45 degrees, both stirrup contribution and concrete contribution increase with increasing applied load in the service load stage.

The characteristic angle α depends on crack length and crack width as well as the tensile strength of the concrete. If the boundary crack grew during the service load stage, the concrete contribution usually decreased and the characteristic angle α was larger than 45 degrees. The crack width affects the interface shear transfer, and that transfer contributes directly to the concrete shear component. If the crack width was larger than a critical value, then interlock was negligible and the result was a high characteristic angle α. In most cases, the crack length did not change significantly after cracking occurred, and therefore, the crack width, or the interface shear transfer component, was the most important factor influencing the characteristic angle.

The amount and strength of the shear reinforcement control the crack width and effectiveness of the interface shear transfer component. Plotted in Figure 101 are the relationships (a) between the characteristic angle α and the stirrup strength $\rho_v f_{yv}$ and (b) between the characteristic angle α and the ratio $\rho_v f_{yv} / \sqrt{f'_c}$, with the latter relationship capturing the influence of concrete strength. Both plots show that the characteristic angle decreased from 90 degrees to 28 degrees as $\rho_v f_{yv}$ or $\rho_v f_{yv} / \sqrt{f'_c}$ increased. The characteristic angle for the stirrup reinforcement ratio ranged from 35 to 60 degrees.

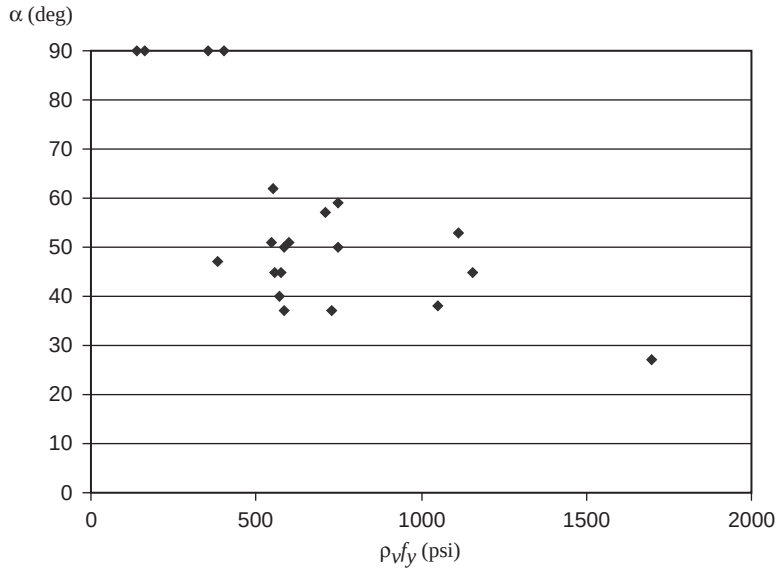

(a) $\rho_V f_y$ versus characteristic angle α

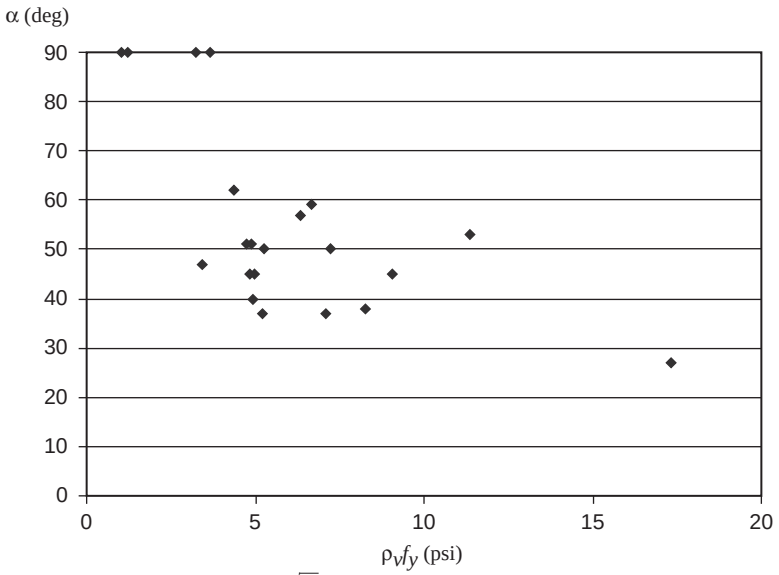

(b) $\rho_v f_y / \sqrt{f'_c}$ versus characteristic angle α

Figure 101. Influence of shear reinforcement on characteristic angle α.

2.7.5 Comparison with LRFD Prediction

Table 28 summarizes the shear forces at the inclined section of selected CFBDs for the ultimate load resisted by each girder. The sectional forces M and V were calculated from the value of the uniform load supported by the beam at failure. The contributions of the shear reinforcement V_s and the concrete V_c were computed using the procedure described in Section 2.7.2. The stirrup strength was calculated as $\rho_v f_s = V_s/(b_w L_c)$, where b_w equals 6 inches and L_c is the value given in Table 26.

Comparisons between the θ, V_c, and V_s values determined from the free bodies selected from the test girders and the values of the same quantities calculated from LRFD predictions are given in Table 29. The ratio of the measured crack angle θ_{test} to the angle θ_{LRFD} predicted by the LRFD procedure ranges from 0.93 to 1.27, and the mean of the ratio $\theta_{test}/\theta_{LRFD}$ is 1.09, with a COV of 0.09. In the derivation of the LRFD method, it is possible that the angle of diagonal compression is derived as flatter than the actual crack angle due to the effects of interface shear transfer.

The LRFD section design model for shear was derived from the MCFT. The MCFT assumes that the concrete contribution to shear strength is limited by the resistance to shear slip along cracks. The ratio of the measured concrete contribution $V_{c,test}$ to the LRFD prediction $V_{c,LRFD}$ is also shown in Table 29.

Table 28. Shear components at ultimate load for selected free body diagrams.

Free Body Diagram	Load (kips/ft)	M (k-ft)	V (kips)	V_s (kips)	V_c (kips)	V_p (kips)	$\rho_v f_s$ (psi)
G1E	26.03	5,058.2	392.4	196.0	196.4	0.0	357
G1W	30.09	5,689.7	464.0	224.0	199.1	40.9	404
G2E	33.79	6,907.0	486.3	393.3	93.0	0.0	710
G2W	38.74	7,286.5	600.0	393.3	172.3	34.4	749
G3E	35.68	7,042.4	530.6	352.6	178.0	0.0	600
G3W	38.82	7,751.8	571.3	298.3	273.0	0.0	553
G4E	42.74	7,619.5	688.4	382.4	306.0	0.0	773
G4W	42.74	7,796.4	676.0	544.6	131.4	0.0	983
G5E	23.70	5,621.9	282.0	121.7	160.3	0.0	161
G5W	19.90	4,189.0	277.9	101.0	176.9	0.0	140
G6E	38.32	5,634.8	566.6	280.8	285.8	0.0	586
G6W	27.66	5,096.0	435.2	240.7	194.5	0.0	549
G7E	33.47	6,382.2	512.7	332.2	180.5	0.0	587
G7W	44.76	9,235.4	427.7	237.8	189.8	0.0	382
G7FS	44.76	10,934.3	167.8	51.5	116.3	0.0	93
G8E	43.73	5,785.9	661.2	276.8	384.4	0.0	571
G8EB	43.73	7,965.7	510.8	332.2	178.7	0.0	555
G8WP	32.70	5,175.2	487.3	276.8	210.5	0.0	576
G9E	32.80	5,749.4	534.4	384.7	149.7	0.0	753
G9W	37.19	5,497.5	623.6	195.0	387.8	40.9	583
G10E	33.93	4,993.2	608.5	324.4	284.1	0.0	731
G10W	42.85	7,252.8	709.2	405.5	261.5	42.2	746

No failure occurred for G4E and G4W.
$\rho_v f_s = V_s/(b_w L_c)$.
b_w = 6 inches.
L_c was given in Table 26.

Table 29. Comparison between test results and LRFD predictions.

Girder	Test			LRFD Prediction			$\frac{\theta_{test}}{\theta_{LRFD}}$	$\frac{V_{c,test}}{V_{c,LRFD}}$
	θ_{test} (deg)	$V_{c,test}$ (kips)	$\rho_v f_s$ (psi)	θ_{LRFD} (deg)	$V_{c,LRFD}$ (kips)	$\rho_v f_{yv}$ (psi)		
G1E	27.2	196.4	357	23.2	121.0	389	1.17	1.62
G1W	28.2	199.1	404	24.9	118.9	389	1.13	1.67
G2E	26.4	93.0	710	25.5	109.0	745	1.04	0.85
G2W	29.8	172.3	749	27.8	106.3	745	1.07	1.62
G3E	26.0	178.0	600	23.7	132.1	565	1.10	1.35
G3W	27.3	273.0	553	23.7	132.1	565	1.15	2.07
G4E*	28.4	306.0	773	28.5	118.0	1,113	1.00	-
G4W*	28.4	131.4	983	28.5	118.0	1,113	1.00	-
G5E	21.1	160.3	161	21.8	189.0	169	0.97	0.85
G5W	23.7	176.9	140	21.8	189.0	140	1.09	0.94
G6E	30.1	285.8	586	23.7	118.1	557	1.27	2.42
G6W	29.9	194.5	549	25.9	113.5	557	1.15	1.71
G7E	25.9	180.5	587	24.2	113.5	577	1.07	1.59
G7W	23.6	189.8	382	23.7	117.2	577	1.00	1.62
G7FS*	25.9	116.3	93	23.9	135.4	119	1.08	-
G8E	30.1	384.4	571	23.7	120.9	577	1.27	3.18
G8EB	25.1	178.7	555	23.7	120.9	577	1.06	1.48
G8WP	30.0	210.5	576	23.7	120.9	577	1.27	1.74
G9E	27.8	149.7	753	30.0	83.6	1,040	0.93	1.79
G9W*	35.7	387.8	583	-	-	1,690	-	-
G10E	30.8	284.1	731	28.8	93.2	751	1.07	3.05
G10W	29.2	261.5	746	27.6	91.2	751	1.06	2.87
						Average	1.09	1.80
						COV	0.09	0.38

*No shear failure occurred.

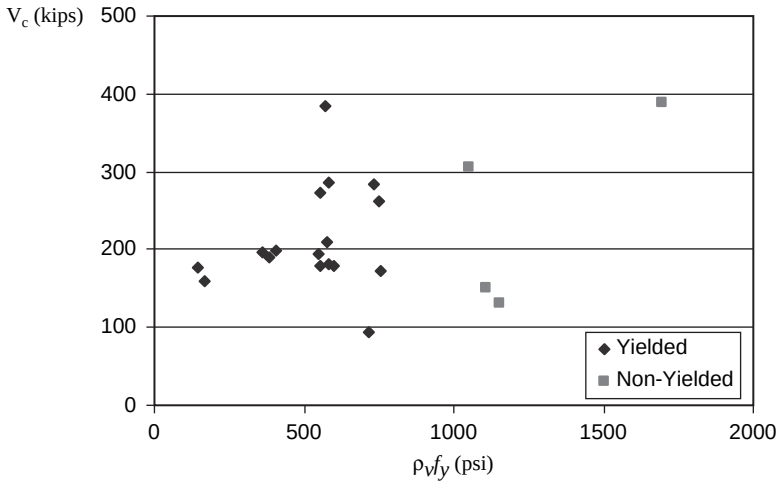

Figure 102. Influence of shear reinforcement on concrete contribution.

The ratios ranged from 0.85 to 3.18, with almost all values being greater than 1.0. The mean of the ratios is 1.80, and the COV is 0.38. The high mean suggests that either the LRFD method underestimates the interface shear transfer resistance or that the top and bottom flanges contribute significantly to shear resistance. Such contributions are not included in the MCFT.

It is also useful to examine the concrete contribution to shear resistance at ultimate capacity as a function of the strength of the shear reinforcement. The results of that correlation are shown in Figure 102. There is an increase in the concrete contribution with increasing amounts of shear reinforcement. The points for G4E, G4W, and G9W are lower than they would be if it had been possible to continue the loading of these members until shear failure occurred.

2.7.6 Significance of This Evaluation

Selected crack-based free body diagrams and measured stirrup strains were used to assess what portion of the applied shear load was carried by the transverse reinforcement and then, by subtraction, what remaining component was carried by the concrete. The results indicate that the amount of stirrup reinforcement had a significant effect on the concrete contribution, and this suggests that the level of resistance provided by interface shear transfer is influenced by the amount of shear reinforcement provided. This result is consistent with what would be suggested by the MCFT in that crack opening stiffness would affect slip resistance. In the LRFD method, the effect of transverse reinforcement on opening stiffness is neglected in an effort to provide a hand-based design procedure. The assumptions made in this derivation are shown by test results to be conservative. A complicating factor in the assessment of V_c is understanding what portion of this resistance is provided by the uncracked compression zone at the top of the member and what portion is provided by the bottom bulb. This subject deserves further research.

2.8 Shear Friction Tests

2.8.1 Introduction

The LRFD Sectional Design Model is derived from the MCFT, in which the concrete contribution to shear resistance is limited by interface shear transfer resistance. The underlying MCFT relationship for evaluating interface shear slip resistance is a function of crack width, crack roughness, concrete strength, and the resistance to crack opening provided by the longitudinal reinforcement (*30*). One of the motivations for NCHRP Project 12-56 was that shear cracks in HSC specimens could be much smoother than in a normal strength concrete structure, and this increased smoothness could lead to much less interface shear transfer resistance than assumed in the derivation in the LRFD Sectional Design Model.

The results from the tests on the HSC girders provided the data necessary to evaluate the safety of the LRFD Sectional Design Model, but they did not provide data that can be directly used to evaluate the appropriateness of the extension of the MCFT relationship for shear slip resistance to HSC structures. To this end, 18 shear transfer test specimens were cast in conjunction with the large concrete bridge girders for this project. These shear transfer specimens were cast using the same concrete materials as those used to cast the first six girders, and they contained the same quantity of reinforcement as used in the webs of the first six girders. The remaining sections describe the details of the shear transfer test specimens, the test setup, the instrumentation, and the test results.

2.8.2 Design of Test Specimens

The experimental variables considered during the construction of the 18 test specimens included:

- **Concrete strength:** The original intent of the study was to look at specimens cast with 10, 14, and 18 ksi concrete.
- **Reinforcement spacing:** The shear reinforcement across the cracks was spaced at intervals varying from 6 to 12 inches. Normal deformed bars were used for all the tests, and those bars were No. 3, No. 4, or No. 5 bars, depending on the specimen.
- **Angle of reinforcing bars:** The shear reinforcement was oriented at either 25 degrees or 35 degrees from the plane of the face of cracking. This orientation was intended to accommodate the fact that diagonal cracking in the test girders was likely to occur at between 25 degrees and 35 degrees to the longitudinal axis of the girder.

Table 30 and Figure 103 present the dimensional and reinforcement details for all 18 test specimens. The designator of each specimen was selected so that it could serve as an identifier that described all relevant details of the specimen. The first two characters indicate the girder with which the specimen was cast (for example, "g1" indicates a specimen that was cast with Girder 1). The next two characters, "sh" and "sl," indicate whether the specimen represented a region of the girder subjected to higher shear stress (closest shear design section to support) or lower shear stress (farther shear design section from support), respectively. The next numeral indicates the number of reinforcing bars in the location of that shear stress level. Note there are two locations in each specimen, such that the number 2 indicates there are a total of 4 bars in that particular specimen. The bar size is indicated by the next entry in the code with 3, 4, or 5 corresponding to the customary U.S. bar size designation. The final entry is the angle of the orientation of the reinforcing bars relative to normal from the shear plane, either 25 degrees or 35 degrees. Additional specimen information is included in Table 30, including the yield strength of the reinforcing bars, the spacing of the shear reinforcement (s), and the length of the shear plane (L). Figure 103 shows pertinent dimensional information that corresponds to values in Table 30 for each specimen. The thickness for the shear plane for each specimen was 6.5 inches.

2.8.3 Instrumentation and Testing Details

The first step in testing a specimen was to attach Whittemore targets to the surfaces of the specimen in order to measure initial crack widths. A total of eight targets were attached to both sides of the specimen in a rectangular configuration that was 12 inches high and 10 inches wide. The rectangle was oriented such that its center corresponded with the mid-length of the shear plane. This configuration of targets allowed for two measurements of initial crack width on each side of the specimen. Initial crack widths are referenced by their location (top or bottom) and by which side of the specimen they were taken on (Krypton side or LVDT side, as described later). The next step in the testing procedure was to

Table 30. Test specimen details.

specimen	L (in)	Label A	s (in)	Θ (°)	fy (ksi)
g1sh_2_4_25	26.5	2- #4 (0.4 in^2)	12	25	70.0
g1sl_1_4_25	26.5	1- #4 (0.4 in^2)	12	25	70.0
g1sh_2_4_35	29.25	2- #4 (0.4 in^2)	12	35	70.0
g1sl_1_4_35	29.25	1- #4 (0.4 in^2)	12	35	70.0
g2sh_2_5_25	24.25	2- #5 (0.62 in^2)	11	25	79.3
g2sl_1_5_25	18.75	1- #5 (0.62 in^2)	8.5	25	79.3
g2sh_2_5_35	26.875	2- #5 (0.62 in^2)	11	35	79.3
g2sl_1_5_35	20.75	1- #5 (0.62 in^2)	8.5	35	79.3
g3sh_2_4_25	17.625	2- #4 (0.4 in^2)	8	25	67.8
g3sl_2_4_25	26.5	2- #4 (0.4 in^2)	12	25	67.8
g3sh_2_4_35	19.5	2- #4 (0.4 in^2)	8	35	67.8
g3sl_2_4_35	29.25	2- #4 (0.4 in^2)	12	35	67.8
g4sh_2_5_25	13.45	2- #5 (0.62 in^2)	6	25	64.6
g4sl_2_5_35	14.625	2- #5 (0.62 in^2)	6	35	64.6
g5sh_1_3_25	22.125	1- #3 (0.11 in^2)	10	25	76.5
g5sh_1_3_35	24.375	1- #3 (0.11 in^2)	10	35	76.5
g6sh_2_5_25	26.5	2- #5 (0.62 in^2)	12	25	64.7
g6sh_2_5_35	29.25	2- #5 (0.62 in^2)	12	35	64.7

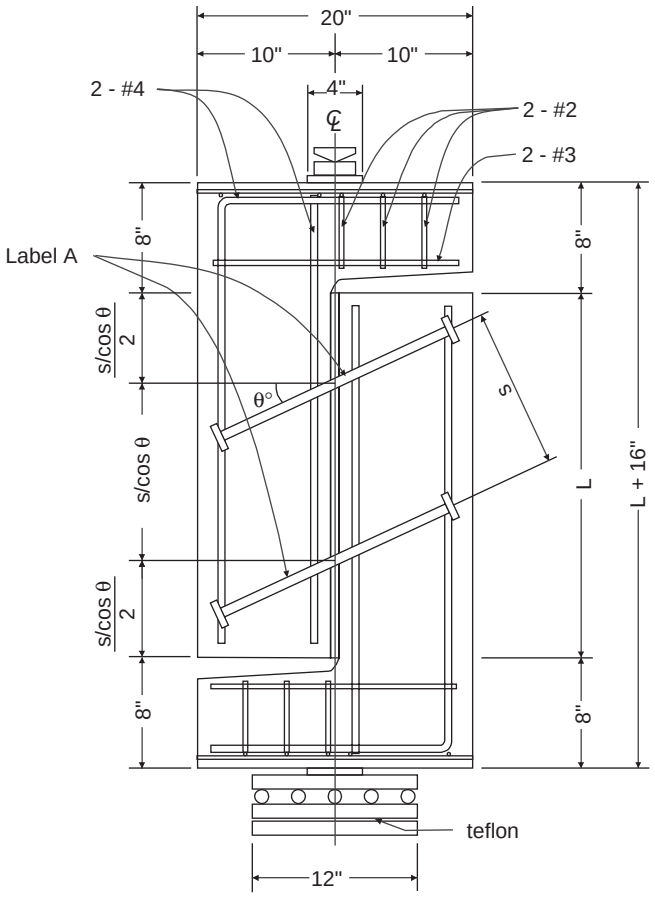

Figure 103. Test specimen geometry.

precrack the test specimen. To accomplish this, each specimen was placed in the testing frame in a horizontal orientation with 1-inch diameter round bars placed into the triangular grooves that had been cast into the faces of the specimen. Figure 104 shows a photograph of one specimen positioned in the testing machine for precracking. Forcing the round bars into the triangular grooves generated a splitting force sufficient to initiate cracking. Load was applied to a specimen in a controlled manner in an effort to minimize the width of the initial cracks. After precracking, the initial crack width was measured using a Whittemore gage at all four locations.

Next, three LVDTs were installed on one face of the test specimen, two for measuring crack opening at distances of 7.5 inches above and below mid-height (6 inches above and below mid-height for the G4 specimens) and one for measuring slip at mid-height. The specimen was then placed in the testing frame in a vertically oriented manner with rollers on the bottom surface and a swivel on the top. Krypton targets were then affixed to the other side of the test specimen to also measure displacements during the test. Twelve targets were affixed to each specimen, with six on each side of the shear plane arranged in a grid at a spacing of 7.5 inches for all of the specimens except the G4 specimens. In G4 specimens, the

Figure 104. Precracking set-up.

vertical spacing was reduced to 6 inches. Figure 105 presents a photograph of a specimen positioned in the testing machine for a shear friction test.

The specimens were loaded in a 600-kip servo-controlled hydraulic testing machine that was operated in displacement control. The loading procedure was as follows. Specimens were preloaded with 1 kip of force before any data acquisition equipment was activated. Displacement was increased at a rate of 0.02 inch (0.5 millimeter) per minute until the total

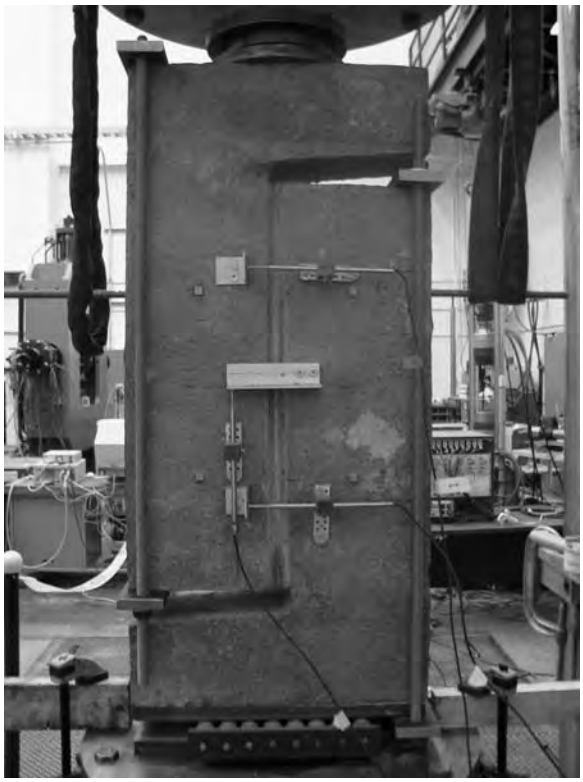

Figure 105. Shear friction test set-up.

load on the specimen reached 10 kips. Then, from that point on, the loading rate was decreased to 0.008 inch (0.2 millimeter) per minute. Finally, the loading rate was increased to 0.016 inch (0.4 millimeter) per minute after the applied load reached 5 percent less than the peak load obtained during the test. Specimens were loaded until the slip along the crack reached 0.4 inch (10 millimeters) or until a reinforcing bar ruptured.

The data for the tests was acquired using two PC-based data acquisition systems that each recorded data at a sampling rate of 2 Hz. The first data acquisition system ran a program written using National Instruments's LabVIEW and was responsible for acquiring data for the load and position of the testing machine and the data for crack width and slip from the three LVDTs. The second data acquisition system was responsible for collecting the data for the 12 Krypton targets. This data consisted of the three-dimensional position of each target located on the specimen to an accuracy of ±0.001 inch (0.02 millimeter). The testing of an individual specimen typically took about 1 hour to complete.

2.8.4 Summary of Experimental Results

Of the 18 specimens, 16 were tested successfully and failed in shear at the desired location. Two specimens (g2sh_2_5_35 and g4sl_2_5_35) did not reach the peak shear loads because other parts of the specimen first failed in flexure. Upon determining that flexure might be a problem in more heavily reinforced specimens, additional external flexural reinforcement was added to subsequent specimens to ensure that the desired shear failure could be achieved. The two specimens from Girder 6 were enhanced with external reinforcement, and peak shear loads were obtained, but flexural problems were encountered before the specimens reached 0.4 inch (10 millimeters) of shear slip. Figure 106 shows shear stress versus crack opening, shear stress versus crack slip, and crack opening versus crack slip results for each of the 18 test specimens. The crack opening plots are offset by the initial crack width for each specimen. Care was taken during precracking to ensure that initial crack widths were kept to a minimum. However, in many of the lightly reinforced specimens it was difficult to control the initial crack width. The scales for crack slip and crack opening are constant in all the figures so that relative comparisons can be made between these figures. The scale for shear stress varies because there is a wide range of values for maximum shear stress for the specimens. Maintaining the constant scales makes it evident that Specimens g2sh_2_5_35 and g4sl_2_5_35 did not reach peak loads and that the two Girder 6 specimens were unable to be taken to the same level of crack opening and crack slip as the other specimens.

Table 31 shows the primary test results from each of the 18 specimens. Values reported include the initial crack width at all four measuring points, as well as the maximum applied load and the corresponding maximum shear stress. Again, it should be noted that the applied load values reported for the g2sh_2_5_35 and g4sl_2_5_35 specimens are not maximums, as denoted by the asterisk in Table 31.

2.8.5 Interpretation of Experimental Results

In an effort to make meaningful comparisons with code predictions for the shear strength of the test specimens, it was necessary to make some assumptions. The specimens that were tested had reinforcing bars that crossed the shear plane at an angle. As a result, the effective clamping force provided by the reinforcing steel was adjusted to compensate for the angle of the bars. Similarly, the angled bars would also have a component of their resistance that would act along the shear plane. To compensate for this, it was assumed that the bars yielded when peak load was reached, and then the component of the resistance of the bar along the shear plane was determined based on this assumption and subtracted from the total applied load, thereby allowing for a net shear stress to be calculated. Table 32 presents a more detailed analysis of the experimental results, including the foregoing assumptions mentioned and comparisons with LRFD code predictions. An explanation of the contents of Table 32 is now presented.

The effective clamping stress ($\rho_v f_y^{**}$), as adjusted for the angle of the reinforcing bars, is shown in Column 3 of Table 32. This value was calculated by multiplying the value for clamping stress ($\rho_v f_y$) in Column 2 by the cosine of the angle in Column 4. Similarly, the net shear stress (Column 6) was calculated by multiplying the clamping stress ($\rho_v f_y$) from Column 2 by the sine of the angle from Column 4 and subtracting it from the maximum shear stress shown in Column 5. The effective clamping stress was used for predicting the strength of the test specimens using the LRFD specifications and was compared with the experimental values for net shear stress.

The predicted strength of the test specimens was determined using Section 5.8.4, "Interface Shear Transfer—Shear Friction," from the LRFD specifications. According to the LRFD specifications, the nominal shear resistance of the interface plane, V_n, shall be taken as:

$$V_n = cA_{cv} + \mu\left[A_{vf} f_y + P_c\right] \qquad (5.8.4.1-1)$$

where:

A_{vf} = area of shear reinforcement crossing the shear plane and

P_c = permanent net compressive force normal to the shear plane.

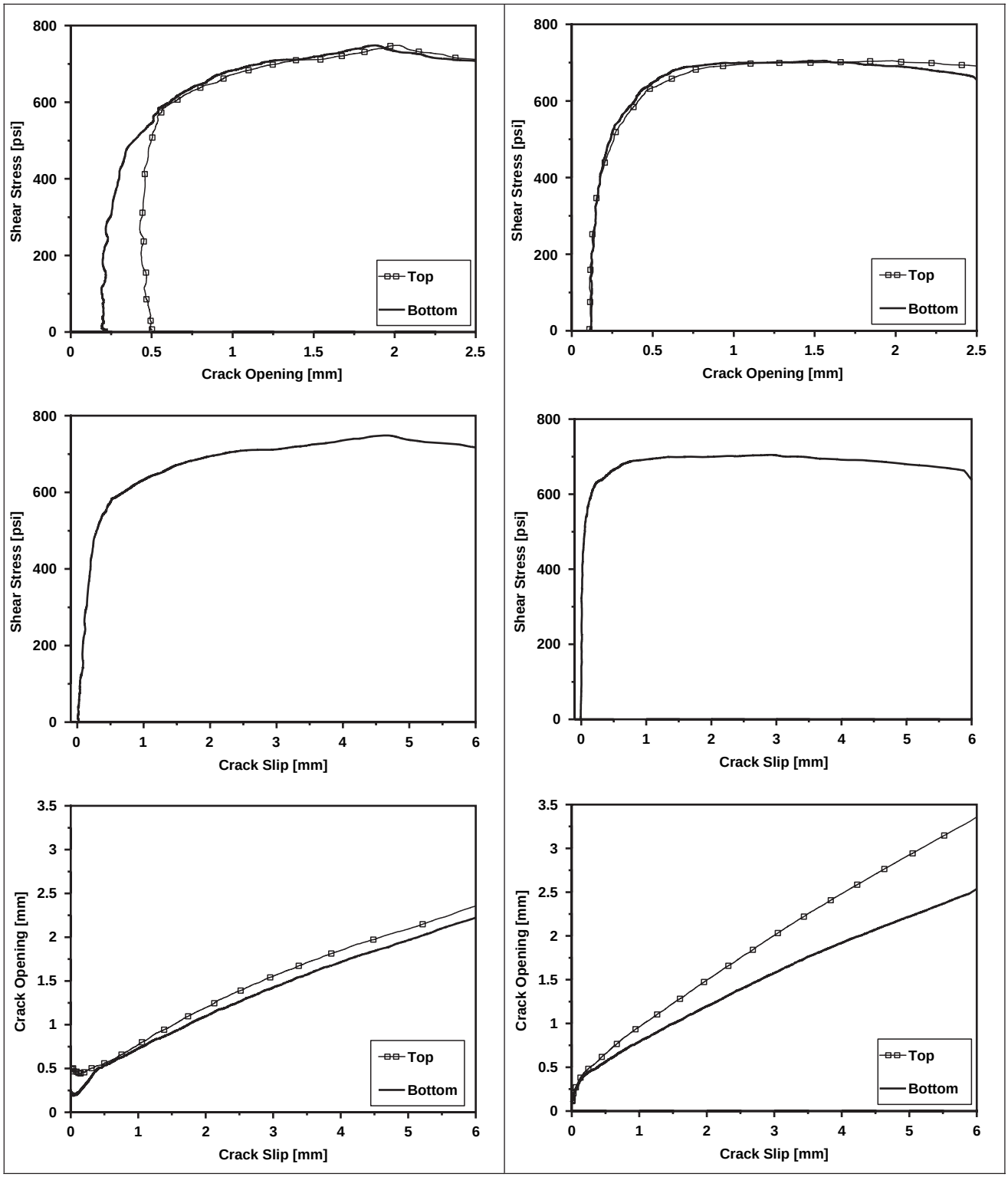

(a) G1SH_2_4_25

(b) G1SH_2_4_35

Figure 106. Experimental results.

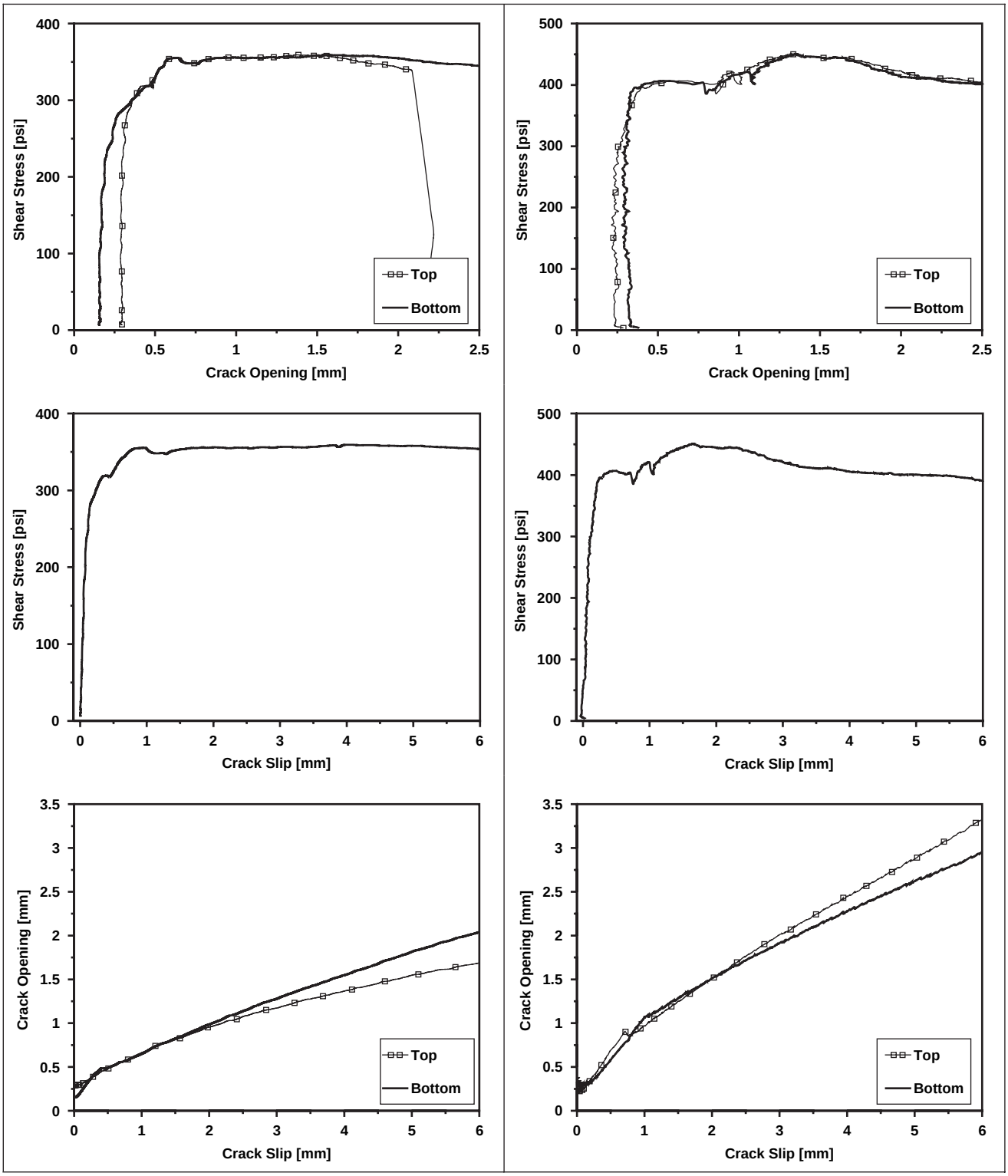

(c) G1SL_1_4_25

(d) G1SL_1_4_35

Figure 106. (Continued).

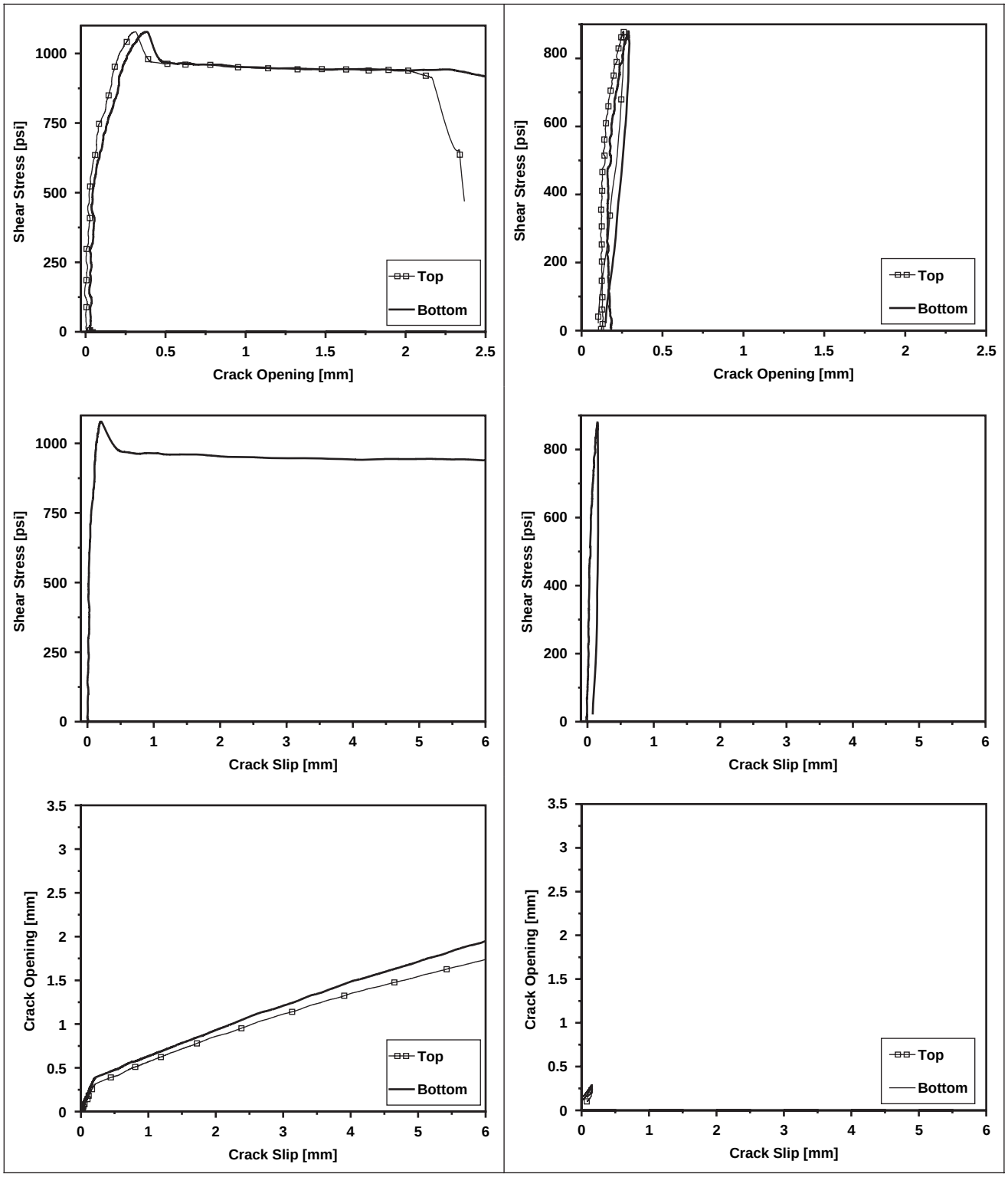

(e) G2SH_2_5_25

(f) G2SH_2_5_35

Figure 106. (Continued).

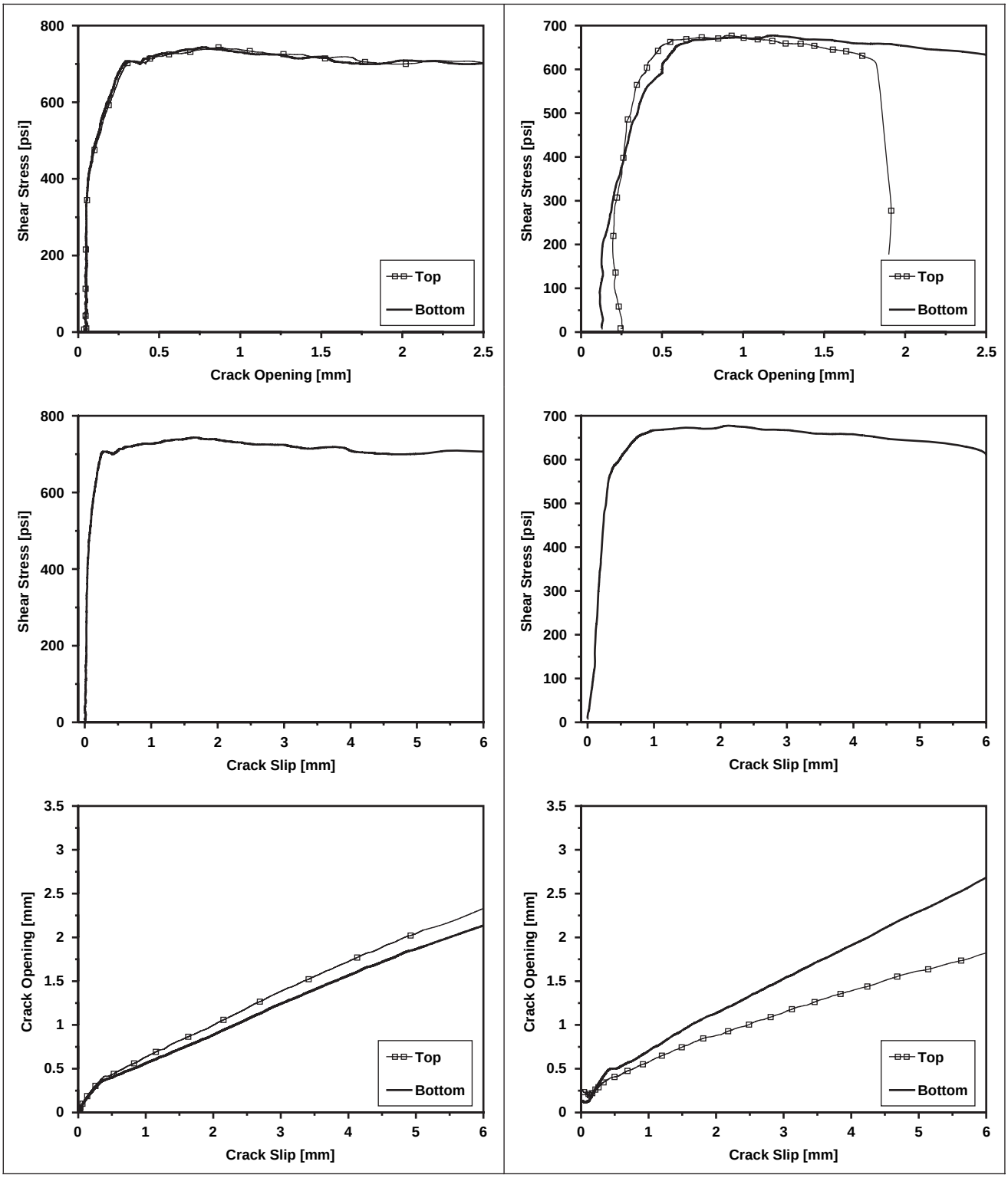

(g) G2SL_1_5_25

(h) G2SL_1_5_35

Figure 106. (Continued).

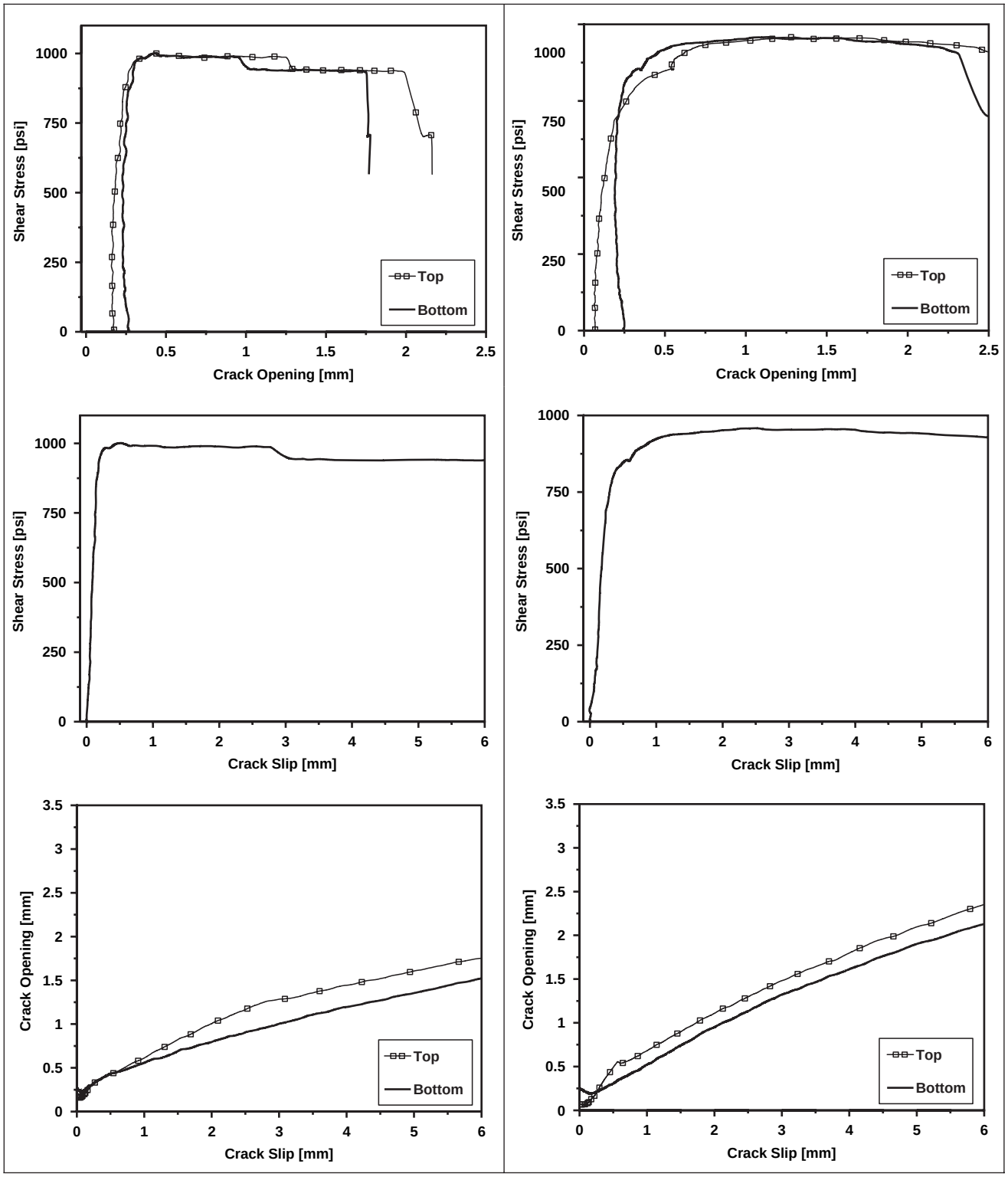

(i) G3SH_2_4_25

(j) G3SH_2_4_35

Figure 106. (Continued).

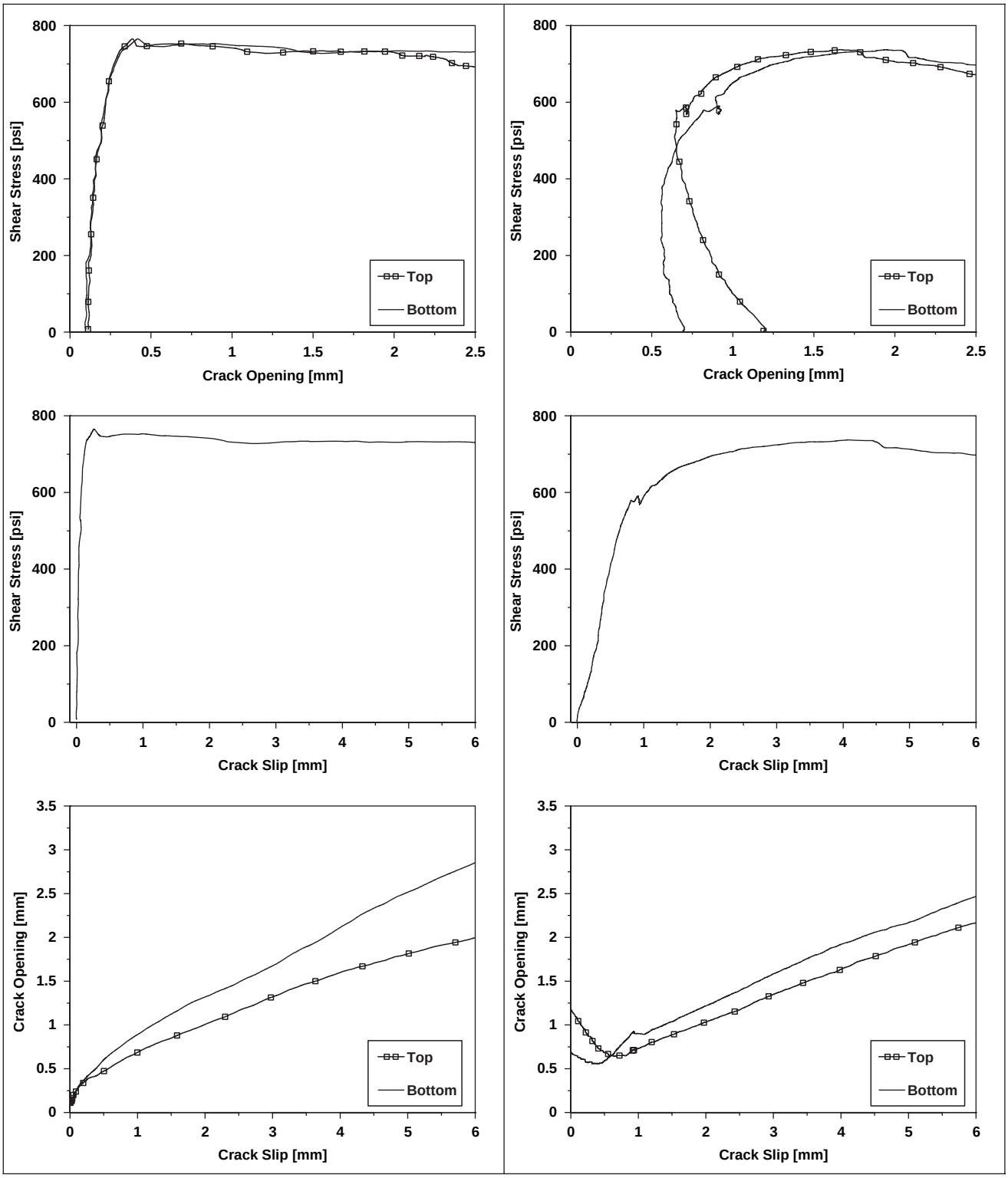

(k) G3SL_2_4_25

(l) G3SL_2_4_35

Figure 106. (Continued).

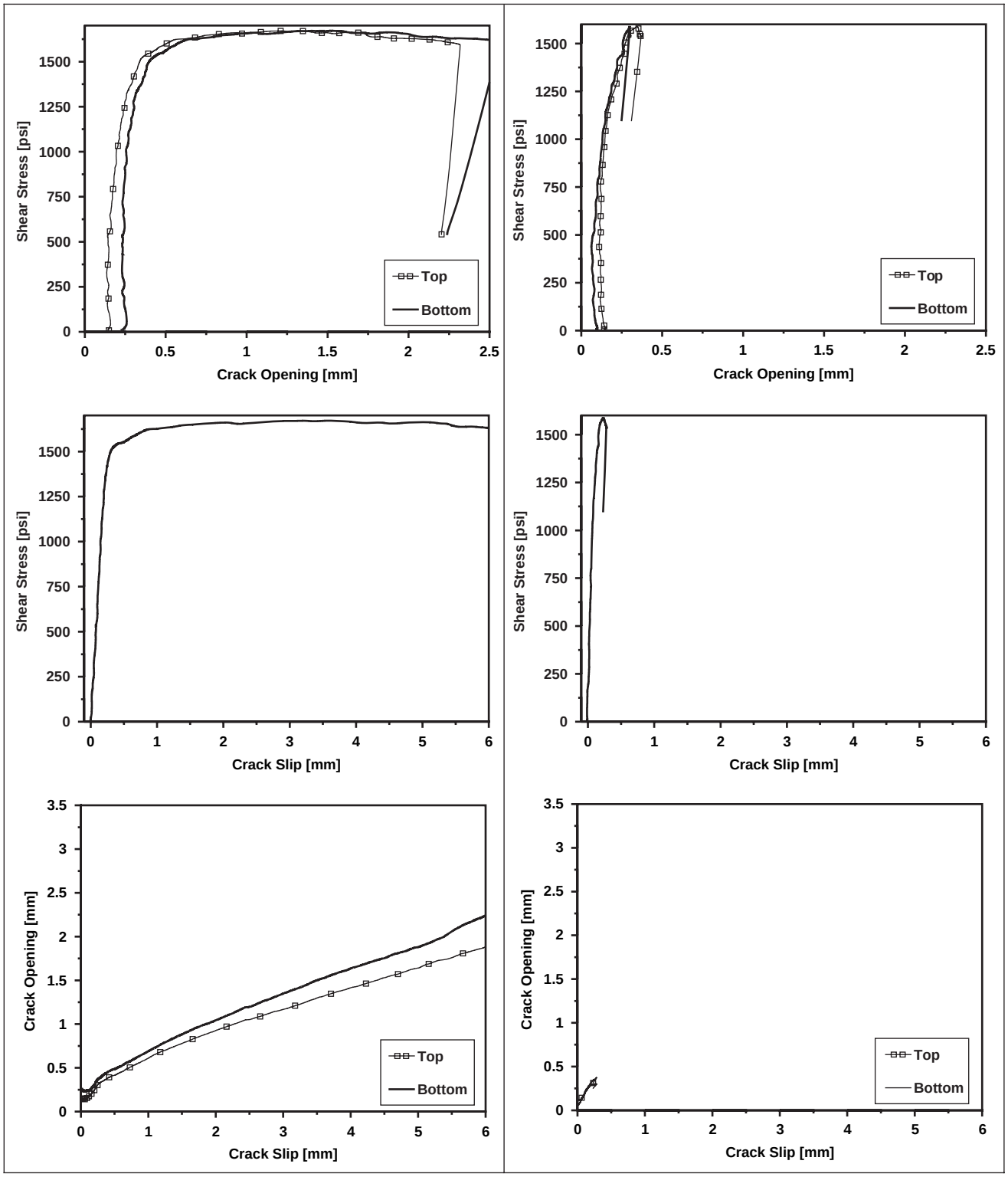

(m) G4SH_2_5_25

(n) G4SL_2_5_35

Figure 106. (Continued).

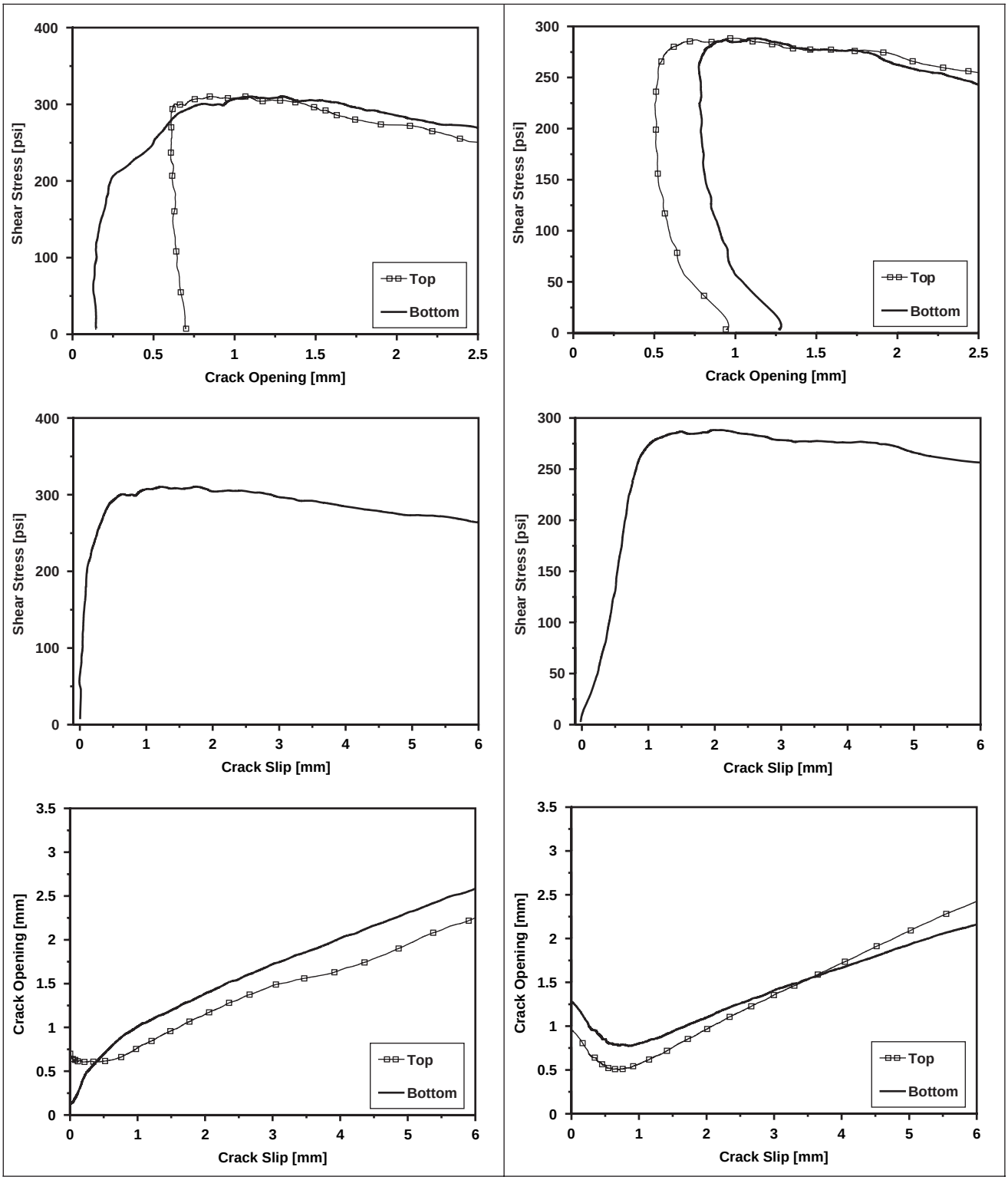

(o) G5SH_1_3_25

(p) G5SH_1_3_35

Figure 106. (Continued).

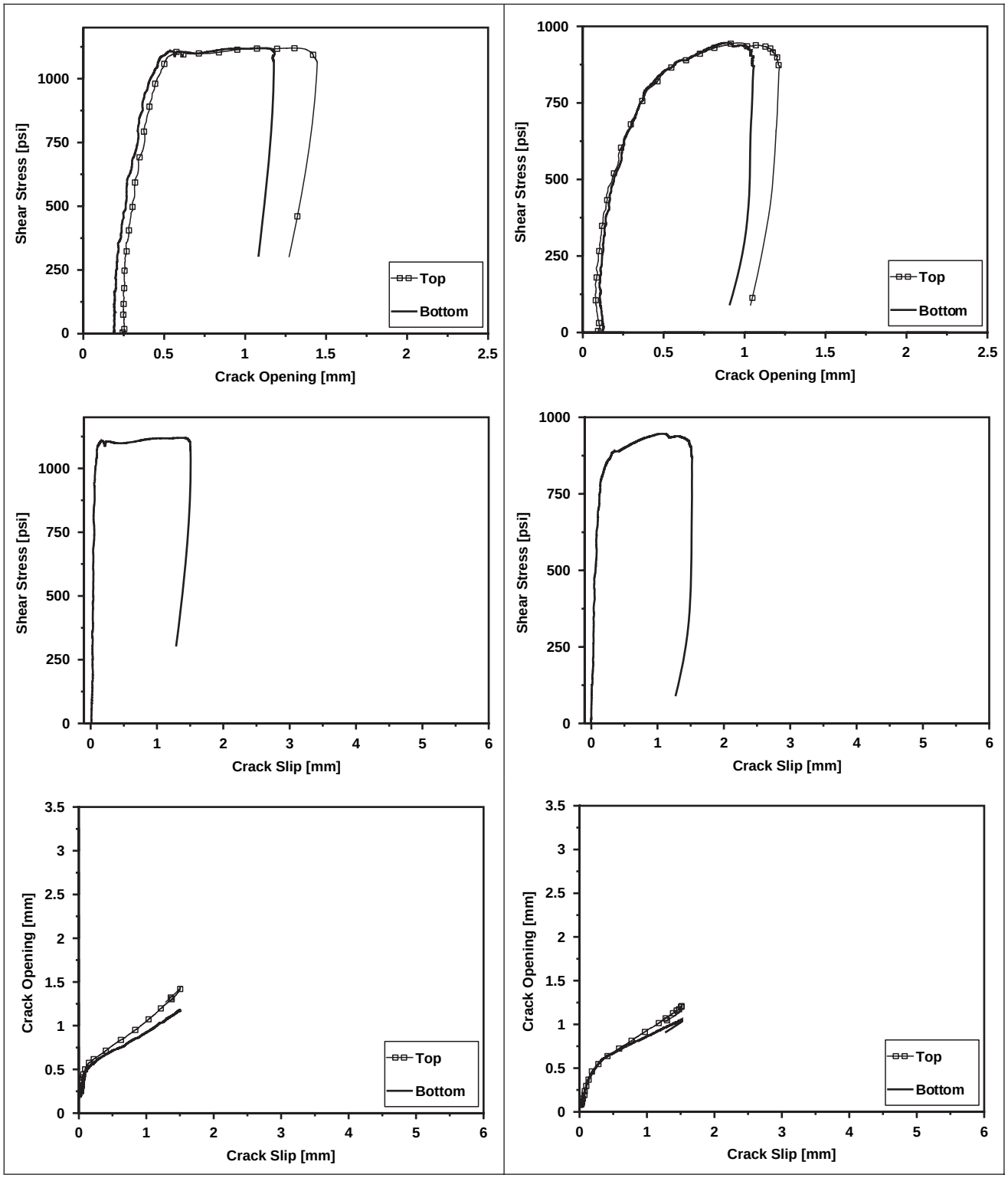

(q) G6SH_2_5_25

(r) G6SH_2_5_35

Figure 106. (Continued).

Table 31. Test results.

specimen designation	initial crack widths (mm)				A_{cv} (in^2)	A_{sv} (in^2)	r_v (%)	f_y (ksi)	f'c (ksi)	Max Load (kips)	Max shear stress (psi)
	lvdt side		krypton side								
	top	bottom	top	bottom							
g1sh_2_4_25	0.48	0.19	0.43	0.15	172.3	0.8	0.46	70.0	13.46	128.9	749
g1sl_1_4_25	0.30	0.16	0.28	0.13	172.3	0.4	0.23	70.0	13.46	61.9	359
g1sh_2_4_35	0.12	0.13	0.13	0.12	190.1	0.8	0.42	70.0	13.46	134.0	705
g1sl_1_4_35	0.26	0.36	0.10	0.22	190.1	0.4	0.21	70.0	13.46	85.7	451
g2sh_2_5_25	0.00	0.03	0.06	0.05	157.6	1.24	0.79	79.3	14.17	169.9	1078
g2sl_1_5_25	0.03	0.04	0.24	0.25	121.9	0.62	0.51	79.3	14.17	90.6	744
g2sh_2_5_35*	0.14	0.19	0.04	0.09	174.7	1.24	0.71	79.3	14.17	153.7	880
g2sl_1_5_35	0.26	0.12	0.47	0.32	134.9	0.62	0.46	79.3	14.17	91.4	678
g3sh_2_4_25	0.17	0.27	0.08	0.17	114.6	0.8	0.70	67.8	16.6	114.7	1001
g3sl_2_4_25	0.12	0.10	0.10	0.32	172.3	0.8	0.46	67.8	16.6	131.9	766
g3sh_2_4_35	0.06	0.24	0.20	0.39	126.8	0.8	0.63	67.8	16.6	121.5	958
g3sl_2_4_35	1.20	0.70	0.71	0.24	190.1	0.8	0.42	67.8	16.6	140.2	738
g4sh_2_5_25	0.14	0.23	0.02	0.09	87.4	1.24	1.42	64.6	16.6	146.2	1672
g4sl_2_5_35*	0.15	0.11	0.15	0.11	95.1	1.24	1.30	64.6	16.6	150.9	1587
g5sh_1_3_25	0.69	0.14	0.93	0.41	143.8	0.22	0.15	76.5	17.51	44.7	311
g5sh_1_3_35	0.96	1.29	0.53	0.65	158.4	0.22	0.14	76.5	17.51	45.7	288
g6sh_2_5_25	0.24	0.18	0.22	0.13	172.3	1.24	0.72	64.7	13.5	192.8	1120
g6sh_2_5_35	0.11	0.12	0.25	0.28	190.1	1.24	0.65	64.7	13.5	179.9	946

* Specimen did not reach ultimate load

Table 32. Comparison of test results with predictions.

specimen designation	$\rho_v f_y$ (psi)	$\rho_v f_y$** (psi)	angle (°)	max shear stress (psi)	net shear stress (psi)	LRFD Φv_n (psi)	LRFD$^+$ Φv_n (psi)	v_{ci} MCFT w=.3 mm (psi)	v_{ci} MCFT w=.75 mm (psi)	v_{test} / Φv_n	v_{test} / Φv_n^+	v_{test} / v_{ci} w=.3 mm	v_{test} / v_{ci} w=.75 mm
g1sh_2_4_25	325	295	25	749	611	355	517	330	175	1.72	1.18	1.85	3.50
g1sl_1_4_25	163	147	25	359	291	223	385	330	175	1.31	0.76	0.88	1.66
g1sh_2_4_35	295	241	35	705	536	307	469	330	175	1.74	1.14	1.63	3.07
g1sl_1_4_35	147	121	35	451	366	199	361	330	175	1.84	1.02	1.11	2.10
g2sh_2_5_25	624	565	25	1078	814	599	761	338	179	1.36	1.07	2.41	4.54
g2sl_1_5_25	403	366	25	744	573	419	581	338	179	1.37	0.99	1.69	3.20
g2sh_2_5_35*	563	461	35	880	557	505	667	338	179	1.10	0.83	1.65	3.11
g2sl_1_5_35	365	299	35	678	469	359	521	338	179	1.31	0.90	1.39	2.62
g3sh_2_4_25	473	429	25	1001	801	476	638	366	194	1.68	1.26	2.19	4.13
g3sl_2_4_25	315	285	25	766	632	347	509	366	194	1.82	1.24	1.73	3.26
g3sh_2_4_35	428	351	35	958	713	405	567	366	194	1.76	1.26	1.95	3.68
g3sl_2_4_35	285	234	35	738	574	300	462	366	194	1.91	1.24	1.57	2.96
g4sh_2_5_25	916	830	25	1672	1285	720	999	366	194	1.78	1.29	3.51	6.62
g4sl_2_5_35*	843	690	35	1587	1104	711	873	366	194	1.55	1.26	3.01	5.69
g5sh_1_3_25	117	106	25	311	261	185	347	376	199	1.41	0.75	0.69	1.31
g5sh_1_3_35	106	87	35	288	227	168	330	376	199	1.35	0.69	0.60	1.14
g6sh_2_5_25	466	422	25	1120	923	470	632	330	175	1.96	1.46	2.79	5.28
g6sh_2_5_35	422	346	35	946	704	401	563	330	175	1.76	1.25	2.13	4.03

* Specimen did not reach ultimate load

** clamping force adjusted for angle of bars

$^+$ Proposed LRFD equation

The nominal shear resistance, V_n, used in the design shall not be greater than the lesser of:

$$V_n \le 0.2 f'_c \, A_{cv} \qquad (5.8.4.1-2)$$

or

$$V_n \le 0.8 A_{cv} \qquad (5.8.4.1-3)$$

Equation 5.8.4.1-1 was adjusted in the following manner to allow for comparison with the experimental data:

$$\phi v_n = \phi\left(c + \mu[\rho_v f_y^{**}]\right) \qquad (46)$$

where:

ϕ = strength reduction factor and
v_n = nominal shear stress over the shear plane.

Values for c and μ were obtained from Section 5.8.4.2, "Cohesion and Friction," with c taken as 100 psi and μ taken as 1.0. Because all of the specimens were precracked prior to testing in shear and the surfaces were not intentionally roughened to an amplitude of 0.25 inch or more, the correct application of the LRFD specifications would require that c be taken as 75 psi and μ as 0.60. However, as explained later, the former values gave reasonable agreement with the test data, and so it was not necessary to use the more conservative values for concrete not intentionally roughened.

Equation 46 was used in all cases except one, where ϕv_n exceeded 720 psi, which is the upper limit permitted by Equation 5.8.4.1-3. Column 7 in Table 32 presents the predicted value of shear stress (ϕv_n) based on Section 5.8.4 of the LRFD specifications, as described above.

An additional prediction was made based on a recent proposed code change to the LRFD specifications in WAI 57. Under the proposed change, the value of c corresponding to that used to calculate the values of Column 7 in Table 32 would be increased to 280 psi, and μ would remain at 1. An upper limit of 1,800 psi for v_n would also be provided, similar to Equation 5.8.4.1-3 from the existing code. Due to the lower levels of shear reinforcement present in the test specimens, this upper limit was never invoked. Column 8 presents the predictions of shear stress (ϕv_n) based on this method, which is denoted as LRFD$^+$ in Table 32.

One final comparison was made with v_{ci} predictions from the MCFT (*3*). According to the MCFT, the shear stress that can be carried across a crack (v_{ci}) is a function of crack width (w) and aggregate size (a) and is given by the following equation (*29*).

$$v_{ci} = \frac{2.16\sqrt{f'_c}}{0.31 + \dfrac{24w}{a + 0.63}} \text{ (in inches and psi)} \qquad (47)$$

Evaluations of the shear stress according to the MCFT were made using crack widths of 0.0118 inch (0.3 millimeter) and 0.0295 inch (0.75 millimeter). The resultant v_{ci} values are displayed in Columns 9 and 10 of Table 32. Columns 11 through 14 present the ratios of the experimental values for shear stress divided by the various predicted values.

Figure 107 shows a plot of the net shear stress normalized by the square root of the concrete strength versus crack opening (crack width) for the test specimens. The experimental net shear stress curves were determined by estimating the strain in the reinforcing steel based on displacement data from the Krypton machine. This allowed for the contribution of the steel to resisting slip along the crack to be removed from the total load applied to the specimen. Comparisons are made to the v_{ci} curves that are also normalized by the square root of concrete strength for aggregate sizes of 0 inch and 1/2 inch. The results illustrate that the interface shear transfer resistance that can be provided by the concrete is larger than that calculated using the v_{ci} expression in the MCFT for crack widths up to 0.04 inch (1 millimeter) in all cases tested and for crack widths up to 0.08 inch (2 millimeters) in most cases.

Figure 108 presents a plot of the interface shear resistance versus the clamping stress. The experimental results are presented in comparison with the existing expression of the LRFD specifications as well as the proposal from the T10 Work Action Item (WAI 57). These results illustrate that the current provisions are conservative and that the WAI proposal is also conservative when clamping stresses exceed 0.4 ksi and c and μ values are chosen as described below.

2.9 Deformation Patterns in End Regions

2.9.1 Introduction

The LRFD specifications permit the use of the LRFD Sectional Design Model for the shear design of regions between the support and the first critical section from the support. For that design, the shear force to be used is that at the first critical section. As discussed in Chapter 1 and demonstrated by the test data from earlier in this chapter, this approach may not be appropriate because the Sectional Design Model was derived based on the assumptions that plane sections remain plane and that there is a uniform field of diagonal compression over the depth of a member. However, in the behavior of end regions, there is a very complex flow of forces due to discontinuities introduced by the vertical reaction force, the anchorage of the prestressing strands, and the stress-free surface at the actual end of a simply supported member. Of particular concern is that the funneling of the diagonal compression field from above a support into the support must lead to a magnification in the principal compressive stress in the web above a support, and this could lead to premature crushing of the concrete as well as large horizontal shear stresses between the lower bulb and web of the girder near the support.

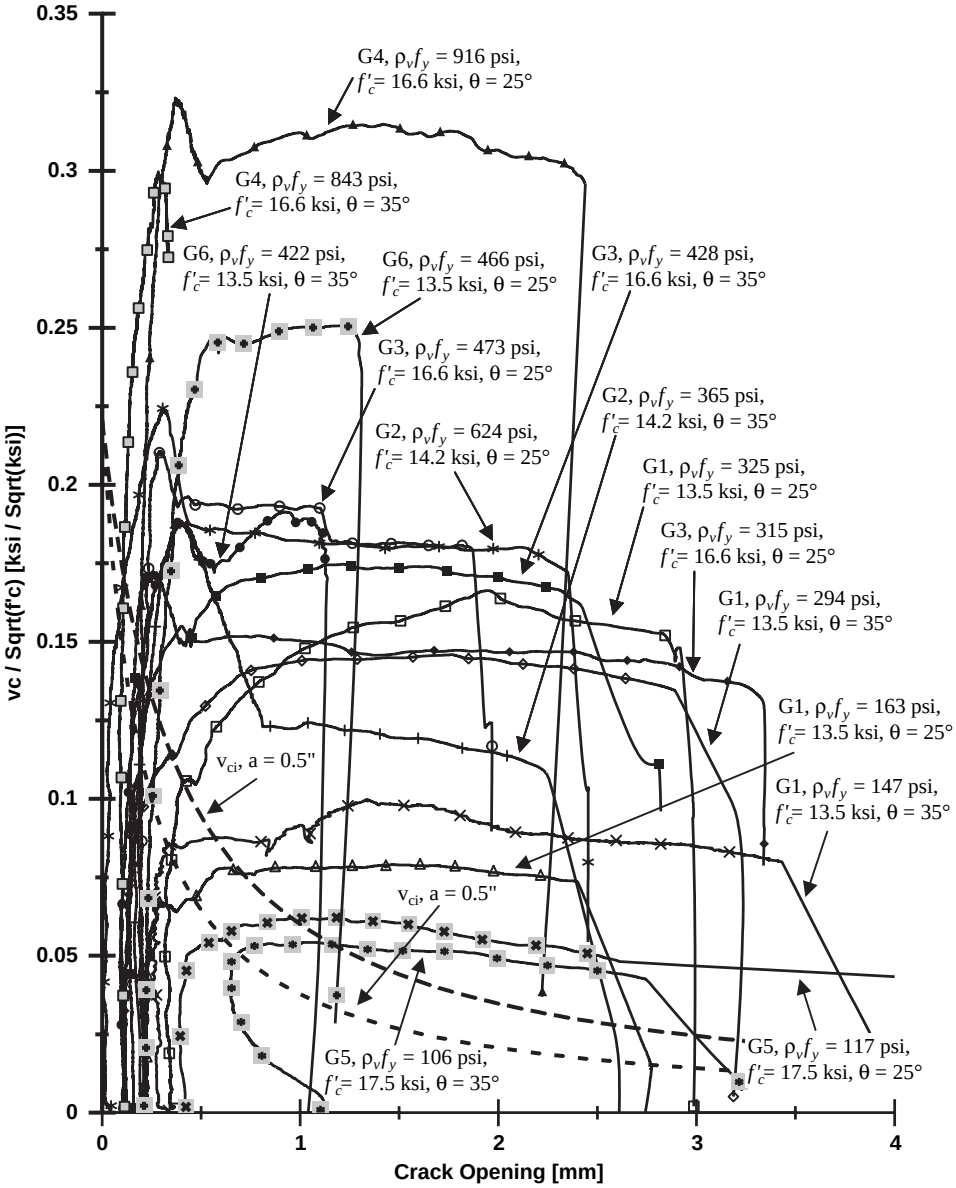

Figure 107. Comparison of test results with V_{ci} predictions.

Many assumptions that are involved in the LRFD Sectional Design Model can be assessed and validated by examining the detailed deformation patterns in the end regions of girders. The deformation pattern in these regions was recorded by the Krypton Dynamic Measurement Machine (DMM) and concrete surface strain gages. Section 2.9.2 describes the methodology that was used to acquire and analyze this detailed data from the Krypton system. This information is used to examine the behavior of the west end of Girder 10, the results and interpretation of which are presented in Sections 2.9.3 and 2.9.4. Section 2.9.5 presents an analysis of selected concrete surface strain gage results.

The remainder of Section 2.9 summarizes the primary relevant observations from the tests on the behavior of end regions. It does not provide a complete analysis of all test data. Such detailed analysis is considered beyond the scope of this project and will be reported subsequently in the technical literature.

2.9.2 Instrumentation Layout and Methodology

Detailed displacement measurements were taken for the end regions of girders using the Krypton DMM system. The Krypton DMM system is capable of measuring the three-dimensional position of infrared LED targets to an accuracy of ±0.0008 inch (0.02 millimeter). This level of accuracy allows strain measurements to be discerned from displacement

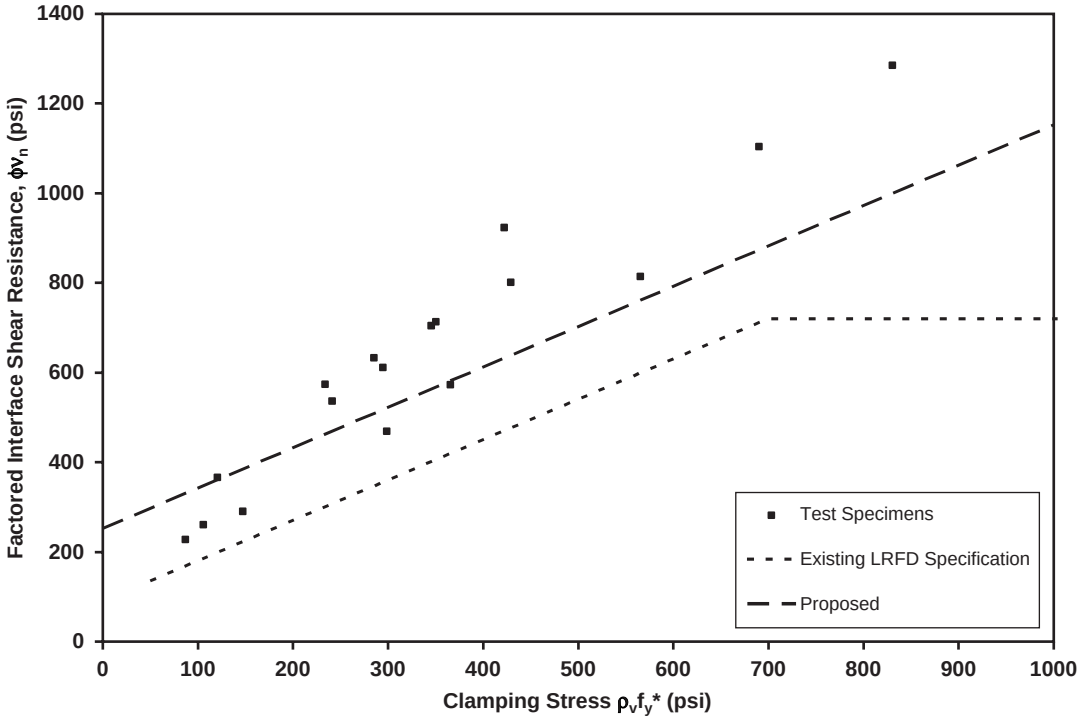

Figure 108. Comparison of test results with LRFD predictions.

measurements provided that there is a sufficient gage length between the LED targets.

The circles in Figure 109 represent the typical layout of Krypton targets in the end region of a girder. The typical layout consisted of 99 targets arranged in 9 rows and 11 columns. The rows were spaced at 5-inch intervals covering the central 40 inches of the 45-inch clear height of the web. The columns were spaced at 10-inch intervals over a 100-inch length of the web that started 5 inches behind the center line of the support and extended 95 inches towards mid-span. The decision was made to space the targets at 5 inches vertically and 10 inches horizontally because greater deformations and variability in the distribution of measurements were expected in the vertical direction. Displacement measurements were acquired at a rate of 1 per second for each LED throughout the duration of a typical test, and the displacement data were correlated with the applied load data.

The number of targets placed on a girder affords a myriad of analysis possibilities. At the most basic level, displacement measurements for every target can be evaluated. Further analysis of the displacements with some additional postprocessing can provide the linear strain between any

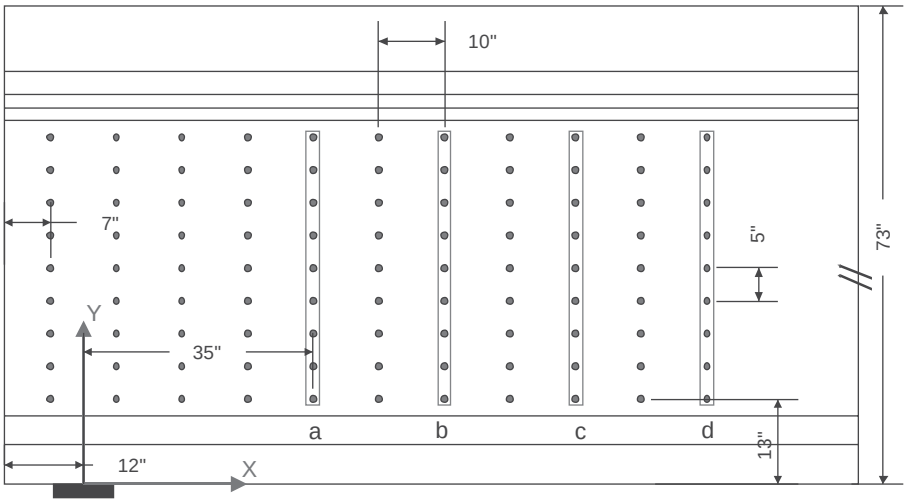

Figure 109. Layout of Krypton targets for selected vertical strain measurements.

two targets located on the girder. This result is especially useful for evaluating distributions of vertical, horizontal, and diagonal strains. Strains between individual targets can also be combined to calculate the magnitude and direction of principal strains. Combining detailed strain distributions with crack patterns, data obtained from concrete surface gages, and strain gages embedded on shear reinforcement can provide significant insight into the behavior of end regions. It should be noted that the data presented in this section does not take into account strains that are a result of the release of the prestressing strands or strains caused by the construction of the cast-in-place deck. The Krypton targets were applied to the girder immediately prior to testing. The Krypton data can be used in conjunction with analysis results to estimate strain as a result of both initial prestressing and the applied uniformly distributed laboratory loading.

2.9.3 Experimental Results

The experimental results included in this report are presented first, with a figure highlighting which Krypton targets were used to derive the results, followed by plots of the results obtained from these targets. Results derived from the analysis of selected vertical, horizontal, shear, and diagonal strains are presented in this section. All strains calculated using displacement information from the Krypton system were determined using the following method. First, the distance between the two targets of interest was calculated at each entry in the data file. Next, an average value was calculated from the first 20 entries of the calculated distance. This value represented the original distance between targets and was used as a baseline to determine the change in the distance between the targets of interest. Finally, the strain was calculated by dividing the change in distance by the original distance. A moving average algorithm was then implemented to smooth the data. All strain results that are reported in this section are referenced to the location of the targets used to calculate the strain value. The coordinate axis located at the left side of Figure 109 was used to describe the coordinate system used for the locations of the strain measurements. The coordinate value used to describe the location of a particular strain corresponds to the mid-point between the two targets that were used to calculate that strain value. Figures that include references to the applied load are based on the six load levels of 1.2 kips/ft, 10 kips/ft, 20 kips/ft, 30 kips/ft, 40 kips/ft, and 42.8 kips/ft. The level of 1.2 kips/ft corresponds to the dead load of the girder and the testing equipment, while the applied load of 42.8 kips/ft is the load acting on Girder 10 immediately before its west end failed.

Figure 109 shows a typical end region of a girder with the location of the Krypton targets marked. The four groups of targets that are outlined in vertical rectangles were used to evaluate vertical strain distributions along those lines over the height of the web. Each line of nine targets allows for the calculation of eight strains with a gage length of 5 inches each. Figure 110 displays the plots that correspond to the locations labeled (a) through (d) on Figure 109. The vertical axis of each plot in Figure 110 represents the height up the web corresponding to the location of the strain measurement. The horizontal axis is the value of measured strain in microstrain. Each line on the plot represents the strain distribution at a particular applied load, as indicated by the legend. As expected, a large variation of the strain throughout the depth of the web was observed. High values of strain correspond to the location of larger cracks in the web of the girder. Figure 111(a) shows the distribution of average strain along the length of the end region for each column of targets. The average strain was calculated by using the displacements from the top and bottom targets in each column. The horizontal axis represents the location along the length of the girder referenced to the centerline of the support, and the vertical axis represents the measured value of the average strain in microstrain. Each line on the plot shows the strain distribution that corresponds to the applied load indicated in the legend. Figure 111(b) displays the applied load versus the average strain for each of the four columns of targets (a) through (d) indicated in Figure 109.

Figure 112 displays a typical girder end region, with the locations of the Krypton targets marked. The targets outlined in horizontal rectangles were used to measure horizontal strain distributions at the bottom and the mid-height of the web. Each line consists of 11 targets, and that configuration allows for 10 individual strain measurements to be calculated, each with a gage length of 10 inches. Figures 113(a) and (b) present the horizontal strain distributions corresponding to the labels (a) and (b) in Figure 112. In the Figure 113 plots, the vertical axes represent the measured horizontal strain values in microstrain, while the horizontal axes represent the horizontal position along the length of the girder where the strain measurements were taken in inches. Each line in the plots represents the horizontal strain distribution corresponding to an applied load, as indicated in the plot legend. Figure 114 displays the average horizontal strain values for the horizontal lines labeled (a) and (b) in Figure 112. The vertical axis represents the applied load, and the horizontal axis represents the measured average horizontal strain. As expected, the average horizontal strain at the bottom of the web exceeds the average horizontal strain at mid-height.

Figure 115 displays the typical layout of Krypton targets on the end region of a girder. The targets that are outlined in large diagonal rectangles labeled (a) and (b) are used to calculate average shear strain values based on a 40-inch by 40-inch square section of the web. The targets that are outlined in small diagonal rectangles labeled (c) and (d) were used to calculate

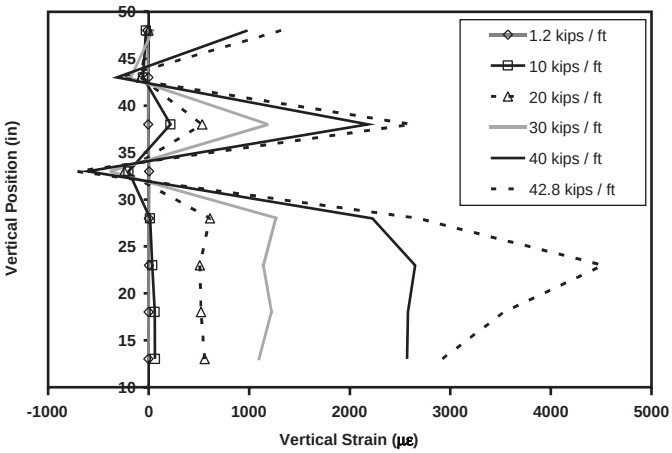

(a) Distribution at x = 35"

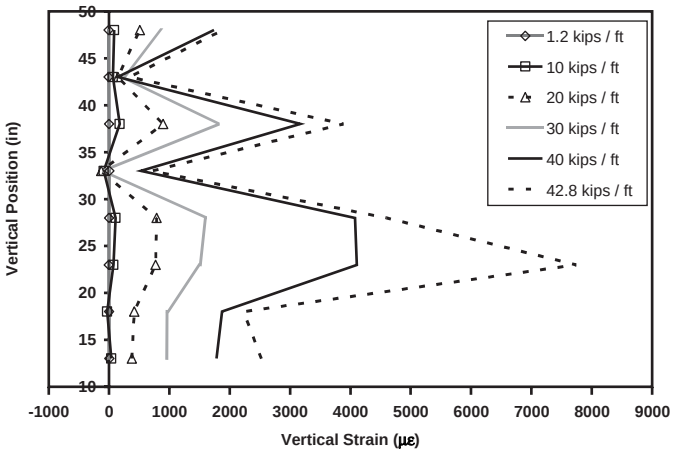

(b) Distribution at x = 55"

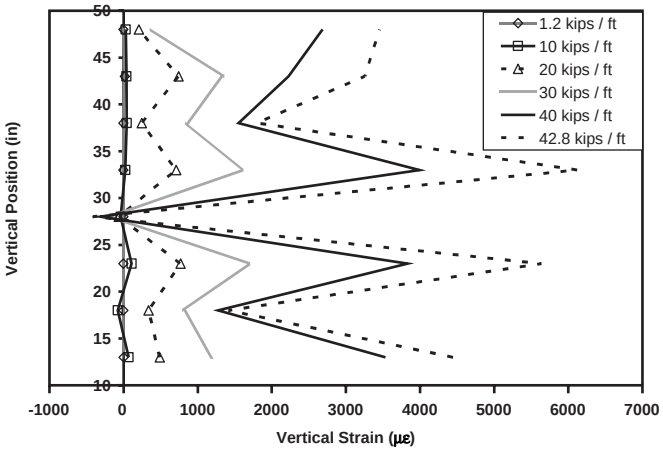

(c) Distribution at x = 75"

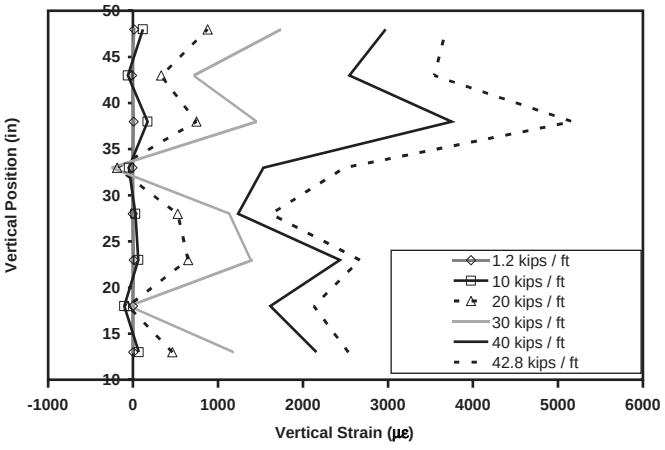

(d) Distribution at x = 95"

Figure 110. Vertical strain distributions in Girder 10.

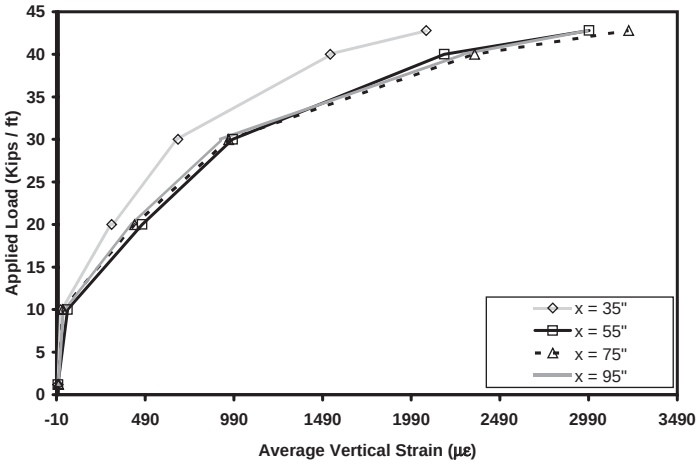

(a) Average Vertical Strain Distribution

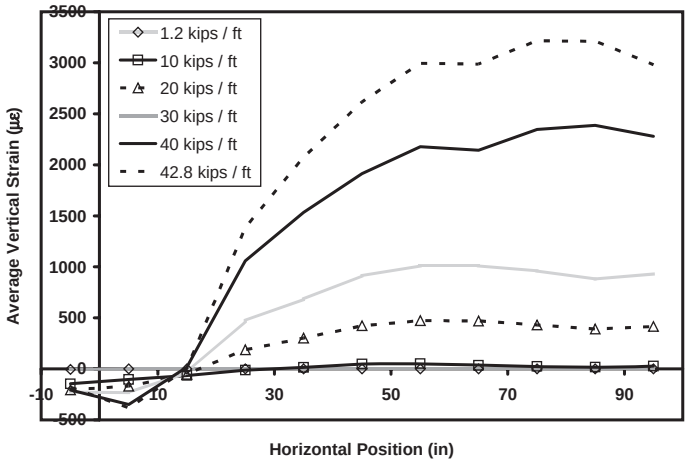

(b) Applied Load versus Average Vertical Strain

Figure 111. Average vertical strain in Girder 10.

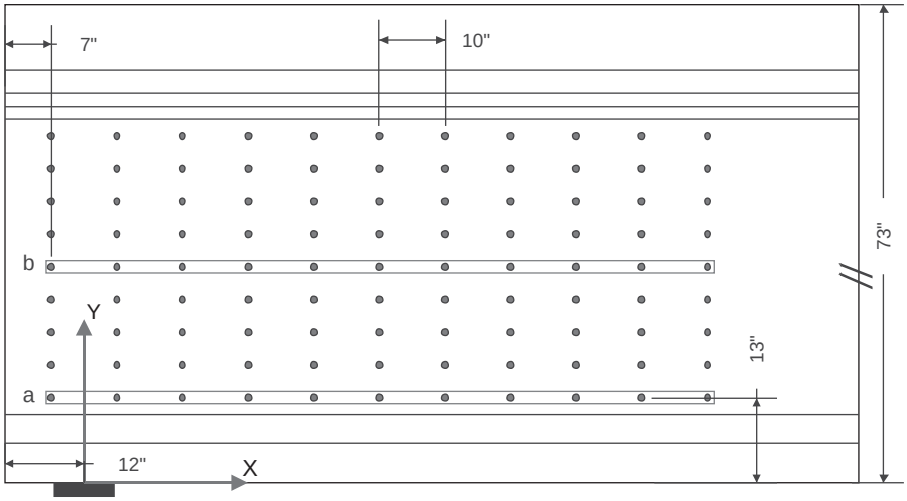

Figure 112. Layout of Krypton targets for selected horizontal strain measurements.

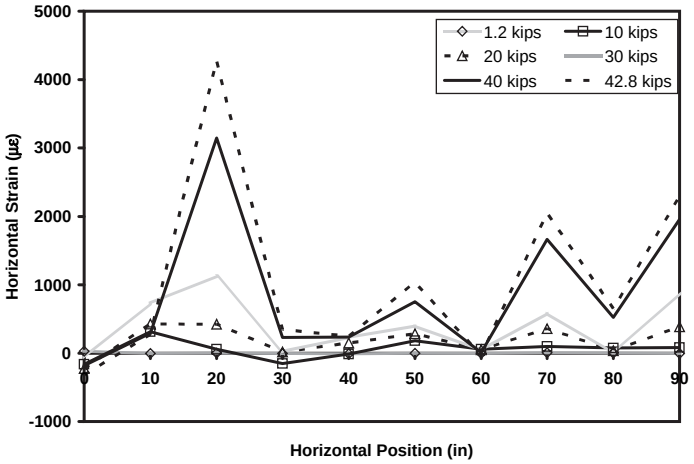

(a) Distribution at y = 13”

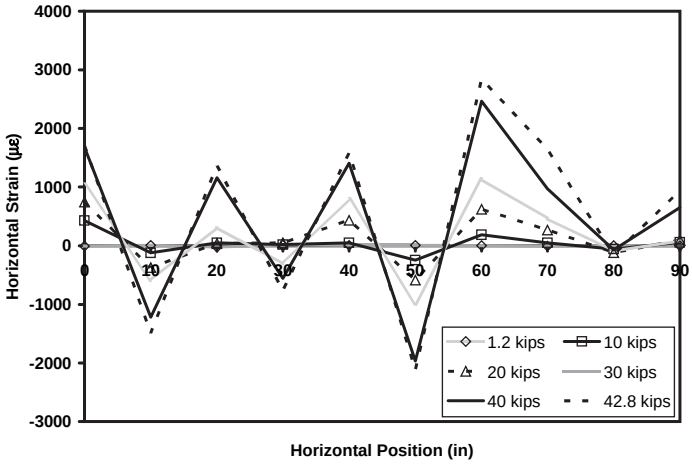

(b) Distribution at y = 33”

Figure 113. Horizontal strain distributions in Girder 10.

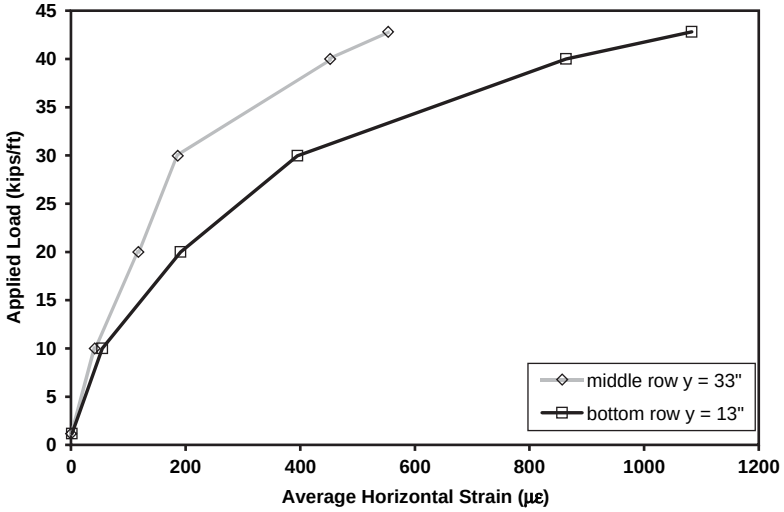

Figure 114. Applied load versus average horizontal strain in Girder 10.

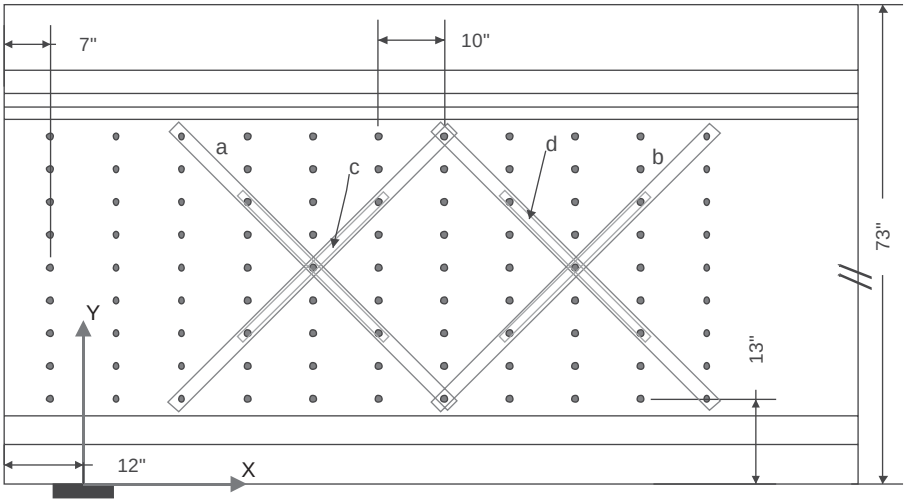

Figure 115. Layout of Krypton targets for selected shear strain measurements.

average shear strains based on a 20-inch by 20-inch square section of the web that is aligned with the midheight of the web. Figure 116 displays the average shear strain values corresponding to the different measurement configurations (a) through (d). The vertical axis represents the applied load, while horizontal axis represents the measured average shear strain.

Figure 117 highlights which targets in the typical layout were used to measure diagonal compressive strains. The left diagonal rectangle, labeled (a), which is oriented at a 45-degree angle, includes five targets and allows for the measurement of four compressive strain values. The right diagonal rectangle, labeled (b), which is oriented at a 26.5-degree angle, includes nine targets and allows for the measurement of eight compressive strain values. Figures 118(a) and 118(b) show the compressive strain distributions corresponding to the lines labeled (a) and (b) in Figure 117. The horizontal axes represent the horizontal distances along the length of the girder where the strain measurement was taken. The vertical axes represent the value of the diagonal compressive strain in microstrain. Each line on the plot represents the distribution of diagonal compressive strain for an applied load value, as indicated in the legend. Figure 119 shows the average diagonal compressive strain along lines (a) and (b) from Figure 117. The vertical axis represents the applied load, while the horizontal axis represents the value of the average diagonal compressive strain.

Figure 120 shows which targets in the typical layout were used to measure the distribution of diagonal tensile strain. The diagonal rectangles that are labeled (a) and (b) each include five targets that were used to measure four diagonal

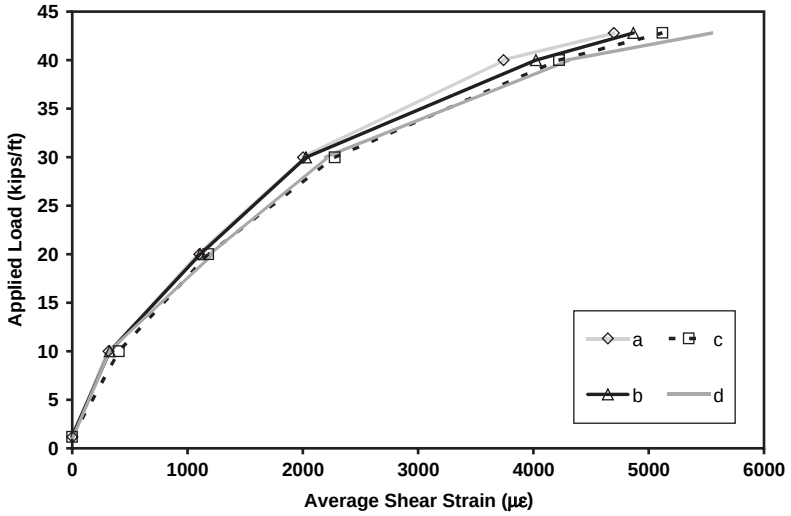

Figure 116. Applied load versus average shear strain in Girder 10.

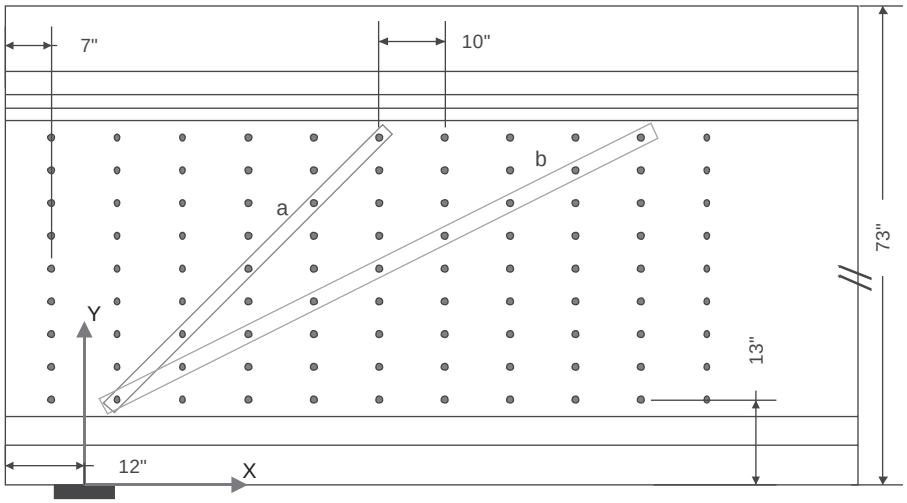

Figure 117. Layout of Krypton targets for selected diagonal strain measurements.

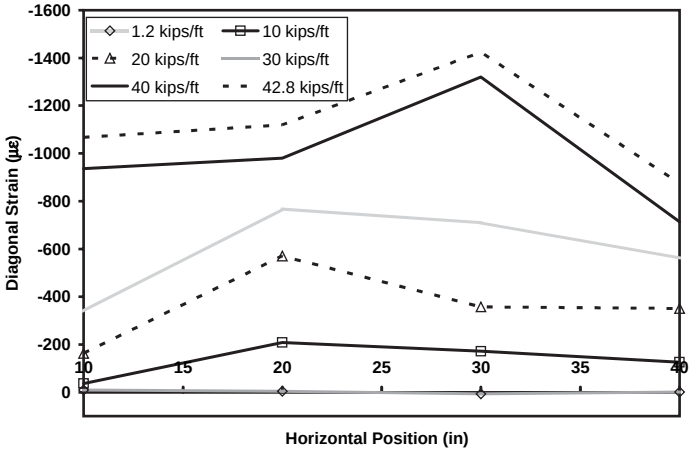

(a) Distribution at 45 degrees

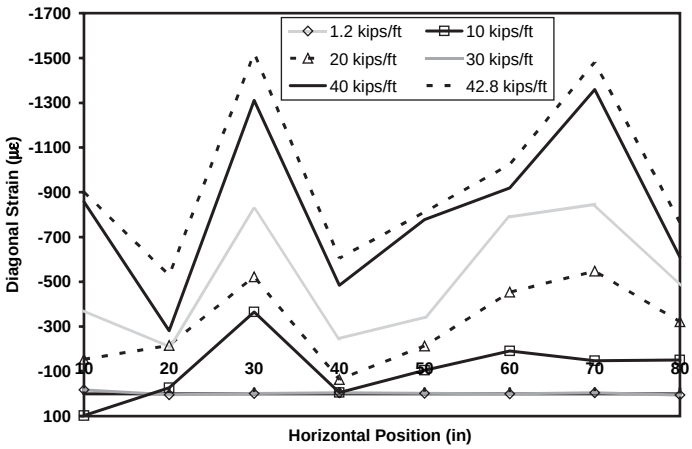

(b) Distribution at 26.5 degrees

Figure 118. Diagonal compressive strain distributions in Girder 10.

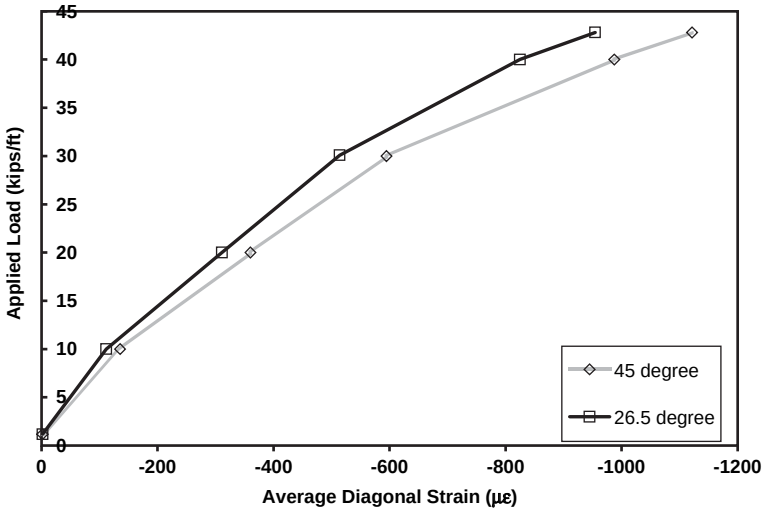

Figure 119. Applied load versus average diagonal compressive strain in Girder 10.

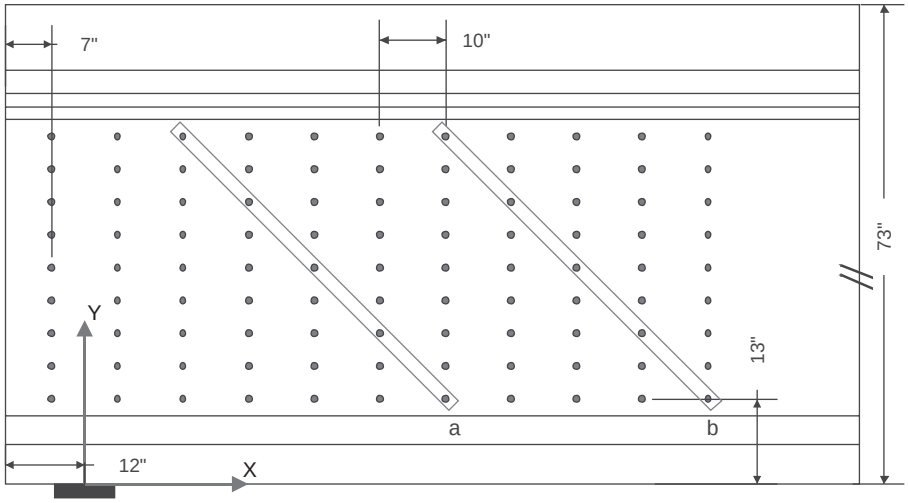

Figure 120. Layout of Krypton targets for selected diagonal strain measurements.

strain values and are oriented along a 45-degree angle. Figures 121(a) and 121(b) show the diagonal tensile strain distributions that correspond to the labels (a) and (b) in Figure 120. Again, the horizontal axes represent the horizontal position of the strain measurement along the length of the girder. The vertical axes represent the value of the diagonal tensile strain. Each line on the plot displays the distribution of the diagonal tensile strain corresponding to a value of the applied load, as indicated in the legend. Figure 122 shows the average diagonal tensile strain along the lines (a) and (b). Again, the vertical axis represents the applied load, while the horizontal axis represents the average value of the diagonal tensile strain.

2.9.4 Interpretation of Results

Further inspection of the experimental results presented in Figure 110 provides insight into the distribution of vertical strains through the height of the girder web and along the length of the girder. Figure 110 shows a positive correlation between the vertical position and horizontal position of the maximum vertical strains in the girder web. This indicates that a plane of weakness forms at an angle along a group of shear cracks, as is expected. This observation correlates well with other test observations. In Figure 111(a), it is observed that the average vertical strain just before failure is at a maximum value for the measurements taken at a distance of 75 and 85 inches from the support and decreases for the measurement taken 95 inches from the support. It is also of interest to note that the average vertical strain at a distance of 15 inches from the support is essentially zero throughout the entire loading sequence. This result confirms the rationality of the design assumption that the shear reinforcement used at the first critical section is sufficient for the region from the support to this section.

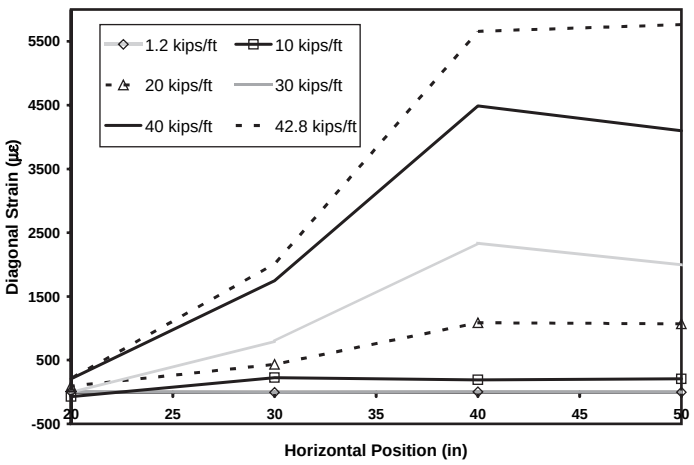

(a) Distribution for line a

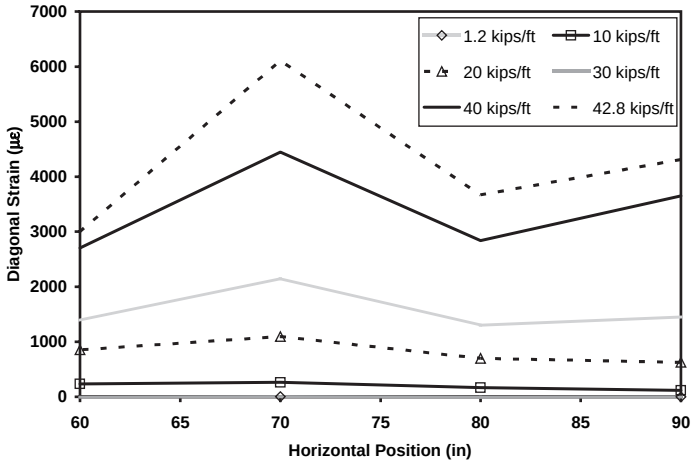

(b) Distribution for line b

Figure 121. Diagonal tensile strain distributions in Girder 10.

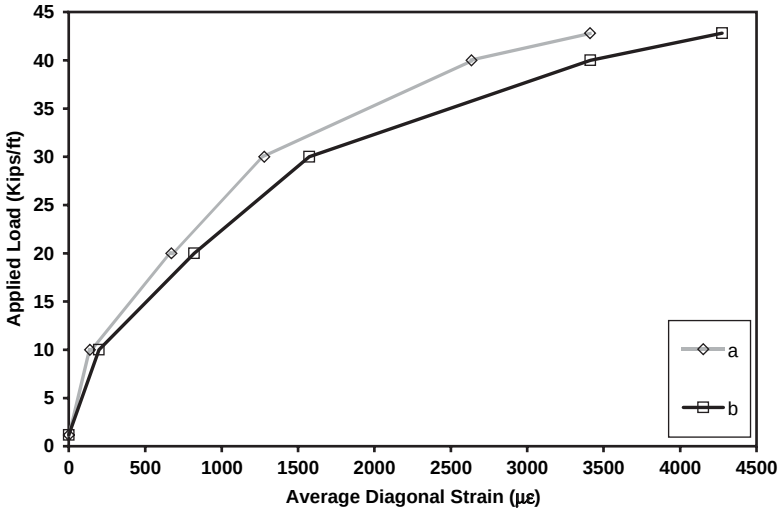

Figure 122. Applied load versus average diagonal tensile strain in Girder 10.

An inspection of the horizontal strain distributions presented in Figure 113(a) indicates that a significant increase in the horizontal strain at a horizontal distance of 20 inches from the support precedes the failure of the girder. This evidence supports the observation that a loss of prestress and excessive demand on the longitudinal reinforcement is exhibited prior to the failure of a typical girder. The horizontal strain distributions in Figure 113(b) show less of a trend because of the spacing of shear cracks crossing the line along which measurements were taken. However, Figure 114 shows that the average strain associated with Figure 113(b) is in tension and increases with the applied load.

Figure 116 compares the shear strain values obtained from the large measurement field with the values from the small measurement field. The figure indicates that the shear strains measured from the small measurement field are consistently greater than those obtained from the large measurement field but that overall they are reasonably close. This result indicates that the top and bottom edges of the web are restrained by the top flange and bottom bulb, respectively, of the girder, and, because of its depth, the middle of the web is able to experience greater shear strains than the boundaries.

Comparisons of the diagonal compressive strains shown in Figures 118 and 119 indicate that the average compressive strain along the 45-degree line is greater than the average compressive strain along the 26.5-degree line. This would lead one to believe that the greatest average compressive strain would occur at an angle between 26.5 degrees and 45 degrees. However, the distribution of straining along the 26.5-degree line had higher peak compressive strain values than the distribution along the 45-degree line. Again, these strains do not consider pretest strains.

The distribution of diagonal tensile strain in Figure 121(a) illustrates that there is very little diagonal tensile strain in the top of the web near the support. This is consistent with other experimental test findings, such as the minimal cracking in this region because forces are flowing into the support via a direct strut. Figure 122 shows that the average tensile strain corresponding to the (b) distribution is greater than that corresponding to the (a) distribution. This result could be artificially influenced by the low values included in the (a) distribution closer to the support. Averaging the 3 largest values from the (a) distribution provides an average strain value close to the average strain value of the (b) distribution just before failure.

2.9.5 Concrete Surface Strain Gage Measurements

This section presents the data collected by selected concrete surface strain gages. It illustrates the measured concentration of compressive straining that occurred due to the funneling of the diagonal compression forces into the support, as well as the factors that influenced the measured magnification in straining.

Figure 123 presents the positions of selected strain gages on Girder 10 and the measured change in strain in these gages due to the imposed loading. At the onset of diagonal cracking, the rate of compressive straining in gages close to the support increased more rapidly than in gages further from the support. The east end of Girder 10 anchored 34 straight strands, of which eight were debonded, while the west end of Girder 10 anchored 34 strands, of which 10 were draped and splayed over the depth at the end of the girder. As shown, the average magnification of the straining in the west end region

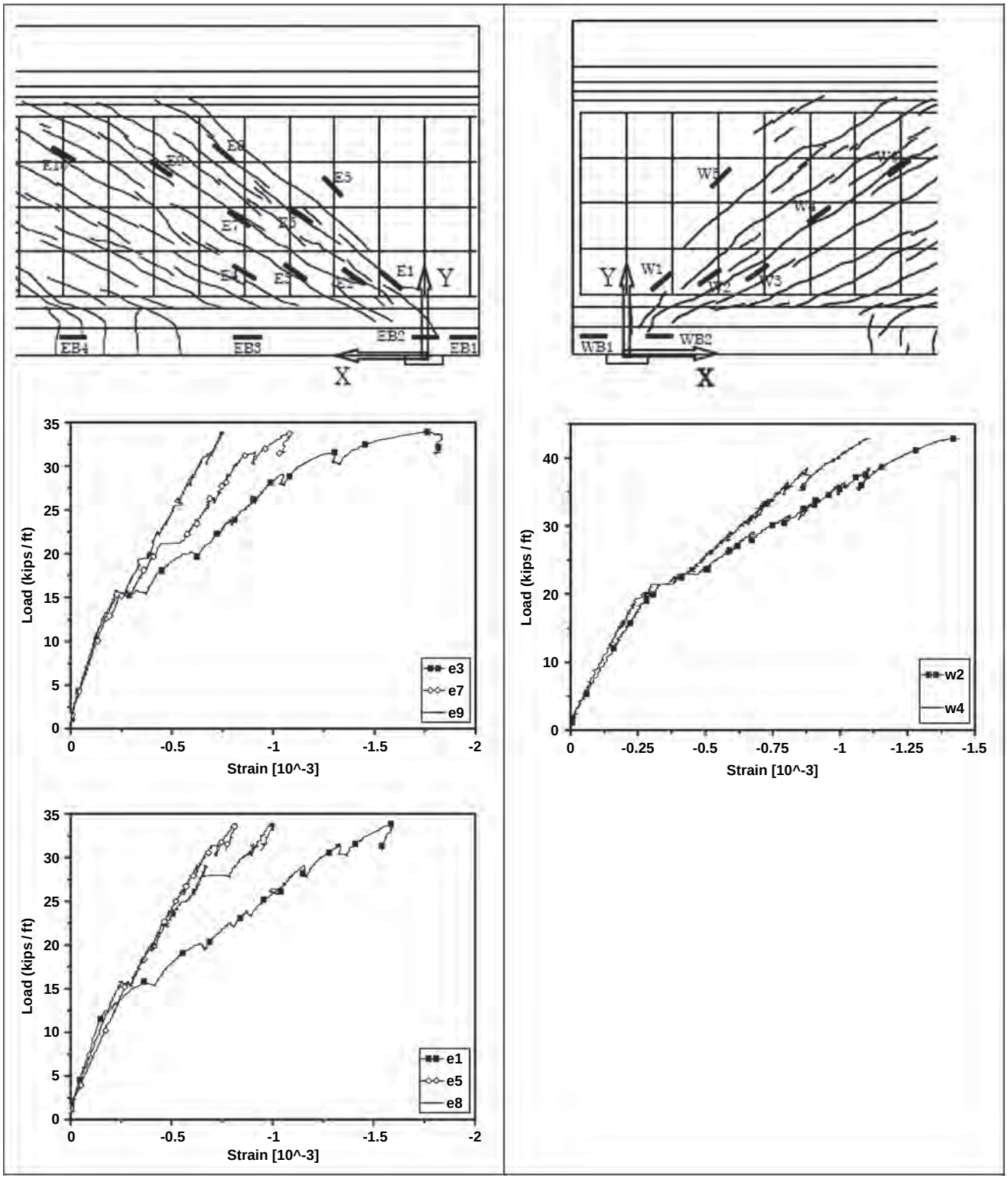

(a) 10 East

(b) 10 West

Figure 123. Measured concrete surface strains in Girder 10.

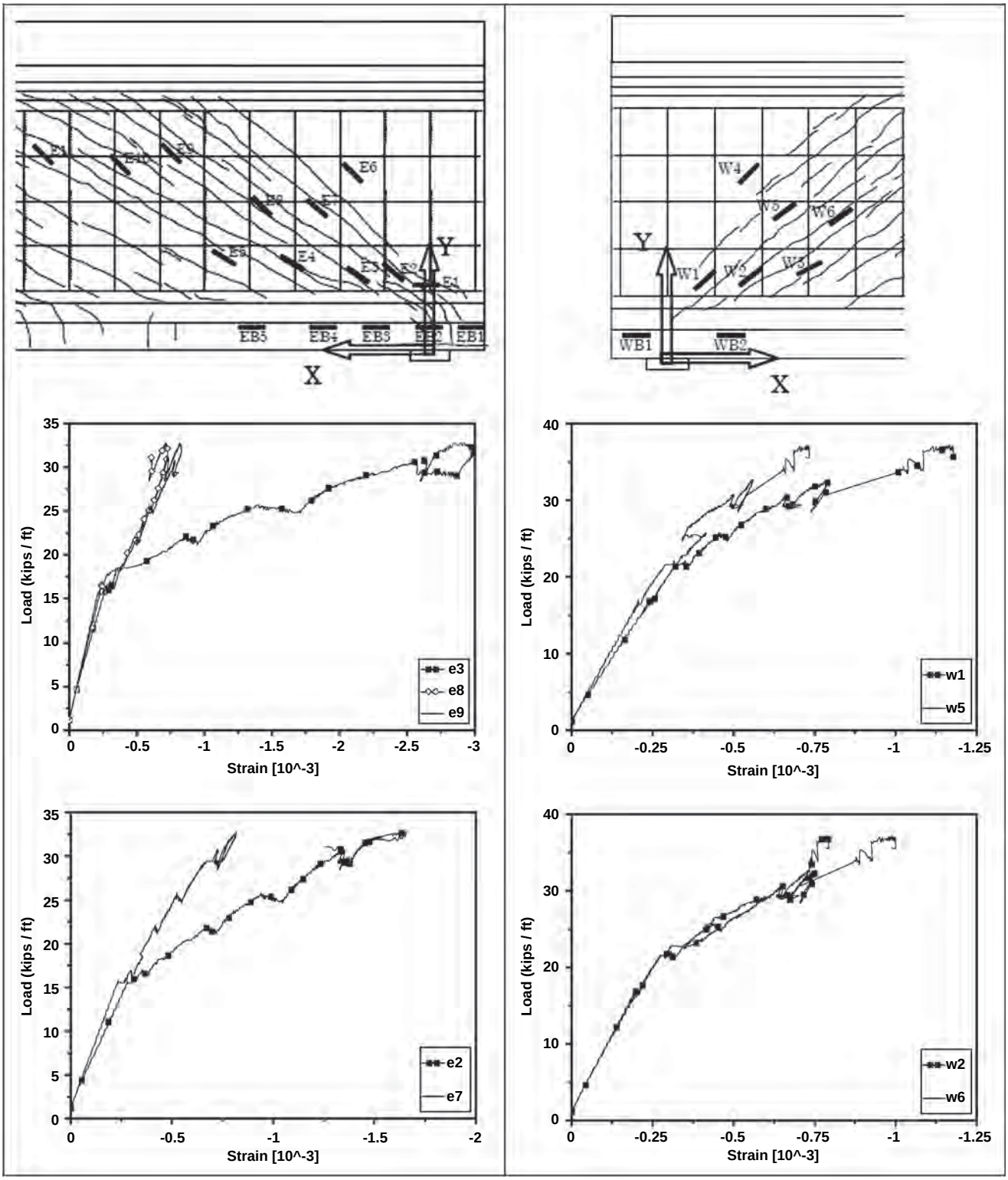

(c) 9 East (d) 9 West

Figure 124. Measured concrete surface strains in Girder 9.

is smaller than in the east end due to the effectiveness of the draping and splaying of the strands at providing a larger region for anchoring of the diagonal compressive force.

Figure 124 presents the position of selected strain gages in Girder 9 and the measured change in strain in these gages due to the imposed loading. The east end of Girder 9 anchored 34 straight strands, while the west end of Girder 9 anchored 34 strands, of which 10 were draped and splayed as was done in Girder 10. The observations are very similar in Girder 9 as in Girder 10, but the extent of the beneficial effect of draping and splaying strands is more pronounced. This result suggests that there is a detrimental effect for the anchoring of the diagonal compressive force when some of the tendons are debonded.

Because prestressing alone can introduce significant compressive stresses at the base of the web, the likely pretest strains should be taken into consideration when reviewing the results of concrete surface strain gauges, particularly the results of gages near the base of webs and on the bottom bulb. These pretest strain levels are predicted from the finite element analyses reported in Section 2.10.

2.10 Prediction of Behavior of Girders Using Finite Element Analyses

2.10.1 Overview

This section presents the behavior of the girders as predicted using nonlinear finite element analyses. The analyses were conducted using the program Vector2, which fully implements the MCFT. This section summarizes the Vector2 program (2.10.2), the development of the geometric model of the girders (2.10.3), the characteristics of the selected material models (2.10.4), material properties (2.10.5), and the overall load-deformation response predictions (2.10.6) for all girders. It then provides selected results of the analyses, including strain distributions prior to loading (2.10.7), cracking strengths and crack patterns (2.10.8), modes of failures (2.10.9), shear deformations (2.10.10), shear slip (2.10.11), and strain and deformation patterns (2.10.12). Many of these predictions are then compared with the results of the experimental testing program that were documented in Sections 2.4 through 2.9. These comparisons are used to assess the effectiveness of Vector2 at predicting overall strength, load-deformation response, mode-of-failure, and distribution of straining. If Vector2 is deemed to be successful, then the result is extremely significant, for it implies that this program can be reliably used for predicting the response of somewhat similar members that were not tested in this research program. This will be particularly important if design cases are identified for which there are concerns about the appropriateness of using the LRFD Sectional Design Model.

2.10.2 The Vector2 Program

Vector2 is a nonlinear finite element program for the analysis of two-dimensional reinforced concrete structures. The theoretical bases of Vector2 are the MCFT (*2*) and the Disturbed Stress Field Model (DSFM) (*31*). The program was principally developed by Professor Frank Vecchio and his students over the last 20 years and was previously known as Trix.

The MCFT and DSFM are analytical models for the response of a two-dimensional membrane structure subjected to in-plane normal and shear stresses. The models account for the average or smeared stress-strain relationships in cracked concrete, as well as perform an equilibrium check of conditions at crack locations. The DSFM differs from the MCFT in that it takes into consideration the deformation associated with slip along the crack faces. As a result, unlike the MCFT, the DSFM does not assume that the angle of principal stress corresponds to the angle of principal strain.

Vector2 computes the response of structures by using constitutive relationships, including compression softening, tension stiffening, tension softening, and tension splitting (*28*). For each constitutive relationship, Vector2 provides several choices, as have been developed by prominent researchers. Therefore, Vector2 has the capacity to predict the response of a wide range of two-dimensional concrete structures.

One of the main objectives of the girder tests was to study the shear behavior of the web. Because the primary behavior of the web is similar to that of a two-dimensional panel, and because the main objective of Vector2 is to analyze such elements, Vector2 is an appropriate tool for analyzing the behavior of these girders. Vector2 provides for the use of constant strain triangular elements, four-node quadrilateral elements for smeared reinforced concrete elements, and two-node linear truss elements for discrete reinforcement modeling. Because, in general, the finite element analysis for structural concrete requires relatively dense meshing, using a low-order element is appropriate. Vector2 solves the nonlinear problems using a secant stiffness algorithm, which is usually adopted for monotonic loading, and the path-independent nonlinear elasticity due to its robustness and simplicity. This approach provides good convergence stability for postpeak behavior.

2.10.3 Modeling of Girders

Because Vector2 is a two-dimensional continuum analysis program, the variations in width of the bulb-tee had to be taken into account by using elements of different thicknesses. This results in some simplification of the cross section, as shown in Figure 125. The area and moment of inertia are only marginally different in the model than in the real member.

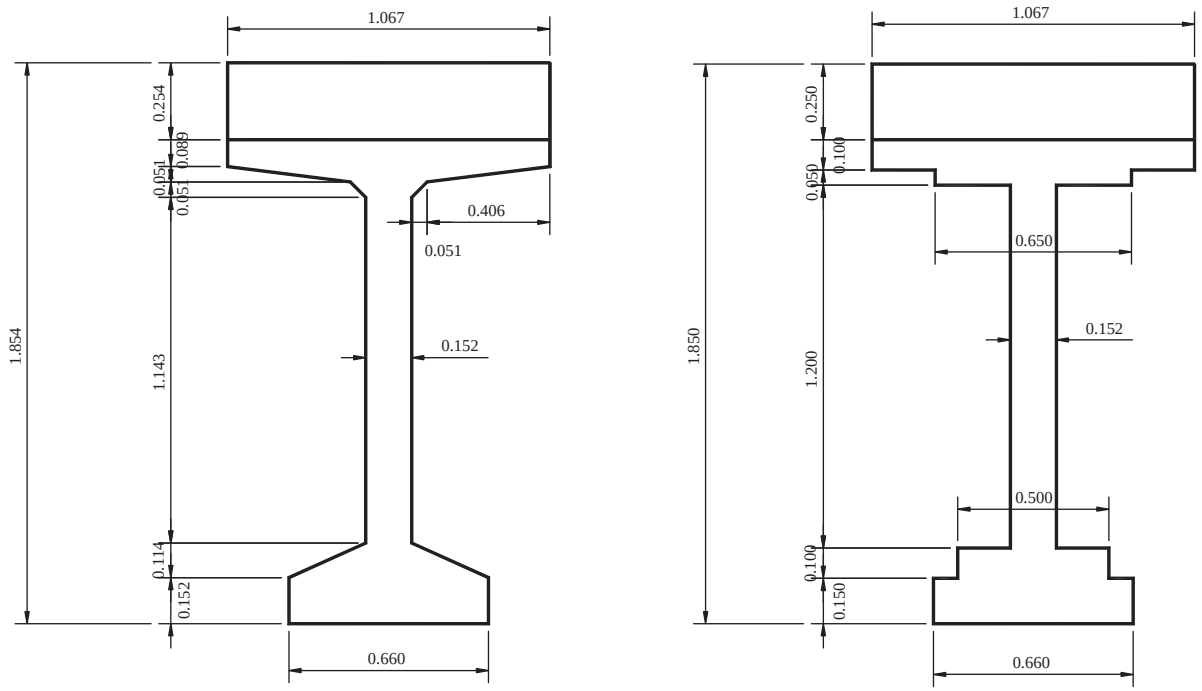

Figure 125. Comparison of cross sections used in experiments and analysis (in millimeters).

Only one-half of the length of girders was modeled at any one time in order to decrease solution time. The typical analysis model is shown in Figure 126. Because the transverse reinforcement was well distributed, it was modeled as smeared reinforcement. The prestressing strands were modeled as discrete truss bars to facilitate the application of prestrains and to account for transfer lengths. Longitudinal reinforcement in the web was also modeled as discrete truss bars, because it is unreasonable to assume that such reinforcement is distributed over the web evenly. The bold lines in Figure 126 indicate the locations of the discrete reinforcement.

The load was assumed to be uniformly distributed over the 44-foot loaded length, as was used in the physical experiments. In Vector2, point loads along the nodes in the upper flange were applied to simulate the uniformly distributed load. In the tests, there were some uneven load cases, such as in the east side of Girder 6 and the west side of Girder 9. In these cases, small shear forces exist at midspan of the girders due to the nonsymmetric load pattern. This force was accounted for in the analyses by applying upward nodal forces at the right side boundary of the model. The load distributions used in the analyses are shown in Figure 127.

The prestress is applied in the form of prestrain. Prestrain is calculated based on the experimentally measured effective prestress prior to loading. The prestrain is applied to the prestress

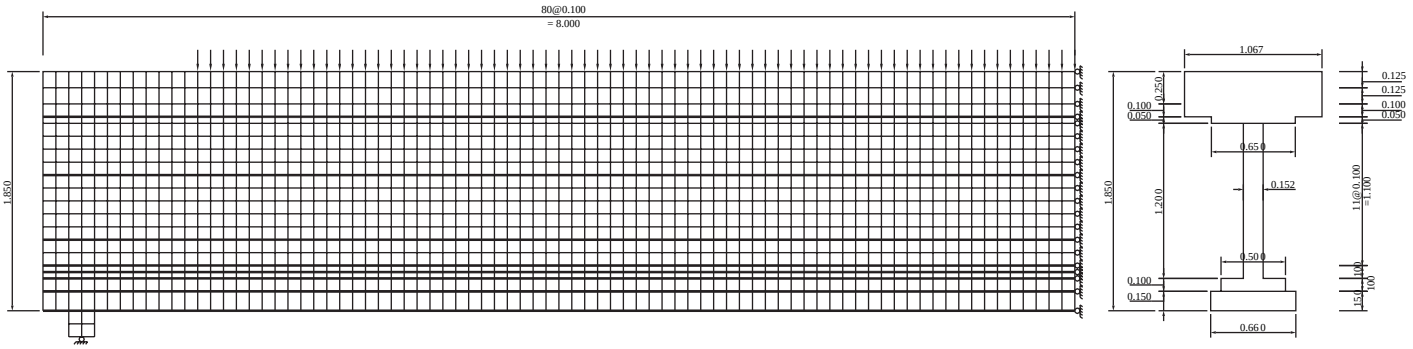

Figure 126. Typical analysis model (in millimeters).

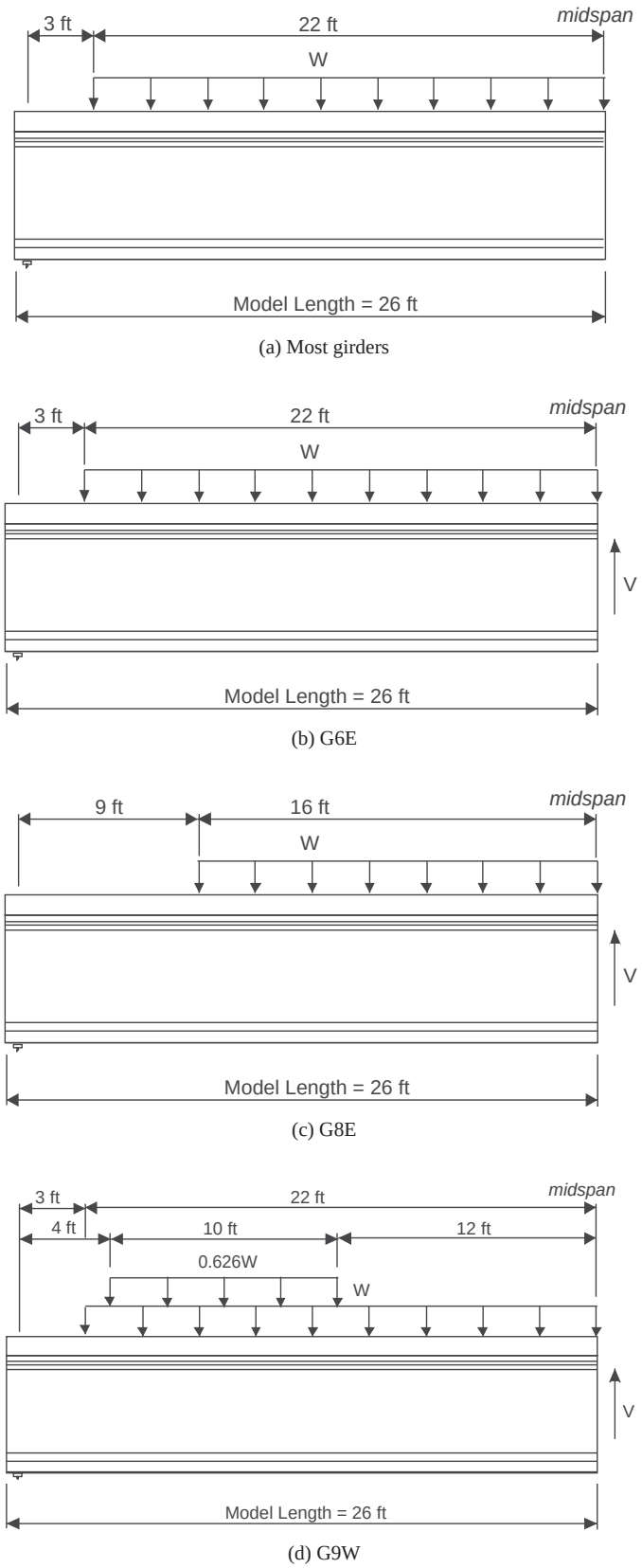

Figure 127. Loading pattern in modeling.

tendons, and thus the strain offset between the concrete element and the strands effectively models the effect of prestressing. The transfer length of the prestressing tendon was considered to be $50d_b$ from the actual end of the girder. Within the transfer length, the prestrain was applied in the manner of stepwise increments.

In the experiments, steel bearing plates were used to avoid stress concentration above the supports. However, in Vector2, only reinforced concrete material can be used for membrane elements, and thus it was not possible to model steel bearing plates directly. If such support conditions are modeled in terms of a one-point roller boundary condition, spurious stress concentrations can result. Therefore, fictitious bearing plate elements were made up of relatively strong reinforced concrete. This fictitious plate prevented the local stress concentration and distributed the stress to the girder in a manner similar to the steel plate.

One of the most important model parameter selections in Vector2 is that of estimating the crack spacing because the crack width is taken as the principal tensile strain multiplied by the crack spacing. The crack width controls the ability of the shear stress to be transferred across the crack. In these analyses, average crack spacing was computed according to CEB-FIP model code 1990 (*32*). The calculation example of average crack width used in the analysis is shown in Table 33, in which s_m refers to the mean crack spacing. Average crack spacing is defined for the x-axis and y-axis.

2.10.4 Material Models

As mentioned previously, Vector2 provides a selection of constitutive relationships that can be used in the analyses for the compression prepeak response, the compression postpeak response, compression softening, the tension stress-strain relationship, and tension softening. To obtain the most reliable results from the analyses, the most appropriate material model should be selected. The models selected for use in this analysis are described in the following sections.

Compression Prepeak Response

The compression prepeak response model is used for the computation of the principal compressive stress before the strain reaches the strain corresponding to the peak compressive stress. The selected relationship is for the uniaxial response, but may be subsequently modified according to the selected compression-softening relationship. Because HSC was used in the girders, and because the strength of the concrete has a large effect on the compressive response, the selected material model should account for that characteristic. For this purpose, the Popovics model for HSC (*33*) was

Table 33. Calculation example of average crack spacing.

Section number	Axis	db	15db	clear cover	maximum spacing	s	k1	k2	As	Acef	rho_ef	sm (mm)
1	x	19.1	287	41	254	254	0.4	0.25	2840	266750	0.011	313
	y	15.9	239	475	102	102	0.4	0.25	2388	102030	0.023	1038
2	x	28.7	431	36	193	193	0.4	0.25	3876	106700	0.036	191
	y	15.9	239	475	102	102	0.4	0.25	2388	102030	0.023	1038
3	x	0	0	0	0	0	0.4	0.25	0	0	0.000	0
	y	15.9	239	266	102	102	0.4	0.25	2388	102030	0.023	621
4	x	0	0	0	0	0	0.4	0.25	0	0	0.000	0
	y	15.9	239	17	102	102	0.4	0.25	2388	45600	0.052	85
5	x	15.2	228	43	51	51	0.8	0.25	840	50000	0.017	278
	y	15.9	239	199	102	102	0.4	0.25	2672	102030	0.026	479
6	x	15.2	228	43	51	51	0.8	0.25	3640	99000	0.037	179
	y	15.9	239	279	102	102	0.4	0.25	2672	102030	0.026	639
7	x	19.1	287	41	254	254	0.4	0.25	2840	266750	0.011	313
	y	12.7	191	475	152	152	0.4	0.25	5676	1080770	0.005	1222
8	x	28.7	431	36	193	193	0.4	0.25	3876	102030	0.038	187
	y	12.7	191	475	152	152	0.4	0.25	5676	1080770	0.005	1222
9	x	0	0	0	0	0	0.4	0.25	0	0	0.000	0
	y	12.7	191	266	152	152	0.4	0.25	5676	1080770	0.005	805

selected because it adequately shows the large linear range of response that occurs before peak stress for HSC.

Compression Postpeak Response

The compression postpeak response model accounts for ductile behavior and strength enhancement due to confinement of the concrete by transverse stresses. Because the webs of the girders are unconfined in the out-of-plane direction, ductile behavior does not occur in that direction. Consequently, the postpeak part of the Popovics model for HSC (*33*), which has a steep descending branch, is used. The typical relationship is shown in the Figure 128(a) and is expressed by Equation 48:

$$f_{ci} = \left(\frac{\varepsilon_{ci}}{\varepsilon_p}\right) f_p \frac{n}{n-1+\left(\frac{\varepsilon_{ci}}{\varepsilon_p}\right)^{nk}} \quad \text{for } \varepsilon_{ci} < 0 \tag{48}$$

where

f_{ci} = principal compressive stress;

ε_{ci} = principal compressive strain;

ε_p = strain corresponding to the peak compressive stress, f_p;

f_p = peak concrete compressive stress;

e_1, e_2 = parameters in compression-softening model;

β_d = compression-softening reduction factor;

ε_{c1} = average concrete axial strain in the principal tensile direction;

ε_{c2} = average concrete axial strain in the principal compressive direction;

ε_0 = strain corresponding to the peak compressive stress, f'_c;

f^a_{c1} = average concrete tensile stress determined by tension-stiffening effect;

ε_{cr} = concrete cracking strain;

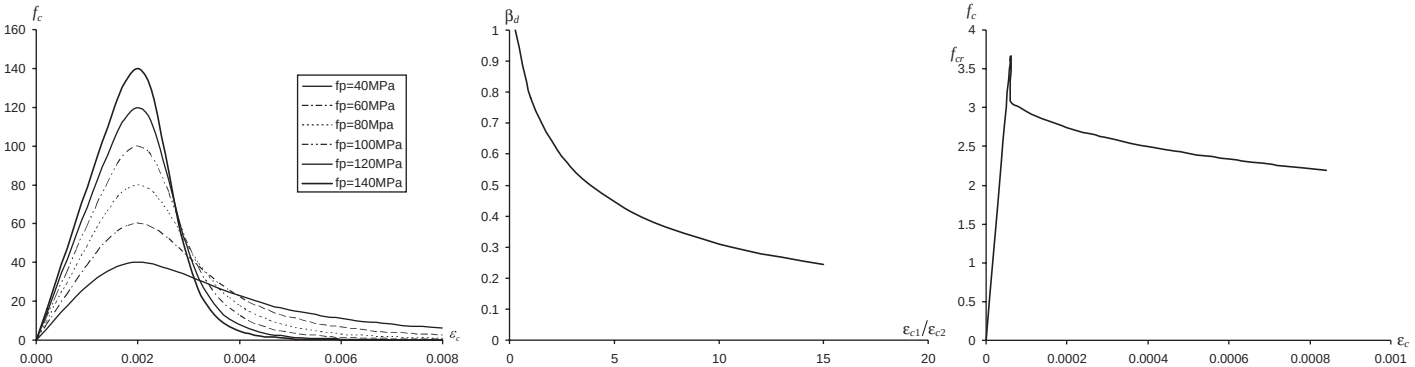

(a) Compressive Response (b) Compression Softening (c) Tension Stiffening

Figure 128. Constitutive relationships.

$$n = 0.80 + \frac{f_p}{17} \qquad (f_p \text{ in MPa}); \text{ and}$$

$$k = \begin{cases} 1.0 & \text{for } \varepsilon_p < \varepsilon_{ci} < 0 \\ 0.67 + \frac{f_p}{17} \geq 1.0 & \text{for } \varepsilon_{ci} < \varepsilon_p < 0 (f_p \text{ in MPa}) \end{cases}$$

Compression Softening

Compression softening is the softening and weakening of the compressive response due to transverse tensile straining. In the original MCFT formulation, the softening was only a function of transverse strain, but more recent shear tests on HSC elements (*34*) found that the use of a compression-softening relationship that includes a concrete strength factor provided for better results. Therefore, two modified models—a strength and strain-softened model, and a strength-only softening model—were proposed, and it was concluded that a strength and strain-softened model gave more accurate predictions for HSC elements. Hence, in this study, the strength and strain-softened model, which is also known as the Vecchio 1992-A (e_1/e_2) model, is used. The relationship is shown in Figure 128(b). The relationship is given by Equation 49:

$$\beta_d = \frac{1}{1 + C_s \times C_d} \leq 1$$

$$C_d = \begin{cases} 0 & \text{if } r > 0.28 \\ 0.35(r - 0.28)^{0.80} & \text{if } r > 0.28 \end{cases}$$

$$r = -\frac{\varepsilon_{c1}}{\varepsilon_{c2}} \leq 400 \qquad (49)$$

$$C_s = \begin{cases} 1 & \text{if sheer slip not considered} \\ 0.55 & \text{if sheer slip considered} \end{cases}$$

$$f_p = \beta_d f_c'$$

$$\varepsilon_p = \beta_d \varepsilon_0$$

Tension Stiffening

After concrete cracks, the concrete is still effectively bonded to the reinforcement between cracks and can carry significant tensile stresses. This action is referred to as the "tension-stiffening effect" and is accounted for by using an average tensile stress in the concrete even when the principal tensile strain is greater than the cracking strain. The tension-stiffening effect is largest for members in which there is a significant amount of deformed bar reinforcement. For these analyses, the research team selected the tension-stiffening relationship proposed by Bentz (*35*), which is a modification of the tension-stiffening model of Collins and Mitchell (*36*). Additional information on this model is available in Bentz's "Sectional Analysis of Reinforced Concrete Members" (*35*). The typical curve is shown in the Figure 128(c). The relationship is given by Equation 50:

Table 34. Selected material models.

Material Model Category	Selected Model
Compression Prepeak Response	Popovics (High Strength)
Compression Postpeak Response	Popovics (High Strength)
Compression Softening	Vecchio 1992-A (e_1/e_2)
Tension Stiffening	Bentz 1999
Element Slip Distortion	Not considered

$$f_{c1}^a = \frac{f_{cr}}{1 + \sqrt{3.6m \times \varepsilon_{c1}}} \text{ for } 0 < \varepsilon_{cr} < \varepsilon_{c1} \qquad (50)$$

where the parameter m accounts for bond and depends on the ratio of the area of the concrete to the bonded surface area of the reinforcement.

Slip Distortion

The essential difference between the DSFM and the MCFT is that the DSFM removes the shear stress limit at the crack surface of the MCFT and replaces it with a slip distortion relationship. Several models have been proposed to address the slip-shear stress relationship at a crack. The relationship developed by Walraven (*37*) depends on the shear stress at a crack surface only, whereas the Hybrid III relationship computes the slip distortion as the maximum of the Walraven estimate and a constant orientation lag. If this option is activated, Vector2 employs the DSFM, while if no slip distortion is selected, then the MCFT is used. In this study, the MCFT was selected and a specific element slip distortion relationship was not used because the shear equation of the LRFD specifications is based on the MCFT, and that the comparison is meaningful. Therefore, 1.0 was used for C_s in the compression-softening model.

The selected main material models are summarized in Table 34. The default values of the programs were used for any other required material models.

2.10.5 Material Properties of the Girders

While the material models were presented in the previous section, the detailed material properties used in those material models are given in this section. Because the variables for the selected material models were limited to the peak stress f_c' and its corresponding associated strain, ε_c, those values were obtained from the uniaxial cylinder test results completed as part of the girder test program. The values for those quantities are given in Table 35.

2.10.6 Prediction of Capacity and Mid-Span Deflection

Vector2 was not only able to provide a detailed prediction of the behavior of the test girders, but also able to simply predict the overall capacity of each test girder. Table 36 com-

Table 35. Properties of concrete.

Girder number	Girder f'_c (ksi)	Girder $\varepsilon_c(\mu\varepsilon)$	Slab f'_c (ksi)
G1	12.1	3000	4.5
G2	12.6	2600	8.6
G3	15.9	3300	3.6
G4	16.3	3400	6.3
G5	17.8	2700	6.1
G6	12.7	2800	9.2
G7	12.5	3200	4.5
G8	13.3	3200	7.0
G9	9.6	2400	6.0
G10	10.6	2600	5.4

pares the measured capacities of the girders with the strengths predicted using various methods, including Vector2, R2K, the LRFD specifications, and the AASHTO Standard Specifications. As explained in Section 2.10.3, some girders were not subjected to uniformly distributed loads over the standard 44-foot length. This fact was taken into consideration in the derivation of the calculated values shown in Table 36. The mean value and the coefficient of variation of $w_{test}/w_{Vector2}$ excludes the result for Girder 4 because that girder failed in flexure due to premature debonding of an external plate.

In general, Vector2 was able to predict the capacity of the test girders to within 10 percent. Although Vector2 typically overestimated the capacity, the coefficient of variation of the strength ratio with Vector2 was only 0.08. That value is remarkably good for predictions of the behavior of complex structural concrete members. This success suggests that Vector2 can be used to predict the capacity of members when it is not possible to test experimentally; thus, Vector 2 can address other important design considerations.

Despite the generally excellent strength predictions by Vector2, the predicted behavior of the west side of Girder 8 was poor. In this experiment, two back-to-back aluminum plates were inserted in the web of the girder to create a shear plane of weakness and to minimize aggregate interlock effects. In order to model this experimental setup in the analysis correctly, a contact-type element that would resist normal compressive forces and not resist tension and shear forces should have been used. However, this type of element was not provided in Vector2, and thus the elements on each side of the plate were simply separated in the numerical model. As a result, the analysis tool showed difficulties such as overlap in early load stages or excessive separation of elements at later load stages. This result is far from the experimental observations and was undoubtedly the cause of considerable error in the strength prediction.

In addition to predicting girder strength, Vector2 was used to calculate the overall load-deformation response of the girders. While shear distortion contributes little to mid-span displacement, the mid-span deflection can be a good indicator of the usefulness of an analysis tool for evaluating global stiffness. Figure 129 presents a comparison of predicted and measured load versus mid-span displacement relationships

Table 36. Comparison of prediction of ultimate strength (kip/ft).

Girder		Test	Vector2	R2K	LRFD	STD	$w_{test}/w_{Vector2}$	w_{test}/w_{R2K}	w_{test}/w_{LRFD}	w_{test}/w_{STD}
G1	East	26.03	26.73	23.14	24.47	19.46	0.97	1.12	1.06	1.34
	West	30.09	30.16	23.71	24.72	20.29	1.00	1.27	1.22	1.48
G2	East	33.79	37.70	36.90	35.08	25.59	0.90	0.92	0.96	1.32
	West	38.73	37.70	37.57	33.60	26.15	1.03	1.03	1.15	1.48
G3	East	35.68	35.64	29.68	31.98	25.73	1.00	1.20	1.12	1.39
	West	38.82	38.38	29.68	31.98	25.73	1.01	1.31	1.21	1.51
G4	East	42.65[a]	50.72	43.28	43.43	33.20	0.84	0.99	0.98	1.28
	West	42.65[a]	50.72	43.28	43.43	33.20	0.84	0.99	0.98	1.28
G5	East	23.70	21.25	21.86	19.31	16.31	1.12	1.08	1.23	1.45
	West	19.91	23.30	21.70	17.80	15.75	0.85	0.92	1.12	1.26
G6	East	38.32	40.44	34.29	34.88	25.76	0.95	1.12	1.10	1.49
	West	27.85	30.16	29.95	27.67	20.91	0.92	0.93	1.01	1.33
G7	East	33.47	34.96	28.41	30.69	24.82	0.96	1.18	1.09	1.35
	West	33.47	34.96	28.41	30.69	24.82	0.96	1.18	1.09	1.35
G8	East	43.72	42.49	36.35	39.74	34.26	1.03	1.20	1.10	1.28
	West	32.70	41.81	31.46	34.85	25.92	0.78	1.04	0.94	1.26
G9	East	32.80	37.70	37.83	36.63	25.33	0.87	0.87	0.90	1.29
	West	37.19	41.81	50.74	43.46	25.61	0.89	0.73	0.86	1.45
G10	East	33.93	36.33	31.56	29.09	24.40	0.93	1.08	1.17	1.39
	West	42.85	39.07	34.85	31.89	26.63	1.10	1.23	1.34	1.61
						Mean[b]	0.96	1.08	1.09	1.39
						Standard Deviation	0.08	0.16	0.12	0.10
						COV	0.09	0.14	0.11	0.07

[a] Maximum applied load, not an ultimate load.
[b] Except for G4.

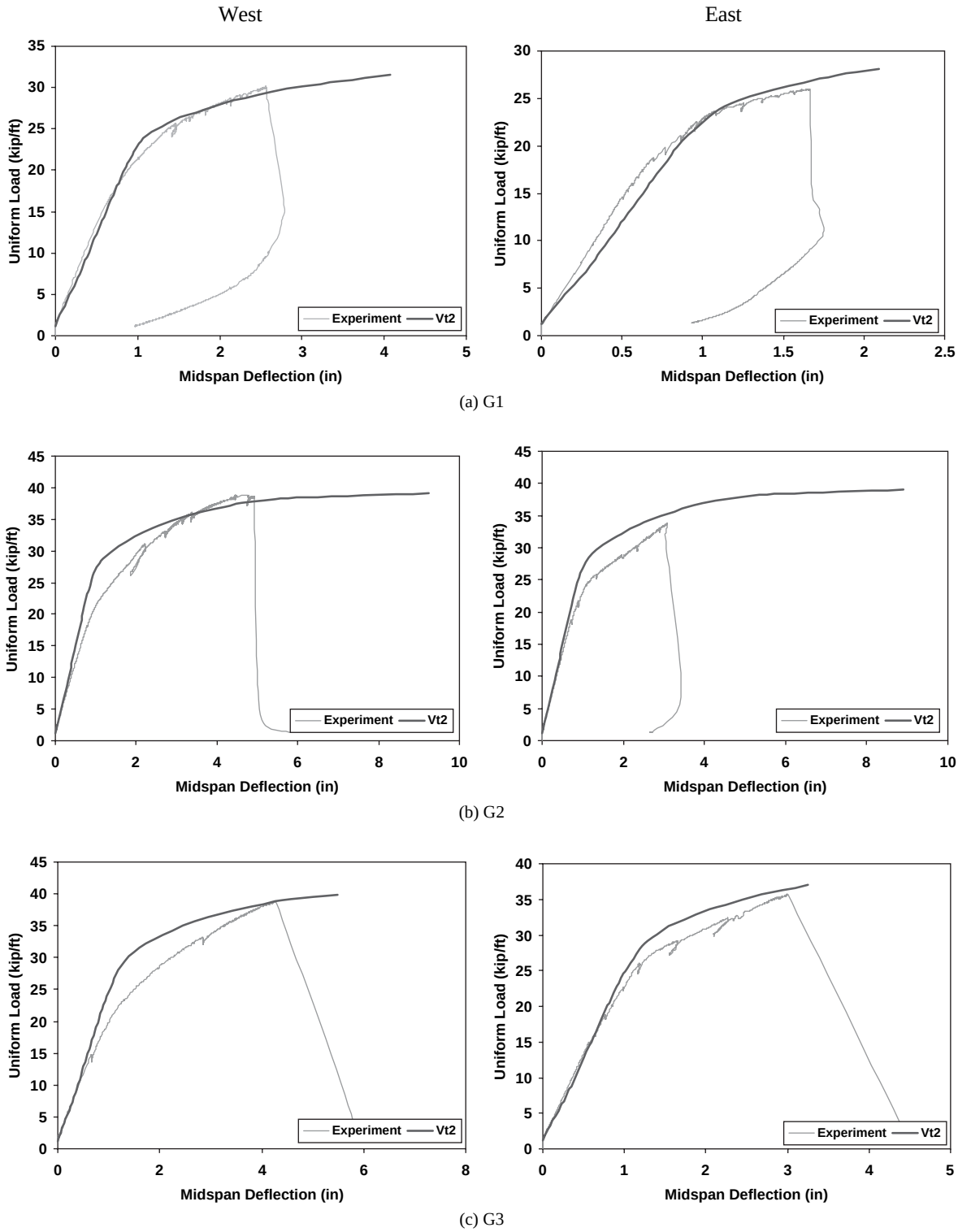

(a) G1

(b) G2

(c) G3

Figure 129. Load-deflection at mid-span.

for all of the test girders. As shown in the figure, the experimental result and the prediction are reasonably close in most cases, both in the elastic region and in the inelastic region. Even though the quality of prediction is excellent, Vector2 predicts that the girder is more ductile than the measured result in about half the cases.

2.10.7 Predicted Strain Distribution Prior to Loading

The experimental results reported in Sections 2.4 through 2.9 presented the change in strains and deformations in the test girders due to the application of the uniformly distributed load.

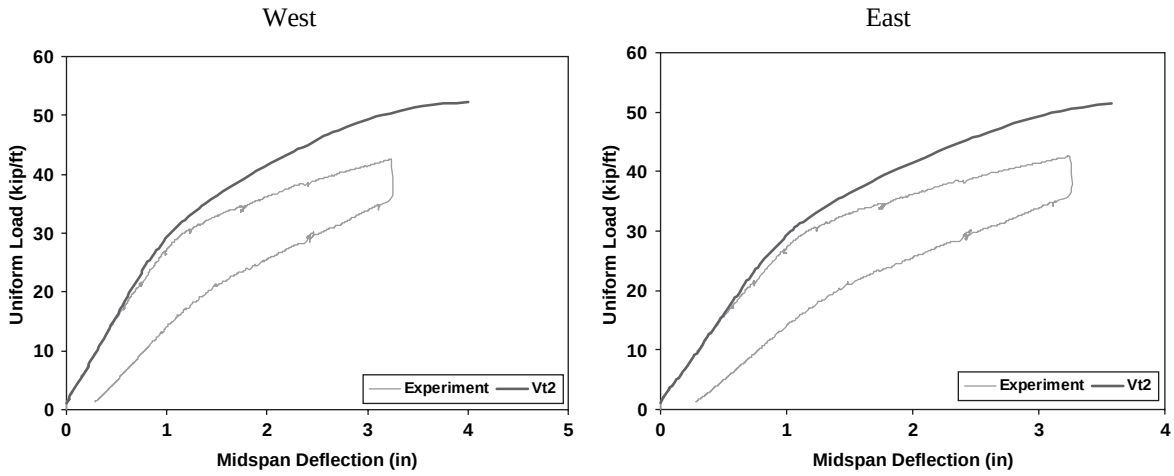

(d) G4

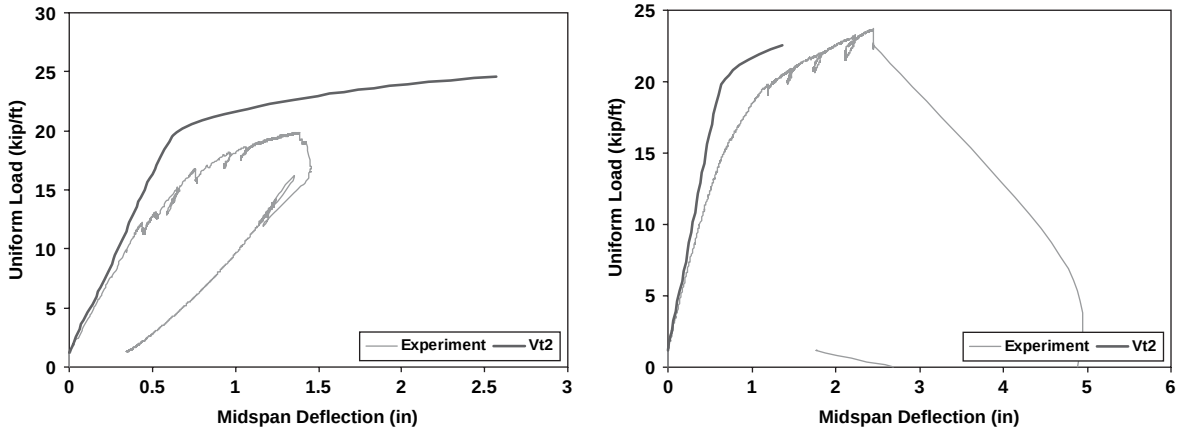

(e) G5

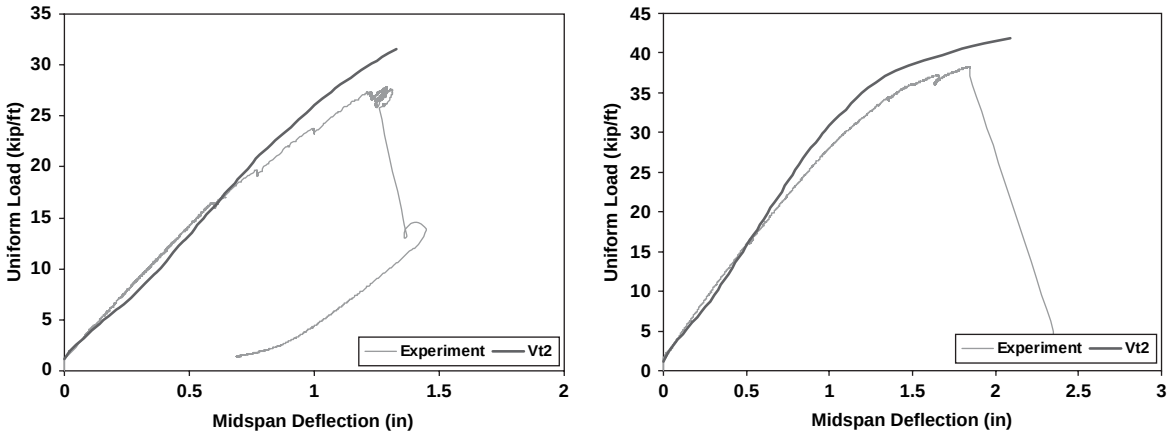

(f) G6

Figure 129. (Continued).

Since these changes do not account for the strains due to the effects of prestressing, Vector2 was used to predict the effects of the prestressing strains that occurred prior to loading.

The effect of the prestressing force can be documented in diagrams that describe the state of strain, including the principal compressive strain, ε_2, and vertical strain, ε_y. Selected analyses were conducted on numerical models of the girders without the top slab in order to obtain these pretest states of strain. In this section, four representative girders were selected to estimate the level of initial strains, two for the upper and lower bounds of the initial strains and two for evaluation of the effects of inclined prestressing tendons.

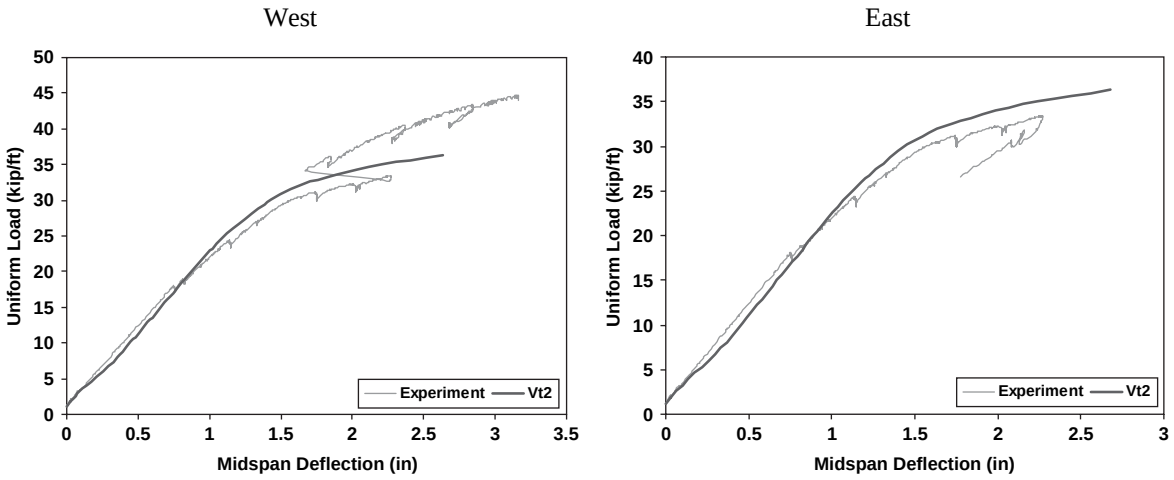

(g) G7

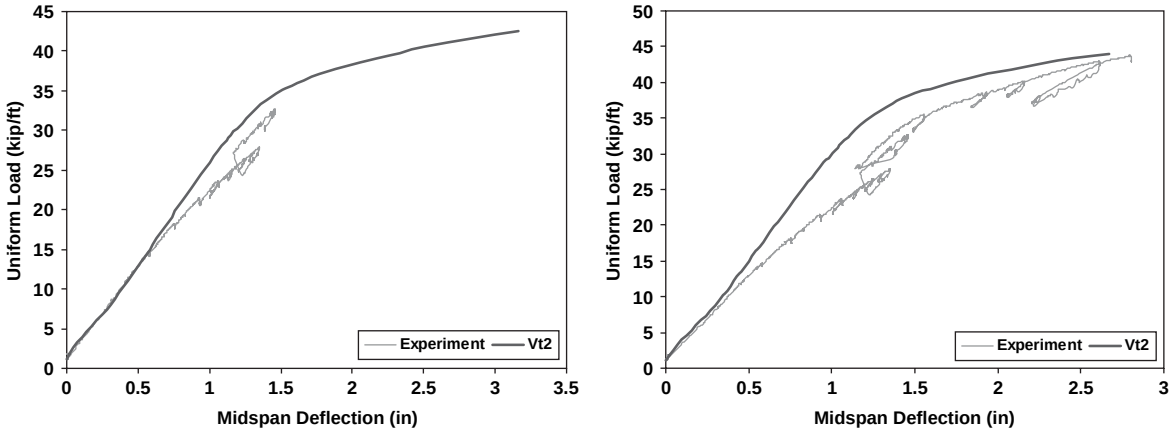

(h) G8

Figure 129. (Continued).

The elastic strains due to prestressing were calculated first because it was reasonable to assume that all materials were in an elastic state. Note that the principal compressive strain is directly proportional to the prestressing force and its direction is close to horizontal. It is also useful to note that vertical strains develop through the Poisson's effect and, thus, are directly proportional to the principal compressive strain. The resulting initial strains due to prestressing are presented in Table 37. The strain levels were calculated for the girder without a slab and were evaluated at the bottom of the web at midspan. To evaluate the upper and lower bounds of initial strains, two girders were selected and the distribution of strains due to prestressing were evaluated. As indicated in Table 37, the results from Girder 5 were selected as a lower bound, and those from Girder 7 were selected as an upper bound.

To evaluate the effects of the inclined prestressing tendons on the initial strain, the west halves of Girder 2 and Girder 10 were selected for examination. Because the west half of Girder 9 was very similar to the west half of Girder 10, it was to be expected that the strain distribution for those two girders would also be very similar.

For the west parts of Girders 2, 5, 7, and 10, the vertical strains are shown on the left and the principal compressive strains are shown on the right in Figure 130. The results are for girders without the slab and with consideration of self-weight. All strains are in millistrain. The lines of the lower part of the vertical strain results for the girders indicate the presence of truss element representing the prestressing tendons. They do not indicate the strain levels in the concrete or reinforcement. For Girders 5 and 7, the results presented in Figure 130 suggest that the vertical strains are influenced by cracking in the end region of the girder, since outside of that region there is very little vertical strain. By contrast, results for Girders 2 and 10 indicate that the initial cracking of the end region is reduced and small vertical strains develop in the remaining parts of the girder. As is the case for the vertical strains, the elastic state of strain dominates in most of the region for the principal compressive strain diagrams. Moreover, in the end region, very little compressive strain develops. Therefore, initial vertical strains in the web can be ignored, and initial

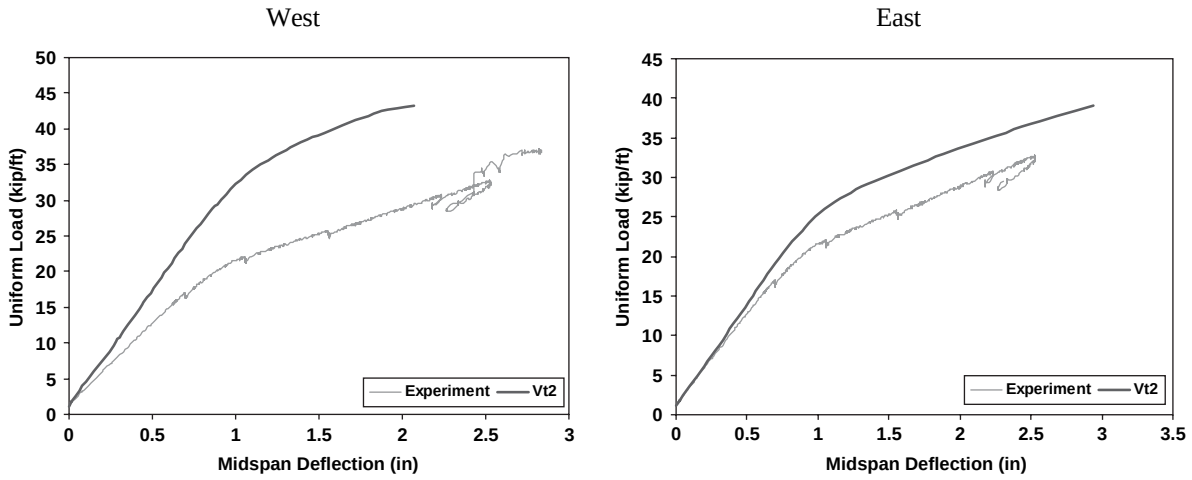

(i) G9

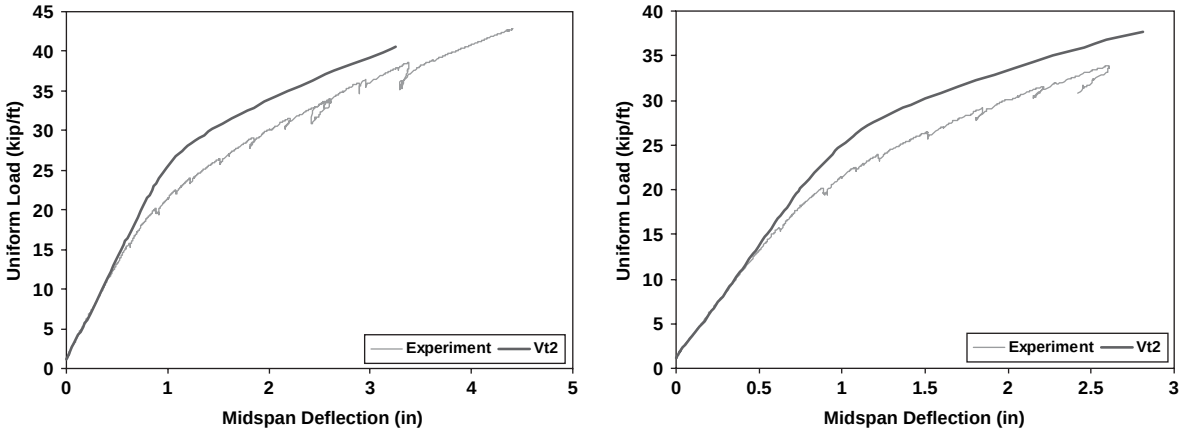

(j) G10

Figure 129. (Continued).

principal compressive strains can be calculated assuming that strains remain in the elastic range of behavior.

2.10.8 Cracking Patterns

One of the most desirable features for a finite element analysis program for structural concrete members is the ability to accurately predict cracks and their locations, directions, and average widths because the stiffness, shear transfer efficiency, and global behavior of concrete members are strongly affected by cracking. Thus, a program should not be considered effective if it cannot accurately predict the state of cracking, even if its ability to predict strength is reasonably accurate.

Figure 131 shows the crack patterns of the final load steps for several girders and, thereby showing the ability of program Vector2 to predict cracking properly. The final loading steps were

Table 37. Strains due to prestress.

Girder	# of Strand	Effective Strain (με)	Prestress Force (*k*)	Eccen. (in)	Moment (k.in)	Elastic Modulus (ksi)	ε_x (με)	ε_y (με) (= ν*ε_x)
G1	34	6,318	1,329	24.355	32,356	6,270	581	0.105
G2	40	6,262	1,549	23.720	36,744	6,398	656	0.118
G3	44	6,141	1,671	24.320	40,641	7,187	637	0.115
G4	40	5,970	1,477	23.720	35,031	7,277	550	0.099
G5	24	6,525	968	29.120	28,203	7,605	383	0.069
G6	44	6,588	1,793	24.302	43,567	6,424	765	0.138
G7	44	6,735	1,833	24.302	44,539	6,373	788	0.142
G8	44	6,407	1,743	24.302	42,370	6,574	727	0.131
G9	36	6,667	1,484	23.009	34,154	5,585	709	0.128
G10	36	6,823	1,519	23.009	34,953	5,869	691	0.124

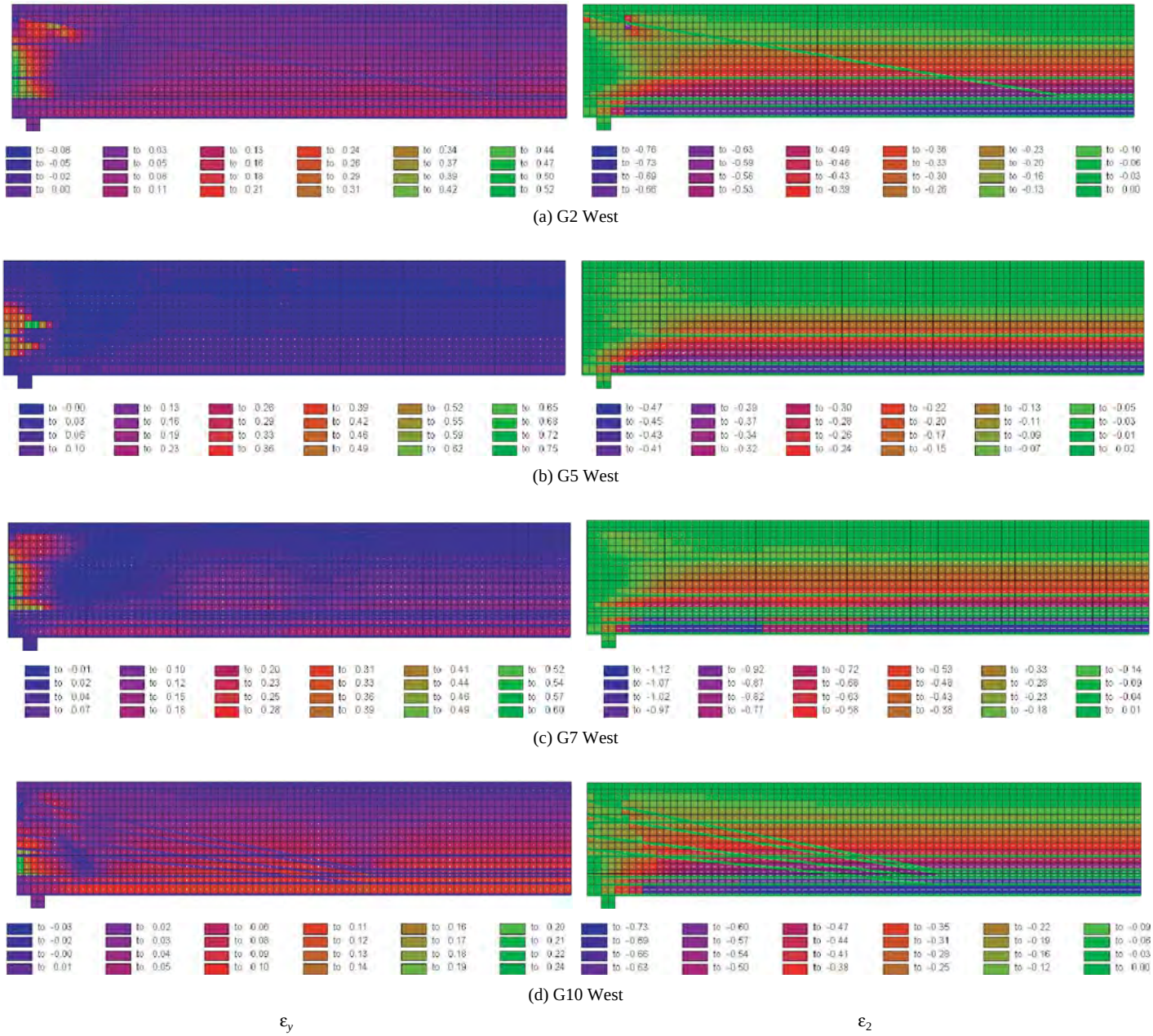

(a) G2 West

(b) G5 West

(c) G7 West

(d) G10 West

ε_y ε_2

Figure 130. Strain distribution prior to loading.

chosen for comparisons with the program predictions because, at such stages, the final crack patterns are fully established and obvious. In Figure 131, the thickness of a given line represents the crack width; a thin line is for a crack predicted to have a width less than 0.04 inch (1.0 millimeter), the line of midwidth is for a crack 0.04 to 0.08 inch (1.0 to 2.0 millimeters), and the thick line is for a crack wider than 0.08 inch (2.0 millimeters). More detailed diagrams for the experimentally measured development of cracking are reported in the appendices. There is good agreement between measured and predicted results in Figure 131.

Figure 132 shows detailed comparisons between the measured and predicted crack patterns for the east half of Girder 3, thereby showing the ability of Vector2 to predict crack development. The comparison shows that Vector2 successfully predicts crack locations, directions, and widths for each step in the loading history of the girder. As discussed previously, the first web-shear cracks occurred at a load of 19.2 kip/ft in the analysis, a value that is reasonably close to the experimentally observed first cracking load of 16.2 kip/ft. By Load Stage 3, both the experimental results and the analysis showed well-developed web-shear cracks and a similar extent of flexural cracking. By Load Stage 4, the flexural cracking in the girder had developed a little more in the analyses than in the experiment, and flexure-shear cracking was occurring in both the experiment and the analysis. By Load Stage 5, the extent of the exper-

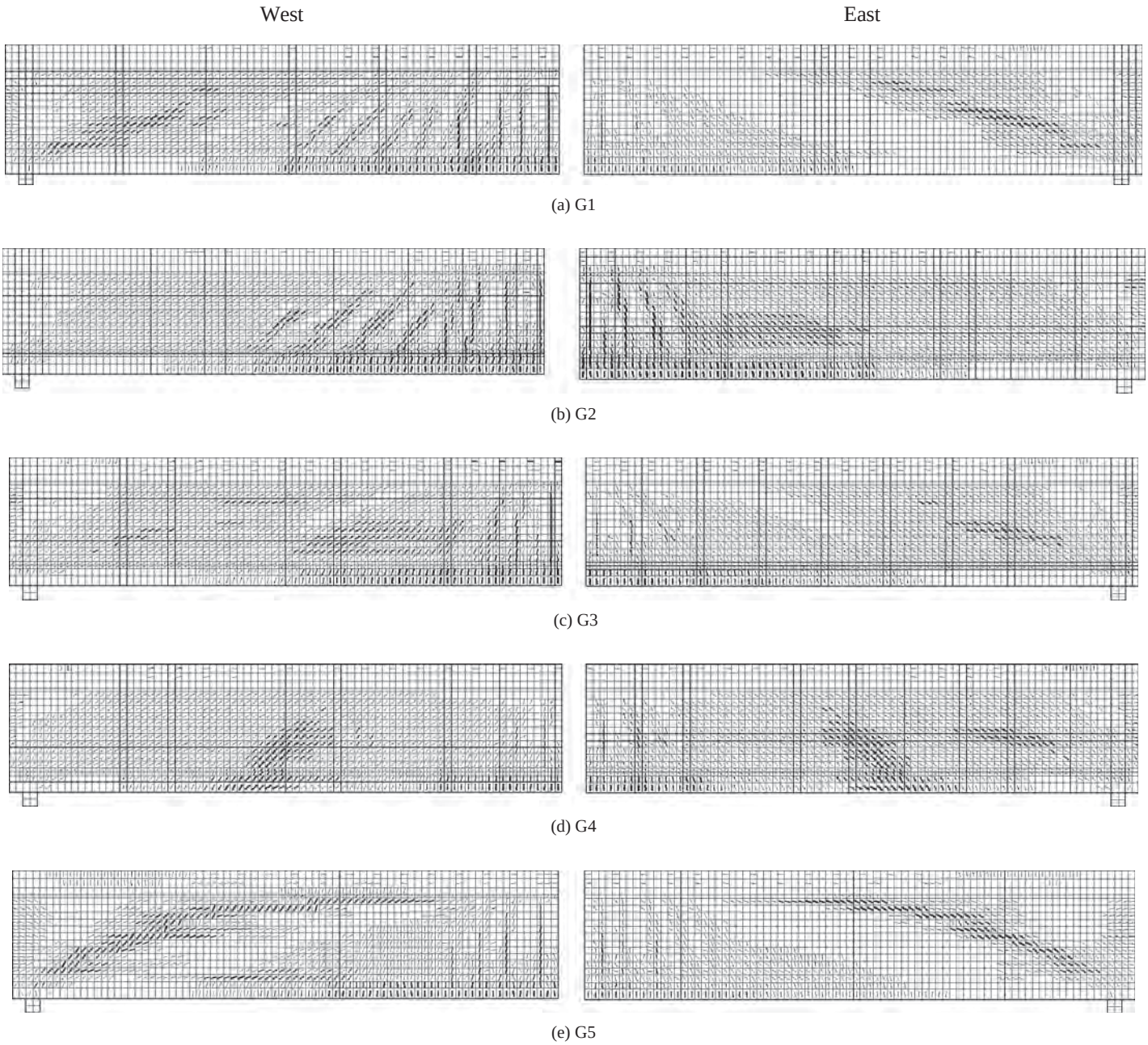

Figure 131. Crack patterns at final step.

imentally measured web-shear cracking and flexure-shear cracking, as well as the crack widths, were well predicted by the program, with the fan-shape of the web-shear cracks being very similar from the measurements and from the analyses.

2.10.9 Mode of Failure

To further evaluate the utility of using Vector2 for conducting analytical studies on the shear performance of HSC girders, this section compares the modes of failure predicted by this program with those measured in the experiments. As is the case with experimental test data, the predicted behavior from the analyses had to be carefully examined in order to correctly assess the predicted mode of failure. To this end, Figure 133 shows the vital signs calculated by Vector2 for the final load step of representative girders for each failure mode. The vital signs include the ratio of the maximum current compressive stress to the possible peak stress for the concrete (shown in the left side of Figure 133) and the ratio of the current steel strain to the yield strain for the reinforcement (shown in the right side of Figure 133). These two ratios help to explain the cause of failure and can be used for selecting the predicted mode of failure.

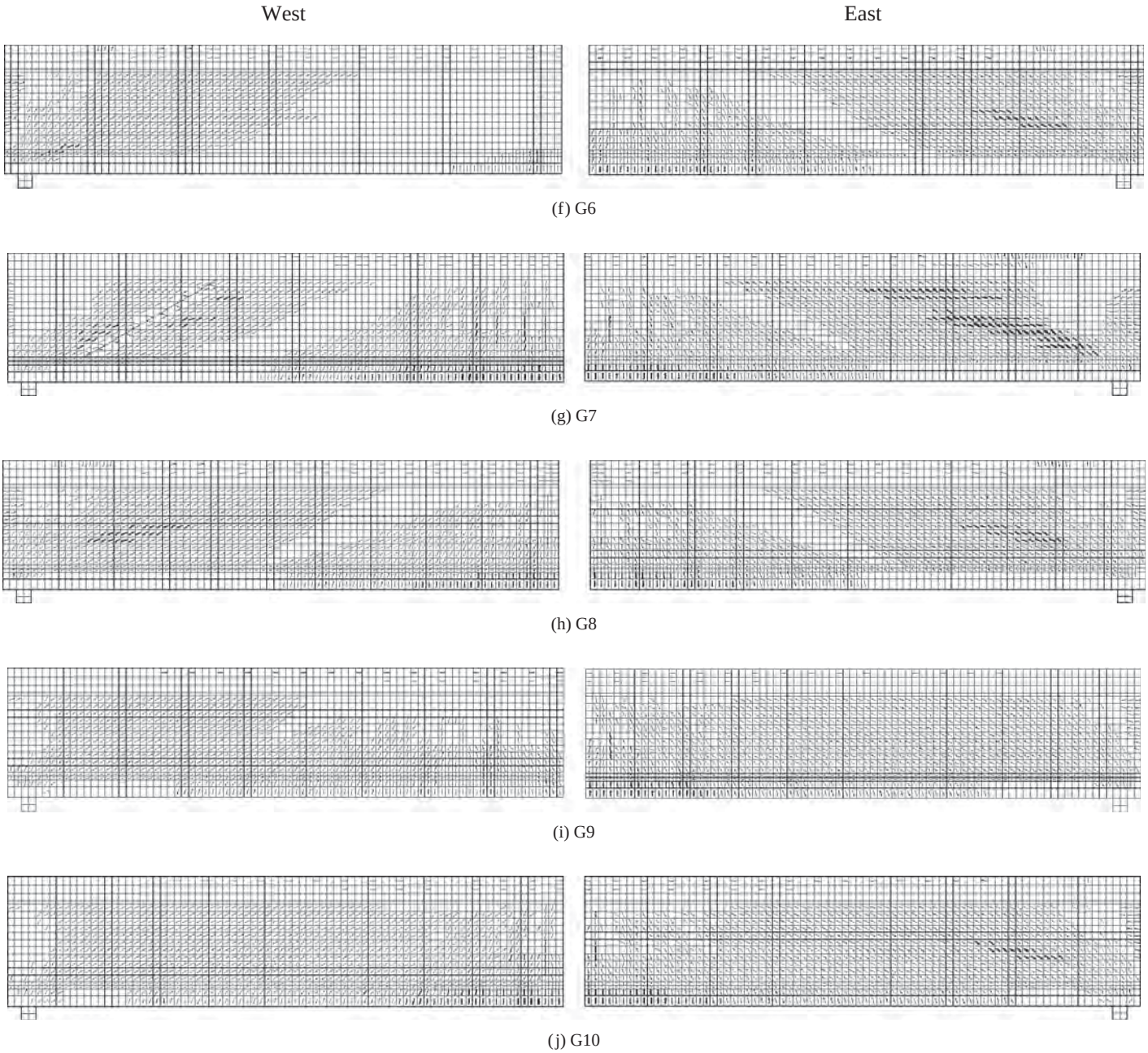

Figure 131. (Continued).

Figure 133(a) shows the two ratios for the west half of Girder 1. The compressive stress ratio is shown on the left side, and the reinforcement strain ratio is shown on the right side. From the left graph, it is evident that the compressive stress above the support reached its peak value, while from the right graph it can be seen that the strains in most of the stirrups have already exceeded their yield strain. Therefore, it can be concluded that the predicted mode of failure is local crushing above the support following extensive yielding of the shear reinforcement. For comparison, Figure 133(b) shows the example of the predicted diagonal tension failure of the west end of Girder G5. In the right graph, the yielding of the stirrup is concentrated over a very narrow band. Moreover, it can be seen that the strain ratio within the band is extremely high. In the left graph, many elements in the band have lost their stiffness due to the large crack width and show very low compressive stresses. Lastly, Figure 133(c) shows the predicted failure mode of local crushing prior to stirrup yielding for the east end of Girder 9. In the left graph, the elements above the support have reached their possible peak stress over a relatively wide area. The right graph indicates that the reinforcing steel above the

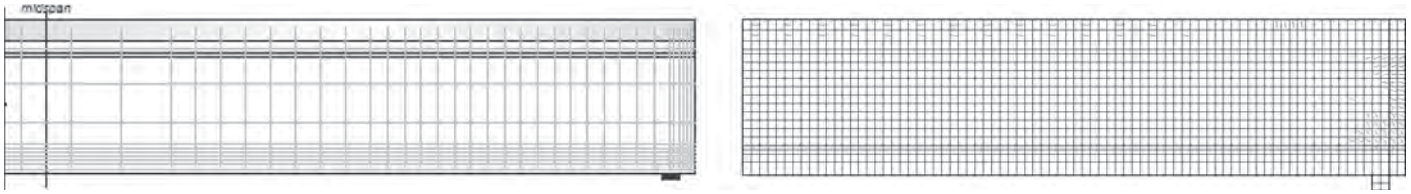

(a) Load Stage 1 (Load = 14.9 kip/ft, w_{cr}- experiment: 0mm, Vector2: 0.01mm)

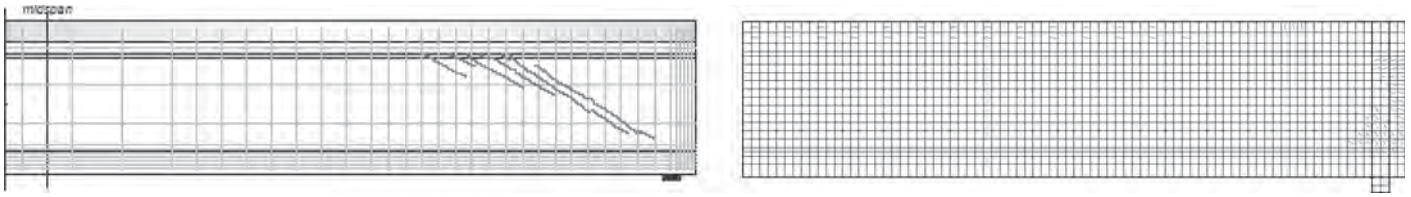

(b) Load Stage 2 (Load = 16.2 kip/ft, w_{cr}- experiment: 0.2mm, Vector2: 0.01mm)

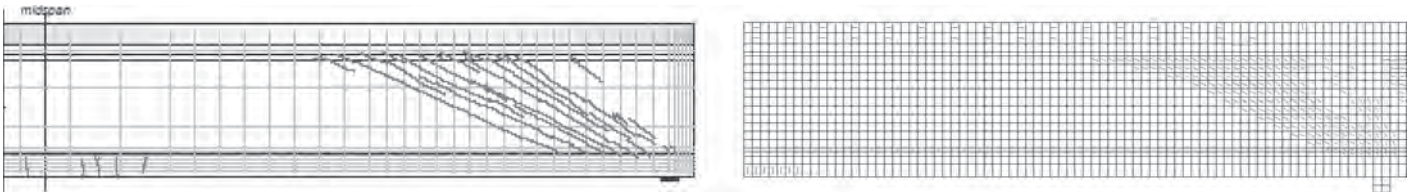

(c) Load Stage 3 (Load = 26.1 kip/ft, w_{cr}- experiment: 0.35mm, Vector2: 0.40mm)

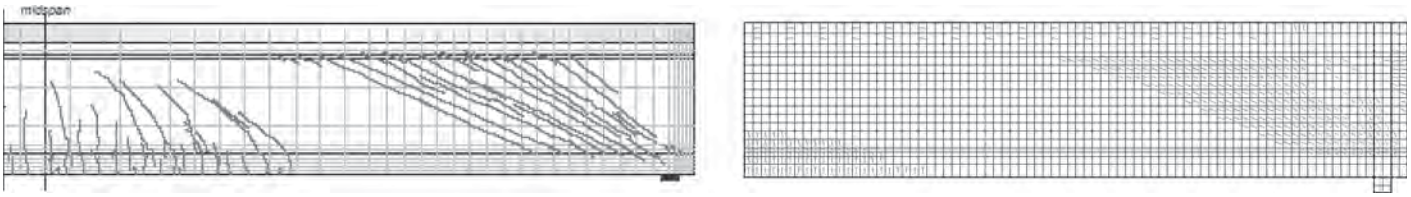

(d) Load Stage 4 (Load = 28.2 kip/ft, w_{cr}- experiment: 0.5mm, Vector2: 0.48mm)

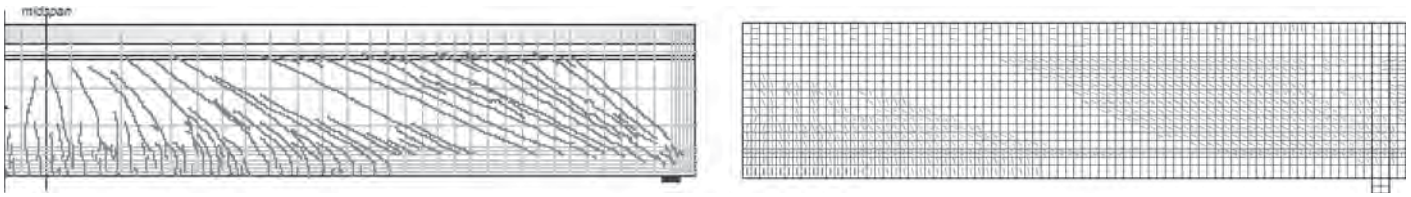

(e) Load Stage 5 (Load = 32.4 kip/ft, w_{cr}- experiment: 0.55mm, Vector2: 0.85mm)

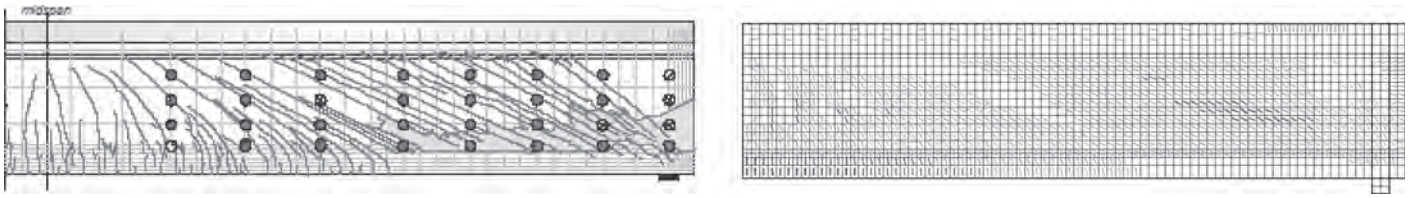

(f) Load Stage 6 (Load = 35.7 kip/ft, w_{cr}- experiment: 0.75~1.5mm, Vector2:1.0~2.0mm)

Figure 132. Crack development of east part of Girder 3.

Current Compressive Stress/Possible Peak Stress | Current Stirrup Strain/Yield Strain

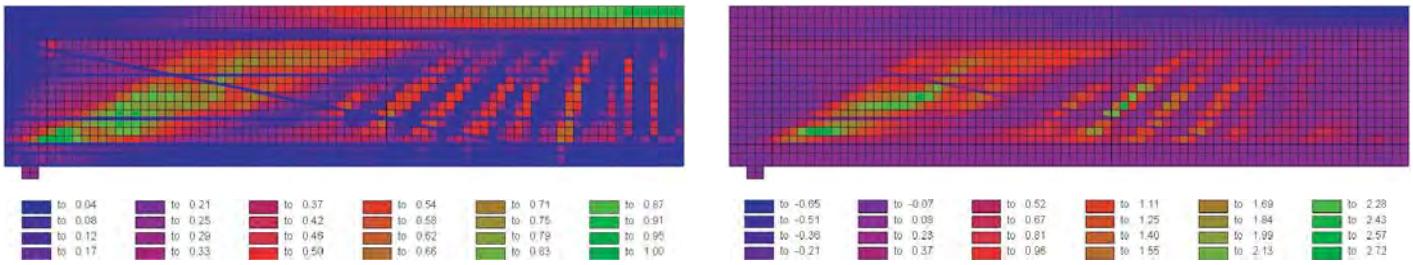

(a) Stirrup yielding followed by local crushing (G1 west)

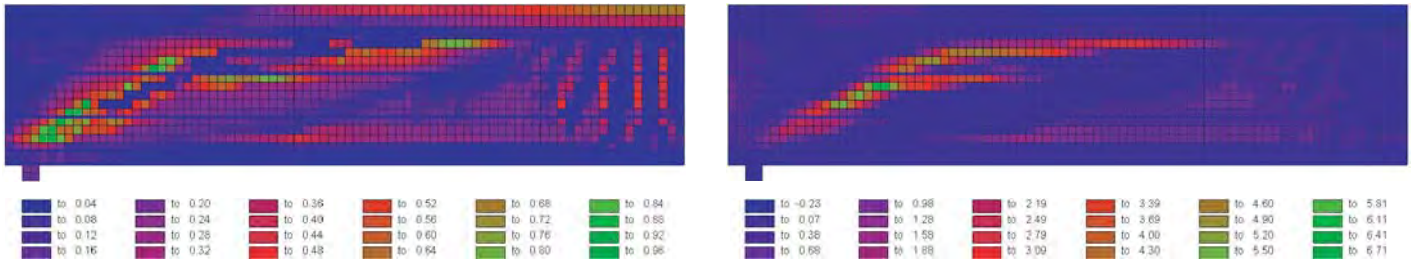

(b) Diagonal tension (G5 west)

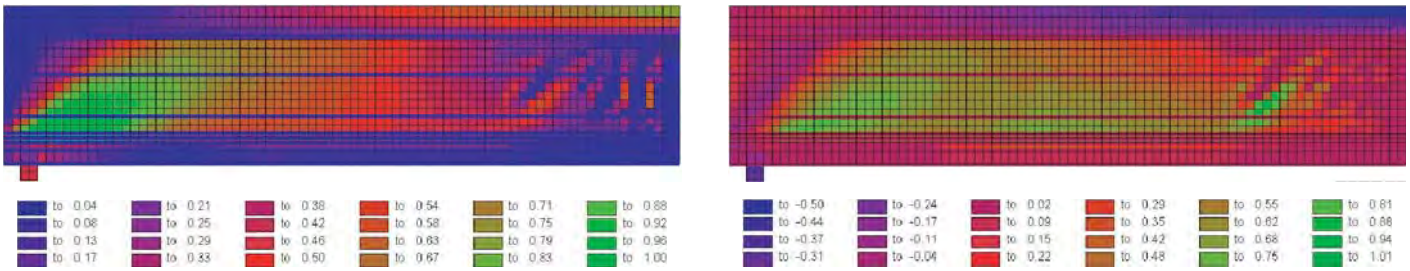

(c) Local crushing almost without stirrup yielding (G9 east)

Figure 133. Vital signs of girders.

support has reached its yield strain but that the region is very small and the strain level is relatively small. It is evident that the cause of failure is therefore not yielding of the transverse reinforcement.

The above examples illustrate that the cause of failure can be identified relatively clearly from the analyses. On the basis of these vital signs, the mode of failure for each girder was predicted, and the results are summarized in Table 38. These predicted modes of failure are reasonably close to those determined from the measured and observed experimental responses. While Girder 4 did not fail in shear, the predicted mode of failure from the analyses is presented for reference.

Table 38. Comparison of mode of failure.

Mode of Failure	Girder
Stirrups yielding followed by local crushing	G1,G2,G3,G4,G6,G7,G8,G10
Diagonal tension (Local stirrup yielding)	G5
Local crushing before stirrup yielding	G9

2.10.10 Shear Deformations

A comparison is now made of the predicted and measured shear strains of the girders immediately inside of the support. The region of the girder whose response was measured by the set of LVDTs closest to the support is used for this comparison. LVDTs WD1 and WD3 were used for calculating the measured shear strains in the west end of the girders, while LVDTs ED1 and ED3 were used for calculating those in the east end. Comparisons of measured and predicted results are shown in Figure 134 for both ends of all the test girders. While Vector2 frequently overestimated the length of the region of elastic response, it did reasonably well at predicting the stiffness of the region of inelastic response.

2.10.11 Shear Slip at Crack Surface

One of the main components of the concrete contribution to shear resistance is assumed to be interface shear transfer across diagonal cracks. For this mechanism, the direction of

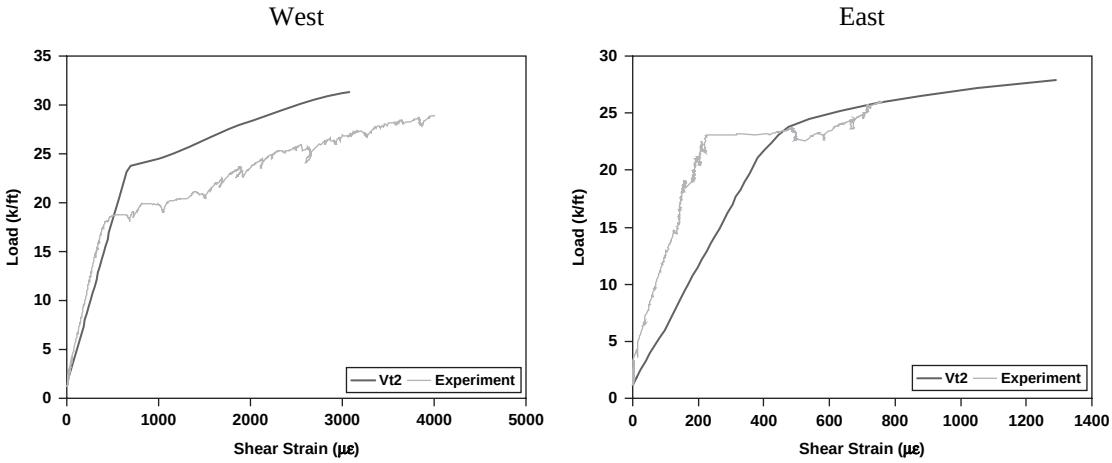

(a) G1

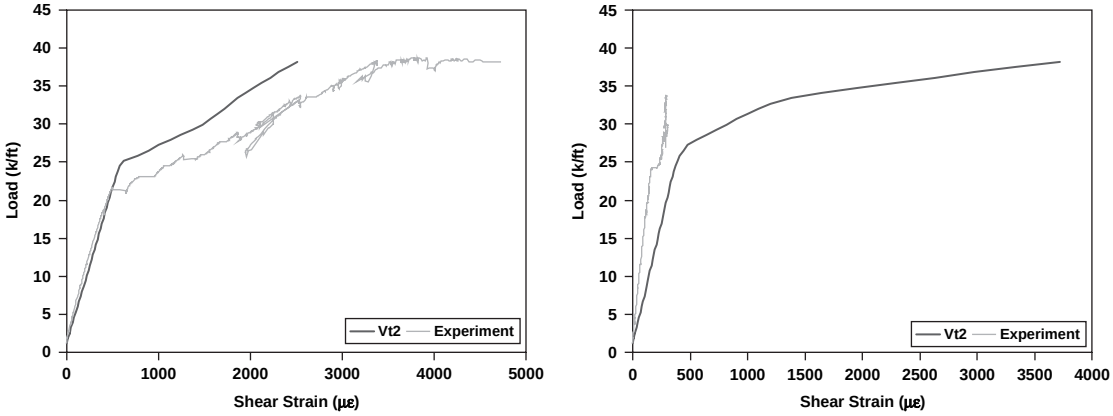

(b) G2

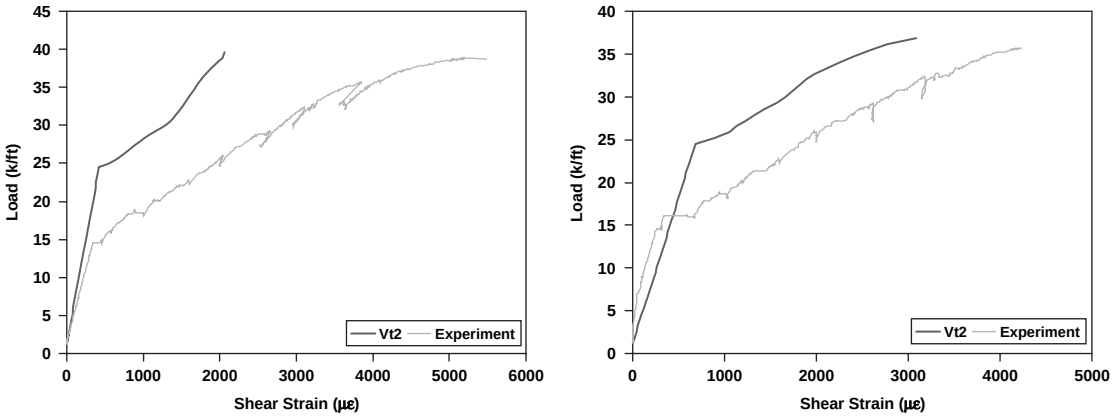

(c) G3

Figure 134. Shear deformations of web.

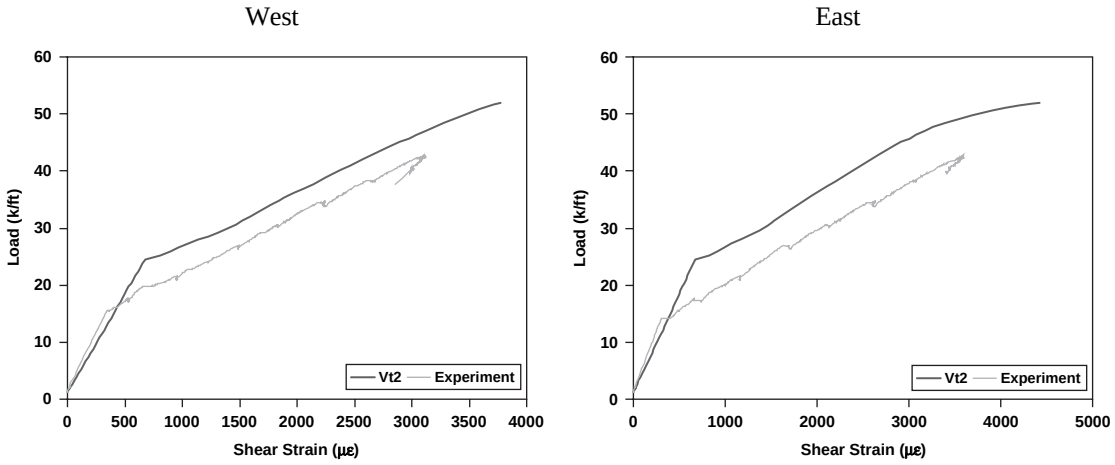

(d) G4

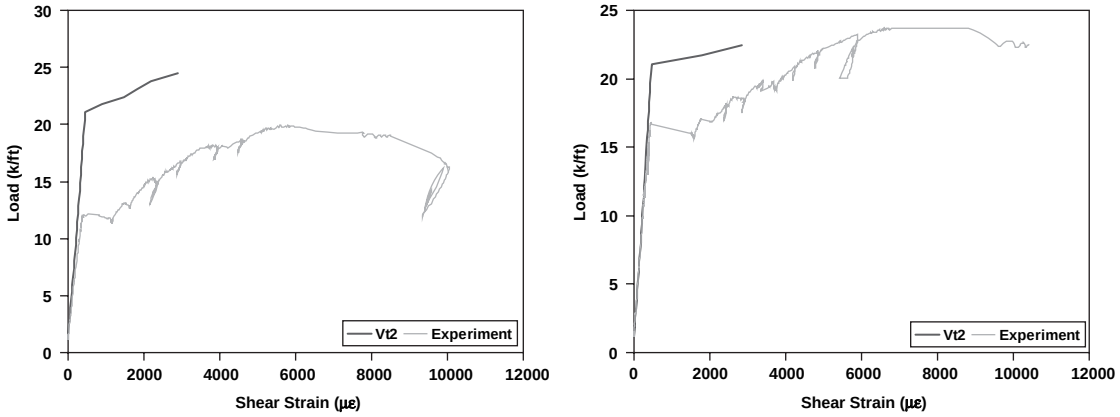

(e) G5

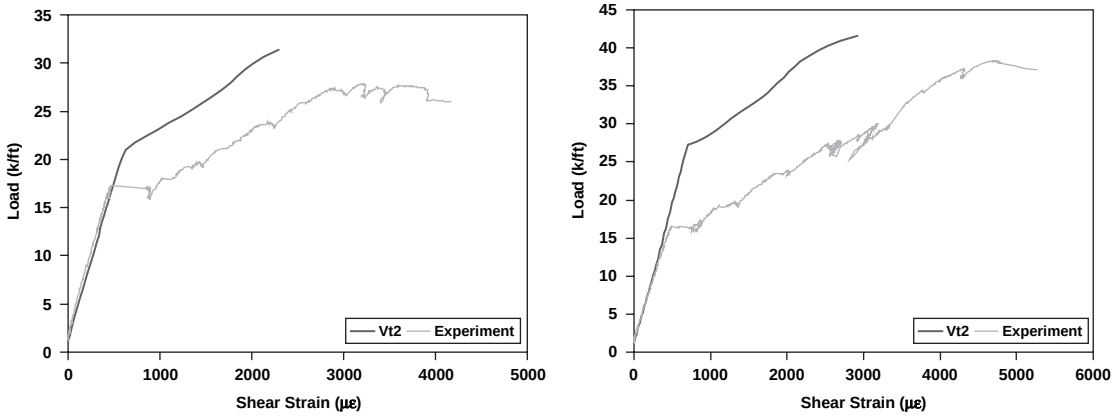

(f) G6

Figure 134. (Continued).

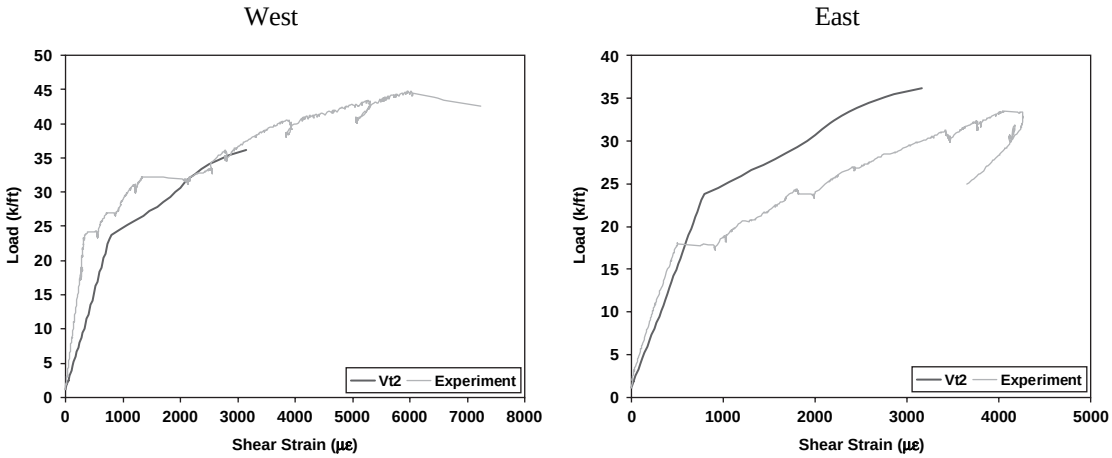

(g) G7

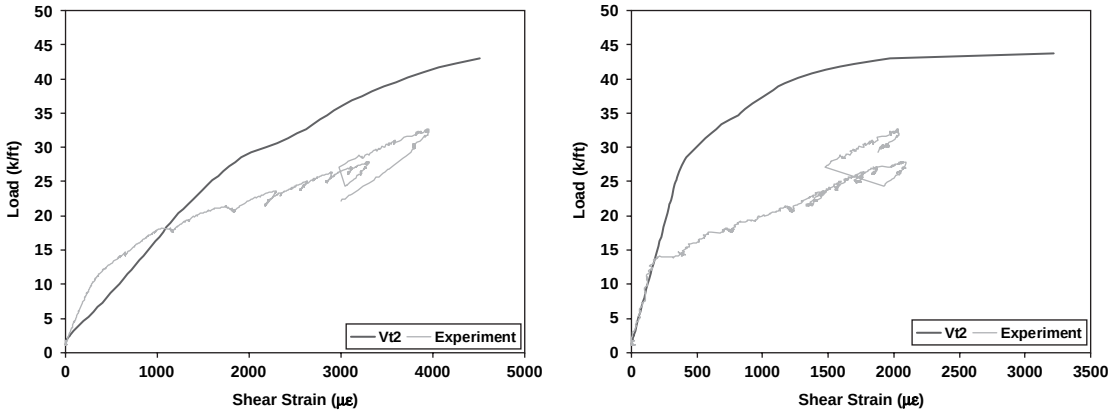

(h) G8

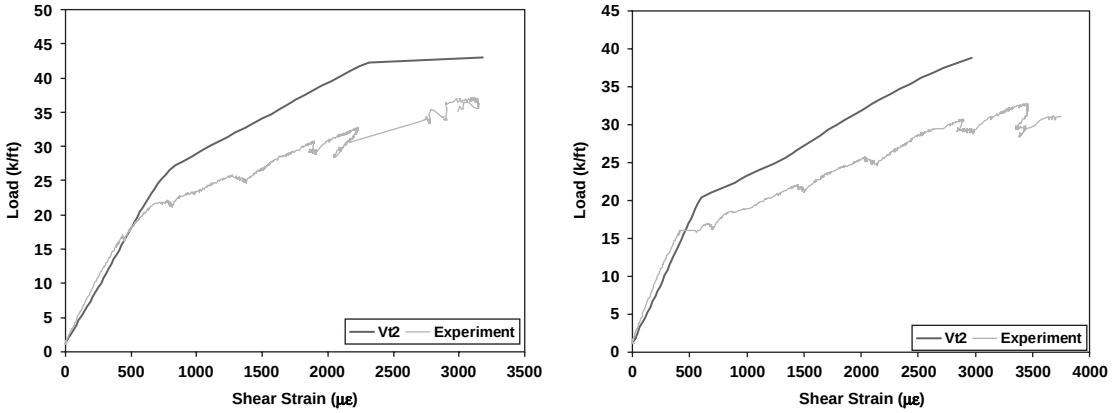

(i) G9

Figure 134. (Continued).

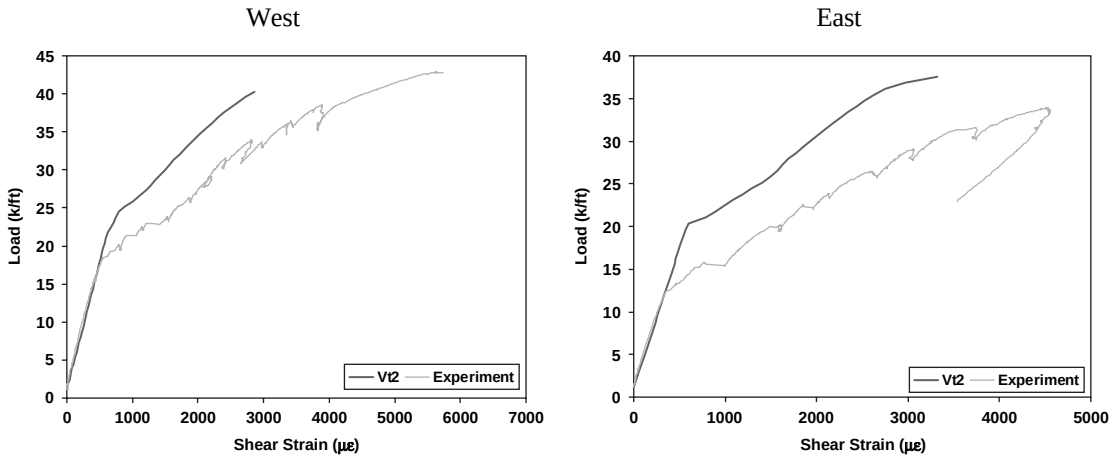

(j) G10

Figure 134. (Continued).

shear friction is assumed to be coincident with the external shear force. However, the experimental observations showed that shear slip frequently occurred in the direction reverse to that which is customarily assumed. It is useful to use Vector2 to more closely examine the cause of this experimental observation and to assess its implications.

Because shear slip at cracks is not considered when the MCFT is used, shear stresses along cracks are shown instead in this comparison. The shear stresses at crack surfaces were evaluated along a 30-degree line drawn from the inside face of the support for the east end of Girder 3. The resultant predicted stresses are given in Figure 135. For the load step, w = 30.15 kip/ft and the shear stresses along the crack are positive, while for the final load step, w = 35.64 kip/ft and most of the stresses are negative. The results of the analyses indicate that the lower part of the crack moved upward due to the anchorage of the significant prestressing force in the earlier load step. However, as the loading was increased, the

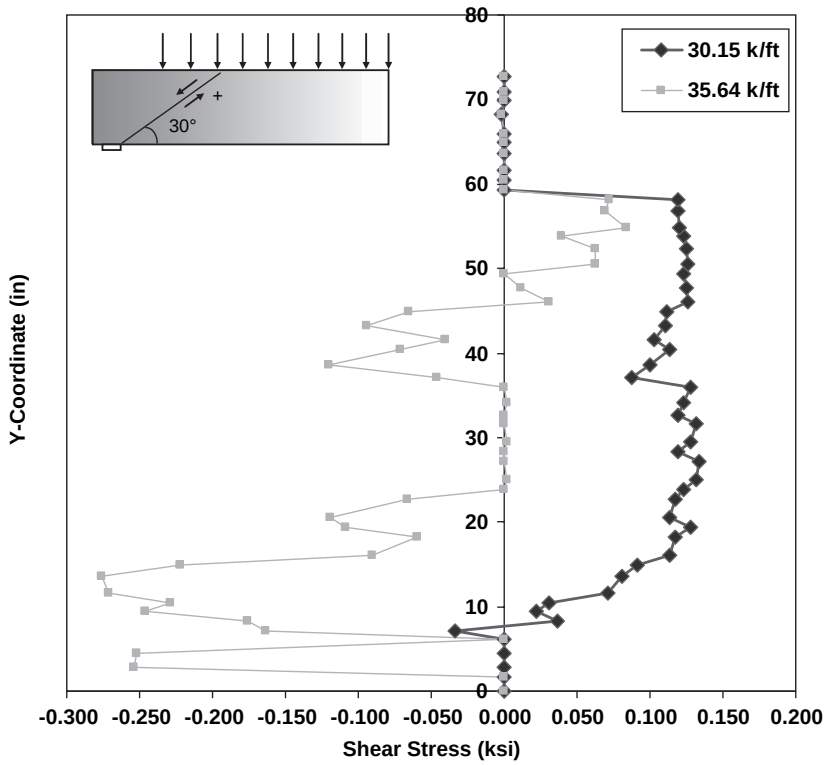

Figure 135. Shear stress at crack.

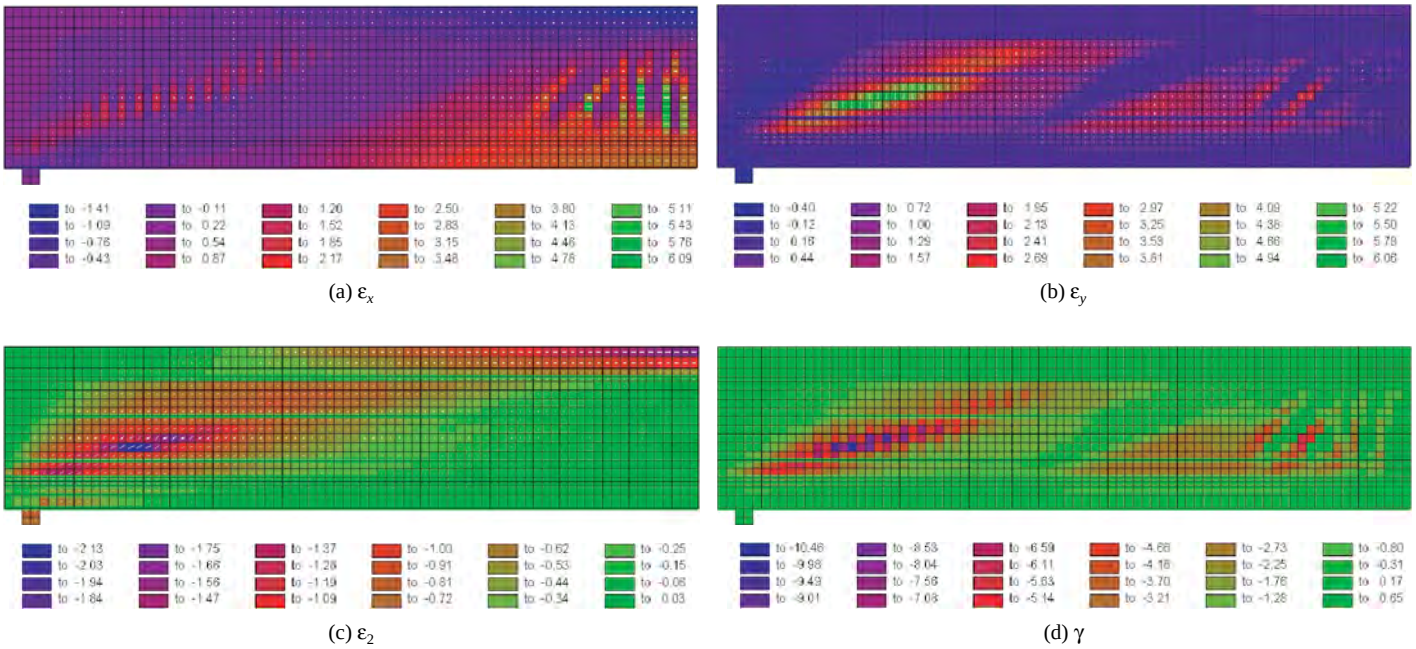

(a) ε_x (b) ε_y

(c) ε_2 (d) γ

Figure 136. Strain at final load step.

shear force induced by the external force overcame the prestressing force and the direction of shear slip was reversed. Because Vector2 uses nonlinear elasticity theory, such accumulated plastic deformation is not addressed properly, which means that the reversed stress direction does not always indicate that the direction of shear slip deformation is reversed also. However, the prediction from the analytical model indicates that the direction of shear slip has begun to reverse. Note that shear stress is in the traditional direction in the upper part of the web.

2.10.12 Strain Patterns

Vector2 can also be used to predict the distribution of straining. The selected components are horizontal strain ε_x, vertical strain ε_y, principal compressive strain ε_2, and shear strain γ for the east half of Girder 3 at the final load step, as shown in Figure 136. Figure 136(a) shows that the largest horizontal strain increases are mainly due to the applied bending moment and are located around mid-span. By contrast, as shown in Figure 136(b), the largest vertical strains develop in the midheight of the web near the end region and are due to diagonal tensions. This result is consistent with the data presented in Section 2.9. Figure 136(c) shows that a compressive strut above the support has developed, and the strain in some parts of the strut have exceeded the peak strain. Thus, there has been softening due to lateral cracking. Figure 136(d) shows, as expected, that large shear strains develop near the end region due to the web-shear cracking.

2.10.13 Summary

A nonlinear finite element program, Vector2, was used to predict the behavior of the test girders. This program uses the MCFT for modeling shear behavior and can be considered to provide a complete MCFT prediction of the load-deformation response of the test girders. For these analyses, a modified Popovics expression was used for modeling the compressive stress-strain response for high-strength concrete. Vector2 was shown to be very effective at predicting the strength, strain patterns, modes of behavior, and overall load-deformation responses of the test girders. Consequently, Vector2 could be used to study the shear behavior of HSC girders with properties other than those of the girders tested in this program and could be useful for subsequent parametric investigations. Vector2 was also used to predict the distribution of the elastic strains due to prestressing. Such values are useful for evaluating the total strain in the test girders in combination with the strains due to loading, as presented in previous sections of Chapter 2.

CHAPTER 3

Interpretation, Appraisal, and Applications

3.1 Overview

This chapter discusses the potential impact of project findings on bridge design practice, as well as safety and economy, with a focus on extending the existing LRFD specifications to HSC. These findings are derived from the review of barriers to the use of HSC that was presented in Section 2.1, the analysis of the experimental database presented in Section 2.2, and the results of the experiments on the HSC girders and shear friction test specimens that were conducted as part of this research project. As previously described, this experimental research program was designed to furnish the necessary basic data for the extension of the existing LRFD shear design provisions to HSC. The goal was to identify any potential areas of shear design in which an extension of the existing provisions to HSC could lead to unconservative designs. This goal was achieved by conducting tests that covered a wide range of shear design stress levels, strand anchorage details, supplementary end reinforcement details, and different concrete strengths such that the different mechanisms of shear resistance could be evaluated and the different possible modes of failure investigated.

There is often the assumption that the extension of existing provisions to HSC can be justified based purely on the measured strengths of members with increasing concrete strengths. However, that approach can readily mask fundamental differences in behavior that occur with increasing concrete strengths. Therefore, in addition to measuring strengths, a key objective of this program was to collect detailed data on the measured response so that a complete evaluation could be made of the applicability to HSC of the behavioral model and underlying assumptions upon which the LRFD shear provisions are based. As a result, some of the implications of the research findings that are presented in this chapter, and the accompanying proposed changes to the LRFD specifications, are based on the detailed analyses of the measured responses of the test specimens in addition to their overall measured strengths. Section 3.2 addresses the extension of the LRFD Sectional Design Model to HSC for evaluating the concrete and shear reinforcement contributions to shear resistance. Section 3.3 examines the extension of other provisions, including the AASHTO Standard Specifications and the newly proposed AASHTO LRFD simplified shear design provisions to HSC. Section 3.4 addresses minimum shear reinforcement requirements, and Section 3.5 covers the maximum shear design stress limit. Performance under service load levels is discussed in Section 3.6, the design of end regions in Section 3.7, and interface shear transfer resistance in Section 3.8. Proposed changes to the LRFD specifications are discussed in Section 3.9, and then specifics of the proposed revisions are discussed in Section 3.10. Finally, the implications of the proposed changes to the LRFD specifications on bridge design practice are given in Section 3.11.

3.2 Extension of LRFD Sectional Design Model to HSC (S5.8.3)

By one line of reasoning, extension of the LRFD Sectional Design Model to HSC would be warranted if the strength ratios (V_{test}/V_{LRFD}) for members cast with concrete with a compressive strength greater than 10 ksi were not less than for members cast with concrete strengths less than 10 ksi. However, as explained in Chapter 1, the extension of the LRFD specifications to HSC concrete is complicated by the desire to more fully validate the use of the LRFD Sectional Design Model because it has not been as thoroughly tested by field experience and through experimental research as the flexure-shear/web-shear models of the AASHTO Standard Specifications. The aspects of the LRFD specifications that required careful evaluation were the values of the diagonal compression θ used in the LRFD tables, the contribution of the concrete to shear strength as controlled by the parameter β, the use of the staggered shear design concept, the minimum shear reinforcement requirement, the design of end regions

by the Sectional Design Model, and the maximum shear design stress permitted by the Sectional Design Model. As described in Chapter 1, the extension to HSC in many of these cases increases the importance of questions related to the accuracy of the LRFD Sectional Design Model.

This section continues with an assessment of the suitability of the LRFD Sectional Design Model for the design of reinforced and prestressed concrete members for all strengths of structural concrete. The suitability of the tabular values for β and θ that control the contribution of the concrete and the reinforcement to capacity are examined first. Next, the accuracy of the crack spacing assumption that was used in the derivation of Table 5.8.3.4.2-1 for evaluating β and θ for members with shear reinforcement is examined, followed by an assessment of the MCFT relationship for shear friction resistance. Finally, the expression for calculating longitudinal strain at middepth, ε_x, is compared with test data because this quantity is the key parameter from which the capacity of a section to resist shear is evaluated. Each of these aspects of the design provisions begins with an assessment based on the results of the girders tested in this research program followed by an assessment based on prior experimental test data. This same order of assessment is also followed in each subsection of Chapter 3 in which the evaluation of other LRFD specifications is presented. The shortcomings in available data for making these assessments are discussed in Chapter 4 in the section on suggestions for future research.

Section 2.4 reported the measured capacities of the girders tested in this research program and compared these measured strengths with shear strengths calculated by the LRFD Sectional Design Model. The results demonstrated that these LRFD specifications provided an accurate estimation of shear strength for the broad range of member details and modes of failure investigated in this program. For the test girders, the mean strength ratio (V_{test}/V_{LRFD}) was 1.11 and the COV was 0.10. The one exception was members designed for very high shear design stress levels, as discussed more fully in Section 3.5. In this comparison, the use of the staggered shear design concept was limited to evaluations of the shear design force between the face of the support and the first critical design section at $d_v\cot\theta/2$ from the support. If the staggered shear design concept were to have been employed for the maximum permissible distance of $d_v\cot\theta$ from the support, then the overall strength ratio would have decreased to 0.79 and the COV would have increased to 0.14. These results indicate that the LRFD method can be unconservative if the staggered shear design concept is employed over the entire design span. Therefore, the use for that concept should be discontinued.

The accuracy and safety of the LRFD Sectional Design Model and its extension to HSC for other classes of members were assessed in Section 2.2, in which previous experimental test data were presented for reinforced concrete and prestressed concrete members both with and without shear reinforcement. As illustrated in Figure 13 for 1,287 reinforced concrete members and Figure 15 for 587 prestressed concrete members, the LRFD Sectional Design Model was generally conservative, with a mean strength ratio well above 1.0 and an acceptably small fraction of the test results falling beneath the strength ratio of 1.0. Because the strength reduction factor is 0.9 for shear, only the values beneath a strength ratio of 0.9 warrant considerable attention. For that criterion, only two test results are particularly unconservative, with strength ratios of around 0.6. These members are from the tests of Jacob and Russell (*38*), in which the webs were only 3 inches thick. While these results are noteworthy, they do not affect the overall evaluation of the performance of the LRFD specifications.

A particularly significant series of tests not presented in the shear database are the tests sponsored by the Louisiana Transportation Research Center, led by Bruce et al. (*39*), and conducted at the Construction Technologies Laboratory. In this research program, six fatigue and shear experiments were conducted on 72-inch deep prestressed concrete bulb-tee girders that were cast with concrete compressive strengths 9.3 and 14.6 ksi. In all of the shear experiments, the shear failure load was above the capacity calculated by the AASHTO Standard Specifications and the LRFD specifications. Thus, it was concluded that these provisions are extendable up to concrete strengths of 13 ksi.

Figures 13 and 15 identified members without shear reinforcement. In the use of the LRFD specifications for calculating the capacity of members with $f'_c > 10$ ksi, the same approach was taken as used in the Canadian Standards Association (CSA) method, where the aggregate size is reduced to zero when the compressive strength of the concrete is greater than 10 ksi. This action is to account for the effect of smoother shear cracking in HSC structures (as opposed to the rougher shear cracking in normal-strength concrete structures) on reducing interface shear capacity. The strength ratio (V_{test}/V_{LRFD}) was also evaluated in *NCHRP Report 549* for a selected group of reinforced and prestressed members that were considered to be more representative of the types of members to be designed by the LRFD specifications. All of these members contained at least the LRFD-required minimum amount of shear reinforcement, were at least 20 inches deep, and had a shear-span-to-depth ratio greater than 1.7. For the 64 selected reinforced concrete members, the mean strength ratio was 1.21 and the COV was 0.179. For the 83 selected prestressed concrete members, the mean strength ratio was 1.23 and the COV was 0.145. From an assessment of the LRFD Sectional Design Model using the test data generated and reviewed in this project, the provisions are considered to be safely extendable to HSC members with concrete strengths up to 18 ksi.

An assessment of the underlying basis of the LRFD specifications can be made through an examination of the calculated and measured angle of diagonal compression, the crack spacing, the interface shear transfer resistance, and the longitudinal strain at middepth (ε_x). In the LRFD Sectional Design Model, the contribution of the shear reinforcement is taken as proportional to the cotangent of the angle of diagonal compression θ. As discussed in Chapter 1, one of the potential concerns with the use and extension of the LRFD specifications to HSC is that this method suggests that the contributions of the shear reinforcement can be considerably larger, up to two or three times as large as the contributions calculated using the AASHTO Standard Specifications. Table 15 presented the ratio of the cotangent of the angle of diagonal cracking in the web-shear zone to the cotangent of the LRFD-calculated angle of diagonal compression. The mean of these cotangent ratios is 0.91 with a COV of 0.08 for LRFD angles that ranged from 21.8 to 30 degrees. This result indicates that the LRFD approach is slightly unconservative unless there is an interface shear stress acting across the crack in such a direction so as to contribute to shear resistance. As discussed in Section 2.7, the direction of observed shear slip indicates that interface shear transfer at loads close to failure was occurring in the direction opposite to that which would contribute to shear resistance. Consequently, it is concluded that the LRFD estimation of diagonal compression leads to a modest 10-percent (on average) overestimation of the contribution of shear reinforcement to resistance.

In the derivation of the LRFD specifications, the spacing of shear cracks in members with at least the minimum required amount of shear reinforcement is taken as 12 inches when calculating the shear slip resistance along a crack face. Table 11 listed the average measured spacing of cracks for the test girders. The average spacing of the web-shear cracks at the ultimate load was 4.5 inches, and the average spacing of the flexure-shear cracks at the ultimate load was 6.0 inches. The corresponding maximum average spacings were 6.0 and 9.2 inches. Thus, the LRFD specifications assumption of 12 inches for crack spacing is conservative, since shear slip resistance is calculated to decrease with an increase in crack spacing.

Section 2.8 presented the results and interpretation of the shear friction experiments. The overall finding was that the interface shear transfer resistance provided by the concrete in the HSC shear friction tests was larger than the resistance calculated using the expression for v_{ci}, which was used in the derivation of the LRFD Sectional Design Model, for crack widths up to 0.04 inch (1.0 millimeter) in all tested cases and for crack widths up to 0.08 inch (2.0 millimeters) in most cases. As shown in Table 18, the crack widths measured in the girder tests, in both the web-shear and flexure-shear regions at the time of failure, were typically less than 0.04 inch (1.0 millimeter) and always less than 0.08 inch (2.0 millimeters). Thus, the results from the shear friction tests in combination with the measured crack widths for the test girders also indicate that the shear friction resistance relationship used in the derivation of the LRFD Sectional Design Model is conservative.

Finally, there is the issue of the LRFD equation for ε_x as given in Equations 15 and 16. This strain is a key parameter because it determines the column in Table 5.8.3.4.2-1 (of Section 5.8.3 of the LRFD specifications) from which the values for β and θ are selected. In the experiments, a displacement transducer was located at the middepth of the web to monitor the development of longitudinal straining in the first critical design region. The center position of this transducer was within a few inches of $d_v\cot\theta/2$ from the support. A comparison of the calculated and measured values for ε_x was presented in Figure 90. The results illustrate that, while the magnitudes of the calculated and measured ε_x prior to predicted tensile crack were reasonably close, after cracking the LRFD relationship did not accurately predict the development of straining. An explanation for this inaccuracy is that in the LRFD equation, plane sections are assumed to remain plane, but in the test girder it was observed that there could be large longitudinal straining in the web due to web-shear cracking, while the top flange and bottom bulb remained uncracked. At the ultimate design load, the difference between the LRFD-calculated strain and the measured longitudinal strain at middepth was typically less than 500 microstrain, but in a few cases the differences were closer to 1,000 microstrain, with the measured strain typically being much larger than the design strain. According to Table 5.8.3.4.2-1, this could result in a change in β of up to 0.8 and in θ of up to 10 degrees.

3.3 Extension of Other Shear Design Methods to HSC

While the focus of NCHRP Project 12-56 was the extension of the LRFD specifications to HSC, it is useful to examine whether the experimental test data collected from the girder tests supports the use of HSC in other shear design approaches. This examination was done in Section 2.4 for the AASHTO Standard Specifications, the 2004 Canadian Standards Association (CSA) provisions, the program Response 2000 (R2K), and the proposed LRFD simplified specifications developed in NCHRP Project 12-61 and presented in *NCHRP Report 549*. Table 8 presented the ratios of the measured shear strengths to code-calculated strengths. The results suggested that all of these methods were sufficiently conservative to use for the design of HSC members. The LRFD, CSA, and R2K methods all yielded similar mean strength ratios of around 1.1, with COVs of 0.10. This is not surprising because they are all based on the MCFT. The AASHTO Standard Specifications

were about 20 percent more conservative, with a mean strength ratio of 1.31 and the lowest COV of 0.08. The proposed simplified LRFD provisions had a mean strength ratio midway between the methods based on the MCFT and the AASHTO Standard Specifications, but it had the largest COV of 0.18.

The strength ratios presented in Table 8 do not provide a comprehensive evaluation or comparison of these different methods for calculating shear capacity because those ratios are the strength ratios from 20 tests only. *NCHRP Report 549* presented a comparison of the strength ratios for R2K, CSA, AASHTO Standard Specifications, the LRFD specifications, the Japanese Society of Civil Engineers, and the German DIN standard for a broad array of test data consisting of 878 reinforced and 481 prestressed concrete members. From this review, it was observed that the LRFD and CSA approaches were best able to predict the capacity of the members in this database. The mean of the strength ratios for both of these approaches was very consistent across the different categories of selected members (reinforced concrete with A_v, reinforced concrete without A_v, prestressed concrete with A_v, and prestressed concrete without A_v), with the range in strength ratios for both methods for all categories being only 1.19 to 1.46. The smallest COV was for the 160 prestressed concrete members with shear reinforcement of 15.4 percent for the LRFD method and 14.7 percent for the CSA method. The COV for the AASHTO Standard Specifications method was a poor 37.1 percent, but this result was principally due to the poor performance of these design provisions in predicting the capacity of reinforced concrete members that did not contain shear reinforcement. Both the mean and COV of the AASHTO Standard Specifications method for reinforced concrete and prestressed concrete members with shear reinforcement were good.

NCHRP Report 549 also discussed the shortcomings in available test data. In particular, concern was expressed that more than 90 percent of the test data were only useful for evaluating the shear design of the first critical section in simply supported members. Expressed another way, there is a scarcity of test data to evaluate shear design provisions for the majority of the length of members, particularly for areas where the moment-to-shear ratio (M/V_d) is greater than 4, in flexure-shear regions, near points of inflection in continuous members, and in regions of negative moment and high shear. For this reason, *NCHRP Report 549* evaluated shear design provisions over the entire length of members where the capacity of members was calculated using the best available analysis methods. The results of this work suggest that the AASHTO Standard Specifications could be somewhat unconservative in negative moment regions and near points of inflection in continuous members. The proposed simplified provisions were developed for members with minimum shear reinforcement to overcome these shortcomings, as well as to take advantage of the more accurate variable angle truss model for evaluating the contribution of shear reinforcement to capacity. It should be noted that the AASHTO Standard Specifications have also been shown to be quite unconservative for large reinforced concrete members without shear reinforcement and that they are particularly unconservative for HSC members without shear reinforcement.

As presented in Section 2.5, the results of this research program were also used to evaluate the expressions for web-shear and flexure-shear cracking strength that are in the AASHTO Standard Specifications. Table 13 compared measured and calculated web-shear cracking strengths and illustrated that the AASHTO Standard Specifications slightly underestimated the cracking strength, with the mean ratio of V_{crack}/V_{cw} being 1.14. While the COV was 0.18, this result was considered to be modestly low given the variability that exists in the tensile cracking strength of concrete. Table 16 compared measured and calculated flexure-shear cracking strengths. In this case, the AASHTO Standard Specifications slightly overestimated the cracking strength, with a mean ratio of V_{crack}/V_{ci} of 0.90 and with a COV of 0.11.

3.4 Minimum Shear Reinforcement Requirements (S5.8.2.5)

One of the motivations for this project was the concern that interface shear transfer resistance would be substantially reduced in HSC due to the presence of smoother cracks than in normal-strength concrete. This effect was expected to be of the largest concern in members containing only minimum shear reinforcement, where the largest and widest shear cracks are expected along with the least resistance to crack opening, and with the concrete contribution being a very large portion of the total resistance. One member, Girder 5, was cast with only the minimum required amount of shear reinforcement. Its shear performance was excellent. Stirrup strains at ultimate resistance reached in excess of several times the yield strain, and stirrups in some locations ruptured before the final girder failure occurred at a load in excess of the LRFD-calculated shear strength. The average spacing of shear cracks in Girder 5 was less than 8 inches and therefore less than the assumption of a 12-inch spacing that was used in the derivation of the LRFD specifications.

The performance of members from the large experimental database presented in Section 2.2 was also used to examine the shear performance of members cast with a broad range of concrete strengths. The results presented in Figure 25 show that the LRFD specifications were typically conservative for members cast with very light amounts of shear reinforcement, including amounts that were somewhat less than the minimum required amount of shear reinforcement by the LRFD

specifications. As is discussed in Section 3.6, the LRFD minimum required amount of shear reinforcement may be somewhat conservative for strength, but it is not conservative when serviceability issues are considered.

3.5 Maximum Shear Design Stress Limit

In the AASHTO Standard Specifications, the maximum allowable shear design stress is limited by the contribution of the shear reinforcement v_s, which is equal to $8\sqrt{f_c'}$ (in psi units). This initial limit was selected based on experimental test data. It was intended to guard against a diagonal compression failure, as well as to help ensure good girder performance under service load levels. With the introduction of the LRFD Sectional Design Model, the maximum allowable shear design stress was increased to $0.25f_c'$ (+ v_p). The upper limit in the LRFD specifications was based on its derivation from the MCFT, in which a particular compression-softening model is used to check that diagonal compressive failure does not occur. For a reinforced concrete beam, the ratio of the maximum shear design stress limit of the LRFD specifications to that of the AASHTO Standard Specifications increases from approximately 1.7 for 6-ksi concrete, to 2.3 for 10-ksi concrete, and to 3.2 for 20-ksi concrete. One of the NCHRP Project 12-56 objectives was to evaluate the safety of this new upper shear design stress limit for a range of concrete strengths and modes of failure. One of the potential concerns was the appropriateness of this upper limit when the Sectional Design Model is used for the design of end regions in which there is a magnification of the diagonal compressive stress as the diagonal compression funnels to a support. This effect was a concern because the Sectional Design Model assumes that there is a uniform field of diagonal compression over the depth of a member, and that condition does not exist if a girder is supported on the bottom flange only. Another concern with the higher design shear stress limit was the condition of the member under service load levels, as is discussed in Section 3.6.

As discussed in Sections 2.9 and 2.10, when the support was at the bottom of the beam, there was significant magnification of the diagonal compressive strain (and thus the stress) along the diagonal strut that intersected with the support. The compressive strain where the bottom of the strut intersected with the lower flange was commonly more than twice the compressive strain in the same strut at the top of the web. As reported in Sections 2.4, 2.6, and 2.7, several members that were cast with heavy amounts of shear reinforcement exhibited localized diagonal crushing in the end regions near the support prior to yielding of a band of shear reinforcement in the shear zone. In some cases, the member failed in diagonal compression at the intersection of the web and lower flange prior to any measured yielding of the transverse reinforcement.

Any level of localized crushing prior to significant yielding of the shear reinforcement is considered to be a significant problem for two reasons. First, if the transverse reinforcement has not yielded prior to failure, then it is inappropriate to use the yield stress of the reinforcement when evaluating the contribution of transverse reinforcement to capacity. Second, localized crushing can easily be missed in a physical examination and can lead to a brittle failure. For most designs, a member will reach its flexural capacity prior to its shear capacity. However, if for some loading case the shear rather than the flexural capacity controls, it is far better that this shear capacity be limited by yielding of the shear reinforcement than by some other mechanism. Yielding is a condition easy to identify in regular inspections and easy to alleviate through external strengthening. The mechanism of shear failure by stirrup yielding is more ductile than other shear failure mechanisms and also allows for load redistribution prior to failure. Based on the results of the experiments performed in this project, it is concluded that shear failure due to localized diagonal compression failure and shear slip can be avoided if the maximum shear design stress limit is kept less than $0.18f_c'$ in members for which the diagonal compression needs to funnel into the support, as may be the case at the ends of simply supported members. Provided that the $0.18f_c'$ stress level is not exceeded, any shear failure should be preceded by yielding of the shear reinforcement.

The safety of the maximum shear design stress limit was also examined in Figures 19 through 22. Figure 20 illustrated that there have been a limited number of shear tests conducted in which sufficiently large amounts of shear reinforcement have been used to generate failures under shear stresses that are in excess of $0.25f_c'$. Figure 20 also illustrated that far more of these types of tests have been conducted for prestressed concrete than for reinforced concrete members. Figures 21 and 22 presented the ratio of the measured shear capacity to the LRFD-calculated shear capacity for these same reinforced concrete and prestressed concrete members that contained relatively large amounts of shear reinforcement. The overall results indicate that the LRFD Sectional Design Model is typically conservative, but that there are some cases in which it is somewhat unconservative. Because the detailed experimental test data are not available for all of these cases, it is not known if localized crushing was observed in any of these cases or if the transverse reinforcement yielded prior to failure.

The conditions investigated in the girder tests conducted in this research program represent a near worse case situation, because a significant source of the diagonal compressive strain and stress in the region of localized failure at the base of the web was a result of the heavy prestressing forces that were principally anchored in the bottom bulb but that also induced a very large stress in the lower part of the web. The

location of that stress coincided with the location where the compressive stresses introduced by the funneling of the diagonal compression into the support were also the largest.

3.6 Serviceability

As described in Section 3.5, the LRFD Sectional Design Model permits members to be designed for much higher shear stresses than those permitted in the AASHTO Standard Specifications. Coupled with the use of HSC, this stress increase has a significant impact on the types of behavior that are expected under service load level. The following observations stem from the results presented in Section 2.5, where the development of cracking over the loading history of the members was reported, and in Section 2.6, where the measured reinforcement strains were reported.

Figure 77 illustrated that web-shear cracking occurred at 33 to 87 percent of the shear design strength of the members. As expected, cracking occurred at the smallest percentage of shear design strength in those members designed for very high shear stress ratios (v/f'_c values), which were in Girders 4 and 9. Whether or not this shear cracking is acceptable depends on the environment of use, the ratio of dead to live load, and the strains in the reinforcement at the onset of diagonal cracking. In some states, particularly where members are exposed to chlorides, prestressed concrete solutions are sought because there is the expectation that these members will remain uncracked under service load levels. Since a member can be cracked in shear under service load levels when the LRFD Sectional Design Model is used, the designer may wish to use AASHTO Standard Specifications expressions for V_{cw} and V_{ci} to check for cracking under service load levels, because those expressions were found to provide reasonably reliable estimates of diagonal cracking forces.

While the onset of cracking can be a concern for durability reasons, a potentially larger concern is the immediate and large increases in transverse reinforcement strains that can occur in reinforcing steel upon the initiation of diagonal cracking. As was shown in Table 19 and Figure 86, the maximum stirrup strain typically increased from less than 100 microstrain to near the yield strain in some members at the onset of diagonal cracking. The largest strains immediately after diagonal cracking were typically observed in the members cast with the highest strength of concrete and low quantities of shear reinforcement. This result was to be expected because the energy released is proportional to the cracking strength of the concrete, and the stress gain in the transverse reinforcement is expected to be inversely proportional to the volume of the reinforcement available to absorb this energy. Thus, there may be a significant fatigue concern for members cast with HSC if shear cracking occurs under service load levels.

3.7 Design of End Regions

The LRFD Sectional Design Model permits the region between the inside face of the support and the first critical shear section from the support to be designed for the same shear force as that at this first critical section. The same practice was followed in the design of the test girders. Based on the pattern of reinforcement strains presented in Table 19, it is concluded that this practice is satisfactory for the design of shear reinforcement. However, the use of the LRFD Sectional Design Model for end region design may not be suitable for guarding against a diagonal compression failure. This is because, in the development of the LRFD method, it was assumed that there is a uniform field of diagonal compression, whereas in end regions, as reported in Sections 2.5, 2.9, and 2.10, there is a funneling of diagonal compressive stresses to the support. This funneling can lead to a magnification of more than two in the compressive strains and stresses from what those strains and stresses would have been without funneling. The overall strength results and the discussion of modes of failure presented in Section 2.4 illustrates that most failures were precipitated by localized diagonal compression failures. This localization effect was particularly a problem in members designed to resist very high shear stresses and in members for which diagonal compression failures were observed to occur before yielding of the shear reinforcement.

As discussed in Section 3.5, one possibility for guarding against diagonal compressive failures in end regions is to simply reduce the allowable maximum shear design stress to $0.18f'_c$ in members not cast integral with, or continuous over, supports. Another option is to design end regions by the strut-and-tie method presented in Section 5.6.3 of the LRFD specifications. With this method, the detailed geometry of the end support can be taken into consideration. With the use of wide supports, distributed horizontal reinforcement, and/or draping of strands, shear design stresses higher than $0.18f'_c$ can be sustained provided that the end region is appropriately detailed using strut-and-tie procedures.

The LRFD method requires a direct check of the longitudinal tension capacity at the inside face of a support. At a simple support, the principal tension demand is due to shear. For members in which the angle of diagonal compression, θ, is quite flat, this demand can be very significant and can exceed the tensile capacity provided by bonded straight strands at the inside face of the support. In the LRFD specifications, in these cases, (a) longitudinal deformed bar reinforcement needs to be added, (b) some strands need to draped so as to increase the capacity at the location where they would cross a diagonal crack, or (c) more shear reinforcement needs to be provided to increase the angle of the diagonal compression strut. Based on the results of the tests on the HSC girders, the first two

methods were found to be effective. The measured longitudinal deformed bar strains presented in Figures 87 and 88 illustrate that the tensile demand was very close to, but did not exceed, the available tensile capacity when the LRFD procedures were followed. Members with draped strands showed a significant decrease in the demands placed on the longitudinal deformed bar and prestressing strands, as presented in Section 2.6 and Appendices 1, 2, 9, and 10. However, an increase in the magnitude of the shear reinforcement did not significantly influence the angle of diagonal compression in the end region, probably because of compression strut funneling effects discussed previously.

Another significant aspect of end region behavior that warrants consideration in design is the significant horizontal shear stress created between the bottom bulb and the base of the web. The act of anchoring a large amount of prestressing in the bottom bulb induces a shear stress between the bulb and the web as that compression spreads out over the depth of the member. From the results of the finite element analyses, these stresses ranged from 0.4 to 0.8 ksi. Upon application of the distributed loading, the effect was to significantly increase these horizontal shear stresses. The finite element analyses showed that these stresses at failure ranged from 2.7 to 4.4 ksi, with typical values being around 3.6 ksi. From the experiments, the effect of this high shear stress was quite evident in the development of flatter cracks near the interface of the bottom bulb and web. These stresses are well in excess of those permitted for interface shear transfer, as discussed in Section 5.8.4 of the LRFD specifications, unless account is taken of the net compression acting normal to the shear plane in the test girders. The maximum interface shear stress that was able to be developed at this web to bottom flange location must have depended on compression stresses that resulted from the spread of the compressive force from the support out into the beam. Currently, the LRFD specifications would allow only that part of the compressive force associated with dead load to be considered in evaluating the horizontal shear strength at the web to bottom flange interface. By contrast, the test beams were able to develop the capacities that they developed only because the full compressive force from the reaction was effective. Additional discussion on this action is presented in Appendix 11.

3.8 Interface Shear Transfer

In the LRFD Sectional Design Model, the concrete contribution to shear resistance is limited by the interface shear transfer resistance across a crack. In the MCFT, from which magnitudes of β, θ, and thus V_c were derived, this resistance was taken to increase with crack roughness and in proportion to $\sqrt{f'_c}$ and to decrease with crack width. As described in Section 1, the crack width increases in proportion to ε_x and the flatness of the crack and is calculated using an assumed crack spacing of 12 inches. A primary motivation for this project was that the smoother and more widely spaced cracks that are expected in HSC structures could lead to less interface shear transfer than assumed in the derivation of LRFD Sectional Design Model.

Most of the results presented in Chapter 2 indicate that the LRFD method for evaluating the concrete contribution to shear resistance is conservative. In Section 2.8, in which the interface shear transfer resistance was evaluated from shear friction tests, the capacity over the range of crack widths measured in the girder tests was equal to or greater than the expression for slip resistance, v_{ci}, that was used in the derivation of the LRFD Sectional Design Model. This result is comforting because the shear friction test results on which the LRFD method was based had either no reinforcement crossing the shear plane or had shear reinforcement that was perpendicular to the plane only. By contrast, the shear friction specimens tested in this program had shear reinforcement crossing the shear plane at angles similar to those for the crack planes in the test girders. In Section 2.5, in which crack spacings were discussed, the spacing of the cracks in the web was measured to be closer than that assumed in the LRFD specifications for members with shear reinforcement. Since crack widths increase in proportion to the spacing between cracks, this LRFD assumption should lead to conservative designs. In Section 2.7, in which the components of resistance were evaluated from the shear free body diagrams, the measured concrete contribution to resistance, V_c, at the ultimate limit state was generally larger than the calculated capacity for V_c determined by the LRFD specifications.

While all of the test data described above appear to suggest that the LRFD method for evaluating the concrete contribution to shear resistance by interface shear transfer is conservative, some observations seem to contradict the reasonableness of the LRFD methodology for the evaluation of the concrete contribution to resistance. In nearly all of the experiments, the direction of shear slip along the shear cracks in the first shear design region was opposite to the direction required for an interface shear transfer contribution to shear resistance. The magnitude of this "reverse direction" slip was largest near the bottom of the web and close to the support. The same direction of slip was predicted by the nonlinear finite element analyses, and the direction is due to displacements introduced by the anchorage of the large amounts of prestressing strands used in the beams. In many parts of the girders, no slip was observed across the cracks. In these cases, it was not possible to tell whether the interface shear transfer was in a direction such that it contributed to shear resistance. The results of the finite element analyses as presented in Section 2.10 predict that, while reverse shear slip

was expected in the lower web near the support, normal shear slip was expected in the upper part of the web and farther away from the support. In addition to interface shear transfer, the other significant source for the concrete contribution to shear resistance is shear transfer in the uncracked compression zone at the top of the member, as well as shear transfer in any uncracked region of the bottom bulb. The magnitude of these potential contributions is highly dependent on other geometric parameters not considered in the LRFD specifications.

3.9 Summary of Proposed Changes to LRFD Specifications

Section 2.1 identified barriers to the extension of the LRFD specifications to HSC, summarized the changes recently made to the specifications, and identified changes for which additional information was required. The review of previous shear test data and the experiments conducted in this project were used to fully address several outstanding items as well as provide insight into other items. The list of outstanding items that are considered fully addressed in this project are Article 5.8.2.5, Minimum Transverse Reinforcement; Article 5.8.3.2, Sections Near Supports; Article 5.8.3.3, Nominal Shear Resistance; and Article 5.8.3.4, Procedures for Determination of β and θ. This list of items for which the data collected and reviewed in this project provide insight include also Article 5.4.2.7, Tensile Strength, Article 5.6.3.3.3, Limiting Compressive Stress in Strut; Article 5.8.2.8, Design and Detailing Requirements; Article 5.8.4.1, General on Interface Shear Transfer—Shear Friction; Article 5.9.1.5, Crack Control; Article 5.9.5.4, Refined Estimates of Time-Dependent Losses; and Article 5.11.2, Development of Reinforcement.

Sections 3.2 through 3.8 discussed the most significant issues for the extension of the LRFD specifications to HSC. The remainder of Section 2.9 presents suggested code changes, and Section 3.10 shows these code changes in LRFD format. Section 3.11 concludes Chapter 3 with a description of the anticipated impact of the proposed changes on bridge design practice.

3.9.1 Items Fully Addressed by This Project

Article 5.8.2.5 Minimum Transverse Reinforcement

The current requirements are considered extendable to HSC, and their use will lead to the design of members with a shear capacity that is equal to or greater than the nominal strength calculated by the LRFD specifications when there is a limit on f'_c of 18 ksi.

Article 5.8.3.2 Sections Near Supports

The commentary to the LRFD specifications currently endorses the concept that the region between the face of the support and the first critical section up to $d_v\cot\theta/2$ from the support can be designed for the shear force at $d_v\cot\theta/2$ from the support only. However, the results of this research program, as documented in Section 2.4, indicate that the general use of the staggered shear design approach, as illustrated in Figure C5.8.3.2-4, should not be permitted. Therefore, it is proposed that this endorsement of that option be eliminated from the commentary in the changes to the LRFD specifications that are presented in the next section of this report.

Article 5.8.3.3 Nominal Shear Resistance

A change in the commentary is proposed so that when the design shear stress is greater than $0.18f'_c$ in the end region of a member that either is not cast integral with the support or is not continuous over a support, this end region must be designed using the strut-and-tie provisions in Section 5.6.3.

Article 5.8.3.4 Determination of β and θ

Subject to the elimination of the staggered shear design approach and a check of end region behavior when $v_u > 0.18f'_c$, the tabular values for β and θ in Table 5.8.3.4.2-1 for members that contain at least the minimum required amount of shear reinforcement are considered appropriate for use in design of HSC members with strengths up to $f'_c = 18$ ksi. The tabular values for β and θ in Table 5.8.3.4.2-2 are appropriate for members with less than the minimum amount of shear reinforcement for use in design of HSC members with strengths up to $f'_c = 18$ ksi, providing that the aggregate size is set to zero when $f'_c > 10$ ksi. The resulting proposed changes to the LRFD specifications in the LRFD format are presented in the next section.

3.9.2 Items Partially Addressed by This Project

The impact of project findings on the following articles is not considered sufficient to either fully support or refute the extension of these articles to HSC. Nevertheless, it is useful to examine what the data from this project indicate.

Article 5.4.2.7 Tensile Strength

In this article, the direct tensile strength is taken as $0.23\sqrt{f'_c}$ where f'_c is in ksi units. From the modulus of rupture test results presented in Table 5, the mean ratio of the measured tensile strengths to $0.23\sqrt{f'_c}$ is 1.24, with a COV of 0.18. Thus,

these test data generally support an extension of this provision to HSC.

Article 5.6.3.3.3 Limiting Compressive Stress in Strut

In this article, the maximum allowable compressive stress in struts, f_{cu}, is

$$f_{cu} = \frac{f'_c}{0.8 + 170\varepsilon_1} \leq 0.85 f'_c$$

Using a longitudinal tensile strain in the reinforcement of 0.002 and a horizontal nodal zone width of 9 inches, the calculated stress in the diagonal compressive stress in each of the experiments was found to be in excess of $0.85f'_c$. Therefore, the results of these tests support the extension of this provision to HSC.

Article 5.8.2.8 Design and Detailing Requirements

As shown in Table 6, the yield strengths in the regular deformed bar transverse reinforcements ranged from 64.6 to 79.3 ksi, and the yield strength of the welded wire reinforcement was 92.2 ksi. The full yield strength of the reinforcement was used in calculating the contribution of the shear reinforcement in all cases. The use of these values without a limit on the yield stress was found not to have any effect on the overall safety of the LRFD Sectional Design Model. A primary objective of Article 5.8.2.8 in limiting yield strengths of transverse reinforcement is to ensure good maintenance conditions and crack control under service load levels. As described in Sections 2.5, 2.6, and 3.6, many factors are considered to have negative effects on conditions under service load levels. Relative to these effects, the limiting of the yield strength of the transverse reinforcement to values less than those used in these experiments is not expected to have a significant effect on ensuring good behavior under service load levels. Owners who are concerned about the possibility of shear cracking under service loads should make separate checks to determine if such cracking is likely. Limiting the yield strength that can be used for the transverse reinforcement to reduce that possibility is not appropriate.

Article 5.8.4.1 Interface Shear Transfer—Shear Friction: General

As presented in Section 2.8 of this report, the current LRFD relationship for interface shear transfer resistance was observed to lead to conservative estimates of the concrete shear stress at failure in the shear friction experiments for test specimens cast with concrete strengths up to 18 ksi. A more extensive independent review of interface shear transfer has been conducted, as described in WAI57, and on the basis of that review some new cohesion and friction coefficients were recommended. Based on the results of the shear friction experiments conducted in this project, these new coefficients were found to be reasonably conservative when the clamping stress $\rho_v f_y$ exceeded 200 psi. Below this level of clamping stress, the new coefficients were found to be somewhat unconservative.

Article 5.9.5.4 Refined Estimates of Time-Dependent Losses

This article of the LRFD specifications presents a refined method for computing time-dependent losses resulting from prestressing. Based on the measured material properties and measured elastic shortening, the calculated time-dependent losses were computed using this refined estimation method and results presented in Figure 96. The comparison showed that the refined estimates of time-dependent losses agreed reasonably well, on average, with the experimental data.

Article 5.9.1.5 Crack Control

This article introduces the AASHTO Standard Specifications relationships for web-shear and flexure-shear cracking as a means of evaluating cracking and fatigue concerns under service load levels.

Article 5.11.2 Development of Reinforcement and Article 5.11.4.2 Bonded Strand

The longitudinal and transverse reinforcement provided in these tests girders was designed to satisfy LRFD requirements. Since significant slip or bond-splitting cracks did not develop prior to the design shear strength being realized in the test girders, without any limit being placed on the value of f'_c used in development length calculations, one conclusion is that the development rules in the LRFD specifications appear to be reasonable.

The transfer lengths of the 0.6-inch diameter prestressing strands were measured by taking Whittemore readings, with one reading taken immediately before and one reading taken immediately after strand release. From the strain profile of the elastic shortening, the average transfer length was about 23 inches, which is about two-thirds of the LRFD-calculated value.

3.10 Proposed Changes in LRFD Specifications Format

The proposed changes to the third edition of the LRFD specifications with 2005 Interim Revisions are presented in Table 39. Additions to the specifications are underlined, and deletions are marked with a strikeout. Only subsections of Article 5 with proposed changes are presented in the table.

Note that the desired changes may be impacted by the outcome of WAI 108 and WAI 110.

3.11 Implications for Bridge Design Practice

This project on the extension of the LRFD shear design provisions to HSC is one of several NCHRP projects that are aimed at the more general extension of Article 5 on Concrete Structures to HSC. The significant benefit of the proposed extension of the shear design provisions is principally realized when the more general extension of the entire LRFD specifications have been realized. This general extension will enable the same size structural section to be used to span longer distances or support heavier loads, or allow a smaller-size structural section to be used in place of the larger-size structural normal-strength concrete section or steel section. This extension is expected to provide substantial first cost savings as well as reduced life cycle costs due to the potential for enhanced durability of HSC concretes.

Outside of these benefits, the impact of the proposed changes to the LRFD specifications that were described and presented in Sections 3.9 and 3.10 are expected to have the following effects:

- The proposed change in the commentary of Article C5.8.3.3 requires that an end region in a simply supported member be designed by the strut-and-tie method when the design shear stress is in excess of $0.18f'_c$. This requirement is expected to prevent the design of structures in which localized diagonal crushing and/or significant cracking develops along the interface between bulbs and webs before the calculated nominal shear capacity of the member is reached. In many cases, shear design stresses in end regions higher than $0.18f'_c$ can be reached with improved detailing, such as the provision of increased longitudinal deformed bar reinforcement in the end region and the draping and flaring of strands over the depth of that region.
- Changes in the commentary of Article C5.9.1.5 will allow designers to check whether the member is likely to be cracked under service load levels. This ability will decrease potential corrosion and fatigue problems.
- Removal of the staggered shear design concept in Article 5.8.3.2 is an important improvement for both normal and HSC structures. It will help to prevent overstressing of a region under service load levels and will help ensure that the calculated nominal shear capacity provides for safe estimates of capacity.
- The overall results of this project serve to endorse the safety of the LRFD Sectional Design Model for the shear design of reinforced and prestressed concrete structures. This extensive review and the aforementioned changes are expected to improve confidence in the validity of the LRFD shear methodology. Coupled with the use of HSC, this design approach should encourage the development of new and innovative structures.

Table 39. Proposed changes to the third edition of the LRFD specifications with 2005 Interim Revisions.

5.8.3 Sectional Design Model

5.8.3.1 General

The sectional design model may be used for shear design where permitted in accordance with the provisions of Article 5.8.1. The values used for concrete compressive strength in Article 5.8.3 shall not exceed 18.0 ksi except that strengths for lightweight structural concrete shall not exceed 6.0 ksi.

C5.8.3.1

In the sectional design approach, the component is investigated by comparing the factored shear force and the factored shear resistance at a number of sections along its length. Usually this check is made at the tenth points of the span and at locations near the supports.

See Article 5.10.11.4.1c for additional requirements for Seismic Zones 3 and 4.

The extension of Article 5.8.3 to concrete compressive strengths of 18.0 ksi for normal weight concretes is based on *NCHRP Report 579*.

5.8.3.2 Sections Near Supports

The provisions of Article 5.8.1.2 shall be considered.

Where the reaction force in the direction of the applied shear introduces compression into the end region of a member, the location of the critical section for shear shall be taken as d_v from the internal face of the support as illustrated in Figure 1.

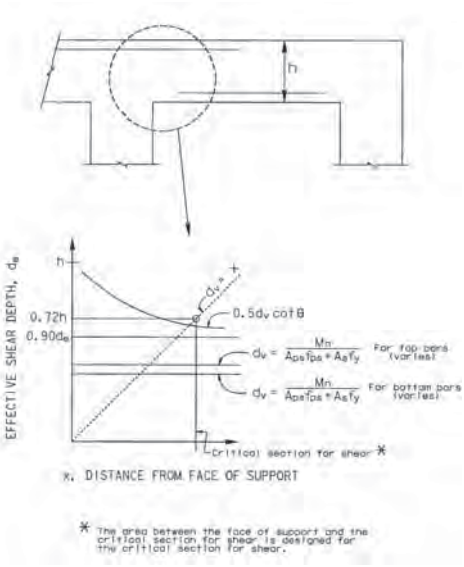

Figure 5.8.3.2-1 Critical Section for Shear.

C5.8.3.2

Loads close to the support are transferred directly to the support by compressive arching action without causing additional stresses in the stirrups.

The traditional approach to proportioning transverse reinforcement involves the determination of the required stirrup spacing at discrete sections along the member. The stirrups are then detailed such that this spacing is not exceeded over a length of the beam extending from the design section to the next design section out into the span. In such an approach, the shear demand and resistance provided is assumed to be as shown in Figure C1. There are, however, more theoretically exact stirrup designs. Knowledge of these may help to reconcile published research to traditional design practice.

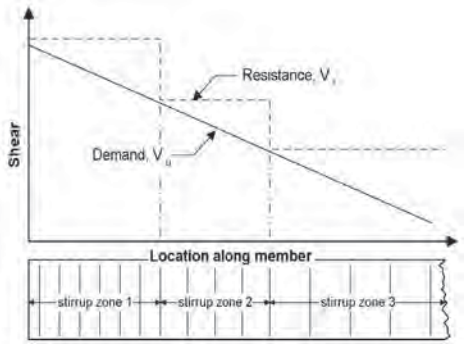

Figure C5.8.3.2-1 Traditional Shear Design.

Table 39. (Continued).

Otherwise, the design section shall be taken at the internal face of the support. Where the beam-type element extends on both sides of the reaction area, the design section on each side of the reaction shall be determined separately based upon the loads on each side of the reaction and whether their respective contribution to the total reaction introduces tension or compression into the end region.

For post-tensioned beams, anchorage zone reinforcement shall be provided as specified in Article 5.10.9. For pretensioned beams, a reinforcement cage confining the ends of strands shall be provided as specified in Article 5.10.10. For nonprestressed beams supported on bearings that introduce compression into the member, only minimal transverse reinforcement may be provided between the inside edge of the bearing plate or pad and the end of the beam.

Unlike flexural failures, shear failures occur over an inclined plane and a shear crack typically intersects a number of stirrups. The length of the failure along the longitudinal axis of the member is approximately d_v cot θ. Each of the stirrups intersected by this crack participates in resisting the applied shear. The relationship between the location of the design section and the longitudinal zone of stirrups that resist the shear at that design section is a function of the vertical position of the load applied to the member, including its selfweight. Ideally, the design section could be located by determining where the vertical centroid of the applied loads intersects a shear crack inclined at an angle θ as shown in Figure C2.

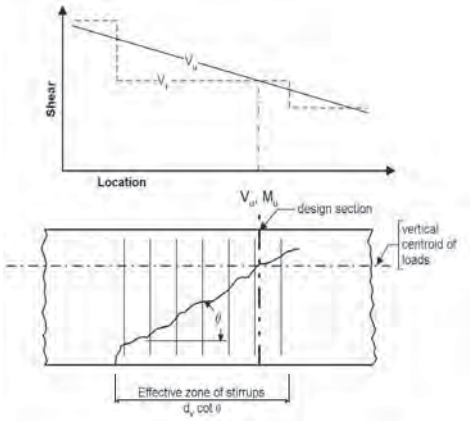

Figure C5.8.3.2-2 Theoretical Shear Design Section Location.

For typical cases where the applied load acts at or above the middepth of the member, it is more practical to take the traditional approach as shown in Figure C1 or a more liberal yet conservative approach as shown in Figure C3. The approach taken in Figure C3 has the effect of extending the required stirrup spacing for a distance of $0.5d_v \cot \theta$ toward the bearing.

Table 39. (Continued).

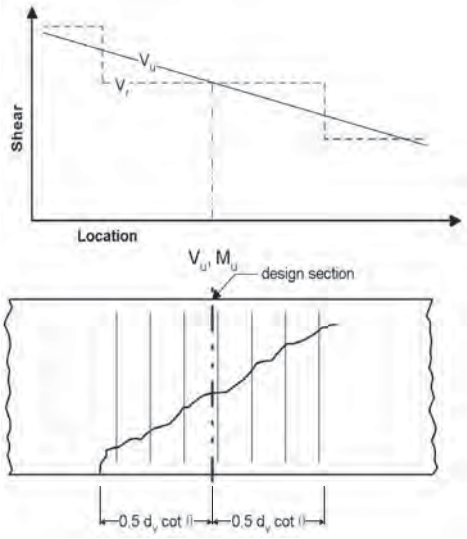

Figure C5.8.3.2-3 Simplified Design Section For Loads Applied at or Above the Middepth of the Member.

If the significant portion of the loads being resisted by the member are applied at a bearing resting on top of the member, the shear failure zone extends for a distance of approximately $d_v cot\theta$ beyond the point of load application as shown in Figure C4. The previous arguments suggest that ~~As with the previous case,~~ all of the stirrups falling within the failure zone may be assumed effective in resisting the applied shear force. and therefore the use of this staggered shear design philosophy was endorsed by the Commentary through the 2006 Edition of the Specifications. However, based on the test data and its analysis, as provided in *NCHRP Report 579*, the use of that philosophy should be discontinued and the traditional approach of Figure C1 used.

Table 39. (Continued).

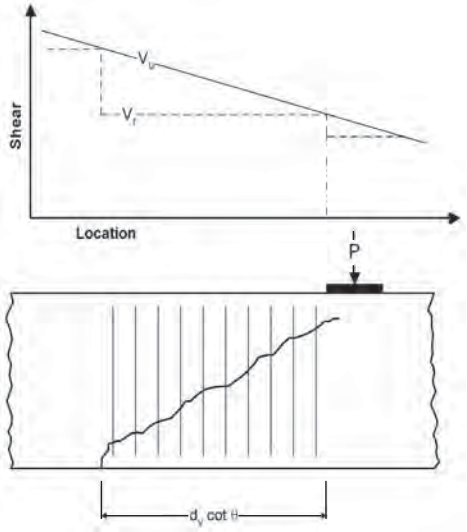

Figure C5.8.3.2-4 Effective Transverse Reinforcement to Members Subjected Primarily to Concentrated Loads.

If the shear stress at the design section calculated in accordance with 5.8.2.9 exceeds $0.18f'_c$ and the beam-type element is not built integrally with the support, its end region shall be designed using the strut-and-tie model specified in Article 5.6.3.

Figure C5 shows a case where an inverted T-beam acts as a pier cap and the longitudinal members are supported by the flange of the T. In this case, a significant amount of the load is applied below the middepth of the member, and it is more appropriate to use the traditional approach to shear design shown in Figure C1.

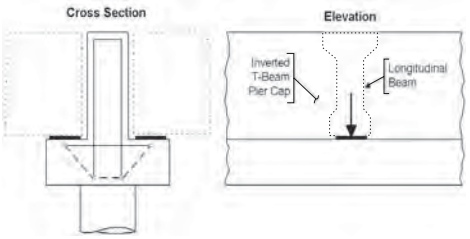

Figure C5.8.3.2-5 Inverted T-Beam Pier Cap.

The T-beam pier cap shown in Figure C5 acts as a beam ledge and should be designed for the localized effects caused by the concentrated load applied to the T-beam flange. Provisions for beam ledge design are given in Article 5.13.2.5.

Where a beam is loaded on top and its end is not

Table 39. (Continued).

	built integrally into the support, all of the shear funnels down into the end bearing. Where the beam has a thin web so that the shear stress in the beam exceeds $0.18f'_c$, there is the possibility of a local diagonal compression or horizontal shear failure along the interface between the web and the lower flange of the beam. Usually the inclusion of additional transverse reinforcement cannot prevent this type of failure, and either the section size must be increased or the end of the beam must be designed using a strut-and-tie model. For a beam to be built integrally with the support, a substantial part of the funneling of the shear down into the end bearing must be through the depth of the supporting member.
5.9.1.5 Crack Control Where cracking is permitted under service loads, crack width, fatigue of reinforcement, and corrosion considerations shall be investigated in accordance with the provisions of Articles 5.5, 5.6, and 5.7. For concrete beams not subject to significant axial tension, the shear cracking strength can be taken as the lesser of V_{ci} and V_{cw}, where f'_c may be taken up to 18 ksi and: V_{ci} = diagonal cracking shear strength when inclined cracking results from combined shear and moment (kip) V_{cw} = diagonal cracking shear strength when inclined cracking results from excessive principal tensions in the web (kip) • V_{ci} shall be determined by $$V_{ci} = 0.02\sqrt{f'_c}\,b_v d_v + V_d + \frac{V_i M_{cr}}{M_{\max}} \geq 0.06\sqrt{f'_c}\,b_v d_v$$ (5.9.1.5-1) where: V_d = shear force at section due to unfactored dead load and includes both DC and DW (kip) V_i = factored shear force at section due to externally applied loads occurring simultaneously with M_{max} (kip)	

Table 39. (Continued).

M_{cr} = moment causing flexural cracking at section due to externally applied loads (kip-in)

M_{max} = maximum factored moment at section due to externally applied loads (kip-in)

M_{cr} shall be determined by:

$$M_{cr} = (I_c/y_t)(0.2\sqrt{f'_c} + f_{pe} - f_d) \quad (5.9.1.5\text{-}2)$$

where:

I_c = moment of inertia of section resisting externally applied factored loads (in^4)

y_t = distance from centroidal axis of gross section resisting externally applied factored loads, neglecting reinforcement, to extreme fiber in tension (in)

f_{pe} = compressive stress in concrete due to effective prestress forces only (after allowance for all prestress losses), at extreme fiber of section where tensile stress is caused by externally applied loads (ksi)

f_d = stress due to unfactored dead load, at extreme fiber of section where tensile stress is caused by externally applied loads (ksi)

In Eq. 5.9.1.5-2, M_{max} and V_i shall be determined from the service load combination causing maximum moment at the section.

- V_{cw} shall be determined by

$$V_{cw} = (0.1\sqrt{f'_c} + 0.30 f_{pc}) b_v d_v + V_p \quad (5.9.1.5\text{-}3)$$

where:

Table 39 (Continued).

f_{pc} =	compressive stress in concrete (after allowance for all prestress losses) at centroid of cross section resisting externally applied loads or at junction of web and flange when the centroid lies within the flange (ksi). In a composite member, f_{pc} is the resultant compressive stress at the centroid of the composite section, or at junction of web and flange, due to both prestresss and moments resisted by precast member acting alone.

CHAPTER 4

Conclusions

4.1 Introduction

This chapter summarizes all major observations and conclusions from this project. The summary is not limited to an examination of the LRFD specifications, but covers all aspects of the design and behavior of the tests conducted and reviewed in this project.

4.2 Conclusions

Four primary issues for normal-weight concretes with f'_c values up to 18 ksi were addressed by this research: (1) the validity of the angle for diagonal compression θ used in the LRFD tables; (2) the validity of the concrete contribution as controlled by the parameter β; (3) minimum shear reinforcement requirements; and (4) maximum shear strength limits. The principal conclusions reached on those issues were as follows:

- Issues (1) and (2): The LRFD tabular values for θ and β are safe to use for the design of members with f'_c up to 18 ksi. Similarly, the alternative shear design provisions that are incorporated for the first time in the fourth edition of the LRFD specifications are also applicable for the design of members with f'_c up to 18 ksi.
- Issue (3): The minimum shear reinforcement requirements were valid for f'_c up to 18 ksi.
- Issue (4): The maximum shear stress limit needs to be restricted to $0.18f'_c + v_p$ unless the end region of the member is designed by strut-and-tie procedures or the end of the member is built integrally into its support. The research also found that use of the staggered shear design concept of the LRFD commentary should be discontinued.

The foregoing principal conclusions are part of the more detailed conclusions that are presented below in Sections 4.2.1 through 4.2.11. These detailed conclusions are derived from the detailed observations and findings that were presented in Chapter 2. They are organized by subject headings that correspond to the associated topic heading in Chapter 2. Additional information on any of these conclusions can be obtained by referring back to the referenced section of Chapter 2.

4.2.1 Evaluation of LRFD Sectional Design Model by Shear Database (Section 2.2)

This project began with an analysis of existing test data from a shear database that contained shear test results from 1,874 tests on reinforced and prestressed concrete members. The ratio of measured to LRFD-calculated shear strength, herein referred to as the "shear strength ratio," was compared for these tests results and then used to examine the influence of several design variables on the shear strength ratio. From this review, the following primary observations and conclusions were made:

1. **Concrete Compressive Strength:** Through an examination of the influence of concrete compressive strength on the shear strength ratio (V_{test}/V_{LRFD}), it was concluded that the LRFD Sectional Design Model was just as accurate and conservative for members cast with HSC as it was for members cast with normal-strength concrete. This conclusion is considered to be equally valid for reinforced and prestressed concrete members, with and without shear reinforcement, and either precast or cast-in-place concrete members.
2. **Maximum Shear Stress Limit:** There was limited test data from which to evaluate the shear strength ratio for members containing very high levels of shear reinforcement. Nevertheless, the available data suggested that the higher shear design strength permitted in the LRFD specifications is reasonable.
3. **Minimum Shear Reinforcement:** The test data suggested that the minimum shear reinforcement requirements in

the LRFD specifications are appropriate for ensuring that the calculated nominal shear capacity of the member is achieved.

4. **Size Effect in Shear:** The Sectional Design Model contains a factor to account for the size effect in shear for members without shear reinforcement and in which the values for β and θ are a function of the spacing of the layers of crack control reinforcement. This approach was found from the existing test data to be effective at accounting for the size effect in shear.
5. **Longitudinal Reinforcement Ratio:** The shear strength ratio (V_{test}/V_{LRFD}) increases with increasing levels of longitudinal reinforcement. For members with very light amounts of longitudinal reinforcement, the LRFD provisions were somewhat unconservative.
6. **Field Structures Versus Laboratory Structures:** The types of members tested in laboratories do not well represent the types of structures built in the field. As a consequence, an evaluation of code shear design provisions purely through a comparison with prior experimental test data is insufficient. The farther a design case is from the types of members tested in laboratories, the greater is the uncertainty that the accuracy of code provisions can be empirically determined from test data. Some of the primary differences between field and laboratory structures are summarized below:
   i. Members in the field are typically slender ($L/d > 10$) and support distributed loads, while members tested in laboratories are typically stocky and support one or two point loads.
   ii. Members in the field are often large and continuous and contain flanges, while members tested in laboratories are typically small, simply supported, and rectangular.
   iii. Members in the field typically contain shear reinforcement, while the majority of members tested in laboratories do not contain shear reinforcement.
   iv. Members in the field are designed to fail in flexure, while members in laboratories are over-reinforced in flexure, often to extreme limits, in the regions of potential shear failure.
   v. Members in the field need to be designed for shear over their entire length, while members in laboratories are typically designed to fail in shear near supports.
   vi. For examining the validity of extending the LRFD Sectional Design Model to HSC, tests on large prestressed concrete members designed for low to very high levels of shear reinforcement are required. This conclusion, which resulted from the review of the large experimental shear database, was the impetus for the specific testing program conducted in this project.

4.2.2 Evaluation of LRFD Sectional Design Model by Girder Tests (Section 2.4.1)

The following conclusions are made from Section 2.4.1:

1. The LRFD Sectional Design Model provided relatively accurate estimates for the shear capacities of the 63-inch deep bulb-tee girders that were tested in this research program and that had concrete strengths that ranged from 10- through 18-ksi concrete. This conclusion was valid regardless of whether straight, draped, or debonded strands were used in the girders.
2. A slight exception to the foregoing observation was that the LRFD specifications become slightly unconservative for members designed to resist shear stresses exceeding approximately $v = 0.18f'_c$. This unconservatism was due to the funneling into the support of the diagonal compressive stresses above the support. That funneling led to local diagonal crushing and very high horizontal shear stresses at the interface between the bottom bulb and the base of the web.
3. Design of the end regions of a beam—including consideration of the consequences of using draped strands, debonded strands, and added deformed bar longitudinal reinforcement—had a significant effect on the overall shear strength of the girders. The use of draped strands, particularly strands that were distributed over the depth of the web of the girder in its end region, significantly improved the shear capacity and performance under service load levels of the end region.

4.2.3 Evaluation of Other Codes and Methods from Girder Tests (Section 2.4.2)

The measured strengths of the test girders were also compared with capacities calculated by the AASHTO Standard Specifications, the program R2K, CSA A23.3-04, and the AASHTO simplified proposed specifications. The last of these are contained in the fourth edition of the LRFD specifications (2007) in Article 5.8.3.4.3, "Simplified Procedure for Prestressed and Nonprestressed Sections." From those comparisons, the following observations are drawn:

1. All four methods predicted the capacity of the test girders to an acceptable level of accuracy.
2. The strength ratios from the LRFD and CSA methods produced very similar results, as was expected because both methods were derived from the MCFT and use the longitudinal strain at mid-depth to characterize the condition of the member in shear.
3. The AASHTO Standard Specifications method was the most conservative and had the lowest COV. The ratio of

the measured to code calculated nominal shear strengths ranged from 1.12 to 1.50.
4. The program R2K had the lowest average strength ratio.
5. The proposed simplified provisions provided a safe estimate of the capacity of all test girders that failed in shear. It was particularly conservative at predicting the capacity of Girder 5, which contained minimum shear reinforcement only. These provisions were intentionally more conservative for lightly reinforced members to guard against serviceability and fatigue problems.

For the above calculations, because the girders were subjected to uniformly distributed loads, the shear forces varied along the length of the span and each successive shear design region was designed for the shear force acting at the section in the middle of that region. If, instead, the staggered shear design concept of the LRFD commentary had been employed over the entire length of the member so that the member was designed for the lowest shear force in each successive shear design region, then it was observed that the shear capacities calculated by the LRFD, R2K, CSA, and simplified proposed provisions were somewhat unconservative.

4.2.4 Modes of Failure (Section 2.4.4)

The capacities of the members were limited by yielding of shear reinforcement, localized diagonal compressive failure of the concrete, concrete horizontal shear resistance between the bottom bulb and the base of the web, shear slip resistance along cracks, bond strength of the reinforcement, the diagonal compressive strength across a region of distributed crushing, or some combination of the above. The most brittle modes of failure were observed in the members designed to resist the higher shear stresses, and in those modes the failure was precipitated by a sudden localized diagonal compressive failure or a horizontal shear-compression failure between the bottom bulb and the web. In those cases, there was an explosive compressive failure of the web and a large relative shear displacement between the bottom bulb and the web. More ductile shear failures were observed in members that contained light amounts of shear reinforcement and in which failures occurred away from the end region. The discussion of modes of failure is presented in Section 2.4.4 and in Appendix 11.

4.2.5 Cracking (Section 2.5)

Section 2.5 presented the measured cracking loads, crack angles, spacing of cracks, and crack widths. Measured values were compared with the shear cracking loads calculated using the AASHTO Standard Specifications, with crack angles calculated using Mohr's circle of stress and the angles of diagonal compression calculated using the LRFD specifications, and with the spacing of cracks predicted using the CEB-FIP model. Some of the key observations from those comparisons were as follows:

1. Typically web-shear cracks occurred very suddenly, along straight lines, and with a significantly loud "pop."
2. The first web-shear crack usually occurred within a longitudinal distance equal to the overall height of the member from the center of the support. The closer the crack was to the end of the member, the steeper was the crack angle as the effect of the longitudinal prestressing decreased as the end of the member was approached.
3. The angle of web-shear diagonal cracking in the first shear design region (a flexural region in the terms of Article 5.8.1.1 of the LRFD specifications) was reasonably constant and substantially flatter than the first web-shear crack. The crack angles ranged from 23 to 32 degrees, with an average angle of 27.8 degrees.
4. The angle of web-shear diagonal cracking was accurately predicted using Mohr's circle of stress.
5. The angle of web-shear diagonal cracking in the first shear design region was typically a little steeper than the angle of diagonal compression calculated from Table 5.8.3.4.2-1 of the LRFD Sectional Design Model. Consequently, the LRFD method may overestimate the contribution of the shear reinforcement in this region unless there are significant shear stresses acting on the faces of the cracks.
6. The angle of potentially critical flexure-shear cracks can be upward of 60 degrees, which suggests that the contribution of the shear reinforcement by most codes of practice is likely to be overestimated in flexure-shear regions.
7. The spacing of shear cracks in the web was on average about half the values predicted using the CEB-FIP expression for crack spacing.
8. The AASHTO Standard Specifications provided a reasonably accurate and somewhat conservative estimate of the web-shear cracking load, V_{cw}, even when the full value of f_{pc} was used in the calculations.
9. First web-shear cracking was observed to occur at between 33 and 87 percent of the LRFD shear design stress. Values for first cracking can be a much lower percentage of the shear design stress than would have been possible with the use of Standard Specifications because the LRFD specifications permit members to be designed for shear stresses up to $0.25f'_c$.
10. The AASHTO Standard Specifications marginally overestimated the flexure-shear cracking loads V_{ci}.
11. The flexural cracking loads were reasonably well predicted by M_{cr} when the tensile cracking stress was taken as $7.5\sqrt{f'_c}$ (in psi units).

12. Upon initiation of web-shear cracking, the first measured web-shear crack width ranged from 0.012 inch (0.3 millimeter) to 0.02 inch (0.5 millimeter). The initial crack widths were larger for members with less shear reinforcement. Flexure-shear cracks opened faster than web-shear cracks once flexure-shear cracking occurred. After flexural cracking occurred, the maximum crack width increased linearly with increasing external moment.

4.2.6 Reinforcement Strains (Section 2.6)

The strains in the transverse and deformed bar longitudinal reinforcement of the test girders were extensively measured. While it is recognized that the magnitudes of measured reinforcement strains highly depend on the location of a gage relative to the nearest crack, the measured strains are still useful for evaluating the demands on the test girders. For the measured strains, the following observations and conclusions were drawn:

1. Prior to first shear cracking, the strains in the stirrups were small and less than 30 microstrain, which corresponds to a stress of less than 1 ksi.
2. Immediately after occurrence of web-shear cracking, strains in some gages jumped to very close to the yield strain. With the development of additional web-shear cracks, similarly large jumps in stirrup strains were observed.
3. There was a dramatic variation in strain in some stirrups, with a gage near a crack measuring strains greater than the yield strain, while gages farther from the same crack measured less than 100 microstrain (<5 percent of yield). However, prior to failure, yielding progressed until it extended over the height of the stirrups in the field of web-shear cracking.
4. For members with the least amount of shear reinforcement, $\rho_v f_y$, the increase in stirrup strains at the onset of web-shear cracking and the strains prior to failure were the largest, and in some cases were greater than 10,000 microstrain. By contrast, the members with the largest amount of shear reinforcement failed when the maximum stirrup strains were only slightly beyond yield or somewhat less than yield.
5. The maximum web-shear stirrup strains in the ends with draped strands—G1W, G2W, G9W, and G10W—were lower, at the same magnitude of loading, than the maximum web-shear stirrup strains in the ends of the same girders where the strands were straight.
6. As with the development of web-shear cracking, there was a rapid increase in stirrup strain following the formation of flexure-shear cracking, with strain values that approached the yield strain being measured immediately upon cracking. Unlike the situation for web-shear cracking, the development of a complete pattern of flexure-shear cracks occurred rapidly over a very narrow loading range. Consequently, the measured strains in all gages crossing flexure-shear cracks went from close to zero strain to almost all gages showing strains close to the yield strain, with an increase in loading of around 10 to 15 percent.
7. Within the flexure-shear region, the farther a stirrup was from mid-span, the larger was the shear, the flatter was the flexure-shear crack, and the larger was the magnitude of the stirrup strains.
8. Even when strains in the stirrups in the flexure-shear region were well above failure, there were no signs of impending failure.
9. In general, the strains in the stirrups in the flexure-shear regions were less than the maximum strains in the web-shear regions even though the members were designed to be equally as likely to fail in a web-shear region as they were to fail in a flexure-shear region.
10. The very large longitudinal reinforcement strains that were measured near the support, as reported in Section 2.6, indicate that the tensile force demands specified by LRFD S5.8.3.5 are very real and need to be resisted by appropriately detailed longitudinal reinforcement.
11. The significant levels of straining measured in the confinement cages indicate that those cages provided significant confinement for the anchorage of the prestressing strands.

4.2.7 Mechanisms of Shear Resistance (Section 2.7)

Selected crack-based free body diagrams and measured stirrup strains were used to assess what portion of the applied shear load was carried by the transverse reinforcement and then, by subtraction, what remaining component was carried by the concrete. The results indicated that the amount of stirrup reinforcement had a significant effect on the concrete contribution, and this suggests that the level of resistance provided by interface shear transfer is influenced by the amount of shear reinforcement provided. This finding is consistent with what would be suggested by the MCFT in that crack opening stiffness affects slip resistance. In the LRFD method, the effect of the transverse reinforcement on crack opening stiffness is neglected in an effort to provide a hand-based design procedure. The assumptions made in this derivation are shown by the test results to be conservative. A complicating factor in the assessment of V_c is understanding what portion of this resistance is provided by the uncracked

compression zone at the top of the member and by the bottom bulb.

4.2.8 Interface Shear Transfer (Section 2.8)

Eighteen interface shear transfer experiments on HSC specimens were conducted to evaluate the safety of the expression for interface shear transfer resistance that is used in the MCFT. The results illustrated that the interface shear transfer resistance that can be provided by the concrete is larger than that calculated using the v_{ci} expression in the MCFT for crack widths up to 0.04 inch (1 millimeter) in all cases tested and for crack widths up to 0.08 inch (2 millimeters) in most cases tested. The results also indicated that the current provisions of the LRFD specifications for interface shear transfer in S5.8.4 are conservative.

4.2.9 Behavior of End Regions (Section 2.9)

The distributions of strains and deformations in the end regions were measured using the Krypton Coordinate Measurement Machine and concrete surface strain gages, as described in Section 2.9. The initial examination of this test data resulted in the following observations and conclusions:

1. The vertical straining increases from the support to a maximum at a distance approximately equal to the depth of the member from the support. This result confirms the rationality of the design assumption that the shear reinforcement used at the first critical section is sufficient for the region from the support to this first critical section.
2. An inspection of the horizontal strain distributions at the base of the girder indicated that a significant increase in the horizontal strain at a horizontal distance of 20 inches from the support preceded the failure of the girder. This evidence supports the observation that a loss of prestress and excessive demand on the longitudinal reinforcement is exhibited prior to the failure of a typical girder.
3. The distribution of the diagonal tensile strains illustrated that there was very little diagonal tensile strain in the top of the web near the support. This result is consistent with other experimental test data, such as the observation that there is little cracking in this region because forces are flowing directly into the support via strut action.
4. The results from the concrete surface strain gage readings indicate that there can be a twofold increase in the compressive strain from the top to the bottom of the strut that runs to the support. This observation is consistent with the observed pattern of cracking that also illustrated a funneling of the compression to the support. The effect of using draped strands was to decrease the magnification of the compressive strains.

4.2.10 Capabilities of Finite Elements Methods (Section 2.10)

The program Vector2, which is a two-dimensional continuum analysis tool that fully implements the MCFT, was used to predict the overall strength, load-deformation response, mode of failure, and distribution of strains in each of the test girders. A comparison with the test data was made to both assess the accuracy of the MCFT and evaluate whether Vector2 can be used to reliably predict the response of somewhat similar members that were not tested in this research program.

Vector2 was able to predict the capacity of the test girders to within 10 percent. Although Vector2 typically somewhat overestimated the capacity, the COV of the shear strength ratio with Vector2 was only 0.08. Vector2 was also able to well predict the overall load-deformation response, but generally underestimated the stiffness of these girders. There was generally good agreement between the predicted and measured cracking loads, locations, and angles. Vector2 also proved to be effective at predicting the test girders' observed mode of failure. Vector2 frequently overestimated the length of the region of elastic shear stress versus shear strain response, but did reasonably well at predicting the stiffness of the inelastic portion of this response. Vector 2 was able to predict the reverse direction of shear slip that was observed at the base of the web near the support. It was generally effective at predicting distributions of horizontal, vertical, and principal strains.

The relatively good agreement between the behavior of the test girders and the predictions of Vector2 indicate that the MCFT is an effective model for capturing the complexity of the behavior of these test girders and that Vector2 can be used for providing reliable analytical predictions for the behavior of similar types of structures. This finding may be particularly useful if there is concern about the applicability of the LRFD Sectional Design Model for the many design situations in which there is little experimental test data.

4.2.11 Miscellaneous Conclusions

The following miscellaneous conclusions were made:

1. Shear cracking has little effect on the overall load-deformation response of the test girders (Section 2.4.5).
2. The LRFD expression for longitudinal strain at mid-depth provides a rough estimate only of the actual straining at

the mid-depth of the first critical shear design section (Section 2.6.7).

3. The shear stress versus shear strain response can be characterized as a tri-linear relationship consisting of one line to represent the stiffness prior to cracking, another line to represent the stiffness between shear cracking and yielding of the shear reinforcement, and a third line to represent the stiffness between yielding of the shear reinforcement and when the ultimate capacity is reached. Post cracking stiffness values can be predicted based on the modular stiffness ratio of the concrete and the reinforcement and the percentage of shear reinforcement used in the girder.

4.3 Background Statement to Suggested Research

There is an underlying and simple model for calculating axial and flexural capacities such that test strengths can usually be predicted to within 10 to 20 percent regardless of the size of the member or material strengths. By contrast, there is considerable debate about (a) how best to design members for shear, (b) what maximum and minimum shear stress design limits are appropriate, and (c) what factors influence shear capacity. This debate is further complicated by the complex flow of forces in end regions.

The only aspect of shear behavior upon which there is international agreement is the use of the parallel chord truss model for evaluating the contribution of transverse reinforcement to shear capacity. However, there is no international agreement on the appropriate angle for diagonal compression in this truss, the appropriate way to calculate the shear depth of the truss, and the appropriate way to characterize the contributions of concrete to shear resistance in a flexural member. The developments of the Compression Field Theory and the subsequent MCFT have been among the most significant advances in modeling shear behavior in the last 100 years. However, these approaches can be fully implemented only in two-dimensional continuum analysis tools, and, even then, there are uncertainties as to how best to predict crack spacing and crack width and how to evaluate interface shear transfer resistance. Furthermore, the methods fail to account for shear slip along cracks, as is now done in the Disturbed Stress Field Model; therefore, their application to structures without well-distributed reinforcement in two directions is debatable. For the purposes of structural design, the challenge has been how to use the MCFT for the design of typical structures such as the flexural members examined in this study. In flexural members, there can be both a linear and a nonlinear variation in strain over the depth of the member, and there are significant top and bottom flanges that restrain the deformations of the web. These effects are combined with the effects of a concentrated prestressing force. The LRFD Sectional Design Model was carefully derived from the MCFT, but the assumptions necessary to develop the hand-based sectional design procedure, and its potentially wide range of applications, limit the general applicability of the method.

The shear provisions for the bridge and building codes of practice in the United States differ from those in other nations. The differences include ways in which the contribution of the transverse reinforcement is evaluated by different methods, as well as the calculated concrete contributions to capacity and to the maximum shear design stress limits. Researchers also differ on the mechanics of shear resistance. These differences in codes and among researchers, especially the very large differences in codes, are a cause for considerable concern. Because the test data upon which provisions are validated does not well represent the types of structures built in the field, the true capacity of members in the field is unfortunately relatively uncertain. The life safety issues raised by this uncertainty suggest that systematic efforts should be undertaken to determine how best to design members for shear. Those efforts should continue until researchers agree on a method for calculating the nominal shear strength that can provide predictions within 20 percent of the measured shear strengths, as validated by comprehensive, weighted, and extensive test data. Current research practices, in which several hundred uncoordinated shear tests on structural concrete members are conducted each year, most of which are on members not representative of those used in practice, will not necessarily answer the life safety questions raised by the shear design issue.

4.4 Suggested Research and Changes to the Code Development Practice

Based on the review of experimental research and familiarity with how changes to code provisions are made, the following suggestions are made for new directions in experimental research on shear strength and the development of code shear provisions:

1. It is estimated that there have been between 6,000 and 10,000 shear tests on beams, but few of these results are ever used by researchers in the design of a research program or by members of code committees in the extension of shear provisions. Thus, there is the need for a national and/or international database of test results that is fully maintained and available to the research, design, and regulatory communities. The creation of this database will require the development of, and agreement upon, standards

for test data acceptance. Such standards must define the checks necessary against anchorage failures and flexural failures, as well as those needed to ensure that proper boundary conditions were provided.

2. This experimental database needs to be compared with the types of members built in the field and the results used to set a national agenda for the types of experiments that are required. It is anticipated that 90 percent of the tests currently conducted each year are redundant, adding little to the collective understanding of shear behavior. As previously stated, most shear tests in laboratories are on small members (<18 inches overall depth) that have rectangular cross sections, are stocky, are loaded at one or two points, are simply supported, are over-reinforced in flexure, and are designed to fail within one or two effective depths from the end of the member. By contrast, most members in the field are large, support distributed loads at the time of maximum shear loading, and are designed for shear over their entire length. Furthermore, many of these members have flanges, are slender, and are continuous over supports.
3. New standards are required for material testing to be done in conjunction with large-scale shear tests. This testing needs to include the measurement of the compressive response, tensile strength, and fracture characteristics of the concrete, and the full stress-strain relationships of all reinforcing materials.
4. A new standard is needed for ensuring appropriate support conditions in test set-ups. This need is illustrated by the difficulties apparent in the test girders in the funneling of the compressive forces into the end supports. Standards need also to be established for the measurements of load, displacements, and strains.
5. It would also be useful to establish a program that enabled the testing to failure of more realistically sized and loaded members that are not well represented in the experimental database of laboratory test results. This would lead to a better assessment of the conservatism and safety concerns with present codes. It is expected that these tests would be on structures being removed from the field, members that are rejected for use in the field, or unused inventory from producers.

References

1. American Association of State Highway and Transportation Officials, *AASHTO LRFD Bridge Design Specifications*, 3rd ed., Washington, D.C. (2004).
2. Vecchio, F. J., and Collins, M. P., "The Modified Compression Field Theory for Reinforced Concrete Elements Subjected to Shear." *Journal of the American Concrete Institute,* Vol. 83, No. 2 (1986).
3. American Association of State Highway and Transportation Officials, *Standard Specifications for Highway Bridges*, 17th ed., Washington, D.C. (2002).
4. Collins, M. P., Mitchell, D., Adebar, P. E., and Vecchio, F. J., "A General Shear Design Method." *ACI Structural Journal,* Vol. 93, No. 1 (1996).
5. American Association of State Highway and Transportation Officials, *AASHTO LRFD Bridge Design Specifications*, 2nd ed., Washington, D.C. (1998). Including interim revisions for 1999 through 2003.
6. Canadian Standards Association, *Design of Concrete Structures, CSA A23.3-04.* (2004).
7. Hawkins, N. M., Kuchma, D. A., Mast, R. F., Marsh, M. L., Reineck, K.-H., *NCHRP Report 549: Simplified Shear Design of Structural Concrete Members*, Transportation Research Board (2005).
8. Mitchell, D., and Collins, M. P., "Diagonal Compression Field Theory—A Rational Model for Structural Concrete in Pure Torsion." *ACI Journal,* Vol. 71 (1974).
9. Sozen, M. A., and Hawkins, N. M., Discussion of report of ACI-ASCE Committee 326, "Shear and Diagonal Tension." *ACI Journal*, Vol. 59, No. 9 (September 1962).
10. Ritter, W., "Die Bauweise Hennebique." *Schweizerische Bauzeitung,* Vol. 33, No. 7, Zurich, (February 1899).
11. Rureyen A. K., and Frosh, R. J., "Concrete Shear Strength: Another Perspective." *ACI Structural Journal*, Vol. 100, No. 5 (2003).
12. Bazant, Z. P., and Kazemi, M. T., "Size Effect on Diagonal Shear Failure of Beams without Stirrups." *ACI Structural Journal*, Vol. 88, No. 3 (1991).
13. Mörsch, E., "Der Eisenbetonbau—Seine Theorie und Anwendung (Reinforced Concrete Construction—Theory and Application)." 5th Ed., Wittwer, Stuttgart, Vol. 1, Part 1 (1920).
14. Mörsch, E., "Der Eisenbetonbau—Seine Theorie und Anwendung (Reinforced Concrete Construction—Theory and Application)." 5th Ed., Wittwer, Stuttgart, Vol. 1, Part 2 (1922).
15. EC 2-1-1, *Eurocode No. 2: Design of Concrete Structures—Part 1: General Rules and Rules for Buildings.* prEN 1992-1-1 (2004).
16. DIN 1045-1, *Deutsche Norm: Tragwerke aus Beton, Stahlbeton und Spannbeton—Teil 1: Bemessung und Konstruktion. S. (Concrete, reinforced and prestressed concrete structures—Part 1: Design)*. Normenausschuss Bauwesen (NABau) im DIN Deutsches Institut für Normung e.V. Beuth Verl. Berlin (July 2001).
17. Collins, M. P., and Kuchma, D. A., "How Safe Are Our Large, Lightly Reinforced Concrete Beams, Slabs, and Footings?" *Structural Journal,* Vol. 96, No. 4 (July-August 1999).
18. Shioya, T., Iguro, M., Nojiri, Y., Akiyama, H., and Okada, T., "Shear Strength of Large Reinforced Concrete Beams, Fracture Mechanics: Application to Concrete." *ACI SP-118*, American Concrete Institute, Detroit (1989).
19. Moody, K. G., Viest, I. M., Elstner, R. C., and Hognestad, E., "Shear Strength of Reinforced Concrete Beams, Part 1—Tests of Simple Beams." *Journal of the American Concrete Institute,* Vol. 51, No. 4 (December 1954).
20. Angelakos, D., Bentz, E. C., and Collins, M. P., "The Effect of Concrete Strength and Minimum Stirrups on the Shear Strength of Large Members." *ACI Structural Journal,* Vol. 98, No. 3 (2001).
21. ACI-ASCE Committee 426, "The Shear Strength of Reinforced Concrete Members—Chapters 1 to 4," *Proceedings ASCE, Journal of the Structural Division,* Vol. 99, No. ST6 (June 1973).
22. Russell, H. G., Miller, R. A., Ozyildirim, H. C., and Tadros, M. K., "Compilation and Evaluation of Results from High Performance Concrete Bridge Projects," Interim Report, submitted to FHWA, U.S. Department of Transportation (May 2001).
23. Collins, M. P., and Rahal, N. R., "Experimental Evaluation of ACI and AASHTO-LRFD Design Provisions for Combined Shear and Torsion." *ACI Structural Journal,* Vol. 100, No. 3 (2003).
24. Bentz, E. C., and Collins, M. P., "Response 2000." http://www.ecf.utoronto.ca/~bentz/r2k.htm (2000).
25. Elzanaty, A. H., Nilson, A. H., and Slate, F. O., "Shear Capacity of Prestressed Concrete Beams Using High-Strength Concrete," *ACI Structural Journal*, Vol. 83, No. 3 (1986).
26. ACI Committee 318, *Building Code Requirements for Structural Concrete (ACI 318-02) and Commentary (ACI 318 R-02)*. American Concrete Institute, Farmington Hills (2002).
27. Comité Européen du Béton (European Committee for Concrete)–Fédération Internationale de la Précontrainte FIP (International Federation for Prestressing) (CEB-FIP), *Model Code for Concrete Structures: CEB-FIP International Recommendations*, 3rd ed. (1978).
28. Won, P. S. and Vecchio, F. J., "VecTor2 & FormWorks User's Manual." http://www.civ.utoronto.ca/vector (2002).

29. Bhide, S. B., and Collins, M. P., "Influence of Axial Tension on the Shear Capacity of Reinforced Concrete Members." *ACI Structural Journal,* Vol. 86, No. 5 (1989).
30. Walraven, J. C., and Reinhardt, H. W., "Concrete Mechanics—Part A: Theory and Experiments on the Mechanical Behavior of Cracks in Plain and Reinforced Concrete Subjected to Shear Loading." *Heron*, Vol. 26, No. 1A (1981).
31. Vecchio, F. J., "Disturbed Stress Field Model for Reinforced Concrete: Formulation." *ASCE Journal of Structural Engineering*, Vol. 126, No. 8 (2000).
32. Comité Européen du Béton (European Committee for Concrete)–Fédération Internationale de la Précontrainte FIP (International Federation for Prestressing) (CEB-FIP), *Mode Code 1990, 1993 (MC90)*, Thomas Telford, London (1993).
33. Porasz, A., "An Investigation of the Stress-Strain Characteristics of High Strength Concrete in Shear." M.A.Sc. Thesis, University of Toronto (1989).
34. Vecchio, F. J., Collins, M. P., and Aspiotis, J., "High-Strength Concrete Elements Subjected to Shear." *Structural Journal*, Vol. 91, No. 4 (1994).
35. Bentz, E. C., "Sectional Analysis of Reinforced Concrete Members," Ph.D. Thesis, Department of Civil Engineering, University of Toronto (2002).
36. Collins, M. P., and Mitchell, D., *Prestressed Concrete Structures*, Response Publications, Canada (1997).
37. Walraven, J. C., "Fundamental Analysis of Aggregate Interlock." *Journal of the Structural Division-ASCE,* Vol. 107, No. 11 (1981).
38. Jacob, J., and Russell, B., "Effects of Horizontal Web Reinforcement on Shear Capacity, Shear Ductility and Strand Anchorage." Paper presented at the 78th Transportation Research Board Annual Meeting (1999).
39. Bruce, Robert N., Russell, H.G., and Roller, J., "Fatigue and Shear Behavior of HPC Bulb-Tee Girders," Report No. FHWA/LA.05/395, Louisiana Transportation Research Center (February 2005).

Appendices

The following appendices are not published herein, but are available online, along with a data-viewing program, at www.trb.org/news/blurb_detail.asp?id=7443:

1. Presentation of Experimental Results for Girder 1
2. Presentation of Experimental Results for Girder 2
3. Presentation of Experimental Results for Girder 3
4. Presentation of Experimental Results for Girder 4
5. Presentation of Experimental Results for Girder 5
6. Presentation of Experimental Results for Girder 6
7. Presentation of Experimental Results for Girder 7
8. Presentation of Experimental Results for Girder 8
9. Presentation of Experimental Results for Girder 9
10. Presentation of Experimental Results for Girder 10
11. Other Aspects of Girder Behavior and Analysis
12. Collection, Analysis, and Use of Existing HSC Information
13. Presentation of Shear Database

Notation

The notation conforms to that of Section 5.3 of the LRFD specifications. However, some new symbols are needed to describe terms used in various models, and in several instances modifications are needed to the basic LRFD definition to better describe subsets of that term.

A_c = area of concrete on flexural tension side of member
A_{cr} = area of crack plane
A_{ct} = area of concrete in tension
A_{cv} = area of concrete resisting shear transfer
A_g = gross area of concrete section
A_p = area of prestressing strands
A_{ps} = area of prestressing steel on flexural tension side of member at ultimate load
A_s = area of nonprestressed tension reinforcement on flexural tension side of member at ultimate load
A_{sl} = area of tensile reinforcement that extends d beyond section considered and is anchored there effectively
A_v = area of transverse reinforcement within distance s
$A_{v,\min}$ = area of minimum required transverse reinforcement
a = shear span length
a_g = maximum aggregate size
b = width of compression face of member
b_v = width of interface; web width including adjustment for presence of ducts
b_w = web width
c_x = distance between midsection and longitudinal reinforcement
c_y = distance between midsection and transverse reinforcement
d = distance from compression face to centroid of tension reinforcement
d_b = bar diameter
d_{bx} = bar diameter of longitudinal reinforcement
d_{by} = bar diameter of transverse reinforcement
d_v = effective shear depth
e_1, e_2 = parameters in compression-softening model
E_c = modulus of elasticity of concrete
E_p = modulus of elasticity of prestressing steel
E_s = modulus of elasticity of reinforcing bars
f_1 = stress in direction 1 = principal tensile stress
f_2 = stress in direction 2; principal compressive stress
f'_c = concrete compressive strength
f^a_{c1} = average concrete tensile stress determined by tension-stiffening effect
f_{c1} = concrete stress in direction 1
f_{c2} = concrete stress in direction 2
$f_{c2\max}$ = maximum value of concrete stress in direction 2 when there is tension in direction 1
f_{ci} = principal compressive stress
f_{ck} = characteristic concrete cylinder compressive strength (EC2 method)($\approx 0.9f'_c$)
f_{cr} = concrete stress at tensile cracking
f_{ct} = concrete tensile stress
f_{cx} = concrete stress in direction x
f_d = stress due to unfactored dead load
f_p = peak concrete compressive stress
f_{pc} = compressive stress in concrete after all prestress losses have occurred either at the centroid of the cross section resisting live load or at the junction of the web and flange when the centroid lies in the flange
f_{pe} = effective stress in the prestressing steel after losses; compressive stress in concrete due to effective prestress forces only at extreme fiber of section where tensile stress is caused by externally applied loads
f_{po} = E_p times the locked-in difference in strain at ultimate load between the prestressing tendons and the surrounding concrete
f_{ps} = stress in prestressing steel
f_{pu} = tensile strength of prestressing steel

f_r = concrete modulus of rupture
f_s = stress capacity in the longitudinal deformed bar reinforcement
f_{sx} = steel stress in direction x
f_{sxcr} = steel stress in the x-direction reinforcement at the crack location
f_{sy} = steel stress in direction y
f_{sycr} = steel stress in the y-direction reinforcement at the crack location
f_t = tensile strength of concrete
f_v = shear stress; stress in shear reinforcement; vertical stress
f_x = stress in direction x
f_y = yield strength of reinforcing bars; stress in direction y
h = overall thickness or depth of member
I = moment of inertia of the section resisting externally applied factored loads
I_c = moment of inertia of uncracked concrete
L = span of member center to center of supports
M = moment
M_{cr} = cracking moment
M_f = ultimate moment = factored moment at the section
$M_{\max}$ = maximum factored moment at section due to externally applied loads
M_n = nominal flexural resistance of section
M_u = ultimate moment; factored moment at section
N_f = factored axial force
N_u = factored axial force
$N_v = V\cot\theta$
n = modular ratio
S_e = elastic stiffness parameter of shear behavior
S_{t1} = stiffness parameter of shear behavior
S_{t2} = stiffness parameter of shear behavior
s = stirrup spacing
$s_{\max}$ = maximum permitted spacing of transverse reinforcement
s_{mx} = average crack spacing in longitudinal direction
s_{my} = average crack spacing in transverse direction
$s_{m\theta}$ = average crack spacing for angle θ
s_x = crack spacing parameter
s_{xe} = crack spacing parameter
s_z = crack spacing parameter
s_{ze} = crack spacing parameter
$T_{\min}$ = minimum tensile capacity required for reinforcement on flexural tension side of member at $d_v\cot\theta$ from design section
V = shear
V_c = shear at inclined cracking; nominal shear resistance provided by concrete
V_{ca} = shear carried by aggregate interlock
V_{cc} = shear in compression zone
V_{ci} = shear at flexure-shear cracking
V_{code} = nominal shear strength of member as evaluated by a specific code method or procedure
V_{cr} = shear carried by residual tensile stresses in concrete
V_{cw} = shear at web-shear cracking
V_d = shear carried by dowel action; shear force at section due to unfactored dead load
V_f = factored shear force
V_i = factored shear force at section due to externally applied loads occurring simultaneously with $M_{\max}$
V_{LRFD} = shear capacity evaluated using LRFD specifications
V_n = nominal shear resistance of section considered
$V_{n,\max}$ = maximum allowable nominal shear capacity
V_p = component in the direction of the applied shear of the effective prestressing force
V_r = factored shear resistance = ϕV_n
V_s = shear resistance provided by transverse reinforcement
V_{STD} = shear capacity evaluated using AASHTO Standard Specifications
V_{test} = shear resistance measured at ultimate capacity in test
V_u = factored shear force at section
v = factored (design) shear stress
v_{ci} = interface shear stress at a crack
$v_u = V_u/b_v d_v$
$v_{u\text{test}} = V_{\text{test}}/b_v d_v$ or $V_{\text{test}}/b_w d_w$
v_{xy} = shear stress
w = crack width
w_{cr} = distributed load at inclined cracking
y_t = distance from neutral axis to extreme tension fiber for uncracked section
β = factor relating effect of longitudinal strain on the shear capacity of concrete, as indicated by the ability of diagonally cracked concrete to transmit tension
β_d = compression-softening reduction factor
γ_{xy} = shear strain
ε_0 = strain corresponding to the peak compressive stress f'_c
ε_1 = strain in concrete in direction 1; principal tensile strain
ε_2 = strain in concrete in direction 2
ε_{c1} = average concrete axial strain in the principal tensile direction
ε_{c2} = average concrete axial strain in the principal compressive direction
ε_{ci} = principal compressive strain
ε_{cr} = concrete cracking strain

ε_p = strain corresponding to the peak compressive stress, f_p
ε_t = strain at level of longitudinal reinforcement on tension side of member
ε_x = strain in direction x; longitudinal strain at mid-depth of section
ε_y = strain in direction y; strain at yield of reinforcing steel
θ = angle of inclination of diagonal compressive stress
ρ_l = longitudinal reinforcement ratio = $[A_s + A_{ps}]/b_w d$
ρ_{sx} = steel ratio for direction x
ρ_{sy} = steel ratio for direction y
ρ_v = ratio of area of vertical shear reinforcement to area of gross concrete area of a horizontal section = $A_v/b_w s$
ρ_x = steel ratio for x-direction
ρ_y = steel ratio for y-direction
ϕ = resistance factor
ϕ_p = strength reduction factor for prestress

Abbreviations and acronyms used without definitions in TRB publications:

AAAE	American Association of Airport Executives
AASHO	American Association of State Highway Officials
AASHTO	American Association of State Highway and Transportation Officials
ACI–NA	Airports Council International–North America
ACRP	Airport Cooperative Research Program
ADA	Americans with Disabilities Act
APTA	American Public Transportation Association
ASCE	American Society of Civil Engineers
ASME	American Society of Mechanical Engineers
ASTM	American Society for Testing and Materials
ATA	Air Transport Association
ATA	American Trucking Associations
CTAA	Community Transportation Association of America
CTBSSP	Commercial Truck and Bus Safety Synthesis Program
DHS	Department of Homeland Security
DOE	Department of Energy
EPA	Environmental Protection Agency
FAA	Federal Aviation Administration
FHWA	Federal Highway Administration
FMCSA	Federal Motor Carrier Safety Administration
FRA	Federal Railroad Administration
FTA	Federal Transit Administration
IEEE	Institute of Electrical and Electronics Engineers
ISTEA	Intermodal Surface Transportation Efficiency Act of 1991
ITE	Institute of Transportation Engineers
NASA	National Aeronautics and Space Administration
NASAO	National Association of State Aviation Officials
NCFRP	National Cooperative Freight Research Program
NCHRP	National Cooperative Highway Research Program
NHTSA	National Highway Traffic Safety Administration
NTSB	National Transportation Safety Board
SAE	Society of Automotive Engineers
SAFETEA-LU	Safe, Accountable, Flexible, Efficient Transportation Equity Act: A Legacy for Users (2005)
TCRP	Transit Cooperative Research Program
TEA-21	Transportation Equity Act for the 21st Century (1998)
TRB	Transportation Research Board
TSA	Transportation Security Administration
U.S.DOT	United States Department of Transportation